THE CRETACEOUS IGNEOUS PROVINCE OF THE SVERDRUP BASIN, CANADIAN ARCTIC: FIELD RELATIONS AND PETROCHEMICAL STUDIES

by

MARIE-CLAUDE WILLIAMSON

Submitted in partial fulfillment of the requirements
for the Degree of Doctor of Philosophy
at Dalhousie University, December 1988.

Department of Geology
Dalhousie University
Halifax, Nova Scotia
Canada B3H 3J5

Copyright (C) Marie-Claude Williamson, 1988

DALHOUSIE UNIVERSITY

FACULTY OF GRADUATE STUDIES

The undersigned hereby certify that they have read and recommend to the Faculty of Graduate Studies for acceptance a thesis entitled " The Cretaceous Igneous Province of the Sverdrup Basin, Canadian Arctic: Field Relations and Petrochemical Studies"

by Marie-Claude Williamson

in partial fulfillment of the requirements for the degree of Doctor of Philosophy.

©

Dated September 8, 1988

External Examiner _____

Research Supervisor _____

Examining Committee _____

_____

_____

_____

D A L H O U S I E U N I V E R S I T Y

DATE December 18th 1988

AUTHOR Marie-Claude Williamson

TITLE The Cretaceous Igneous Province of the Sverdrup Basin, Canadian Arctic: Field Relations and Petrochemical Studies.

Department or School Geology

Degree Ph.D. Convocation January Year 1989

Permission is herewith granted to Dalhousie University to circulate and to have copied for non-commercial purposes, at its discretion, the above title upon the request of individuals or institutions.

[redacted]

Signature of Author

THE AUTHOR RESERVES OTHER PUBLICATION RIGHTS, AND NEITHER THE THESIS NOR EXTENSIVE EXTRACTS FROM IT MAY BE PRINTED OR OTHERWISE REPRODUCED WITHOUT THE AUTHOR'S WRITTEN PERMISSION.

THE AUTHOR ATTESTS THAT PERMISSION HAS BEEN OBTAINED FOR THE USE OF ANY COPYRIGHTED MATERIAL APPEARING IN THIS THESIS (OTHER THAN BRIEF EXCERPTS REQUIRING ONLY PROPER ACKNOWLEDGMENT IN SCHOLARLY WRITING) AND THAT ALL SUCH USE IS CLEARLY ACKNOWLEDGED.

Dédié à Mark et Nicole;
à ma famille;
et aux pionniers de l'Opération Franklin.

Once in his life a man ought to concentrate his mind upon the remembered earth. He ought to give himself up to a particular landscape in his experience; to look at it from as many angles as he can, to wonder upon it, to dwell upon it.

He ought to imagine that he touches it with his hands at every season and listens to the sounds that are made upon it.

He ought to imagine the creatures there and all the faintest motions of the wind. He ought to recollect the glare of the moon and the colors of the dawn and dusk.

N. Scott Momaday

TABLE OF CONTENTS

		Page
	TABLE OF CONTENTS	v
	LIST OF ILLUSTRATIONS	ix
	LIST OF TABLES	xiii
	LIST OF PLATES	xv
	ABSTRACT	xvii
	ABBREVIATIONS AND SYMBOLS USED	xviii
	ACKNOWLEDGEMENTS	xix
CHAPTER 1	INTRODUCTION	
1.1	Problem and Objectives	1
1.2	Methodology and Thesis Organization	6
CHAPTER 2	GEOLOGICAL SETTING	
2.1	Introduction	8
2.2	Regional Setting	9
2.2.1	Arctic Geological Provinces	9
2.2.2	Major Structures in the Canada Basin	12
2.2.3	The Mesozoic Tectonic History of the Canadian Arctic and Alaska	14
2.3	The Sverdrup Basin	18
2.3.1	Mesozoic Stratigraphy	18
2.3.2	Igneous History	22
2.4	Study Area and Representative Sampling	28
CHAPTER 3	FIELD RELATIONS - EXTRUSIVE ROCKS	
3.1	Introduction	30
3.2	Field Characteristics of Cretaceous Volcanic Successions	30
3.2.1	Volcanic Rocks in the Isachsen Formation	30
3.2.2	The Strand Fiord Formation	36
3.2.3	Volcanic rocks in the Hassel Formation	47

		Page
3.3	Eruptive style in Cretaceous Volcanic Intervals	57
3.3.1	Volcanic rocks in the Isachsen and Hassel Formations	57
3.3.2	The Strand Fiord Formation	59
3.4	Summary and Discussion	66
CHAPTER 4	FIELD RELATIONS - INTRUSIVE ROCKS	
4.1	Introduction	71
4.2	East Axel Heiberg Island and Eureka Sound	73
4.2.1	The Lightfoot River Dyke Swarm	73
4.2.2	The Buchanan Lake and Eureka Sound Area	75
4.3	Northeastern Ellesmere Island	77
4.3.1	Tanquary Fiord area	77
4.3.2	North Shore of Lake Hazen and Piper Pass	85
4.4	Comparative Summary	91
4.5	Correlation with Volcanic Episodes	93
CHAPTER 5	PETROLOGY AND GEOCHEMISTRY OF EXTRUSIVE ROCKS	
5.1	Introduction	102
5.2	Characteristics of Cretaceous Volcanic Successions	104
5.2.1	Volcanic Rocks in the Isachsen Formation (Group 1)	104
5.2.2	The Strand Fiord Formation (Group 2)	108
5.2.3	Volcanic rocks in the Hassel Formation (Group 3)	131
5.3	Comparison of Early Cretaceous Volcanic Successions	135
5.3.1	Alteration Effects	135
5.3.2	Compositional Types	138
5.3.3	Tectonic Discrimination Diagrams	142
5.4	Petrology of the Strand Fiord basalts	145

		Page
5.4.1	Phase Equilibria	146
5.4.2	Compositional Variations	149
5.4.3	Petrogenesis	156
5.5	Summary and Discussion	176
CHAPTER 6	PETROLOGY AND GEOCHEMISTRY OF INTRUSIVE ROCKS	
6.1	Introduction	181
6.2	Characteristics of Intrusive Rocks	182
6.2.1	Groups A and B: East Axel Heiberg Island and Eureka Sound	182
6.2.2	Groups C and D: Northeastern Ellesmere Island	190
6.3	Petrochemical Studies	199
6.3.1	Alteration Effects	199
6.3.2	Intradyke or -sill Chemical Variations	202
6.3.3	Interdyke or -sill Chemical Variations	206
6.3.4	Compositional Types	209
6.3.5	Cluster Analysis	216
6.4	Summary and Conclusions	216
CHAPTER 7	COMPOSITIONAL VARIATIONS OF IGNEOUS ROCKS AND THEIR SIGNIFICANCE	
7.1	Introduction	218
7.2	Significance of Compositional Diversity	218
7.2.1	Crustal Contamination	219
7.2.2	Source Characteristics	227
7.3	Tectonic Controls on Magma Genesis	234
7.3.1	Episodicity	234
7.3.2	Spatial Distribution of Compositional Types	236
CHAPTER 8	TECTONOMAGMATIC EVOLUTION OF THE SVERDRUP BASIN	
8.1	Introduction	241
8.2	Tectonic Setting	244
8.2.1	Tectonic and Thermal History of the Sverdrup Basin	244
8.2.2	Origin and Age of the Canada Basin	246

		Page
8.3	Tectonomagmatic Model	251
8.4	Regional Implications	261
	APPENDIX A	267
	APPENDIX B	302
	APPENDIX C	326
	BIBLIOGRAPHY	396

LIST OF ILLUSTRATIONS

Figure		Page
1.1	Location of the Sverdrup Basin in the Canadian Arctic Archipelago	2
2.1	Geological provinces of the Canadian Arctic Archipelago (after Trettin, 1987)	10
2.2	Map showing the position of major structures in the Amerasian and Eurasian Basins (after Srivastava, 1985)	13
2.3	Major depositional and tectonic events in the western Queen Elizabeth Islands (from Kerr, 1981)	15
2.4	Mesozoic stratigraphic succession in the central and eastern Sverdrup Basin (after Balkwill, 1978)	20
2.5	Volcanic stratigraphy in Cretaceous strata of the east-central Sverdrup Basin (from Embry and Osadetz, in press)	23
2.6	Location of the study area	26
3.1	Sampling stations for extrusive rocks	31
3.2	Detailed volcanic stratigraphy of the Strand Fiord Formation along the south shore of Bunde Fiord, northern Axel Heiberg Island	40
3.3	Reconstruction of volcanic and volcaniclastic facies in the Artharber Creek section, northern Axel Heiberg Island	41
3.4	Stratigraphic sections of the Strand Fiord Formation in the type area, western Axel Heiberg Island	45
3.5	Examples of intraflow structures in flood basalts (from Long and Wood, 1986)	48
3.6	Simplified cross-sections of lava tubes (from Greeley, 1987)	60
3.7	Eruptive and depositional setting at the margin of a basaltic plateau	65

Figure		Page
3.8	Eruptive style in a region of "basaltic plains" volcanism (from Greeley, 1982)	68
4.1	Sampling stations for intrusive rocks	72
4.2	Geology and sampling stations in the Lightfoot River area	74
4.3	(a) Geology and sampling stations in the Buchanan Lake area	76
	(b) Field relationships between intrusive units	78
4.4	Geology and sampling stations, Tanquary Fiord	82
4.5	Geology and sampling stations, Lake Hazen	87
4.6	Geology and sampling stations, Piper Pass	88
4.7	Results of $^{40}Ar/^{39}Ar$ step-heating analyses by Avison (1987) on samples from Buchanan Lake	97
4.8	Results of $^{40}Ar/^{39}Ar$ step-heating analyses by Avison (1987) on samples from Lake Hazen and Piper Pass	98
5.1	Pyroxene compositions in selected Group 2 basalts	115
5.2	Type and relative proportions of phenocrysts in Group 2B basalts at Artharber Creek	118
5.3	Percentage change of major and trace elements relative to TiO_2 in altered volcanic rocks	137
5.4	Classification diagrams for volcanic rocks	140
5.5	Primitive mantle-normalized diagrams for selected volcanic rocks	141
5.6	(a) Plot of $^{87}Sr/^{86}Sr$ initial ratios vs. Sr	144
	(b) Ti-Zr-Y tectonic discrimination diagram	
5.7	Projections of whole rock compositions for Group 2 basalts in the tetrahedron plag-oliv-diops-quartz	147

Figure		Page
5.8	Variations in the contents of Al_2O_3, CaO, FeOT, TiO_2 and MgO in a basaltic liquid undergoing gabbro fractionation	150
5.9	Two-element variation diagrams for Group 2 basalts	151
5.10	Chondrite-normalized rare earth patterns for Group 2 basalts	155
5.11	Test of petrogenetic processes using log-log plots of compatible and incompatible element concentrations in basaltic rocks	160
5.12	Log-log diagrams of Ni and Cr vs. La, Hf and Th for Group 2 basalts	162
5.13	Examples of the effects of perfect fractional crystallization and AFC on log-log diagrams of Ni or Cr vs. La, Th and Nb	167
5.14	Plot of $^{87}Sr/^{86}Sr$ initial ratios vs. Sr contents	173
6.1	Pyroxene and feldspar compositions in Group C and D gabbros	196
6.2	Percentage change of major and trace elements relative to TiO_2 in altered intrusive rocks	201
6.3	Examples of compositional changes due to internal differentiation	204
6.4	Two-element variation diagrams for Group B, C and D intrusives	207
6.5	Classification diagrams for intrusive rocks	210
6.6	Primitive mantle-normalized diagrams for selected intrusive rocks	213
6.7	Ti-Zr-Y discrimination diagram for intrusive rocks	214
6.8	Chondrite-normalized rare earth patterns for selected intrusive rocks	215
7.1	Th-Hf-Ta diagram of Wood (1980)	221
7.2	(a) Plot of Th/Hf vs. $^{87}Sr/^{86}Sr$ isotopic ratios (b) Plot of Th/Hf vs. SiO_2	224

Figure		Page
7.3	Plot of eNd vs $^{87}Sr/^{86}Sr$ initial ratios	225
7.4	Petrogenetic grid of Takahashi and Kushiro (1983)	228
7.5	Plots of Zr vs. Y and Zr vs. Nb for igneous rocks of the study area	232
7.6	Geographic distribution of compositional types across the eastern Sverdrup Basin	237
7.7	TiO_2-Nb/3-Th discrimination diagram of Holm (1985) for within-plate basalts	239
8.1	Major Cretaceous tectonic provinces of Arctic North America and northern Greenland (from Balkwill el al, 1983)	242
8.2	Crustal cross-section from northern Ellef Ringnes Island to the Canada Basin (after Sweeney, 1986b)	248
8.3	Plate tectonic reconstructions and rotation model for the opening of the Amerasian Basin (from Jackson et al, 1986)	250
8.4	(a) Variation in the degree of partial melting of a pyrolite mantle according to temperature and depth (from Keen, 1987) (b) Tectonomagmatic evolution of the Sverdrup Basin	254
8.5	Schematic model for the combined evolution of parallel rift basins developed in continental crust (after Salveson, 1978)	257

LIST OF TABLES

Table		Page
1.1	Physical aspects of selected basalt plateaus	3
2.1	Evidence supporting the origin of the Canada Basin by rotation of the Arctic-Alaska plate	17
2.2	Summary of age determinations on mafic intrusive rocks of the Sverdrup Basin	24
3.1	Eruptive setting of the Strand Fiord Formation, western Axel Heiberg Island	64
4.1	Summary of Cretaceous magmatic cycles: eastern and central Sverdrup Basin	100
5.1	Sampling information for extrusive rocks	103
5.2	Representative whole rock geochemical data for Group 1 and 3 basalts	107
5.3	Representative mineral analyses, Group 2A	111
5.4	Type and proportions of phenocrysts in the Group 2B basalts	116
5.5	Representative mineral analyses, Group 2B	123
5.6	Range, means and standard deviations for major and trace elements, Group 2A	128
5.7	Additional trace element data for the Group 2A basalts at Twisted Ridge	130
5.8	Range, means and standard deviations for major and trace elements, Group 2B	132
5.9	Additional trace element data for Group 2B basalts at Celluloid Creek	134
5.10	Sr-isotopic compositions of selected Group 1, 2 and 3 basalts	143
5.11	Results of mass balance calculations	158
5.12	(a) Summary of partition coefficients used in trace element modelling (b) Contamination model end-members	166
6.1	Chemical analyses, Group A	184

Table		Page
6.2	Additional trace element data, Group A	185
6.3	Chemical analyses, Group B (chilled margins of sills)	188
6.4	Other representative chemical analyses, Group B	189
6.5	Selected mineral analyses, Groups C and D	192
6.6	Chemical analyses, Groups C and D	197
6.7	Additional trace element data, Groups C and D	198
7.1	Composition, location and age of igneous rocks	220

LIST OF PLATES

Plate		Page
1	Cross-section of a lava tube, Blue Mountains, northwestern Ellesmere Island	34
2	The Strand Fiord Formation at Celluloid Creek, northern Axel Heiberg Island	37
3	Structures at the base of a lava flow in the Strand Fiord Formation, south shore of Bunde Fiord	37
4	Valley and ridge topography, type area at Strand Fiord, western Axel Heiberg Island	43
5	The Strand Fiord Formation at Dragon Cliff	43
6	Type II intraflow structures in ponded flood basalts, type area at Strand Fiord	49
7	Type III intraflow structures, type area at Strand Fiord	49
8	Invasive flow along Split Mountain ridge, type area at Strand Fiord	51
9	Type II intraflow structures at Bastion Ridge, type section of the Strand Fiord Formation	51
10	Variations in intraflow structures along strike, south shore of Strand Fiord	53
11	Pillow lavas and tubes at Castle Mountain, type area at Strand Fiord	53
12	Invasive flows along coastal cliff sections, Index Ridge Peninsula, Strand Fiord	55
13	Scoriaceous tops, Index Ridge Peninsula	55
14	Cross-cutting relationships observed on the north shore of Buchanan Lake	79
15	Thin, feldspar-phyric dyke cutting through a sill, south shore of Buchanan Lake	79
16	Sills exposed along Rollrock River, head of Tanquary Fiord	83

Plate		Page
17	Cliff section along the Macdonald River, head of Tanquary Fiord	83
18	Sills in the Piper Pass area, northeastern Ellesmere Island	89
19	Three-fold structural division in the Dark Crystal sill, Piper Pass	89
20	Lithologic variations in a composite intrusion near Lake Hazen	94
21	Textural character of clinopyroxene oikocrysts in Group 2 basalts	109
22	Olivine phenocrysts and glomeroporphyritic texture, Group 2B basalt at Celluloid Creek	119
23	Glomeroporphyritic texture, Group 2B basalt at Artharber Creek	119
24	Poikilitic texture of plagioclase phenocrysts, Group 2B basalt at Artharber Creek	121
25	Melt inclusions in resorbed phenocryst, Group 2B basalt at Artharber Creek	121
26	Relict olivine enclosed in augite, Group 2B basalt at Artharber Creek	126
27	Relict cores of olivine in plagioclase phenocrysts, Group 2B basalt at Artharber Creek	126

ABSTRACT

Field, petrological and geochemical studies of Cretaceous igneous rocks in the Sverdrup Basin, Canadian Arctic, have defined the timing and character of continental magmatism, during tectonic rejuvenation.

One hundred and forty-six whole-rock chemical analyses were obtained on samples of volcanic and intrusive rock in the study area. Two compositional types of volcanic and intrusive rocks were identified: LREE-enriched basaltic lavas and gabbros of subalkaline affinity, with moderate to high TiO_2 contents; and high-TiO_2, olivine-normative gabbros and ferrobasaltic lavas of mildly alkaline character. Compositional differences between these igneous rock types are interpreted in terms of variable degrees of partial melting of a heterogeneous mantle source, combined with the selective interaction of tholeiitic magmas with crustal melts. Detailed petrogenetic studies of basaltic lavas, erupted during the peak of Early Cretaceous volcanic activity, suggest a complex origin involving a combination of fractional crystallization, magma mixing, and the selective assimilation of upper crustal rocks. The AFC process also accounts for the range of $^{87}Sr/^{86}Sr$ and $^{143}Nd/^{144}Nd$ initial isotopic ratios observed (0.70563-0.70913; 0.51188-0.51207).

The timing and character of Cretaceous magmatism are interpreted in terms of the crustal stratigraphy and locus of extensional movements, during renewed rifting in the eastern part of the Sverdrup Basin. Tectonic rejuvenation is linked to the development of the Sverdrup and Canada Basins as conjugate rift systems, during extension that eventually led to the formation of the polar continental margin. Voluminous magmatism of subalkaline character occurred in areas close to the Sverdrup Basin depocentre, where maximum lithospheric thinninng favoured greater degrees of partial melting of mantle material and interaction with the upper crust. More alkaline magmas showing little or no evidence for contamination, were emplaced beneath thicker, cooler crust, along the southern margin of the basin. A progressive widening of the tectonic zone to the north is consistent with extension along the adjacent rifted margin. Tectonic movements in parts of this extensional zone triggered the emplacement of alkali basalt-trachyte-rhyolite suites, during the final phase of volcanic activity in the Late Cretaceous.

SYMBOLS AND ABBREVIATIONS USED

CFB	Continental Flood Basalts
REE	Rare Earth Elements L- Light H- Heavy
LILE	Large-ion Lithophile Elements
IRT	Initial Rifting Tholeiites
MORB	Mid-Ocean Ridge Basalts
TR	Twisted Ridge section
BR	Bastion Ridge section
GFS	Glacier Fiord Syncline section
CC	Celluloid Creek section
AC	Artharber Creek section
AFC	Assimilation-Fractional Crystallization
PPL	Plane-polarized light
XPL	Cross-polarized light
β	Stretching factor (lithosphere)

ACKNOWLEDGEMENTS

I wish to thank N.J. McMillan, whose interest prompted the initiation of this study; and my supervisors, G.K. Muecke and D.B. Clarke, for their guidance and support throughout the project. I would also like to thank the Institute of Sedimentary and Petroleum Geology (Geological Survey of Canada) in Calgary, which provided a substantial part of the funding for laboratory and field work, and access to their facilities to complete the project; and the Polar Continental Shelf Project, for aircraft and logistic support in the field. Part of the research was financed through an operating grant from the Natural Sciences and Engineering Research Council of Canada to Dr. G.K. Muecke.

I would like to thank Ashton Embry and Kirk Osadetz who helped me organize the field work between 1983 and 1985, allowing me to work out of their field camps, and kindly providing the background stratigraphic information and their own data whenever necessary. The field work could not have been undertaken without their cooperation and previous work in the area. Karen Wallace-Dudley and Mark Williamson are thanked for able assistance in the field. I am particularly indebted to Gunter Muecke for his great enthusiasm and expertise, most appreciated during our 1984 and 1985 expeditions. For technical help, I am grateful to R. Mackay, D. Merrett, K. Cameron and M. Parikh in Halifax; C. Thompson, K. Nairn, W. Pickering, R. Larush, and A. Pascual, in Calgary; and Dr. Peter Dulski, of the Hahn-Meitner Institut in Berlin. The staff at the I.S.P.G. Library were particularly helpful during the final stages of writing, and I thank them for their help and encouragement.

Mes meilleurs souvenirs vont aux professeurs et aux étudiants du Département de Géologie, à l'Université de Montréal, et en particulier aux membres de l'équipe du Laboratoire de Géochimie Isotopique, 1985-87, qui m'ont communiqué leur science et leur enthousiasme: Chris Brooks, John Ludden, Gilles Gauthier, Pierre Thibault, Claude Gagné, Michel Boily et Ole Stecher.

I. INTRODUCTION

1.1 Problem and Objectives

Continental flood basalts (CFB) and associated intrusions, are the most extensive manifestation of intraplate magmatism on earth (Basaltic Volcanism Study Project, 1981). The Cretaceous volcanic-intrusive province of the Sverdrup Basin, in the Canadian Arctic (Fig. 1.1), was emplaced over a period of approximately 60 million years (Embry and Osadetz, in press; Avison, 1987). Estimates of the volume of magma erupted are similar to those reported for western U.S. Cenozoic provinces such as the Columbia River Plateau (10,000 to 20,000 km^3; Table 1.1). The volume of magma intruded as sills or dykes is at least ten times larger, resulting in the predominantly intrusive character of the province, comparable to parts of the East Greenland Province or the early Jurassic Karoo and Ferrar dolerites of South Africa and Antarctica.

The Sverdrup Basin is a large epicontinental basin with a depositional history that spans 250 million years from the Early Carboniferous to the Tertiary. Limited volcanic activity associated with the initial rifting event took place early in the history of the basin. During the final depositional stage in the Cretaceous, voluminous tholeiitic magmas systematically intruded the Mesozoic succession and lava flows were erupted episodically.

This first comprehensive study of igneous rocks in the Sverdrup Basin follows recent advances in better defining the nature of Cretaceous rifting events in and around the Arctic Ocean. Stratigraphic

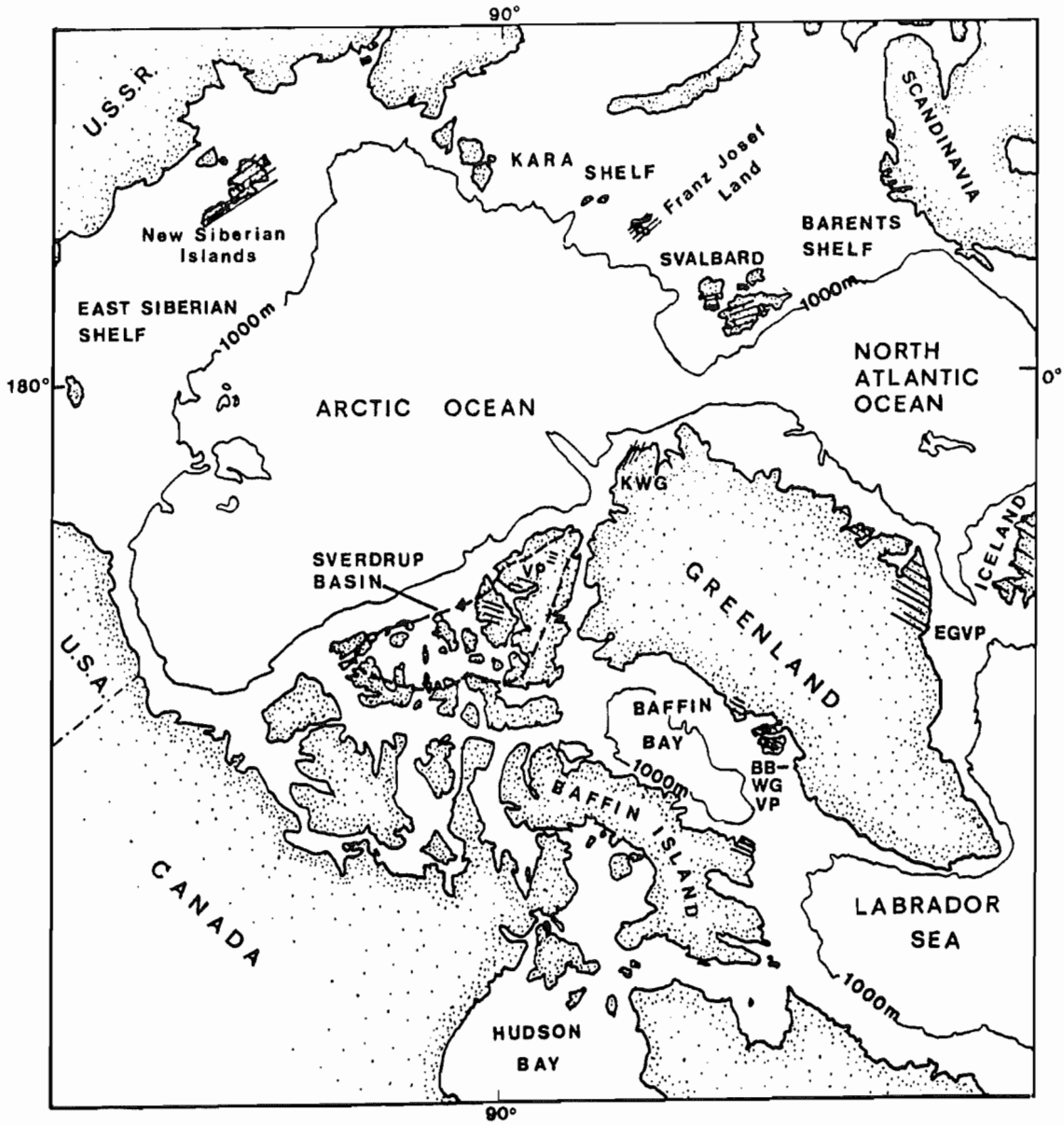

Figure 1.1 Location of the Sverdrup Basin, in the Canadian Arctic Archipelago. The Cretaceous igneous province is best exposed in the east-central part of the Basin (VP). Other areas of Mesozoic-Cenozoic igneous activity in Arctic and North Atlantic regions include: The Baffin Bay-West Greenland Volcanic Province (BB-WGVP), the East Greenland Volcanic Province (EGVP), the Kap Washington Group (KWG), Svalbard, and Iceland. Johnson and Rich (1986) report Cretaceous volcanic activity on Franz Josef Land and the New Siberian Islands. Modified from Srivastava (1985).

TABLE 1.1
PHYSICAL ASPECTS OF SELECTED BASALT PLATEAUS (1)

BASALT PLATEAU	AGE	MAXIMUM AND AVERAGE THICKNESS	PRESENT AND POSSIBLE ORIGINAL AREA	APPROXIMATE VOLUME	FLOW THICKNESS
Columbia River Province	17 - 6 m.y.	1000 m +	200,000 km^2	2-3 x $10^5 km^3$	10 - 45 m
Deccan Traps Province	65 - ?50 m.y.	max. 2000 m min. 100 - 200 m	500,000 km^2	7 x $10^5 km^3$	
Sverdrup Basin	125 - 90 m.y.	Strand Fiord Formation max. 800 m	Extrusives (L. Albian) 30,000 km^2 Intrusives: ?	1-2 x $10^4 km^3$ Sills 1 x $10^5 km^3$?	10 - 60 m max. 100 m
Paraña Basin	119 - 149 m.y.	1500 - 1800 m average 650 m	1,200,000 km^2 original 2,000,000 km^2	6.5 x $10^5 km^3$	aver. 50 m max > 100 m
Karoo Province	166 - 206 m.y.	8000 - 9000 m average ?1000 m	140,000 km^2 original 2,000,000 km^2	?	aver. 10 m (?) sills to 1000 m
Siberian Platform	216 - 248 m.y.	3500 m average 1000 m	> 1,500,000 km^2	6 x $10^5 km^3$ (9 x $10^5 km^3$ incl. intrusions)	aver. 30 m
Lake Superior Basin (Keweenawan)	1100 - 1120 m.y. (-1200?)	8000 - 12000 m average 5000 m	100,000 km^2 original 125.000 km^2?	> 3 x $10^5 km^3$	3 - 30 m aver. 25 m max. 400 m

(1) Modified from Table 1.2.2.1, Basaltic Volcanism Study Project (1981) with additional information from Hooper (1982) and this study.

and geophysical data from Alaska, the Canadian Arctic Islands and polar ice stations suggest that the Canada Basin opened during the Early (?) Cretaceous from a pole of rotation located near the Beaufort Sea (e.g. Sweeney, 1985; Jackson et al., 1986). This led to a re-examination of the Cretaceous volcanic stratigraphy in the central part of the Sverdrup Basin and renewed interest in its tectonic significance.

The association of CFB provinces with the initial rifting attending continental breakup and the formation of new ocean basins is well documented (e.g. Burke and Kidd, 1980). In detail, however, the physical processes operating in this environment were poorly understood. Renewed interest in continental basalts during the 1980's has provided insight into the petrology and geochemistry of igneous rocks from extensional settings, with implications for the nature of the subcontinental mantle, role of crustal assimilation, and relative timing of magmatic and rifting events. As in any rifting environment, the progression of magmatism in time and space is a critical aspect of the igneous history. There is increasing evidence that the nature of the erupted or intruded magmas is closely related to the locus of extension and thermal state of the lithosphere at the time of rifting. The type of feeders or "plumbing system" also plays an important role in determining the style of volcanism and the physical processes operating on the ascending magmas.

In many continental igneous provinces, the overall picture is that of an apparently monotonous succession of igneous rocks which in fact records a highly complex history. In the case of the Sverdrup Basin, the study of igneous rocks is facilitated by excellent exposure and stratigraphic control. Specific aspects of rift-related magmatism can

elements were determined for 60 samples at the geochemical division of the Hahn-Meitner Institut, Berlin. Between 1985 and 1987, the author performed isotopic analyses on selected samples at the Laboratoire de Géochimie Isotopique, Université de Montréal.

After extensive sampling of intrusive rocks in 1984, it became apparent that radiometric dating of the sills was essential and deserving of separate attention. To this end, a suite of samples was dated by Avison (1987) at Dalhousie University using $^{40}Ar/^{39}Ar$ step-heating analysis. In addition, trend analyses of dykes in the Sverdrup Basin and a preliminary geochemical study were performed by Jollimore (1986).

This thesis is divided into three parts, corresponding to field relations, petrochemical studies and tectonic interpretation respectively. For the purpose of clarity, descriptions and data on volcanic and intrusive rocks were kept separate. Chapter 2 is a brief summary of the geological and tectonic setting of the study area. Chapter 3 presents the field observations on volcanic rocks and an interpretation of the eruptive style. Field relations of intrusive rocks are presented in Chapter 4, and a comparison made between relative or stratigraphic ages of igneous rocks and the limited number of radiometric dates obtained by Avison (1987). The association between intrusive and extrusive rocks is examined and a working hypothesis formulated before proceeding to Part II, petrology and geochemistry. In Chapter 5, a classical approach to the study of volcanic rocks is used, with discussions on mineralogical, geochemical and isotopic data. The mineralogical and geochemical data on intrusive rocks are presented in Chapter 6 in the form of a reconnaissance study, with emphasis on the

be examined such as the spatial-temporal association between intrusive and extrusive rocks, the role of crustal assimilation, and the nature of extensional events in a basin setting, that led to voluminous magmatism during the Cretaceous.

With the above in mind, the aims of this study are:

1. to determine the field relations of intrusive and extrusive rocks, and to clarify their relative age and associations;

2. to examine the petrology and geochemistry of a representative suite of volcanic and intrusive rocks and to determine their petrogenesis;

3. to integrate the data in a general tectonomagmatic model for the Sverdrup Basin;

4. to discuss the implications of the study for the nature and timing of rift-related magmatism in Arctic regions and along the eastern Canadian continental margin.

1.2 Methodology and Thesis Organization

The field work for this study took place between 1983 and 1985. The primary objective was to collect field observations and samples from volcanic successions and intrusive rocks exposed on Axel Heiberg and Ellesmere Islands. A total of 146 samples was examined in detail during the study. Petrographic observations were made on all the samples and mineralogical data obtained for a representative suite of volcanic rocks and some intrusive rocks. Whole-rock geochemical data include the major elements and 16 trace elements and were obtained at Dalhousie University and at the XRF Facility, St.-Mary's University, Halifax. Rare earth

effects of in situ differentiation, and the geographic distribution of compositional types across the study area. The pertinent data are reviewed in Chapter 7, in a discussion on the role of crust and mantle processes during magma genesis. A tectonomagmatic model for the evolution of the Sverdrup Basin is described in Chapter 8.

II. GEOLOGICAL SETTING

2.1 Introduction

This chapter outlines the geological and tectonic setting of the Canadian Arctic Islands, addressing in particular the origin, evolution and igneous history of the Sverdrup Basin. The main purpose of the review is to acquaint the reader with previous studies in the area and provide the geological framework for the following chapters. A brief description of Arctic geological provinces and major structures in the Canada Basin is followed by a summary of Mesozoic tectonic events in Arctic regions. The age and distribution of igneous rocks in the Sverdrup Basin are discussed, as well as current interpretations of the tectonic setting based on stratigraphic and geophysical studies.

In the classification of Bally (1987), the Sverdrup Basin is included with other basins that developed within rigid lithosphere, and straddle an ocean-continent boundary (e.g. Atlantic-type margins, Rio Grande rift). To date, the only two models that have been proposed to explain the onset of voluminous magmatic activity during the Cretaceous both invoke rifing events that occurred during the depositional history of the basin. However, the nature and timing of extensional movements in this complex setting remain unclear - can all the magmatism be related to the initial rifting and subsidence history of the basin (Balkwill, 1983); or was igneous activity related to passive margin development and tectonic events in the Canada Basin (Embry and Osadetz, in press)? The evidence used in these models is described in Section

2.3.2 and re-examined in Chapter 8, in the light of new results from this study.

2.2 Regional Setting

2.2.1 Arctic Geological Provinces

The Canadian Arctic Islands contain several geologic provinces that exhibit a general "northward-decreasing" age. These provinces record a complex geological history including:

- the formation of mobile belts and tectonic accretion of an "exotic" terrane during the lower Paleozoic;
- the depositional and magmatic history of a major, long-lived sedimentary basin that was active in the late Paleozoic and throughout the Mesozoic;
- a regional compressive event which occurred in the Cenozoic and contributed to the present day exposures on Axel Heiberg and Ellesmere Islands.

A generalized map of the stratigraphic and structural framework is shown on Figure 2.1. North of the 75th parallel, Precambrian crystalline terranes are exposed mainly on southeast Ellesmere Island and Devon Island. Most of the units are inferred to be of Hadrynian-Helikian age and to underlie the early Paleozoic fold belts (Trettin and Balkwill, 1979). To the north, the Canadian Shield is overlain by a shallow to non-marine, Proterozoic and Phanerozoic carbonate and clastic sequence belonging to the Arctic Platform and Franklinian Basin. The Arctic Platform consists of Phanerozoic

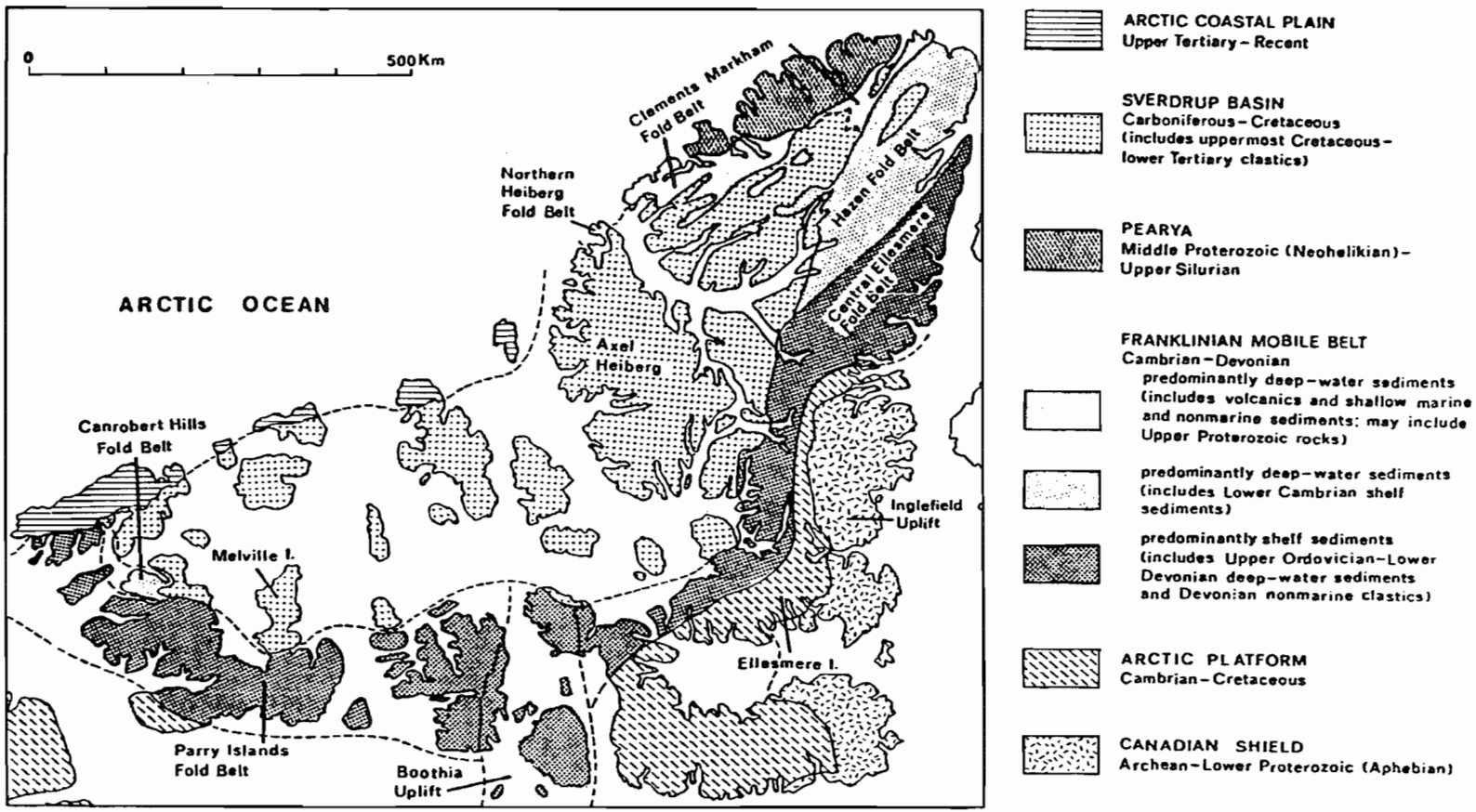

Figure 2.1 Geological provinces of the Canadian Arctic Archipelago. Modified from Trettin (1987); with structural features of Harrison and Bally (submitted manuscript).

successions that have not been folded or thrust-faulted on a regional scale. The sedimentary sequence is divided into a lower-middle Paleozoic succession and a Mesozoic-Paleogene succession (Trettin, in press). The Franklinian mobile belt preserves early Phanerozoic sedimentation in the Franklinian basin. The stratigraphic succession includes a shelf province and a deep-water basin of Early Cambrian to Early Devonian age. These strata were subsequently deformed by the Ellesmerian orogeny (Mid-Devonian to late Early Pennsylvanian) and forms an arcuate belt exposed throughout the Arctic Islands (Fig. 2.1). ***Pearya***, on northernmost Ellesmere and Axel Heiberg Islands, is divisible into four successions that include basement rocks of Grenvillian age, platformal sediments of late Proterozoic (?) to earliest Ordovician age and mafic-ultramafic complexes of Early (?) to Middle Ordovician age, overlain by a volcanic-sedimentary sequence of Middle Ordovician to Late Silurian age. The sequence is interpreted as a composite terrane that accreted to the Franklinian deep water basin in the Late Silurian (Trettin, 1987 and in press).

In the Early to Late Mississipian, the Sverdrup Basin developed over areas underlain by deformed Franklinian strata. During a long depositional history, the basin accumulated marine and non-marine clastic, carbonate and evaporite strata, and was influenced by episodic magmatic activity of an intrusive and extrusive nature (Balkwill, 1978). In the eastern part of the Canadian Arctic Archipelago, strata of the Sverdrup Basin underwent widespread tectonism during the Tertiary Eurekan Orogeny. These units are now partly overlain by a clastic wedge of Cenozoic age constituting the Arctic Coastal Plain.

2.2.2 Major Structures in the Canada Basin

Recent work shows that the geological evolution of the Canadian Arctic Islands during the Mesozoic is closely tied to tectonic events in the Canada Basin. The following is a brief description of the major structures illustrated on Figure 2.2 and a summary of the present knowledge concerning their mode of origin.

The Arctic Ocean is divided into the Amerasian Basin and Eurasian Basin, and is cut by three subparallel ridges, the Alpha-Mendeleev Ridge, the Lomonosov Ridge and the Nansen Ridge. The Canada Basin is bounded by the Alpha-Mendeleev Ridge, the Alaskan and Canadian polar continental margins, and the Chukchi Shelf. Both the Amerasian and Eurasian basins are floored by oceanic crust overlain by up to 5 km of sediment (e.g. Oliver et al., 1955; Hall, 1973; Baggeroer and Falconer, 1982). Spreading along the Nansen Ridge during the Tertiary formed the Eurasian Basin and caused a fragment of the Barents Shelf to rift and form the Lomonosov Ridge (e.g. Srivastava, 1985). The history of the Amerasian Basin is still poorly understood. Recent progress is in large part attributable to multidisciplinary studies of the Alpha Ridge, the largest structure in the Canada Basin. Geophysical surveys of the ridge suggest that crestal morphology, sediment-basement structures and average crustal velocities are similar to those of oceanic plateaus (Forsyth et al., 1986; Jackson et al., 1986). The volcanic nature of the Alpha Ridge is also indicated by mineralogical and geochemical data on igneous rocks recovered from dredge hauls (Van Wagoner et al., 1986). The age of the Alpha Ridge is constrained to pre-Late Campanian (approximately 75 Ma) based on magnetic measurements, heat flow

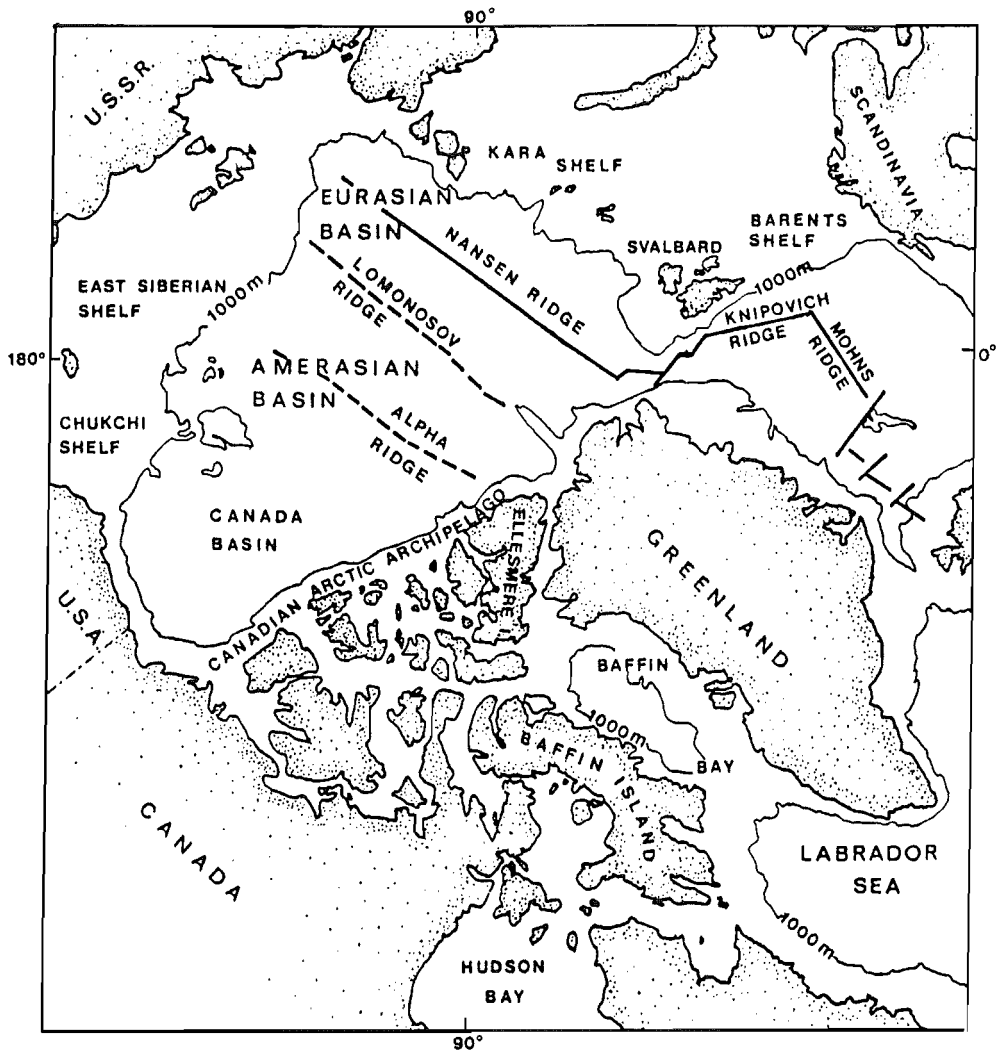

Figure 2.2 Map showing the position of major structures in the Amerasian and Eurasian Basins. Dashed line, extinct ridge; full line, active ridge. Modified from Srivastava (1985).

estimates and biostratigraphy of sediment cores (e.g. Sweeney and Weber, 1986). The origin of the ridge could therefore be tied to the opening of the Canada Basin (e.g Jackson et al., 1986).

2.2.3 The Mesozoic Tectonic History of the Canadian Arctic and Alaska

The plate tectonic history of Arctic regions is highly complex and still controversial. There are several options for palinspastic reconstructions (e.g. Carey, 1955; Tailleur and Brosgé, 1970; Harland and Gayer, 1972; Morel and Irving, 1978; Scotese et al., 1979; Smith et al., 1981), most of which are summarized in the classification scheme of Harland et al. (1983).

The Precambrian to Neogene tectonic evolution of the Arctic involves the opening and closure of the Iapetus Ocean, relative motions between Eurasia and North America, the formation of the Urals during the collision of Siberia with the Russian Platform, possible motions of Alaska with respect to North America, and the opening of the North Atlantic and Eurasian Basin. In the Canadian Arctic Islands, these events are viewed by Kerr (1981) as involving a constructional phase, followed by the fragmentation of the resulting protocontinent. Figure 2.3 is a simplified diagram illustrating the timing of major depositional and tectonic events. The constructional phase involved the formation of large sedimentary basins of Paleozoic age on crystalline Precambrian basement (Franklinian geosyncline), ending in the Late Devonian-Mississipian at the close of the Ellesmerian Orogeny (Trettin and Balkwill, 1979; Kerr, 1981). The development of the Sverdrup Basin

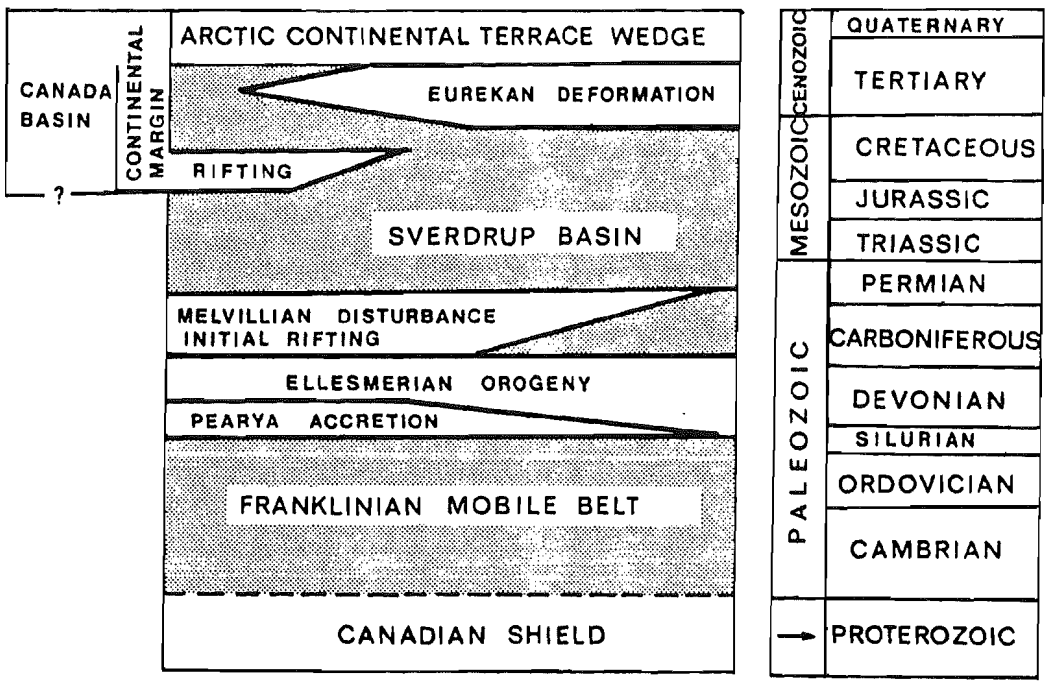

Figure 2.3 Simplified diagram illustrating major depositional and tectonic events in the western Queen Elizabeth Islands. Grey shading outlines major depositional provinces. Thick lines indicate tectonic events. Modified from Kerr (1981, Fig. 4) according to Trettin (in press).

in the upper Paleozoic and lower Mesozoic is marked by a period of relative tectonic stability, as evidenced by the presence of shelf or basin sequences in other Arctic regions (e.g. Harland et al., 1983). Of main interest here are the late Mesozoic rifting events and continental (?) displacements that led to the opening of the Canada Basin.

Carey (1958) was first to propose the concept of a triangular tension rift or "Arctic Sphenochasm", apically opposed to the Alaskan orocline. The implied rotation of the Alaska North Slope and adjacent Siberian margin away from Arctic Canada was later favoured by Hamilton (1970) who recognized a late Paleozoic continuity between the Uralides and Ellesmerides of northern Greenland and the Canadian Arctic Islands. Other models for the origin of the Amerasian Basin require movement along major transform faults (e.g. Herron et al., 1974; Jones, 1980), the complex interaction of micro-continents involving the Kula (proto-Pacific) plate (Churkin and Trexler, 1980) or the motion of Alaska away from the Lomonosov ridge (Dutro, 1981). Recent syntheses of Arctic Mesozoic tectonics favour the rotation model (e.g. Harland et al., 1983; Burke, 1984; McWhae, 1986).

Geophysical, structural and stratigraphic evidence that support rotation of the Arctic Alaska plate are listed in Table 2.1. Several features are compatible with the progressive development of a passive margin, such as early tensional faulting and local uplift, followed by subsidence and deposition along the margin. According to Sweeney (1985), continental breakup may have occurred between about 131 and 113 Ma. Sea-floor spreading from the start of the long normal magnetic interval to magnetic anomaly 33 time (125?-79 Ma) could provide an explanation for the absence of well-defined marine magnetic anomalies

TABLE 2.1
EVIDENCE SUPPORTING THE ORIGIN OF THE CANADA BASIN
BY ROTATION OF THE ARCTIC-ALASKA (AA) PLATE (1)

GEOPHYSICAL	STRUCTURAL	STRATIGRAPHIC
1. Paleomagnetic measurements in the Brooks Range, Alaska: Newman *et al.*, 1977, challenged by Hillhouse and Gromme, 1982.	1. Normal dip-slip faults off northern Alaska - movement of the Rapid Fault Array (Young *et al.*, 1986).	1. Uplift and erosion along the Barrow Arch and Sverdrup Basin (thermal effects during rifting?; *eg.* Embry and Osadetz, in press).
2. Sea-floor spreading anomalies in southern Canada Basin (Vogt *et al.*, 1982).	2. Development of the Banks and Eglinton Basins (Embry *et al.*, in prep.).	2. Uplift of the Brooks Range and presence of mafic-ultramafic complexes at the plate edge (Tailleur, 1973).
3. Possible extinct spreading axis (Taylor *et al.*, 1981).	3. Presence of transverse structures (transform faults?) perpendicular to the margin: Canadian Arctic Islands (Vogt *et al.*, 1982) and Alaska (Grantz et al., 1979).	3. Break-up unconformity along the western part of the polar margin (Meneley, 1975; Balkwill, 1978; Embry *et al.*, in prep.).

(1) Modified from Harland *et al.* (1983)

next to the continental margin (e.g. Vogt et al., 1982). Despite this recent influx of data from airborne geophysical surveys and ice stations, the evolution of the polar continental margin remains a subject of controversy. In the Canadian Arctic Islands, the geometry of rifting is still poorly understood and the timing of the possible strike-slip displacements along its length is a serious challenge to the rotational hypothesis (Oldow et al., 1987). Evidence for rifting within the Sverdrup Basin is reviewed in the following section.

2.3 The Sverdrup Basin

2.3.1 Mesozoic Stratigraphy

The Sverdrup Basin is a northeast-trending, elongate structural depression, approximately 1300 km long and 350 km wide (Balkwill, 1978, 1983). The basin contains up to 13 km of sedimentary rocks of Carboniferous to Tertiary age which overlie deformed strata of the lower Paleozoic Franklinian Geosyncline. The succession is concordant in the axial parts of the basin and unconformable along the margins. Since the first formal definition by Fortier (1957), the Sverdrup Basin has been described in several accounts (e.g. Thorsteinsson and Tozer, 1960, 1970; Fortier et al., 1963; Plauchut, 1971; Balkwill, 1978). Excellent stratigraphic summaries are presented in Balkwill (1978), Nassichuk and Davies (1981) and Balkwill et al. (1983). The reader is referred to Thorsteinsson (1974) for detailed descriptions of Carboniferous and Permian stratigraphy in the study area. More relevant to the present

work, is a brief overview of the Mesozoic succession of the Sverdrup Basin as it contains the igneous rocks described in this study.

The 9 km thick Mesozoic succession is well studied from exposures of broadly folded strata on Axel Heiberg and north-central Ellesmere Islands, and borehole data from the central and western parts of the basin. A schematic diagram of Mesozoic stratigraphic nomenclature in the eastern and central parts of the Sverdrup Basin is shown on Figure 2.4. The sequence is interpreted as a series of regional transgressive-regressive cycles often separated by unconformities at the basin margins (Embry, unpubl. man.). The cyclic nature of the depositional sequence is attributed to eustatic sea level changes at 4-6 Ma intervals. Variable rates of sediment supply throughout the Mesozoic are caused by episodic uplift of cratonic areas to the south and east. Other influences on stratigraphy include Carboniferous evaporite diapirism (Nassichuk and Davies, 1981) which caused local uplift and erosion as early as the Triassic.

The present outline of the basin coincides approximately with the extent of the Ellesmerian orogeny (Fig. 2.1). A distinctive morphological feature is the Sverdrup Rim (Meneley et al., 1975) which constitutes the northwestern margin of the basin and trends parallel to the present continental shelf edge. This recurrent positive element influenced depositional patterns during the late Paleozoic, but its role during the Mesozoic is still poorly understood.

The Sverdrup Basin is underlain by continental crust that has been thinned by stretching. The sedimentary thickness ranges from 9 to 17 km and the underlying crystalline basement varies from 18 to 33 km (Forsyth et al., 1979; Sobczak and Overton, 1984). According to Bally and

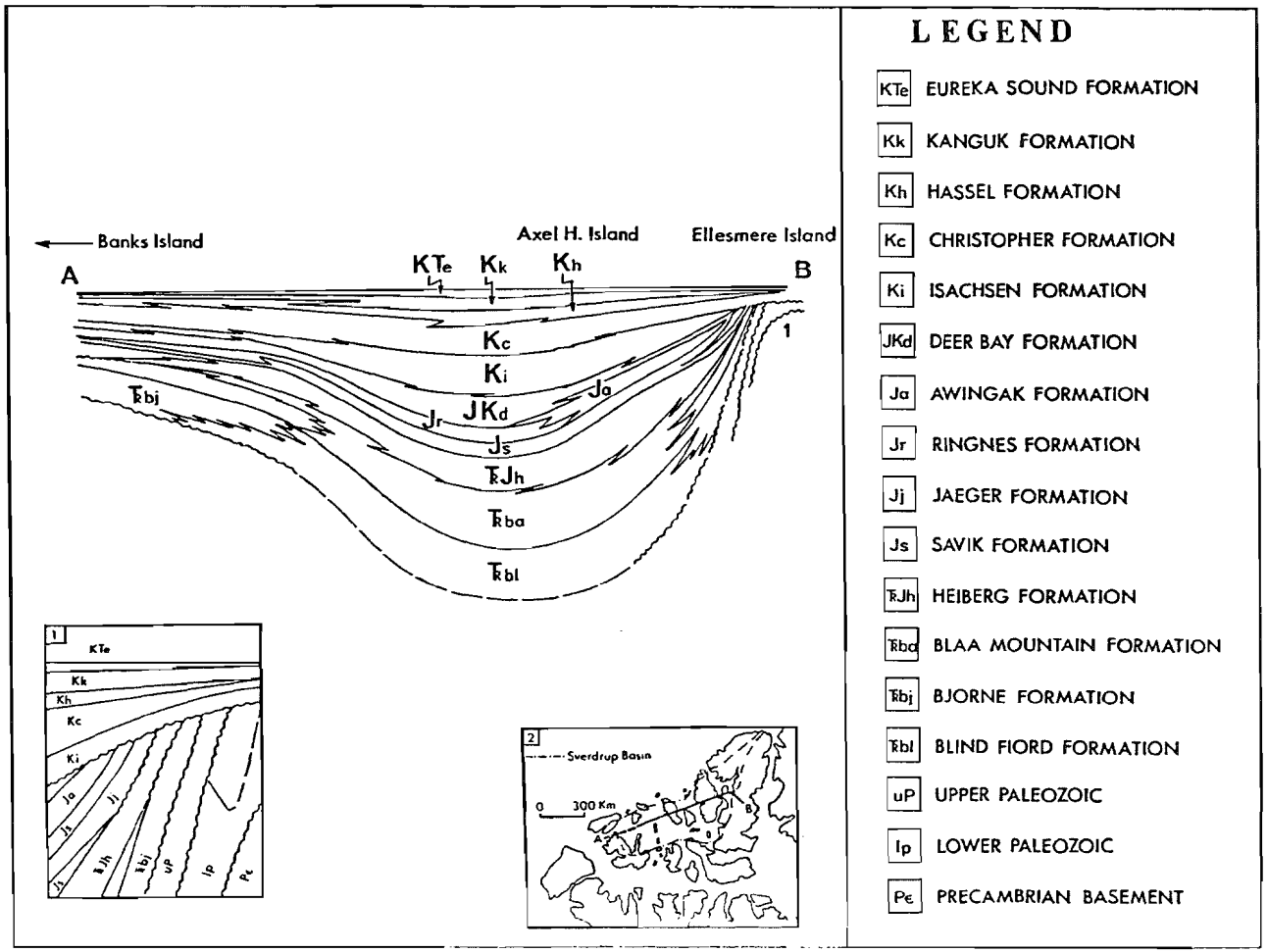

Figure 2.4 Schematic representation of the Mesozoic stratigraphic succession in the central and eastern parts of the Sverdrup Basin. Insets show the detailed stratigraphic sequence in west-central Ellesmere Island [1] and location of the transect in the Queen Elizabeth Islands [2]. Modified from Balkwill (1978).

Snelson (1980), the Sverdrup Basin is an episutural basin on attenuated continental crust. More recent classification schemes emphasize the features characteristic of passive margin basins (Balkwill and Fox, 1982; Bally, 1987).

2.3.2 Igneous History

Previous Work

- Extrusive Rocks

Igneous rocks of the Canadian Arctic Archipelago were first described by Bugge (1910) from collections made during the Second FRAM Expedition and later included in maps compiled by workers of the Geological Survey of Canada. In the Sverdrup Basin, the oldest volcanic rocks recognized are of Carboniferous age and occur in the Nansen Formation (Thorsteinsson, 1974). The best known occurrences of extrusive rocks in the east-central Sverdrup Basin are the volcanic successions of the Late Cretaceous Strand Fiord Formation on Axel Heiberg Island (e.g. Souther ***in*** Fortier et al., 1963; Thorsteinsson and Trettin, 1971). Recently, major contributions on Cretaceous volcanic rocks in the Sverdrup Basin have included a description of the volcanic stratigraphy (Embry and Osadetz, in press), a field study of the eruptive style in the Strand Fiord Formation (Ricketts et al., 1985), the first detailed description of the Hansen Point volcanics on northern Ellesmere Island (Trettin and Parrish, 1987), paleomagnetic studies on Cretaceous igneous rocks (Wynne et al., in press), and geochemical studies of volcanic rocks in the Lake Hazen area (Osadetz and Moore, in press).

Cretaceous volcanic intervals are shown in a time-stratigraphic framework on Figure 2.5. Each occurrence is correlated with a depositional (and tectonic) cycle (Embry and Osadetz, op. cit.). Cycles 1 and 2 occur in the Early Cretaceous Isachsen Formation. The first cycle contains lava flows of Valanginian to Early Barremian age found in the Paterson Island Member at two localities on Axel Heiberg Island. Volcanic rocks of Late Barremian-Aptian age occur in the Walker Island Member at several localities in northwestern and central Axel Heiberg Island. A thin volcanic succession in an undivided portion of the Isachsen Formation is found in the Blue Mountains area and included in Cycle 2 (Fig. 2.5).

Volcanic successions of Late Albian-Early Cenomanian age (Cycle 3, ibid.) include the Strand Fiord Formation, a thick, uninterrupted succession of basaltic flows erupted at the peak of Cretaceous volcanic activity; and thin flows in strata of the Hassel Formation on northeastern Ellesmere Island. Volcanic rocks of Cycle 4 were erupted or intruded from Late Cenomanian to Maastrichtian and unconformably overlie Paleozoic strata on northern Ellesmere Island (Trettin and Parrish, 1987).

The stratigraphic data on Cretaceous volcanic successions suggest that effusive activity was intermittent over a period of approximately 40 Ma, and limited to the eastern and central parts of the Sverdrup Basin. At the time of writing, absolute ages of volcanic rocks were available for Cycles 3 and 4 (Trettin and Parrish, 1987; and Late Cretaceous ages listed in Table 2.2, from Avison 1987).

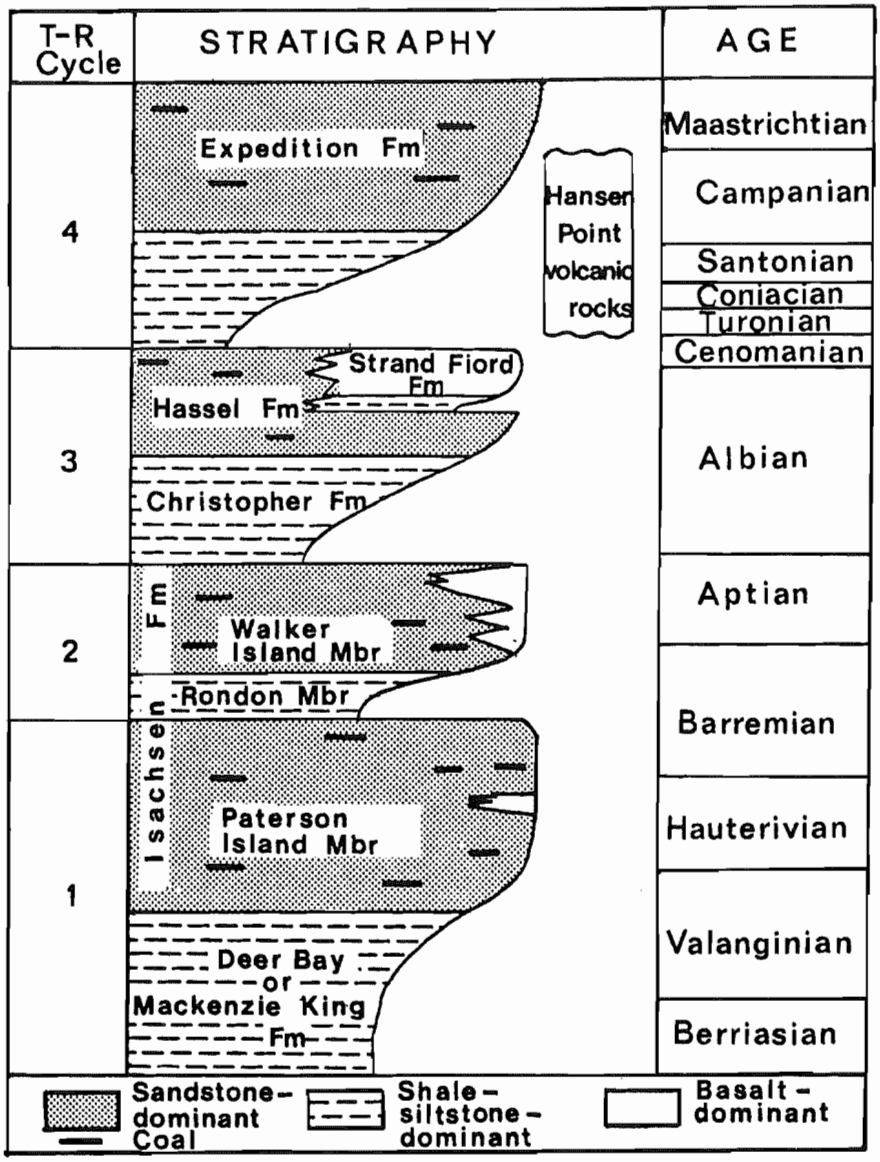

Figure 2.5 Schematic representation of the volcanic stratigraphy in Cretaceous strata of the Sverdrup Basin, Axel Heiberg and northern Ellesmere Islands. Volcanic successions are found in all four transgressive-regressive cycles recognized by Embry (unpubl. man.). Redrawn after Embry and Osadetz (in press).

TABLE 2.2
SUMMARY OF AGE DETERMINATIONS ON
MAFIC INTRUSIVE ROCKS OF THE SVERDRUP BASIN

	LOCATION	ROCK TYPE	METHOD	AGE	SOURCE
Southwest	Sabine Peninsula, Meville Island	Dyke	K/Ar	123 ± 6 Ma	[2]
	Panarctic et al. Drake Point D-68		K/Ar		[2]
	Cored Interval 4685 m	Sill		152 ± 6 Ma	
	Drill Cuttings 4929 - 4947 m	Sill		131 ± 6 Ma	
	Deer Bay Formation Ellef Ringnes Island	Intrusive Sheet	K/Ar	102 - 110 Ma	[1]
	Ringnes Formation Amund Ringnes Island	Sill	K/Ar	144 Ma	[3]
	Panarctic Amund Central				
	Dome H-40; 1967 m	Mafic Rocks	K/Ar	114 Ma	[3]
	Dome H-40; 1987 m	Mafic Rocks		132 Ma	
	Blaa Mountain Formation Cornwall Island	Sill	K/Ar	118 Ma	[3]
	Grinnell Peninsula, Devon Island	Dykes	K/Ar	112- 114 Ma	[3]
Northeast	Buchanan Lake	Sill	Ar-40/Ar-39	126 ± 2 Ma	[4]
	Axel Heiberg Island	Dyke		113 ± 6 Ma	[4]
	Piper Pass, NE Ellesmere Island	Sill	Ar-40/Ar-39	91 ± 2 Ma	[4]

[1] Larochelle et al. (1965)
[2] Balkwill and Haimila (1978)
[3] Balkwill (1983)
[4] Avison (1987)

- Intrusive Rocks

Mafic sills and slightly discordant intrusive sheets systematically intrude upper Paleozoic and Mesozoic rocks of the Sverdrup Basin. These intrusions are particularly abundant in thick, incompetent shale and siltstone sequences of Triassic age on Axel Heiberg Island. Dykes are abundant and prominent swarms are included on 1:250,000 geological maps published by the Geological Survey of Canada. Intrusive rocks on Axel Heiberg Island were first formally included in the Mesozoic stratigraphy during Operation Franklin (Fortier et al., 1963). Blackadar (1964) described over 100 specimens collected mainly from basic intrusions on Ellef Ringnes, Amund Ringnes, Axel Heiberg, Ellesmere and Cornwall Islands (Fig. 2.6). Osadetz and Moore (in press) studied the distribution and geochemistry of intrusive rocks in the Tanquary Fiord and Lake Hazen areas.

The age of intrusive rocks has never been systematically investigated. K-Ar dates obtained on igneous rocks in the western part of the basin range from about 180 to 90 Ma and are summarized in Table 2.2. The ages obtained by Avison (1987) on sills and dykes from the east-central Sverdrup Basin are all Cretaceous. Sills from the same area were sampled for paleomagnetic studies and yield Early Cretaceous paleopoles (Jackson and Halls, 1983).

Tectonic Setting

During the Early Cretaceous, renewed rifting and subsidence in the Sverdrup Basin may have occurred contemporaneously with the incipient opening of the Canada Basin. As a result, there is at present no agreement on the type of extensional tectonics that led to igneous activity during the Cretaceous. Specific models refer to episodic

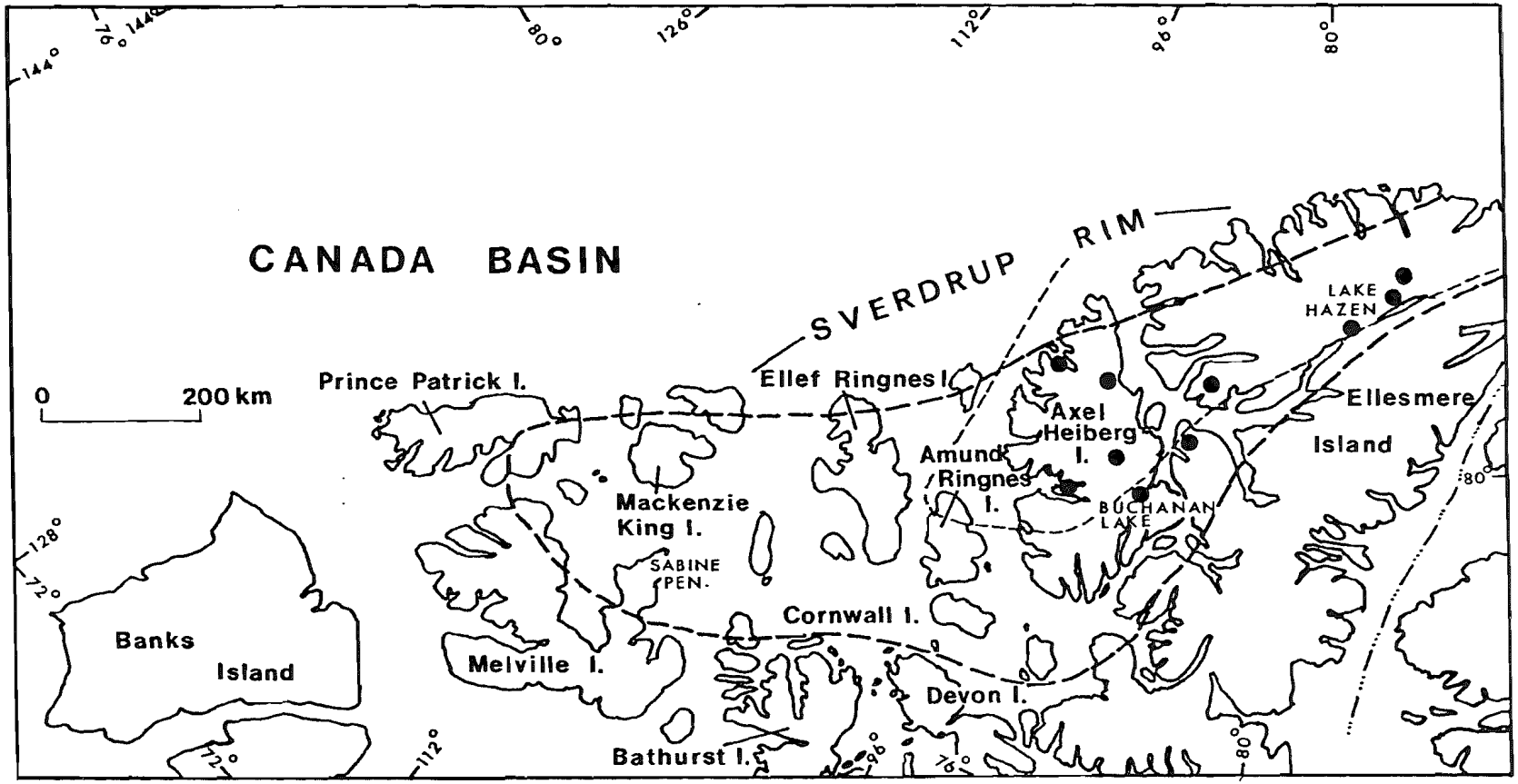

Figure 2.6 Location of the study area in the Canadian Arctic Archipelago. Long-dashed line: limits of the Sverdrup Basin. Short-dashed line: general area of Cretaceous volcanic rocks in the east-central part of the basin. Filled circles: sampling stations, 1983,-84 and -85.

rifting and subsidence within the basin (Balkwill, 1983), continental breakup and passive margin development (Embry and Osadetz, in press) or tectonic events in the Amerasian Basin (e.g. Forsyth et al., 1986).

The consistent orientation of structural elements in the western part of the Sverdrup Basin led Balkwill and Fox (1982) to propose the existence of an incipient rift zone extending from western Ellef Ringnes Island to Sabine Peninsula (Fig. 2.6). Normal faults, linear magnetic anomalies, gabbro dykes, aligned evaporitic domes and modern earthquake epicentres were interpreted to define a broad tectonic belt striking northeastward toward the Sverdrup Rim. The magnetic anomalies are interpreted as subvertical gabbro dykes that were probable feeders to the intrusions observed on Sabine Peninsula and northern Ellef Ringnes Island (Fig. 2.6). The relative age of these structural elements is poorly constrained. Overall, the range of radiometric dates obtained on some of the igneous intrusions represents critical evidence for the proposed timing of crustal dilation events. These authors envisage a period of initial rifting and volcanism (Carboniferous) followed by passive thermal subsidence and recurrent episodes of subsidence, deposition and mafic intrusion throughout the Mesozoic (190 to 86 Ma, with errors of 6 Ma +).

A different approach is used by Embry and Osadetz (op. cit.) to describe the tectonic events in the east-central the Sverdrup Basin. Stratigraphic evidence is presented for a regional correlation between the four Cretaceous volcanic episodes and regional T-R cycles in the basin (see preceding section). The progressive truncation of Early Cretaceous and older strata along the northwest margin of the basin is interpreted as evidence of major uplift along the Sverdrup Rim during

the Early Cretaceous (e.g. Table 2.1). The onset of volcanic activity is correlated with the main rifting phase of the Canada Basin. The nature of a genetic link between the Alpha Ridge and Cretaceous volcanic rocks in the east-central Sverdrup Basin (Ricketts et al., 1985; Forsyth et al., 1986; Embry and Osadetz, in press) remains speculative.

2.4 Study Area and Representative Sampling

The location of the Sverdrup Basin along a developing passive margin during the late Mesozoic explains the disparity of tectono-magmatic models proposed. In fact, the early rifting and subsidence history of the basin and formation of the polar continental margin clearly form a continuum of extensional events that should be reflected in the nature and timing of igneous activity. The approach to field work was therefore to sample igneous rocks of different ages, geographic distribution and mode of emplacement.

Representative sampling in such a large igneous province was a serious consideration at the start of the project. The episodic nature and geographic distribution of Cretaceous volcanic activity is well established in the eastern part of the Sverdrup Basin. Little is known, however, on the ages of spatially associated intrusions (which are far more voluminous) and whether these can be correlated in time with the volcanic episodes. The limits of the study area were chosen to include volcanic successions in three of the cycles of Embry and Osadetz (in press) ranging in age from Valanginian to Early Cenomanian. The region extends from western Axel Heiberg Island to the northern limit of the Hazen Trough and shows excellent exposure (Fig. 2.6). Abundant sills

and dykes are found throughout this area, none of which was dated during previous work. Sills were, therefore, sampled at several stations along the *c*. 400 km transect from Buchanan Lake to Piper Pass (i.e. Lake Hazen area on Fig. 2.6). Some of the best-exposed sections coincide with those sampled for paleomagnetic studies (Jackson and Halls, 1983), providing some constraints on the age of emplacement. A systematic study of dykes in the study area was beyond the scope of this thesis. However, a prominent dyke swarm on eastern Axel Heiberg Island was sampled for geochemical studies.

III. FIELD RELATIONS - EXTRUSIVE ROCKS

3.1 Introduction

The principal objective of this chapter is to describe and interpret the field observations on the extrusive rocks of the Isachsen, Strand Fiord and Hassel Formations. The data concern mainly the lava flows and their internal structures, and the associated volcaniclastic rocks.

The field relationships provide the spatial and temporal framework in which the results from geochemical studies are later integrated. Also of importance to petrochemical studies is a sound interpretation of the eruptive and depositional styles observed. This aspect was not a primary objective of the study; however, it is relevant to many of the physical processes discussed in Chapter 5. Particular attention is given to the eruptive style in the Strand Fiord Formation. Several modes of volcanic eruption and deposition are discussed, with reference to previous interpretations and similar occurrences elsewhere.

3.2 Field Characteristics of Cretaceous Volcanic Successions

3.2.1 Volcanic Rocks in the Isachsen Formation

Several samples were collected from a thick flow of Valanginian to Early Barremian age at the base of a section in the Geodetic Hills (Field work by K. Osadetz and G.K. Muecke; location on Fig. 3.1). A

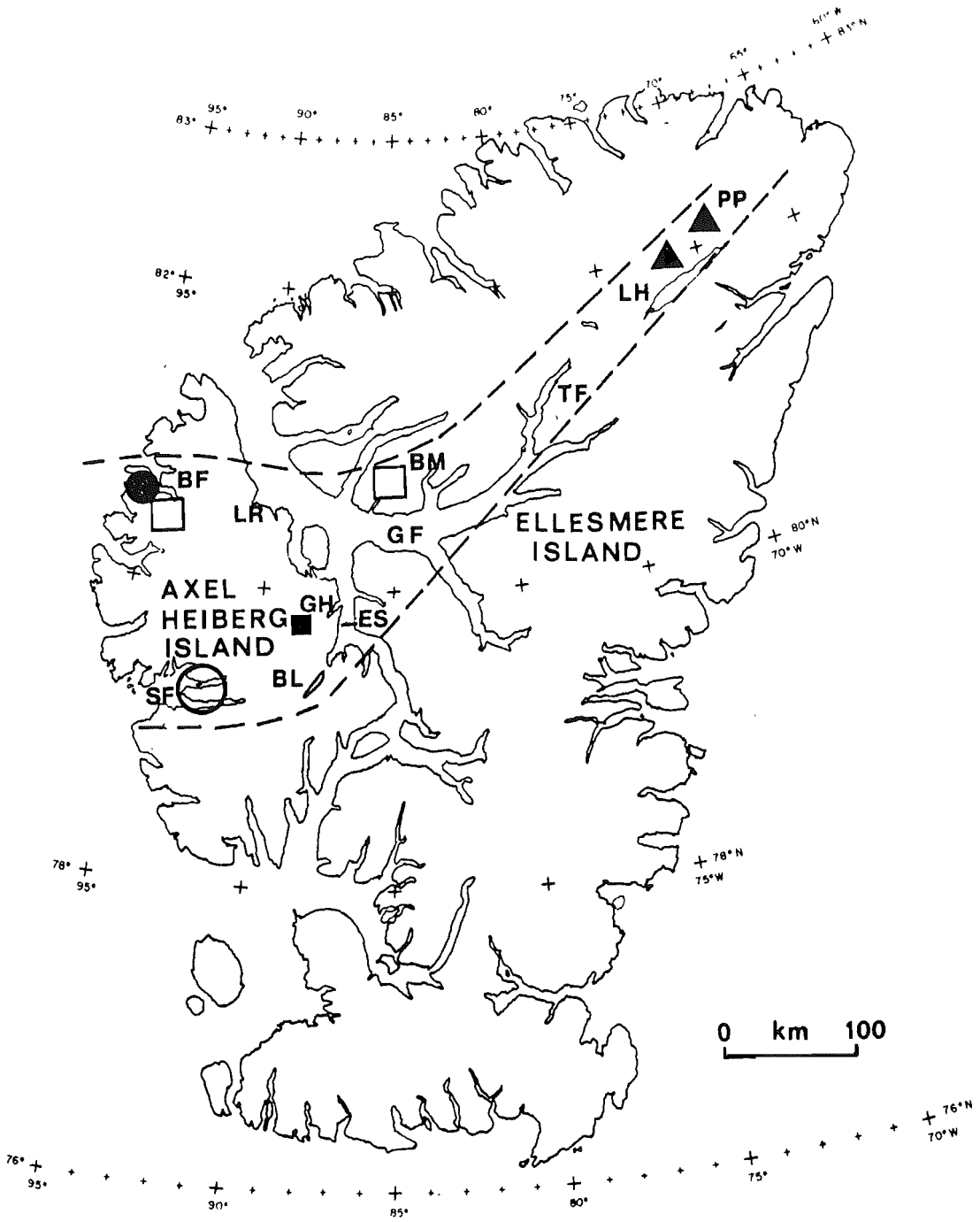

Figure 3.1 Sampling stations for extrusive rocks on Axel Heiberg and northeastern Ellesmere Islands. Square, volcanic rocks in the Isachsen Formation; circle, Strand Fiord Formation; triangle, volcanic rocks in the Hassel Formation. Dashed line, approximate limits of the study area. BF - Bunde Fiord, BL - Buchanan Lake, BM - Blue Mountains, ES - Eureka Sound, GF - Greely Fiord, GH - Geodetic Hills, LH - Lake Hazen, LR - Lightfoot River, PP - Piper Pass, SF - Strand Fiord, TF - Tanquary Fiord.

schematic representation of the stratigraphy is shown on Figure A.1 (a; note that this and all other stratigraphic sections through the Isachsen Formation are located in Appendix A). At this locality, the basal lava flow is overlain by fluvial sandstones of the Paterson Island Member that were subsequently intruded by sills. The age of the basal and uppermost volcanic units is constrained to Late Hauterivian or Early Barremian by the presence of the Rondon Member higher in the section (Embry and Osadetz, in press). The basal flow (#1 on Fig. A.1 a) consists of glomerophyric basalt overlying massive, buff-weathering sandstones. Intraflow structures include a zone of blocky lava at the base, a thick columnar unit and a locally fractured, amygdaloidal flow top. It is overlain by the host sedimentary rocks, two sills and a semi-concordant intrusion fed by a thin dyke. Two flows occur at the top of the section. Flow #2 is a composite lava flow showing a distinctive, chilled intraflow contact with a rubbly top of scoracious fragments or blocks in a fine-grained matrix. The top flow unit (#3) consists of highly vesicular basaltic lava. It displays a thin, basal scoriaceous zone that grades into light grey, finely crystalline and xenocrystic lava.

Volcanic rocks of Late Barremian-Aptian age in the Walker Island Member (Fig. 2.5) were sampled at three stations. At Camp Five Creek, on northern Axel Heiberg Island, the Walker Island Member largely consists of basaltic flows interlayered with quartzitic sandstones and minor pyroclastic and volcaniclastic rocks (field work by G.K. Muecke; Fig. A.1 b). The lava flows are 5 to 30 m thick and display simple structures. The bases of the flows are commonly amygdaloidal or sheared, and may contain pipe vesicles, scalloped protrusions

(spiracles?) or wood fragments and tree stumps up to 60 cm in diameter (Embry and Osadetz, in press). Massive, thick-bedded sandstones form the predominant lithology between lava flows. Some of the sandstones are interlayered with shales and many are lensoid, causing some variation of facies along strike. Three of the lava flows are underlain by thin coal beds (Fig. A.1 b). The top of the succession consists of an uninterrupted sequence of flows.

The third section in the Isachsen Formation was sampled in the Blue Mountains area, northwestern Ellesmere Island (stratigraphic sections and sampling intervals are shown on Fig. A.2). At this locality, the Isachsen Formation is undivided and composed of sandstone, minor shale, siltstone and conglomerate. The section measured on the east side of the syncline is overturned and consists of four thin, highly altered amygdaloidal lava flows totalling 14 meters in thickness. The equivalent section on the opposite side of the valley consists of a single massive unit approximately 15 meters thick that was examined at two localities. At section (a) (Fig. A.2), internal structures include a massive base with blocky joints, overlain by thick irregular columns and a hackly weathered top. An outcrop of section (b) on the west side of the valley is only accessible at its basal contact with sandstones. There is no evidence of a scoriaceous top; structures consist of columnar joints and the possible presence of two cooling units of similar thickness. At the base of the unit, the rock face contains a semi-circular section of homogeneous, light grey, highly amygdaloidal lava in sharp contact with the host igneous rock (Plate 1). The semi-circular area is interpreted to represent a section through a lava tube (cross-sectional area is 9 m^2; chilled margin is 10-15 cm thick).

PLATE 1

Cross-section of a lava tube exposed at the base of a basaltic flow in the Isachsen Formation, Blue Mountains area of northwestern Ellesmere Island. The cross-sectional area is 9 m^2 and consists of pale grey, very fine-grained and highly amygdaloidal lava (circular vesicles filled with calcite). The contact with the host igneous rock is indicated by a black arrow (10-15 cm chilled margin). The enclosing dark grey basaltic flow consists of two cooling units (irregular contact shown by dotted line). The lava tube shows no evidence of channel-roofing, downcutting or multiple injection and drainback of lava during successive eruptions. It may have formed without a channel phase, via lava toes at the front and sides of a pahoehoe flow (see Fig. 3.6 a).

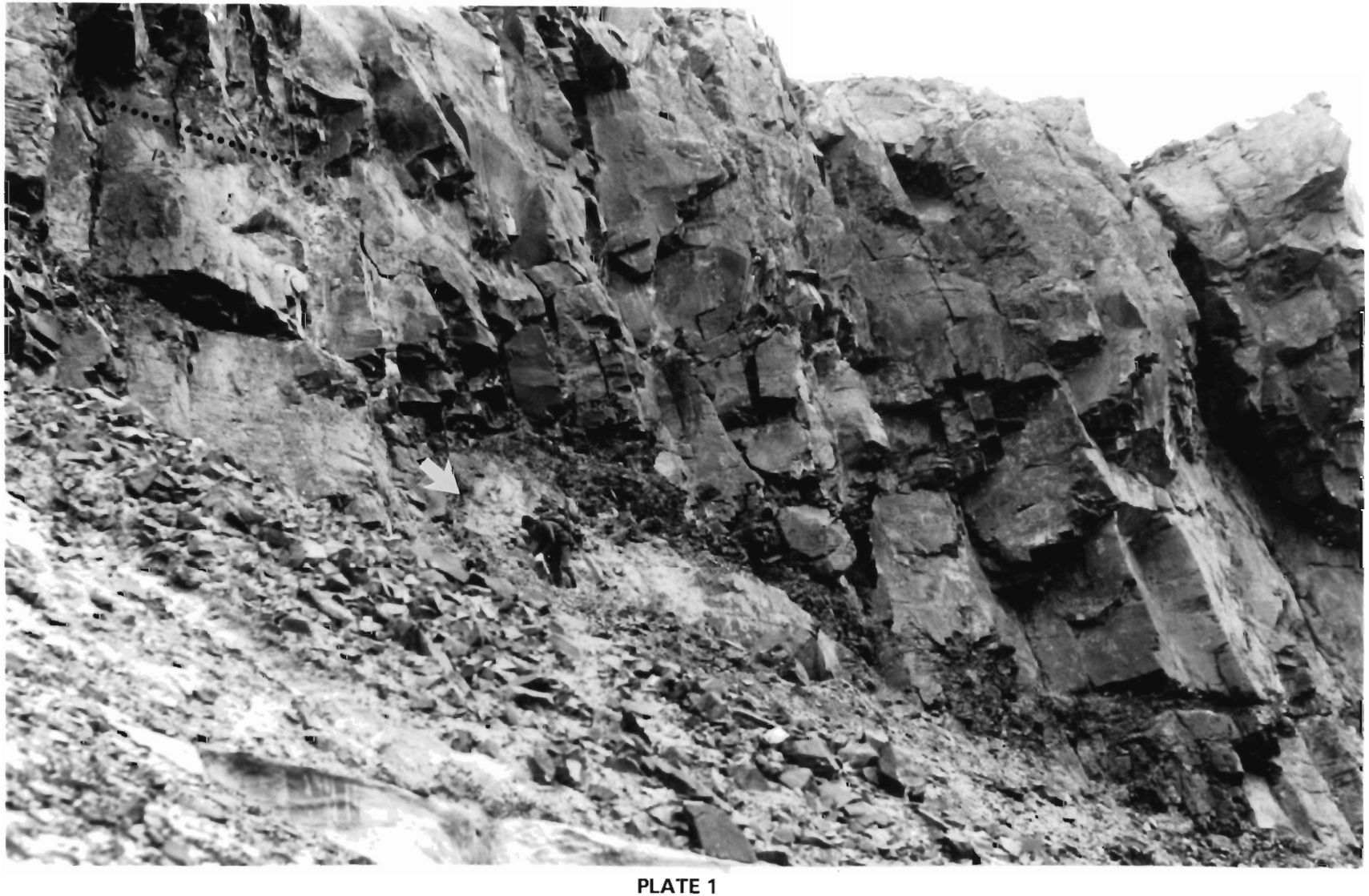

PLATE 1

3.2.2 The Strand Fiord Formation

Northern Axel Heiberg Island

The stratigraphy in the Bunde Fiord area is similar to that of axial successions found in other parts of the Sverdrup Basin (e.g. Fisher, 1984). Cretaceous strata consist of the Isachsen Formation (as illustrated on Figure A.1), overlain by the Christopher, Hassel and Strand Fiord Formations (sequence partially reproduced on Fig. A.3). Structural evidence suggests that an extensional phase produced steep normal faults of Late Cretaceous to Middle Eocene age in this area. The Tertiary Eurekan Orogeny gently deformed all the strata and produced large-scale steep reverse faults (Fisher, 1984).

Sections through the Strand Fiord Formation were measured at ***Celluloid Creek*** (K. Osadetz, unpubl.) and along the coast, on the south shore of Bunde Fiord (ref. ***Artharber Creek***). The volcanic stratigraphy and sampling intervals are illustrated on Figures A.3 and 3.2. The sequence of basalts unconformably ovelies marine sandstones of the Hassel Formation, a reasonable indication that they are equivalent to the Strand Fiord Formation in the type area on western Axel Heiberg Island. However, the correlation has not been confirmed using biostratigraphic or radiometric data.

The lava flows in both sections are rather thick (20-30 metres), and generally display columnar jointing and red oxidized flow tops (Plates 2 and 3). The Celluloid Creek succession is remarkably uniform in structure (Plate 2; Fig. A.3) and consists of an uninterrupted sequence of 28 basaltic flows, with a total thickness of 785 + metres

PLATE 2

PLATE 3

PLATE 2

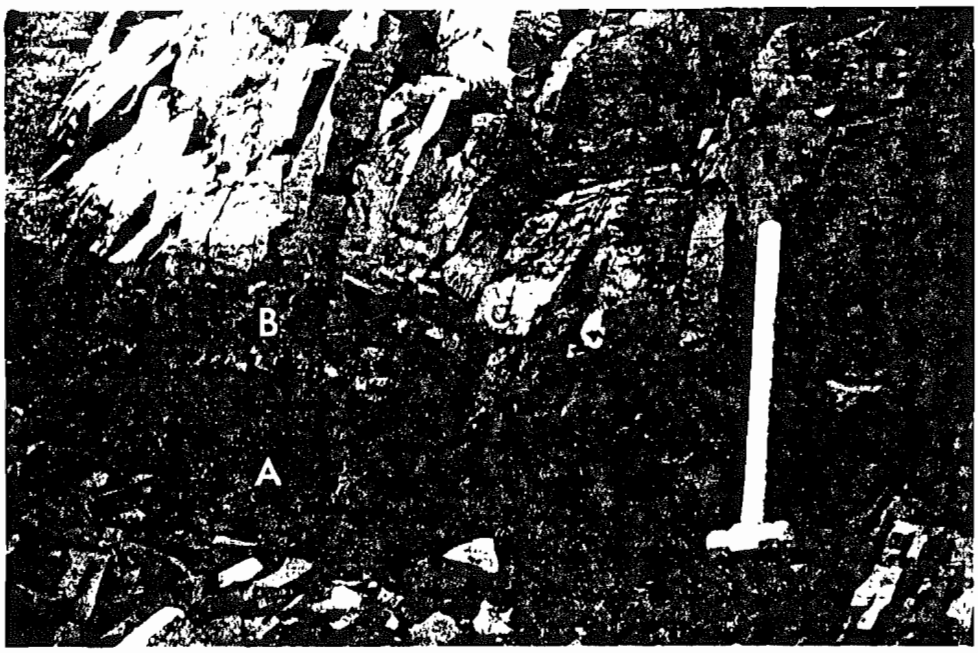

PLATE 3

(Embry and Osadetz, in press). Lava flows were emplaced as single cooling units of massive to amygdaloidal lava.

The Artharber Creek succession is 293 + metres thick and consists of eighteen units that are shown in some detail on Figure 3.2 (95% flows and 5% volcaniclastic rocks of basaltic composition). A total of 11 basaltic lava flows were measured, that contain up to 20-30% euhedral plagioclase phenocrysts. The volcaniclastic rocks are crystal-bearing lapilli-tuffs (classification of Cas and Wright, 1987) of probable pyroclastic origin. The basal deposit, for example, is a nonbedded, nonsorted assemblage of angular scoriaceous clasts with chilled margins, fragments of massive basaltic lava and varying amounts of euhedral feldspar phenocrysts (2-3 mm) in a matrix of ash. The overlying greyish-green tuff also contains crystals.

The section was measured from east to west along the coast. Further along strike, flow # 2 is in contact with a thin, lensoid flow of sparsely amygdaloidal, blocky lava with a prominent flow top (Fig. 3.2). At the level of flow # 5, a laterally discontinuous volcanic breccia deposit is associated with several thin flows. The sequence of deposits is depicted graphically on Figure 3.3. Two thin flows were emplaced over the volcanic breccia before subsequent sheet floods buried the deposits. Flow #6 grades laterally to a thin highly porphyritic, rubbly and altered lava flow with an extensive flow top, in contact with flow #7 (Fig 3.2). All the variations in volcanic facies are observed within a narrow zone, suggesting that deposits were emplaced in a topographic depression, or channel.

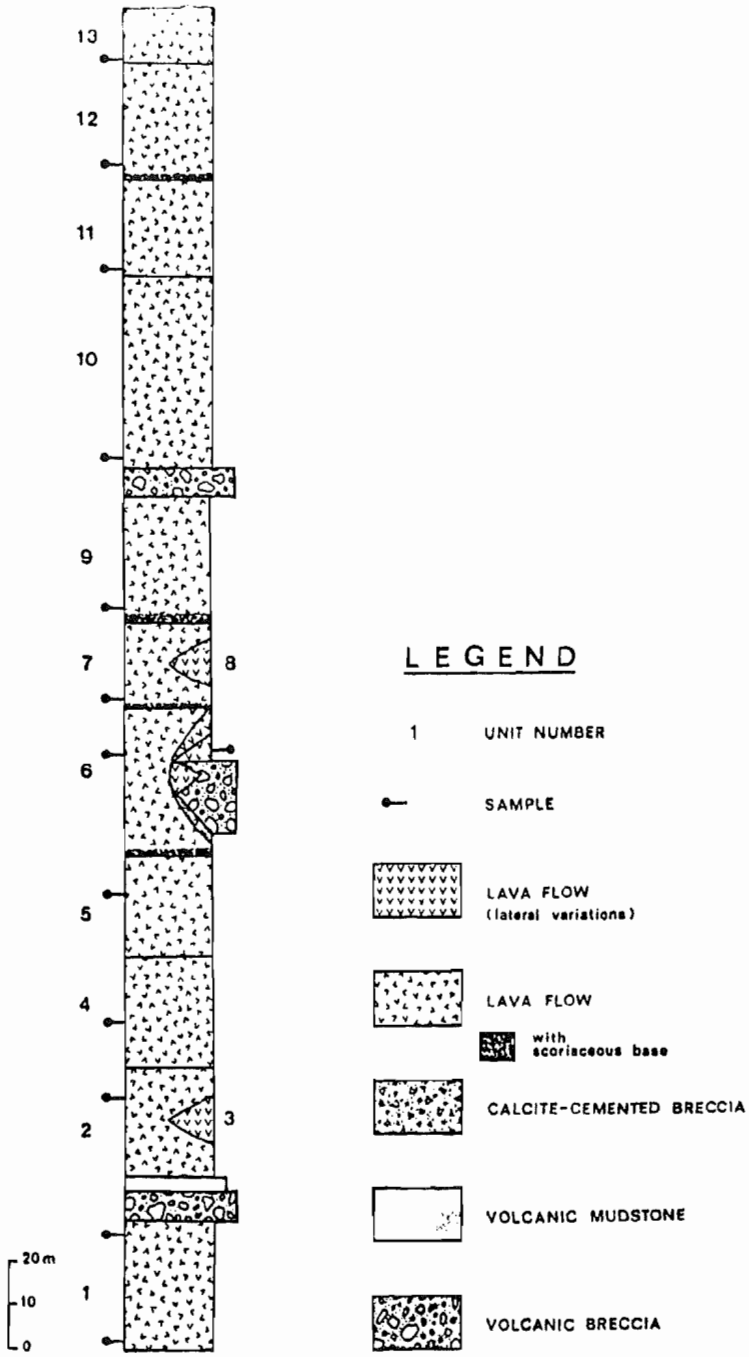

Figure 3.2 Detailed volcanic stratigraphy of the Strand Fiord Formation along the south shore of Bunde Fiord, northern Axel Heiberg Island (ref. ***Artharber Creek***).

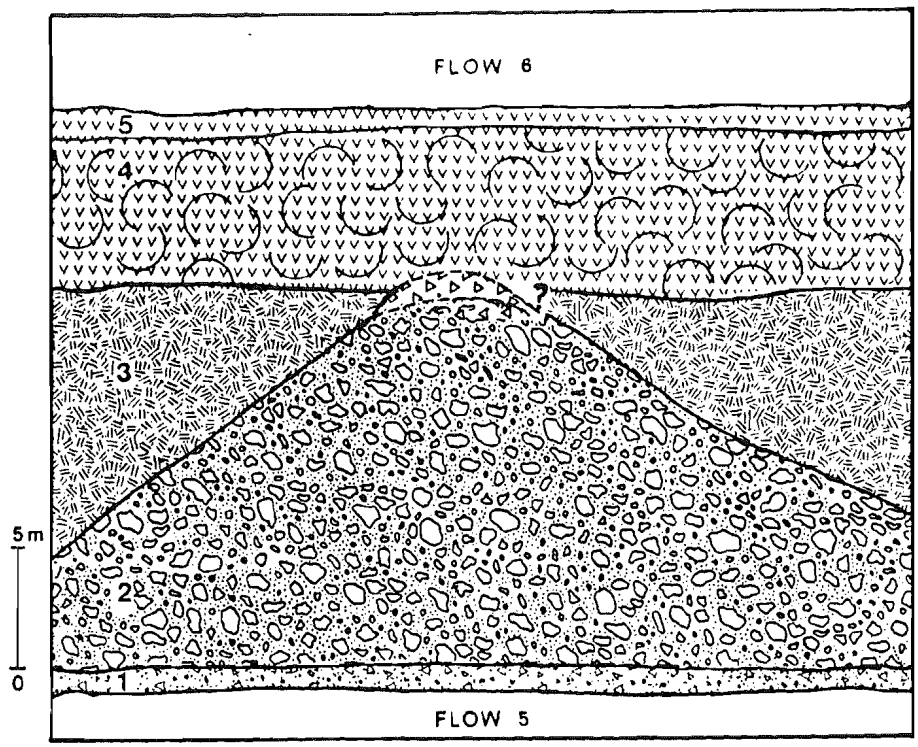

Figure 3.3 Schematic reconstruction of volcanic and volcaniclastic facies located along strike in the Artharber Creek section, as inferred from contact relationships. The central volcanic breccia deposit is similar to other crystal-bearing volcaniclastic deposits identified in the sequence and distinct from the underlying calcite-cemented breccia. The volcanic breccias are mixtures of spatter, cinder and clinkery flow that could have been rafted from a vent ("breccia tops" of Wright 1984) or produced by a spatter cone or rampart. The intermittent nature of the pyroclastic activity, and the presence of thin flows with a compound structure distinct from the thick enclosing sheet flows suggests an origin from a secondary (central) vent. The presence of euhedral feldspar phenocrysts in some of the breccias, thin flows and overlying ponded basalt flows is an indication that the magmas erupted were tapped from the same conduits.

[1] Calcite-cemented breccia
[2] Volcanic breccia
[3] Finely crystalline flow
[4] Highly feldspar-phyric, rubbly flow
[5] Thin, massive flow

Western Axel Heiberg Island

In the type area on western Axel Heiberg Island, the Strand Fiord Formation uncomformably overlies silty shales of the Bastion Ridge Formation and is in turn overlain by black, bituminous shales of the Kanguk Formation (Ricketts et al., 1985). In this area, Mesozoic strata are broadly folded in the form of doubly plunging anticlines and synclines, and are locally cut by diapiric anhydrite of the Otto Fiord Formation. The volcanic succession outcrops along spectacular, but poorly accessible ridges throughout the area (Plate 4) and is more rarely found along stream cuts. The lava flows display conspicuous jointing and average 10 metres in thickness (maximum 60 metres). The sequence is in places remarkably uniform (Plate 5) and lava flows are interlayered with marine siltstones at the base.

A schematic representation of three sections chosen for study is shown on Figure 3.4. The Bastion Ridge section consists of three lithological types (recognized at several other locations by Ricketts et al., 1985): basaltic flows, volcanic breccias, and black shales that locally support sandstone lenses. The Twisted Ridge section consists entirely of flows beyond the first 60 metres. Of the four cross-sections chosen for geochemical studies, two lie in the area of thickest exposures while others are located on the south shore where the total succession amounts to less than 50-100 metres and includes volcaniclastic sediments (Souther *in* Fortier et al., 1963; Ricketts et al. 1985).

In the Strand Fiord area, all the flows observed show features typical of ponded flood basalts (basal colonnade, entablature and vesicular top; e.g. Swanson and Wright, 1980). Unlike pahoehoe and aa

PLATE 4

Valley and ridge topography south of Expedition Fiord, western Axel Heiberg Island. The view is to the west from the type section of the Strand Fiord Formation at Bastion Ridge.

PLATE 5

Exposure of the Strand Fiord volcanic succession along Dragon Cliff, north shore of Expedition Fiord. The cliff is 500 metres high. Note the range in width and height of columnar joints throughout the section; and the recessive, scoriaceous flow tops (arrowed).

PLATE 4

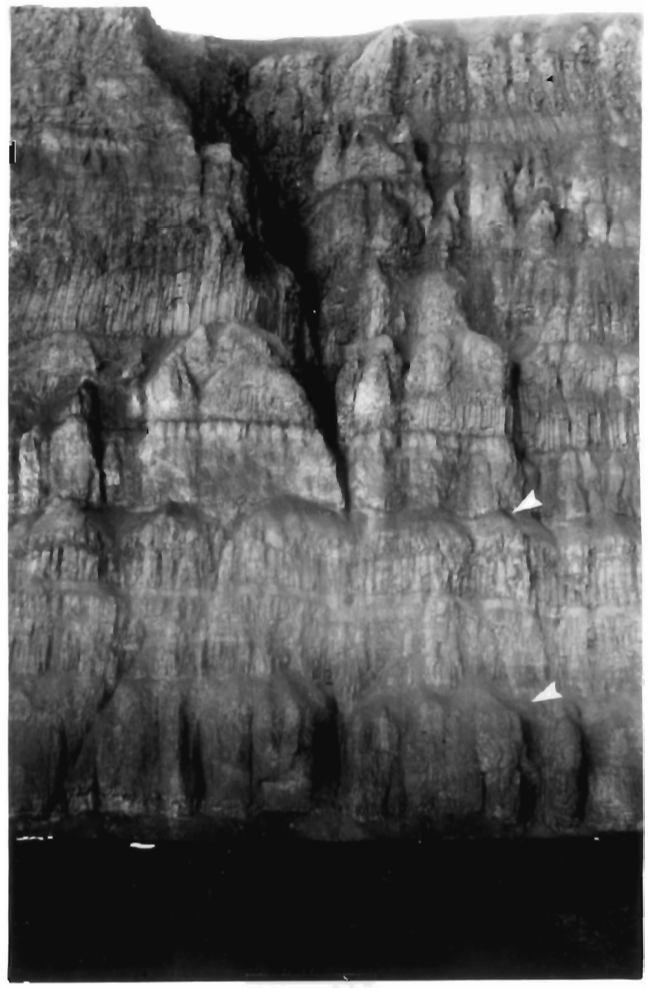

PLATE 5

Figure 3.4 Schematic stratigraphic sections of the Strand Fiord Formation in the type area, western Axel Heiberg.
[1] Dragon Mountain
(from Ricketts et al., 1985)
[2] Twisted Ridge section
[3] Bastion Ridge section
[4] Glacier Fiord Syncline stream section

In the northern part of the type area, traverses along ridges above cliff faces provide the best exposures for sampling and observing intraflow structures. Cliff erosion permits each individual flow to be identified from the presence of a scoriaceous top; and beds of welded pyroclastic ejecta or volcanic breccia provide additional markers. Accurate measurements of flow thicknesses, however, could not be obtained beyond the first 50 to 60 metres along section [2]; and most volcanic units in section [3] are averaged to 10 metres. This approach to sampling in the northern part of the study area was chosen to maximize the range of petrological and geochemical data along single sections and would not be viable without the background stratigraphy provided by Ricketts et al. (1985).

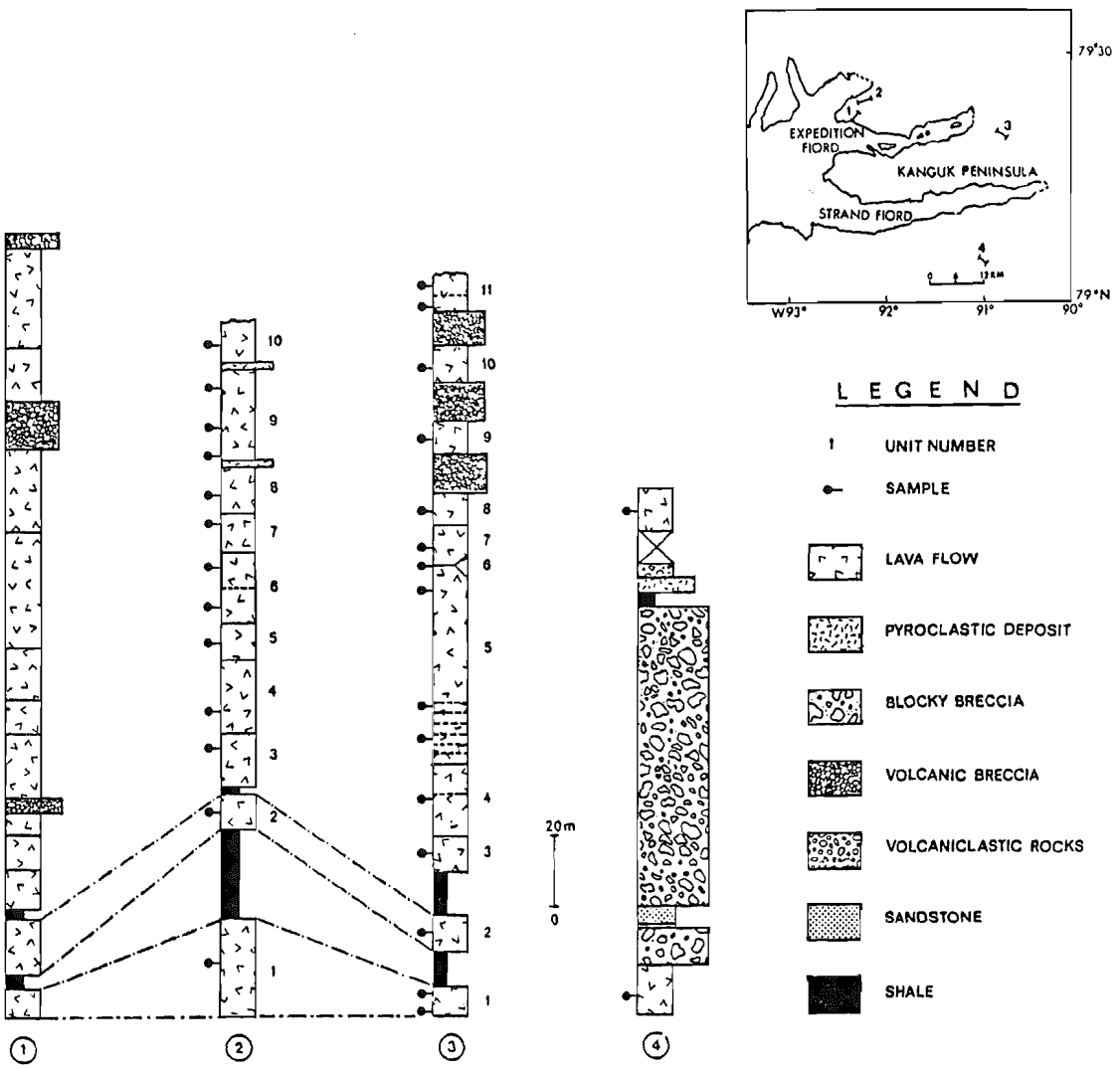
79°30
EXPEDITION FIORD
KANGUK PENINSULA
STRAND FIORD
79°N
W93°
92°
91°
90°
LEGEND
UNIT NUMBER
SAMPLE
LAVA FLOW
PYROCLASTIC DEPOSIT
BLOCKY BRECCIA
VOLCANIC BRECCIA
VOLCANICLASTIC ROCKS
SANDSTONE
SHALE
20m
0

FIGURE 3.4

flows which exhibit structures acquired during flow, flood basalts are characterized by extremely rapid emplacement and display structures that result from cooling in a stagnant pond (Wright, 1984). Several authors have proposed classifications of intraflow structures in successive cooling units (Tomkieff, 1940; Spry, 1962; Swanson, 1967). The nomenclature adopted here is that of Long (1978) and is based on fracture morphology and textural character (Fig. 3.5). Excellent exposures of Type II and III flows can be found on the Kanguk Peninsula (e.g. Plates 6,7,9 and 10). A Type II flow ideally consists of alternating colonnade and entablature tiers; Type III flows exhibit a lower colonnade and a single entablature. Both types may show an upper colonnade (Long and Wood, 1986).

Pillow lavas and tube pillows were observed at one locality along a stream near Castle Mountain (Plate 11). The pillows are spheroidal structures up to 50 cm in diameter which show radial arrangements of calcite-filled amygdales in cross-section. They are underlain by flattened, elongate tube pillows up to 2 m across. The matrix consists of spalled glassy lava.

3.2.3 Volcanic Rocks in the Hassel Formation

Cretaceous strata in the Lake Hazen and Piper Pass areas (Fig. 3.1) include a condensed section of the Isachsen Formation, shales of the Christopher Formation and a volcanic-sedimentary sequence in the Hassel Formation. The volcanic rocks are grouped with other successions of Late Albian-Early Cenomanian age in Cycle 3 of Embry and Osadetz (in press; see Fig. 2.5). The lava flows form easily accessible cuestas and

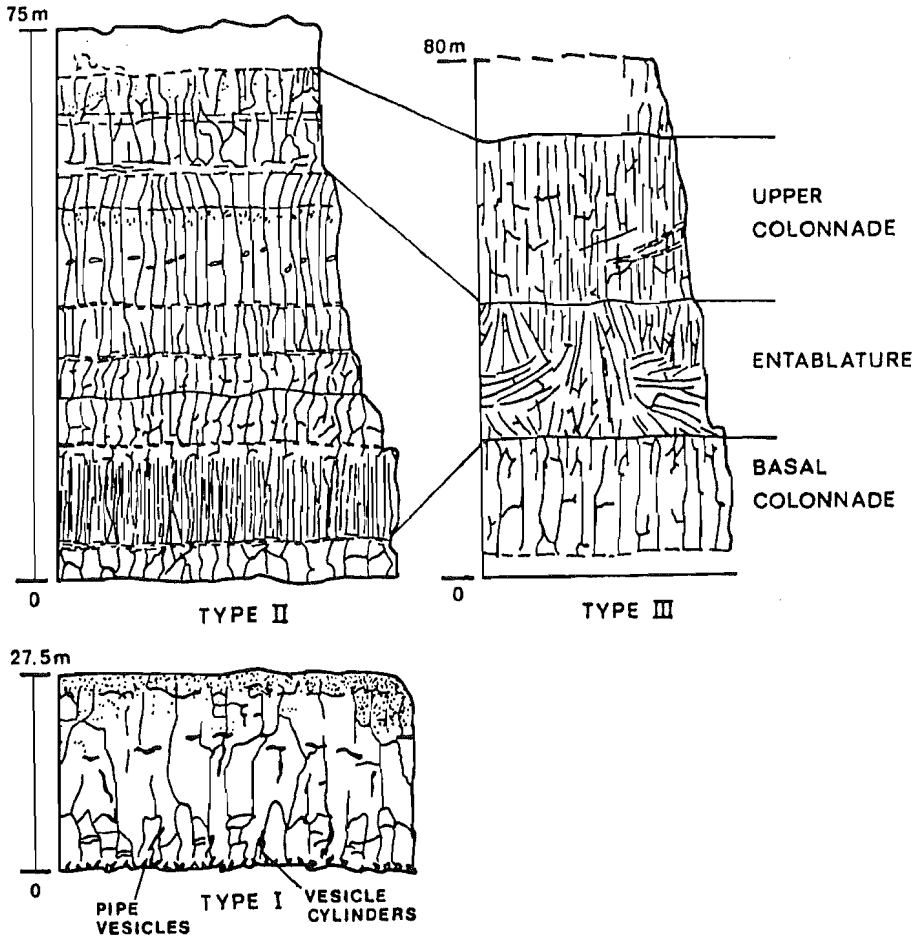

Figure 3.5 Intraflow structures in Type I, Type II and Type III flows of Long (1978; modified from figures 2 and 3 of Long and Wood, 1986).

PLATE 6

A Type II flow along the Bastion Ridge section. Tiers of thin columns form the entablature, in contact with thicker columns at "C" (arrowed).

PLATE 7

Spectacular exposure of Type III flow along the south shore of Strand Fiord. A: basal colonnade B: entablature with curvicolumnar jointing C: vesicular flow top.

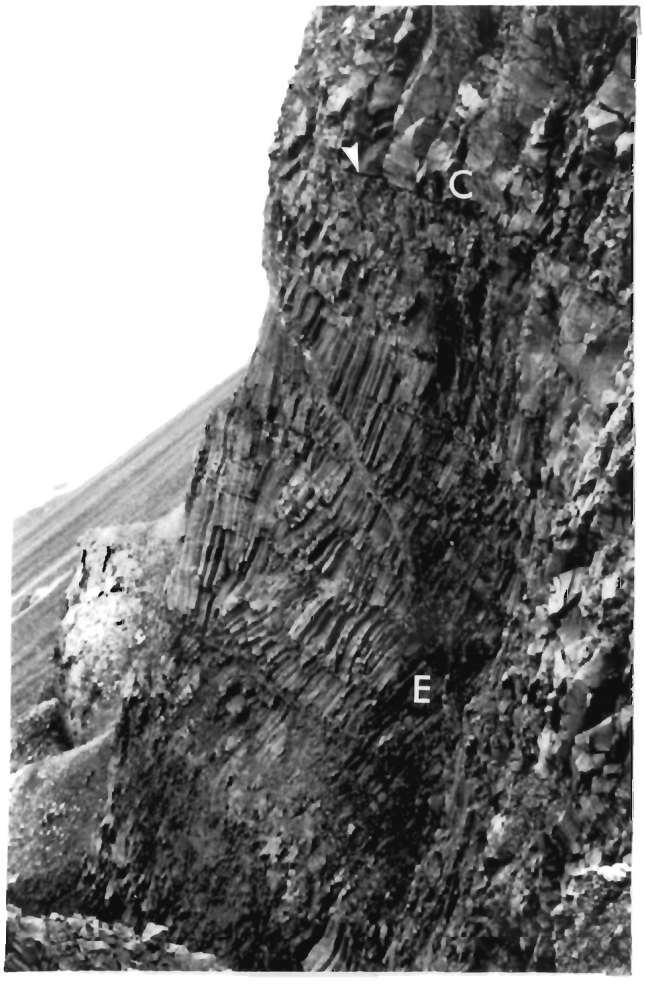

PLATE 6

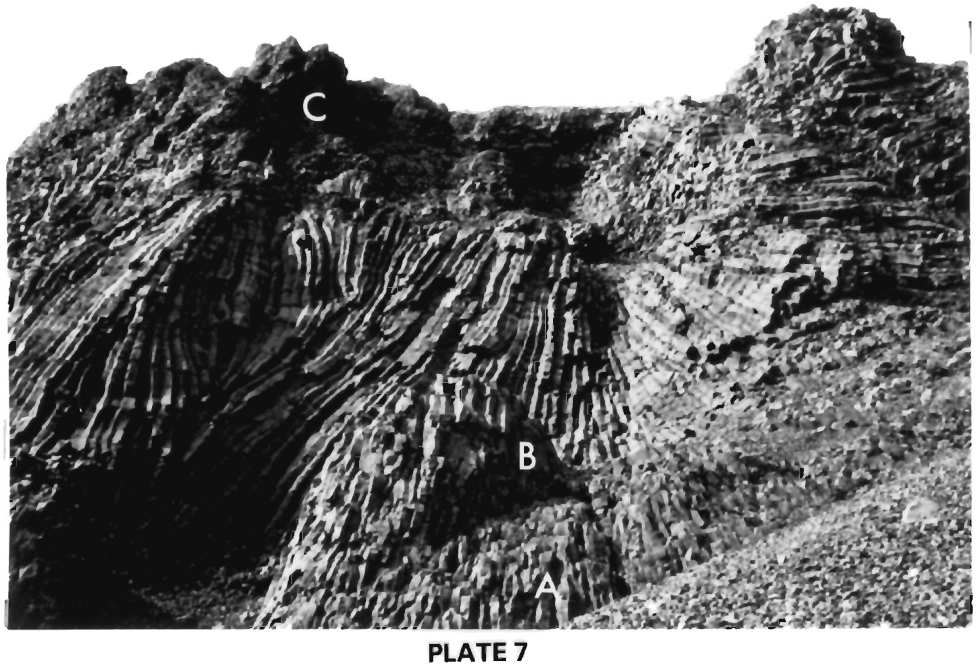

PLATE 7

PLATE 8

Invasive flow at the base of the Strand Fiord volcanic succession along Split Mountain Ridge, western Axel Heiberg Island. Buff sandstones of the Hassel Formation are visible to the left and in the background. The basaltic flow (A) is 20 metres thick and massive up to the contact with a 60 metre bed of dark grey fossiliferous shales (B) belonging to the Bastion Ridge Formation. The thickness of the flow varies along strike and in places two units are observed. It appears from observations made during several traverses that two separate invasive flows occur at the base of the Strand Fiord Formation in the northern part of the type area (see Fig. 3.4, sections 1-3). It is likely, however, that lava advancing into unconsolidated sediments will form laterally discontinuous lenses and rafts which complicate the stratigraphy (e.g. Plate 12). There is some debate as to the exact mode of emplacement of these flows: whether the magma intruded the sediments and solidified before reaching the surface; or whether it "burrowed" into the unconsolidated sedimentary pile because of density contrasts (Camp, 1981).

PLATE 9

A thick basaltic flow (>40 m) along the type section at Bastion Ridge, displaying some features of the Type II flow of Long (1978): a poorly-developed lower colonnade (A); well-defined entablature (B); central colonnade (C); hackly entablature (or pseudocolumnar zone of Tomkieff, 1940) (D); and thick vesicular flow top (E). Type II flows are typically thick units (45-76 m) where the textures of alternating entablature and colonnade may vary regardless of position within the flow (Long and Wood, 1986).

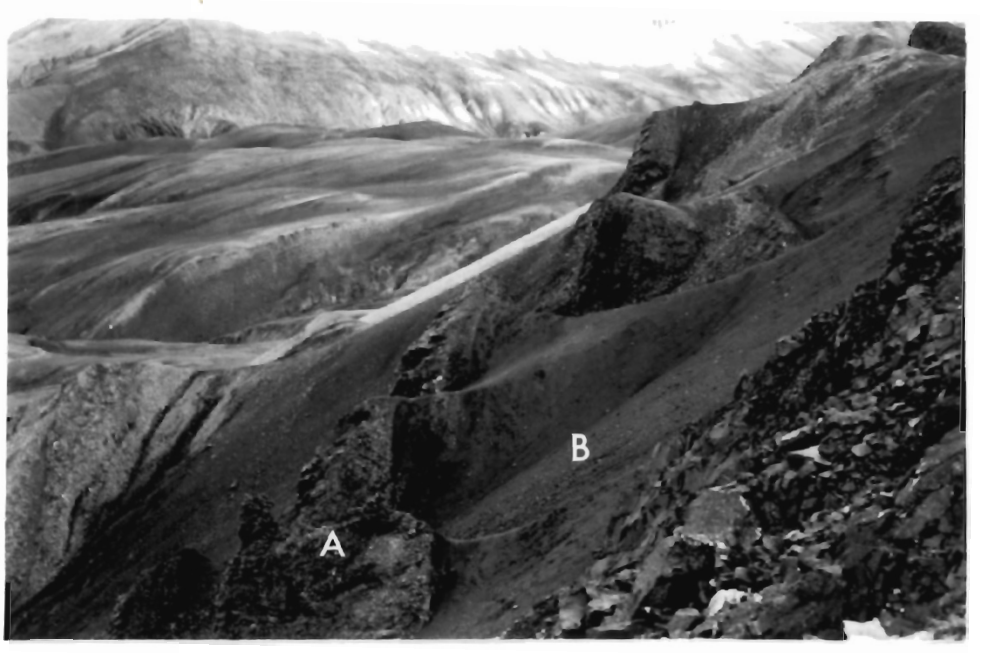

PLATE 8

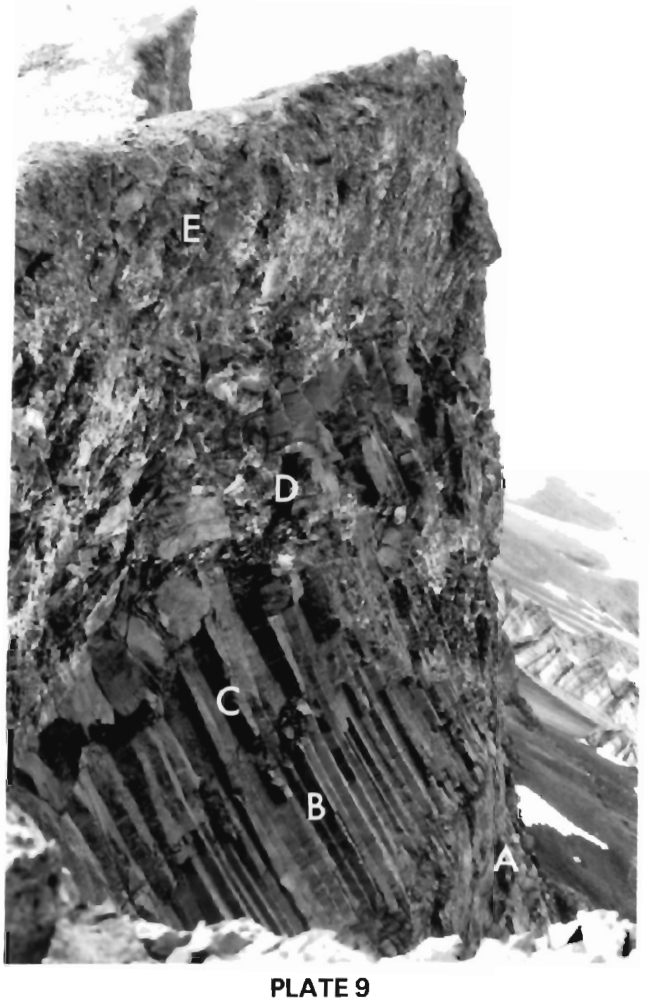

PLATE 9

PLATE 10

The same flow as illustrated on Plate 7 displays variations in the structure of the entablature further along strike. The base of the lava flow is in contact with shales of the Bastion Ridge Formation. Here the basal colonnade (bc) is still visible but fanning columns are replaced by alternating tiers of thin columns. The observed changes in intraflow structures are probably caused by variations in paleotopography, underlying substrate, rates of cooling along the advancing front of ponded flows, or a combination of these. Note the assistant geologist, arrowed for scale at center-right.

PLATE 11

Pillow lavas in the Strand Fiord Formation, exposed at Castle Mountain, on Kanguk Peninsula. The transition to tube pillows is shown by arrows. The pillows are spheroidal structures up to 50 cm in diameter, with amygdaloidal cores and a selvage. Tubes are up to 2 m across. Note the hammer for scale. Pillow tubes derived from fissure-fed flood eruptions are formed when the thin crust at the convex edge of a subaqueous lava front stretches and splits, creating a series of self-sealing lava tubes. Massive or pillowed lava will overlie the tube pillows, depending on flow velocity (Baragar, 1984). The cross-section illustrated shows that the lava tubes spread laterally at a very slow rate, producing a wall of pillows above the tubes.

PLATE 10

PLATE 11

PLATE 12

Invasive Strand Fiord Formation basaltic flow visible along coastal cliff sections, Index Peninsula. The basal flow (A) is in sharp contact with the overlying buff sandstones and grey siltstones (B: Bastion Ridge Formation), suggesting a sill-like relation with the sedimentary rocks. Invasive flows are formed as lava advances into a topographic low and burrows into unconsolidated sediments. Several examples have been described in the Columbia River Basalts of the western U.S. (e.g. Schmincke, 1967; Byerly and Swanson, 1978), particularly along the margins of the plateau and in local structural basins where sediment availability is the greatest. A thin flow to the left (C) likely represents a portion of "rafted" basaltic lava.

PLATE 13

Well-developed scoriaceous tops of basaltic flows (T's) exposed further along the Index Ridge Peninsula. Note the very sharp contact between the two flows and preferential erosion of vesicular lava. This photograph to contrast with the contact between an invasive flow and the ovelying sedimentary rocks shown on Plate 12.

PLATE 12

PLATE 13

mesas in both areas. The stratigraphy at three localities is reported by Osadetz and Moore (in press). The thickest sequence consists of two flows separated by fine, quartzose sandstones interlayered with silty shales and thin coal beds; a single flow unit outcrops at all other localities. Despite their proximity, the sections provide insufficient data for stratigraphic correlation.

Volcanic rocks in the Hassel Formation were re-sampled to provide material for age determinatins and geochemical studies (sampling stations shown on Fig. 4.5, next chapter). The unit exposed near Lake Hazen (ref. ***Tropical Ridge***, Fig. 4.8, next chapter) displays internal cooling structures but no evidence of extrusion such as an amygdaloidal flow top. A section through the volcanic sequence at Piper Pass (ref. ***Arctic Hare Mesa***) is graphically represented in Appendix A (Fig. A.4). The most common structures in massive flows are regularly-spaced columns. Pillow lavas are found locally. On a south-facing section of the Mesa, the central portion of a 27 m thick flow consists of smooth lava with curved, billowy structures in sharp, irregular contact with a massive columnar base.

3.3 Eruptive Style in Cretaceous Volcanic Intervals

3.3.1 Volcanic Rocks in the Isachsen and Hassel Formations

The small number of sections of Early Cretaceous volcanic rocks precludes any modelling of the paleoenvironment of eruption. Based on their studies of several sections through the Walker Island Member, Embry and Osadetz (in press) envisage quiescent subaerial eruptions onto

subsiding delta plains, with some areas undergoing sporadic, mildly explosive activity from cinder cones. The field observations reported here suggest the episodic eruption of Type I flows of Long (1978; Fig. 3.5 a) in areas of active sediment accumulation, and are consistent with the proposed interpretation.

One of the difficulties encountered during field studies of Isachsen basalts is the distinction between sills and flows (e.g. Fig. A.1 a). In several areas, the succession consists almost entirely of a regular series of massive units interlayered with quartzitic sandstones. The units do not display a scoriaceous top, and their thin, glassy margins and segregated layers of vesicles render them indistinguishable from sills. Some of the massive units could represent "invasive flows" (***sensu*** Byerly and Swanson, 1978). Invasive flows display a massive structure and chilled margins, or locally intrude the overlying sediments in the form of apophyses and small dykes. However, unlike sills intruded at depth, the flows occur in the correct stratigraphic position with respect to the overlying lava pile and are emplaced during rapid flow through poorly consolidated sediments (Wright, 1984). There appear to be several possible cases of invasive flows in successions of Early Cretaceous age. Nonstratified, nonsorted breccias in the Isachsen Formation near Strand Fiord are interpreted as the result of rising magma reacting with meteoric water at very shallow depths, causing autobrecciation upon extrusion (Ricketts, 1985). A surface-fed flow invading unconsolidated sediments and spreading laterally could also surface as a breccia (Balkwill, 1983). This is worth considering in future field-based studies of these rocks in the study area.

The presence of a lava tube in basaltic flows at Blue Mountains (Plate 1) provides additional information. According to Greeley (1987), the presence of lava tubes reflects a distinct style of volcanism involving prolonged periods of eruptive activity, and moderate rates of effusion of relatively fluid lava that has not greatly degassed. In the Blue Mountains example, there is no evidence of channel-roofing, downcutting or multiple injection and drainback of lava during successive eruptions (compare Plate 1 and Fig. 3.6). The tube likely formed via lava toes at the front or sides of slow-moving pahoehoe flows (e.g. Swanson, 1973; Greeley, 1987). The lava tube may have acted as a conduit for highly amygdaloidal basalt flows exposed on the opposite side of the valley.

In the Hassel Formation, on northeastern Ellesmere Island, the intraflow textures and the presence of pillow lavas in one sequence indicate that surface-fed flows were probably of pahoehoe type and locally entered water. These observations are consistent with the delta plain environment suggested by Trettin et al. (1982) and Osadetz and Moore (in press).

3.3.2 The Strand Fiord Formation

Northern Axel Heiberg Island

Interpretation of the eruptive style at Bunde Fiord, northern Axel Heiberg Island, is constrained by the small number of cross-sections available. The two sections measured at Bunde Fiord display a similar eruptive style. The flows generally show a simple structure and are of similar thickness at both localities. More variety in intraflow

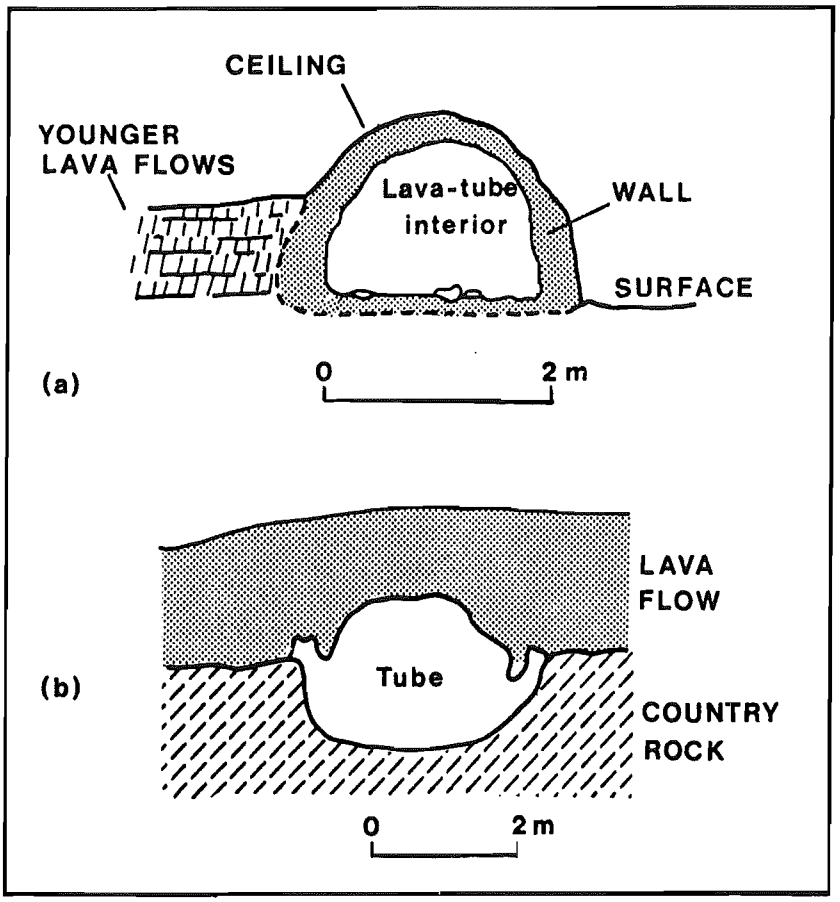

Figure 3.6 Simplified cross-sections of lava tubes (redrawn from Greeley, 1987).
(a) Lava tube formed without a channel phase via lava toes at the front and sides of slow-moving pahoehoe flows.
(b) Lava tube showing evidence of downcutting and lateral erosion of the country rock.

structure is found along the coast where several flows consist of a basal columnar unit overlain by a zone of blocky joints and a rubbly top. These data are sufficient to show that columnar basalts form the bulk of the succession and were erupted episodically, probably as flood basalts.

The scoria and ash deposits could represent breccia tops. These are thick accumulations of spatter, cinder and clinkery flow fragments rafted away from a vent on rapidly flowing basalt (Wright, 1984). Alternatively, the deposits could have originated independently from a (secondary) spatter cone or rampart. This is suggested by facies variations in the volcanic pile along strike where volcanic breccia constitutes a channel-fill that was later buried by thin compound flows, and eventually, by thick basalt floods. The fact that some of the glassy spatter has preserved euhedral crystals suggests that their provenance is closely related to that of the basaltic flows (i.e. same plumbing system).

Western Axel Heiberg Island

The field studies by Ricketts et al. (1985) provide the first and only detailed account of the volcanic stratigraphy in the type area at Strand Fiord. The lavas are described as non-channelized sheets of aa and pahoehoe flows that progressively thin to the south and east, where up to half of the succession consists of volcaniclastic rocks. No direct evidence of subaqueous eruption was found but the authors suggest that lavas accumulated rapidly both as surface-fed and subaqueous sheet-flows. Laharic debris flows were produced by surface weathering of the volcanoes. The lateral facies variations and progressive thinning of the sequence are interpreted as evidence for the presence of a broad,

low volcanic edifice (Hawaiian or Galapagos type shield volcanoe), parts of which were reworked in a beach and shoreface environment.

Field observations reported here suggest that the lavas were erupted subaerially as flood basalts and occasionally flowed into lakes and sluggish streams. The two basal units illustrated on Figure 3.4 (a to c) are interpreted to represent invasive flows. Well-defined scoriaceous tops are characteristically absent. Rather, the flows consist of massive, fine-grained basalt in sharp contact with the enclosing shales. This is observed on the cliff face along Index Ridge, where scoriaceous flow tops ordinarily form well-visible recessive beds in the overlying succession (compare Plates 12 and 13); and at Split Mountain Ridge, where the same units are equally massive but locally display a thin band of amygdales at the upper contact with dark grey fossiliferous shales (Plate 8). Camp (1981) reports several occurrences of invasive flows in areas of active sediment accumulation at the margins of the Columbia River Plateau.

The origin of the basal flows provides a possible explanation for the presence of the Chaotic Breccia described by Ricketts et al. (1985) and examined by the author in 1983. The breccia is of unique character in the area and consists of an unsorted mixture of angular blocks of basaltic lava and baked siltstone in a highly contorted mass of spalled glassy lava. It is in partial contact with the overlying lava flow. Ricketts et al. (1985) proposed two possible origins: by debris flow; or intrusion of magma at shallow levels in proximity to a vent. An alternative explanation is that the blocky breccia formed at the front of an advancing flow of invasive character. Balkwill (1983) describes a similar lava flow-breccia relationship on Amund Ringnes Island.

The presence of ponded and invasive flows, evidence of local subaqueous eruption, and rapid thinning of the sequence, suggest a distal environment at the margin of a basaltic plateau. All the elements of the previous model are compatible with this setting without invoking the presence of a constructional edifice. The dissected topography at a plateau margin explains both the intraflow structures and the presence of a transitional zone where flows interact with available sediment and water.

The field observations from this study are merged in Table 3.1 with aspects of the facies described by Ricketts et al. (1985); a sketch depicting the paleoenvironment is shown on Figure 3.7.

Facies 1: The northern part of the study area typically displays 95% lava flows and 5% pyroclastic and volcaniclastic rocks. The latter are clearly subordinate and were observed to consist of welded lapilli tuffs and volcanic breccia. Facies 1 is therefore predominantly volcanic, and typically consists of ponded flows, best described in terms of Types II and III of Long (1978).

Facies 2: This facies is characterized by both volcanic and volcaniclastic rocks that are the direct result of magmas interacting with poorly consolidated sediments and water, at the plateau margin. Flows might be observed to be invasive, and brecciate laterally. Local evidence of flows entering water and forming pillow lavas suggest the presence of ephemeral lakes or perched ponds. In this transitional zone, the volcanic element still predominates.

Facies 3: Further from the margin, there is clear evidence of reworking in a beach or shallow marine environment. A detailed description of this facies is found in Ricketts et al. (1985).

TABLE 3.1
ERUPTIVE SETTING OF THE STRAND FIORD FORMATION,
WESTERN AXEL HEIBERG ISLAND

FACIES	CHARACTER	COMPONENTS	ERUPTIVE AND DEPOSITIONAL ENVIRONMENT
1. Volcanic	Distal	Ponded flows Rare Lapilli Tuffs Rare Volcanic Breccia	Basalt Plateau Margin
2. Volcanic and Volcaniclastic	Distal	Ponded Flows Invasive Flows Pillow Lavas Volcanic Breccia Blocky "Chaotic" Breccia [1]	Transitional environment from plateau margin to area of active sediment deposition (ephemeral lakes and channels, sluggish streams, etc.)
3. Epiclastic [1]	Distal	Volcanogenic Sandstones and Conglomerate Coal Beds Mudstone	Littoral, Shallow Marine

[1] From Ricketts *et al.*, 1985

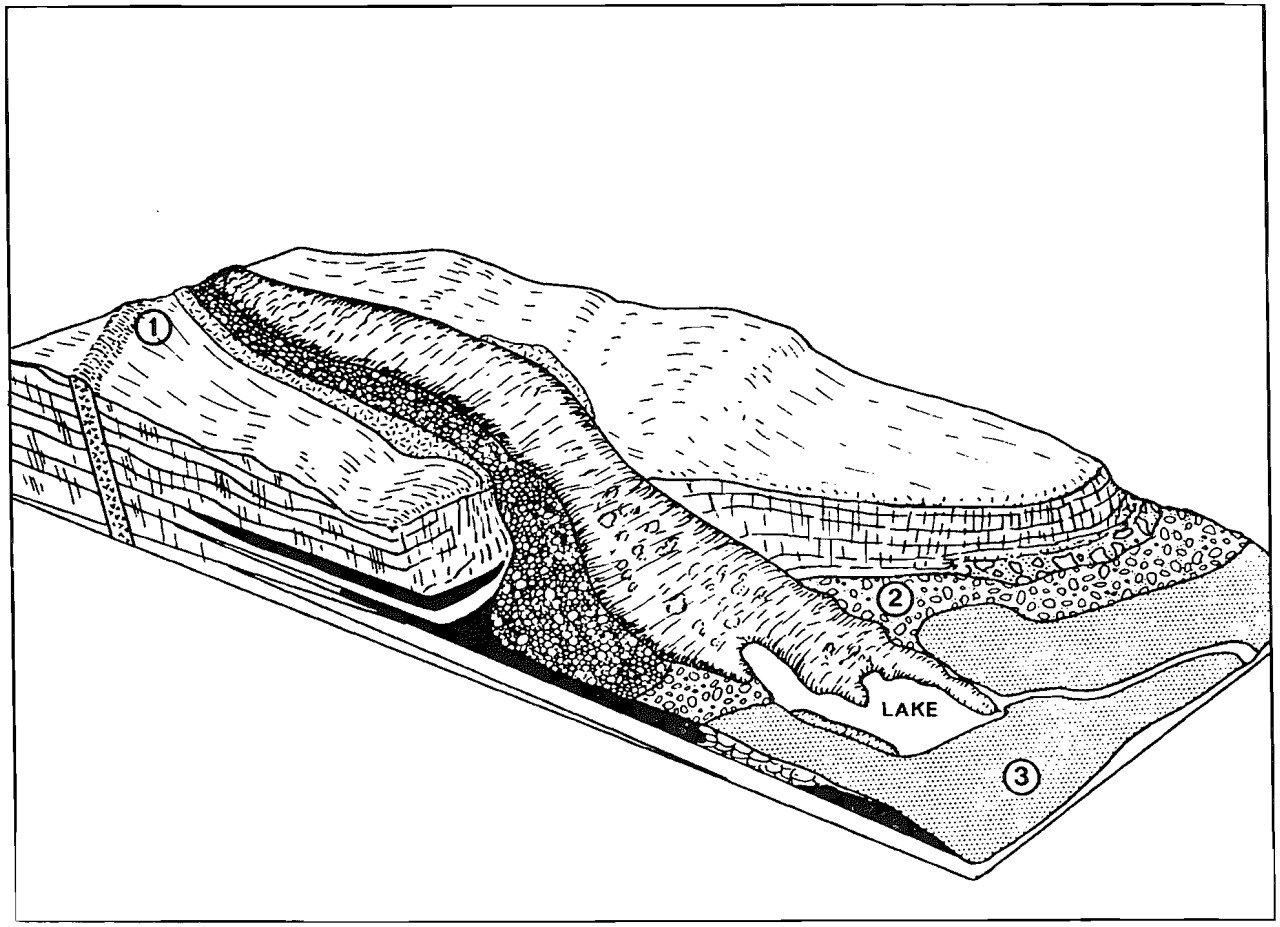

Figure 3.7 Block diagram illustrating some features of the eruptive and depositional environment at the margin of a basaltic plateau. Numbers correspond to the facies described in Table 3.1. Patterns depicting lithological types are shown in the legend of Figure 3.4. The surface of recent basaltic floods is shown by dashed/curved lines.

3.4 Summary and Discussion

This chapter has described the field relations of extrusive rocks in the Isachsen and Strand Fiord Formations. Direct evidence of the style of eruption in the Isachsen Formation is scarce. Lava flows resemble pahoehoe type compound flows or Type I flood basalts of Long (1978). The flows were emplaced in areas of active sediment accumulation, as witnessed by the presence of sedimentary interbeds and sill-like bodies that could represent invasive flows. Interaction between surface-fed magmas and poorly-consolidated sediments is further suggested by the occurrence of thick volcanogenic breccias at some localities (Ricketts, 1985). On the basis of stratigraphic studies, Embry and Osadetz (in press) propose that Isachsen lavas were emplaced during prolonged, quiescent eruptions onto subsiding delta plains.

The lava flows in the Strand Fiord Formation show features typical of flood basalts. The style of eruption is distinct between successions on northern Axel Heiberg Island and in the type area at Strand Fiord. The thickest lava piles occur to the north and consist of flows with simple structures and oxidized flow tops. On western Axel Heiberg Island, the lava flows display complex intraflow structures as a result of ponding and quenching. None of the flows examined displays a reddened flow top, suggesting a relatively short time interval between eruptions. Facies variations in the type area are characterized by a transitional zone where a change in eruptive and depositional patterns is observed, from predominantly volcanic to volcanic and volcaniclastic.

The rapidly changing succession in the type area at Strand Fiord is indicative of a distal plateau margin environment. The presence of a northward-thickening plateau implied by the model is consistent with the position of the source postulated by Embry and Osadetz (in press). In this context, the conspicuous absence of oxidized flow tops in the type area would link the emplacement of these distal flows to an increase in the rate of effusion at the source (Walker, 1972). However, unequivocal evidence of near-vent facies in the Bunde Fiord area (beds of welded spatter, breccia tops) is scarce and warrants further investigation.

According to Wright (1984), the presence of widespread columnar basalt flows that have interacted with water and sediment, and filled the existing topography, is a reasonable indication of flood basalt or "basaltic plains" volcanism. The resulting basalt plateau is usually fed from parallel linear fissure systems. In a basaltic plains environment, lavas are fed both from fissures and low shields, or domes, cinder cones, etc (Greeley, 1982; Fig. 3.8). The products of eruption are thus usually more varied (e.g. silicic lavas) and no flooding of the plain by a single volcanic event ever occurs.

The physical and textural characteristics of the Strand Fiord volcanics are best explained in terms of a flood basalt setting, where lavas are emplaced rapidly, are ponded in topographic lows, and are uniformly basaltic. However, it is worth considering that flood and basaltic plains environments are end-members, and that the latter type is relatively more common (Greeley, 1982; Wright, 1984). The facies variations observed in the Bunde Fiord area could, for example, be explained by the interaction of fissure-fed basalt floods with thin,

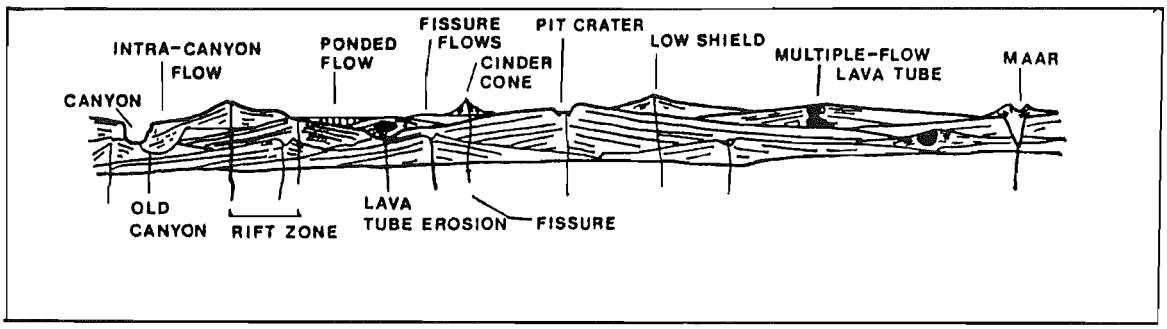

Figure 3.8 Eruptive style in a region of basaltic plains volcanism (redrawn from Greeley, 1982; fig. 4a). The predominant lava type is pahoehoe basalt, in flow units that rarely exceed 3 to 10 m in thickness. Thicker flows (greater than 10 m) may represent flood type eruptions, or more frequently, the ponding of lavas in low-lying regions and as intracanyon flows. Primary forms include low shields, often with summit pit craters; flows fed by large lava tubes between shields; fissures, which can produce thin flows or, more rarely, cinder-spatter-cones during point-source eruptions; and maar craters resulting from groundwater and magma interactions.

channeled flows erupted from a central vent. Point-source eruptions along fissures could produce cinder-and-spatter cones.

The setting of Late Albian volcanism in the Sverdrup Basin is added evidence that no unique model can apply to the eruptive style of continental flood basalt provinces (CFB) and variations thereof. The types of vents associated with flood basalt eruptions especially, are no longer thought to consist solely of large-scale fissures exposed as dyke swarms. Recent field-based studies on Iceland rifts, the Deccan Traps and western U.S.A. Cenozoic Provinces, amongst others, indicate that catastrophic flooding by basaltic lavas can occur from a system of linearly arranged fissures (Swanson et al., 1975), a primary central edifice (Beane et al., 1986; Devey and Lightfoot, 1986), a combination of fissures and shield volcanoes (e.g. Helgason, 1983) or a region where several types of vents are juxtaposed (Greeley, 1982). This has direct consequences on the types of flows erupted. A classic CFB province such as the Deccan Traps of India, for example, predominantly exhibits compound aa and pahoehoe flows (Walker, 1972) erupted from central vents or a primary volcanic edifice (Agashe and Gupte, 1972; Beane et al., 1986).

In the type area at Strand Fiord, the volcanic style is remarkably similar to that of the Columbia River Plateau as reported by Swanson and Wright (1980), Wright (1984) and Long and Wood (1986; references therein). On northern Axel Heiberg Island, the eruptive style closely resembles that of feldspar-phyric basalt lavas of the West Greenland Tertiary volcanic province described by Clarke and Pedersen (1976; fig. 333). Based on these analogies and the available field evidence, it

appears likely that the Strand Fiord basalts were erupted from a linear system of vents, now exposed as dykes on Axel Heiberg Island.

IV. FIELD RELATIONS - INTRUSIVE ROCKS

4.1 Introduction

In this chapter, field observations on intrusive rocks are described and used to constrain the relative age of sills and dykes as indicated by cross-cutting or feeder relationships in different parts of the study area. The field data are then combined with absolute age determinations of key units (Avison, 1987) and trend analyses of dykes (Jollimore, 1986) to establish a chronology of intrusive magmatism in the east-central Sverdrup Basin. The results are compared with the stratigraphic ages for extrusive rocks (Section 2.3.2). The proposed "integrated" magmatic events provide the working hypothesis for petrochemical studies.

Sills and dykes were measured and sampled in four areas along the length of the study area (Fig. 4.1). For descriptive purposes, the units are grouped and described according to their geographic location and predominant style of intrusion, as: Igneous rocks of the Lightfoot River Dyke Swarm (A); Buchanan Lake and Eureka Sound area (B); Tanquary Fiord area (C) and Lake Hazen-Piper Pass area (D). In each of the areas described, intrusive rocks were sampled at regular intervals between contacts with the host sedimentary rocks. Tables containing the sampling information are included in Appendix A.

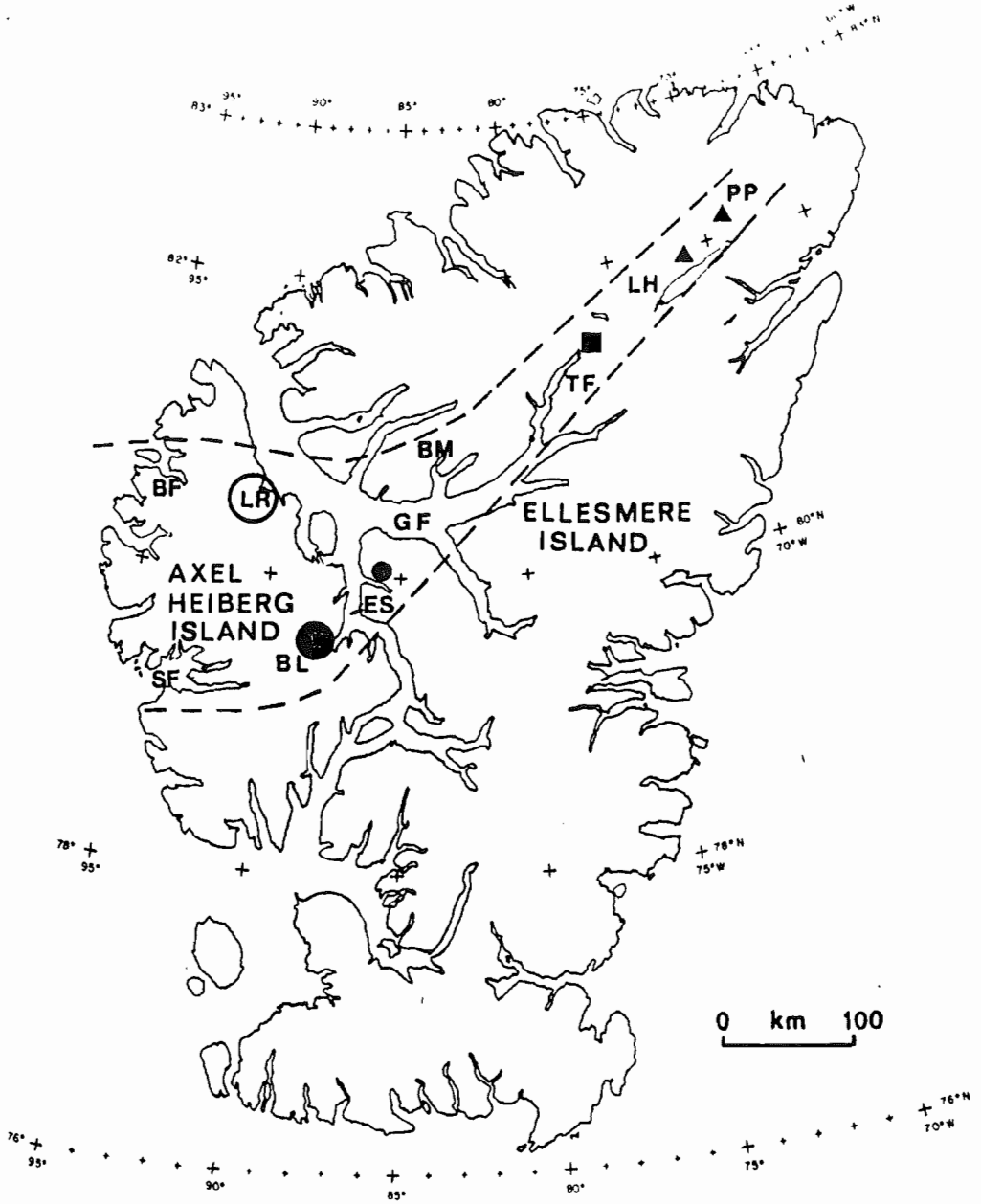

Figure 4.1 Sampling stations for intrusive rocks on Axel Heiberg and northeastern Ellesmere Islands. Open circle, Group A: Lightfoot River Dyke Swarm; filled circle, Group B: Buchanan Lake and Eureka Sound intrusives; square, Group C: Tanquary Fiord intrusives; triangle, Group D: Lake Hazen and Piper Pass intrusives. Dashed line: approximate limits of the study area. BF - Bunde Fiord, BL - Buchanan Lake, BM - Blue Mountains, ES - Eureka Sound, GF - Greely Fiord, LH - Lake Hazen, LR - Lightfoot River, PP - Piper Pass, SF - Strand Fiord, TF - Tanquary Fiord.

4.2 East Axel Heiberg Island and Eureka Sound

4.2.1 The Lightfoot River Dyke Swarm

The Lightfoot River flows from west to east across the north-central part of Axel Heiberg Island. The presence of sills and dykes of gabbro in this area was first reported by N. J. McMillan (in Fortier et al., 1963) during a geological traverse from Lightfoot River to Wading River. The intrusions were observed to cut all the bedrock formations and be particularly abundant in older Mesozoic strata. The group of dykes chosen for study occurs along a 25 km wide belt north of the Lightfoot River (Fig. 4.2). Individual units can be traced up to 40 km on air photographs. The dykes cut indiscriminantly through carbonate rocks of the Nansen Formation and Triassic shale and siltstone sequences.

Ten dykes and five sills were sampled in this area. The dykes vary in thickness between 1 and 60 m and show a similar attitude (NNW - vertical or dipping west at high angles). The sills vary in thickness between 5 and 15 + m and intrude the Triassic Blind Fiord or Blaa Mountain Formations. In the eastern part of the area, these units straddle the contact between the two formations. At this locality, broad folds obscure the contact relationships between thin, semi-concordant sills and the host rocks.

Two of the dykes show well-developed structures along one of the margins. Dyke 9 (Appendix A) is 21.5 metres wide with well-exposed chilled margins (30-50 cm wide). A zone of flow banding occurs one metre from the east-facing margin, consisting of 2 to 5 cm-wide layers

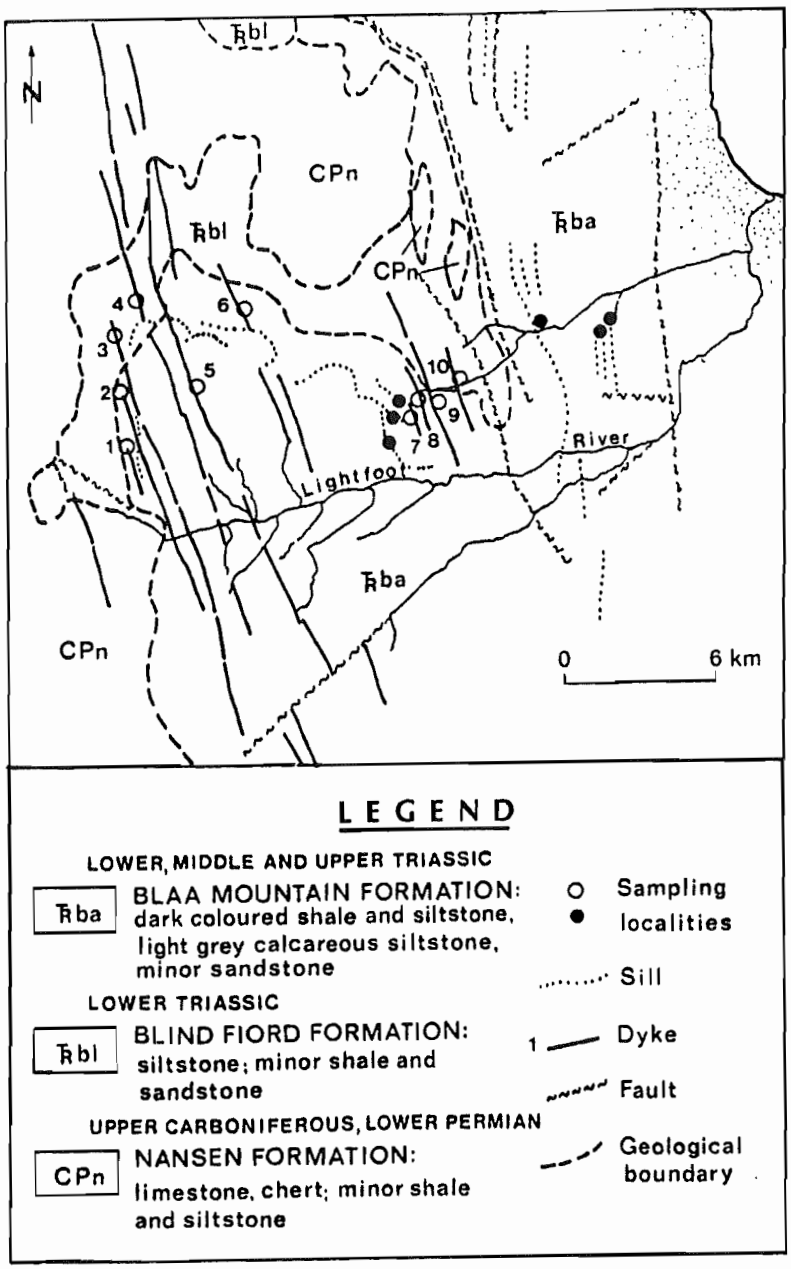

Figure 4.2 Simplified geological map of the Lightfoot River area. Modified from G.S.C. Map 1310A, Bukken Fiord, 1:250 000. Thin dykes and sills observed during field work were added to the original compilation (list in Appendix A).

of coarser felsic material. The central portion of the dyke and west margin do not show layering. Dyke 5 is 60 metres wide and displays crude zoning within 10 to 15 metres of the west wall. The zones include poorly-defined areas of coarser-grained, melanocratic gabbro and irregular veins of fine-grained pale grey diabase in sharp contact with the host rock. The latter are generally oblique to the dyke wall and may represent disrupted or truncated layers (e.g. Irvine, 1979). The eastern half of the dyke is medium-grained with a homogeneous texture and shows no evidence of internal differentiation.

North of the Lightfoot River, dykes are seen to postdate the sills (a thick sill that forms a resistant ridge is cut by dykes 4, 5 and 6; Fig. 4.2). In this respect, they provide examples of a second intrusive event in the area.

4.2.2 The Buchanan Lake and Eureka Sound Area

Prior to Operation Franklin (Fortier et al., 1963), Schei (1904) of the FRAM Expedition was the first to report the presence of basic rocks in Mesozoic strata of Axel Heiberg Island. Souther (1963) described abundant sills along the Buchanan Lake shores as "tabular bodies" of diabasic gabbro intruding Triassic strata of the Blind Fiord, Blaa Mountain and Heiberg Formations.

The southern shore of Buchanan Lake provides a semi-accessible succession where 18 units were sampled and measured wherever possible (Fig. 4.3 a). The sills vary in thickness between 1 and 50 + m. and intrude fissile black shales of the Blaa Mountain Formation. Most of the units are massive and display columnar joints. They are generally

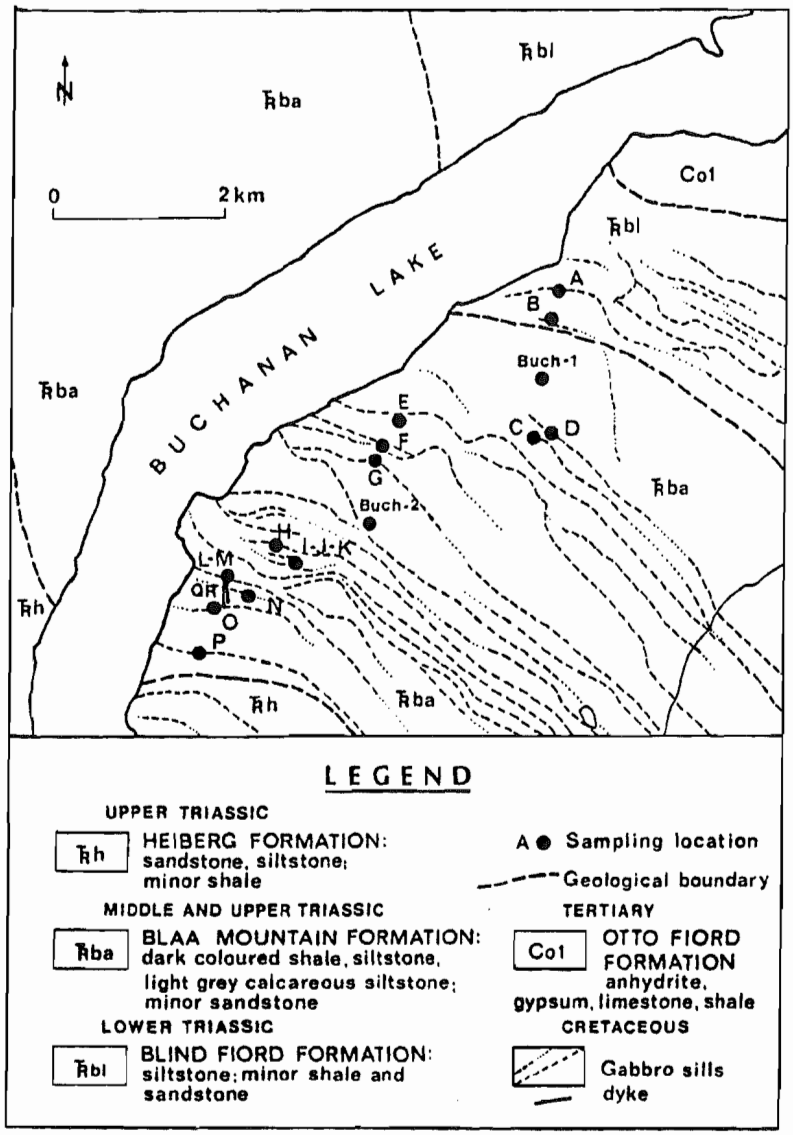

Figure 4.3 (a) Simplified geological map of the Buchanan Lake area showing sampling stations (A-R) and prominent sills (drawn from air photographs according to GSC Map # 1302A, Eureka Sound North).

concordant or slightly discordant, as previously reported by Souther (1963). One of the units sampled is lensoid and cross-cuts the sedimentary rocks at a moderate angle (Dyke J; Appendix A).

The style of intrusion is illustrated on Figure 4.3 (b). Some of the sills intrude the shales in a step-like fashion; others are cut by thin, irregular dykes. Two populations of sills can be distinguished on the basis of colour, thickness and internal structure. The presence of darker, massive sills is consistent with the possibility of a second younger magmatic event. Two feldspar-phyric dykes cutting through a sill (Plate 15) were sampled to provide an upper age limit to the magmatism. The dykes also cut calcite-filled amygdales and veins near the top contact with shales, suggesting that two intrusive events were well separated in time.

To complete the data base in the Eureka Sound area, four sills averaging 27 m in thickness were sampled at Blacktop Mountain, near the Eureka weather station (Fig. 4.1). The sills are massive and show well-developed columnar jointing. They intrude shales of the Blaa Mountain Formation. No evidence was found at this locality, of dykes cross-cutting the sills (G. K. Muecke, pers.comm., 1987).

4.3 Northeastern Ellesmere Island

4.3.1 Tanquary Fiord Area

Geological reconnaissance work in the Tanquary Fiord area was first undertaken by Troelsen in 1940 (1950). Field studies by workers of the Geological Survey of Canada followed in 1957-1958 (Christie, 1964); in

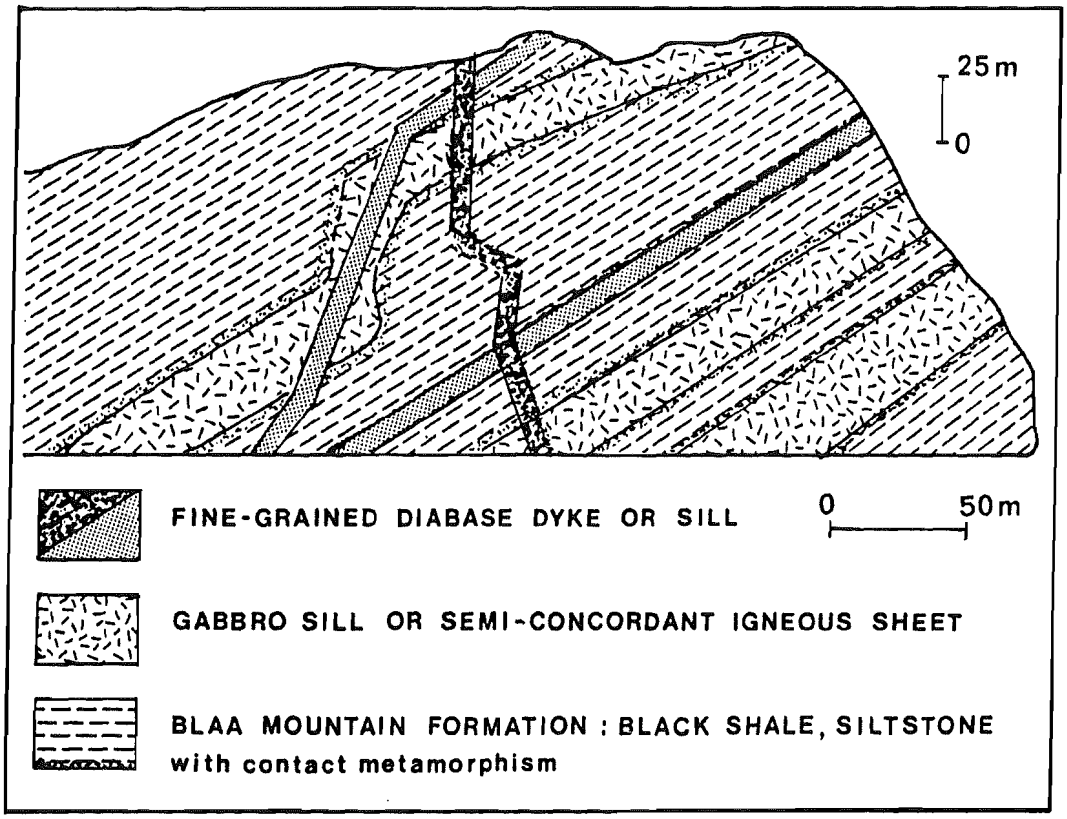

Figure 4.3 (b) Schematic profile of a cliff on the northern shore of Buchanan Lake, showing field relationships between intrusive units. At this locality, sills and dykes intrude shales of the Blaa Mountain Formation near the contact with the Blind Fiord Formation. Sills vary in thickness between 1-2 m and 50 m +. Intrusive sheets often penetrate the country rock in "steps". Most of the larger sills display columnar joints. There are at least two generations of cross-cutting dykes which appear characteristically darker than the sills. Dark, fine-grained sills are structurally and texturally distinct from thick gabbro sills and semi-concordant, hydrothermally (?) altered igneous sheets.

PLATE 14

Profile of a cliff on the northern shore of Buchanan Lake, showing field relationships between intrusive units. At this locality, sills, slightly discordant intrusive sheets , and dykes intrude shales of the Blaa Mountain Formation near the contact with the Blind Fiord Formation (partial view of the cliff section illustrated diagrammatically on Fig. 4.3 b). Arrows point to examples of thick, altered sills (white) and thin, darker units (black). Baked shales at the contact with igneous rocks form whitish bands that are clearly visible on this section.

PLATE 15

Thin feldspar-phyric dyke cutting through a sill, south shore of Buchanan Lake. Note the contrasting position of cooling joints in both units. $^{40}Ar/^{39}Ar$ step-heating analysis of the dyke rock (Q/R of Avison, 1987) provided an age of 113 Ma for this intrusive event, equivalent to Cycle 2 of Embry and Osadetz (in press; see Fig. 2.5).

PLATE 14

PLATE 15

1962 (Tozer, 1963; Thorsteinsson and Trettin, 1971; Thorsteinsson, 1974); in 1963 and 1966 (Nassichuk and Christie, 1969); and in 1967 (Trettin, 1971). Reconnaissance mapping of the area was started in 1975 and resulted in a preliminary geological map of the area (Mayr et al., 1982a).

The stratigraphic sequence in the Tanquary Fiord and Lake Hazen areas is influenced by the presence of the Grant Land Uplift, a major Tertiary structure that overthrusts Paleozoic (and younger) strata onto Mesozoic (and older) strata (Osadetz, 1982). At the head of the fiord, the Cambrian Grant Land Formation overthrusts upper Paleozoic and Mesozoic strata of the Sverdrup Basin along the Lake Hazen Fault Zone (Christie, 1964). This thrust extends to Piper Pass. A simplified geological map of the area is shown on Figure 4.4.

Field data on intrusive rocks were first reported by Osadetz and Moore (in press) and provide the best account of cross-cutting relationships between sills and dykes. Dykes are abundant and were observed to cut all pre-Tertiary Formations. Their density is particularly high in the vicinity of the Airforce Glacier where they trend east-west. The units are generally thin (approximately 1 m) and can be traced for up to 5 km along strike. Lower Paleozoic strata do not contain sills and are rarely cut by subvertical dykes. The structural relationship of dykes to sills is complex: some dykes cross-cut the sills, whereas others act as feeders or originate from concordant intrusions.

Sills were sampled at two localities near the head of Tanquary Fiord (Fig. 4.4). A composite section along the Rollrock River valley (Plate 16) provided samples for 8 sills (Fig. A.5 in Appendix). The

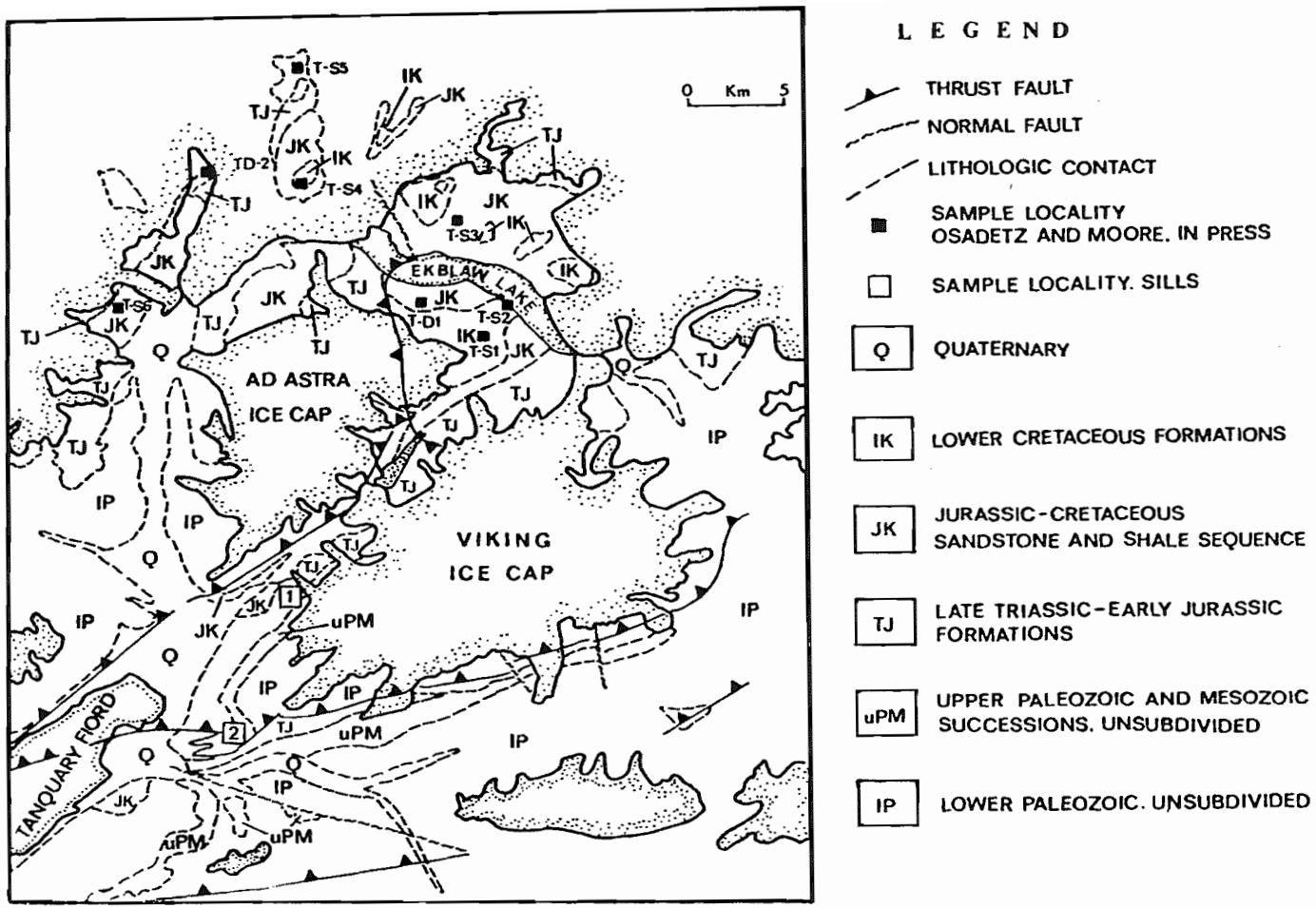

Figure 4.4 Simplified geological map of the Tanquary Fiord and Ekblaw Lake areas (modified from Osadetz 1982 and Mayr et al., 1982a). Sills were sampled at two localities (open squares) along the Rollrock and Macdonald Rivers. Localities for samples analysed by Osadetz and Moore (in press) are shown as filled squares (Squares, T-S* sills; T-D* dykes).

PLATE 16

Photograph of the section sampled along Rollrock River, at the head of Tanquary Fiord ([1] on Fig. 4.4). A total of eight sills were measured (schematic representation on Fig. A.5, Appendix). The view is northeast towards Rollrock Glacier and Ekblaw Lake.

PLATE 17

Cliff section along the Macdonald River, showing sharp, conformable contacts between sills and Triassic-Jurassic strata of the Sverdrup Basin. The thickness of individual sills ranges from 5 to 30 metres.

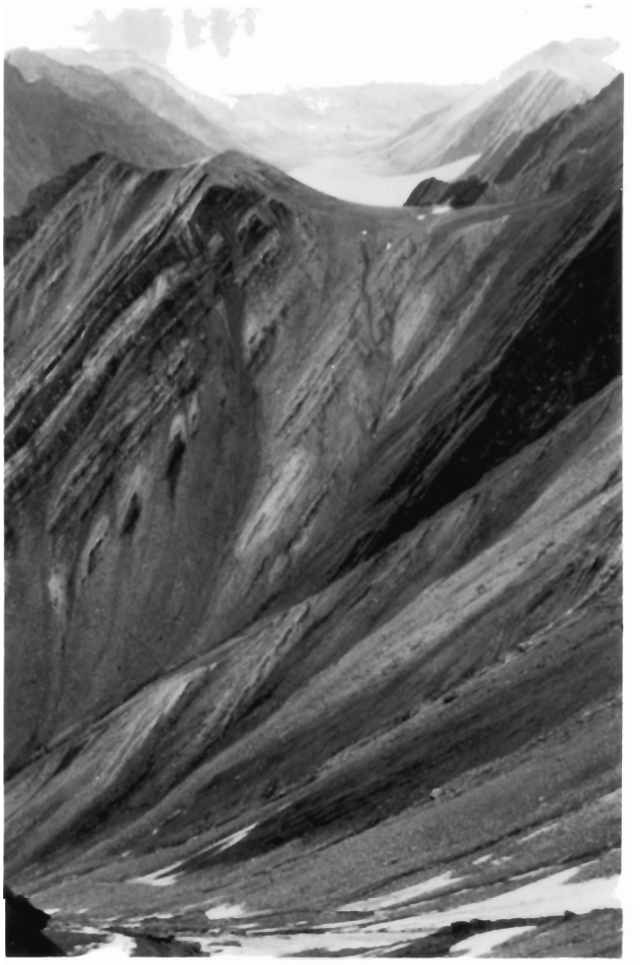

PLATE 16

PLATE 17

sills display sharp, conformable contacts with competent sandstone units and consist of massive, fine to medium-grained gabbro. The progressive increase in grain size from the margins to the centre is not accompanied by visible evidence of compositional differentiation. Some sills split along strike and thinner top units intrude the sedimentary rocks in steps.

Three sills that also intrude Permo-Triassic strata were sampled along the Macdonald River, (Fig. 4.4). At this locality, the contacts with sedimentary rocks are poorly exposed. Cliff outcrops, however, suggest that the sills are perfectly concordant intrusions (Plate 17).

No cross-cutting dykes were observed. Only one sill is cut by thin dykes in the Rollrock River section (Fig. A.5).

4.3.2 North Shore of Lake Hazen and Piper Pass

The first geological reconnaissance work on northern Ellesmere Island was done in 1875-1876 by members of a British naval expedition led by Admiral Sir George Nares (Feilden and de Rance, 1878). Field work resumed in the 1940's and 50's. R.L. Christie (1964) produced the first comprehensive geological map of the area based on field work in 1957 and 1958. Reconnaissance mapping in this area was completed between 1975 and 1982 by workers of the Geological Survey of Canada, and resulted in preliminary maps of part of the Lady Franklin Bay area, Clements Markham Inlet and Robeson Channel areas (Trettin et al., 1982; Mayr et al., 1982b).

The Lake Hazen area occupied a basin margin stratigraphic setting throughout the upper Paleozoic and Mesozoic. Simplified geologic maps

are shown on Figures 4.5 and 4.6. The contacts between formations are usually disconformable (Trettin et al., 1982). Upper Paleozoic and Mesozoic strata from Lake Hazen to Piper Pass are wedged between faulted or lithologic contacts with lower Paleozoic rocks to the northwest and the Tertiary Eureka Sound Formation to the southeast. Cretaceous strata include a condensed section of the Isachsen Formation, shales of the Christopher Formation and a volcanic-sedimentary sequence in the Hassel Formation (the latter grouped with other successions of Late Albian-Early Cenomanian age in Cycle 3; see Fig. 2.5). A relatively small number of intrusive rocks outcrop in upper Paleozoic and Mesozoic strata of the Lake Hazen area. Intrusive rocks are abundant and well-exposed in the Permian Trold Fiord Formation near the Turnabout Glacier and Piper Pass (Fig. 4.6).

Samples from sills and dykes were collected at several localities. The sills examined in the Piper Pass area vary in thickness between 10 and 90 + m. Units are uniformly massive and columnar-jointed, and display a gradual coarsening of the gabbroic mineral assemblage from the margins to the centre. A three-fold structural division of cooling units is observed in the ***Camp*** and ***Dark Crystal*** sills. In the ***Dark Crystal*** sill, the units display columns of similar morphology and length, separated by cross-joints that form two major discontinuities (Plate 19). Columnar joints develop when the magma contracts during cooling. However, three-fold structural divisions are rarely observed in intrusive sheets (Spry, 1962). The presence of three zones in the Piper Pass sills may result from downward percolation of water into the interior of the sill via cooling fractures, a mechanism invoked by Long

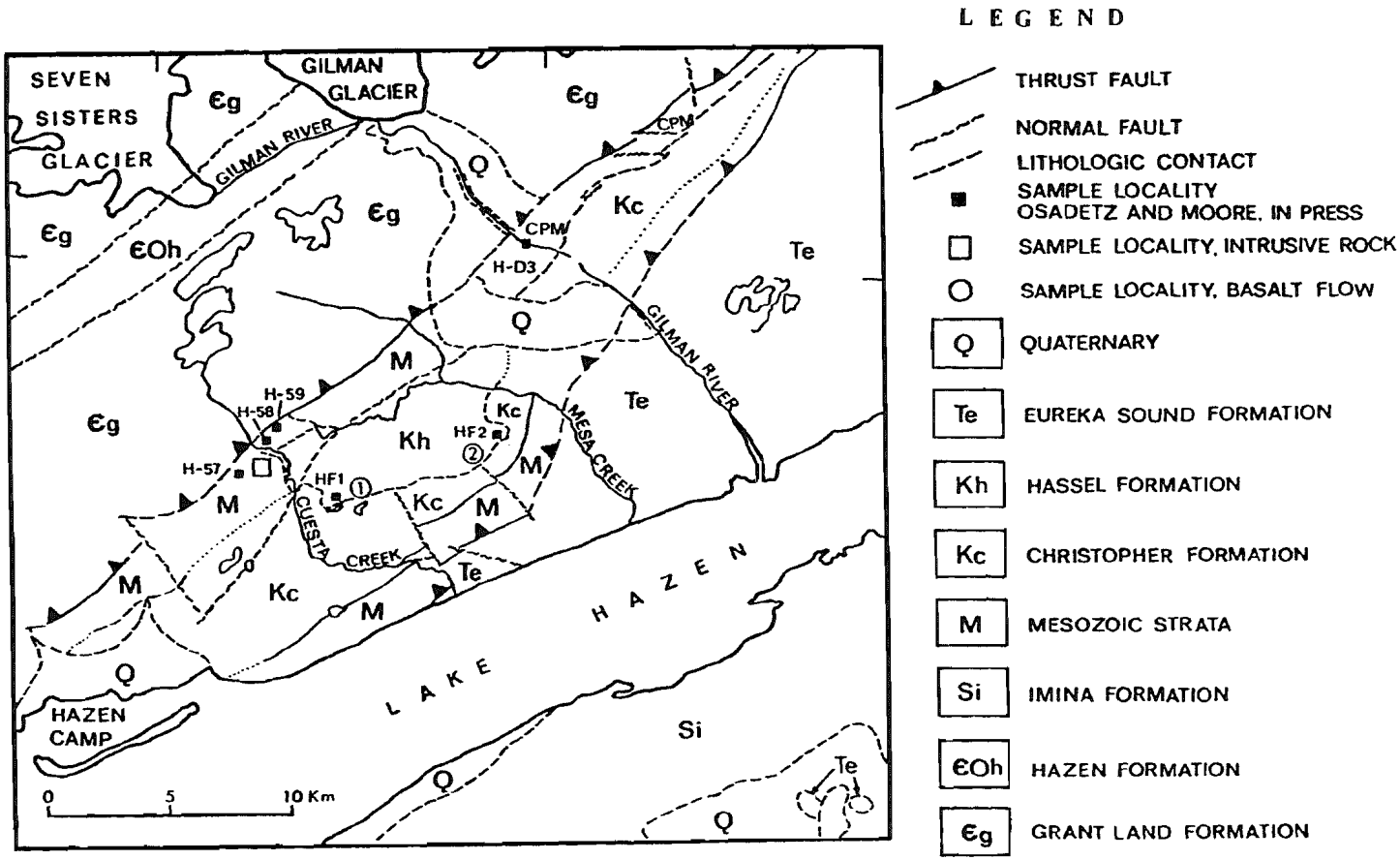

Figure 4.5 Simplified geological map of the Lake Hazen area (modified from Trettin et al., 1982). Sampling localities for this study are shown by an open square or circle. Localities for samples analysed by Osadetz and Moore (in press) are also indicated (symbols as in Fig. 4.4; H-F* lava flows; H-S* sills; H-D* dykes).

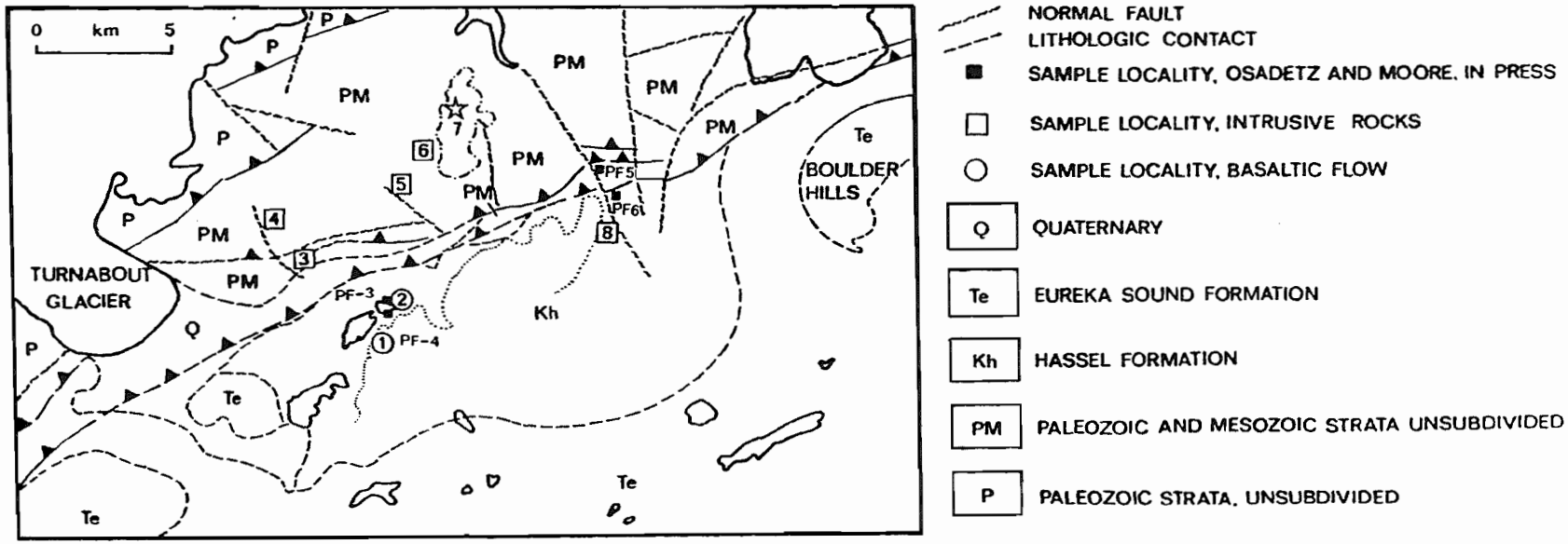

Figure 4.6 Simplified geological map of the Piper Pass area (modified from Mayr et al., 1982b). Key to sections sampled for this study: [1] ***Lake Sections***; [2] ***Arctic Hare Mesa***; [3] ***Turnabout Sill***; [4] ***Dark Crystal***; [5] ***Mount Doom***; [5] ***Camp Sill***; [6] ***Camp Sill Extension***; [7] ***Star Intrusive***; [8] ***Piper Pass Sills***. Localities for samples analysed by Osadetz and Moore (in press) are also shown (symbols as in Fig. 4.4; P-F* = lava flows in the Hassel Formation).

PLATE 18

View to the southwest from the Star Intrusive Complex. The photograph is taken from Sill 1. In the foreground, dykes 1 to 3 (see Fig. 4.9). The Dark Crystal (1) and Mount Doom sills (2) are visible in the background ([4] and [5] on Fig. 4.7).

PLATE 19

A rare example of three-fold structural division in an intrusive sheet, observed along a section of the Dark Crystal sill near Piper Pass. The sill measures 90 metres. It consists of three cooling units of medium to coarse-grained gabbro separated by cross-joints along two major discontinuities (arrowed). Internal chilled contacts were not found. The three-fold division could result from the percolation of water into the interior of the sill via cooling fractures (e.g. Long and Wood, 1986).

PLATE 18

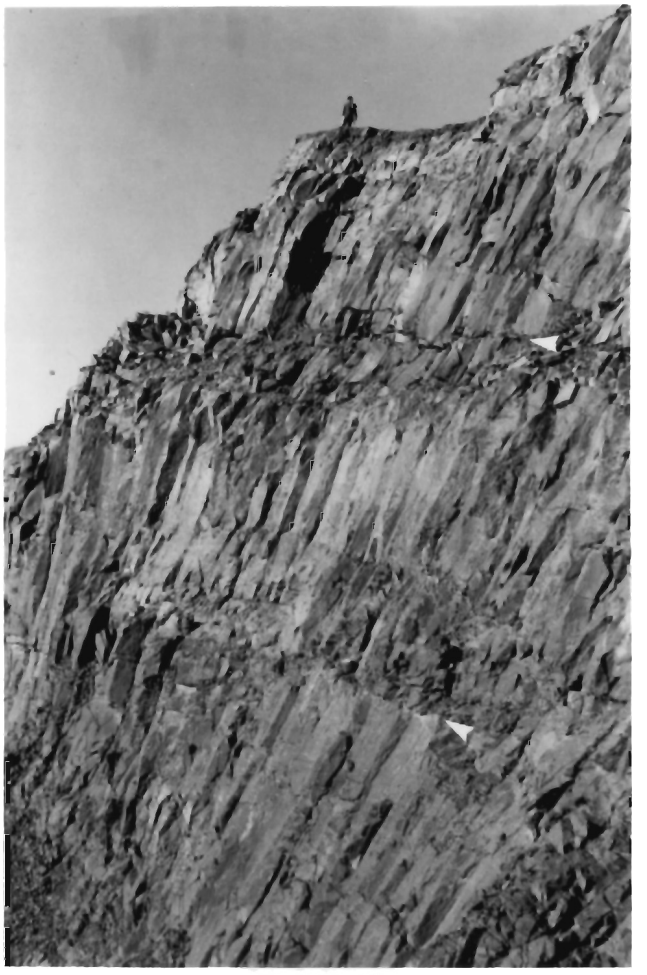

PLATE 19

and Wood (1986) to explain the intraflow structures of ponded flood basalts.

No dykes were observed to cross-cut sills or emanate from them except at the southern tip of Piper Pass ([7] on Fig. 4.6). At this locality, a star-shaped complex of feeder dykes and sills intrudes an outlier of Permian strata (Plate 18). A plan view of the intrusives (Fig. 4.8) shows that all the dykes originate from a single, steeply dipping feeder dyke that can be traced along the south wall of the adjacent stream. Two thin dykes and a sill are branches related to splitting of the main feeder.

The ***Star Intrusive*** dykes were the only discordant intrusions identified in the Piper Pass area. The field evidence gathered so far suggests that they are remnants of magmatic conduits in a volcanic-intrusive complex. No dykes can be traced to volcanic flows in the Hassel Formation. However, a shallow sill near Cuesta Creek is locally highly vesicular and fed by a thin dyke ([3] on Fig. 4.5).

4.4 Comparative Summary

The principal differences among sampling localities concern the mode of emplacement and internal differentiation of intrusive rocks. On eastern Axel Heiberg Island, igneous rocks form semi-concordant sheets emplaced in thick Triassic shale and siltstone sequences. Poorly-consolidated shales are often bleached near the contact with igneous rocks. In one or two cases, hornfelsed pelitic sediments form rafts along the contact with thick sills. Igneous rocks from stations on northeastern Ellesmere Island were emplaced in sandstone-dominated

facies. Intrusive sheets are generally concordant and there is little evidence of magma-sediment interaction.

The visible effects of differentiation in dykes and thick intrusive sheets demonstrate the need for a careful examination of geochemical analyses from the margins to the centre of units. The possibility of crustal assimilation appears strongest in the Buchanan Lake and Lightfoot River areas.

In the Lightfoot River area (Fig. 4.2), two of the thickest dykes show layering parallel to dyke walls or inhomogeneities in composition and texture towards the centre of the intrusion. The discovery of a partially assimilated xenolith in the central part of Dyke 5 is the only direct evidence of contamination by the surrounding country rocks.

Three of the sills examined at Buchanan Lake (Fig. 4.3 a) show visible internal differentiation on the outcrop. Sill A is massive up to 24 m, where it displays a zone of leucocratic, pegmatitic diabase (G.K. Muecke, pers. comm. 1985; Avison, 1987). Sill E (Appendix A) is 28 m thick with sharp and conformable basal and upper contacts. From the margins to the centre of the sill, there is a transition from fine-grained, massive diabase to coarser, leucocratic and altered gabbro with conspicuous acicular pyroxenes. Sill M contains at least five units with variable textures.

The thickest sill measured along the Macdonald River near Tanquary Fiord, displays a mafic base that grades into a coarser, more altered leucocratic gabbro with a distinct ophitic texture. The layered intrusion near Ekblaw Lake (TS-6 on Fig. 4.4; Osadetz and Moore, in press) was not re-sampled for this study.

A composite intrusion at a locality west of Cuesta Creek, near Lake Hazen, is characterized by a coarse, pyroxene-rich base overlain by fine-grained leucogabbro (Plate 20). The basal unit is aphanitic at the contact with a massive sill showing well-developed columnar jointing.

4.5 Correlation with Volcanic Episodes

Four episodes of Cretaceous volcanism are recognized in the Valanginian-Maastrichtian interval (Fig. 2.5). The presence of widespread intrusive rocks raises the question of contemporaneity: were sills and dykes intruded in the Sverdrup Basin during several episodes, or are they related to a single event? Do the dykes at Buchanan Lake and Lightfoot River represent feeders to some of the volcanic rocks? The apparent association of intrusive and extrusive rocks in northeastern Ellesmere Island (Osadetz and Moore, in press) suggests that intrusive activity may also be episodic throughout the Sverdrup Basin.

$^{40}Ar/^{39}Ar$ step-heating analyses were performed at Dalhousie University on key units of the Buchanan Lake, Lake Hazen and Piper Pass area (Avison, 1987). Dates calculated from the $^{40}Ar/^{39}Ar$ ratio of each fraction of argon released in an igneous rock (or mineral separates) ideally yield a plateau that indicates an age more or less equal to the time of crystallization, if cooling temperatures remained below closure temperatures. Partial loss of gas as a result of reheating usually disrupts the plateau. However, a new plateau can be established by episodic complete out-gassing, yielding useful information on regional thermal events.

PLATE 20

Lithologic variations through a composite intrusion differentiated at its' base, West Cuesta Creek, Lake Hazen area ([3] on fig. 4.4). The dashed line indicates the sharp contact between the differentiated base and auto-intruded, massive unit above. The transition between a coarse, pyroxene-rich basal unit and the overlying leucocratic gabbro is gradual. Note the difference in the effects of weathering between the mafic base (arrowed) and greyish, felsic upper zone. The leucocratic unit decreases in grain size near the contact with massive, fine-grained diabase.

PLATE 20

The samples from the Buchanan Lake area belong to Sill A and Dyke Q (see Fig. 4.3 a). The objective was to analyse biotite, mafic and felsic separates, and whole-rock samples of the sill to determine which fraction in chilled or coarse, central portions of the sill provides the best spectra. Dyke Q was chosen because it clearly represents a second intrusive event and would provide an upper limit to the age of magmatism in this part of the Sverdrup Basin.

The results are shown in Figure 4.7. The most reliable ages for Sill A samples were obtained from the biotite separate. The mafic and felsic fractions all displayed internally discordant $^{40}Ar/^{39}Ar$ spectra. Avison (1987) interprets the true age of sill A as being 126 $^{+/-}$ 2 Ma. Spectra of a whole-rock sample from the feldspar-phyric Dyke Q yielded an age of 113 $^{+/-}$ 6 Ma. Avison (1987) concludes that Sill A was intruded in the Hauterivian. Dyke Q was intruded approximately 15 Ma later, during the Late Barremian-Aptian volcanic episode or Cycle 2 (ibid.).

The igneous rocks chosen from the Lake Hazen and Piper Pass areas include a sample from the cuesta of volcanic rocks at Lake Hazen ([1], Fig. 4.5) and two samples from Sill #4 of the Star Intrusive Complex ([7], Fig. 4.6). The results are shown in Figure 4.8. All three whole-rock samples yielded ages of 91 or 92 $^{+/-}$ 2 Ma. The age of the volcanic flow is somewhat younger than expected from stratigraphic considerations (Cycle 3, Late Albian-Early Cenomanian). The coincident ages of the lava flow and dykes confirm the presence of a volcanic-intrusive complex in the Lake Hazen-Piper Pass area. The age of intrusives in the Tanquary Fiord area, however, is still uncertain and the correlation

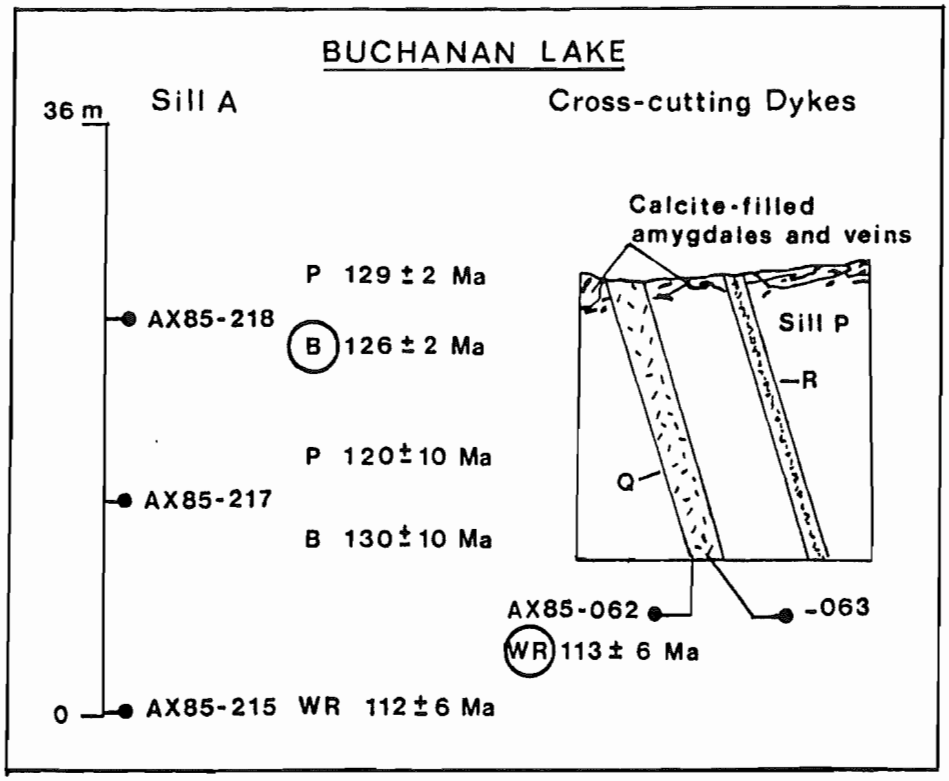

Figure 4.7 Results of $^{40}Ar/^{39}Ar$ step-heating analyses performed by Avison (1987) on a sill and cross-cutting dyke from Buchanan Lake (locations on Fig. 4.3 a). P: plagioclase and B: biotite separates; WR: whole rock. The ages retained in the final interpretation are circled.

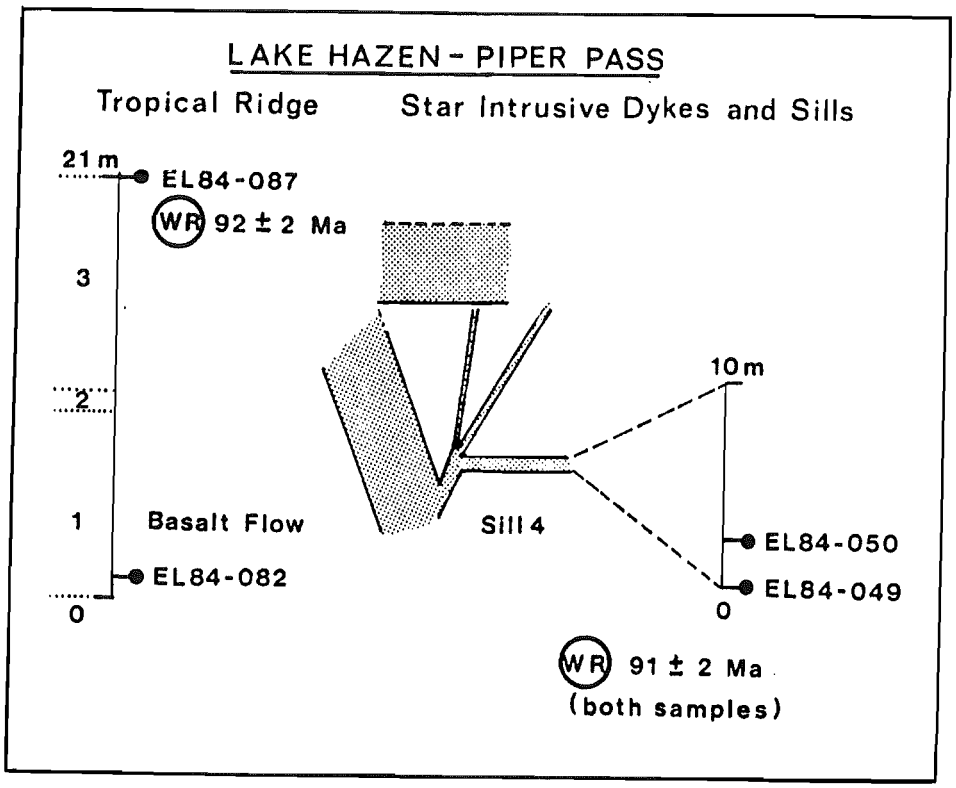

Figure 4.8 Results of $^{40}Ar/^{39}Ar$ step-heating analyses performed by Avison (1987) on samples from a basalt flow in the Lake Hazen area (ref. ***Tropical Ridge***); and sill 4 of the ***Star Intrusive***, Piper Pass area (locations on Figs. 4.5 and 4.6). Symbols as in Figure 4.7. Intraflow structures are [1] well-developed, regularly-spaced columns; [2] hackly unit; [3] massive unit with no internal structures.

with igneous rocks near Piper Pass (Osadetz and Moore, in press) is speculative.

The age of intrusive rocks in the Lightfoot River area remains an open question, constrained to some degree by the studies of Jollimore (1986). An analysis of dyke swarms in the Sverdrup Basin was carried out using 1:250,000 maps of the Arctic Islands. Jollimore (1986) concludes that the Sverdrup Basin underwent two major dyking episodes. The trends deduced from analysis are observed in all stratigraphic horizons prior to and including the Cretaceous, indicating that both events occurred during the Cretaceous period. Each event produced two trends (or swarms). The Lightfoot River dykes form part of the strong northerly trend which is most pronounced along the western margin of Ellesmere Island and in northern and eastern Axel Heiberg Island (Balkwill and Fox 1982; Jollimore 1986). There is a progressive change to an east-west trend in the western part of the basin.

The relative ages of the two dyking episodes are not known. However, the Lightfoot River dykes could represent a linear system of feeders linked to the emplacement of the Late Albian basaltic plateau (Chapter 3). The correlation was tested by Jollimore (1986) who examined a set of geochemical analyses of dykes in this area. The preliminary study indicates that the dykes are compositionally indistinguishable from basaltic lavas of the Strand Fiord Formation and may indeed represent feeders. This aspect is discussed in Chapter 7.

Table 4.1 is a summary of the stratigraphic and radiometric ages available at the time of study. The new dates by Avison (1987) provide a basis for comparing the petrology of intrusive and extrusive rocks in the study area. The significance of the associations shown on Table 4.1

TABLE 4.1
SUMMARY OF CRETACEOUS MAGMATIC EVENTS:
EASTERN AND CENTRAL SVERDRUP BASIN

EXTRUSIVE ROCKS		INTRUSIVE ROCKS
VOLCANIC EPISODE (1)	**AREA**	**$^{40}Ar/^{39}Ar$ STEP HEATING ANALYSIS (2)**
IV		
Late Cenomanian-Maastrichtian	Northern Ellesmere Island	
HANSEN POINT VOLCANICS (3)		
Turonian	Lake Hazen→	Basalt Flow 92 ± 2 Ma
	Piper Pass→	Sill/Dyke #4 91 ± 2 Ma
BASALT FLOWS IN THE HASSEL FORMATION		
III	**West and North Axel Heiberg Island**	
Late Albian-early Cenomanian	Eastern Axel Heiberg→	?Lightfoot River Dykes (4)
STRAND FIORD FORMATION		
II	**Axel Heiberg Island**	
Late Barremian-Aptian	Buchanan Lake→	Dyke Q 113 ± 6 Ma
BASALT FLOWS IN THE ISACHSEN FORMATION	**- Walker Isl. Member**	
I	**Eastern Axel Heiberg Island**	
Valanginian-Early Barremian	Buchanan Lake→	Sill A 126 ± 2 Ma
BASALT FLOWS IN THE ISACHSEN FORMATION	**- Paterson Isl. Member**	

(1) Embry and Osadetz, in press
(2) Avison, 1987
(3) Trettin and Parrish, 1987
(4) Jollimore, 1986

Note: Radiometric and palynological age determinations on volcanic rocks from northern Ellesmere Island suggest that Cycle IV of Embry and Osadetz (in press) consists of two distinct pulses, and that igneous rocks are no older than Campanian (G.K. Muecke, pers. comm., 1988)

is limited because of the reconnaissance nature of the dating project. The identification of several magmatic episodes, however, provides the best available working hypothesis for petrological and geochemical studies.

V. PETROLOGY AND GEOCHEMISTRY OF EXTRUSIVE ROCKS

5.1 Introduction

Geochemical studies of continental flood basalts from thick, monotonous volcanic piles are often hindered by the lack of stratigraphic control. One of the advantages of a basin setting is that it enables the time-sequence of eruptions to be known, thus providing a solid framework for petrochemical studies.

The sampling information for Early Cretaceous volcanic successions in the east-central Sverdrup Basin is summarized in Table 5.1. In the first part of this chapter, all three groups are compared using petrographic, mineralogical and geochemical data. Despite the small number of samples available for Groups 1 and 3, the data were sufficient to characterize each eruptive episode. Geochemical studies of the Group 3 basalts were particularly useful in establishing spatial-compositional differences between successions from the centre and southern margin of the basin (Fig. 3.1).

The Strand Fiord basalts (Group 2, Table 5.1) should ideally form a continuous series, or at least display a similar petrogenetic history if individual successions were once part of a single basaltic plateau (Chapter 3). In the second part of the chapter, the petrogenesis of the Group 2A and 2B basalts is examined in detail, with particular attention given to trace element and isotopic evidence for fractionation, mixing and crustal assimilation processes. As expected, the study reduces some of the uncertainty concerning the stratigraphic correlation between the Bunde Fiord and Strand Fiord successions. The discussion that follows

TABLE 5.1
SAMPLING INFORMATION FOR EXTRUSIVE ROCKS

VOLCANIC EPISODE (1)	REFERENCE	# OF SAMPLES
IV	NE Ellesmere Island	
Late Cenomanian-early Turonian	GROUP 3	4
BASALT FLOWS IN THE HASSEL FORMATION		
III	Axel Heiberg Island	
Late Albian-early Cenomanian	GROUP 2B (north)	19
	GROUP 2A (west)	32
STRAND FIORD FORMATION		
II	Ellesmere Island	
	GROUP 1C*	2
	Axel Heiberg Island	
Late Barremian-Aptian	GROUP 1B	6
BASALT FLOWS IN THE ISACHSEN FORMATION - Walker Isl. Member		
I	Axel Heiberg Island	
Valanginian-Early Barremian	GROUP 1A	5 (sills) 2 (lava flow)
BASALT FLOWS IN THE ISACHSEN FORMATION - Paterson Isl. Member		

(1) Embry and Osadetz, in press
*Lava flows in undivided Isachsen Formation, Blue Mountains.
Note: The relative stratigraphic position of Groups 1B vs. 1C and 2A vs. 2B is not known.

examines the possible causes for the increasing complexity of petrogenetic processes operating in the north-central Sverdrup Basin during the Early Cretaceous.

5.2 Characteristics of Cretaceous Volcanic Successions

5.2.1 Volcanic rocks in the Isachsen Formation (Group 1)

Petrography and Mineralogy

The following is a summary of mineralogical and textural features. More complete descriptions and a list of mineralogical data can be found in Appendices A and B.

a/ Group 1A is represented by two samples from the basal flow at Geodetic Hills (see Chapter 3). The rocks consist of sparsely plagioclase-phyric, hypocrystalline basaltic lava with an intergranular and intersertal texture. Compositions of groundmass plagioclase are in the range An_{52-58}. Both augite ($Wo_{32}En_{36}Fs_{32}$) and pigeonite ($Wo_{14}En_{45}Fs_{41}$) coexist in the groundmass. The opaque phase consists of ilmenite.

b/ The Group 1B samples consist of glomeroporphyritic basaltic lava with well-preserved intergranular to (rarely) sub-ophitic groundmass textures. Phenocryst point-counts suggest a relatively narrow range between 16 and 23 percent by volume (Appendix A). The volume of plagioclase phenocrysts decreases up section with a corresponding increase in the amount of clinopyroxene phenocrysts. Phenocrysts of calcic plagioclase are clear, seriate, partially resorbed crystals (0.25-1.75 mm) that display multiple normal zoning from core to rim.

Frequent reverse oscillatory zoning was noted in two of the samples (AX85-263, 264). Compositions range from An_{53} to An_{81}. The basal flow displays the widest range of groundmass compositions and most calcic phenocryst cores, and there is a general trend to a narrower compositional range and less calcic plagioclase with stratigraphic height. Clinopyroxene phenocrysts consist of anhedral plates of augite (~ 0.5 - max. 2mm) with minute inclusions in the core or at the periphery of crystals. Most phenocrysts are zoned and show fritted edges. Ca-rich pyroxenes predominate in all the basalts. Augite and subcalcic augite or pigeonite coexist in the groundmass of two of the samples (Appendix B).

Some of the flows at the base of the succession are sparsely olivine-phyric. The phenocrysts are anhedral clay pseudomorphs of olivine (iddingsite) that rarely exceed 1 mm in size. Altered grains of olivine are present in the groundmass of some of the flows. Fe-Ti oxides occur only in the groundmass, as interstitial lamellar to skeletal crystals or subequant grains. Compositions in two of the flows include both titanomagnetite and ilmenite. Apatite occurs in some of the basalts as an accessory phase.

b/ The Group 1C samples were collected from thin volcanic successions in the Blue Mountains area. Samples from two highly amygdaloidal flows on the eastern side of the valley are sparsely glomeroporphyritic, seriate basalts (Appendix B). In EL84-256A, phenocrysts consist of partly sericitized plagioclase with strong oscillatory zoning and clinopyroxene phenocrysts with or without inclusions in their cores. Groundmass phases include abundant plagioclase and clinopyroxene, carbonate pseudomorphs of olivine and opaque oxide grains. Calcite is

conspicuous in the angles between crystals, in vesicles and as a replacement phase of olivine grains. Samples of a massive basaltic lava flow on the opposite side of the valley (EL85-107, Appendix A) show a similar mineralogy and texture, but less alteration of the primary mineralogy.

Representative analyses of plagioclase, clinopyroxene and Fe-Ti oxides are listed in Appendix B. The range of groundmass plagioclase compositions is An_{55-62} in EL84-256A, and An_{43-54} in EL84-107. The high-Ca pyroxene in both samples is augite. Opaque oxides in EL84-256A consist exclusively of ilmenite.

Chemical Analyses

Representative whole-rock analyses of Group 1 basalts are shown on Table 5.2. All the samples consist of evolved tholeiitic basalts with SiO_2 between 49 and 53% and Mg numbers varying from 35 to 50. TiO_2 values are relatively constant in the 2-3% range, and K_2O is variable between 0.2 and 1.2 %.

The Group 1A sample shows a marked enrichment in P_2O_5, Ba and Sr. Group 1B basalts display low and variable Rb (Table 5.2 and Appendix C) and Sr contents between 200 and 300 ppm. Ni (25-50 ppm) and Cr (20-100) show maximum concentrations in flows with the highest MgO. Group 1C samples contain 3% TiO_2, higher Rb, low values of Cr and Ni, and MgO in the range 4-5%.

All the Group 1 samples can be classified as quartz-normative tholeiites (CIPW norms, Appendix C).

TABLE 5.2
REPRESENTATIVE WHOLE ROCK GEOCHEMICAL DATA
FOR GROUP 1 AND 3 BASALTS

(WT %)	GROUP 1A	GROUP 1B (N=6)	GROUP 1C	GROUP 3
SiO_2	52.98	51.10-52.37	49.64	50.52
TiO_2	3.39	2.13-2.72	3.42	3.40
Al_2O_3	13.35	13.27-14.72	13.28	12.62
FeOt	11.98	10.99-13.34	12.90	13.74
MnO	0.21	0.17-0.23	0.21	0.26
MgO	4.35	4.68-6.01	5.05	3.91
CaO	8.59	8.98-11.33	10.81	7.85
Na_2O	3.12	2.33-2.65	2.86	2.70
K_2O	0.85	0.24-0.77	0.74	1.60
P_2O5	0.65	0.22-0.30	0.36	1.16
$(H_2O_T+CO_2)$	2.50	2.20-4.08	n.d.	0.80
Mg #	43.2	42.6-53.4	45.1	37.4
(PPM)				
Rb	15	*-19	22	41
Sr	416	196-326	279	519
Ba	1208	142-276	384	1060
V	317	327-495	441	185
Cr	33	17-89	37	n.d.
Ni	32	25-47	25	14
Cu	31	106-156	44	18
Zn	138	95-119	128	135
Y	53	29-49	39	32
Zr	289	159-253	195	180
Nb	31	12-33	20	26

Representative analyses are: Group 1A, AX85-242;
Group 1C, EL85-107; Group 3, EL84-010; from Appendix C.
n.d.: not determined; *: below detection limit

5.2.2 The Strand Fiord Formation (Group 2)

Petrography and Mineralogy

Group 2A

Hand samples from the Strand Fiord Formation in the type area are generally aphyric, very fine-grained basaltic lavas. Microscopic examination reveals that approximately 20 % of the samples are sparsely to highly microphyric, and that 40 % are hypocrystalline basalts (see Fig. A.3). The most abundant type of phenocryst is plagioclase, with a size range of 0.4 to 1 mm. Normal and reverse oscillatory zoning, minor resorption and melt inclusions are only present in unusually large crystals (e.g. AX83-067, Twisted Ridge). Augite is associated with plagioclase and typically consists of smaller anhedral plates (0.3-0.6 mm) with sector zoning and opaque inclusions in the cores of crystals. Oikocrysts of augite hosting plagioclase laths are also present (Plate 21). Pseudomorphs of olivine are rare and occur as microphenocrysts in three of the samples.

The groundmass consists of intergranular, often intersertal aggregates of plagioclase, clinopyroxene, altered grains of olivine, opaque oxides and altered volcanic glass. The centre of thick, ponded flows contains up to 40% devitrified glass, as also reported for Columbia River Basalts by Long and Wood (1986).

Representative groundmass plagioclase analyses are listed in Table 5.3. Compositions range from An_{42} to An_{64} and are more albitic in two of the samples (An_{15-34}). In all the samples examined, the Ca-rich pyroxene is augite. Unlike microphenocryst compositions, groundmass clinopyroxenes in several flows at Bastion Ridge show wide variations in

PLATE 21

Textural characteristics of clinopyroxene oikocrysts in Group 2 basalts with varying degrees of crystallinity. No systematic differences in mineral compositions were observed between clear pyroxene phenocrysts and oikocrysts in these lavas. Clockwise from top left: AX83-063 Group 2A at Twisted Ridge; AX83-023, Group 2A at Bastion Ridge; AX85-075 and AX85-081, Group 2B at Artharber Creek.
Scale is 1 mm. PPL.

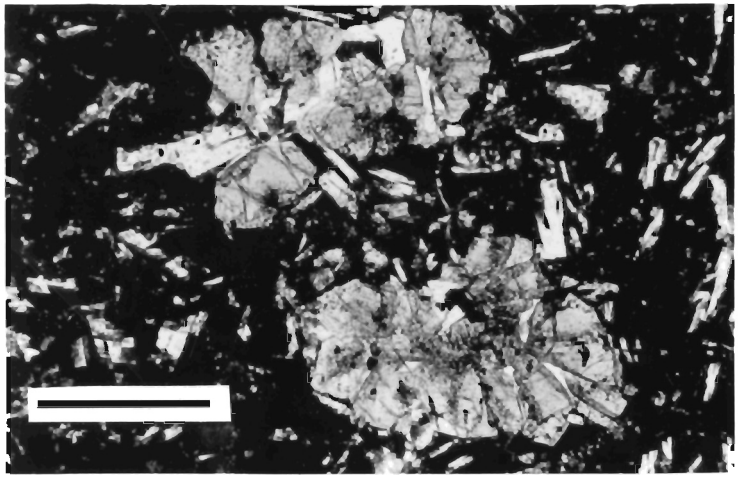

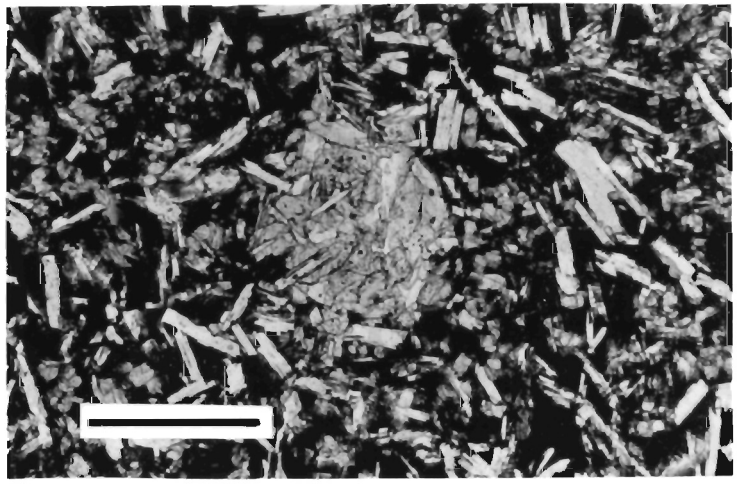

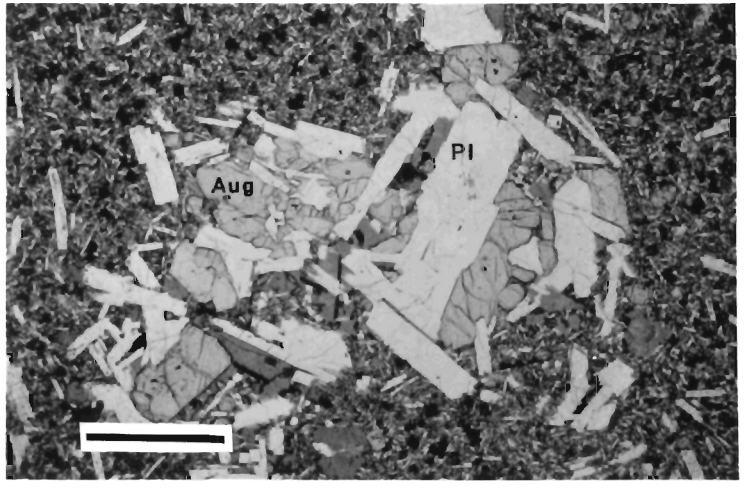

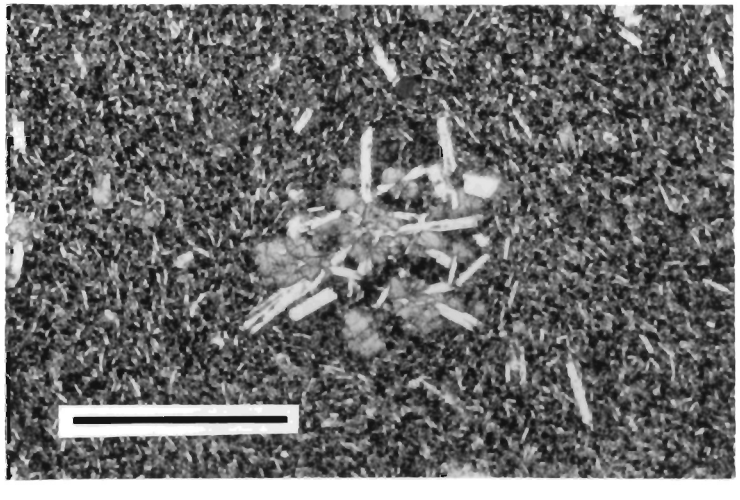

PLATE 21

TABLE 5.3
REPRESENTATIVE MINERAL ANALYSES*, GROUP 2A

PLAGIOCLASE

	AX83-032A	AX83-011B	
	G	G	G
SiO_2	52.78	55.39	52.56
Al_2O_3	29.65	26.09	28.17
CaO	13.02	10.50	13.08
Na_2O	4.47	5.76	4.46
K_2O	0.34	0.46	0.33
Total	100.26	98.20	98.60
Mol per cent			
An	61	49	61
Ab	38	49	37
Or	1	2	2

	AX83-056A	AX83-060		
	G	G1	G2	G3
SiO_2	57.18	52.03	55.71	52.21
Al_2O_3	25.42	28.95	26.89	29.61
CaO	9.12	13.62	10.60	13.64
Na_2O	6.45	4.12	5.85	4.14
K_2O	0.60	0.26	0.55	0.27
Total	98.77	98.98	99.60	99.87
Mol per cent				
An	42	64	49	64
Ab	54	35	48	35
Or	4	1	3	1

* Representative analyses of single grains except in the case of AX83-032A groundmass pyroxene, next page (average of 7 analyses).
Symbols: G, groundmass (analyses are numbered to illustrate variations in mineral chemistry); P_C, core; P_R, rim of phenocryst; MP microphenocryst.
Next page: FeO*, total iron as FeO.

TABLE 5.3 (continued)

PYROXENE

	AX83-032A		AX83-011B	
	G	MP_C	MP_R	G
SiO_2	51.70	50.36	52.13	51.66
TiO_2	0.78	1.11	0.83	0.98
Al_2O_3	1.71	4.91	1.75	1.80
Cr_2O_3	0.00	0.00	0.24	0.12
FeO*	11.16	8.75	10.58	11.63
MnO	0.12	0.00	0.08	0.16
MgO	15.01	15.47	15.33	14.42
CaO	19.37	19.59	20.22	19.92
Na_2O	0.07	0.00	0.00	0.00
Total	99.92	100.19	101.16	100.69
Si	1.933	1.859	1.922	1.927
Ti	0.022	0.031	0.023	0.027
Al^{IV}	0.067	0.141	0.077	0.073
Al^{VI}	0.008	0.073	0.000	0.007
Cr	0.000	0.000	0.007	0.004
Fe	0.348	0.271	0.326	0.363
Mn	0.004	0.000	0.002	0.005
Mg	0.836	0.851	0.843	0.802
Ca	0.776	0.775	0.799	0.796
Na	0.005	0.000	0.000	0.000
X atoms	0.781	0.775	0.799	0.796
Y atoms	1.218	1.226	1.201	1.207
Z atoms	2.000	2.000	2.000	2.000

TABLE 5.3 (continued)

PYROXENE

	AX83-056A				AX83-060	
	MP_C	MP_R	G1	G2	G1	G2
SiO_2	52.41	52.62	51.46	53.29	50.19	53.95
TiO_2	0.82	0.77	1.32	0.49	1.13	0.09
Al_2O_3	3.02	1.42	1.72	1.46	2.41	4.08
Cr_2O_3	0.17	0.00	0.00	0.00	0.02	0.04
FeO*	8.30	10.99	15.51	10.46	12.27	9.69
MnO	0.11	0.17	0.29	0.13	0.39	0.32
MgO	16.51	16.13	13.86	16.63	13.63	30.60
CaO	19.23	17.93	16.43	17.99	18.86	0.27
Na_2O	0.00	0.16	0.18	0.11	0.33	0.05
Total	100.57	100.19	100.77	100.56	99.23	99.09
Si	1.924	1.953	1.936	1.964	1.900	1.906
Ti	0.023	0.021	0.037	0.014	0.032	0.002
Al^{IV}	0.076	0.047	0.064	0.036	0.100	0.094
Al^{VI}	0.054	0.015	0.012	0.028	0.008	0.076
Cr	0.005	0.000	0.000	0.000	0.001	0.001
Fe	0.255	0.342	0.488	0.322	0.389	0.286
Mn	0.003	0.005	0.009	0.004	0.013	0.010
Mg	0.903	0.892	0.777	0.914	0.769	1.611
Ca	0.756	0.713	0.662	0.710	0.765	0.010
Na	0.000	0.012	0.013	0.008	0.024	0.003
X	0.756	0.725	0.675	0.718	0.789	0.013
Y	1.243	1.275	1.323	1.282	1.212	1.984
Z	2.000	2.000	2.000	2.000	2.000	2.000

Fe and Mg contents (Fig. 5.1 a). Disequilibrium crystallization as a result of variable cooling rates in some of the lava flows is a possible cause for the variations observed (e.g. Coish and Taylor, 1979). No systematic differences in composition were found between augite microphenocrysts and oikocrysts in the same sample.

Most of the opaque oxides in these basalts are too fine-grained for analysis. This problem is compounded in glass-rich lavas where individual grains cannot be distinguished. A rapid scan of compositions in several holocrystalline samples suggests that the opaque phase is titanomagnetite.

Group 2B

The uppermost flows in the Celluloid Creek succession are holocrystalline basaltic lavas with varying amounts of plagioclase, augite and olivine phenocrysts (Table 5.4). The total amount of phenocrysts in individual flow units varies between 5 and 14 percent and is observed to decrease to 0-2 percent in the top flows. The most abundant phenocrysts consist of euhedral plagioclase crystals with strong normal zoning, while clinopyroxene and olivine usually occur in amounts less than 1%. Augite crystals are either uniform, platy crystals with inclusions in the cores or oikocrysts hosting randomly-oriented plagioclase laths (Plate 21). Olivine phenocrysts are iddingsitized (or partly carbonatized), and in rare cases show a euhedral morphology and some relict cores. The texture is commonly glomeroporphyritic and seriate.

The groundmass mineralogy in all the flows consists of the assemblage plagioclase, olivine, clinopyroxene and Fe-Ti oxides. Minor glass altered to clays occurs in some of the basalts.

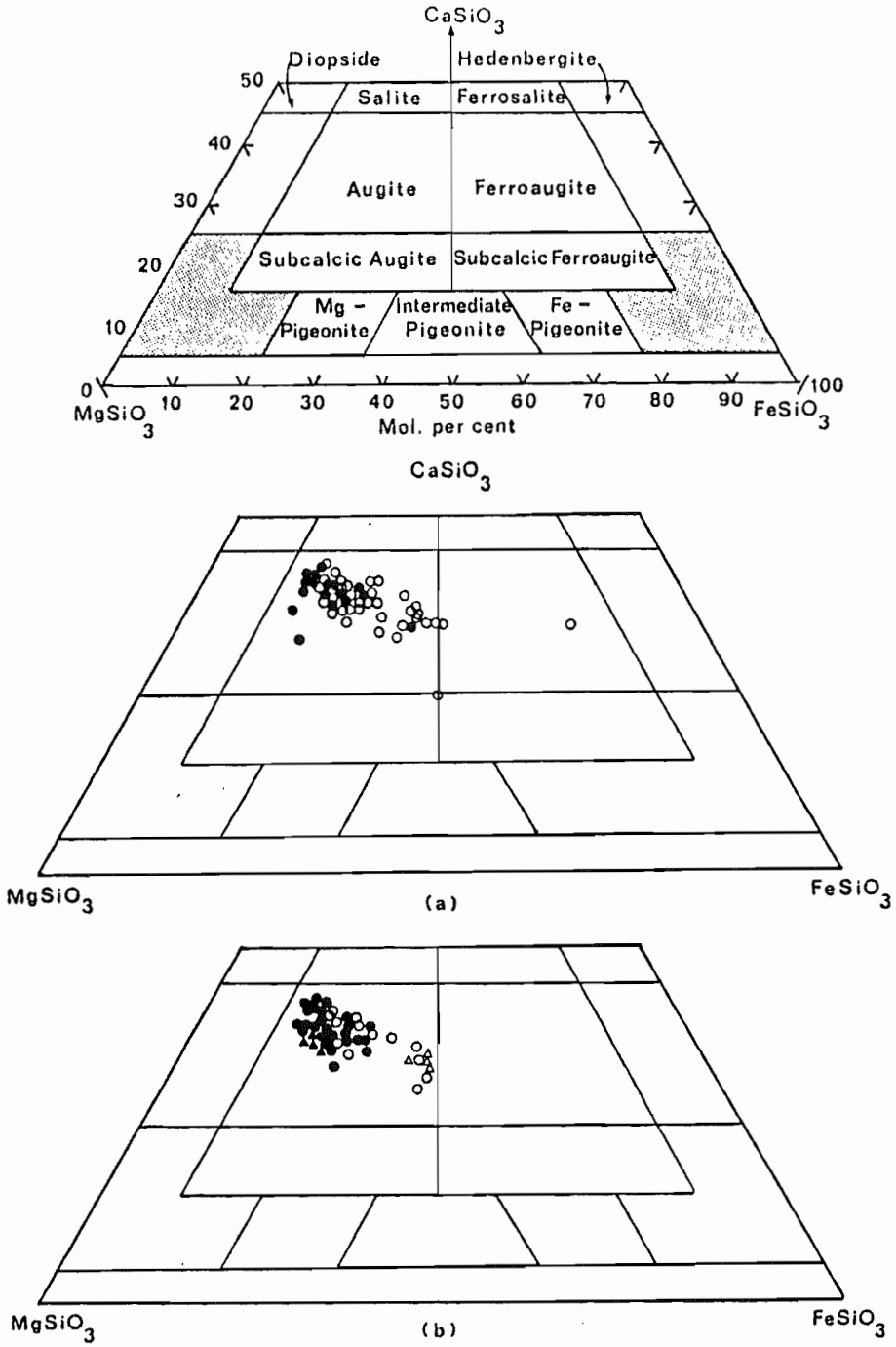

Figure 5.1 The pyroxene quadrilateral, illustrating the range of compositions in selected Group 2 basalts.
(a) Group 2A basalts at Bastion Ridge. Microphenocryst, filled circle; Groundmass, open circle.
(b) Group 2B basalts at Celluloid Creek and Artharber Creek. Phenocryst, filled circle; Groundmass, open circle. Triangles are compositions of cores and rims of phenocrysts in sample BND83-017.

TABLE 5.4
TYPE AND PROPORTIONS OF PHENOCRYSTS IN GROUP 2B LAVAS

SAMPLE#	PLAG	AUG	OLIV	TI-MAG	TOTAL
		CELLULOID CREEK			
BND83-017	60.4	32.4	7.2	-	13.9%
BND83-016	75.5	16.3	8.2	-	4.9%
BND83-015	91.6	4.8	3.6	-	8.3%
BND83-012	65.9	21.3	12.8	-	9.4%
BND83-009	84.5	-	8.7	6.8	10.3%
		ARTHARBER CREEK			
AX85-075	57.1	36.5	6.4	-	6.3%
AX85-078	43.2	43.2	13.6	-	8.8%
AX85-080	65.4	24.7	9.9	-	10.1%
AX85-082	63.5	29.7	6.8	-	7.4%
AX85-086(1)	86.5	10.4	3.1	-	19.3%
AX85-087	66.7	23.6	9.7	-	7.2%
AX85-091	87.2	12.8	-	-	14.9%
AX85-094	86.3	12.0	1.7	-	11.7%
AX85-095	43.7	32.8	23.5	-	6.4%

(1) Also contains sparse, resorbed oxyhornblende phenocrysts.

Volcanic rocks in the Artharber Creek succession are holocrystalline basaltic lavas characterized by ubiquitous euhedral plagioclase phenocrysts which are also found in the associated pyroclastic deposits (Table 5.4). The proportion of phenocrysts increases in the central portion of the volcanic sequence. The uppermost lava flows are sparsely phyric or aphyric (Fig. 5.2).

Plagioclase phenocrysts occur in a wide range of sizes (0.5-3 mm) and form monomineralic (more rarely polymineralic) clusters, giving the basalts a glomeroporphyritic, often seriate texture (Plate 23). The largest plagioclase crystals show disequilibrium textures, such as partial resorption, melt inclusions and complex reverse oscillatory zoning (Plates 24, 25). Plagioclase microphenocrysts are euhedral and may show simple normal or reverse zoning. Augites usually occur as microphenocrysts (seriate to 1mm) of three types: anhedral plates with minute, opaque inclusions, oikocrysts such as described for the Celluloid Creek basalts, and rare, clear and unzoned crystals of larger size (e.g. AX85-096). Iddingsite pseudomorphs of olivine phenocrysts are rare (1%).

The groundmass in most of the flows consists of a holocrystalline, intergranular aggregate of abundant plagioclase and clinopyroxene, rare altered olivines and opaque oxides. Many show a microcrystalline or cryptocrystalline texture. Three of the flows are hypocrystalline (less than 5% devitrified glass).

Representative compositions of plagioclase, clinopyroxene and Fe-Ti oxides in the Group 2B samples are shown in Table 5.5. The range of compositions in Celluloid Creek basalts is An_{50}-An_{66} for groundmass plagioclase (three samples). A larger data base for Artharber Creek

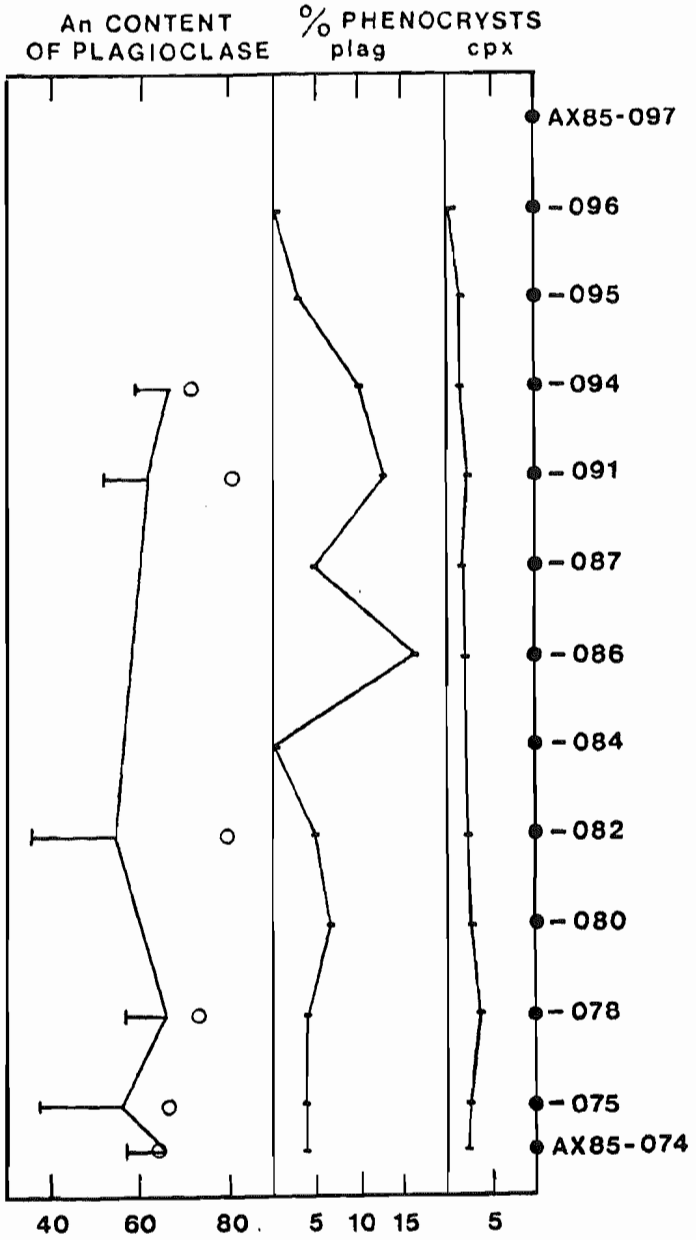

Figure 5.2 Relative proportions of plagioclase and clinopyroxene phenocrysts in Group 2B basalts at Artharber Creek. The An content of plagioclase in selected samples is shown as (bar) minimum and maximum in groundmass plagioclase and (circle) maximum in cores of plagioclase phenocrysts.

PLATE 22

Partially preserved olivine phenocrysts (arrowed) in glomeroporphyritic texture with plagioclase (Pl) and augite (Aug). The groundmass shows an intergranular, holocrystalline texture. BND83-009, Group 2B at Celluloid Creek.
Scale is 1 mm. PPL.

PLATE 23

Glomeroporphyritic texture typical of Group 2B lavas at Artharber Creek. The groundmass in these lavas is often microcrystalline. Note the alignment of inclusions along compositional zones (plagioclase crystal at bottom, centre) or cleavages (centre, left). Relict oxyhornblende phenocryst is arrowed (AX85-086).
Scale is 1 mm. PPL.

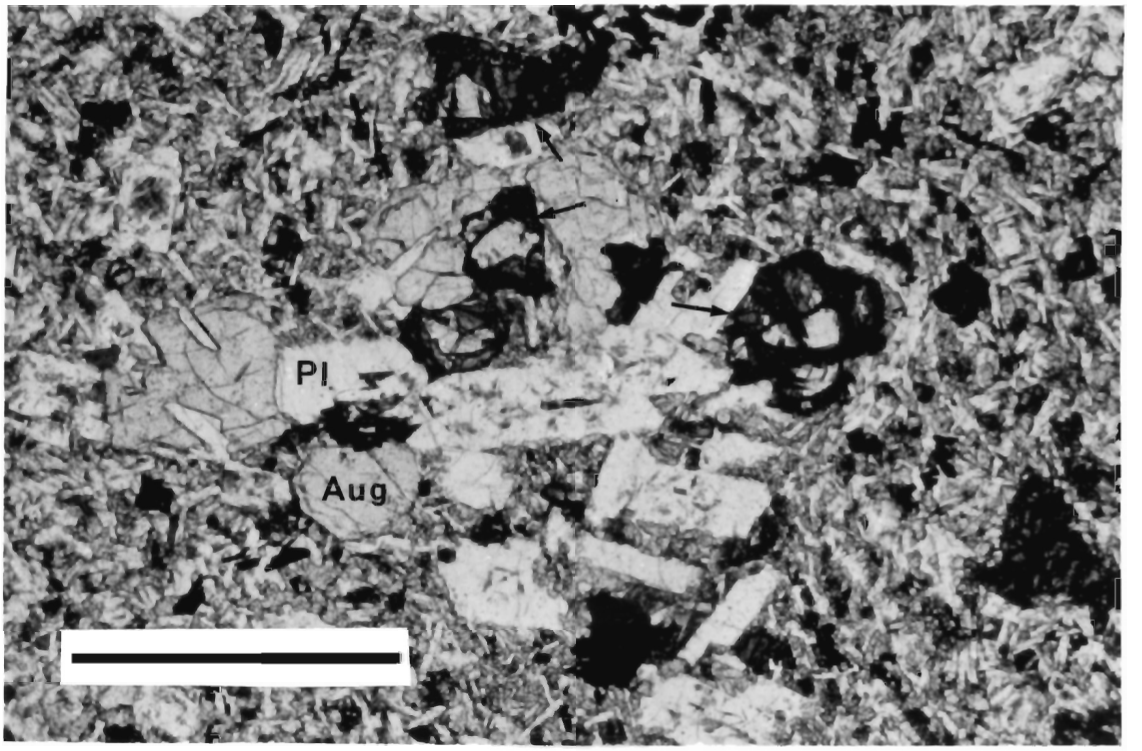

PLATE 22

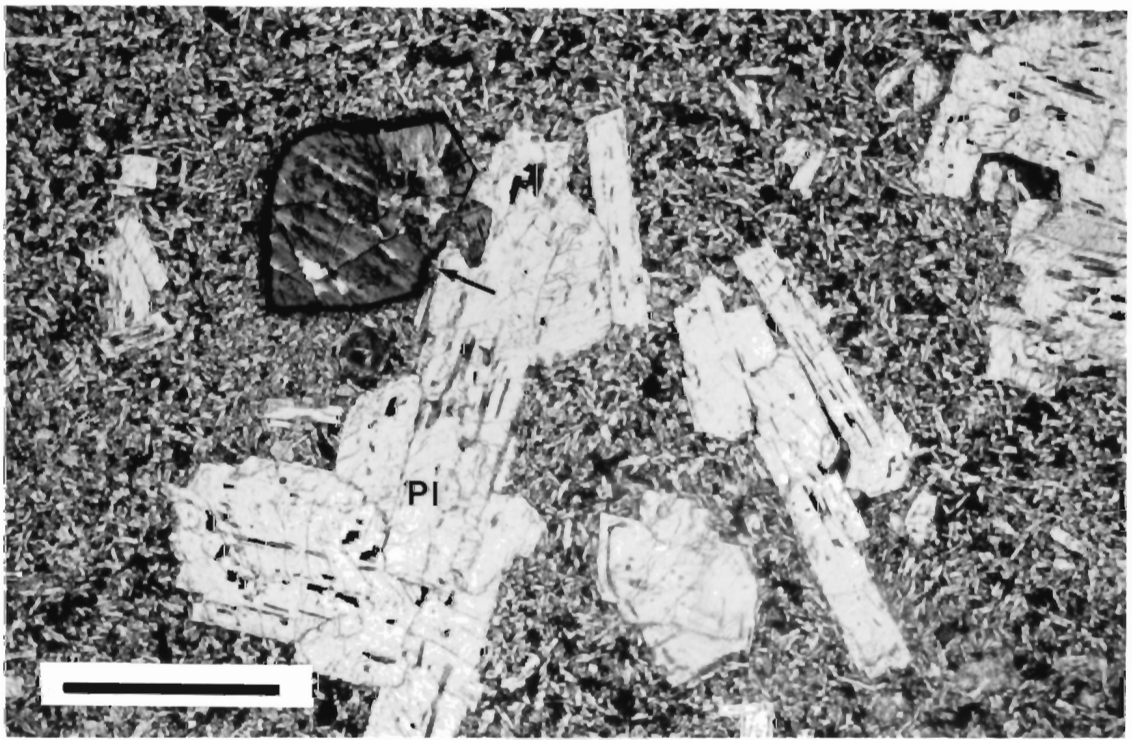

PLATE 23

PLATE 24

Poikilitic texture in a single, large plagioclase phenocryst. Minute inclusions consist of pyroxene and trapped melt. AX85-074 (basal flow), Group 2B at Artharber Creek.
Scale is 1 mm. XPL.

PLATE 25

Hypocrystalline basalt showing prominent melt inclusions in a partially resorbed, complexly zoned phenocryst. This type of texture, typical of Group 2B basalts at Artharber Creek, is regarded as evidence for compositional disequilibrium during magma mixing. AX85-077, Group 2B at Artharber Creek.
Scale is 1 mm. XPL.

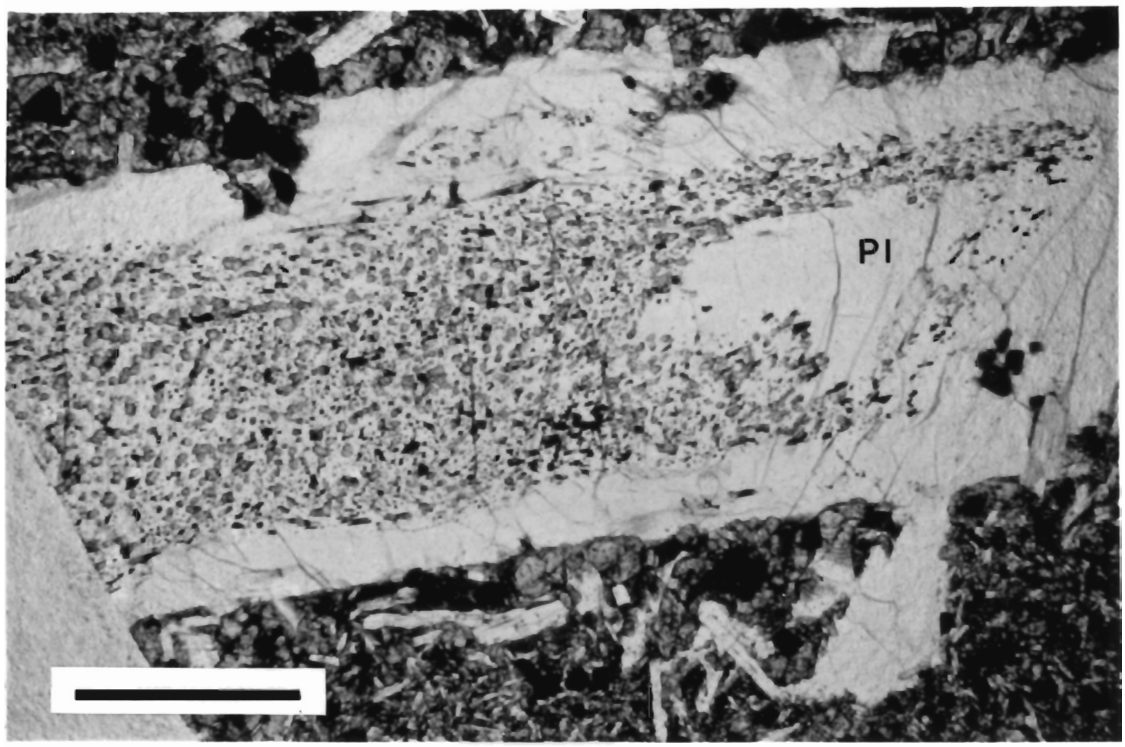

PLATE 24

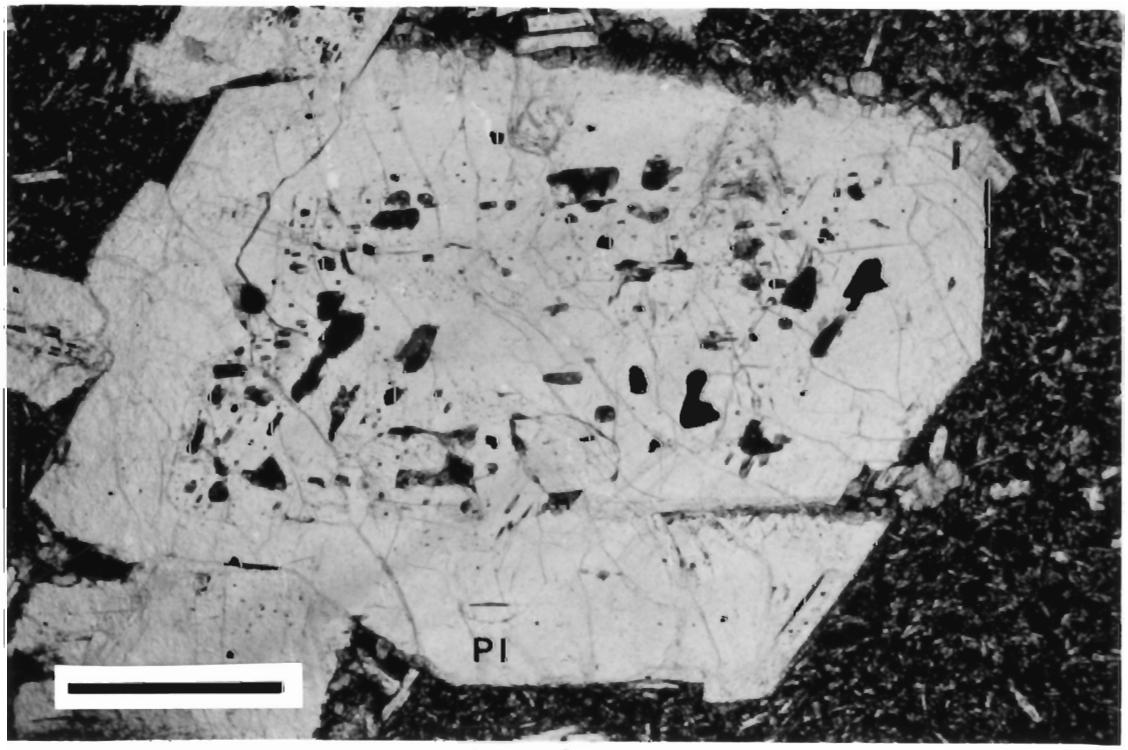

PLATE 25

TABLE 5.5
REPRESENTATIVE MINERAL ANALYSES*, GROUP 2B

PLAGIOCLASE

	BND83-012			BND83-016		AX85-075	
	G	P_C	P_R	G	P_C	P_R
SiO_2	53.92	47.64	49.98	51.84	50.87	54.96
Al_2O_3	28.35	32.21	30.20	29.25	30.70	27.50
CaO	12.06	16.76	15.10	13.40	14.56	10.93
Na_2O	5.23	1.74	3.11	4.19	4.01	5.42
K_2O	0.37	0.12	0.22	0.26	0.22	0.45
Total	99.56	98.47	98.61	98.94	100.36	99.26
Mol per cent						
An	55	84	72	63	66	51
Ab	43	16	27	36	33	46
Or	2	0.01	1	1	1	3

	AX85-091		
	P_C	P_R	G
SiO_2	49.34	51.47	52.24
Al_2O_3	31.92	30.33	29.14
CaO	16.44	14.76	13.26
Na_2O	2.30	3.03	4.28
K_2O	0.02	0.13	0.40
Total	100.02	99.72	99.32
An	80	72	60
Ab	20	27	37
Or	(1)	1	3

* Representative analyses of single grains.
Symbols: G groundmass; P_C, core; P_R, rim of phenocryst; MP microphenocryst; G^M magnetite; G^I ilmenite; FeO* total iron as FeO.
(1) Less than 0.1

TABLE 5.5 (continued)

PYROXENE

	BND83-012			BND83-016		
	MP_C	MP_R	G	P_C	P_R	G
SiO_2	51.86	51.77	51.25	52.07	51.60	50.71
TiO_2	1.06	1.20	0.96	0.61	0.61	0.83
Al_2O_3	3.33	1.68	1.50	2.46	1.44	1.37
Cr_2O_3	n.d.	n.d.	n.d.	0.09	0.00	0.00
FeO*	11.66	13.34	13.79	9.46	12.45	18.85
MnO	0.17	0.31	0.38	0.09	0.14	0.21
MgO	15.88	14.42	13.08	16.29	15.06	12.06
CaO	17.12	18.11	18.86	19.26	17.83	16.03
Na_2O	0.00	0.00	0.42	0.00	0.00	0.00
Total	101.08	100.83	100.24	100.33	99.13	100.06
Si	1.912	1.936	1.930	1.924	1.950	1.948
Ti	0.029	0.034	0.027	0.017	0.017	0.024
Al^{IV}	0.088	0.064	0.068	0.076	0.050	0.052
Al^{VI}	0.057	0.010	0.000	0.031	0.014	0.010
Fe	0.360	0.417	0.435	0.292	0.394	0.606
Mn	0.005	0.010	0.012	0.003	0.004	0.007
Mg	0.873	0.804	0.735	0.897	0.848	0.691
Ca	0.676	0.726	0.762	0.762	0.722	0.660
Na	0.000	0.000	0.031	0.000	0.000	0.000
X atoms	0.676	0.726	0.793	0.762	0.722	0.660
Y atoms	1.324	1.275	1.209	1.242	1.278	1.337
Z atoms	2.000	2.000	1.998	2.000	2.000	2.000

FE-TI OXIDES

	BND83-016		BND83-017	AX85-082	
	G^M	G^I	G^M	G^M	G^I
TiO_2	26.84	46.61	27.61	27.50	51.93
Al_2O_3	1.85	0.11	1.89	1.44	0.09
FeO*	59.89	46.15	61.84	65.89	45.80
MnO	0.76	0.42	1.08	1.02	0.49
MgO	0.41	1.19	0.23	0.04	1.26
Mol per cent					
mt	88.39		89.14	84.68	
usp	11.61		10.86	15.32	

basalts indicates compositions ranging from An_{49} to An_{67}. Two of the flows contain andesine (An_{36-38}). Cores of plagioclase phenocrysts are usually more calcic (An_{70-80}) and this is characteristic in the central part of the succession (Fig. 5.2).

The high-Ca pyroxene in basalts from both successions is augite. Strong zoning of augite phenocrysts to more Fe-rich rims is observed in one sample from the Celluloid Creek succession (Fig. 5.1 b). Fe-Ti oxides are titanomagnetite and, more rarely, ilmenite.

Some particulars concerning olivines are worth noting. Crystalline portions of olivine phenocrysts were found in only one lava flow (BND83-009, Celluloid Creek: Fo_{56}). The crystals are subhedral and occur in clusters with plagioclase and augite (Plate 22). In the Artharber Creek basalts, many olivine phenocrysts are closely associated with plagioclase, and augite to a lesser extent, forming relict cores overgrown by these phases (Plates 26, 27). Strong zoning of olivine microphenocrysts is preserved despite alteration in a flow near the top of the succession (AX85-096, Appendix A).

Chemical Analyses

Thirty-two whole-rock geochemical analyses were obtained for the Group 2A samples, from four successions in the Strand Fiord type area (Chapter 3). Most samples belong to the Bastion Ridge and Twisted Ridge sections. The range, means and standard deviations for major elements and selected trace elements are shown in Table 5.6. Data for the rare earths and HFS elements in the Twisted Ridge basalts are listed in Table 5.7.

This group is characterized by highly uniform chemical compositions, as shown by the low standard deviations for major and

PLATE 26

Seriate basalt displaying relict olivine enclosed in augite phenocryst, suggesting the sequence of crystallization oliv-clinopyroxene-plagioclase. Most of the Group 2 basalts show evidence of cotectic crystallization at low pressure regimes. Note the pattern of inclusions at the periphery of the augite plate. AX85-082, Group 2B at Artharber Creek.
Scale is 0.5 mm. PPL.

PLATE 27

Glomeroporphyritic, microcrystalline basalt showing relict cores of olivine in plagioclase phenocryts. Many of the basalts at Artharber Creek display olivine-plagioclase phenocryst assemblages, with only minor amounts of clinopyroxene. AX85-085, Group 2B at Artharber Creek.
Scale is 1 mm. XPL.

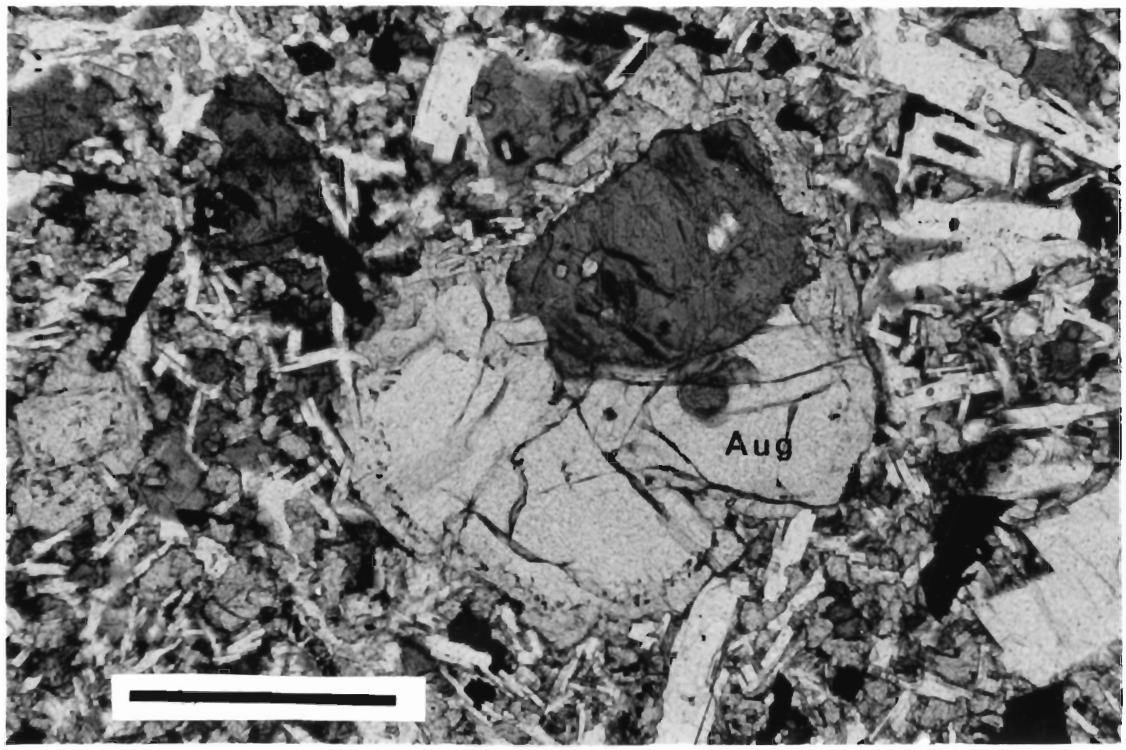

PLATE 26

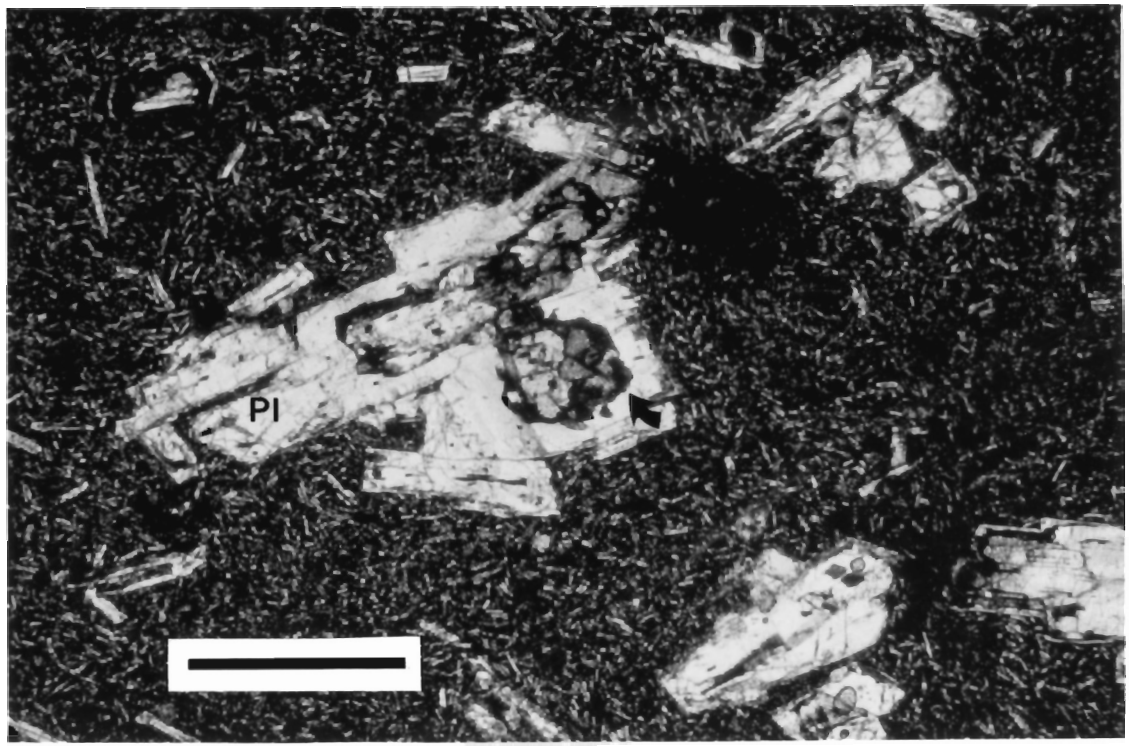

PLATE 27

TABLE 5.6 (a)
RANGE, MEANS AND STANDARD DEVIATIONS FOR
MAJOR AND TRACE ELEMENTS: GROUP 2A

TWISTED RIDGE SECTION (N=13)

(WT%)	RANGE	MEAN	S.D.
SiO_2	48.74-52.33	50.86	1.10
TiO_2	1.97-3.44	2.65	0.52
Al_2O_3	12.99-14.83	13.87	0.58
FeOt	12.52-16.11	13.98	1.26
MnO *			
MgO	3.95-5.45	4.64	0.53
CaO	8.45-10.35	9.20	0.64
Na_2O	2.80-3.79	3.34	0.29
K_2O	0.36-1.04	0.65	0.22
P_2O_5	0.20-0.42	0.29	0.07
$(H_2O_T+CO_2)$	1.68-4.28	2.32	0.68
Mg#	33.9-47.2	41.0	4.7
(PPM)			
Rb	18-60	31	11
Sr	186-253	236	17
Ba	167-365	230	52
V	305-420	339	38
Cr	15-49	28	10
Ni	18-41	31	7
Cu	23-130	67	32
Zn	83-157	124	21
Y	33-51	39	5
Zr	149-272	192	35
Nb	13-27	19	4

* See the section on analytical precision, Appendix C

TABLE 5.6 (b)
RANGE, MEANS AND STANDARD DEVIATIONS FOR
MAJOR AND TRACE ELEMENTS: GROUP 2A

BASTION RIDGE SECTION (N=15)

(WT%)	RANGE	MEAN	S.D.
SiO_2	49.67-52.63	51.24	1.56
TiO_2	1.96-2.90	2.16	0.30
Al_2O_3	12.98-14.72	14.07	0.46
FeOt	10.37-16.44	12.96	1.38
MnO *			
MgO	4.37-5.69	5.13	0.35
CaO	8.39-10.88	10.09	0.76
Na_2O	2.62-4.20	3.09	0.36
K_2O	0.40-1.13	0.64	0.22
P_2O_5	0.23-0.32	0.25	0.02
$(H_2O_T+CO_2)$	1.33-2.41	1.82	0.33
Mg#	35.8-49.7	45.5	3.8
(PPM)			
Rb	10-39	24	8
Sr	229-355	252	30
Ba	162-456	230	65
V	316-472	343	40
Cr	25-64	43	15
Ni	23-51	43	9
Cu	29-110	74	19
Zn	111-142	118	10
Y	36-47	39	3
Zr	171-208	186	10
Nb	14-19	16	2

* See section on analytical precision, Appendix C.

TABLE 5.7
ADDITIONAL TRACE ELEMENT DATA FOR GROUP 2A BASALTS
AT TWISTED RIDGE

	1	2	3	4	5	6	7	8
Sc	42.8	39.3	32.8	34.5	31.9	31.7	33.6	33.0
Hf	4.5	4.1	7.1	5.6	4.9	4.9	6.2	6.2
Ta	1.6	1.7	3.2	2.3	1.5	2.5	2.6	2.8
Th	3.9	3.6	6.4	3.9	4.2	3.9	3.7	3.8
La	16.4	17.3	30.4	22.3	21.1	19.8	21.7	21.6
Ce	38	40	66	48	48	42	48	48
Sm	6.1	5.7	9.3	7.6	6.6	6.6	8.1	8.0
Eu	1.77	1.68	2.33	2.19	1.92	2.01	2.46	2.43
Tb	1.10	1.00	1.30	1.60	1.30	0.95	1.50	1.60
Yb	3.60	3.30	4.50	3.60	3.50	3.80	4.30	4.50
Lu	0.53	0.48	0.66	0.54	0.51	0.51	0.66	0.67
SUM*	67.5	69.5	115.0	85.8	83.0	75.7	86.7	86.8
Ce/Yb_N	2.7	3.1	3.7	3.4	3.5	2.8	2.8	2.7

	9	10	11	12	13
Sc	31.1	36.9	n.d.	33.5	33.9
Hf	5.8	4.4	4.3	5.1	5.0
Ta	4.1	1.2	1.5	1.8	1.9
Th	3.8	2.8	2.4	3.6	3.8
La	20.6	15.4	14.6	19.3	19.1
Ce	44	34	32	41	40
Sm	7.1	6.0	5.7	6.4	6.5
Eu	2.19	1.95	1.73	1.90	1.90
Tb	1.20	0.82	1.10	1.10	1.60
Yb	4.10	3.60	3.00	3.70	3.30
Lu	0.53	0.47	0.47	0.50	0.52
SUM*	79.7	62.2	58.6	73.9	72.9
Ce/Yb_N	2.7	2.4	2.7	2.8	3.1

KEY

1: AX83-056A
2: AX83-057
3: AX83-058
4: AX83-059
5: AX83-060
6: AX83-062
7: AX83-063
8: AX83-064
9: AX83-065
10: AX83-066
11: AX83-067
12: AX83-068
13: AX83-070
*: of rare earths

trace elements. All the basalts are tholeiites with 1 to 2 % normative quartz (CIPW norm, Appendix C).

Nineteen whole-rock geochemical analyses were obtained for the Group 2B samples. The data for major elements and sixteen trace elements are listed in Appendix C. The range, means and standard deviations for major elements and selected trace elements are shown in Table 5.8. Additional trace elements and rare earth data for the Celluloid Creek basalts are listed in Table 5.9.

The major elements show a similar range in both the Celluloid Creek and Artharber Creek successions. Most of the samples consist of highly evolved basaltic lava with SiO_2 between 49-54% and low Mg numbers (37-60). TiO_2 varies from 1.5 to 3.6% and the range of K_2O values is 0.35-1.9%. According to the normative classification of Yoder and Tilley (1962), most samples consist of slightly oversaturated tholeiitic basalts (Appendix C).

The trace element data (Table 5.8) show wide variations in the contents of Rb and Ba, and rather uniform contents of Sr (200 ppm). The range of Ni values is similar in both successions but a wider variation in Cr contents is observed in the Artharber Creek basalts. High field strength elements such as Y, Zr and Nb show similar ranges, with the largest variations occurring in the Celluloid Creek basalts.

5.2.3 Volcanic Rocks in the Hassel Formation (Group 3)

The Group 3 samples (Table 5.1) were collected from cuestas and mesas in the Piper Pass and Lake Hazen areas. All the samples consist of aphyric basaltic lava with a remarkably uniform mineralogy and

TABLE 5.8 (a)
RANGE, MEANS AND STANDARD DEVIATIONS FOR
MAJOR AND TRACE ELEMENTS: GROUP 2B

CELLULOID CREEK SECTION (N=8)

(WT%)	RANGE		MEAN	S.D.
SiO_2	49.37-52.18		50.81	1.11
TiO_2	1.53-3.67		2.38	0.68
Al_2O_3	12.89-14.89		13.88	0.69
FeOt	11.15-16.33		13.35	1.57
MnO *				
MgO	4.01-5.81		5.12	0.68
CaO	8.11-10.95		9.78	1.05
Na_2O	2.21-3.13		2.74	0.30
K_2O	0.35-1.56		0.71	0.40
P_2O_5	0.19-0.41	(N=7)	0.26	0.07
$(H_2O_T+CO_2)$	1.24-3.44		2.10	0.73
Mg#	37.3-51.4		44.5	4.9
(PPM)				
Rb	7-51		22	13
Sr	171-246		206	26
Ba	131-290		181	56
V	295-509		382	66
Cr	11-87		54	26
Ni	24-60		48	12
Cu	48-213		136	66
Zn	88-153		115	19
Y	32-60		42	8
Zr	127-275		174	47
Nb	9-25		15	5

* See the section on analytical precision, Appendix C

TABLE 5.8 (b)
RANGE, MEANS AND STANDARD DEVIATIONS FOR
MAJOR AND TRACE ELEMENTS: GROUP 2B

ARTHARBER CREEK SECTION (N=11)

(WT%)	RANGE	MEAN	S.D.
SiO_2	49.46-53.84	51.83	1.15
TiO_2	1.35-2.86	2.11	0.44
Al_2O_3	12.47-15.28	13.86	0.78
FeOt	9.88-14.19	11.87	1.30
MnO	0.16-0.30	0.20	0.04
MgO	4.17-7.21	5.22	0.77
CaO	7.56-11.47	9.56	0.99
Na_2O	2.19-2.92	2.58	0.23
K_2O	0.50-1.86	0.92	0.41
P_2O_5	0.15-0.30	0.24	0.05
$(H_2O_T+CO_2)$	1.13-3.08	1.98	0.55
Mg#	41.4-60.5	47.9	5.5
(PPM)			
Rb	2-77	30	21
Sr	183-236	211	16
Ba	133-290	197	40
V	234-413	313	51
Cr	2-162	41	43
Ni	24-50	30	8
Cu	69-277	122	64
Zn	78-138	101	15
Y	27-48	38	6
Zr	133-212	167	31
Nb	10-21	15	3

TABLE 5.9
ADDITIONAL TRACE ELEMENT DATA FOR GROUP 2B LAVAS
AT CELLULOID CREEK

	1	2	3	4	5	6	7	8
Sc	49.1	47.1	39.1	37.7	33.0	41.5	41.0	44.0
Hf	4.4	4.2	7.5	4.4	5.8	4.2	3.5	3.3
Ta	1.7	1.4	1.9	1.1	2.1	1.4	1.4	1.0
Th	2.0	1.9	4.0	2.6	5.1	3.1	3.6	2.1
La	13.0	11.9	22.6	15.3	23.8	14.6	13.7	11.4
Ce	30	31	55	36	50	32	29	25
Sm	6.1	5.5	8.6	5.8	7.6	5.5	4.9	4.4
Eu	1.86	1.69	2.57	1.79	2.05	1.66	1.44	1.40
Tb	1.00	1.20	1.90	0.98	1.40	n.d.	1.00	n.d.
Yb	3.80	3.70	5.00	3.50	3.30	3.70	2.90	3.80
Lu	0.55	0.57	0.81	0.55	0.56	0.48	0.39	0.53
SUM*	56.0	56.0	97.0	64.0	89.0	58.0	53.0	46.0
Ce/Yb_N	2.0	2.1	2.8	2.6	3.9	2.2	2.6	1.7

KEY

1: BND83-005
2: BND83-006
3: BND83-007
4: BND83-009
5: BND83-012
6: BND83-015
7: BND83-016
8: BND83-017
*: of rare earths

intergranular (Lake Hazen) or intersertal (Piper Pass) textures. Groundmass phases include plagioclase, clinopyroxene, olivine and opaque oxides. Euhedral apatite crystals (0.1 mm) form a characteristic accessory phase. Plagioclase compositions range from An_{43} to An_{53}. Pyroxenes are generally augitic, with a trend to Fe-rich compositions. Fe-rich groundmass olivines range in composition from Fo_{28} to Fo_{37}. Opaque oxides consist of coexisting titanomagnetite and ilmenite (Appendix B).

A representative chemical analysis is shown on Table 5.2. Group 3 basalts typically show higher TiO_2, K_2O and P_2O_5 than basaltic lavas from older successions, and low Mg numbers. Rb, Sr and Ba contents are higher than in all other samples analysed, with the exception of the Group 1A basalts. The whole-rock compositions of the four samples analysed (Appendix C) are similar to those reported by Osadetz and Moore (in press). Though definitely of tholeiitic affinity, these rocks are better described as ferrobasalts, in the manner adopted by Leeman et al. (1976) for Crater of the Moon Lavas, western U.S.A.

5.3 Comparison of Early Cretaceous Volcanic Successions

5.3.1 Alteration Effects

Petrographic observations indicate that all the samples of basaltic lava are altered to some degree (Appendix A). Volcanic glass and olivines are partially or completely replaced by clay minerals. Plagioclase feldspars and clinopyroxenes usually display incipient alteration in the form of sericitization or replacement by oxides.

Secondary alteration could be caused by a combination of post-emplacement weathering and interaction with groundwaters. The resulting compositional changes include the introduction of water and CO_2, the oxidation of Fe^{2+} to Fe^{3+} and, in some cases, the redistribution of major and trace elements (e.g. Na, K, Ca, Rb, Ba).

The absolute change in the concentration of selected major and trace elements in altered volcanic rocks was examined by assuming that TiO_2 remained constant during the alteration process. Several studies have demonstrated the low solubility of TiO_2 in natural waters (e.g. Loughnan, 1969; Cramer and Nesbitt, 1983 and references therein). The choice of titanium as a reference constituent is particularly relevant in the case of mafic igneous rocks, where it is present in concentrations that permit accurate analysis. The variations in major- and trace-element concentrations in six samples of relatively altered basaltic lava were calculated for anhydrous compositions as percentage change in the ratio element/TiO_2, normalized to that of the least altered rock in the same succession. Relative changes in weight percent are listed in Table C-1 and plotted on Figure 5.3 for samples with increasing wt % ($H_2O_{TOT}+CO_2$).

The profiles for major elements suggest that mobilization of Mg, Ca and K has indeed occurred in strongly altered basaltic rocks. The alteration of volcanic glass in a sample of hypocrystalline basalt may have caused K_2O depletion, although two other glass-rich basalts from Bastion Ridge failed to show similar variations. Some trace elements most likely to be remobilized during alteration include Ba and Rb. Significant variations in Sr, Ni and Cr concentrations occur in some samples but do not correlate well with the alteration index, suggesting

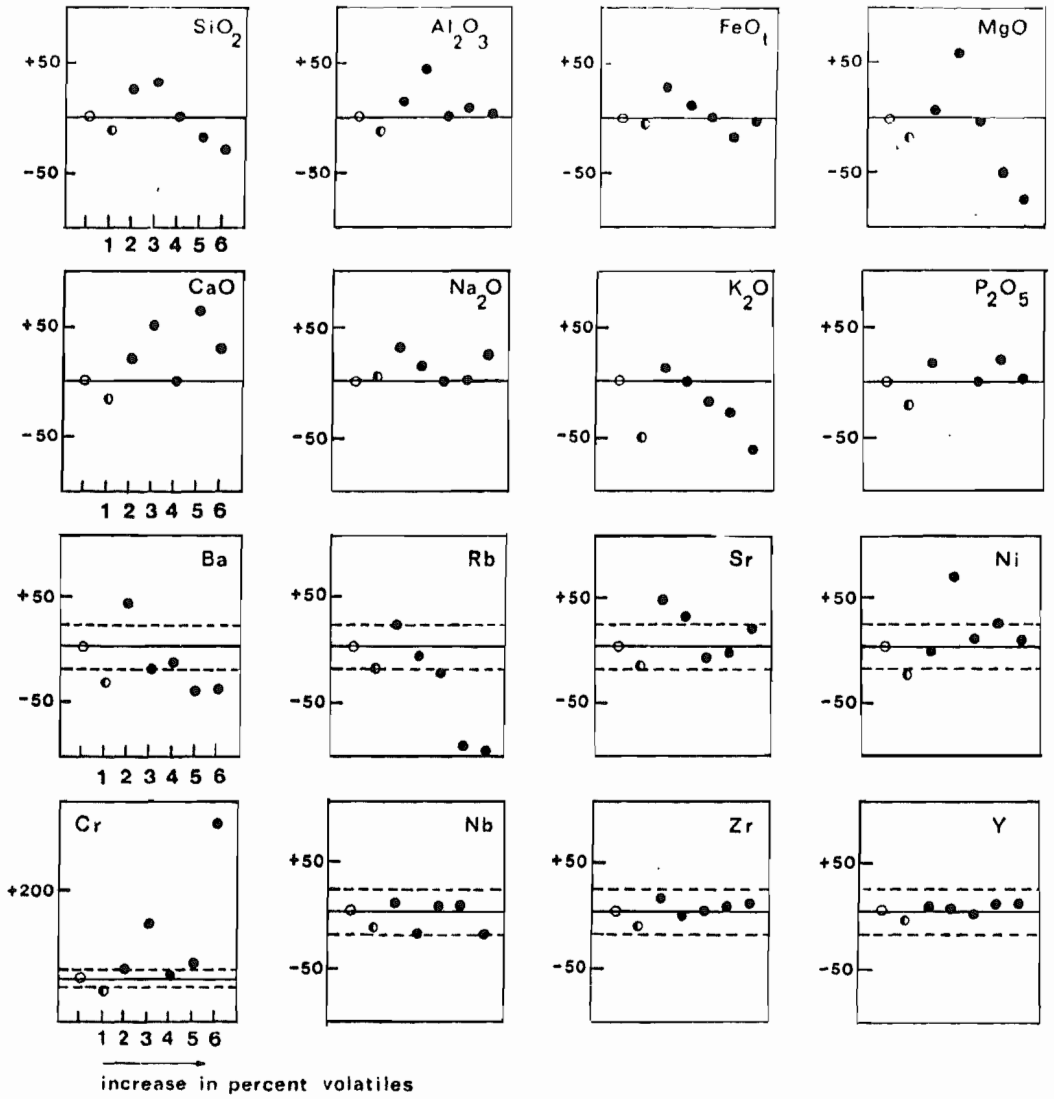

Figure 5.3 Percentage change of major and trace elements relative to TiO_2, in selected volcanic rocks. The ordinate is calculated as % Change = $((X^A/I^A)/(X^{UA}/I^{UA}) - 1) \times 100$ (Nesbitt, 1979) where X = the concentration of any element in the altered (A) and relatively unaltered (UA) samples of basaltic lava from the same succession; and I = the concentration of TiO_2. The dashed lines at 20% change in the ratio are approximate limits of cumulative analytical error for trace element data (i.e. level of significance). Note the change in scale for Cr. The abcissa shows the samples in order of increasing weight % ($H_2O_{TOT}+CO_2$). Symbols: open circle, unaltered rock; half-filled circle, hypocrystalline basalt (40% devitrified glass); filled circle, all other samples of holocrystalline basalt. Key to numbers and corresponding (% $H_2O_{TOT}+CO_2$): [1] AX83-063 (1.76); [2] AX85-082 (3.08); [3] AX83-067 (4.28); [4] AX85-241 (5.12); [5] AX85-265 (10.22); [6] AX83-108 (11.4). Further details are given in Table C-1.

additional processes. Nb, Zr and Y show the least amount of variation with increasing degree of alteration, a result that is consistent with several other studies (e.g. Pearce and Norry, 1979; Ludden et al., 1982; Cramer and Nesbitt, 1983). Similarly, the values for Th, Hf, Ta and La in four samples (Table C-1) indicate that these elements are relatively immobile during alteration.

The samples discussed in this chapter (Tables 5.6 and 5.8) contain between 1 and 3 % ($H_2O_{TOT}+CO_2$). Secondary alteration is limited, and mostly affects olivine grains and volcanic glass. All the major element data discussed are based on volatile-free whole-rock analyses with $Fe_2O_3/(FeO + Fe_2O_3) = 0.15$, and each analysis is tested using the basalt screen of Manson (1967). According to Figure 5.3, these precautions should allow the interpretation of geochemical trends on variation diagrams if special consideration is given to the range of K, Rb, Ba, Ca and Sr values observed. Isotopic analyses were performed on carefully selected holocrystalline basalts.

5.3.2 Compositional types

The volcanic rocks that were sampled belong to three distinct volcanic episodes in the east-central Sverdrup Basin (Table 5.1). However, the stratigraphic correlation between the Strand Fiord basalts in the type area and at Bunde Fiord is poorly constrained (Chapter 3). *T*-tests applied to the means listed in Tables 5.6 and 5.8, and cluster analysis of major element data failed to detect significant compositional differences between the Group 2A and 2B basalts. The

grouping is, therefore, considered valid in the following comparison with Groups 1 and 3.

According to normative classifications, basalts from all three groups are quartz-normative tholeiites with moderate (Groups 1 and 2) to high TiO_2 contents (Group 3). All the samples plot in the field of subalkaline basalts on the alkalies vs. silica diagram (Fig. 5.4 a). A nomenclature plot using normative Ab'-An-Or (Fig. 5.4 b) shows that most of the volcanic rocks correspond to "low" or "medium K" tholeiites. The position of Group 3 basalts suggests a mildly alkaline character.

Despite rather similar major element compositions, volcanic rocks in the study area show marked differences in their trace element contents. All the basalts show the high K, Rb and Ba values that are typical of continental tholeiites (Norry and Fitton, 1983). Rb/Sr ratios, however, are uniformly low in Group 1 basalts (approximately 1-3 X chondritic; compare values listed in Table 5.10). Mantle-normalized diagrams for representative samples from each group are shown on Figure 5.5. The patterns for Group 1 and 2 basalts are similar, with negative anomalies at Sr, P and (in some samples) K. The Group 1 basalts, for example, show a relative enrichment in highly incompatible elements. Marked enrichment in LILE, Nb and the LREE is shown by one sample. AX85-242, from Group 1A, displays a relative enrichment in all the trace elements and a positive spike at Ba.

Despite their overall similarity, the patterns for Group 2A and 2B basalts show a difference in the relative enrichment of Nb and the LREE i.e. a convex anomaly where La is enriched with respect to Nb and Ce in Group 2A basalts, and a slight enrichment of Nb over La and Ce in Group 2B basalts.

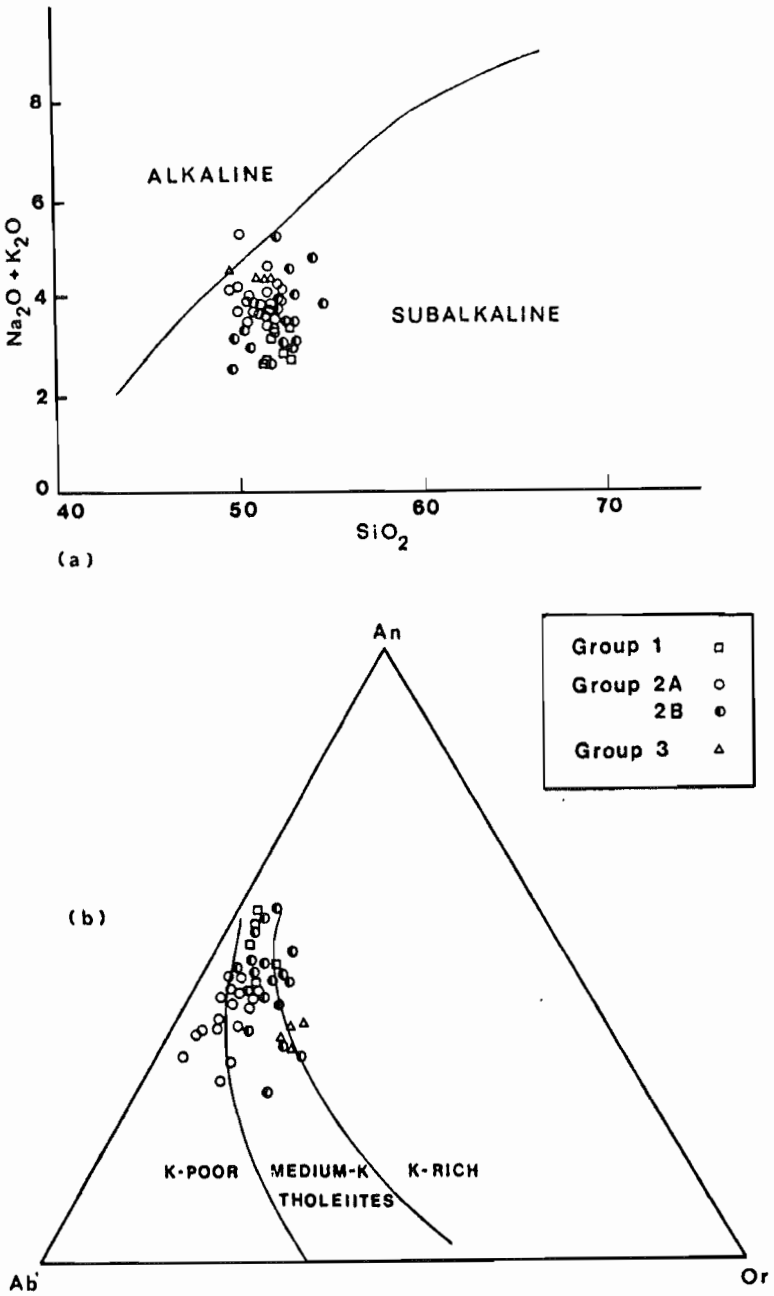

Figure 5.4 Classification diagrams showing the position of samples from Groups 1, 2 and 3 (after Irvine and Baragar, 1970).
(a) Total alkalies vs. silica diagram.
(b) Plot of An-Ab'-Or.

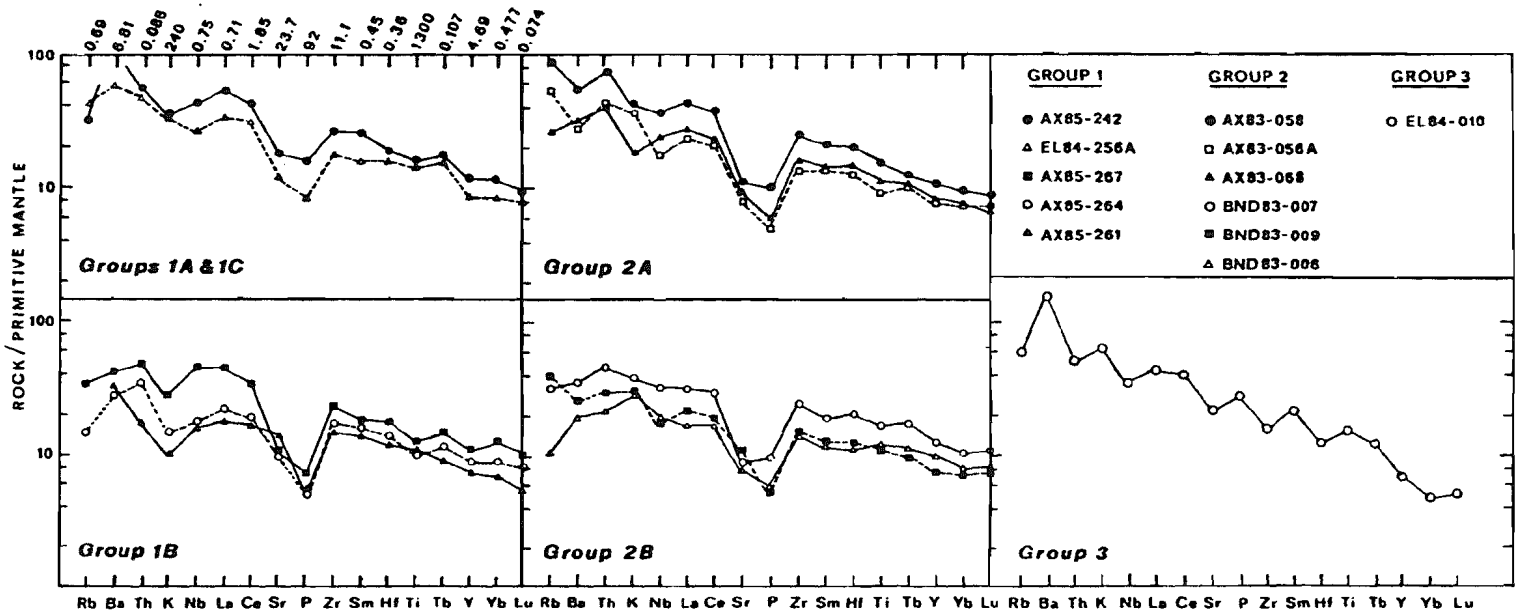

Figure 5.5 Mantle-normalized trace element diagrams for Cretaceous volcanic rocks in the study area. Normalizing values (in ppm) from McDonough et al. (1985).

The Group 3 pattern is markedly different (Fig. 5.5). The Sr anomaly is less pronounced, while K, P and Ti show a positive anomaly. The pattern generally resembles that of alkaline rocks, showing a strong enrichment in highly incompatible elements, and a positive spike at Ba. Unlike most patterns of alkaline rocks, however, the LREE are preferentially enriched over Nb (e.g. Weaver and Tarney, 1983).

Sr isotopic data for a subset of 14 samples are listed in Table 5.10. All the samples of basaltic lava show rather high and variable $^{87}Sr/^{86}Sr_C$ ratios, in the range 0.70532-0.70840. Group 2 basalts display the highest ratios. Variations between the Sr contents and isotopic data provide a means to discriminate among the three volcanic successions (Fig. 5.6 a). In the Group 1 basalts, Sr values display a positive correlation with the $^{87}Sr/^{86}Sr$ ratio. All the Group 2 samples analyzed show uniformly low Sr values and high, variable $^{87}Sr/^{86}Sr$ ratios. The Group 3 basalts show similar $^{87}Sr/^{86}Sr$ ratios and relatively high Sr values. The significance of these trends in terms of the fractionation and assimilation history of the magmas is discussed in Section 5.4.

5.3.3 Tectonic Discrimination Diagrams

The field relations described in Chapter 3 are the best indication that the volcanic rocks were erupted in a continental setting. Accordingly, most of the samples analyzed show Ti/Y and Zr/Y ratios that are typical of within-plate basalts (Pearce and Cann, 1973; Pearce and Norry, 1979; Fig. 5.6 b). Mantle-normalized trace element patterns are also useful in characterizing basaltic rocks from oceanic and

TABLE 5.10
SR ISOTOPIC COMPOSITION OF SELECTED
GROUP 1, 2 AND 3 BASALTS

	Rb/Sr	$^{87}Sr/^{86}Sr_M$	$^{87}Sr/^{86}Sr_C$
GROUP 1			
AX85-242	0.047	0.70711 ± 3	0.70703
AX85-261	n.d.	0.70611 ± 5	0.70624
AX85-264	0.042	0.70604 ± 3	0.70598
AX85-267	0.095	0.70563 ± 3	0.70532
EL84-256A	0.099	0.70652 ± 3	0.70619
GROUP 2			
AX83-056A	0.193	0.70733 ± 3	0.70668
AX83-058	0.262	0.70799 ± 3	0.70706
AX83-060	0.179	0.70848 ± 3	0.70789
BND83-007	0.107	0.70589 ± 3	0.70559
BND83-012	0.109	0.70768 ± 3	0.70737
BND83-016	0.214	0.70913 ± 2	0.70840
BND83-017	0.064	0.70718 ± 2	0.70705
GROUP 3			
EL84-010	0.079	0.70716 ± 3	0.70699
EL84-087	0.069	0.70721 ± 4	0.70708

$( )_M$ measured isotopic ratio

$( )_C$ isotopic ratio corrected to the following ages: Group 1, 113 Ma; Group 2, 95 Ma; Group 3, 92 Ma; and E & A standard = 0.7080.

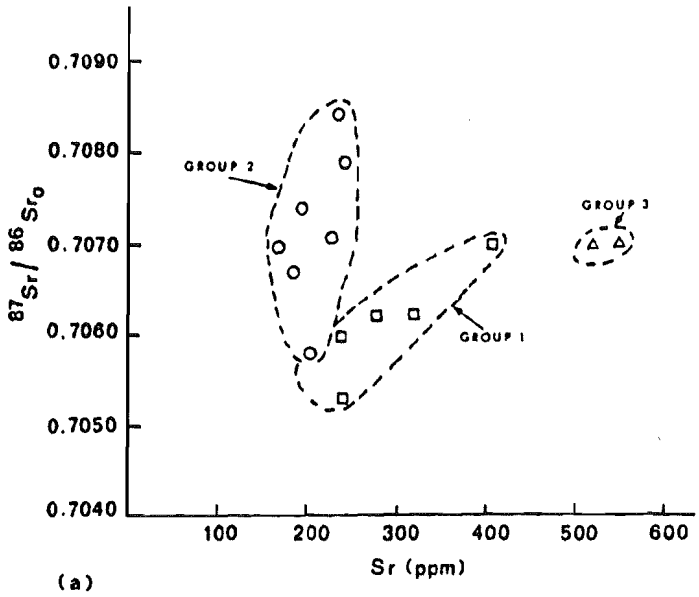

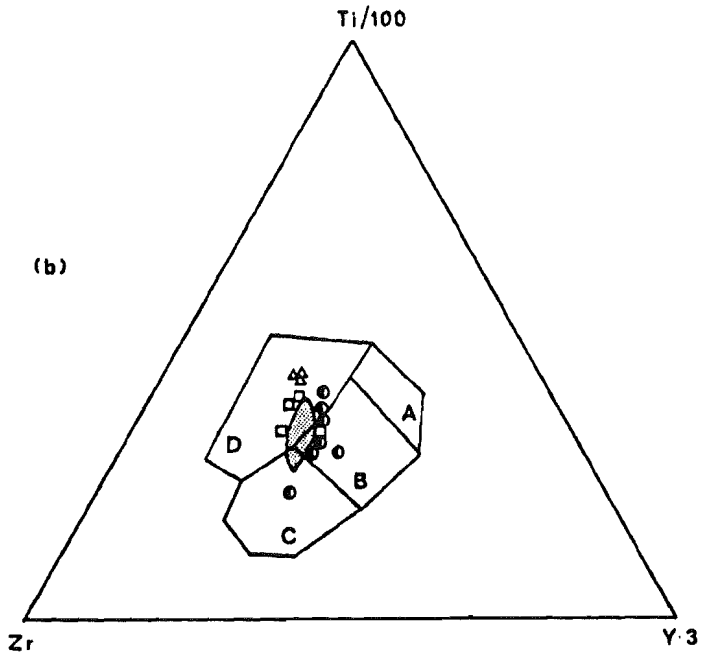

Figure 5.6 (a) Plot of $^{87}Sr/^{86}Sr$ initial ratios vs. Sr (ppm) for selected Group 1, 2 and 3 basalts. Symbols: Group 1, square; Group 2, circle; Group 3, triangle.
(b) Discrimination diagram of Pearce and Cann (1973). Cretaceous volcanic rocks of the Sverdrup Basin plot in the field of within-plate basalts (D) and overlap with compositions of ocean-floor and continental basalts (Field B). The shaded area represents the compositional field of Group 2A basalts. Symbols of data plotting outside this field as in Figure 5.4. Other fields are A+B+C = plate-margin basalts; A+B = island-arc tholeiites; B+C = calc-alkali and shoshonitic basalts; C = ocean-floor and continental basalts.

continental environments (e.g. Norry and Fitton, 1983). Some authors have proposed that these diagrams further discriminate among continental flood basalts (CFB) from a variety of settings (e.g. rifted margin, intracontinental rift, a-tectonic continental setting, etc; Holm, 1985; Marsh, 1987). Holm (1985), in particular, noted the contrast between the negative slope of CFB patterns and the inverted U-shape pattern of tholeiitic basalts from initial rifting regimes in continental settings (IRT). Mantle-normalized trace element diagrams for the Sverdrup Basin volcanic rocks (Fig. 5.5) show the general features of CFB patterns, except for the positive Nb anomaly that is characteristic of the IRT of Holm (1985), and of enriched mid-ocean ridge basalts (E-MORB; Le Roex et al., 1983).

5.4 Petrology of the Strand Fiord Basalts

The Group 2 basalts were sampled in sufficient number to allow a petrogenetic study. In the following section, geochemical data on fifty-one samples are used to discriminate among several processes that may have played a role during petrogenesis (e.g. partial fusion, fractional crystallization, magma mixing, crustal assimilation). In some cases, trends on geochemical diagrams were tested using cluster analysis. These and other statistical data are located in Appendix C.

5.4.1 Phase Equilibria

The pseudo-liquidus phase diagram (e.g. Coombs, 1963; O'Hara, 1968) is a useful method for interpreting the crystallization history of basaltic liquids. Figure 5.7 shows projections of the major element data for Group 2 basalts in the diagram of Walker et al. (1979). The ***Group 2A*** basalts show abundant scatter on the olivine-diopside-quartz projection (Fig. 5.7 a). Some of the samples from Twisted Ridge follow a fractionation trend towards the pseudoinvariant point where liquid and olivine react to form augite + pigeonite + plagioclase. Samples from Bastion Ridge and Glacier Fiord Syncline form a loose cluster of points and project in the primary phase field of diopside.

Sparsely or moderately phyric lavas can be interpreted as liquids if the bulk rock composition is similar to a glass or aphyric rock from the same data set, or if the proportions and composition of the phenocrysts and coexisting glass can be reproduced experimentally under similar conditions of crystallization (Tormey et al., 1987). The type and proportions of phenocrysts in the ***Group 2B*** basalts (Table 5.4) are in agreement with the evolved character of the rocks and suggest differentiation at low pressures. The olivine-diopside-quartz projection of Figure 5.7 (b) illustrates the position of both aphyric and phenocryst-bearing samples in Group 2B. Whole-rock compositions for sparsely to moderately phyric basalts from both successions plot reasonably close to the experimental phase boundary. The path followed by Celluloid Creek basalts indicates fractionation of oliv+plag followed by oliv+plag+cpx at or near 1 atm pressure. The data from Artharber Creek are more scattered and most of the data points are displaced

Figure 5.7: Projections of whole rock compositions for Group 2 basalts in the tetrahedron plagioclase, olivine, diopside, quartz (molecular proportions; experimental phase boundary of Walker et al., 1979).
(a) Projection for Group 2A basalts from plagioclase into the plane diopside-olivine-quartz
(b) Projection for Group 2B basalts. Samples containing more than 10% phenocrysts are indicated by a circled symbol.
(c) Fractionation and mixing paths of ocean-floor tholeiites according to Walker et al., 1979. The heavy dashed line illustrates the fractionation path of a sample that 1/ crystallizes olivine 2/ evolves towards the oliv and cpx (+plag) boundary with falling temperature and 3/ follows this boundary as it precipitates all three phases. According to Walker et al. (1979), mixed batches of such residual liquids would crystallize clinopyroxene before olivine, as shown by the position of the vectors located in the curvature of the 1 atm phase boundary.

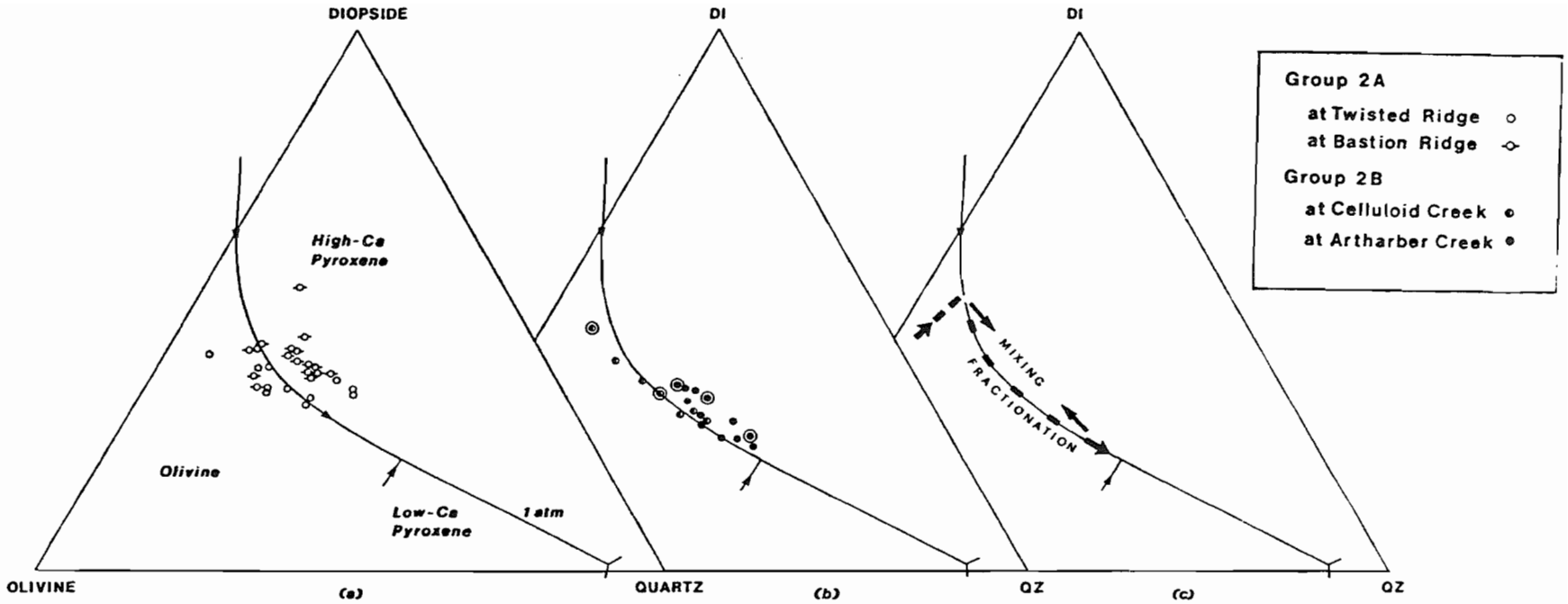
DIOPSIDE
DI
DI
High-Ca
Pyroxene
Olivine
Low-Ca
Pyroxene
1 atm
MIXING
FRACTIONATION
OLIVINE
(a)
QUARTZ
(b)
QZ
(c)
QZ
Group 2A
at Twisted Ridge
at Bastion Ridge
Group 2B
at Celluloid Creek
at Artharber Creek

FIGURE 5.7

towards the primary phase field of diopside. Overall, Group 2B samples plot closer to the pseudoinvariant point than the Group 2A basalts from the type area, suggesting a more evolved character.

The near-cotectic behaviour of all the Group 2 basalts with respect to olivine, clinopyroxene and plagioclase is also evident on other projections using CMAS or recalculated CIPW coordinates. In practice, however, it is difficult to verify the crystallization sequences indicated on Figure 5.7 using petrographic observations, particularly for samples of microcrystalline or altered basalt (see Section 5.2.2). Evidence for the presence of more evolved compositions in Group 2B is examined below.

5.4.2 Compositional Variations

The cotectic mineralogy of the Strand Fiord basalts is consistent with equilibration at low pressures in the crust. The presence of phenocrysts of olivine, plagioclase and clinopyroxene in some of the rocks suggests that fractional crystallization may account for some of the compositional variations observed. The removal of a gabbroic assemblage would lead to a progressive enrichment of Fe relative to Mg, and to the depletion of CaO and Al_2O_3 in successive residual liquids (Fig. 5.8). The most evolved basalts should display the strongest enrichment in incompatible trace elements and the rare earths, resulting in a high degree of correlation between pairs of these elements (e.g. Treuil and Joron, 1976).

Plots of selected major oxides and trace element data against MgO illustrate some of these features in the Group 2 basalts (Fig. 5.9). In

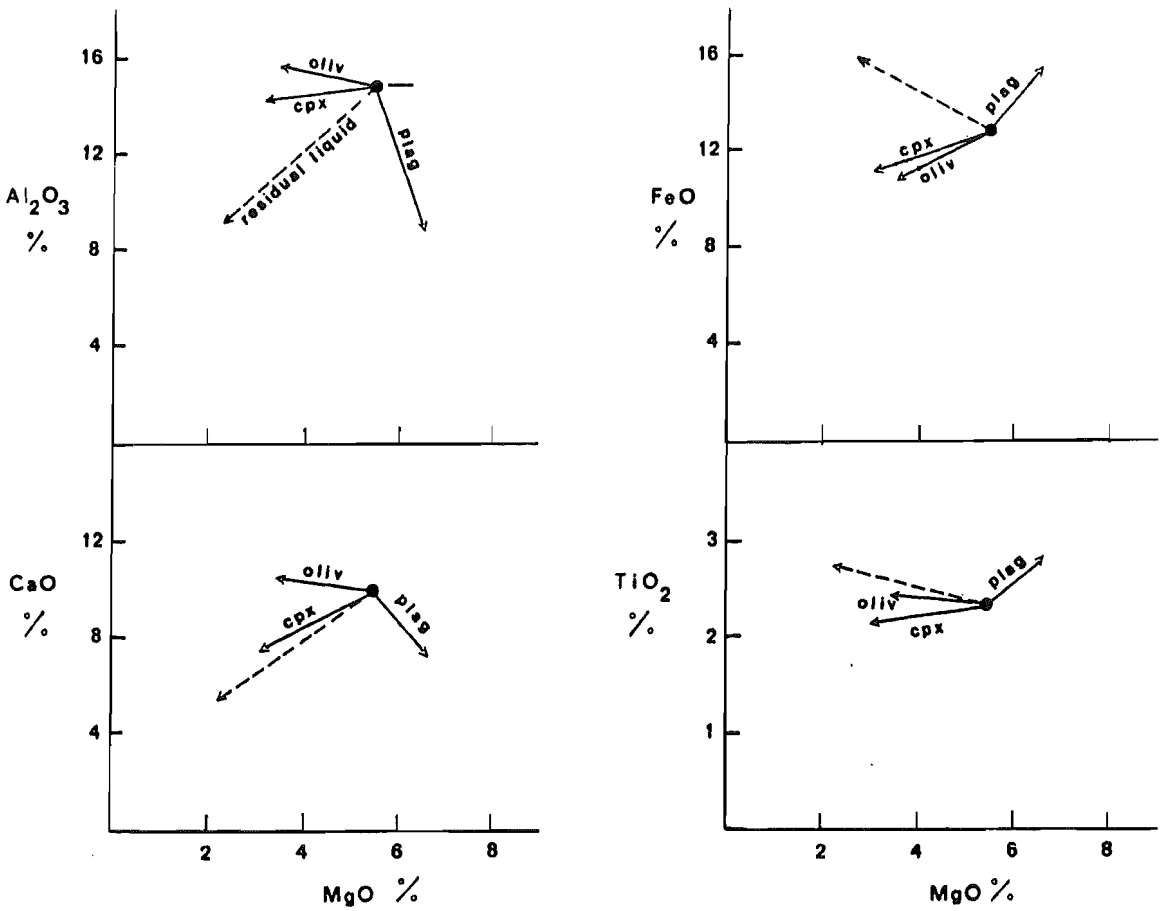

Figure 5.8 Variations in the contents of Al_2O_3, CaO, FeO (total), TiO_2 and MgO in a basaltic liquid undergoing gabbro fractionation. The composition of the residual liquid was obtained by removing olivine, clinopyroxene and plagioclase in the proportions 15:35:50 from a magma with the composition of a Group 2A basalt at Twisted Ridge (AX83-066B, Appendix C). Mineral compositions are for Fo_{65}, An_{60} and augite phenocrysts in sample BND83-015 (Appendix B). The vectors illustrate 40% crystallization.

Figure 5.9 Two-element variation diagrams for Group 2 basalts. A cutoff at 2.5 % ($H_2O_{TOT}+CO_2$) was applied, reducing the data base from 51 to 45 samples.

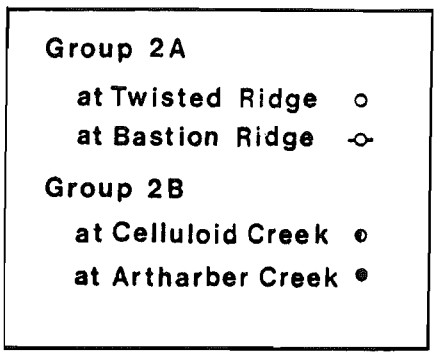

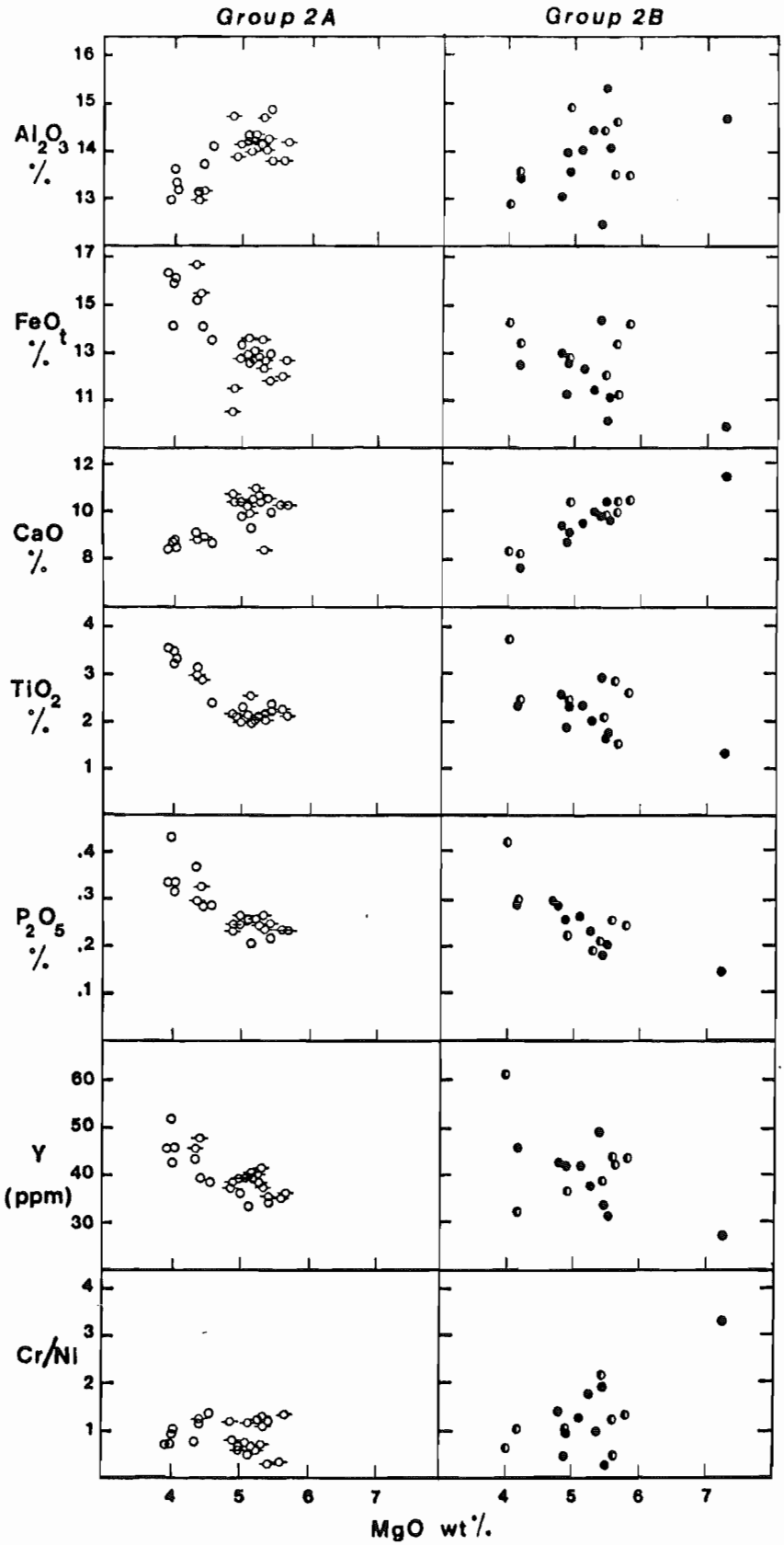

FIGURE 5.9

the ***Group 2A*** samples, the widest compositional range and most fractionated basalts are found at Twisted Ridge (TR), in the northern part of the type area. Little or no variation is present in basaltic lavas sampled to the south and east, at Bastion Ridge (BR) and Glacier Fiord Syncline (GFS). Despite the scatter, the trends for Al_2O_3, CaO, FeO (total), TiO_2 and P_2O_5 are consistent with fractional crystallization of a gabbroic assemblage (compare Figs. 5.8 and 5.9).

No simple liquid line of descent exists for the Group 2A basalts as a whole. This is particularly evident on plots of high-field strength elements vs. MgO (e.g. the enrichment in yttrium in BR-GFS basalts, Fig. 5.9). Cluster analysis also indicates that the TR and BR-GFS suites are distinct on the basis of Ti, Nb, Zr and Y abundances (Table C-7, Test I). It is clear that the Strand Fiord basalts in the type area all belong to the same group, as indicated by the field relations (Chapter 3) and the uniform major element compositions of the samples analysed (Table 5.6). However, the differences in trace element concentrations observed in TR and GR-GFS basalts at MgO values of 5-6 % (Fig. 5.9) cannot be attributed to fractionation alone and must result from other processes, or reflect the composition of their respective parental magmas.

The correlation coefficients for major elements and MgO in the ***Group 2B*** basalts are generally low (Table C-2) and translate into much scatter on variation diagrams, particularly in the case of Al_2O_3 and FeO (Fig. 5.9). The trends for CaO, TiO_2 and P_2O_5 are similar to those displayed by the Group 2A basalts. However, no systematic differences exist in the abundances of incompatible elements, suggesting that

basaltic lavas at Celluloid Creek (CC) and Artharber Creek (AC) are cogenetic (see *r* values of TiO_2-P_2O_5, or Y-, Nb-, P_2O_5-Zr in Table C-2).

Despite similar compositions, the differentiation history of the Group 2 basalts cannot be described in terms of a single process, such as closed system fractionation involving a gabbroic assemblage. This is evident on a plot of Cr/Ni vs. MgO (Fig. 5.9), where some of the Group 2B basalts show a large increase in this ratio for constant values of MgO. The scatter is most evident in Group 2B basalts at Artharber Creek with 51-52% SiO_2. The variations in Cr/Ni could be attributable to differences in the type of fractionating phases, source composition, to some form of contamination, magma mixing, or combinations of these variables. Cr and Ni behave as compatible elements during the fractional crystallization of basaltic liquids, and are strongly partitioned into clinopyroxene and olivine, respectively. Low-pressure crystallization of olivine, for example, would rapidly deplete Ni relative to Cr, whereas the removal of a spinel phase would create the opposite effect. Good correlations between high-field strength elements in the Group 2B samples suggest that the Cr/Ni variations are caused by differences in the types of phases removed, or by magma mixing in crustal reservoirs.

Rare earth data were obtained for the Group 2A basalts at Twisted Ridge and Group 2B basalts at Celluloid Creek (Tables 5.7 and 5.9). The variations in Ta, Hf and rare earth elements in the Celluloid Creek basalts appear to be controlled largely by fractionation. Chondrite-normalized patterns for these samples (Fig. 5.10 b) show a progressive increase in all the rare earths by a factor of 1.4 (HREE) to 1.9 (LREE), consistent with the fractionation of a gabbroic assemblage (Leeman,

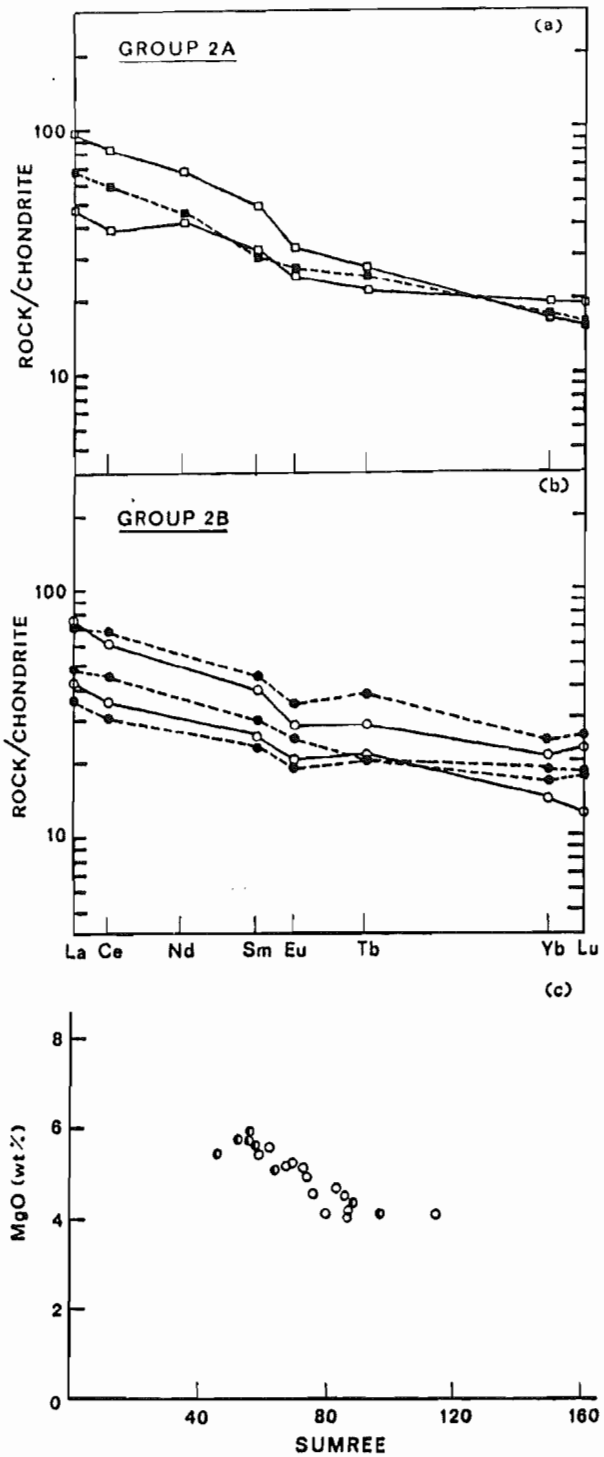

Figure 5.10 Chondrite-normalized rare earth patterns for selected Group 2 basalts (normalizing values from Taylor and Gorton, 1977).
(a) Group 2A basalts at Twisted Ridge.
(b) Group 2B basalts at Celluloid Creek.
(c) MgO vs. SUMREE for selected Group 2A and 2B basalts. Symbols as in Figure 5.7.

1976; Hanson, 1980). The distinct Eu anomaly reflects the role of plagioclase fractionation. Rare earth patterns for the Twisted Ridge samples (Fig. 5.10 a) show a similar degree of LREE enrichment, but only small variations between the most primitive and most differentiated basalts. Despite the differences outlined above, the Group 2A and 2B basalts form a single trend on a plot of MgO vs. SUMREE (Fig. 5.10 c). Processes that could be responsible for the relative enrichment of LREE vs. HREE in some of the Group 2A are discussed in Section 5.5.

5.4.3 Petrogenesis

Mass Balance Calculations

Attempts to derive the most evolved Group 2 basalts by crystal fractionation were generally unsuccessful. The best results were obtained using samples from Group 2A at Twisted Ridge. Least-squares fractionation calculations (Bryan et al., 1969) were applied to samples AX83-066 and -063. Despite a rather low MgO content (5.33%), AX83-066 is one of the most primitive basalts in the series (also shows low FeOt, high CaO, and relatively low contents of the incompatible elements, SUMREE; see Appendix C and Table 5.7). AX83-063 is a more evolved basalt, with lower MgO and CaO, and higher FeOt and TiO_2, showing the expected increase in Nb, Y, Zr and total REE (and decrease in compatible elements) that could result from gabbro fractionation. The fractionation model assumes that phenocrysts were removed from the primitive magma to produce the more evolved composition. In the calculations, the squares of the differences for each oxide component

between the calculated and observed compositions are minimized. The "goodness of fit" is expressed as the sum of the squared residuals.

The results of the mass balance are shown on Table 5.11. The solution is acceptable inasmuch as the type and proportions of cumulate phases are similar to those observed petrographically (Table 5.4). Note that olivine, clinopyroxene and plagioclase are not fractionated in cotectic proportions. The fact that plagioclase dominates in the phenocryst assemblage of most samples (Table 5.4) may result from enrichment caused by density contrasts (Elthon, 1984). Overall, the test generally explains the decrease in Cr, Ni and increase in incompatible elements expected from fractionation of a gabbroic assemblage. The variations in K, however, cannot be explained by fractionation alone (Table 5.11).

The low correlation coefficients for major and trace elements, and the failure of fractionation calculations to explain all the compositional variations in Group 2 basalts suggest the operation of other processes during petrogenesis. These are examined in the next sections by means of trace element and Sr-isotopic data.

TABLE 5.11
MASS BALANCE CALCULATIONS

	PARENT (1)	(obs) (2)	(calc)
WT% *			
SiO_2	49.07	49.63	49.61
TiO_2	2.31	3.43	3.22
Al_2O_3	14.93	12.96	12.94
FeO	12.87	16.08	16.08
MgO	5.49	3.94	3.96
CaO	9.96	8.43	8.47
Na_2O	3.41	3.78	4.09
K_2O	0.68	0.41	0.75
P_2O_5	0.21	0.33	0.30
PPM **			
Rb	23	27	32
Ni	41	28	34
Cr	49	20	24
Nb	14	22	19
La	15.4	21.7	21
Hf	4.4	6.2	6
Th	2.8	3.7	4

MINERALS(3)	% CUMULATE (30 % crystallization)
Olivine Fo_{85}	11
Augite	25
Plagioclase An_{70}	62
Magnetite	2
	100 %

SUM OF SQUARES OF RESIDUALS R = 0.265 (4)

* Weighted input data
** Calculated from the solution for major elements according to partition coefficients in Table 5.12 (a).
(1) AX83-066 Group 2A at Twisted Ridge
(2) AX83-063 Group 2A at Twisted Ridge
(3) Olivine and plagioclase mineral compositions were determined using the GPPMINCO program of Geist et al., 1985.
Augite: analysis 6, Table 13, Deer et al., 1966.
Magnetite: analysis 4, Table 46, Deer et al., 1966.
(4) Values less than 1 are considered reasonable, less than 0.3 is a good fit and less than 0.1 is excellent (GPPMIX Program, Geist et al., 1985).

Trace Element Modelling

Quantitative modelling of trace elements is beset by several difficulties:

- the concentrations observed in samples of basaltic lava likely result from several superimposed processes,
- the samples may not adequately reflect the magmatic processes involved or contain all the mineral phases that were present at each stage,
- precise measurements of partition coefficients are difficult to obtain because of changing physical and chemical conditions, etc.

Despite these limitations, end-member melting and crystallization models are described by simple equations that relate the initial and final concentrations of an element to the bulk distribution coefficient and fraction of liquid remaining (e.g. Neumann et al., 1954; Shaw, 1970). When combined with correlation diagrams, the models allow the distinction between characteristics imposed by the source material(s) and those caused by other processes such as fractional crystallization, batch melting, mixing or crustal assimilation (e.g. Treuil and Joron, 1976; Allegre et al., 1977; Langmuir et al., 1978). Log-log diagrams using compatible vs. incompatible elements are particularly useful: among the processes listed above, Rayleigh fractional crystallization is the only one that causes exponential changes in the concentration of elements in the residual liquids, producing linear arrays rather than curves. This is illustrated on Figure 5.11 for fractional crystallization, equilibrium batch melting and a combination of crystal fractionation and assimilation of crustal rocks (AFC: Taylor, 1980; DePaolo, 1981), assuming that the bulk distribution coefficient D

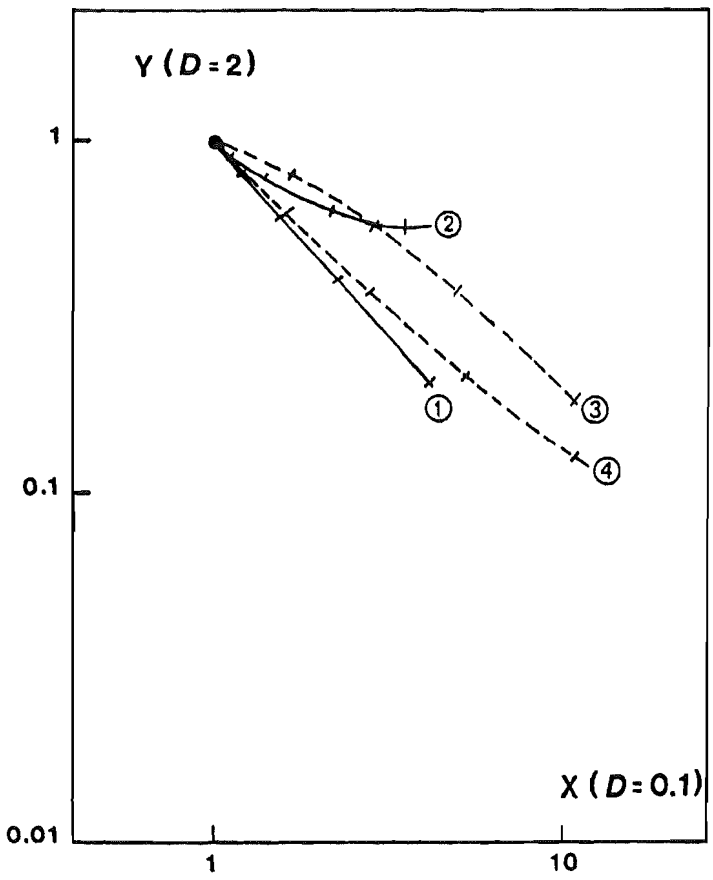

Figure 5.11 Log-log diagram showing variations in the concentrations of compatible trace element Y (D = 2) and incompatible trace element X (D = 0.1) for:
- [1]: perfect fractional crystallization;
- [2]: equilibrium crystallization or batch melting;
- [3,4]: combined crystallization and assimilation (AFC).

C/A, crystallization vs. assimilation rate.
Initial values of X and Y in the magma are 1. Values of X and Y in a hypothetical contaminant are $X^{Cl} = 8$, $Y^{Cl} = 1$.
- [3]: C/A = 10;
- [4]: C/A = 2.5.

Tick marks indicate 20% crystallization.

remains constant. The trajectories for perfect fractional crystallization, batch melting and AFC can be distinguished on this type of diagram. The shift in the position of the AFC curves on either side of a simple fractionation trend is largely controlled by the rate of crystallization vs. assimilation (modelled as C/A = 2.5 and 10 on Fig. 5.11), and by the concentration of elements X and Y in the contaminant.

A qualitative comparison with log-log diagrams for selected Group 2 basalts (Fig. 5.12) suggests that neither batch melting nor perfect fractional crystallization can account for the compositional variations observed. The concentrations of compatible elements (e.g. Ni, Cr) in the TR and CC basalts show the regular decrease caused, for example, by the fractional crystallization process. However, the expected concurrent increase in the concentration of incompatible elements (e.g. Hf, La, Th) is limited to the most primitive basalts in the series. The more evolved basaltic compositions show constant, and occasionally lower, values of these elements. An inflection in the trend is particularly evident on plots using Cr values on the ordinate.

The trends on Figure 5.12 can be produced by a combination of fractional crystallization and assimilation (AFC), however, several assumptions are required.

1. Nature of the Parental Magma(s). The AFC process has been successfully modelled in several studies of basaltic rocks from continental and subduction-related environments (e.g. Mantovani et al., 1984; Singer and Kudo, 1986; Wyers and Barton, 1987). In most cases, high-Mg basalts in the volcanic sequence were identified as parental compositions that were derivatives of primary liquids capable of coexisting with a host mantle. High-Mg basalts are relatively scarce in

Figure 5.12 Log-log diagrams of Ni and Cr vs. La, Hf and Th for Group 2A basalts at Twisted Ridge and Group 2B basalts at Celluloid Creek. Symbols as in Figure 5.7. The circle and arrow show the position of samples used in fractionation calculations, Table 5.11 (also full-line arrow indicating fractional crystallization on insets, Figure 5.13).

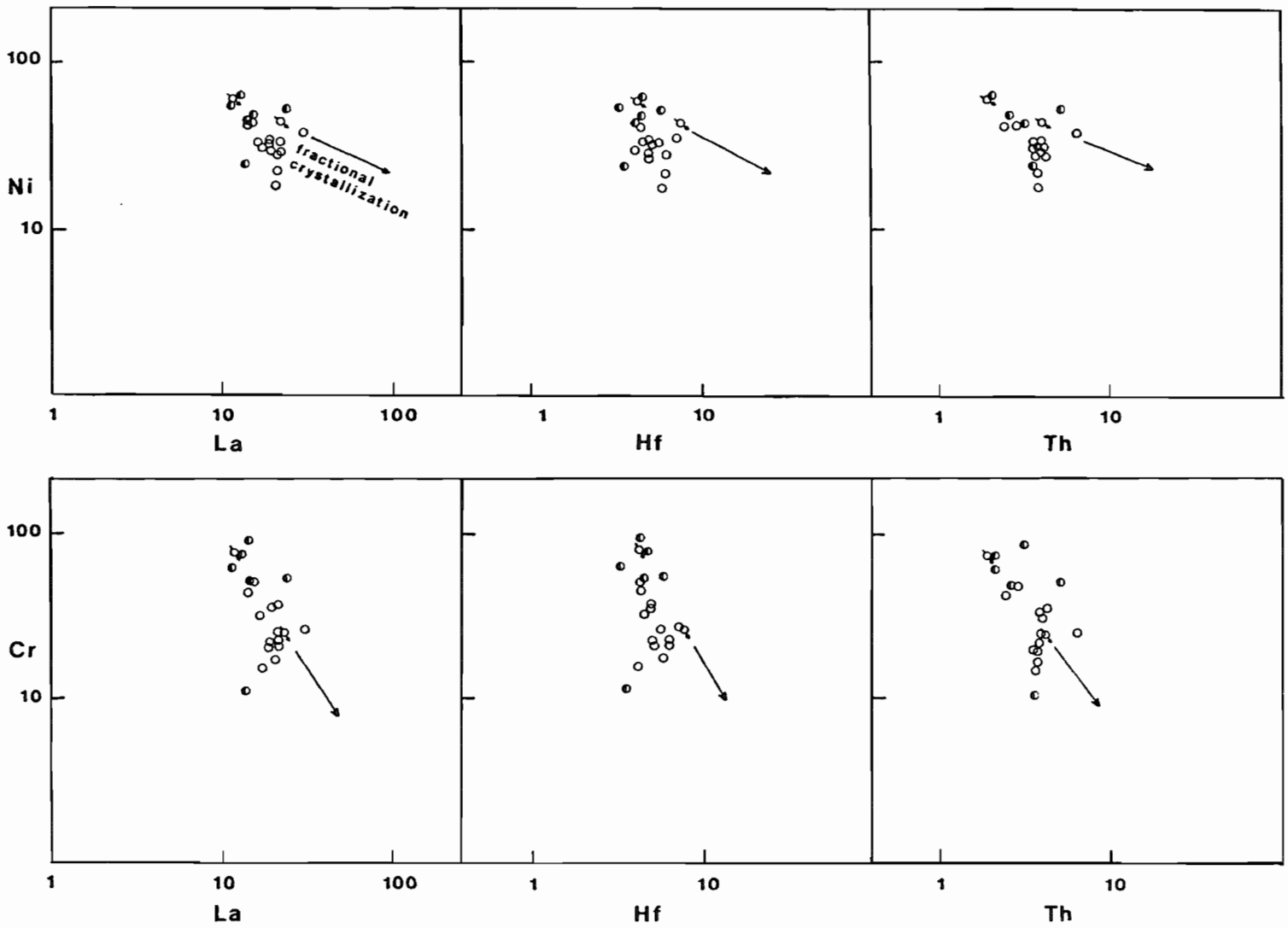
100
Ni
10
fractional
crystallization
1
10
100
La
1
10
Hf
1
10
Th
100
Cr
10
1
10
100
La
1
10
Hf
1
10
Th

FIGURE 5.12

areas of voluminous continental magmatism, a characteristic that also applies to the Sverdrup Basin. This has led some authors to argue that the vast volumes of chemically uniform basalts erupted as CFB's (or MORB's) could be produced by moderate amounts of fusion (e.g. 25%) of a more Fe-rich mantle (e.g. Wilkinson and Binns, 1977). The alternative view is preferred here, i.e. that basaltic compositions in the Sverdrup Basin do not represent primary magmas, but were derived from Mg-rich parental compositions that represent melts of peridotitic mantle. This assumption is supported by experimental studies and quantitative models of basalt magma petrogenesis (e.g. Clarke and O'Hara, 1979). As well, some of the physical processes operating in flood basalt provinces may explain the scarcity of picritic basalts in the continental environment.

- The melts fractionate within the mantle, during ascent or in crustal magma chambers.
- Mixing of primitive melts with their differentiates in open reservoirs (O'Hara, 1977) reduces the opportunity for parental magmas to reach the surface.
- The earth's crust acts as a density filter, trapping picritic liquids at or near the base of the crust and favoring the eruption of more evolved basaltic liquids at the density minimum (Stolper and Walker, 1980).

*2. **Nature of the Contaminant(s).*** Quantitative evaluation of crustal contamination in the Group 2 basalts is limited by the unknown nature of the basement rocks. Crustal cross-sections of the central part of the Arctic Archipelago suggest that the upper crust consists of Proterozoic and Paleozoic strata underlain by Archean rocks (Sweeney, 1986 b). A similar crustal stratigraphy is found in the east-central part of the

Basin where strata of the Arctic Platform and Franklinian basin overlie high-grade Archean terranes (e.g. Trettin, in press). The bulk chemical compositions for the upper and lower crust proposed by Taylor and McLennan (1985) were, therefore, considered adequate end-member contaminants for trace element modelling. Values for selected trace elements are shown in Table 5.12 (b), and illustrate the chemical contrast between granulite facies terrains of the lower crust (depleted in K, Rb, U, Th) and low-grade metamorphic sedimentary or igneous rocks of the upper crust.

3. Major Element Constraints. Relatively large degrees of contamination of primitive basaltic magmas by crustal rocks should result in the production of more siliceous compositions (e.g. Pearce, 1983). The restricted range of major element compositions in Group 2 basalts prevents accurate modelling of crustal contamination using these elements. However, the results presented below concerning trace elements and Sr-isotopic data could be tested using compositions for basalts and basaltic andesites at Artharber Creek.

Figure 5.13 illustrates the essential results of the trace element modelling. Trace element concentrations in two hypothetical parental magmas (PB1 and PB2) are calculated by fractionating olivine from "end-member" picrites (P1 and P2), using a range of Ni, Cr, La and Th values from the literature, and the partition coefficients of Table 5.12 (a). Bulk distribution coefficients are derived assuming the removal of a gabbroic assemblage from PB1 and PB2 to produce more evolved compositions. Details of the calculations and starting compositions are given in Appendix C (Tables C-3 and C-4).

TABLE 5.12 (a)
SUMMARY OF PARTITION COEFFICIENTS USED IN MODELLING

	Rb	Ni	Cr	Hf	La	Th	Nb
Olivine	0.001	10	2.8	0.04	0.03	0.03	0.01
Clinopyroxene	0.001	1.4	10	0.36	0.06	0.04	0.30
Plagioclase	0.07	-	-	0.05	0.15	0.05	0.025
Magnetite	0.01	5	10	0.38	0.29	0.55	1.0

Partition coefficient values were extracted from: Irving, 1978; Cox et al., 1979; Pearce and Norry, 1979; Villemant et al., 1981; Irving and Frey, 1984; and Watson, 1987.

TABLE 5.12 (b)
CONTAMINATION MODEL END-MEMBERS

PPM	C1	C2
Rb	5.3	112
Sr	230	350
Ni	135	20
Cr	235	35
Nb	6	25
Hf	2.1	5.8
Th	1.06	10.7
Ta	0.6	2.2
La	11	30
Rb/Sr	0.02	0.32

C1: Lower continental crust, Taylor and McLennan 1985.
C2: Upper continental crust, Taylor and McLennan 1985.

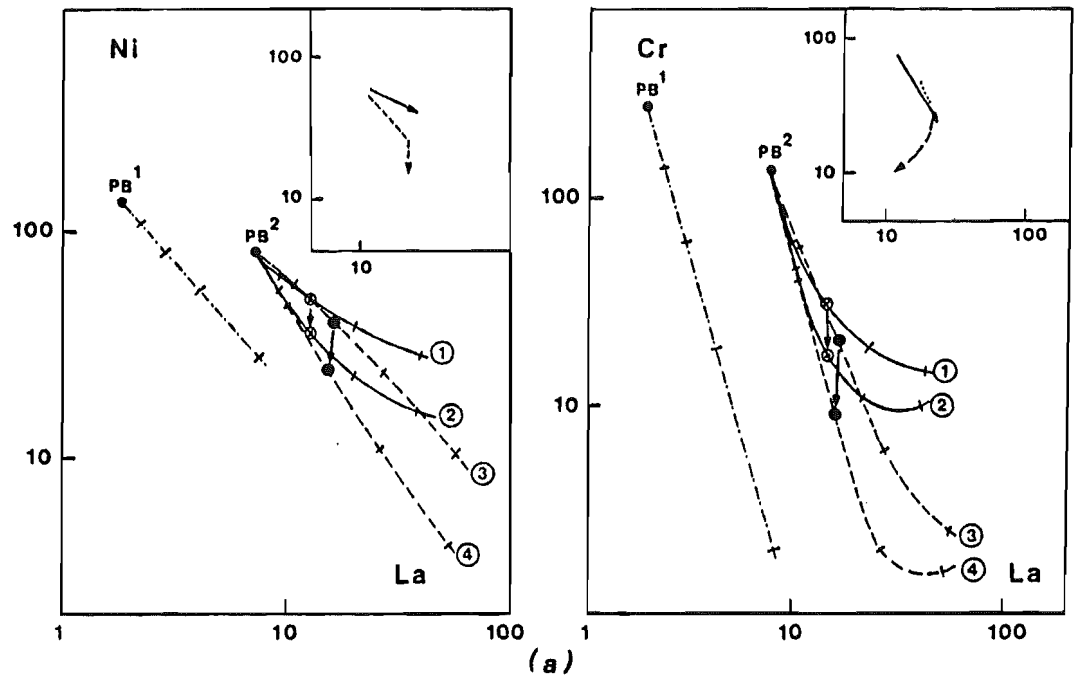

Figure 5.13 Examples of the effects of perfect fractional crystallization (dash-dotted line from PB1) and combined fractionation and assimilation (lines 1 to 4 from PB2) on the concentrations of Ni and Cr vs. (a) La and (b) Th. Values for PB1 and PB2 "parental basalts" are derived by subtracting 20% olivine from picritic basalts with a range of trace element abundances selected from the literature (see Table C-2 for sources). The fractionating assemblage is 0.15 Ol + 0.35 Cpx + 0.5 Plag (Biggar, 1983). AFC calculations were performed according to DePaolo (1981), using the lower (C1) and upper crust (C2) contaminants of Table 5.12 (b). Full lines = C1 contaminant at [1] C/A = 5 and [2] C/A = 2.5. Dashed line = C2 contaminant at [3] C/A = 5 and [4] C/A = 2.5. Tick marks indicate 20 % crystallization. The general trends observed on Figure 5.12 are reproduced on the inset (full line, fractional crystallization; dashed or dotted line, deviations shown by the data). A combination of fractionation and assimilation of crustal rocks could explain the poor correlation between concentrations of compatible (C_Y) and incompatible elements (C_X) observed on Figure 5.12. The trend to lower values of C_Y for relatively constant values of C_X observed in the most evolved basalts could result from an increase in the assimilation rate (lower C/A values) for similar degrees of crystallization undergone by the parental basalt. This is shown by the arrows between open and filled circles at 40 % crystallization on each set of AFC curves. The data for Nb (Figure c) lend further support to the role of AFC in the petrogenesis of Group 2 basalts (curves are not shown, but data are listed for comparison in Table C-4).

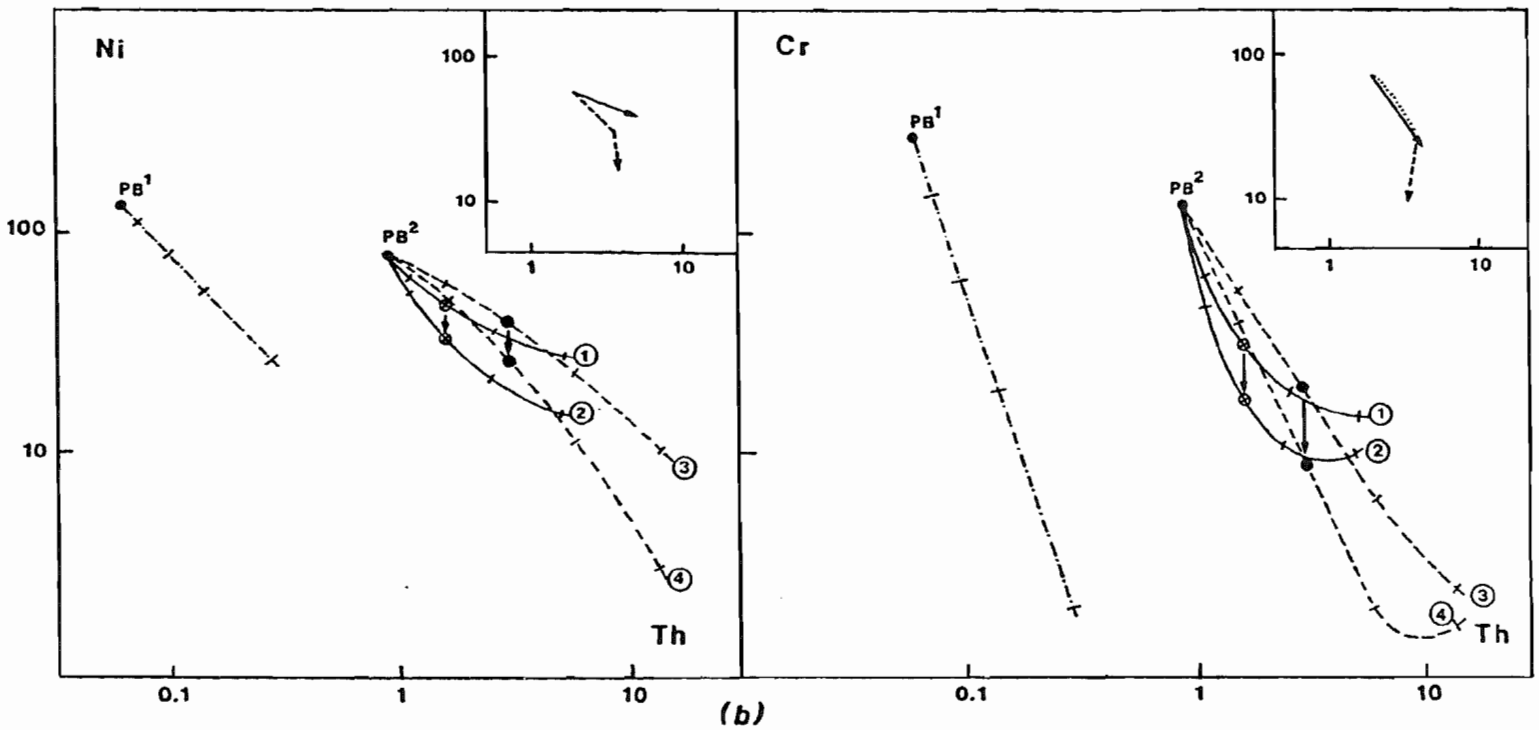

FIGURE 5.13

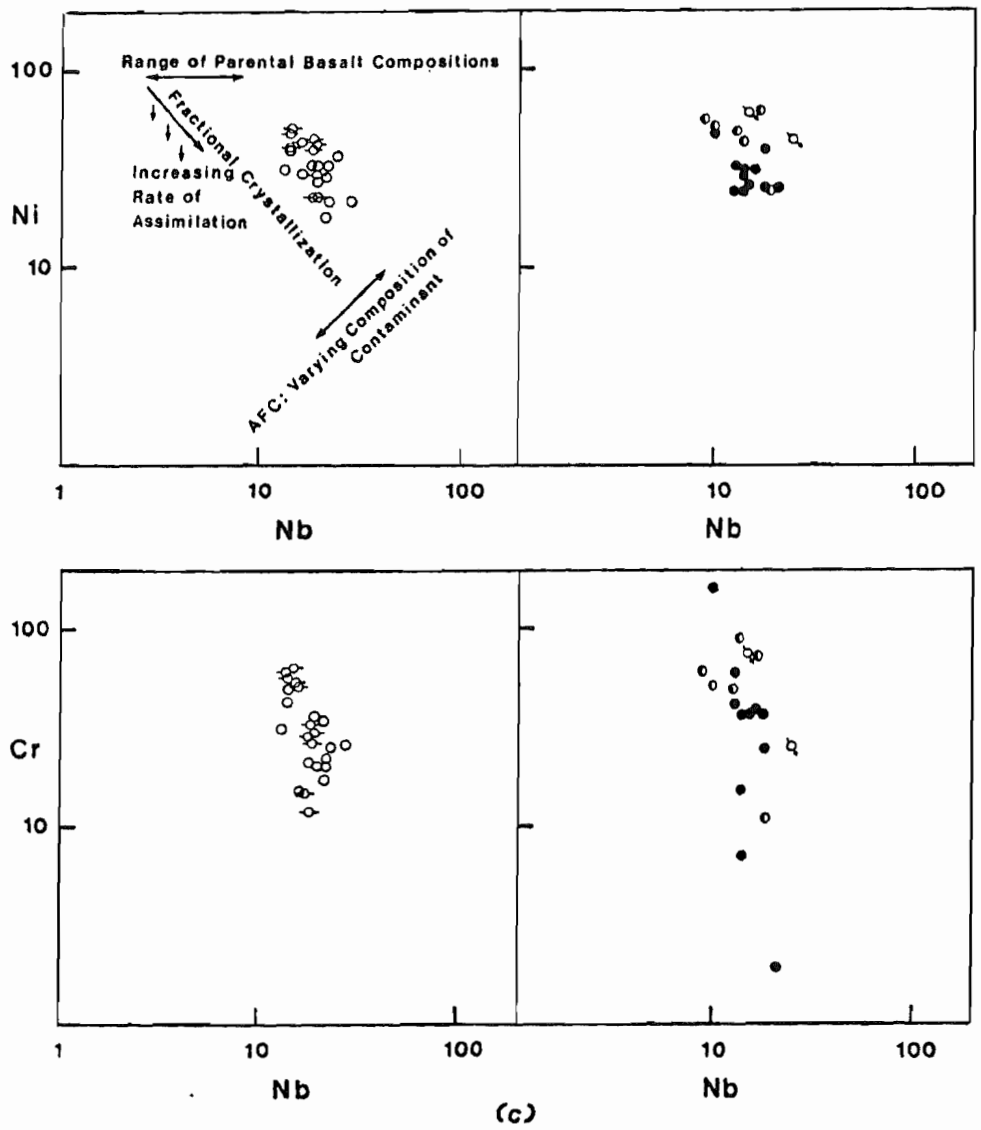
Range of Parental Basalt Compositions
Fractional Crystallization
Increasing Rate of Assimilation
AFC: Varying Composition of Contaminant
100
Ni
10
1
10
100
Nb
10
100
Nb
100
Cr
10
1
10
100
Nb
10
100
Nb
(c)

FIGURE 5.13

None of the model curves on Figures 5.13 (a) and (b) exactly reproduces the trends shown by the data (insets). However, the change from progressively higher concentrations of incompatible elements in the least evolved basalts, to constant or lower values in the most evolved basalts could be caused by an increase in the rate of assimilation. This is shown on Figure 5.13 for a two-fold increase in the assimilation rate, at 40 % crystallization.

The AFC process would effectively lower the correlations among trace elements in the Group 2 basalts (see data for Nb on Fig. 5.13 c). However, other variables must be considered, such as the range of possible parental basalt compositions, nature of the contaminant and role of magma mixing or mafic recharge in open reservoirs.

Role of Magma Mixing

The chemical uniformity of the Group 2 basalts and conspicuous absence of dacitic or rhyolitic lavas in the succession imply that simple two-component mixing involving mafic and silicic magmas is unlikely. Furthermore, textural and mineralogical evidence for disequilibrium phenocryst assemblages or xenocrysts is lacking, as well as the linear trends on element-element variation diagrams which are characteristic of this process, and lead to relatively high correlation coefficients between the element pairs considered (Langmuir et al., 1978). Mixing of mafic magmas and their differentiates during periodic replenishment of open reservoirs, however, cannot be ruled out. Though more difficult to establish, this process might lead to the following characteristics in the erupted basalts:

1. Petrographic: Hybrid lavas may contain phenocrysts showing complex zoning patterns and melt inclusions, features that are considered as

evidence for mixing in basaltic rocks from a variety of settings (e.g. Dungan and Rhodes, 1978; Sakuyama, 1981)

2. Mineralogical: According to Walker et al. (1979), the mixing process is reflected in low-pressure phase equilibria. Their experimental studies suggest that if high-Mg parental basalts 1/ crystallize olivine and 2/ evolve towards and then along the oliv-cpx-plag boundary with falling temperature, then mixed batches of such residual liquids should crystallize clinopyroxene before olivine. The resulting compositions lie in the curvature of the 1 atmosphere phase boundary on the projection from plagioclase into the plane diopside-olivine-quartz (Fig. 5.7 c). After a large number of cycles, the erupted lavas are neither primitive, nor highly differentiated, but reach a steady state corresponding to the perched compositions of O'Hara (1977).

3. Geochemical: O'Hara (1977) and O'Hara and Mathews (1981) have shown that mafic recharge will lead to anomalous enrichment of highly incompatible elements in the hybrid magmas, eventually modifying their ratios after a large number of mixing cycles. Even more diagnostic is the enrichment in compatible trace elements, such as Ni and Cr, which cannot be explained by fractional crystallization, assimilation or a combination of these processes.

The Group 2B basalts at Artharber Creek display all three types of evidence, and may represent hybrid magmas:

1. Some of the basaltic lavas contain phenocrysts of highly calcic plagioclase (Fig. 5.2), with complex zoning patterns and inclusions (Plates 25, 27).

2. Low-pressure phase equilibria are consistent with their origin as mixtures of primitive magmas and more evolved compositions similar to the Celluloid Creek basalts (compare Figs. 5.7 b and c).

3. Magma mixing may provide an explanation for the wide range of Cr values which characterize this volcanic succession (e.g. Cr/Ni ratios on Fig. 5.9, and AC data on Fig. 5.13 c).

The precision of pseudo-liquidus diagrams such as the one proposed by Walker et al. (1979) is limited and, therefore, provides questionable evidence for mixing. A larger data base for Artharber Creek basalts is clearly needed to further support the magma mixing hypothesis. Mixing with more siliceous differentiates could, for example, produce LREE enrichment and HREE depletion with increasing SiO_2 (e.g. McMillan and Dungan, 1986, fig. 7). This type of variation is observed in some of the Group 2A basalts at Twisted Ridge (Fig. 5.10 a). A test of isotopic disequilibrium between the phenocrysts and host rock was beyond the scope of this study, but would further constrain the timing of mixing and assimilation processes in Artharber Creek basalts (e.g. Geist et al., 1988).

Sr-isotopic Evidence

The range of isotopic ratios in the Group 2 basalts is illustrated on Figure 5.14, using a plot of $^{87}Sr/^{86}Sr_C$ vs. Sr contents. Because fractionation cannot alter the $^{87}Sr/^{86}Sr$ ratios, the variations must reflect source characteristics or open system processes involving isotopically distinct materials (country-rock interaction or magma mixing). There is considerable debate concerning the causes of Sr-isotopic diversity in continental igneous suites. Geochemical studies of peridotite xenoliths in alkali basalts have demonstrated that the

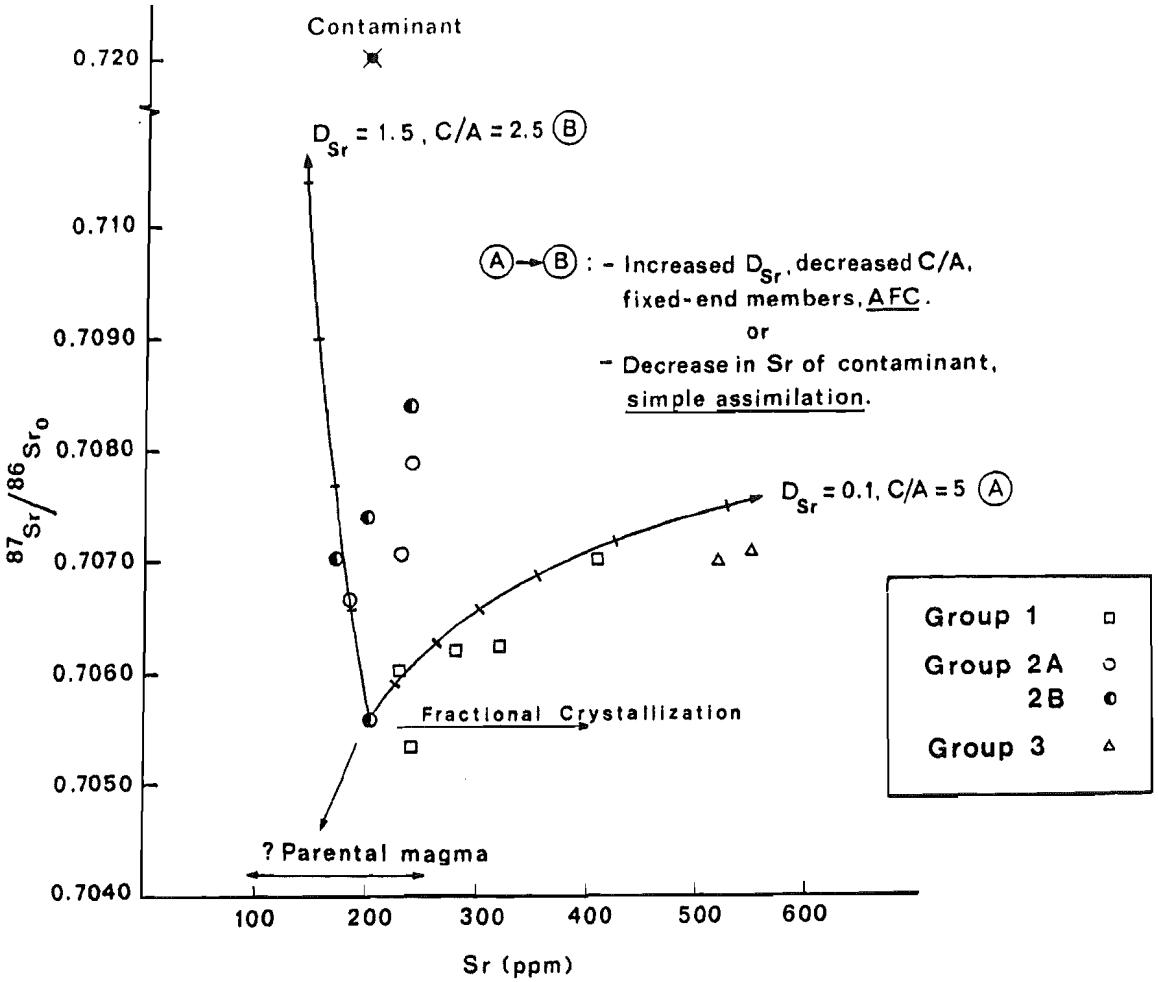

Figure 5.14 Plot of $^{87}Sr/^{86}Sr$ initial ratios vs. Sr contents for selected basalts from Groups 1, 2 and 3. The two trends shown by the data suggest that Early Cretaceous and lower Late Cretaceous volcanic rocks could have evolved from a similar parental magma, either by combined assimilation and fractional crystallization or simple assimilation. The AFC curves were calculated according to DePaolo (1981), using a hypothetical crustal contaminant with $^{87}Sr/^{86}Sr$ = 0.720 and Sr = 200 ppm, and data for one of the least evolved Group 2B basalts ($^{87}Sr/^{86}Sr$ = 0.7056 and Sr = 205 ppm). Tick marks indicate 10 % crystallization. The shift in the position of the curves is determined by the values of the strontium distribution coefficient (D^{Sr}) and rate of crystallization vs. assimilation (C/A). As C/A becomes smaller, the trajectories converge for all values of D^{Sr} toward a simple mixing curve. A similar set of curves can be derived if the Sr content of the contaminant progressively decreases, during simple ***dynamic assimilation*** (Myers et al., 1984).

subcontinental mantle is isotopically heterogeneous. In old subcontinental mantle (e.g. below cratonic areas), variations in Sm/Nd and Rb/Sr ratios resulting from trace element enrichment events could persist for long enough to generate the observed range in isotopic ratios. Subduction-related isotopic and trace element enrichment may also characterize young subcontinental mantle generated during terrane accretion along active plate margins. In many continental suites, however, Sr-isotopic data show a positive correlation with differentiation indices, or the observed time-sequence of eruption (e.g. in western U.S.A. Cenozoic provinces: Menzies et al., 1984, Singer and Kudo, 1986). In these studies, crustal assimilation processes are invoked to explain the observed range in isotopic compositions, as an alternative to partial melting of several discrete, closely-spaced mantle sources.

When considered on their own, Sr-isotopic data for the Group 2 basalts do not provide clear evidence for either of the processes described above. However, a comparison with data for other Early Cretaceous basalts suggests that crustal assimilation is the more likely alternative.

1. It would be highly fortuitous for the two distinct trends on Figure 5.14 to result from mantle heterogeneity. Although volcanic episodes during the Early Cretaceous were well-separated in time, they occurred within the same general area in the north-central part of the Sverdrup Basin.

2. Some of the variations observed can be modelled by AFC processes, assuming fixed compositional end-members. The two curves on Figure 5.14 were calculated according to DePaolo (1981) using a hypothetical

contaminant with $^{87}Sr/^{86}Sr$ = 0.720 (comparable to that in many types of upper crustal rocks e.g. Singer and Kudo, 1986), and a Group 2B basalt as the starting composition. The shift in the position of the curves is determined by values of the strontium distribution coefficient D_{Sr}, and the rate of crystallization vs. assimilation (C/A). Although an infinite number of curves can be derived depending on the composition of parental magmas and contaminants, the calculations illustrate three major points:

- It is conceivable that all the Early Cretaceous basalts were derived from similar parental magmas, and that AFC played a dominant role during petrogenesis. The starting composition used in the calculations, however, is clearly not a true parental composition and may have undergone some degree of crustal contamination (BND83-007, Table 5.10).
- The unusually high and variable Sr-isotopic ratios in the Group 2 basalts could result from a change in the physical conditions of eruption, i.e. higher D_{Sr} values and a greater rate of assimilation vs. crystallization.
- High $^{87}Sr/^{86}Sr$ ratios in the contaminant are required by the AFC model, suggesting that the basalts could have assimilated upper crustal rocks. An alternative would be to invoke a progressive decrease in the Sr content of the contaminant, during dynamic assimilation (Myers et al., 1984). The result is a series of curves similar to those derived by AFC calculations. This solution is unlikely, however, because the range of $^{87}Sr/^{86}Sr$ ratios in the Group 2 basalts would require a contaminant with unrealistically high values of Sr.

5.5 Summary and Discussion

A comparison of samples from three volcanic successions of Early Cretaceous age suggests that they consist of subalkaline basalts (Q-normative tholeiites) with moderate to high TiO_2 contents. All the basalts are within-plate continental tholeiites. Group 1 and 2 basalts are broadly similar in terms of major element chemistry, but show a distinct range of Rb/Sr and $^{87}Sr/^{86}Sr$ ratios. Mantle-normalized trace element patterns resemble those of continental flood basalts, without significant fractionation of HFSE with respect to LREE. The Group 3 basalts form a distinct compositional type. These samples are evolved ferrobasalts with high P_2O_5, Ba and Sr. Trace element patterns resemble those for basaltic rocks of mildly alkaline or alkaline character.

The highly uniform geochemical characteristics of Group 2 basalts in northern and western Axel Heiberg suggest that the stratigraphic correlation between the two areas is probably valid. The suite is characterized by low correlation coefficients for most element-element pairs that should vary concurrently during fractional crystallization. As a result, mass balance fractionation calculations are generally unsuccessful, suggesting the influence of other petrogenetic processes.

The possibility of crustal contamination was examined using trace element and Sr-isotopic data because Group 2 basalts show a restricted range of major element compositions. The combined use of compatible and incompatible trace elements on log-log diagrams indicates that compositional variations in Group 2 basalts can be modelled by a combination of assimilation and fractional crystallization (AFC). In particular, compositional variations in the most evolved basalts can be

explained by an increase in the rate of assimilation for similar degrees of crystallization (30-40%). However, the following constraints apply:

1. Field and petrographic evidence for assimilation (e.g. xenoliths) is lacking in the Group 2 basalts.

2. The AFC model is severely constrained by the unknown nature of parental magmas for this suite. The use of compositions derived from picrites in the trace element modelling is justified on the basis of experimental studies and quantitative models of basalt generation in CFB provinces.

3. The type of contaminant assimilated by the magmas is also unknown. Compositions for the lower and upper crust (Taylor and McLennan, 1985) are used as end-member contaminants in the modelling. The calculations do not provide specific information as to which composition is the most suitable in generating the AFC trends in Group 2 basalts. However, a comparison of Sr-isotopic data for all the Early Cretaceous basalts sampled suggests that contamination by upper crustal rocks could produce the high and variable ratios in Group 2 basalts.

In view of the above limitations, estimates of the amount of crustal contamination undergone by the parental magmas would be highly speculative. Trace element patterns, for example, can be used to determine the degree of enrichment in Th, Ba, Rb, K, Sr, that can result from contamination of a primitive basalt magma by crustal rocks (Pearce, 1983). However, the enrichment caused by assimilation processes may not be perceptible in CFB's, which characteristically show high concentrations of these elements before contamination.

Despite the large number of constraints, and within the limits of the present data base, the AFC model provides the most viable

explanation for compositional variations in the Group 2 basalts. The model also carries some implications for the physical processes that operated during basalt generation in the north-central part of the Sverdrup Basin. For example, what are the changes in the physical conditions of eruption that could have led to enhanced crustal contamination in the later-erupted magmas?

The correlation between crustal assimilation and the time-sequence of eruption during continental magmatism has been addressed in a number of studies. Thermal considerations dictate that magmas ascending through the crust should eventually encounter cooler wallrocks, a process that will contribute to decreased assimilation rates (e.g. DePaolo, 1981). If the volcanic centre remains fixed, small volumes of basaltic magma erupted during the early stages should display the greatest compositional variability as a result of interaction with the enclosing wall-rocks. As the system matures and magmatic conduits become established, subsequent magmas will be insulated from the effects of crustal assimilation and show more coherent geochemical signatures (e.g. Myers et al., 1985).

Field studies in the north-central part of the Sverdrup Basin indicate that volcanic activity peaked during the Late Albian (Chapter 3). There is no evidence for a major shift of the volcanic zone during the Early Cretaceous. The Group 2 basalts were, therefore, erupted from a mature volcanic system.

In continental extensional provinces where later-erupted lavas are the most contaminated, wall-rock assimilation may be caused by:

- longer crustal residence times in areas remote from tectonism or the site of maximum lithospheric thinning (e.g. Singer and Kudo, 1986),

- the underplating of open reservoirs by hot, primitive magma,
- turbulent flow in subvolcanic conduits (Huppert and Sparks, 1985; Kille et al., 1987),
- or rejuvenation of the volcanic plumbing system as a result of a shift in the volcanic zone or a change in the eruptive style (e.g. from central vents to fissure swarms).

Petrographic and geochemical evidence in the Artharber Creek basalts suggests that magma mixing may have operated concurrently with fractionation and assimilation. This is an important observation, as mafic recharge in an open reservoir could provide the additional heat required for assimilation (e.g. O'Hara and Mathews, 1981; Wyers and Barton, 1987). The presence of a broader zone of extensional movements may explain the higher eruption rates and increasing complexity of the system, if primitive magmas were given a renewed opportunity to reach crustal reservoirs and mix with their differentiates. Even without invoking the mixing process, however, it is likely that the emplacement of voluminous flood basalts in a widening tectonic zone involved a change to predominantly fissure-fed eruptions. This process may have enhanced the opportunity for crustal assimilation in newly-established magmatic conduits.

In geochemical terms, this type of evolving magmatic system is best described by Myers et al. (1985):

> "We do, however, note a ***caveat*** to this monotonic advance from small and dirty to big and clean (in arc volcanic plumbing systems). In some instances, a system may become so big and its plumbing so well used that it is unusually hot throughout...In comparison to the original deeper source, the resultant lavas may appear dirty within an otherwise mature system."

Thin successions on northeastern Ellesmere Island reflect minor volcanic activity along the southern margin of the basin during the lower Late Cretaceous. The distinct geochemical character of the basaltic lavas (Group 3) suggests a different petrogenetic history. In Chapter 6, a larger data base for sills and dykes in the same area is used to establish the existence of two compositional types of basic igneous rocks in the east-central Sverdrup Basin.

VI. PETROLOGY AND GEOCHEMISTRY OF INTRUSIVE ROCKS

6.1 Introduction

According to the age determinations summarized in Table 4.1, basic intrusive rocks were emplaced throughout the Early Cretaceous in central and eastern parts of the Sverdrup Basin. The principal aim of this reconnaissance geochemical study was, therefore, to determine the main compositional types, and to establish a comparison with the volcanic rocks. Samples collected from the centre and southern margin of the basin provided an opportunity to examine spatial-compositional variations in all the igneous rocks, regardless of the mode of emplacement.

Because such large volumes of magma were intruded as sills and dykes (Table 1.1), the approach taken is comparable to that used in studies of Phanerozoic flood basalt provinces, where geochemical stratigraphy is the principal means of establishing space-time compositional variations over large areas. In the case of gabbroic rocks, however, several other important variables come into play. Problems of secondary alteration, internal differentiation, and in situ contamination are enhanced as a result of slower cooling rates. The resulting compositional variations must be distinguished from characteristics inherited from the source(s), and modified by fractional crystallization, mixing, wall-rock interaction, etc. The flow rate, for example, is a controlling factor in determining the role of crustal assimilation during magma ascent and emplacement (e.g. Huppert and Sparks, 1985; Kille et al., 1986; Tarney and Weaver, 1987).

The first part of the chapter is descriptive and presents petrographic and geochemical data concerning the four groups of intrusive rocks sampled. The effects of secondary alteration and internal differentiation are examined in the second part, before proceeding to a comparison of compositional types in the central, northern and eastern parts of the study area.

6.2 Characteristics of Intrusive Rocks

6.2.1 Groups A and B: East Axel Heiberg Island and Eureka Sound

Two groups of igneous rocks were sampled in the western part of the study area: dykes of the Lightfoot River area and sills at Buchanan Lake and Blacktop Mountain (locations on Fig. 4.1).

The Lightfoot River Dyke Swarm

Although a large number of dykes intrude the central part of the Sverdrup Basin, Jollimore (1986) recognized two swarms of possible Cretaceous age: the first emplaced along the axis of the basin, and the second in a north-south direction. The dyke swarm at Lightfoot River is part of the latter group and may represent a system of linear feeders related to the emplacement of the Strand Fiord basalts (Chapter 3). The swarm occurs along a 25 km wide belt that can be traced for up to 40 km on air photographs (Fig. 4.2). The dykes are massive and consist of single units that are regularly spaced and vary in thickness from 1 to 60 metres. The age of the Lightfoot River dykes is unknown, however,

the swarm clearly postdates the emplacement of sills and other semi-concordant intrusions in that area.

Group A consists of 15 samples from dykes and 5 samples from sills. Jollimore (1986) reports that all the samples from dykes consist of diabase or gabbro with variable amounts of plagioclase, clinopyroxene and opaque oxides. Portions of the chilled margins of dykes are generally sparsely plagioclase-phyric or contain clusters of plagioclase and augite, suggesting that these phases were the first to crystallize. Towards the centre of dykes, samples vary from fine to medium-grained, with intergranular to sub-ophitic textures, and show a similar primary and secondary mineralogy (Appendix A). Plagioclase crystals (andesine to labradorite) are commonly sericitized and clinopyroxenes consist of augite and are partially or completely replaced by fine clays or intergrown chlorite and biotite. Opaque oxides show an embayed to strongly corroded morphology. Interstitial quartz is found in virtually all the samples. Patches of carbonate and myrmekitic intergrowths are common. Samples from sills in the area are indistinguishable from the dyke rocks on the basis of mineralogy and texture. One notable exception is AX85-005 which contains unaltered grains of olivine.

The geochemical data base for the Lightfoot River area includes ten analyses from Jollimore (1986) as well as additional data acquired for two dykes showing internal differentiation and for the sills mentioned above (Appendix C). In many cases, the samples analysed are from the dyke or sill interior. The range of values for sills and dykes, and analyses from the margin and interior of the two thickest dykes, are shown on Table 6.1. Data for rare earths and additional trace elements are listed in Table 6.2 for a subset of nine samples. The range of

TABLE 6.1
CHEMICAL ANALYSES, GROUP A.

(Wt%)	1	2	3	4	5	6
SiO_2	48.35-53.10	49.78-52.21	49.70	51.14	49.65	50.70
TiO_2	2.14-4.43	2.04-4.40	3.62	3.00	4.32	3.64
Al_2O_3	12.29-15.13	12.21-13.82	13.30	13.74	12.99	14.83
FeOt	11.87-16.04	12.09-14.33	14.21	13.65	13.10	13.10
MnO	0.17-0.26	0.19-0.23	0.24	0.26	0.20	0.19
MgO	3.55-6.27	4.81-6.14	5.01	4.22	5.08	4.14
CaO	7.09-9.36	8.15-10.58	8.35	7.56	8.91	7.09
Na_2O	2.55-3.35	2.24-2.69	3.31	3.62	3.04	3.30
K_2O	0.34-1.47	0.32-1.16	1.14	1.14	0.83	1.26
P_2O_5	0.21-0.67	0.24-0.48	0.41	0.59	0.47	0.67
(H_2O_T +CO_2)	1.68-4.06	2.01-2.84	2.40	2.55	1.91	3.45
Mg#	35.4-47.6	41.3-51.5	42.5	39.3	44.9	39.8
(PPM)						
Rb	9-47	8-39	32	22	26	41
Sr	257-469	225-419	399	313	376	420
Ba	139-616	101-723	582	500	377	242
V	273-515	311-489	444	329	428	372
Cr	6-62	9-77	11	8	45	8
Ni	22-48	28-57	22	21	40	37
Cu	47-205	79-160	52	49	140	173
Zn	68-175	102-148	166	288	113	104
Y	39-64	39-51	39	51	48	59
Zr	195-368	149-295	220	276	301	326
Nb	16-26	12-23	22	26	26	24

KEY

1. Range of values for dykes (N =15)
2. Range of values for sills (N=5)
3. Chilled margin of Dyke 9 (AX85-020, E wall)
4. Interior of Dyke 9 (AX85-019)
5. Chilled margin of Dyke 5 (AX85-037, E Wall)
6. Interior of Dyke 5 (AX85-032)

TABLE 6.2
ADDITIONAL TRACE ELEMENT DATA, GROUP A DYKES

	1	2	3	4	5	6
Sc	35.5	35.9	36.7	34.2	36.6	44.5
Hf	6.5	5.8	7.6	5.6	6.9	5.5
Ta	1.7	1.9	2.0	1.6	1.7	1.6
Th	3.9	2.3	2.6	1.9	2.7	3.7
La	26.9	25.7	24.5	17.0	21.6	25.3
Ce	55.7	54.3	55.6	38.3	48.7	49.8
Sm	8.7	9.1	10.9	8.0	10.4	8.4
Eu	2.71	2.95	3.53	2.87	3.35	2.61
Tb	1.5	1.3	1.8	1.4	1.7	1.6
Yb	4.7	4.4	4.2	3.9	5.0	4.8
Lu	0.7	0.55	0.59	0.51	0.60	0.71
SUM*	100.9	98.3	101.1	72.0	91.4	93.2
Ce/Yb_N	3.0	3.2	3.4	2.5	2.5	2.6

	7	8	9
Sc	37.6	41.5	39.6
Hf	5.0	4.6	4.8
Ta	1.7	1.2	1.9
Th	3.4	2.7	2.0
La	23.8	16.2	24.9
Ce	48.3	35.0	51.9
Sm	7.8	6.9	8.6
Eu	2.61	2.30	3.01
Tb	1.4	1.2	1.5
Yb	4.3	3.9	4.4
Lu	0.62	0.60	0.56
SUM*	88.8	66.1	94.9
Ce/Yb_N	2.9	2.3	3.0

KEY

1: AX85-015
2: AX85-020
3: AX85-026
4: AX85-031
5: AX85-035
6: AX85-040
7: AX85-043
8: AX85-046
9: AX85-048
*: of rare earths

major element contents is similar for dykes and sills in the area (compare 1 and 2, Table 6.1). The SiO_2 and TiO_2 values (48-53%; 2-4%) and relatively low Mg numbers (35-50) suggest that the intrusive rocks consist of evolved, high-Ti gabbros. All the samples display a wide range of K_2O (0.3-1.5%), P_2O_5 (0.2-0.7%) and trace element contents.

Sills and Dykes at Buchanan Lake and Blacktop Mountain

Up to forty sills intrude a 10 km section of Mesozoic strata south of Buchanan Lake (C. Jackson, pers. comm., 1985). Eighteen units were sampled that include sills and thin cross-cutting dykes (Fig. 4.3). The sills vary in thickness between 2 and 50+ metres and consist of massive, concordant or semi-concordant tabular intrusions. Both the chilled margin and interior of units were sampled for geochemical studies. Two sills that showed evidence of internal differentiation were sampled in more detail. Samples from four sills at Blacktop Mountain (Eureka weather station) are also included in this group.

The age determinations on selected samples from Buchanan Lake (Avison, 1987) suggest two pulses of igneous activity in this area. Widespread intrusion of sills may have occurred around 126 Ma, and cross-cutting dykes were emplaced at 113 Ma, an age that corresponds approximately to that of Group 1 basalts. The age of the Blacktop Mountain intrusives is unknown.

Group B consists of 16 samples from the chilled margins of sills and 16 from the interior of units, and includes 3 samples from thin cross-cutting dykes. All the sills show a similar mineralogy that includes abundant plagioclase, augitic clinopyroxene and opaque oxides with an intergranular to sub-ophitic texture. Fine-grained samples of chilled margins often contain phenocrysts of plagioclase and lesser

augite in glomeroporphyritic texture. Pseudomorphs of olivine are rare. Sill interiors show the expected increase in grain size (max. 3mm) and are generally more altered. Common alteration products include sericite after feldspar, chlorite and associated biotite after pyroxene, interstitial quartz, patches of carbonate and rare calcic amphibole. Products of deuteric alteration such as fine-grained biotite occur locally. The sills at Blacktop Ridge show a similar mineralogy and texture.

Samples from thin cross-cutting dykes at Buchanan Lake (Plate 15) are very fine-grained, sparsely plagioclase and olivine-phyric aggregates of plagioclase, augite, olivine and oxides. Plagioclase phenocrysts (1 mm) are clear, show complex oscillatory or sector zoning and occur in clusters. Anhedral olivine phenocrysts are generally less abundant and altered along fractures. Alteration of the groundmass phases is minimal and limited to interstitial glassy areas.

Thirty-five samples from Group B were analysed for major and trace elements. All the data are listed in Appendix C, and selected analyses are shown in Tables 6.3 and 6.4. The range of values for chilled margins is generally representative of the compositional variations in this group. Samples collected at Blacktop Mountain or from the cross-cutting dykes at Buchanan Lake show the highest MgO contents. Geochemical variations from the margin to the centre of units are best observed in sills such as "A" or "E", which display textural evidence of differentiation in the field (Table 6.4).

TABLE 6.3
CHEMICAL ANALYSES, GROUP B

(CHILLED MARGINS OF SILLS, N=16)

(WT%)	RANGE	MEAN	S.D.
SiO_2	49.16-52.0	50.93	0.63
TiO_2	1.79-4.08	2.87	0.70
Al_2O_3	12.36-14.54	13.02	0.50
FeOt	11.73-13.82	12.89	0.65
MnO	0.19-0.25	0.21	0.02
MgO	4.43-6.57	5.48	0.58
CaO	7.50-11.35	9.34	1.01
Na_2O	2.02-3.75	2.77	0.46
K_2O	0.35-1.04	0.60	0.22
P_2O_5	0.18-0.48	0.33	0.10
$(H_2O_T+CO_2)$	0.70-4.24	2.01	1.00
Mg#	40.9-52.8	47.1	3.5
(PPM)			
Rb	9-40	21	8
Sr	127-454	274	88
Ba	83-269	168	57
V	313-494	408	45
Cr	15-128	46	34
Ni	28-65	40	10
Cu	48-219	131	48
Zn	77-211	144	32
Y	32-50	41	5
Zr	144-269	203	42
Nb	10-23	16	4

TABLE 6.4
REPRESENTATIVE CHEMICAL ANALYSES, GROUP B

	1A	1B	2	3	4
SiO_2	51.95	52.78	50.61	56.77	50.76
TiO_2	2.20	2.22	2.38	2.43	1.91
Al_2O_3	13.14	13.70	12.36	12.68	13.88
FeOt	12.70	11.77	12.40	12.67	12.03
MnO	0.21	0.22	0.20	0.25	0.19
MgO	4.92	4.75	6.57	3.12	6.60
CaO	9.21	9.03	10.62	6.31	11.17
Na_2O	2.72	2.85	2.02	3.50	2.17
K_2O	0.56	0.77	0.52	1.27	0.18
P_2O_5	0.26	0.29	0.23	0.60	0.18
(H_2O_T+ CO_2)	2.45	2.21	1.60	3.92	1.78
Mg#	44.8	45.8	52.6	34.0	53.5
(PPM)					
Rb	10	26	18	23	7
Sr	409	248	282	247	200
Ba	145	222	96	220	109
V	426	376	419	135	350
Cr	40	46	94	1	102
Ni	39	33	47	26	49
Cu	174	77	93	22	168
Zn	146	130	125	173	107
Y	42	45	37	70	34
Zr	268	231	160	367	148
Nb	22	22	14	32	11

KEY

1: Interior of sill. (A) Buchanan Lake AX85-239;
(B) Blacktop Ridge EL85-202
2: Chilled margin of differentiated sill E, AX85-223
3: Interior of sill E, AX85-225
4: Representative analysis of cross-cutting dykes (AX85-067, dyke R).

6.2.2 Groups C and D: Northeastern Ellesmere Island

Intrusive rocks were sampled in two areas of the eastern Sverdrup Basin: Tanquary Fiord and the Lake Hazen-Piper Pass area (locations on Fig. 4.1). In both areas, sills intrude upper Paleozoic and Mesozoic strata of the Sverdrup Basin. ***Group C*** consists of samples from ten sills collected at the head of Tanquary Fiord. Most of the intrusions consist of massive, concordant sheets in sharp contact with the host sedimentary rocks. ***Group D*** consists of samples from ten sills and four dykes measured at Lake Hazen and Piper Pass. The sills are generally massive and vary in thickness between 8 and 90 metres. Thick dykes near Piper Pass feed concordant intrusions that systematically intrude Permo-Triassic strata. Differentiated sills are relatively uncommon in the eastern part of the study area. Osadetz and Moore (in press) report the presence of a layered intrusion near Ekblaw Lake, and two more differentiated units were identified during this study, one of which is a composite intrusion (Plate 20). Samples of chilled margins from these intrusions were included in Groups C and D (Appendix A).

The age determinations of Avison (1987) suggest that igneous rocks in the Lake Hazen-Piper Pass area constitute a volcanic-intrusive complex emplaced at *c*. 91 Ma. The age of intrusive rocks near Tanquary Fiord is unknown (Table 4.1).

All the igneous rocks sampled in this area contain plagioclase, augitic clinopyroxene, opaque oxides and olivine (see modal counts, Appendix A). The Group C gabbros are medium-grained and holocrystalline, and may show up to 3% euhedral apatite. Crystals of clinopyroxene typically form reddish-brown elongate prisms with moderate

pleochroism, or display a skeletal morphology. Most of the Group D samples are fine-grained and hypocrystalline, and contain anhedral plates of beige to colourless augite. Plagioclase phenocrysts occur in most samples from chilled margins.

In the Group C gabbros, secondary alteration products consist of clays (after feldspars, augite, olivine and minor interstitial glass), rare amphibole, carbonates or quartz. Clays replace glass and mafic phases, and are often mixed with carbonates in Group D samples. In all the gabbros, textures vary from intergranular to sub-ophitic and are intersertal in samples from chilled margins.

A study of plagioclase and clinopyroxene mineralogy was carried out on selected samples from both groups. Representative analyses for each of these phases are listed in Table 6.5 and plotted in classification diagrams on Figure 6.1. In both groups, plagioclase chiefly consists of labradorite and minor andesine. Despite some overlap in the field of augite, most of the Group C pyroxenes analysed cluster in the field of salite. The Ca-rich pyroxene in the Group D samples is augite.

Major and trace elements were determined on a total of 25 samples from the two areas. All but 3 samples are from the chilled margins of sills or dykes. The range of values and average analysis for each group are listed in Table 6.6. Data for rare earths and additional trace elements are listed in Table 6.7 for a subset of 7 samples. As indicated by average analyses, the range of major element contents is similar in both groups. All the samples consist of evolved high-Ti gabbros with SiO_2 in the range 45-50%, moderately high iron contents (FeOt = 12-15%) and Mg numbers of 42 to 53. Higher P_2O_5 values to a maximum of 1 % in the Group C gabbros reflect the modal content of

TABLE 6.5
REPRESENTATIVE MINERAL ANALYSES*, GROUPS C AND D

PLAGIOCLASE (Group C)

	EL84-218	EL84-222				
	G	G_C	$P1_C$	$P1_R$	$P2_C$	$P2_R$
SiO_2	52.94	56.25	53.30	56.23	59.19	57.30
Al_2O_3	29.36	27.11	28.74	27.33	25.43	26.35
CaO	11.95	9.90	12.11	9.80	7.69	8.93
Na_2O	4.71	5.92	5.07	5.93	7.51	6.85
K_2O	0.70	0.30	0.25	0.33	0.46	0.40
Total	99.66	99.48	99.47	99.62	100.28	99.83
Mol per cent						
An	56	47	56	47	35	41
Ab	40	51	42	51	62	57
Or	4	2	2	2	3	2

	EL84-235			
	P_C	P_R	G1	G2
SiO_2	51.36	56.87	54.29	49.67
Al_2O_3	29.79	26.45	28.79	30.32
CaO	13.28	9.07	11.61	14.88
Na_2O	3.70	6.28	5.14	3.25
K_2O	0.30	0.47	0.36	0.17
Total	98.43	99.14	100.19	98.29
Mol per cent				
An	65	43	54	71
Ab	33	54	44	28
Or	2	3	2	2

* Representative analyses of single grains (these are numbered to illustrate variations in mineral chemistry)
Symbols: G groundmass; P_C, core; P_R, rim of phenocryst
FeO*, total iron as FeO.

TABLE 6.5 (continued)

PLAGIOCLASE (Group D)

	EL84-041			EL84-050		
	G	P_C	P_R	G	P_C	P_R
SiO_2	52.15	51.80	54.49	53.17	51.25	54.87
Al_2O_3	29.49	29.70	26.94	28.48	29.98	27.94
CaO	12.93	13.08	11.27	12.04	13.91	10.97
Na_2O	3.79	3.68	4.94	5.14	4.11	5.83
K_2O	0.12	0.20	0.36	0.38	0.31	0.47
Total	98.48	98.46	98.00	99.21	99.56	100.08
Mol per cent						
An	65	65	55	55	64	50
Ab	34	34	43	43	34	48
Or	1	1	2	2	2	2

	EL84-056	
	G1	G2
SiO_2	53.29	60.30
Al_2O_3	28.23	25.16
CaO	12.14	7.12
Na_2O	4.40	6.77
K_2O	0.36	0.89
Total	98.42	100.24
Mol per cent		
An	59	35
Ab	39	60
Or	2	5

TABLE 6.5 (continued)

PYROXENE (Group C)

	EL84-218		EL84-222		EL84-235
	G_C	G_R	$G1_C$	$G2_C$	G
SiO_2	45.22	46.87	51.50	49.05	45.75
TiO_2	3.68	2.65	0.91	1.90	3.25
Al_2O_3	6.38	4.95	1.88	3.85	6.38
Cr_2O_3	0.00	0.00	0.04	0.04	0.00
FeO*	11.02	11.33	10.61	11.01	10.98
MnO	0.24	0.26	0.40	0.39	0.31
MgO	11.57	11.75	15.68	14.09	12.28
CaO	21.81	21.45	19.30	19.98	21.61
Na_2O	0.49	0.45	0.30	0.48	0.50
Total	100.41	99.71	100.62	100.79	101.06
zSi	1.698	1.772	1.908	1.818	1.701
zAl^{IV}	0.302	0.228	0.092	0.182	0.299
yAl^{VI}	-0.020	-0.007	-0.010	-0.014	-0.020
yTi	0.105	0.076	0.026	0.053	0.092
yFe^{3+}	0.146	0.115	0.071	0.122	0.171
yFe^{2+}	0.121	0.154	0.046	0.059	0.077
yCr	0.000	0.000	0.001	0.001	0.000
yMg	0.648	0.662	0.866	0.778	0.680
xFe^{2+}	0.079	0.090	0.211	0.160	0.093
xMn	0.008	0.008	0.001	0.012	0.010
xCa	0.878	0.869	0.766	0.793	0.861
xNa	0.036	0.033	0.022	0.034	0.036
SUM	4.000	4.000	4.000	4.000	4.000

TABLE 6.5 (continued)

PYROXENE (Group D)

	EL84-041			EL84-050		EL84-056	
	Gl_C	Gl_R	$G2_C$	G1	G2	G1	G2
SiO_2	47.70	49.05	49.64	50.87	49.04	50.57	51.09
TiO_2	2.33	1.64	1.55	1.42	2.16	1.47	0.77
Al_2O_3	4.87	3.94	3.52	3.13	3.94	2.73	1.08
Cr_2O_3	0.07	0.24	0.00	0.15	0.00	0.03	0.00
FeO*	9.59	8.43	8.31	9.21	11.05	9.78	18.67
MnO	0.21	0.24	0.06	0.28	0.25	0.32	0.54
MgO	13.02	14.13	14.42	14.70	13.54	14.66	11.32
CaO	21.31	21.32	21.67	20.38	19.94	20.16	17.04
Na_2O	0.38	0.29	0.30	0.58	0.48	0.30	0.30
Total	99.47	99.28	99.47	100.72	100.40	100.02	100.81
Si	1.793	1.836	1.851	1.911	1.829	1.883	1.951
Ti_{IV}	0.066	0.046	0.043	0.029	0.061	0.041	0.022
Al^{IV}	0.207	0.164	0.149	0.088	0.171	0.117	0.049
Al^{VI}	0.009	0.010	0.006	0.000	0.002	0.003	0.000
Cr	0.002	0.007	0.000	0.003	0.000	0.001	0.000
Fe	0.302	0.264	0.259	0.348	0.345	0.304	0.596
Mn	0.007	0.008	0.002	0.009	0.008	0.010	0.017
Mg	0.730	0.789	0.802	0.892	0.753	0.814	0.645
Ca	0.858	0.855	0.866	0.683	0.797	0.804	0.697
Na	0.028	0.021	0.022	0.036	0.035	0.022	0.022
X	0.886	0.876	0.888	0.719	0.788	0.826	0.719
Y	1.116	1.124	1.112	1.281	1.169	1.173	1.280
Z	2.000	2.000	2.000	2.000	2.000	2.000	2.000

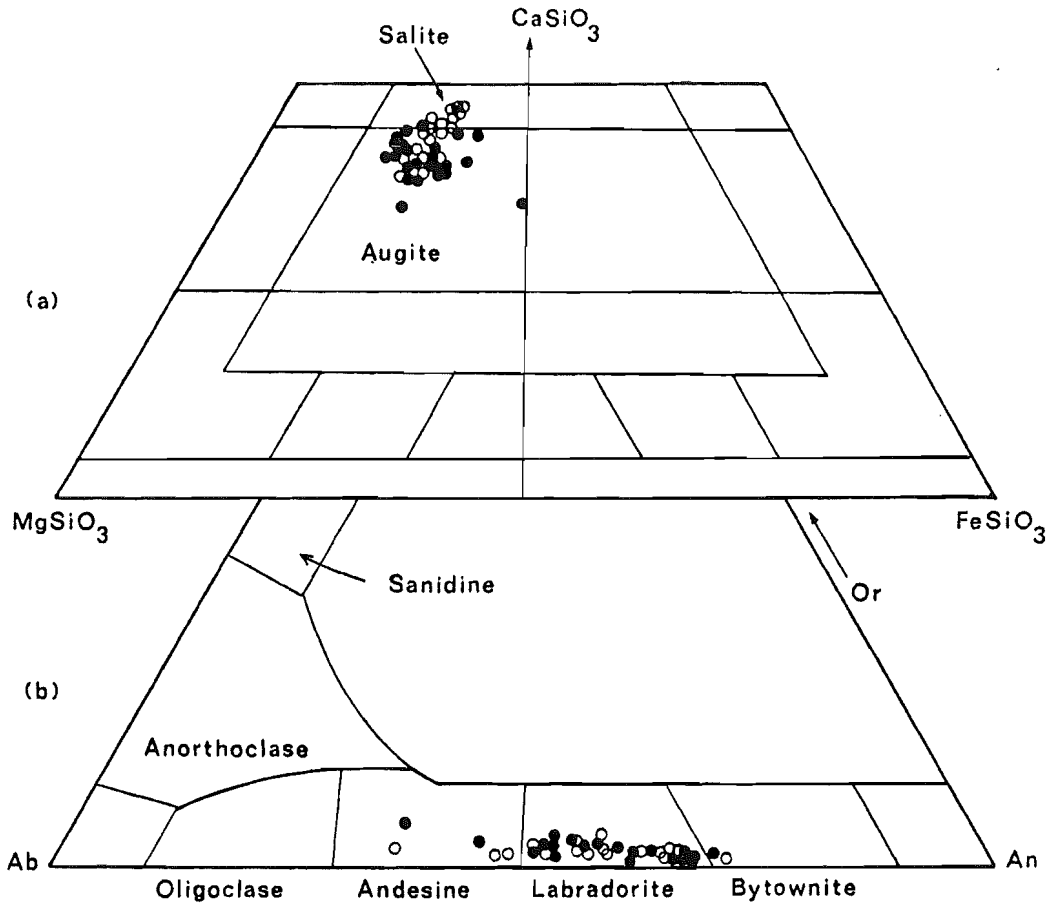

Figure 6.1 (a) Pyroxene compositions in selected samples from Groups C and D, plotted in the pyroxene quadrilateral.
(b) Ab-Or-An plot of feldspar compositions in selected samples from Groups C and D.
Symbols: Open circle, Group C; Filled circle, Group D.

TABLE 6.6
CHEMICAL ANALYSES, GROUPS C AND D

	1	2	3	4	5
SiO_2	45.0-48.8	47.3	46.5-49.9	48.4	47.9
TiO_2	3.1-4.5	3.7	3.2-4.0	3.6	3.7
Al_2O_3	12.8-14.9	14.1	12.6-14.4	13.6	13.8
FeOt	12.3-14.8	13.6	12.8-14.2	13.7	13.7
MnO	0.17-0.25	0.21	0.15-0.21	0.19	0.20
MgO	4.9-6.9	5.7	4.8-5.7	5.2	5.4
CaO	7.5-10.9	9.6	7.8-9.7	9.1	9.3
Na_2O	2.1-4.5	2.9	2.6-4.3	3.0	3.0
K_2O	0.32-1.06	0.71	0.84-1.4	1.07	0.91
P_2O_5	0.42-1.04	0.70	0.37-0.47	0.40	0.53
$[H_2O_T+CO_2]$	2.74-7.68	4.24	0.51-8.79	2.75	3.49
Mg#	43.1-52.9		41.6-47.8		
Rb	9-27	18	16-35	28	24
Sr	382-572	480	461-583	520	502
Ba	129-793	424	291-625	387	404
V	278-448	324	327-420	363	346
Cr	16-63	38	20-107	33	35
Ni	26-66	36	19-68	31	33
Cu	5-43	28	31-104	48	39
Zn	73-156	121	79-169	123	122
Y	26-38	31	27-36	30	31
Zr	139-214	181	189-282	211	198
Nb	22-29	25	30-41	32	29

KEY:

1: Chemical range, Group C (N=11)
2: Average, Group C.
3: Chemical range, Group D (N=14)
4: Average, Group D
5: Average analysis, NE Ellesmere intrusives (N=25)

TABLE 6.7
ADDITIONAL TRACE ELEMENT DATA, GROUPS C AND D

	1	2	3	4	5	6	7
Sc	29.9	29.0	22.1	27.9	30.0	21.7	27.9
Hf	6.0	4.3	4.6	5.3	7.7	5.7	5.2
Ta	2.6	2.1	2.2	2.9	3.7	5.5	2.9
Th	3.4	2.8	3.2	3.2	4.0	3.4	3.4
La	27.9	25.8	24.2	25.6	34.5	26.8	26.7
Ce	58.0	54.0	51.0	51.0	70.0	55.0	55.0
Sm	9.0	8.6	7.7	7.6	10.4	8.1	7.8
Eu	2.57	4.06	2.66	2.41	3.21	2.64	2.50
Tb	1.30	0.91	1.00	1.00	1.10	1.20	1.20
Yb	2.90	2.60	2.40	2.50	3.20	2.40	2.90
Lu	0.39	0.37	0.28	0.32	0.39	0.33	0.34
SUM*	102.1	96.3	89.2	90.4	122.8	96.5	96.4
Ce/Yb_N	5.1	5.3	5.4	5.2	5.6	5.9	4.8

KEY

Group C	Group D
1: EL84-211	5: EL84-050
2: EL84-218	6: EL84-056
3: EL84-235	7: EL84-210
4: EL84-023	*: of rare earths

apatite in these rocks. Both groups show a similar range of Sr and Ba, but K and Rb reach higher values in Group D. Cu contents are unusually low in all but one sample.

6.3 Petrochemical studies

In the following section, geochemical data on eighty samples from dykes and sills are used to establish the major compositional types present across the study area. The effects of secondary alteration and internal differentiation are evaluated before chemical variations among dykes and sills are considered. Tables of correlation coefficients and other statistical data mentioned in the text are located in Appendix C.

6.3.1 Alteration Effects

Secondary alteration is more evident in the intrusive rocks, and affects all the major mineral phases. Plagioclase crystals are partially or completely replaced by sericite or saussurite. Clinopyroxenes are more resistant to alteration but often show incipient replacement by fine clays, intergrown chlorite and biotite and, in rare cases, amphibole. Olivines are usually clay pseudomorphs, except in the case of the Group C and D gabbros: these samples contain an iron-rich, granular variety that is partially replaced by fine-grained oxides rather than clays. Finally, interstitial glass in samples from chilled margins is always replaced by carbonates, clays and/or quartz. This type of alteration is particularly noticeable in samples from the Piper Pass area.

The effects of alteration in selected intrusive rocks were examined using the normalization method described in Chapter 5, i.e. the variations for selected major and trace elements in five samples of altered vs. (relatively) unaltered gabbros were calculated for anhydrous compositions as percentage change in the ratio element/TiO_2. The assumption is that the effects of weathering and deuteric alteration were comparable for magmas intruding similar host rocks in the same area. The results are illustrated on Figure 6.2. The significant variations observed for CaO, the alkalies, Ba, Rb, Sr, Ni and Cr, indicate that these elements are nearly always affected by weathering and deuteric alteration. However, many elements do not show systematic variations as a function of (H_2O_T+CO_2). This was also observed in altered volcanic rocks and suggests differences in the primary mineralogy of samples or mobilization by other processes (e.g. Ba, Cr, Ni on Figs. 6.2 and 5.3). The effect may be enhanced in intrusive rocks because individual samples were chosen from separate sills, with the added uncertainty concerning the age of emplacement. The small degree of variation in Y, Zr and Nb contents suggests that these trace elements constitute reliable geochemical indicators.

The samples of gabbro discussed in this chapter (e.g. Tables 6.1, 6.3, 6.4) generally contain between 1.5 and 4 % (H_2O_{TOT}+CO_2). Samples with higher volatile contents (Table 6.6) were not included on geochemical diagrams using values for CaO, the alkalies or LIL elements. All the data are shown on plots using TiO_2, P_2O_5 and the high-field strength elements.

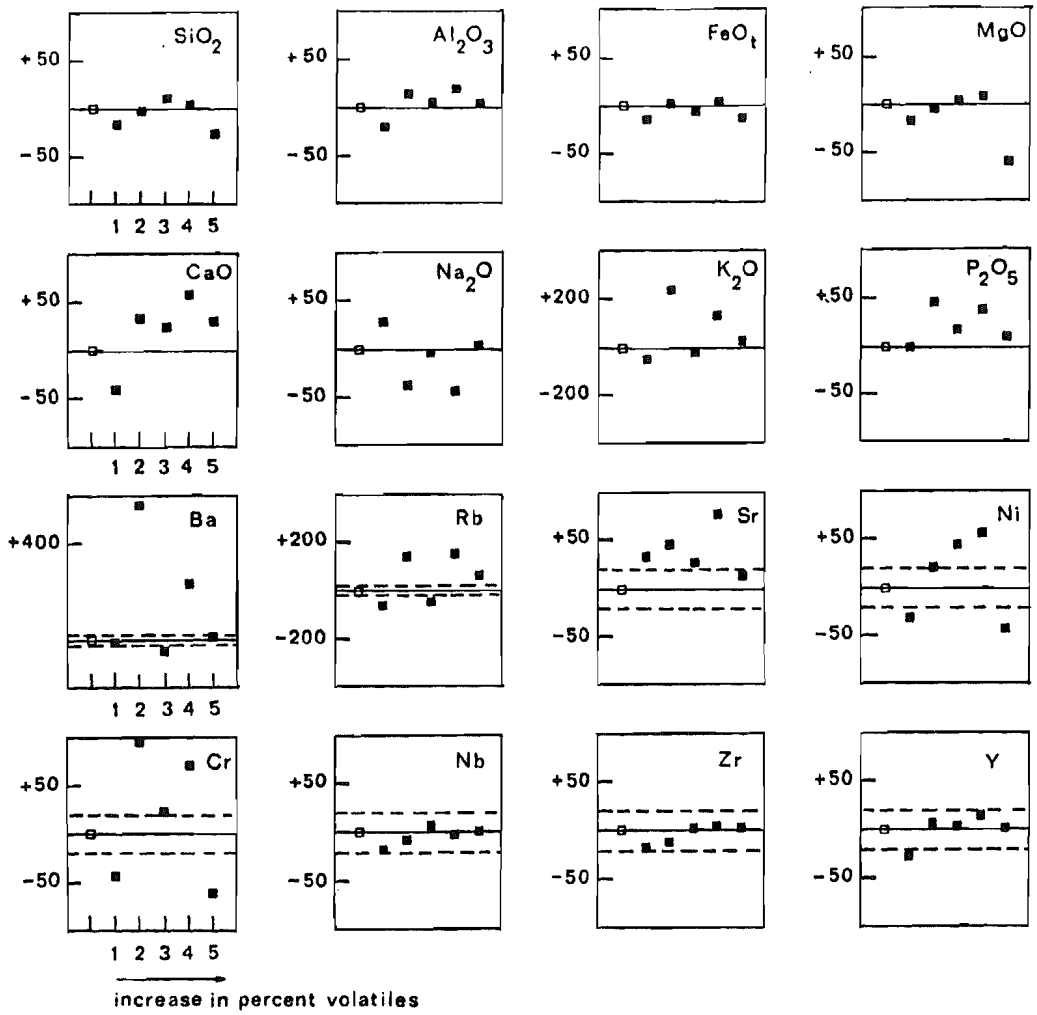

Figure 6.2 Percentage change of major and trace elements relative to TiO_2 in selected samples from Groups B, C and D (ordinate calculated according to Nesbitt, 1979; see caption, Fig. 5.3 for details). A change in ratio greater than 20 % is considered significant for trace element data (shown by dashed lines). Note the change in scale for K_2O, Ba and Rb. The abcissa shows the samples in order of increasing weight % ($H_2O_{TOT}+CO_2$). Symbols: unaltered rock, open square; altered gabbro, filled square. Unaltered and altered rock samples belong to separate sills in the same area; except in the case of [5], where both samples are from the same unit. Key to numbers and corresponding % ($H_2O_{TOT}+CO_2$): [1] AX85-061 (3.73); [2] EL84-245 (4.62); [3] EL84-044 (6.96); [4] EL84-232 (7.68); [5] EL84-052 (14.99). Further details are given in Table C-5.

6.3.2 Intradyke or -sill Chemical Variations

Chemical profiles across individual intrusive bodies provide useful information concerning the processes that operated during the emplacement and cooling of magmas. Compositional variations across dykes or sills can be caused by post-emplacement differentiation, flow segregation, crustal contamination and the relative abundance of subsequently altered glass, or be linked to processes at the source of magmatism, such as the tapping of a zoned magma reservoir, the effects of continuous partial melting, etc. A mafic to felsic trend from the margin to the interior of units usually reflects in situ, post-emplacement crystallization. Chemical variations of this type include an increase in SiO_2, Al_2O_3, the alkalies, FeO, TiO_2 and P_2O_5, and incompatible trace elements, and a decrease in CaO, MgO and compatible trace elements (e.g. Steele and Ragland, 1976). The opposite trend might be caused by the segregation of high-temperature phases away from the margins during laminar flow (Bahttacharji, 1967), resulting in less evolved compositions near the centre of intrusions, or by the concentration of felsic components and some trace elements in early partial melts, causing an enrichment at the dyke margins (Ross, 1983). The effects of crustal assimilation are more difficult to establish, particularly if field evidence is lacking. From thermal considerations, Huppert and Sparks (1985) conclude that a basic magma should selectively assimilate fusible rock types during turbulent flow, and fail to develop a chilled margin. The field evidence of Kille et al. (1986) indicate that this process can indeed operate in dyke-like conduits.

Approximately 10 % of the intrusions sampled showed clear evidence of internal differentiation in the field. The most common type involves a progressive change from fine-grained, dark grey diabase near the margins of sills, to coarser, leucocratic gabbro near the centre. Composite or layered sills are relatively uncommon (see Chapter 4). However, asymmetric layering is characteristic of differentiated dykes in the Lightfoot River area.

Compositional variations were examined in one dyke and two sills. Dyke 5, from the Lightfoot River area, displays crude zoning within 10 to 15 metres of the west wall. The zones consist of irregular veins of fine-grained, pale grey diabase that could represent disrupted or truncated layers. This dyke also contains a partially assimilated xenolith. Both Sills A and E are exposed on the south shore of Buchanan Lake, and show evidence of internal differentiation. Sill A is massive up to 24 metres, where a 4 metre zone of more feldspathic, pegmatitic diabase occurs (poorly defined pods and veinlets showing rapid crystal size variations). Sill E displays a progressive transition from fine-grained, mafic diabase near the margins, to coarser, leucocratic gabbro near the centre.

Chemical profiles across these intrusions are shown on Figure 6.3. Sill E displays a straightforward mafic to felsic trend from the margins to the centre of the intrusion i.e. SiO_2, the alkalies and incompatible trace elements increase, while MgO and CaO decrease. Chemical variations in Sill A are not as marked, but suggest the opposite trend i.e. somewhat less evolved compositions near the centre of the intrusion. The data for Dyke 5 are more complex. Overall, the most evolved compositions occur near the centre of the dyke - this is

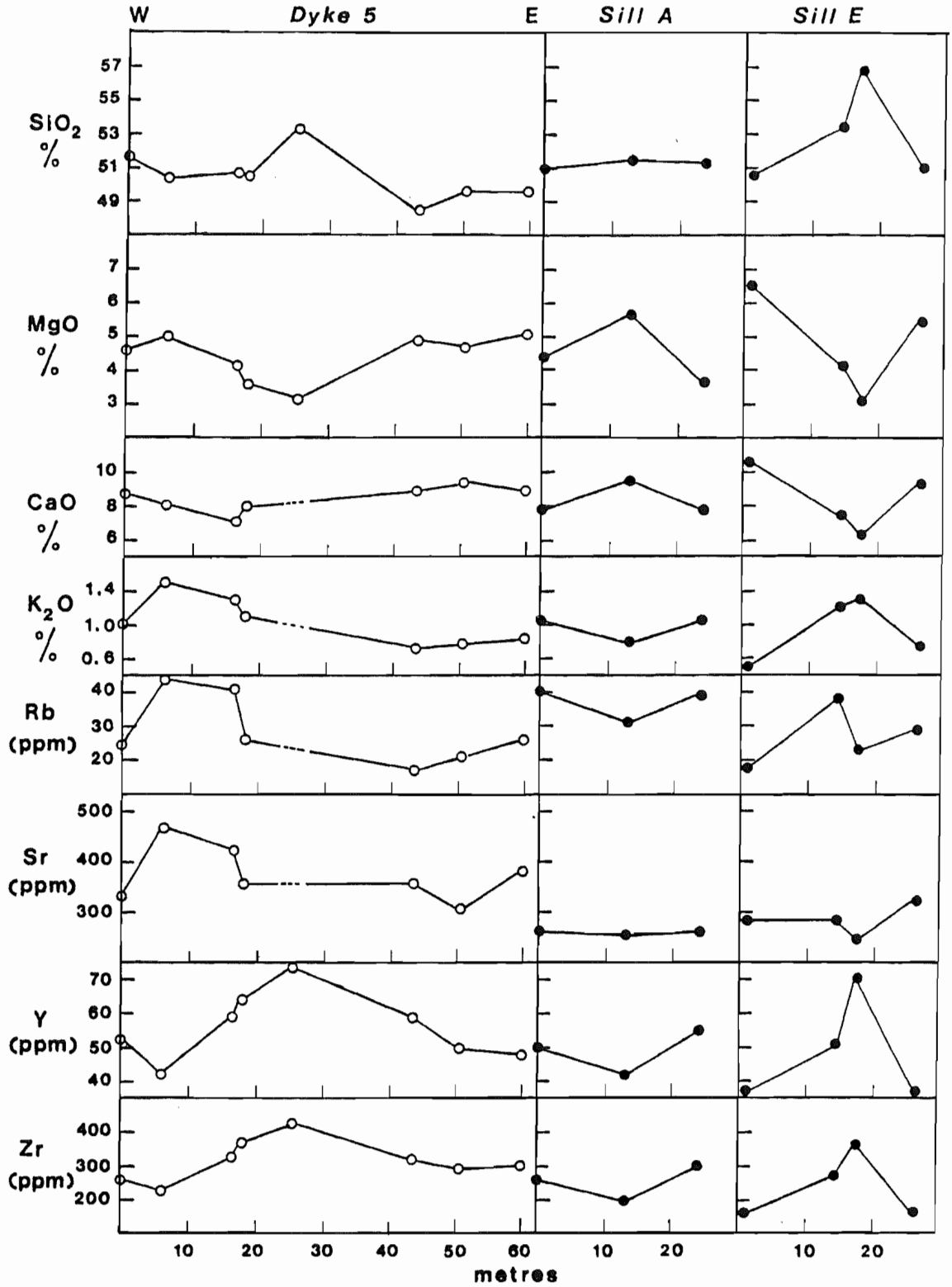

Figure 6.3 Compositional variations across a dyke from the Lightfoot River area, and two sills at Buchanan Lake. Data for CaO, K_2O, Rb and Sr were omitted for AX85-034, a highly altered sample from the centre of the dyke ($H_2O_{TOT}+CO_2$ = 7.6%).

particularly well illustrated by variations in SiO_2, MgO and the high field-strength elements. However, the western margin of the dyke is characterized by a geochemical anomaly where SiO_2, K_2O, Rb and Sr show higher values than along the east margin, while CaO, MgO, Y, Zr and TiO_2 (not shown on Fig. 6.3) are relatively depleted.

The patterns are interpreted as follows:

1. The mafic to felsic trend observed in Dyke 5 and Sill E likely reflects post-emplacement differentiation, i.e. the injection of a single pulse of magma that crystallized as a closed system (Irvine, 1979).

2. In Sill A, the chemical variations are consistent with flow differentiation processes that concentrate early crystallizing phases at the centre of the intrusion, producing felsic margins.

3. The asymmetric chemical variations along the margins of Dyke 5 cannot be as a result of the flow segregation process. Petrographic observations rule out a possible correlation with modal glass content, or the degree and type of secondary alteration. The internal structures along the west wall and the presence of a xenolith suggest that the initial composition of the magma may have been modified by crustal assimilation during ascent and emplacement. Selective enrichment of some elements such as potassium can occur during contamination of basic magmas by continental crust. This process would also affect SiO_2 and LIL elements as a result of their high concentrations in crustal rocks (Pearce, 1983). Compositional variations of this type may be caused by the selective assimilation of highly fusible rock types as a result of turbulent flow in magmatic conduits (e.g. Kille et al., 1986).

6.3.3 Interdyke and -sill Chemical Variations

Pearson correlation coefficients for element-element pairs in Groups A, B and C-D are listed in Table C-6. Few of the coefficients in Groups A and C-D are significant at the 0.1 % confidence level. In contrast, the Group B samples show a much greater number of significant correlation coefficients for major and trace elements.

To illustrate these results, plots of SiO_2, FeO total, CaO, TiO_2, P_2O_5, Y and Cr against MgO are shown on Figure 6.4. In Group B, samples from chilled margins plot along the same trend as those from sill interiors. Most of the variations observed are consistent with gabbro fractionation, for example the progressive enrichment of SiO_2, FeO, TiO_2, P_2O_5 and incompatible trace elements (e.g. Y), and depletion in CaO, Al_2O_3 (not shown) and compatible trace elements (e.g. Cr) in successive residual liquids. The samples from Blacktop Mountain also follow the same trend, and represent some of the least evolved gabbros in this series, along with samples from younger cross-cutting dykes.

As expected from the low correlation coefficients, samples from Groups C and D do not follow any single trend on two-element variation diagrams. In general, the Group C gabbros show the greatest amount of geochemical variation and are somewhat less evolved than the Group D samples. The latter also show low P_2O_5 values (0.37-0.47 %) that contrast with higher, variable contents in the Tanquary Fiord sills (0.42-1.04 %). Low CaO values (enclosed by the dotted line on Fig. 6.4) are only found in samples of chilled margins with substantial amounts of glass (see modal contents, Appendix A). This suggests that leaching

Figure 6.4 Two-element variation diagrams for Group B, C and D intrusives.

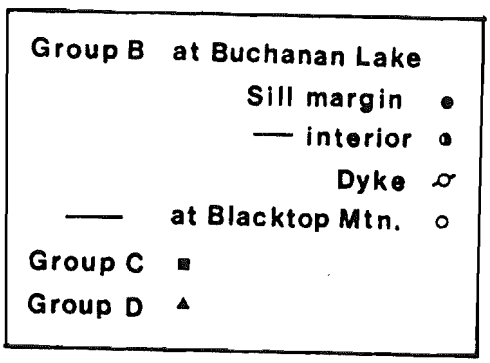

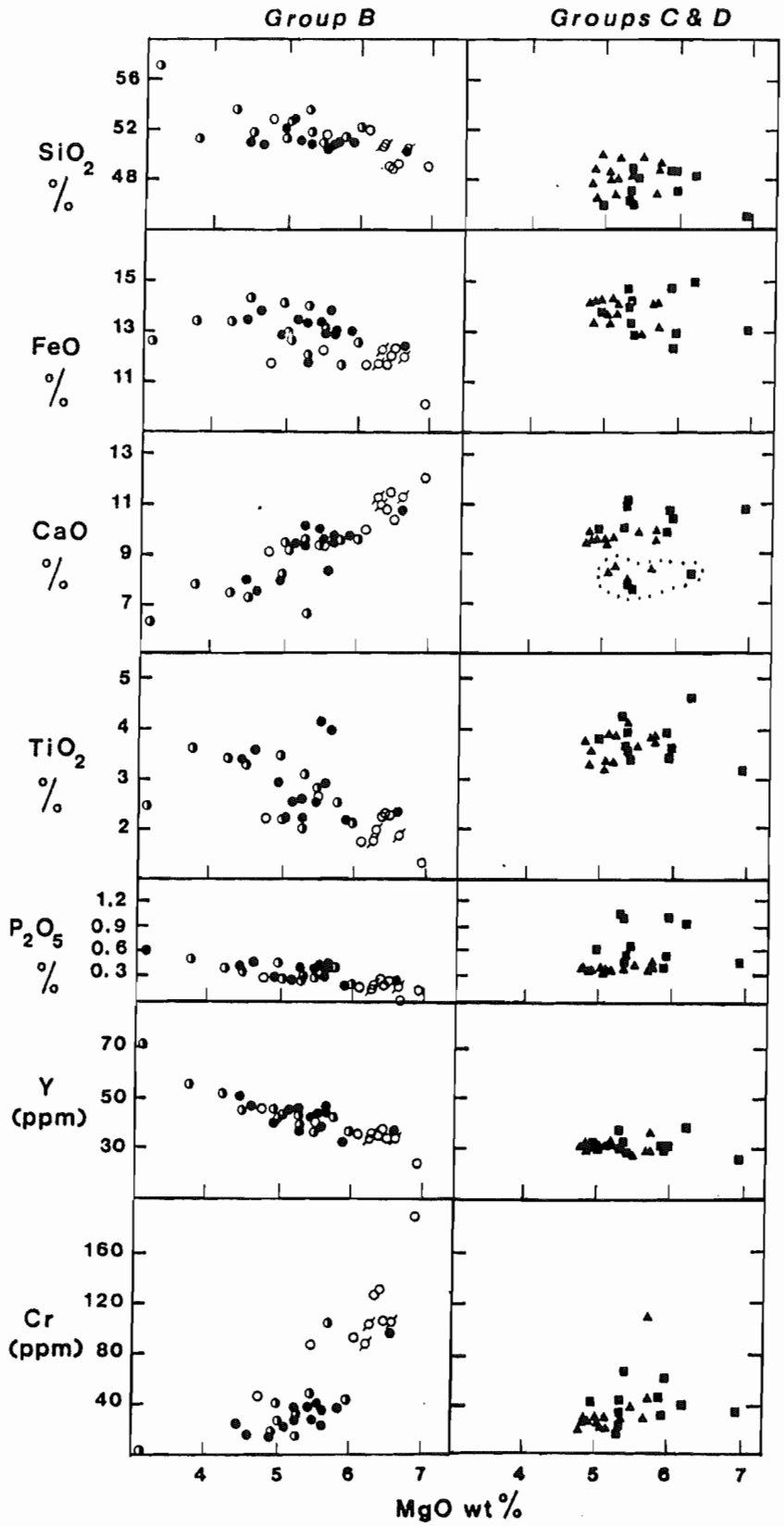
Group B
Groups C & D
SiO2 %
56
52
48
FeO %
15
13
11
CaO %
13
11
9
7
TiO2 %
5
4
3
2
P2O5 %
1.2
0.9
0.6
0.3
Y (ppm)
70
50
30
Cr (ppm)
160
120
80
40
4
5
6
7
MgO wt %

FIGURE 6.4

along the margins of intrusions may have been an additional cause of element mobility in these rocks.

6.3.4 Compositional Types

Samples from all three groups of intrusive rocks are plotted in classification diagrams on Figure 6.5. Despite the differences in intrusive style, sampling location within units, geographic area and ?age, the Group A and B gabbros are broadly similar in composition (compare Table 6.3 with #'s 1 and 2, Table 6.1). Samples from both groups plot in the subalkaline field on the total alkalies vs. SiO_2 diagram (Fig. 6.5 a), and with few exceptions, can be classified as quartz-normative tholeiites (Fig. 6.5 b). According to the alkali-silica classification, the Group C and D gabbros are mildly alkaline. This is consistent with their normative mineralogy (CIPW, Appendix C): the majority of samples are olivine tholeiites, though a small number plot in the nepheline- and quartz-normative fields (Fig. 6.5 b). The wide range of normative compositions is characteristic, as illustrated by the data of Osadetz and Moore (in press).

The cotectic curves for the equilibria oliv + plag + cpx + basaltic liquid at 1 atmosphere and 9 kb (from Thompson, 1982) are also shown on Figure 6.5 (b). All the data for basic intrusive rocks suggest equilibration within the upper crust. The dense cluster of points between the Di-Hy join and the 1 atm cotectic largely consists of compositions for the Group A and B gabbros, and indicates equilibration in near-surface reservoirs. In the case of Groups C and D, magmas may have reached cotectic equilibria at somewhat greater depths in the

Figure 6.5 Classification diagrams showing the position of samples from Groups A, B, C and D.
(a) Total alkalies vs. silica diagram (after Irvine and Baragar, 1970).
(b) Normative ***di***, ***ol***, ***hy***, and ***ne*** or ***qz*** (CIPW, weight per cent; Appendix C). The cotectic curves at 1 atmosphere and 9 kb (anhydrous) are for the equilibria oliv+plag+cpx+liq (data sources in Thompson, 1982). The arrows mark the direction of falling temperature.

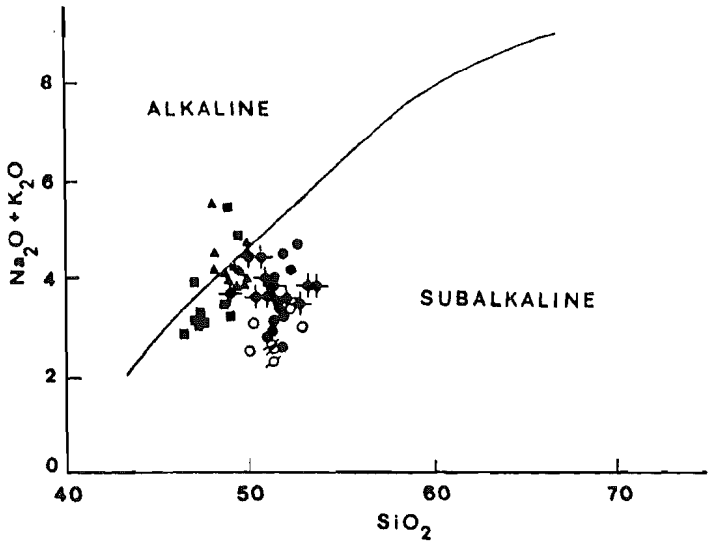

(a)

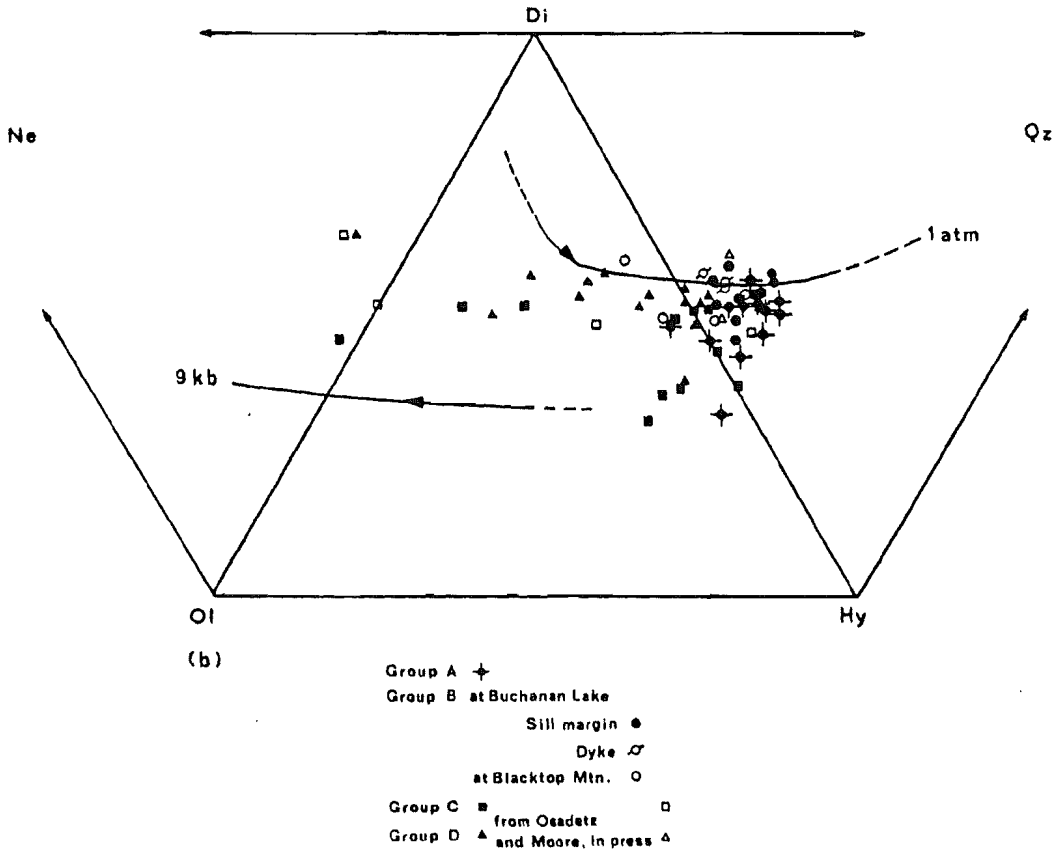

(b)

Group A ✦
Group B at Buchanan Lake
Sill margin ●
Dyke ⌀
at Blacktop Mtn. ○
Group C ■ from Osadetz and Moore, in press □
Group D ▲ from Osadetz and Moore, in press △

FIGURE 6.5

crust, in a pressure range of 5-10 kb. Similar results are obtained using the CMAS projections of O'Hara (1968).

Compositional differences between the subalkaline and mildly alkaline gabbros are more obvious when trace elements are considered. Mantle-normalized trace element patterns for the Group A, C and D intrusives are shown in Figure 6.6. The relative enrichment in Rb and Ba with respect to high-field strength and rare earth elements is most pronounced in the Group A and C gabbros. The spread in data for these two trace elements probably reflects post-emplacement alteration (Fig. 6.2). Group D samples show the smoothest patterns, and enrichment in Nb relative to the LREE. Variable Th contents are only found in the Group A dykes, and differences in P and Ti contents are most pronounced in the Group A and C gabbros.

Normalized trace-element contents in the Group 3 basalts compare favourably with those of Group C. The pattern on Figure 6.6 displays similar geochemical anomalies (probably as a result of fractionation) and relative enrichment of highly incompatible elements (compare with pattern for sample EL84-218, Group C).

Ratios of high-field strength elements and the more pronounced enrichment in LREE (Ce/Yb_N = 5-6) in the Group C and D gabbros are typical of mildly alkaline igneous rocks. The contrast with subalkaline gabbros from Group A is evident on the Ti-Zr-Y diagram (Fig. 6.7), and on plots of chondrite-normalized REE abundances against increasing atomic number (Fig. 6.8).

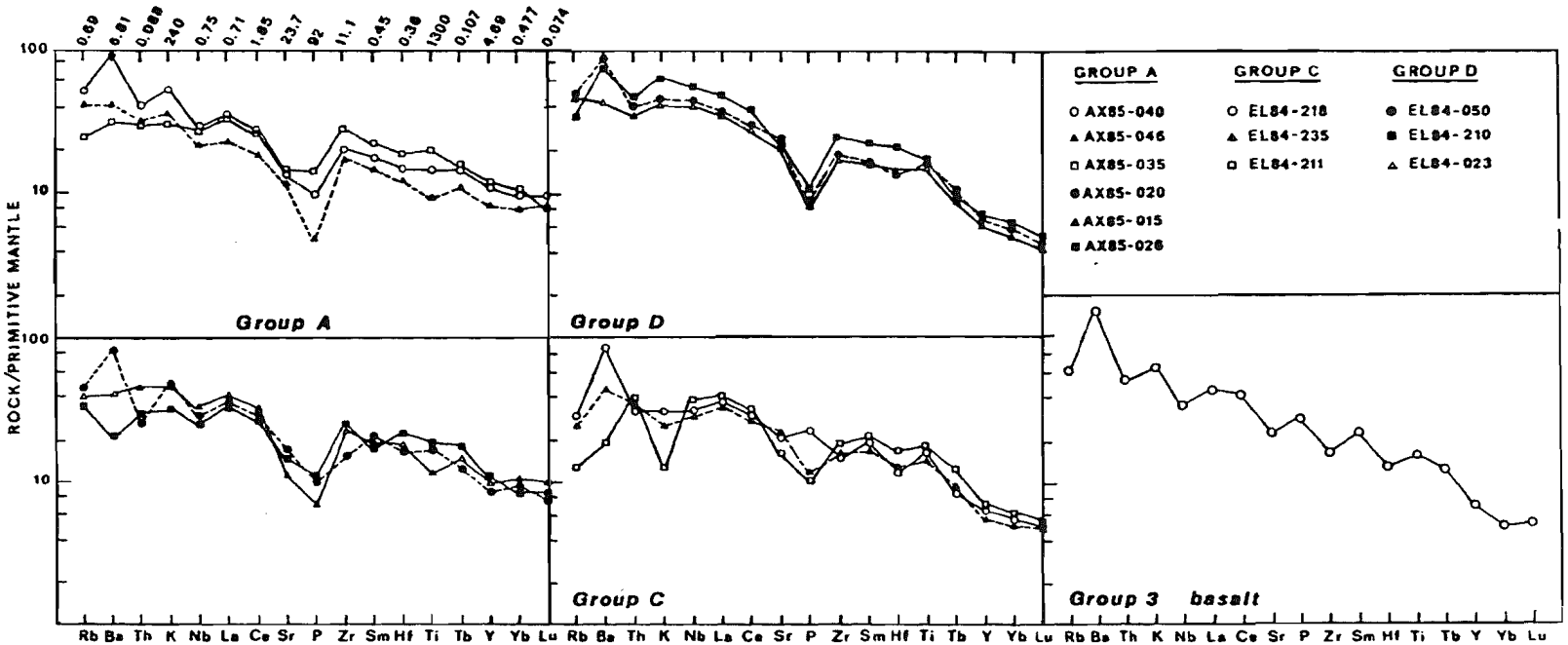

Figure 6.6 Mantle-normalized trace element diagrams for selected samples from Groups A, C and D. The pattern for a Group 3 basalt (EL84-010) is shown for comparison. Mantle-normalizing values (in ppm) are from McDonough et al. (1985).

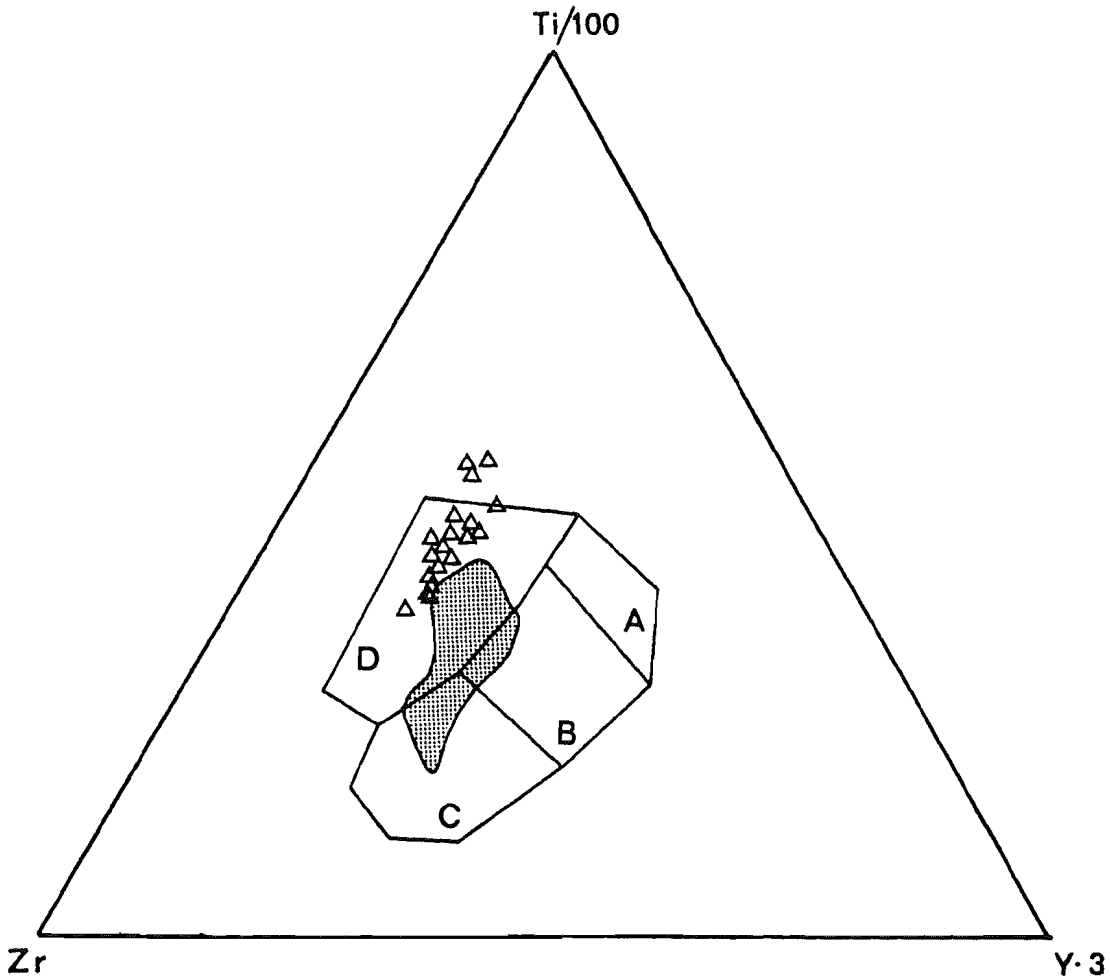

Figure 6.7 Ti-Zr-Y tectonic discrimination diagram of Pearce and Cann (1973). The shaded area represents the compositional field for Group A and B intrusives; triangles correspond to Groups C and D. The rocks show a within-plate affinity (field D), with some overlap in the fields of ocean-floor and continental basalts (B) and calc-alkali basalts (C). Other fields are: A+B+C = plate-margin basalts; A+B = island-arc tholeiites.

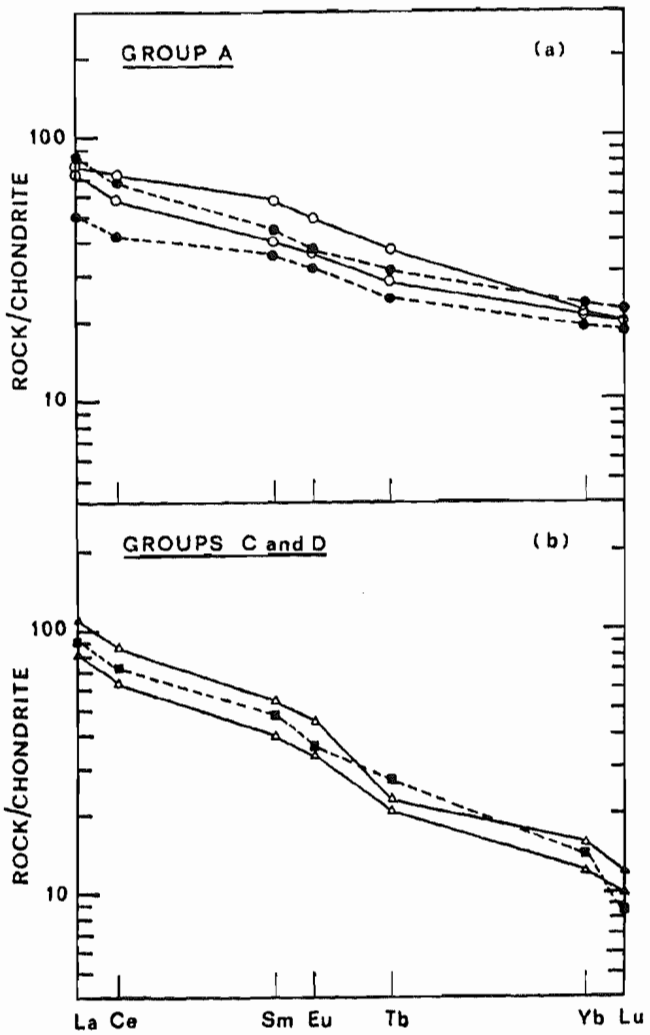

Figure 6.8 Chondrite-normalized rare earth patterns for selected samples from Groups A, C and D (normalizing values from Taylor and Gorton, 1977).

6.3.5 Cluster Analysis

The compositional differences between Groups [A-B] and [C-D] were tested using the K-means method of clustering (McQueen, 1967). A description of the method, and a list of relevant statistics are provided in Table C-7 of the Appendix. As expected from compositional data, values for SiO_2, TiO_2, Y, Zr and Nb best discriminate between the subalkaline and mildly alkaline gabbros. The results suggest that the differences observed are significant, and that the intrusive rocks are divisible into two distinct compositional types.

6.4 Summary and Conclusions

The results of petrochemical studies on eighty samples of basic intrusive rocks from eastern Axel Heiberg Island, the Eureka Sound area, Tanquary Fiord and the north shore of Lake Hazen can be summarized as follows:

1. GROUPS A AND B: Sills and dykes sampled at Lightfoot River (Group A), Buchanan Lake and Blacktop Mountain (Group B) all consist of evolved, LREE-enriched subalkaline gabbros, with moderately high TiO_2 contents. Systematic compositional variations as a result of gabbro fractionation were only observed in the Group B sills at Buchanan Lake and Blacktop Mountain. Data for the margins and interiors of sills follow the same trend on two-element variation diagrams, suggesting that differentiation as a result of post-emplacement crystallization is the main cause of chemical variation within single units. The dykes and sills at Lightfoot River display low correlation coefficients for

element-element pairs. Detailed geochemical studies of the thickest dyke encountered suggest that both fractional crystallization and assimilation may have operated during the emplacement of the dykes.

Despite the evidence for several periods of intrusion in both areas, there is little variation in the geochemistry of dykes and sills from Group [A-B]. Sills at Blacktop Mountain and thin cross-cutting dykes at Buchanan Lake show the least evolved compositions.

2. GROUPS C AND D: Most of the dykes and sills sampled on northeastern Ellesmere Island (Groups C and D) are olivine-normative gabbros with alkaline affinities. No single liquid line of descent was observed on two-element variation diagrams. Although broadly similar in terms of major element chemistry, the two groups show a distinct range of trace element ratios (e.g. Rb/Sr and Zr/P_2O_5). The Group D gabbros show the least amount of chemical variation between units, and somewhat more evolved compositions than Group C.

On the basis of trace element abundances, ferrobasaltic lavas at Lake Hazen and Piper Pass are indistinguishable from high-P_2O_5 gabbros at Tanquary Fiord (Group C). This result was unexpected, considering the close spatial association of basaltic lavas and sills or dykes north of Lake Hazen (Group D).

3. Compositional differences between the [A-B] and [C-D] gabbros are sufficiently large to warrant classification as two distinct compositional types, i.e subalkaline vs. mildly alkaline gabbros. Ratios of trace elements provide the best discriminants (e.g. Rb/Sr = 0.02-0.26 in [A-B] vs. 0.02-0.08 in [C-D] and Ce/Yb_N = 2-3 vs. 5-6). The gabbros can be uniquely classified by K-means clustering of geochemical data (SiO_2, TiO_2, Y, Zr and Nb abundances).

VII. COMPOSITIONAL VARIATIONS OF IGNEOUS ROCKS AND THEIR SIGNIFICANCE

7.1 Introduction

The aim of this chapter is to examine the compositional variations in volcanic and intrusive rocks of the Sverdrup Basin in terms of crust, mantle and tectonic processes. In the classic "inverse" approach used in petrological studies (e.g. Wyllie, 1984), an evaluation of crustal contamination is a prerequisite to any discussion concerning source characteristics. The processes most likely to modify the initial composition of magmas in continental settings have already been mentioned in Chapter 5. In Section 7.2.1 of this chapter, special consideration is given to the variations in Th-Hf-Ta abundances or Sr and Nd isotopic ratios that can result from crustal contamination. A brief discussion on characteristics of the source region(s) follows a review of experimental evidence concerning the generation of tholeiitic and alkaline magmas in continental settings. Some of the tectonic processes that can lead to the compositional variations observed are examined in the final section.

7.2 Significance of Compositional Diversity

Petrological and geochemical studies of extrusive and intrusive rocks (Chapters 5 and 6) have established that:

1. Volcanic rocks emplaced throughout the Early Cretaceous near the central part of the Sverdrup Basin consist of subalkaline basalts.

Volcanic rocks of lower Late Cretaceous age (*ca*. 91 Ma) erupted near the southern margin of the basin consist of mildly alkaline ferrobasalts.

2. Intrusive rocks sampled along a southwest-northeast transect of the study area are divisible into gabbros of subalkaline and mildly alkaline character.

For reference, the age, location and geochemical character of igneous rocks in the east-central Sverdrup Basin are shown in Table 7.1.

7.2.1 Crustal Contamination

The mineralogy and geochemistry of all the igneous rocks studied are consistent with equilibration at shallow depths in the crust (Figs. 5.7 and 6.5). The best evidence for interaction with continental crust comes from trace-element and isotopic studies of the Group 2 basalts (Chapter 5). In the case of intrusive rocks, the effects of crustal contamination were not systematically investigated.

One way of assessing the role of crustal contamination in basic igneous rocks is to examine the behaviour of trace elements which show significantly different concentrations in mantle and crustal rocks. In this respect, Ba, Th and Ta are considered to be sensitive geochemical indicators of crustal contamination (e.g. Wood, 1980; Pearce, 1983). In Figure 7.1, relative abundances of Th, Hf and Ta in igneous rocks of the study area are compared using the tectonic discrimination diagram of Wood (1980; data in Tables 5.7, 5.9, 6.2 and 6.7). Samples from Groups 1 and 2 plot in the field of continental basalts and E-type mid-ocean ridge basalts [B], with some overlap in the field of within-plate alkaline basalts [C]. The increase in Th/Hf and Ta/Hf ratios in some of

TABLE 7.1
COMPOSITION, LOCATION AND AGE OF BASIC IGNEOUS ROCKS

SVERDRUP BASIN

EXTRUSIVE ROCKS

north, centre → south margin; centre, Sverdrup rim → south margin

GROUP	COMPOSITIONAL TYPE	AGE	GEOGRAPHIC LOCATION
3	MILDLY ALKALINE FERROBASALTS	TURONIAN	HASSEL FORMATION NORTHERN ELLESMERE ISLAND
2	SUBALKALINE BASALTS	LATE ALBIAN - EARLY CENOMANIAN	STRAND FIORD FORMATION W. AND N. AXEL HEIBERG ISLAND
1	SUBALKALINE BASALTS	VALANGINIAN - APTIAN	ISACHSEN FORMATION AXEL HEIBERG AND W. ELLESMERE ISLANDS

INTRUSIVE ROCKS

GROUP	COMPOSITIONAL TYPE	AGE	GEOGRAPHIC LOCATION
D	MILDLY ALKALINE GABBROS	91 2 Ma	LAKE HAZEN-PIPER PASS N. ELLESMERE ISLAND
C	MILDLY ALKALINE GABBROS	N.D.	TANQUARY FIORD N. ELLESMERE ISLAND
B	SUBALKALINE GABBRO SILLS AND CROSS-CUTTING DIABASE DYKES	126 2 Ma 113 6 Ma	BUCHANAN LAKE, EUREKA E. AXEL HEIBERG ISLAND, W. ELLESMERE ISLAND
A	SUBALKALINE GABBROIC DYKES	N.D.	LIGHTFOOT RIVER E. AXEL HEIBERG ISLAND

Figure 7.1 The Th-Hf-Ta diagram of Wood (1980), with fields for: [A] N-Type MORB, [B] E-Type MORB and tholeiitic within-plate basalts, [C] alkaline within-plate basalts, and [D] destructive plate-margin basalts. (a) Data for subalkaline volcanic rocks in Groups 1 and 2. (b) Data for subalkaline gabbro dykes in Group A, and mildly alkaline volcanic and intrusive rocks in Groups 3, C and D.
The assimilation of upper crustal rocks causes an increase in the Th/Hf ratio and (to a lesser extent) in the Ta/Hf ratio of basaltic magmas (e.g. Taylor and McLennan, 1985). The arrow indicates the resultant shift of data points, from fields B to C, and towards the Th apex.

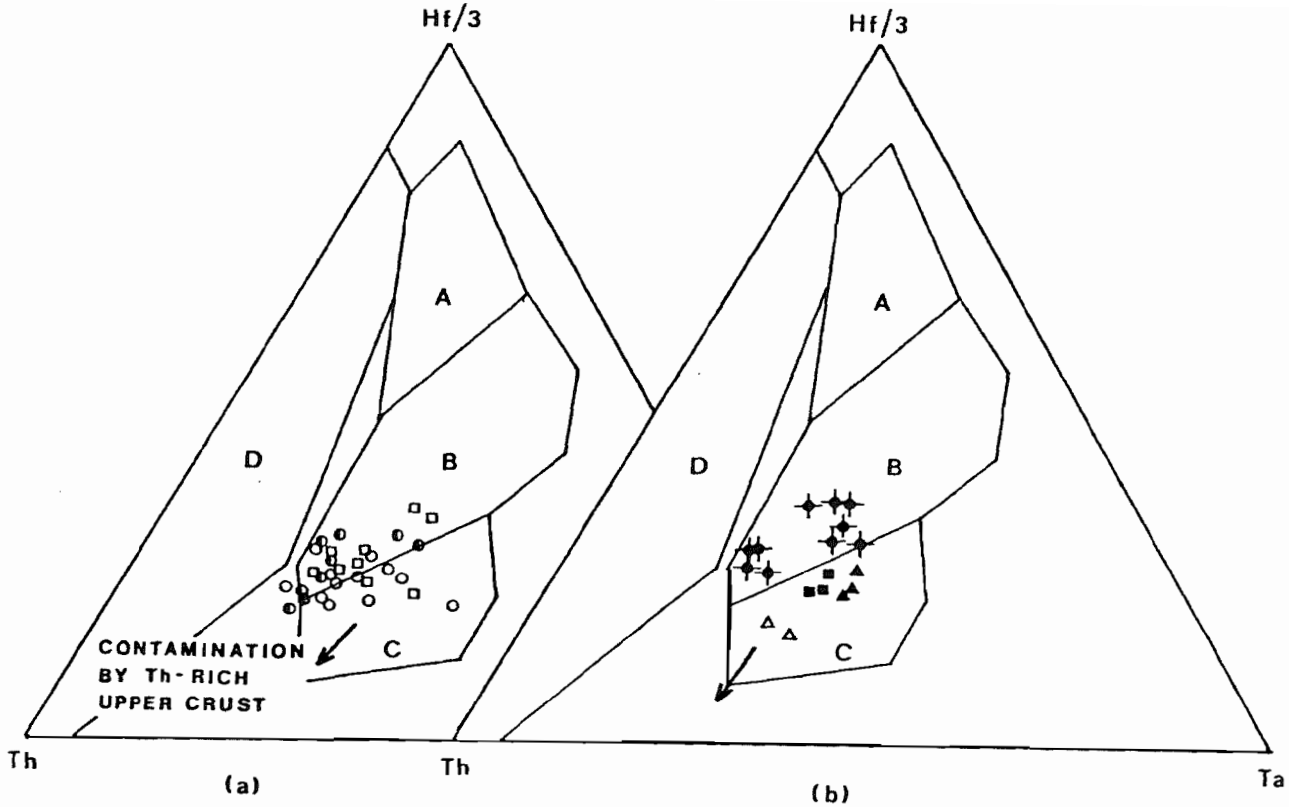

VOLCANIC ROCKS G1 □, G2A ○, G2B ◐, G3 △

INTRUSIVE ROCKS GA ✦, GC ■, GD ▲

FIGURE 7.1

the basalts causes the data points to shift from fields B to C, and towards the Th apex. The data for intrusive rocks and the Group 3 basalts (Fig. 7.1 b) plot in the appropriate compositional fields. However, some of the Lightfoot River dykes and the two samples of basaltic lava display an increase in Th/Hf and Ta/Hf ratios.

There is no apparent correlation between Th and other lithophile elements, at least in the Group 2 basalts for which *r* values are available (Table C-2 in the Appendix). However, the Th/Hf ratio shows a positive correlation with Sr-isotopic data and SiO_2 abundances in volcanic rocks (Fig. 7.2), supporting other evidence for crustal contamination presented in Chapter 5. The correlation is also observed for the Group 3 basalts and Group A samples mentioned above (Fig. 7.2 b).

Variations in Sr and Nd isotopic ratios provide additional constraints on the role of crustal assimilation in the petrogenesis of volcanic rocks (Carter et al., 1978; Hawkesworth and Vollmer, 1979; James, 1981; DePaolo, 1981; Norry and Fitton, 1983; Menzies et al., 1984). Figure 7.3 is a plot of eNd vs. $^{87}Sr/^{86}Sr$ initial ratios for six samples of basaltic lava and one sample from a sill in Group D for which an age and Sr-isotopic data were available (EL84-050, Fig. 4.8 and Appendix C). The isotopic composition of the sill plots within the field of modern mantle values. The volcanic rocks show higher $^{87}Sr/^{86}Sr$ and lower $^{143}Nd/^{144}Nd$ ratios than the mantle array. There are several possible explanations for the isotopic compositions observed.

- Seawater alteration can cause a shift to higher $^{87}Sr/^{86}Sr$ ratios with no concurrent change in Nd-isotopic compositions (e.g. O'Nions et al., 1979).

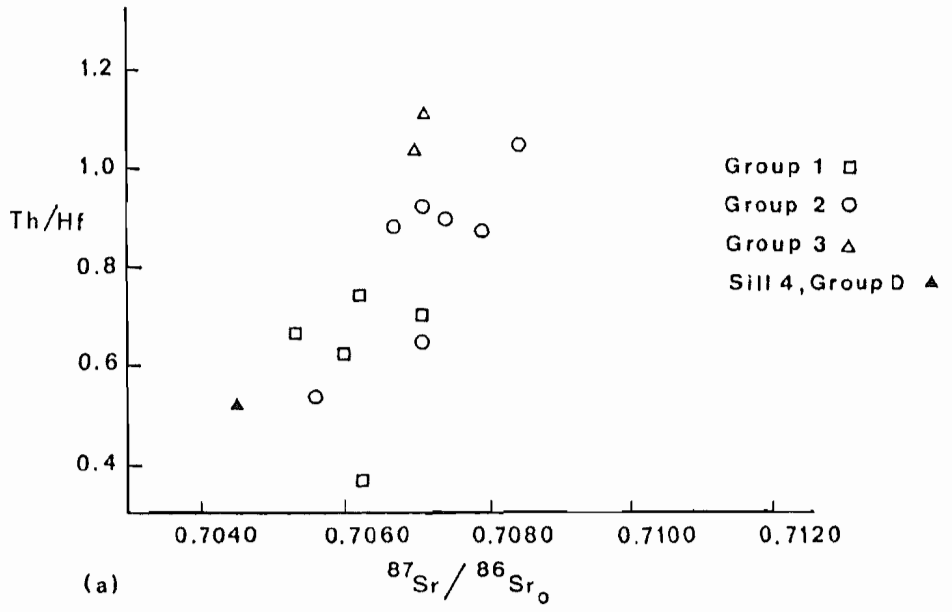

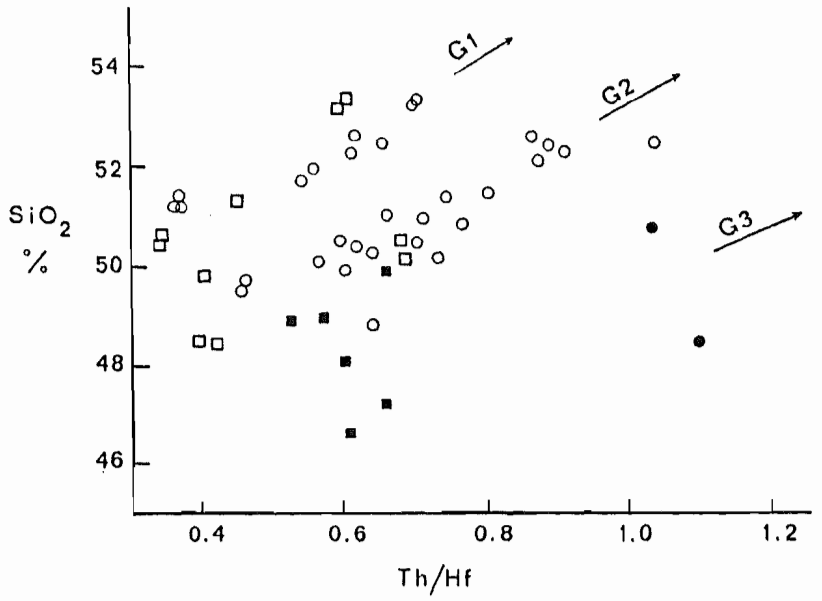

(b) SUBALKALINE Intrusive rocks □
Extrusive rocks ○

MILDLY ALKALINE Intrusive rocks ■
Extrusive rocks ●

Figure 7.2 (a) Plot of Th/Hf vs. $^{87}Sr/^{86}Sr_o$, illustrating a correlation between the two ratios in volcanic rocks of the study area.
(b) Plot of SiO_2 vs. Th/Hf. A positive correlation between SiO_2 and Th/Hf is particularly evident for volcanic rocks. Separate trends reflect progressively lower SiO_2 contents in each group of basalt flows.

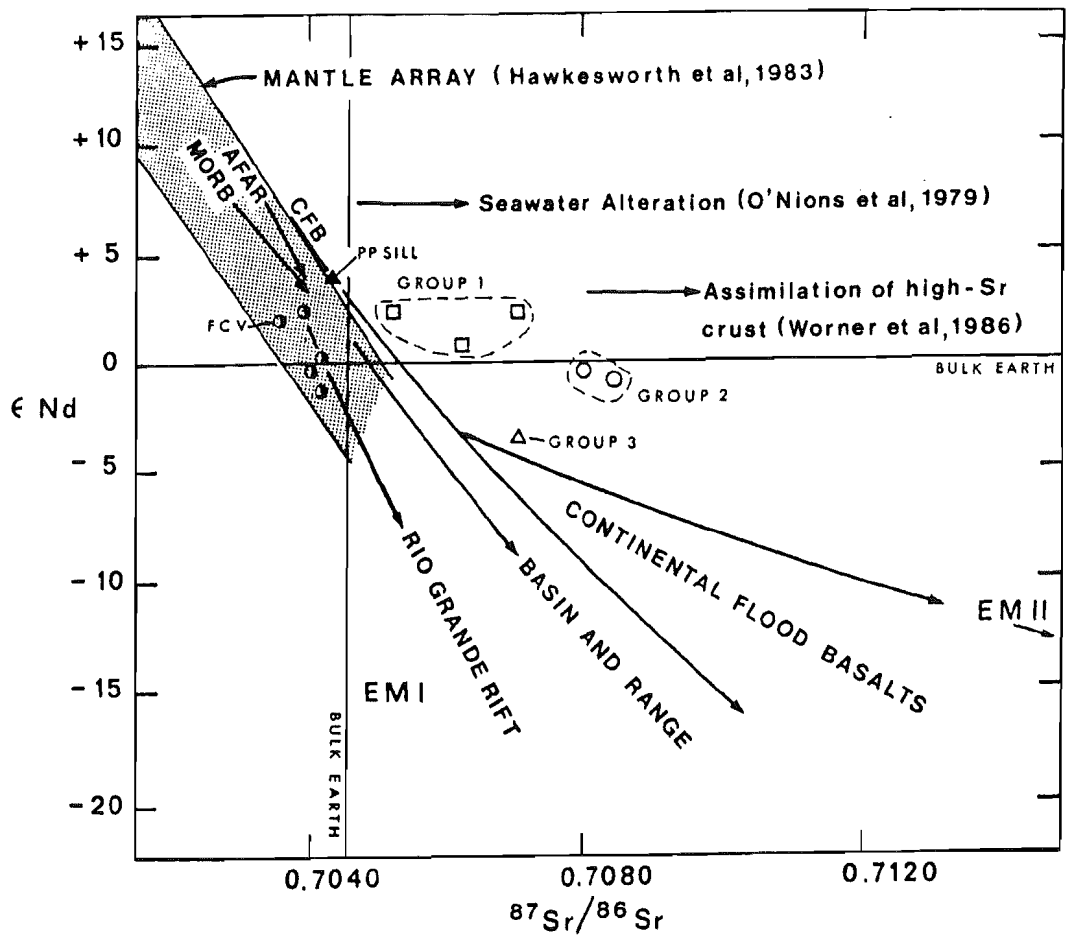

Figure 7.3 Plot of eNd vs. $^{87}Sr/^{86}Sr$ initial ratios for selected volcanic rocks (open symbols), and one sill at Piper Pass (filled triangle). Half-filled circles show the position of samples from the Tertiary Freeman's Cove Volcanics, on Bathurst Island. The suite is bimodal, and includes phonolite, nephelinite, basanite, ***hy***- and ***ne***-normative basalt (isotopic analyses by the author on samples provided by R.H. Mitchell). Isotopic data for the bimodal suite (FCV) and olivine normative gabbro from Piper Pass (PP) are contained within the field of modern mantle values. The shift to more radiogenic Sr and lower $^{143}Nd/^{144}Nd$ in the Group 1, 2 and 3 basalts suggests some form of mixing process, either with crustal melts or an enriched mantle component present in the subcontinental mantle. The position of EM I and EM II components, and trends for MORB's, CFB's and basalts of the Afar Rift, Rio Grande Rift and Basin and Range are from Zindler and Hart (1986). Cretaceous ages used in the calculation of eNd values are listed in Appendix C. See text for explanation.

- Simple bulk assimilation models (e.g. Wörner et al., 1986) suggest that contamination by upper crustal material of chemically undifferentiated and isotopically depleted basalts (e.g. data for MORB or the Afar Rift on Fig. 7.3) will cause a greater increase in radiogenic Sr than contamination by lower crust granulites.
- Hypothetical mixing trajectories for a three-component system (magma, cumulate and upper crustal rocks; James, 1981) resemble the curved arrays produced by some of the data from continental extensional provinces (e.g. the Rio Grande Rift, Basin and Range and Continental Flood Basalts , Fig. 7.3).

Many authors have argued that source contamination also explains the high $^{87}Sr/^{86}Sr$ and low $^{143}Nd/^{144}Nd$ initial ratios in some volcanic suites (e.g. Brooks et al., 1976; Hawkesworth and Vollmer, 1979; Hart, 1985). For example, at least two types of enriched mantle components are required to explain the Sr- and Nd-isotopic data in some ocean-island basalts (e.g. EM I and EM II components of Zindler and Hart, 1986, see Fig. 7.3). These enriched components may also exist within the subcontinental mantle (Wörner et al., 1986) and mix with depleted melts to produce the range of isotopic compositions observed in basalts from continental settings.

Additional isotopic data for each of the volcanic groups are required to characterize these processes more accurately. Despite the evidence for crustal contamination in volcanic rocks, only the mildly alkaline igneous rocks from Piper Pass (sill and ferrobasaltic lavas) follow the trend of chemically differentiated and contaminated continental flood basalts on Figure 7.3. In the case of Group 1 and 2 basalts, contamination by seawater or evaporites cannot be discounted.

7.2.2 Source Characteristics

Direct partial melting experiments have shown that melting of peridotite under different conditions (P, T, volatile content) can produce a wide range of basaltic compositions (e.g. Green, 1973; Kushiro, 1973; Eggler, 1974; Mysen and Boettcher, 1975; Jaques and Green, 1980; Fujii and Scarfe, 1985). This is illustrated in Figure 7.4 by the petrogenetic grid of Takahashi and Kushiro (1983). According to the summary, olivine tholeiites and tholeiitic picrites result from moderate to large degrees of partial melting at pressures greater than 5 kb. The liquids obtained at higher pressures are more olivine rich than those at lower pressures, and the initial melts formed at pressures above 15 kbar are alkali basalts (e.g. O'Hara, 1968). The initial peridotite melt becomes increasingly alkalic and silica-undersaturated as pressure increases at least up to 30 kb (Wendlandt and Eggler, 1980; Takahashi and Kushiro, 1983).

The large volumes of compositionally uniform, low Mg-tholeiites that are characteristic of CFB provinces can originate in several ways (Basaltic Volcanism Study Project, 1981), that include:

1. Extensive crystal fractionation (+/- magma mixing) of primary picritic melts derived from peridotitic mantle (O'Hara, 1968; Clarke and O'Hara, 1979; Walker et al., 1979; Cox, 1980; Francis et al., 1983).
2. Moderate amounts of fusion (+/- crystal fractionation) of (more Fe-rich) peridotitic mantle, either at a eutectic-like invariant point or low temperature cusp on the mantle solidus (e.g. Carmichael et al., 1974; Wilkinson and Binns, 1977; Presnall et al., 1979).

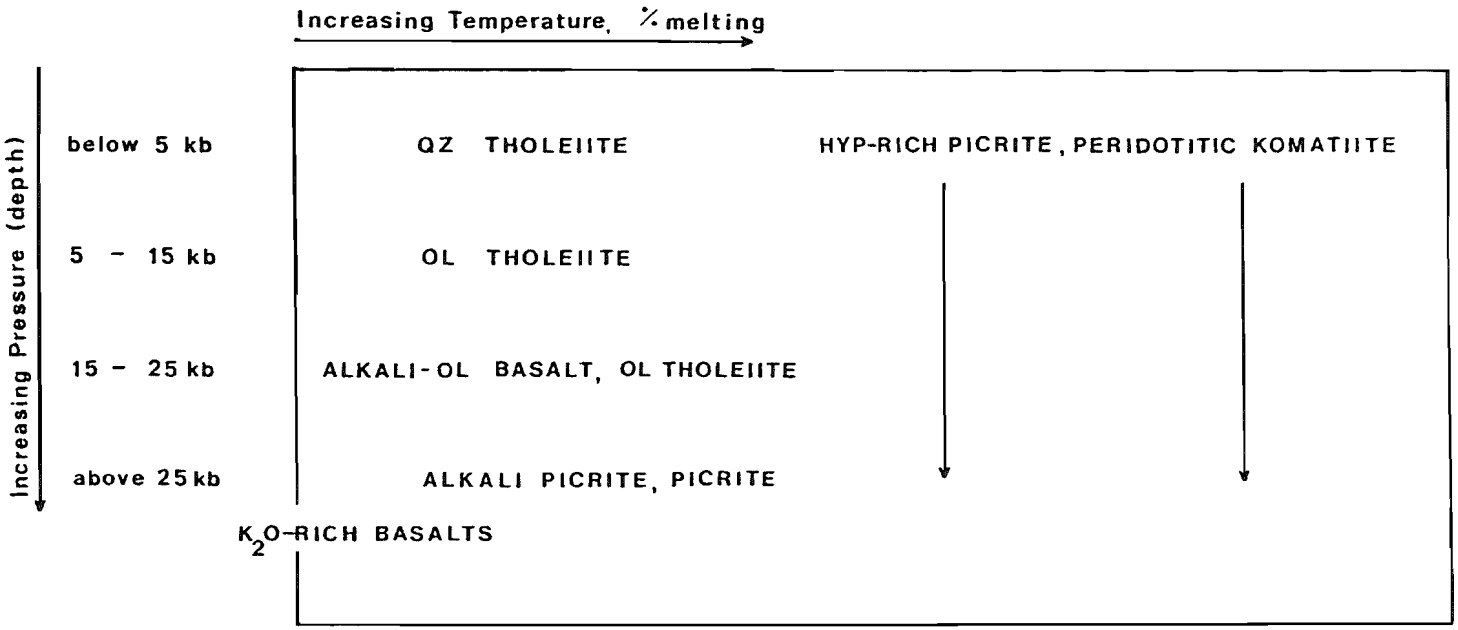

Figure 7.4 Petrogenetic grid of Takahashi and Kushiro (1983), showing the compositional diversity of basaltic magmas formed by partial melting of peridotite (anhydrous) according to temperature, depth and degree of partial melting.

In both types of model, the continental setting and large degrees of partial melting required to produce tholeiitic melts are likely to enhance the opportunity for crustal contamination (e.g during underplating at the base of the lithosphere). Recent studies of continental flood basalts, therefore, emphasize the distinction between crust and mantle geochemical signatures.

In continental flood basalt provinces, highly silica-undersaturated alkalic basalts such as basanites, olivine nephelinites, olivine melilitites and high-K_2O lavas, are volumetrically minor compared to tholeiitic basalts. Alkaline rocks characteristically show high concentrations of incompatible or large-ion lithophile (LIL) elements that contrast with depleted isotopic signatures. Until recently, the extraction from the mantle of very small degrees of partial melt required to concentrate these trace elements (less than 1%) was considered problematic. Although this is now challenged by the work of McKenzie (1984), other processes have since been proposed that include zone refining, wall-rock reaction and metasomatic enrichment of the mantle source.

For rocks of tholeiitic character emplaced in continental settings, most of the debate centres around the cause for the relative enrichment of incompatible trace elements and distinct isotopic character of the igneous rocks, as compared to MORB's. The higher SiO_2, K, Rb, Ba, LREE and $^{87}Sr/^{86}Sr$, and lower $^{143}Nd/^{144}Nd$ isotopic ratios, are explained either in terms of crustal assimilation processes or melting of variably enriched sub-continental lithosphere (e.g. Norry and Fitton, 1983). The presence of LILE-enriched peridotitic xenoliths in continental alkali basalts, for example, suggests that the petrogenesis of voluminous

mildly alkaline and tholeiitic basalts from continental rifts and flood basalt provinces may involve extensive melting of enriched, sub-continental lithosphere. However, studies of alkaline rocks from both oceanic and continental settings (Fitton, 1987) imply a source in the asthenosphere.

Regardless of the type of source region invoked, it is necessary to postulate a recent enrichment of the source peridotite in LREE and other lithophile elements in order to account for the consistent trace element and isotopic enrichment observed in continental basalts of tholeiitic and alkaline character (e.g. Carter et al., 1978; Menzies and Murthy, 1980; Hawkesworth et al., 1984). Even in cases where the magmas are inferred to represent LILE-depleted mantle (e.g. Fitton and Dunlop, 1985), isotopic differences require some form of enrichment process (i.e. producing LILE-enriched domains). At least two types of mechanisms are envisaged:

1. Migration of small volumes of silicate melt (occurring preferentially in the convecting upper mantle).
2. Metasomatic enrichment as a result of the release of H_2O- and alkali-enriched fluids (restricted to continental areas, and often attributed to dehydration processes operating above subduction zones).

According to the above summary, subalkaline and mildly alkaline magmas emplaced in the Sverdrup Basin could have segregated at different depths (and/or) from chemically distinct source regions. This is illustrated to some extent by the ratios of high-field strength elements in these rocks. Although absolute abundances of HFSE can vary during fractional crystallization, systematic variations in ratios of these elements depend on source characteristics. Differences in Zr/Y ratios,

for example, can be attributed to systematic source heterogeneity, variations in the degree of partial melting of a garnet lherzolite source, progressive melting of a single source or eclogite fractionation. Unless minor phases are invoked or mineral-melt partition coefficients vary, Zr/Nb ratios are insensitive to variations in the degree of partial melting and reflect heterogeneities in the mantle source (Pearce and Norry, 1979).

In Figure 7.5, the Zr, Y and Nb abundances in subalkaline volcanic and intrusive rocks are compared with those in gabbros of mildly alkaline character. The differences in Zr/Y ratios are not systematic, but suggest higher values in the mildly alkaline rocks. Zr/Nb ratios are distinctly lower in the mildly alkaline rocks. The differences in Zr/Y ratios between the subalkaline and mildly alkaline rocks can be explained either in terms of melting style of a single source, different sources or batch fractionation processes. Differences in the Zr/Nb ratios may reflect a change in mineral-melt partition coefficients, fractionation of a minor phase, or distinct mantle sources. The batch fractionation process, during the repeated influx of magma in crustal reservoirs, could modify the Zr/Y and Zr/Nb ratios and eventually lead to more alkaline compositions (Clarke et al., 1983; Nielsen, 1987). This type of process is unlikely to have played a determinant role during the emplacement of voluminous magmas of predominantly tholeiitic character in the east-central Sverdrup Basin. However, it may have contributed to the evolution of alkali basalt-trachyte-rhyolite suites along the northern margin of the Sverdrup Basin and on northern Greenland.

Figure 7.5 Comparison of Zr, Y and Nb abundances in subalkaline and mildly alkaline igneous rocks of the study area. (a) Volcanic rocks of subalkaline character include the Group 1 and 2 basalts (enclosed by the dashed line or indicated as open symbols). Data for mildly alkaline basic igneous rocks belonging to Groups 3 (volcanic), C and D (intrusive) are shown as filled symbols. (b) Data for the Group B gabbros (samples of chilled margins) illustrate Zr, Y and Nb abundances in subalkaline basic intrusive rocks of the study area. Data for mildly alkaline igneous rocks as in (a).

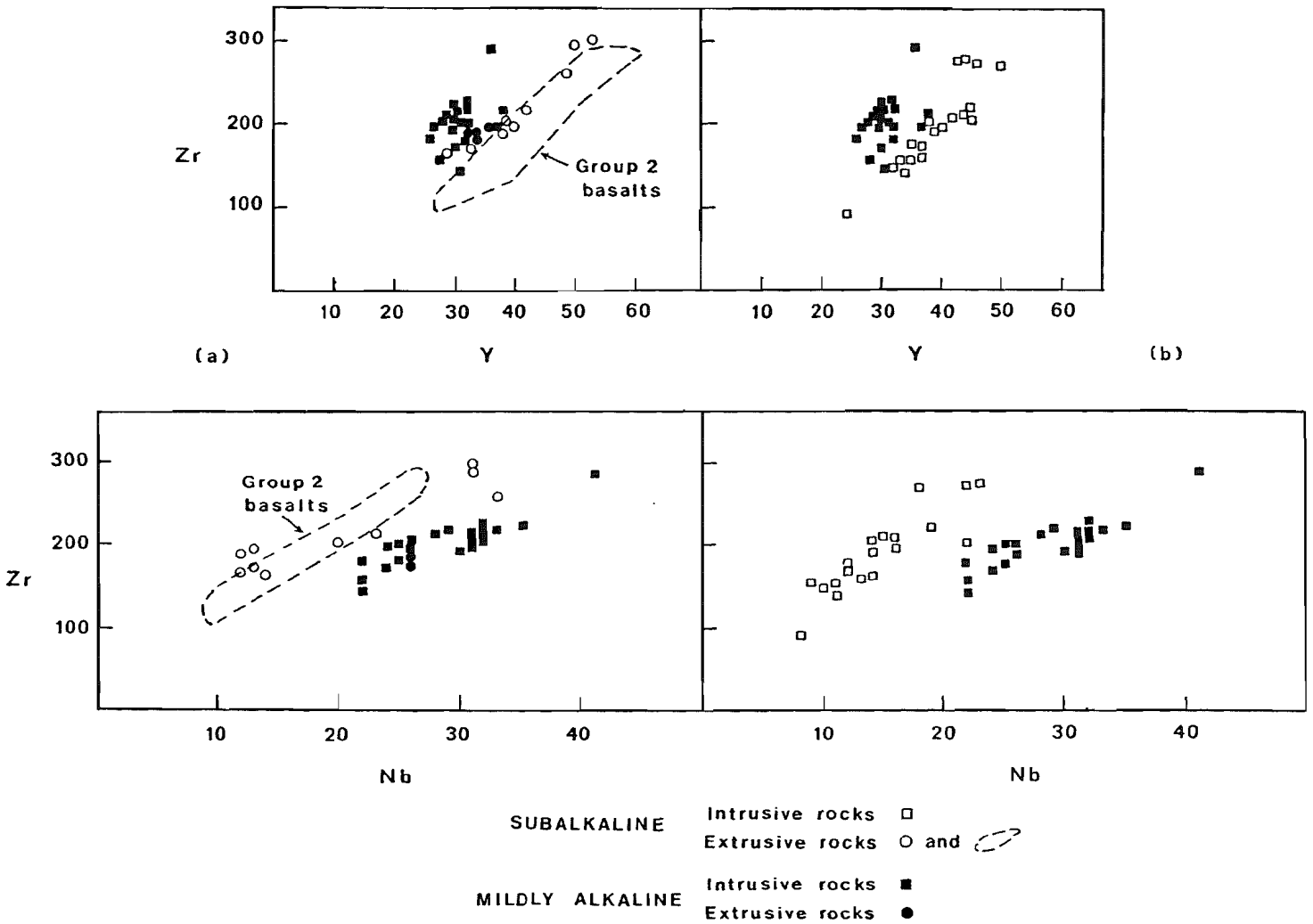
300
200
100
Zr
Group 2
basalts
10 20 30 40 50 60
Y
(a)
(b)
Nb
SUBALKALINE
Intrusive rocks
Extrusive rocks
and
MILDLY ALKALINE
Intrusive rocks
Extrusive rocks

FIGURE 7.5

7.3 Tectonic Controls on Magma Genesis

7.3.1 Episodicity

Whole-rock and mineral compositions of basaltic rocks from different geological settings are often used as a guide in the interpretation of ancient tectonic environments (e.g. Pearce and Cann, 1973; Winchester and Floyd, 1977; Leterrier et al., 1982). In extensional settings, cyclic or episodic igneous activity may coincide with periods of renewed tectonism (e.g. in rift basins, Mohr, 1978; Eaton, 1982; Williams, 1978; Wernicke et al., 1987).

In the eastern Sverdrup Basin, volcanic rocks occur within specific time-stratigraphic intervals (Section 2.3.2, Fig. 2.5). Little is known, however, concerning the timing of intrusive activity. As a premise to geochemical studies, stratigraphic and radiometric ages for intrusive and volcanic rocks were combined in Table 4.1. The resulting magmatic episodes range in age from Early Cretaceous to lower Late Cretaceous.

1. Sills of Hauterivian age at Buchanan Lake represent a major episode of intrusive activity, approximately contemporaneous with minor volcanic activity during the Valanginian-Early Barremian interval (Group 1A basalts, Table 5.1).
2. Cross-cutting dykes in the same area are equivalent in age to the Group 1B basalts (Late Barremian-Aptian).
3. Basic igneous rocks in northeastern Ellesmere Island were emplaced during a single volcanic-intrusive episode in Late Cenomanian-Early Turonian.

4. Dykes in the Lightfoot River area (and others belonging to the same group; Jollimore, 1986) could represent feeders to the Late Albian basalt plateau.

Subalkaline basalts of Early Cretaceous age in the north-central Sverdrup Basin are chemically uniform (Chapter 5). Despite the apparent correlation in the stratigraphic and radiometric ages of igneous rocks from this area (Table 7.1), no evidence was found of a subvolcanic complex or dyke-flow relationship in the field. Although similar in composition to the extrusive rocks, subalkaline gabbros in Groups A and B could have been generated at different times.

Some discrimination among basalts in the Isachsen and Strand Fiord Formations can be achieved using Sr-isotopic data (Fig. 5.6 a). Although isotopic studies of basic intrusive rocks were beyond the scope of this study, Sr-isotopic data were obtained for three samples from Buchanan Lake and Blacktop Mountain, two of which had been dated by Avison (1987, Fig. 4.7). The $^{87}Sr/^{86}Sr$ initial ratio for a sample from Dyke Q at Buchanan Lake is 0.70526. A sample from Sill A yielded a value of 0.70669. The ratio for a sample from Sill D, at Blacktop Mountain, is 0.7048 (details in Appendix C). The ratios obtained for Dyke Q and Sill D are comparable to isotopic data for the Group 1 basalts (Table 5.10). Although the data are too few to be conclusive, the compositional similarity between the Buchanan Lake dykes and Blacktop Mountain sills (Chapter 6) is confirmed by the Sr-isotopic data. These preliminary results suggest that a systematic study of isotopic compositions of subalkaline volcanic and intrusive rocks in the Sverdrup Basin would clarify their association. Although precise

correlations may not be possible, the nature of source regions and the contamination history could be better constrained.

The geochemical correlation among volcanic and intrusive rocks from the southern margin of the basin (Table 7.1) was discussed in the preceding chapter. Although high-Ti gabbros and ferrobasaltic lavas in the area form a single compositional group (shown as type [2] on Fig. 7.1), volcanic rocks from Lake Hazen or Piper Pass and basic intrusive rocks in the Tanquary Fiord area are indistinguishable on the basis of minor and trace element contents (e.g. P_2O_5 and ratios of high-field strength elements). This is an important observation because the age determinations by Avison (1987) provided evidence for contemporaneity of lavas and intrusive rocks at Lake Hazen and Piper Pass. The apparent geochemical correlation between these volcanic rocks and the sills at Tanquary Fiord implies that the latter group was also emplaced during the lower Late Cretaceous (*ca.* 91-92 Ma).

7.3.2 Spatial Distribution of Compositional Types

Figure 7.6 shows the geographic distribution of compositional types in Cretaceous igneous rocks of the east-central Sverdrup Basin. A transition from basic subalkaline to mildly alkaline igneous rocks occurs between the Early Cretaceous and lower Late Cretaceous intervals. Alkali basalt-trachyte-rhyolite suites were emplaced along the Sverdrup Rim during the final phase of volcanic activity in the Late Cretaceous (Trettin and Parrish, 1987; G.K. Muecke, pers. comm. 1988).

There have been many attempts to correlate the geographic distribution of tholeiitic and alkaline rocks in extensional settings

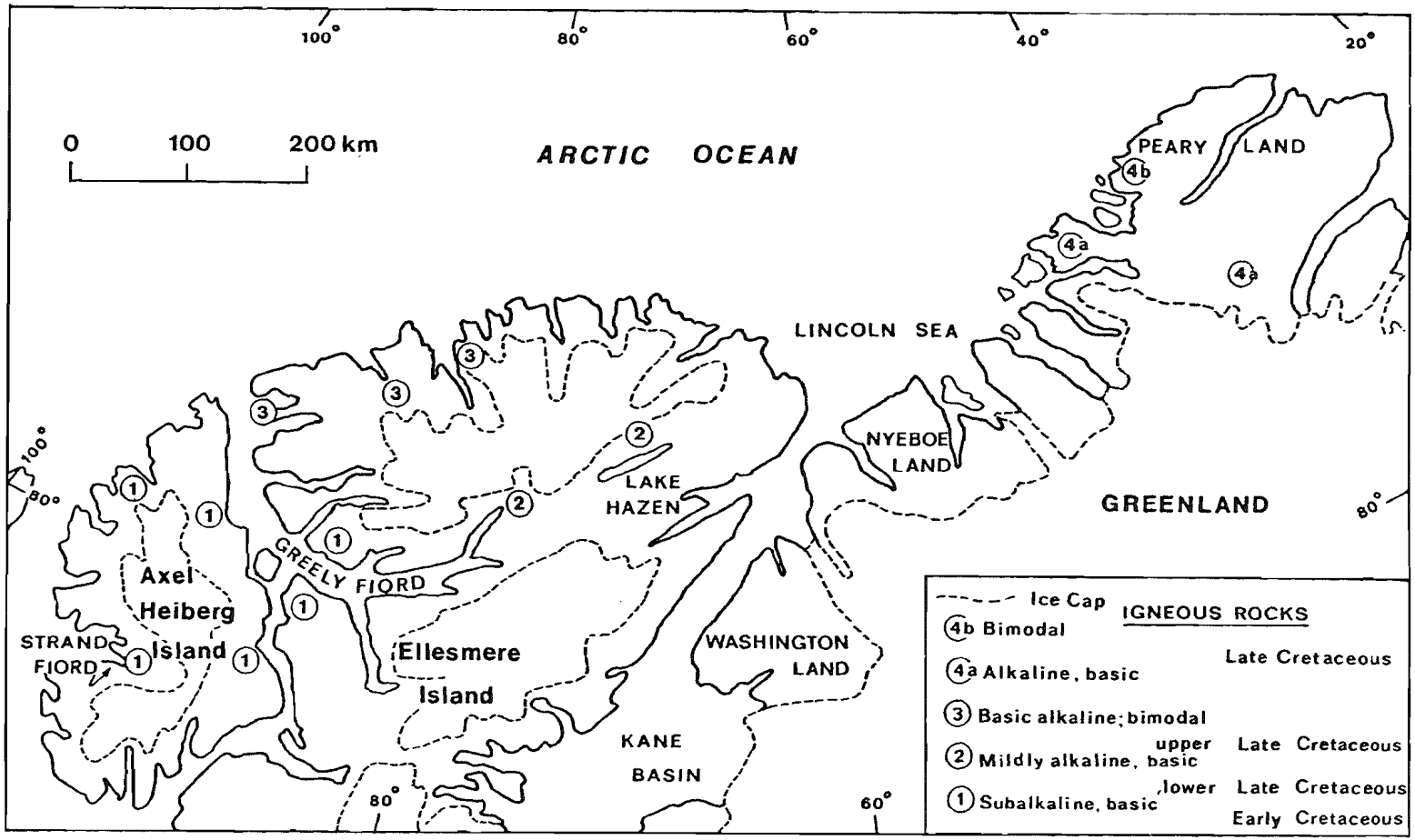

Figure 7.6 Geographic distribution of compositional types in Cretaceous igneous rocks of the eastern Sverdrup Basin and northern Greenland. Sources of data are: [1] and [2] this study; [3] Bates, 1986, Trettin and Parrish, 1987, and G.K. Muecke, pers. comm., 1988; [4a] and [4b] Soper et al., 1982 and Brown et al., 1987.

with variations in the tectonic regime. In some cases, a clear tectonic control can be demonstrated. During continental breakup involving plate separation, for example, vigorous magmatism of tholeiitic character in the continental zone may be followed in time by alkaline igneous activity along the trailing continental margin, long after the spreading centre is established offshore. Where no tectonic control is apparent, the presence of a rising plume of asthenospheric material may be invoked to explain successive cycles of tholeiitic and alkaline magmatism (e.g Hawaii). In his review of magmatism in continental rifts, Williams (1978) found no simple relationships between volcanic events and major faults or between igneous activity and pulses of uplift. Other studies (e.g. Wernicke et al., 1987) suggest that the role of crust and mantle in a basin setting will be determined by the locus of extensional movements and thermal state of the lithosphere at the time of rifting.

The spatial-compositional distribution of Cretaceous igneous rocks, shown in Figure 7.6, implies some form of tectonic control. The migration of volcanic centres with time, for example, may reflect the progression of extensional movements from the depocentral area to the northeastern margin of the basin. Tectonic controls on magma composition, however, are not as evident because of the apparent correlation between trace element signatures and the mode of emplacement of igneous rocks. The tectonic discrimination diagram of Holm (1985), reproduced on Figure 7.7, serves to illustrate this point. Although the distinction between within-plate and plate-margin tholeiites does not apply to igneous rocks of this study, the diagram highlights lower Nb/Th ratios in the volcanic rocks, that could result from selective crustal contamination of the parental magmas. Further investigation of the

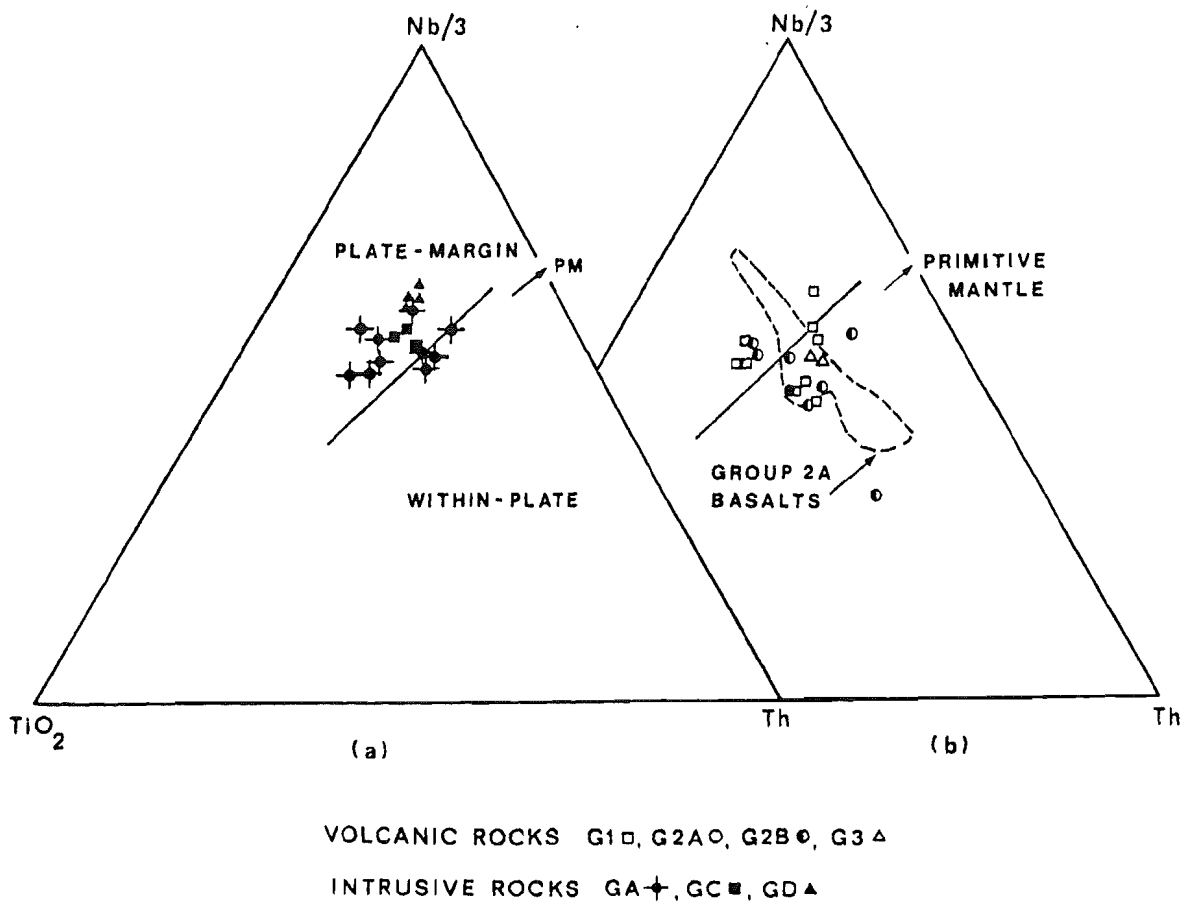

Figure 7.7 The TiO_2-Nb/3-Th diagram of Holm (1985), used here to illustrate the relative contribution of crust and mantle in a basin setting.
(a) Data for basic intrusive rocks in Groups A, C and D.
(b) Data for volcanic rocks in Groups 1, 2 and 3.
Most of the intrusive rocks exhibit Nb/Th ratios that are comparable to values for primitive mantle (from Taylor and McLennan, 1985). Volcanic rocks show a wide range of ratios that could result from the assimilation of crustal rocks. The distinction between within-plate and plate-margin tholeiites does not apply to igneous rocks of this study. However, the apparent correlation between the degree of crustal contamination and the mode of emplacement of igneous rocks is perhaps a characteristic of magmatism in a basin setting. Tectonic implications are discussed in the text.

impact of crustal contamination on intrusive rocks is required to establish a correlation between the degree of assimilation and spatial distribution of igneous rocks across the basin. Although the existence of four volcanic-intrusive episodes (Table 7.1) will be a matter of debate until more intrusive rocks are dated, it is clear that a trend towards more alkaline compositions is present.

VIII. TECTONOMAGMATIC EVOLUTION OF THE SVERDRUP BASIN

8.1 Introduction

An acceptable tectonomagmatic model for the Sverdrup Basin must account for the following observations:

1. The timing of magmatism, i.e. limited volcanism during the Carboniferous and Permian (e.g. Trettin, 1988; Cameron, 1986 and thesis in prep.), followed by renewed igneous activity during the Cretaceous.
2. The geographic distribution of compositional types across the east-central Sverdrup Basin (Fig. 7.6).
3. Evidence for a widening volcanic zone as Cretaceous igneous activity progressed (Sections 5.5 and 7.3.2).

Two types of tectonic controls will be considered:

- Rifting events during the depositional history of the Sverdrup Basin.
- Relative plate motions during the Late Mesozoic, that led to the opening of the Canada Basin and development of the polar continental margin.

Regional implications are discussed in the final section. For reference, the major Cretaceous tectonic provinces of Arctic North America and northern Greenland are shown on Figure 8.1.

Figure 8.1 Major tectonic provinces of Arctic North America and northern Greenland, mid-Early Cretaceous to Late Cretaceous tectonic regime (modified from Balkwill et al., 1983). Areas of Cretaceous igneous activity in the Sverdrup Basin and on northern Greenland are indicated (sources as in Fig. 7.6; data for Alpha Ridge from Van Wagoner et al., 1986). The ocean-continent transect from northern Ellef Ringnes Island to the Canada Basin is illustrated on Figure 8.2. Tectonic elements discussed in the text include the Sverdrup Basin (axis and Sverdrup Rim), Canada Basin and Alpha Ridge. The Baffin Bay-West Greenland Tertiary Volcanic Province is referred to in the text.

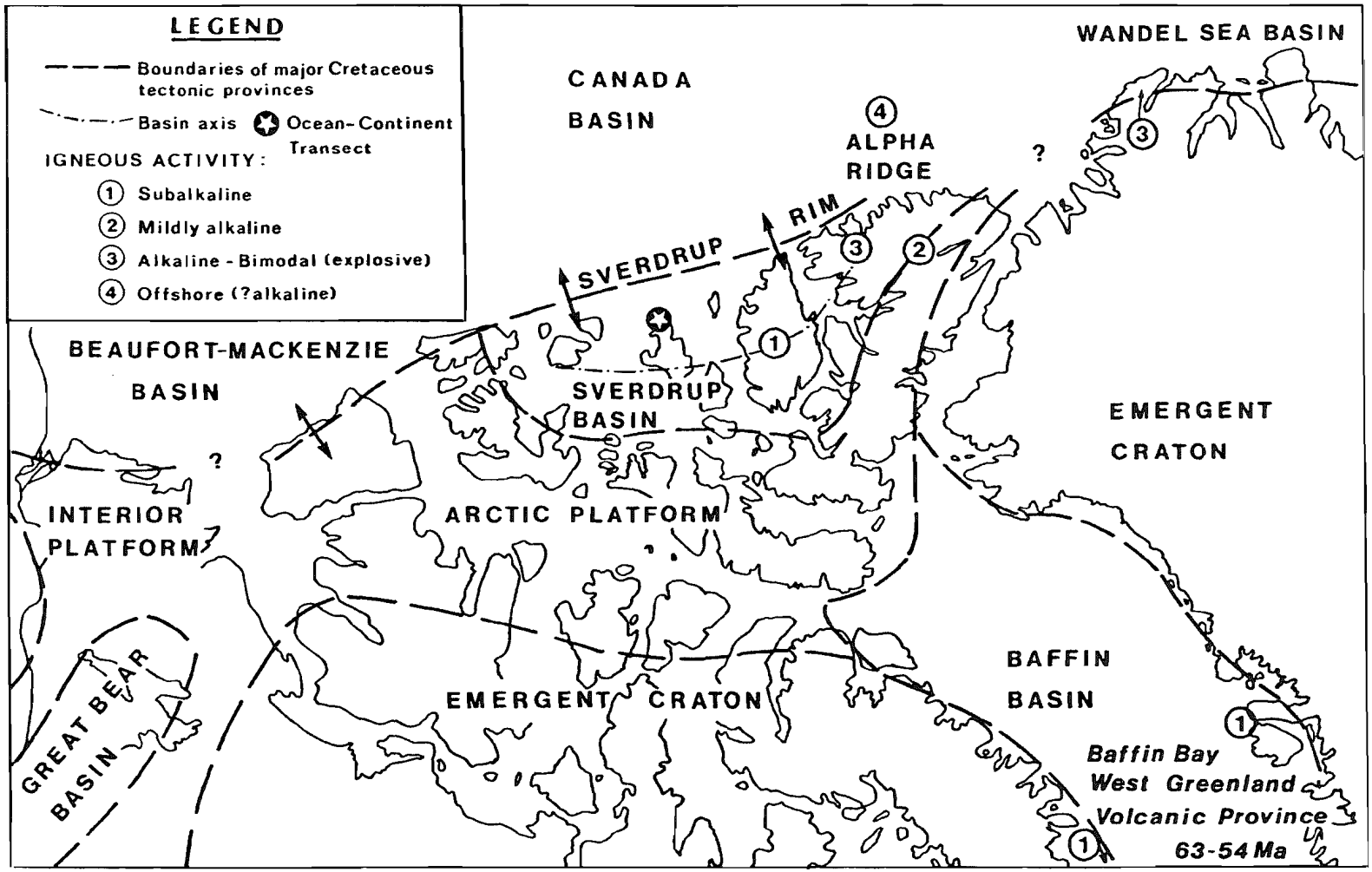
LEGEND
Boundaries of major Cretaceous tectonic provinces
Basin axis
Ocean-Continent Transect
IGNEOUS ACTIVITY:
1 Subalkaline
2 Mildly alkaline
3 Alkaline - Bimodal (explosive)
4 Offshore (?alkaline)
WANDEL SEA BASIN
CANADA BASIN
ALPHA RIDGE
SVERDRUP RIM
SVERDRUP BASIN
BEAUFORT-MACKENZIE BASIN
EMERGENT CRATON
INTERIOR PLATFORM
ARCTIC PLATFORM
GREAT BEAR BASIN
EMERGENT CRATON
BAFFIN BASIN
Baffin Bay West Greenland Volcanic Province 63-54 Ma

FIGURE 8.1

8.2 Tectonic Setting

8.2.1 Tectonic and Thermal History of the Sverdrup Basin

There is general agreement that the Sverdrup Basin evolved as an intracratonic extensional province (Sweeney, 1976; Balkwill, 1978; Bally and Snelson, 1980), bounded to the east and south by the stable platform and craton (Balkwill et al., 1983). From the Early Carboniferous to the Tertiary, the basin received up to 13 km of sedimentary rocks and underwent episodic igneous activity. Balkwill (1978) recognized several phases of subsidence and basin formation:

1. ***Carboniferous-Middle Jurassic:*** Progressive infilling of the depocentral region and southwestern re-entrant by cratonic-derived clastics characterized the initial development of the Sverdrup Basin. A thick sequence of evaporites and marine muds accumulated in the axial region and there is evidence of localized volcanic activity (Cameron, 1986; Trettin, 1988).

2. ***Oxfordian-Late Neocomian:*** Renewed tectonism in the Oxfordian resulted in the deposition of thick successions of muds and sands near the depocentre and important morphological changes in the western part of the Sverdrup Basin. A basin-wide fluvial succession marks the peak of Early Cretaceous clastic infilling.

3. ***Aptian-Maastrichtian:*** This stratigraphic interval records the final episode of foundering and accelerated deposition near the centre the Sverdrup Basin, that caused prolonged depositional overstepping and marine transgression beyond the former basin margins. Igneous activity

peaked during this period. Gradual filling by progressively shallower marine clastics occurred until about middle Maastrichtian.

According to Balkwill and Fox (1982), the consistent orientation of structural elements in the western part of the Sverdrup Basin suggests that the basin was generated by episodic rifting. Seismic refraction and gravity data (Sobczak and Weber, 1973; Forsyth et al., 1979; Sobczak and Overton, 1984) indicate that the underlying crystalline basement has been thinned from a mean thickness of about 37 km to about 30 km in the axial region.

Interpretations of the igneous history of the Sverdrup Basin are based on one of two tectonic models. The results of subsidence analysis done by Sweeney (1977) indicate three depositional stages corresponding to the initial rifting in the Late Paleozoic (330-230 Ma), followed by renewed basin tectonism and foundering in the early Mesozoic (225-124 Ma) and in the late Mesozoic (124-74 Ma). In the subsidence model of Stephenson et al. (1987), a single rifting event during the Carboniferous-Early Permian is invoked to explain all the pre-Valanginian fill of the Sverdrup Basin. Furthermore, an extrapolation of the model to include Cretaceous stratigraphy suggests that thermal subsidence and sediment compaction can account for Valanginian-Campanian sedimentation everywhere in the basin except in the vicinity of Axel Heiberg and western Ellesmere Islands. The authors, therefore, envisage a second (relatively minor) rifting event that occurred during the Early Cretaceous (or earliest Late Cretaceous). This event was limited to the eastern part of the Sverdrup Basin.

On the basis of stratigraphic evidence, Balkwill (1978, 1983) proposed that widespread mafic intrusive activity accompanied episodes

of basin subsidence and deposition in the western and central parts of the Sverdrup Basin. This concept of episodic crustal dilation, foundering and magmatic activity during "rejuvenated thermal subsidence" (Balkwill and Fox, 1982) is consistent with the basin analysis of Sweeney (1977). Embry and Osadetz (in press) specifically address the occurrence of volcanic rocks in four Cretaceous time-stratigraphic intervals in the east-central Sverdrup Basin (Section 2.3.2). They postulate a link between Early Cretaceous volcanic activity, renewed rifting in the eastern Sverdrup Basin (e.g. Stephenson et al., 1987) and the opening of the Canada Basin.

8.2.2 Origin and Age of the Canada Basin

The summary of Arctic tectonics presented in Chapter 2 pointed out some of the controversies surrounding plate reconstructions of Arctic regions during the Mesozoic. More specifically, the timing of opening (i.e. the age of oceanic crust) and plate kinematics that led to the formation of the Amerasian Basin are still debated. Some plate tectonic models for Arctic regions (Section 2.2.3) require strike-slip motion of Alaska along the Canadian polar continental margin (e.g. Jones, 1980; Oldow et al., 1987). The principal argument against strike-slip displacement is that both the Alaskan and Canadian shelves display structures that are typical of rifted, rather than transform, margins. The latter, for example, do not display a broad zone of thinned crystalline continental crust, or deep marginal sedimentary basins (e.g. the Grand Banks, offshore Newfoundland; Keen and Hyndman, 1979). A portion of the Canadian polar margin, off northern Ellef Ringnes Island,

is shown on Figure 8.2. The cross-section is a schematic representation of crustal stratigraphy compiled from geological maps, borehole logs, seismic surveys and gravity data for the Isachsen Peninsula (location on Fig. 8.1) and adjacent continental margin (Sweeney, 1986b). Although highly schematic, the ocean-continent transect illustrates some important stratigraphic features of the Sverdrup Basin and polar continental margin:

1. Variations in crustal stratigraphy occur from the central part to the northwest margin of the Sverdrup Basin. Close to the basin axis, the crust shows evidence of thinning (e.g. Sobczak and Overton, 1984), while thicker continental crust underlies the Sverdrup Rim.
2. Thinned continental crust along the polar continental margin is interpreted as transitional between continental and oceanic domains. As such, it would represent rift-stage crust, and mark the locus of continental breakup (e.g. Keen and de Voogd, 1988).
3. Basic intrusive rocks within the continental tectonic zone overlap the boundary between the Sverdrup Basin and the Arctic Terrace wedge.

Figure 8.3 illustrates some of the plate kinematics involved in the rotation model (Section 2.2.3), as envisaged by Jackson et al. (1986). In this particular reconstruction, continental breakup is initiated in a region adjacent to Ellesmere Island. The rotation of the AA plate about a (migrating) pole located in the Beaufort-Mackenzie Basin results in a fan-shaped magnetic lineation pattern during seafloor spreading. The type of geological and geophysical evidence used to support the rotation model is listed in Table 2.1. Many of the observed stratigraphic features are consistent with passive margin development and suggest that the Alaskan and Canadian continental shelves are conjugate margins.

Figure 8.2 Crustal cross-section from northern Ellef Ringnes Island to the Canada Basin (with no vertical exaggeration), based on geological mapping, borehole logs, seismic surveys and gravity data (after Sweeney, 1986b). Crustal thickening occurs beneath the Sverdrup Rim, separating areas of thinned continental crust near the axis of the Sverdrup Basin and along the margin of the Canada Basin. The presumed Cretaceous age of transitional and oceanic crust in the Canada Basin is still a matter of debate. Basic intrusive rocks within the continental tectonic zone overlap the boundary between the Sverdrup Basin and Arctic Terrace Wedge. Some examples of K-Ar age dates for igneous rocks in the area of the cross-section are listed in Table 2.2.

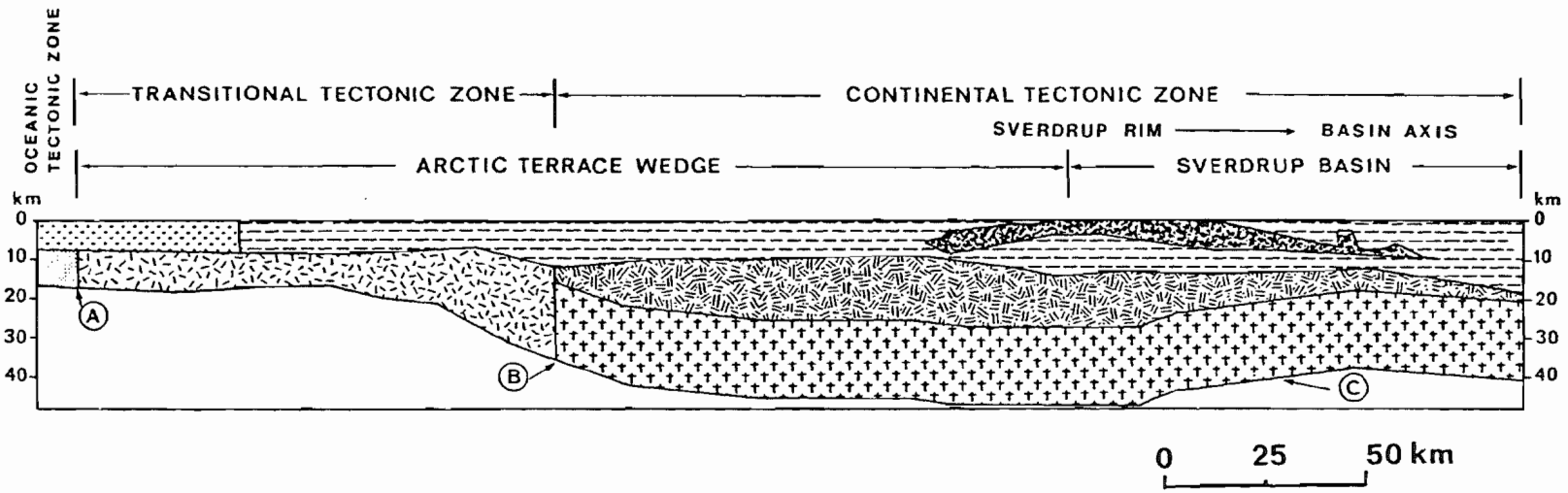

Undifferentiated deep-water sediments

Oceanic crust (of Cretaceous age)

Thinned continental crust (of Cretaceous or pre-Cretaceous age)

Mantle

Igneous rocks of Jurassic-Cretaceous age

Undifferentiated sedimentary rocks

Upper continental crust

Lower continental crust

Assumed boundary between (A) transitional and oceanic crust (B) continental and transitional crust (C) Mohorovičič Discontinuity

FIGURE 8.2

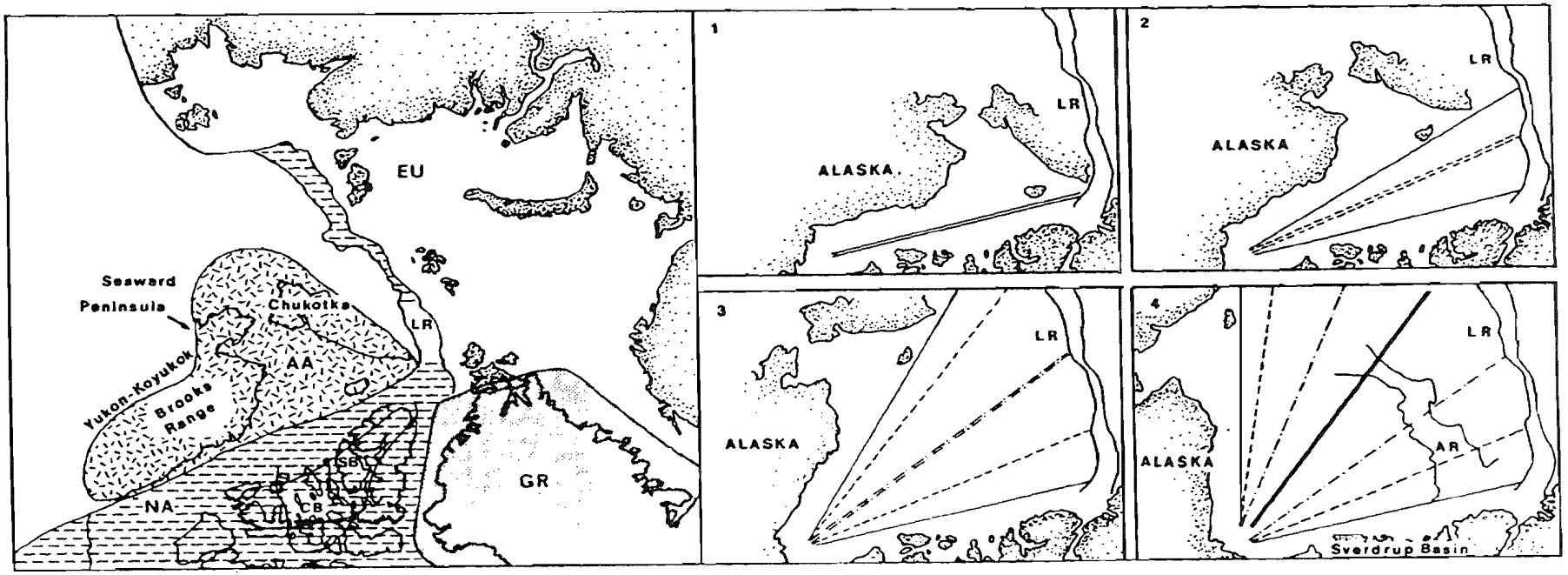

Figure 8.3 An example of plate reconstructions based on the rotation model for the opening of the Amerasian Basin during the Cretaceous (from Jackson et al., 1986). The diagram on the left shows the pre-drift position of the North American (NA), Eurasian (EU), Arctic-Alaska (AA) and Greenland (GR) plates. The Lomonosov Ridge (LR; ?fragment of the Barents Shelf formed during Cenozoic seafloor spreading in the Eurasia Basin) is fitted adjacent to the Eurasia Plate. The Chukchi Plateau (CB) overlaps the southwestern part of the Sverdrup Basin (SB) (challenged by Wynne et al., in press). Diagrams 1 to 4 show the position of the AA plate during counter-clockwise rotation away from NA. Fan-shaped magnetic lineations result from seafloor spreading about a pole located in the Beaufort Sea. In panel [4], AR = Alpha Ridge.

Stratigraphic data indicate that continental breakup occurred during the Valanginian-Albian interval (e.g. Sweeney, 1985). Depth-versus-age curves for the Canada Basin (Lawver and Baggeroer, 1983) suggest that seafloor spreading took place in the interval 125-90 Ma. Poorly-developed magnetic anomalies in the southern Canada Basin are consistent with crustal accretion during the Cretaceous non-reversal period (118-83 Ma; Jackson et al., 1986).

Despite the recent influx of data from polar ice stations, the debate concerning the age and origin of the Canada Basin is not resolved. Recently, the emphasis has shifted to evidence on land for rifting in the Sverdrup Basin and along the north coast of Alaska. The age of oceanic and transitional crust proposed by Sweeney (1986b; Fig. 8.2) implies that the Sverdrup and Canada Basins evolved as parallel rift basins during part of their history. Implications for the tectonic development of the Sverdrup Basin are considered below.

8.3 Tectonomagmatic Model

The two models described in Section 8.2 show agreement on the following points:

1. The Sverdrup Basin evolved as an intracontinental rift with a long history of basin subsidence and deposition.
2. The final stage of evolution of the Sverdrup Basin may have been influenced by plate tectonic reorganizations in Arctic regions, that led to the opening of the Canada Basin and formation of the polar continental margin.

The difference between the two models for the origin of the Cretaceous igneous province is a difference of internal vs. external dynamics. Many of the elements of the model proposed by Balkwill (1978) are consistent with present knowledge concerning rift-related magmatism in sedimentary basins. The best evidence for heat input during extension is igneous activity. Since Gass (1970) first proposed his classic model for the evolution of the Afro-Arabian dome, rift-related volcanism has been recognized in most continental extensional provinces. The nature of the thermal anomaly and its expression during rifting eventually led to the distinction between active and passive rifts. In the first, convective upwelling of the asthenosphere is invoked to explain volcanism and local doming that predate rifting. In the second, lithospheric thinning as a result of extension causes rifting to precede the onset of volcanism and uplift (Sengör and Burke, 1978). In many cases, both tectonic cycles produce a similar set of observations relating to heat flow, subsidence or uplift, extensional movements and igneous activity (Keen, 1985). This difficulty was encountered by Balkwill (1978), who speculated on the presence of a stationary hot spot beneath the Sverdrup Basin but found no evidence of a broad, elevated dome in the stratigraphic succession.

The timing and character of magmatism in extensional provinces (African-type rifts, CFB provinces, or along passive margins) are now viewed in more complex terms, such as the type and relative intensity of extensional movements, diversity of the mantle source and thermal properties of the lithosphere and asthenosphere. A case in point is the model proposed by McKenzie (1978) for the evolution of sedimentary basins, in which lithospheric thinning during simple, uniform extension

results in regional upwelling of asthenospheric material. Following the initial, rapid subsidence, a relatively long-term thermal subsidence occurs as an isostatic response to the cooling of the lithosphere. Implicit in this model is the presence of a broad-based, subcrustal heat anomaly during rifting (Hellinger and Sclater, 1983). Recent advances also constrain the role of partial melting during the rifting process (Foucher et al., 1982). Figure 8.4 (a) for example, shows how progressive thinning of the lithosphere can account for greater degrees of partial melting of mantle material during simple, uniform extension. The stretching factor β equals the ratio of the thickness of both the crustal and subcrustal layers before and after extension. Assuming lithospheric thinning by an amount β , partial melting will occur as a result of decompression during adiabatic uprise of the asthenosphere. Figure 8.4 (a) shows that, for a pyrolite mantle, the solidus intersects the adiabatic thermal gradient for the asthenosphere (Ta) at about 75 km. The degree and depth of partial melting will depend on the amount of extension and thinning, which determines the pressure decrease.

The degree and depth of partial melting in the mantle are important controls during the generation of alkaline or tholeiitic magmas (Section 7.3.1, Fig. 7.2). Such a correlation, between the degree and depth of partial melting in the mantle and the amount of lithospheric thinning, may influence the timing and character of magmatism in extensional settings. A wide rift such as the Sverdrup Basin, with a long depositional and tectonic history, may eventually display sufficient contrasts in the crustal stratigraphy to influence the melting regime in the mantle.

Figure 8.4 (a) Variation in the degree of partial melting of a pyrolite mantle according to temperature and depth. The temperatures within the lower lithosphere are shown for different values of the stretching factor . Ta, temperature of the asthenosphere; Zf, depth at which melting is initiated. The shaded area corresponds to the region of melting. Assuming adiabatic upwelling of the asthenosphere during simple, uniform extension, the depth and degree of partial melting in the mantle varies according to the value of the stretching factor, β [from Keen, 1987).

(b) Tectonomagmatic evolution of the Sverdrup Basin, integrated with the rifting history of the adjacent continental margin. Thick arrows indicate widespread intrusion and the peak of Cretaceous volcanic activity in the north-central Sverdrup Basin. Short arrows illustrate episodic volcanic activity. [Modified from Sweeney, 1986b, according to the subsidence analysis of Stephenson et al., 1987, and data from this study).

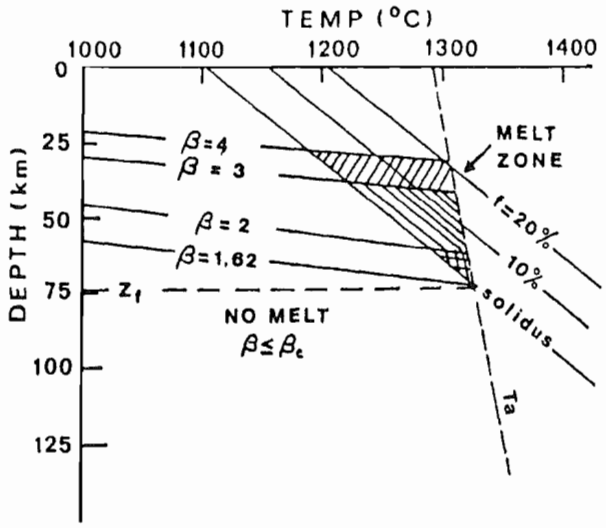
TEMP (°C)
1000
1100
1200
1300
1400
0
25
50
75
100
125
DEPTH (km)
β=4
β = 3
β = 2
β=1.62
z_t
NO MELT
β≤$β_c$
MELT
ZONE
f=20%
10%
solidus
Ta

(a)

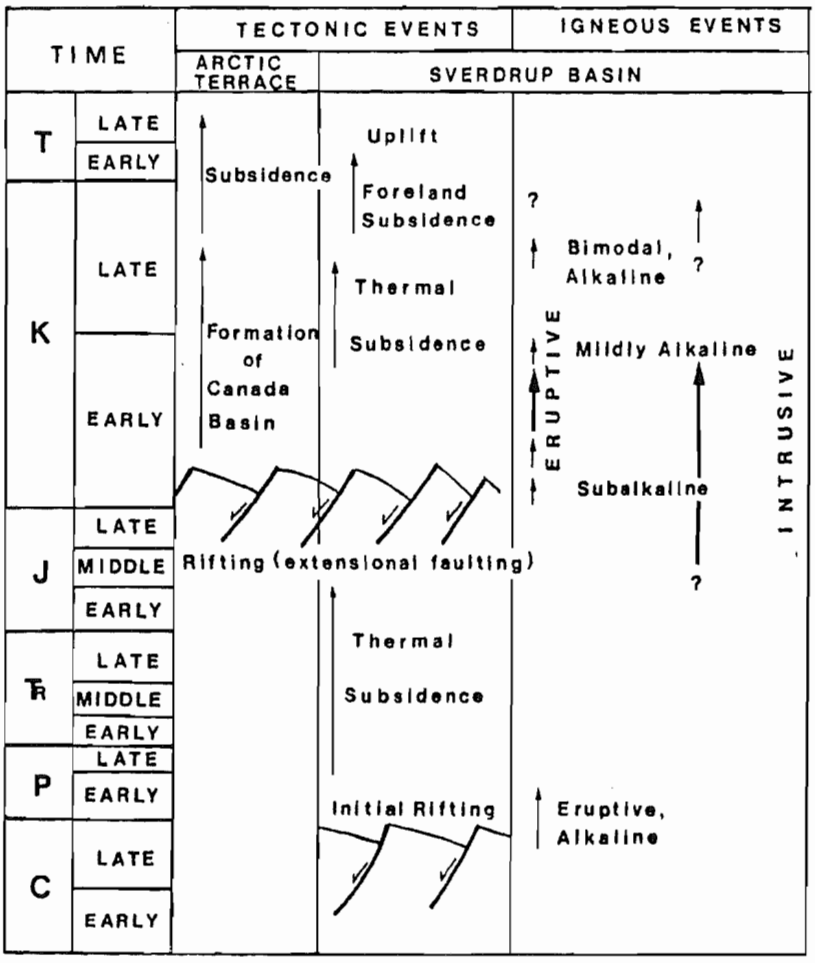
TIME
TECTONIC EVENTS
IGNEOUS EVENTS
ARCTIC TERRACE
SVERDRUP BASIN
T
LATE
EARLY
K
LATE
EARLY
J
LATE
MIDDLE
EARLY
TR
LATE
MIDDLE
EARLY
P
LATE
EARLY
C
LATE
EARLY
Subsidence
Uplift
Foreland Subsidence
Thermal Subsidence
Formation of Canada Basin
Rifting (extensional faulting)
Thermal Subsidence
Initial Rifting
?
Bimodal, Alkaline
?
Mildly Alkaline
Subalkaline
?
ERUPTIVE
INTRUSIVE
Eruptive, Alkaline

(b)

FIGURE 8.4

Figure 8.4 (b) integrates the igneous events in the Sverdrup Basin with the subsidence analysis of Stephenson et al. (1987) and the tectonic evolution of the adjacent continental margin (Sweeney, 1986b). The timing of igneous activity is as follows:

1. Volcanism of alkaline character accompanied the initial rifting event during the Carboniferous-Early Permian.
2. Voluminous magmatism of tholeiitic character in the eastern part of the Sverdrup Basin coincided with, and followed, renewed rifting during the Early Cretaceous.
3. Volcanic activity gradually waned during the Late Cretaceous.

This type of model provides a basis to explain both the timing of igneous events, and the compositional variations observed in the Sverdrup Basin.

1. The eruption of alkaline volcanic rocks during the Carboniferous and Permian was caused by small degrees of melting of mantle material during the initial rifting event.
2. The distribution of compositional types in the eastern part of the Sverdrup Basin (Figs. 7.6 and 8.1) was dependent on the thermal state of the lithosphere at the time of renewed rifting. Subalkaline igneous rocks were emplaced in areas close to the depocentre, where maximum lithospheric thinning favoured greater degrees of partial melting of mantle material. More alkaline magmas were generated beneath thicker, cooler crust along the southern margin of the basin.
3. A widening of the tectonic zone to the north is consistent with extension along the adjacent continental margin. Figure 8.5 is a schematic representation of the evolution of parallel rift basins (after Salveson, 1978): [1] The initial rifting event results in the formation

Figure 8.5 Schematic model for the combined evolution of parallel rift basins developed in continental crust (modified from Hellinger and Sclater, 1983, after Salveson, 1978). The initial rifting event results in the development of Basin I. [2] Crustal attenuation is compensated by mantle upwelling in the region of maximum lithospheric thinning. Partial melting results from adiabatic uprise of the asthenosphere and may be followed by localized volcanic activity. [3] Extension ceases, and the depositional history of the basin is determined by the amount of thermal subsidence that occurs as an isostatic response to lithospheric cooling. Renewed extension promotes the development of a second rift basin in adjacent continental crust. [4] Prolonged extension of the lithosphere leads to the generation of oceanic crust in the newly-formed basin; renewed tectonism and widespread igneous activity in the intracontinental rift basin; and [5] to the formation of a mature continental margin. The thermal state of the subcrustal lithosphere and underlying asthenosphere during the second rifting episode remains speculative. Evidence from the Sverdrup Basin suggests that voluminous tholeiitic magmatism (resulting from relatively larger degrees of partial melting) was limited to areas of maximum lithospheric thinning close to the depocentre. This is consistent with theoretical predictions (Fig. 8.4 a). The presence of both tholeiitic and alkaline igneous rocks along the Sverdrup Rim, however, implies a broadening of the tectonic zone in the direction of the developing passive margin.

EVOLUTION OF PARALLEL RIFT BASINS

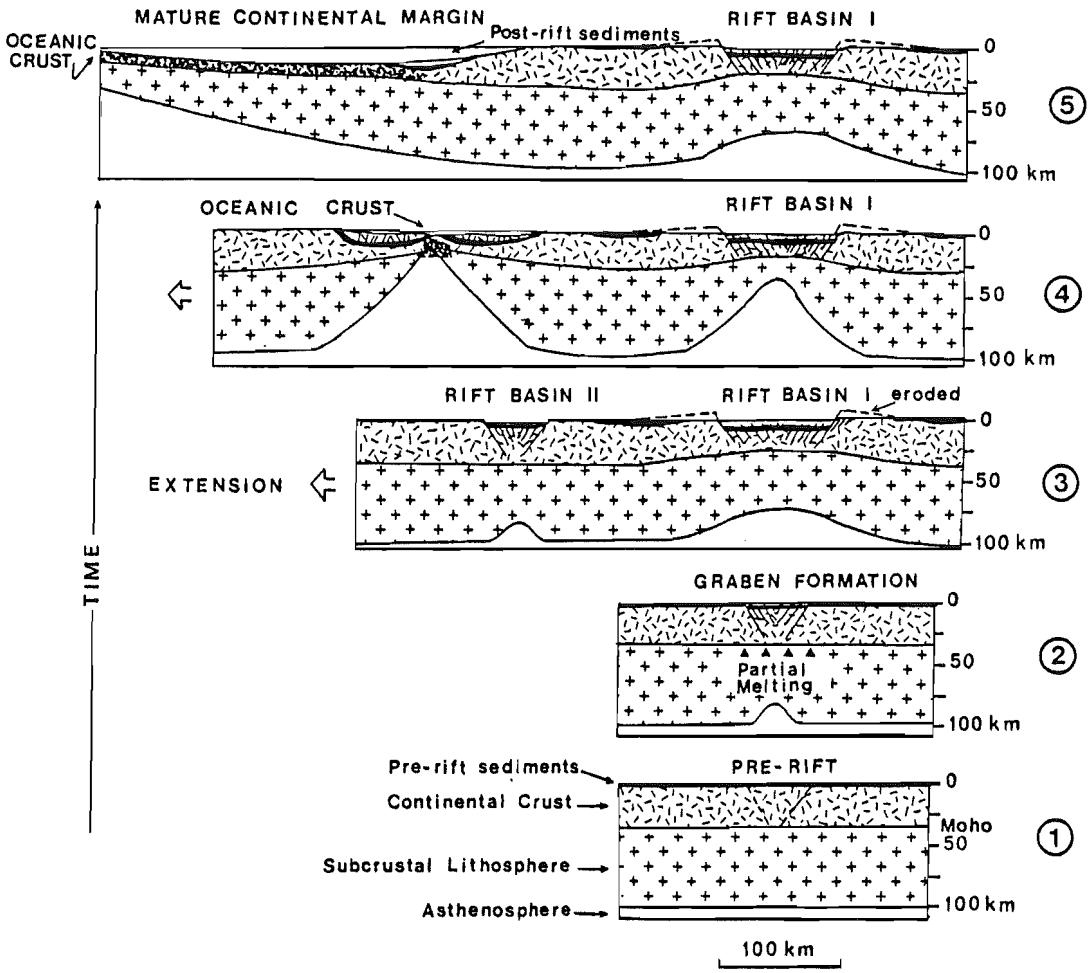

FIGURE 8.5

of an intracontinental basin. [2] Tensional stresses within the lithosphere cause the upper mantle to fail by necking. The compensating rise of the asthenosphere to a lower pressure regime initiates partial melting in the upper mantle. Igneous activity may follow. [3] The main depositional stage occurs during thermal subsidence. Renewed extension promotes the development of a second rift basin in adjacent continental crust. [4] A more robust extensional regime leads to the generation of oceanic crust, and eventually, [5] to the formation of a mature continental margin. This sequence of extensional events results in the type of crustal stratigraphy observed along the ocean-continent transect for the Canadian Arctic Islands (Fig. 8.2).

During renewed rifting (Panel [4] on Fig. 8.5), extensional movements in the continental zone would proceed from the area of greatest lithospheric thinning (basin axis) towards the ocean-continent boundary. In the case of the Sverdrup Basin, a broadening of the tectonic zone caused igneous activity to spread along the northern margin. Tectonic rejuvenation at the northernmost limit of the extensional zone triggered the final phase of volcanic activity during the Late Cretaceous.

The sequence of igneous events on Figure 8.4 (b) allows some speculation regarding the role of the lithosphere and asthenosphere during renewed rifting. An estimate of the total amount of melt produced can be calculated by integrating over the area of melting in Figure 8.4 (a; Foucher et al., 1982; Keen, 1987). Assuming uniform stretching, the amount of partial melt produced during passive upwelling is critically dependent on the potential temperature of the asthenosphere (Ta), initial thickness of the lithosphere and stretching

factor (e.g. White et al., 1987). Estimates of the thickness of partial melt generated are in the order of 5 km, for steadily increasing values of (Keen, 1987). The subsidence analysis of Stephenson et al. (1987) suggests a stretching factor of about 2 for crystalline crust underlying the Sverdrup Basin, a result that is consistent with previous estimates based on gravity modelling (Sobczak and Overton, 1984). The calculations of White et al. (1987) suggest that thinning of 100 km thick lithosphere by this amount will produce approximately 1 km of partial melt (if Ta = 1380 ^{o}C). This is clearly insufficient to account for the volume of magma emplaced within the Sverdrup Basin. Although only approximate, volume estimates for the Cretaceous igneous province (Table 1.1) cannot be explained by partial melting events during simple, uniform extension, unless elevated mantle temperatures or greater lithospheric thinning are invoked. White et al. (1987), propose that an increase by 100-150 ^{o}C in the potential temperature of the asthenosphere is sufficient to account for enhanced melt production at rifted margins in proximity to a hot spot. Alternatively, lateral temperature gradients in extensional settings may induce small-scale convection in the upper mantle, leading to enhanced melt production during convective partial melting (Mutter et al., 1988). This type of melting model is germane to the process of convective thinning of the lithosphere, discussed by other authors (e.g. Yuen and Fleitout, 1985). In wide rifts, such as the Sverdrup Basin, this mechanism can account for maximum lithospheric thinning along one or both edges of the rift zone, where the strongest lateral temperature gradients occur (Keen, 1987).

At the present time, the latter model is more consistent with tectonic rejuvenation than the elevated mantle temperatures requiring

proximity to an asthenospheric plume. Convective thinning of the lithosphere could have contributed to igneous activity along the Sverdrup Rim and enhanced the opportunity for crustal assimilation during the peak of volcanic activity in the north-central part of the basin.

8.4 Regional Implications

The Alpha Ridge

Geological and geophysical investigations of the Alpha Ridge (shown as [4] on Fig. 8.1), during Project CESAR, have led to the following conclusions (Sweeney and Weber, 1986a):

- The ridge is oceanic in nature and was built, at least in part, by volcanic activity.
- The age of the ridge is constrained to the Cretaceous period (120-80 Ma) by paleontological, heat flow and magnetic data.

The results from this study do not provide any direct evidence concerning the nature of the Alpha Ridge. However, some aspects of the tectonomagmatic model described above provide additional constraints on previously proposed models for its origin.

If indeed the Alpha Ridge is a volcanic feature, it represents an igneous event of major proportions. Seismic refraction studies indicate a velocity structure of remarkable lateral (100 km) and vertical (23 km) continuity (Weber, 1986), similar to that of oceanic plateaus (Jackson et al., 1986). Any mechanism invoked for its origin must be able to account for the production of a large amount of partial melt, emplaced either in the form of intrusions or erupted lavas.

This type of problem has already been addressed by a number of workers to explain the origin of thick igneous sequences that form prominent reflectors along some rifted continental margins (e.g. Saunders, 1988). The models invoked suggest that enhanced melt production can occur at or near a hot spot, or during convective partial melting. There is no general consensus regarding the origin of the Alpha Ridge, partly because the data compiled during CESAR are insufficient to end all speculation. Many of the features observed are consistent with the origin of the Alpha Ridge as an aseismic ridge formed by hot spot activity as spreading began in the Canada Basin (Williamson and Van Wagoner, 1985; Van Wagoner et al., 1986). Such a mode of origin is compatible with the plate reconstructions of Jackson et al. (1986; panel [4] on Fig. 8.2). Some workers have proposed that the Cretaceous igneous province is, in fact, a manifestation of hot spot activity at the site of the Alpha Ridge (Ricketts et al., 1985; Embry and Osadetz, in press). The evidence from this study suggests that there is a monotonic progression from subalkaline to mildly alkaline to highly alkaline igneous activity with time, as well as a migration of volcanic centres north and east of the depocentral area, perhaps as far as northern Greenland (Figs. 7.6 and 8.1). The possible genetic link between igneous activity of ?alkaline character offshore and the emplacement of voluminous tholeiitic magmas onshore is, therefore, tenuous at best.

The lack of direct evidence for hot spot activity during the igneous history of the Sverdrup Basin would seem to preclude the development of an aseismic ridge in the Canada Basin. An alternate mechanism is convective partial melting. The position of the Alpha

Ridge (Fig. 8.1) suggests its initiation within a zone of contrasting thermal structure and crustal stratigraphy, at the intersection of the Sverdrup Rim with thinner, ?transitional crust on the adjacent rifted margin. Mutter et al. (1988), proposed that aseismic ridges form when a spreading centre relocates in older oceanic lithosphere. The resulting configuration of isotherms may lead to convective partial melting and enhanced melt production.

Until the age and geochemical characteristics of the Alpha Ridge and volcanic rocks on northern Ellesmere Island are better constrained, no unique model involving lithospheric vs. asthenospheric control can be invoked. The author favours the former at the present time, but acknowledges the lack of evidence to support the model.

Magmatism at Rifted Margins

The present study has focused on the timing and character of intracontinental basin magmatism during tectonic rejuvenation. In the specific case considered, there is evidence to support enhanced igneous activity in the continental zone during renewed extension along the adjacent rifted margin. The tectonomagmatic model proposed for the Sverdrup Basin implies that it evolved as a passive margin basin during the final depositional and tectonic stage in the Cretaceous.

Passive margin basins that are parallel to large ocean basins evolve in two distinct stages, the first of which involves the formation of a continental rift basin (Perrodon, 1985). Some of the characteristics of the Sverdrup Basin igneous province are also found along Atlantic-type margins:

- Voluminous igneous activity of tholeiitic character in the continental zone, often in the form of linear dyke swarms that are emplaced prior to continental breakup.
- Widening of the tectonic zone in the direction of the developing continental margin.
- Presence of three types of basement that define the continental, transitional and oceanic regions (Fig. 8.2).

Cretaceous igneous rocks of the east-central Sverdrup Basin are best compared to the Triassic diabase dykes and sills of Eastern North America, emplaced during the initial phase of igneous activity associated with the opening of the North Atlantic (e.g. Bryan et al., 1977). The discussion about the effects of crustal contamination, presented in Chapters 5 and 7, is particularly relevant to the petrogenesis of continental tholeiites emplaced in this type of extensional setting. In addition, some aspects of the tectonomagmatic model proposed apply to the igneous history of rift basins developed along passive margins.

The evidence presented in this chapter argues in favour of lithospheric control on the spatial-compositional distribution of igneous rocks in the Sverdrup Basin. Other studies of magmatism in intracontinental rifts also conclude that the timing and character of magmatism were determined by crustal stratigraphy and the thermal state of the lithosphere prior to the onset of rifting (e.g. Wernicke et al., 1987). Recent studies of the deep structure of the rifted margin off Eastern Canada suggest that these variables also determine the locus and extent of igneous activity in syn-rift basins adjacent to the ocean-continent boundary (Keen and de Voogd, 1988), and that lithospheric

control may influence the timing and character of magmatism along both "volcanic" and "non-volcanic" continental margins.

Rifted margins are commonly classified as non-volcanic or volcanic, depending on the evidence for widespread igneous activity associated with rifting. The latter usually consists of prominent dipping reflectors along the margin, that are interpreted as thick igneous complexes emplaced during continental breakup (e.g. Hinz et al., 1987). The eastern North American margin is considered to be non-volcanic, in view of the relatively limited igneous activity of alkaline character attributed to fault reactivation. From Late Jurassic to Early Cretaceous, igneous activity was widespread along the newly-formed margin of the western North Atlantic. Petrological studies of igneous rocks from the eastern Canadian continental margin suggest that alkali basalts of intraplate character predominate (Jansa and Pe-Piper, 1988). Magmatism was related to three major tectonic events: the initiation of rifting in the Labrador-Greenland region, plate separation between Iberia and the Grand Banks, and seafloor spreading in the Labrador Sea (Srivastava and Tapscott, 1986).

The presence of seaward-dipping reflectors off the Grand Banks suggests that magmatic underplating or intrusion of the lower crust was confined to areas near the ocean-continent boundary that underwent large amounts of thinning during rifting. Basins formed further landward on the margin do not exhibit these features (Keen and de Voogd, 1988). The new results have important implications for the role of rift-related magmatism during the evolution of passive margins. Samples recovered from drilling through the reflectors suggest that they consist of igneous rocks of tholeiitic character (e.g. Roberts et al., 1984). The

predominance of alkaline rocks in Cretaceous igneous provinces of the eastern Canadian continental margin may, therefore, only be apparent. Jansa and Pe-Piper (1985) have proposed that most of the igneous activity resulted from the reactivation of old fracture zones. The origin of the Cretaceous alkaline suites along the continental margin should be re-examined in terms of the thermal history and crustal stratigraphy of the host basins, particularly in areas close to the ocean-continent boundary.

The synchroneity of magmatism in the Sverdrup Basin and along parts of the eastern Canadian continental margin has led some authors to speculate on the existence of a link in tectonic regimes between the two areas. The evidence from this study indicates that this is not the case: the igneous provinces of similar age located offshore Eastern Canada and in the Sverdrup Basin are related to the opening of two distinct ocean basins. However, waning volcanic activity in both of these provinces during the Late Cretaceous was closely followed by widespread volcanism associated with the opening of Baffin Bay (Fig. 8.1; Clarke, 1969; Clarke and Pedersen, 1976). Crustal attenuation to the northwest and southeast of the Tertiary volcanic province may have played a role in determining the volume and composition of igneous rocks emplaced in the Baffin Bay-West Greenland area. An integrated study of all three provinces would clarify the role of basin magmatism of either tholeiitic or alkaline character in the Sverdrup Basin, Baffin Bay-West Greenland volcanic province and along the eastern Canadian continental margin.

APPENDIX A

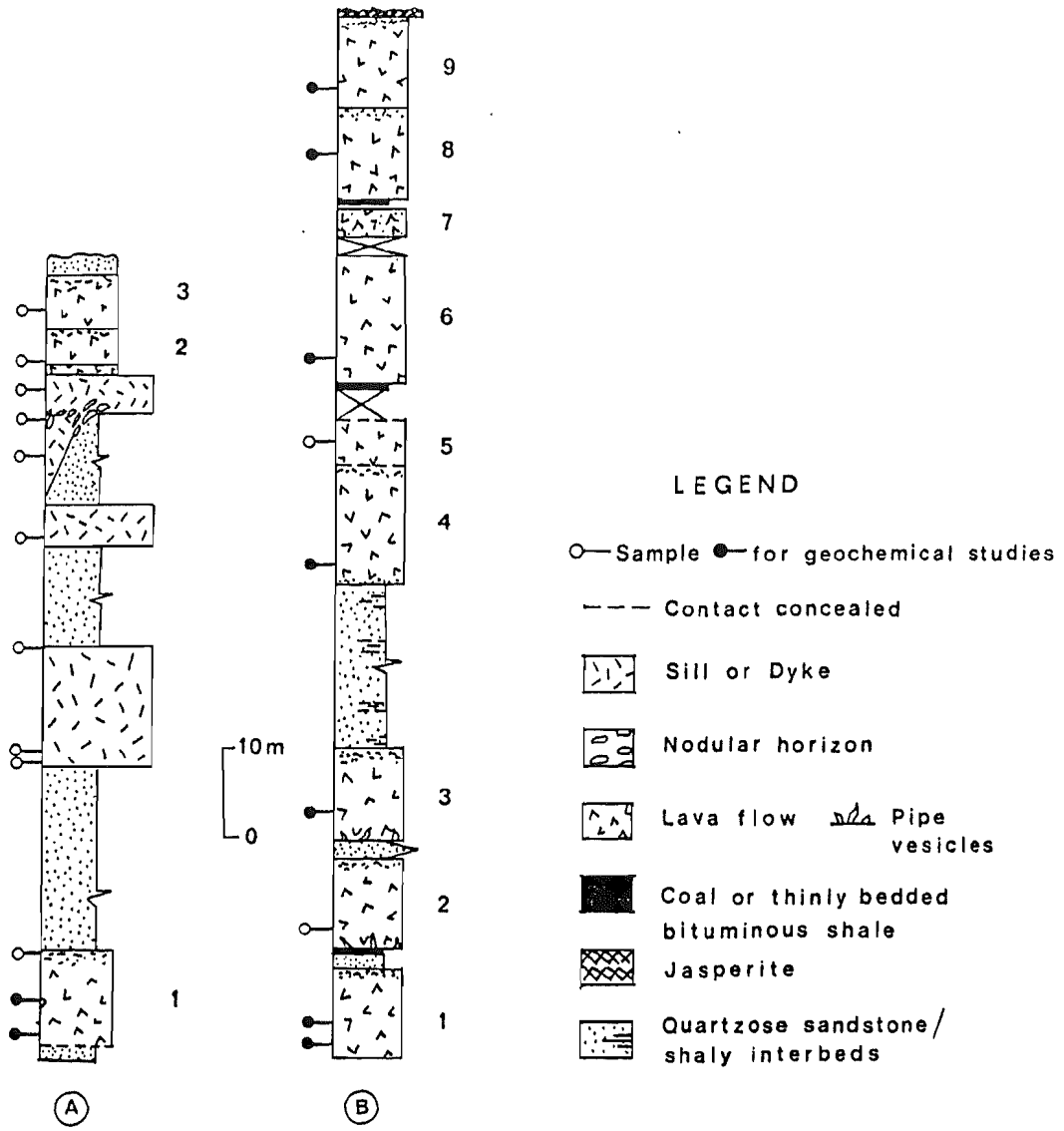

Figure A.1 Schematic representation of sections measured in the Isachsen Formation.
[A] Igneous rocks in the Paterson Island Member, Geodetic Hills, central Axel Heiberg Island.
[B] Volcanic rocks in the Walker Island Member along Camp Five Creek, northern Axel Heiberg Island.
Stratigraphy by K. Osadetz and G.K. Muecke.

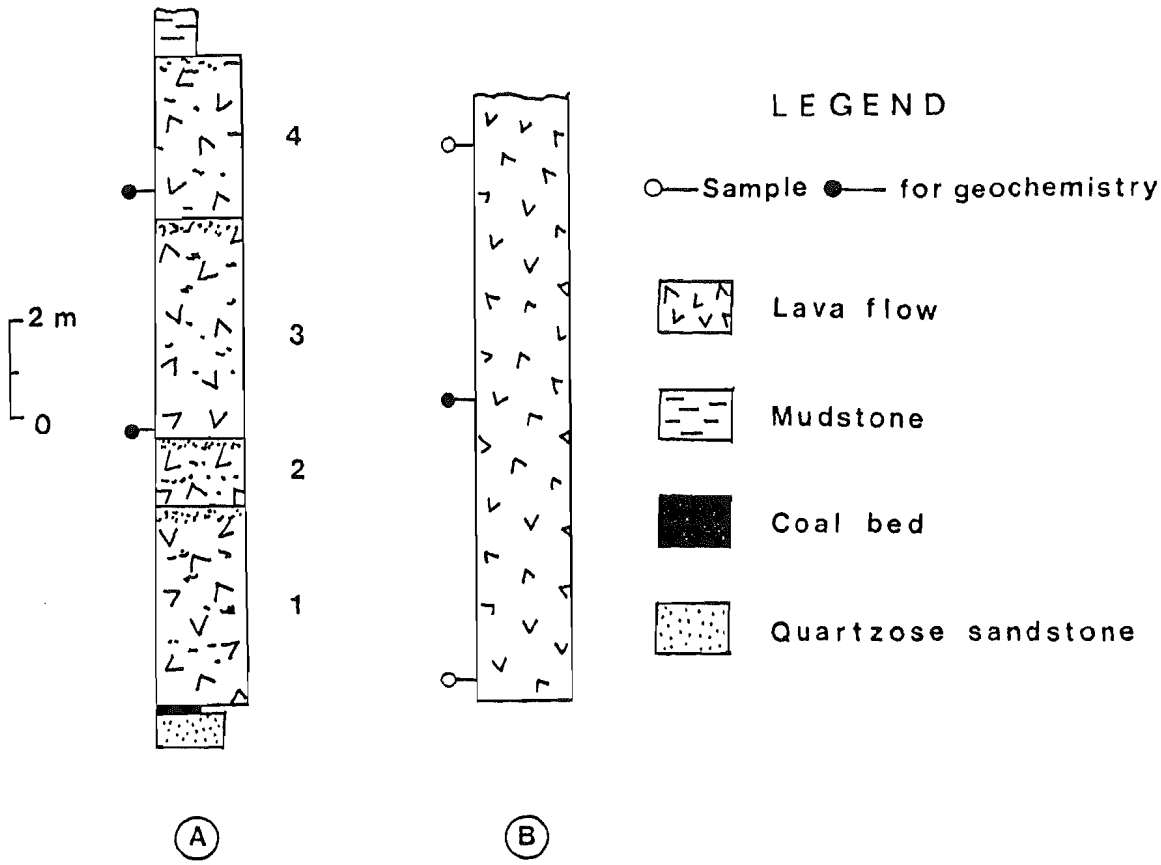

Figure A.2 Schematic representation of sections measured in the Isachsen Formation, Blue Mountains area, western Ellesmere Island.
[A] EL-84 section, Blackwelder Ridge
[B] EL-85 section, Blue Mountains Ridge

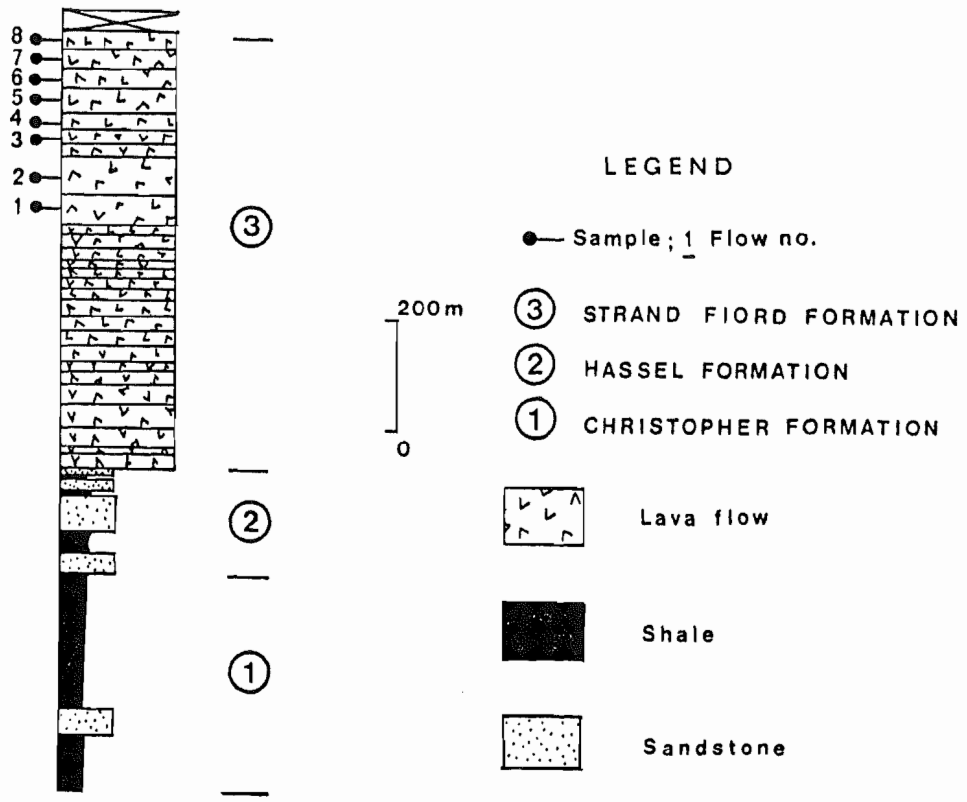

Figure A.3 Schematic representation of the stratigraphic succession along Celluloid Creek, near Bunde Fiord on northern Axel Heiberg Island. Redrawn from measurements by K. Osadetz (unpubl.).

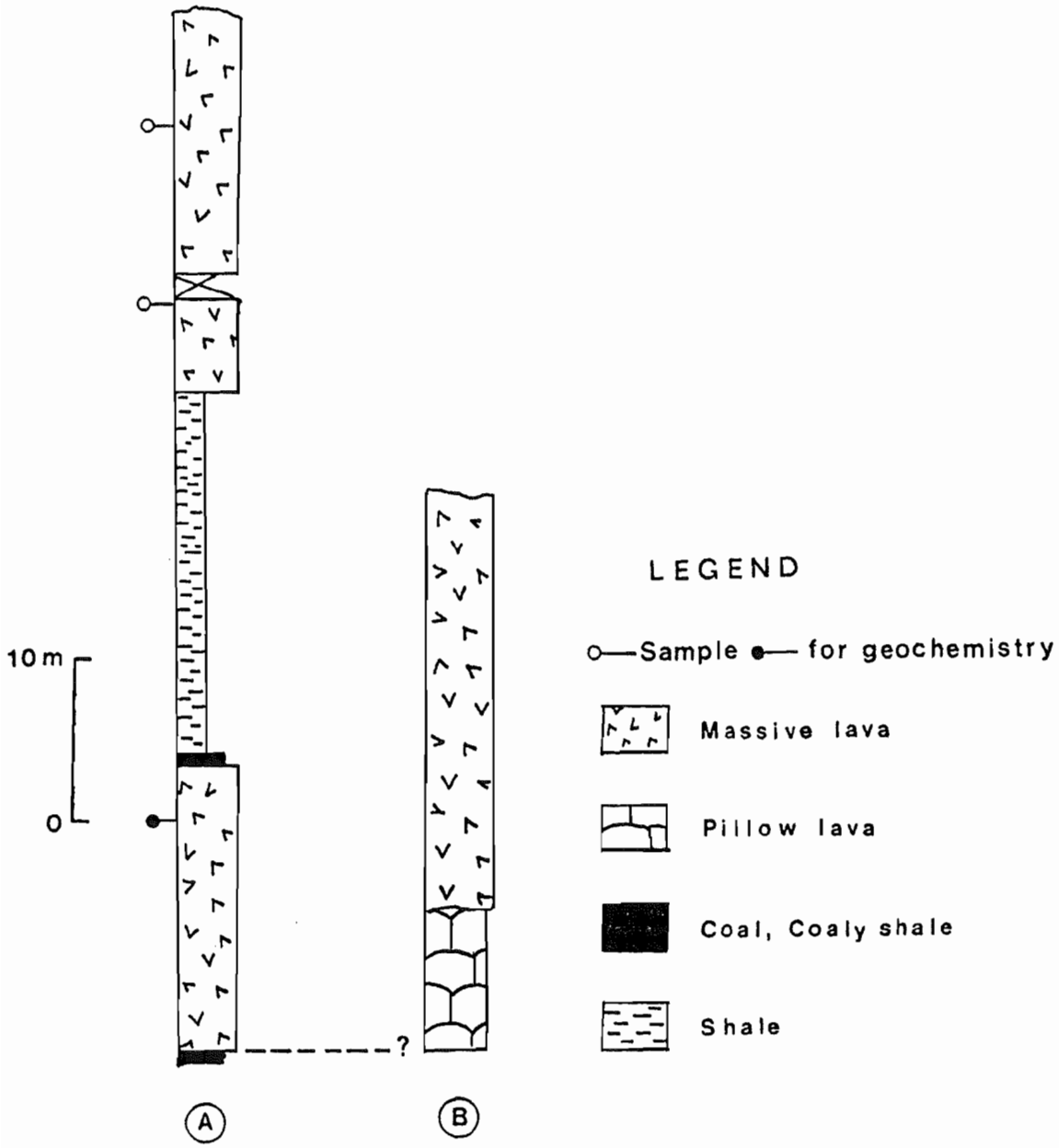

Figure A.4 Schematic representation of the volcanic stratigraphy at two locations on the ***Arctic Hare Mesa***, Piper Pass area of northern Ellesmere Island.

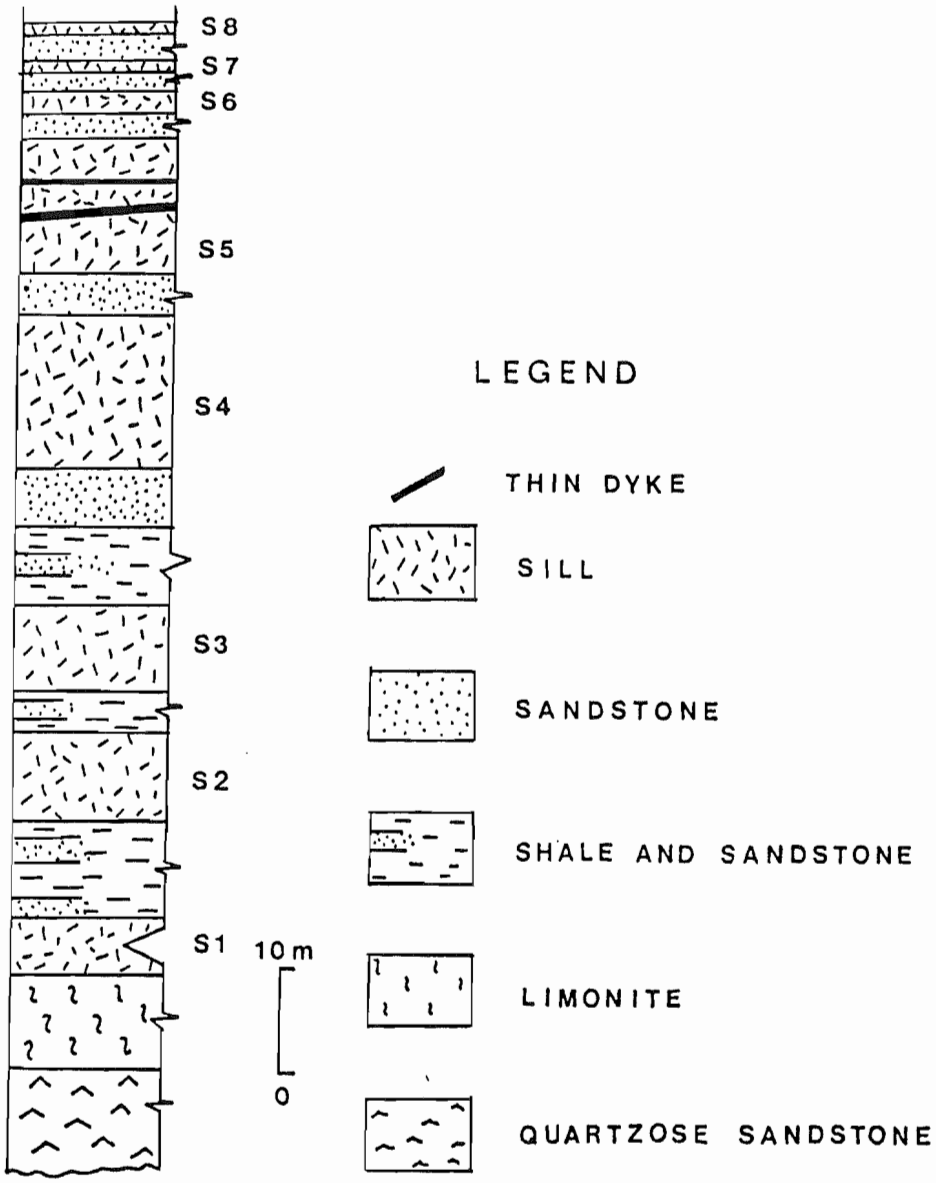

Figure A.5 Stratigraphy along the Rollrock River section, Tanquary Fiord area, northern Ellesmere Island (Appendix A).

LOCATION DATA AND SAMPLING INFORMATION:
EXTRUSIVE ROCKS

GROUP 1A
SECTION: Volcanic rocks in the Isachsen Formation, Geodetic Hills
AREA: Central Axel Heiberg Island 1985
TOPOGRAPHIC MAP # 59H, Strand Fiord
LONG. W89°45'00" LAT. N79°49'03"
GEOLOGICAL MAP # 1301 A, 1:250 000, Strand Fiord
VOLCANIC STRATIGRAPHY: Figure A.1, [1]

GROUP 1B
SECTION: Volcanic rocks in the Isachsen Formation, Camp Five Creek
AREA: Northern Axel Heiberg Island 1985
GEOLOGICAL MAP # 1310A, 1:250 000, Bukken Fiord
AIR PHOTO NO. A16754-160 COORDINATES (29,10)
VOLCANIC STRATIGRAPHY: Figure A.1, [2]

GROUP 1C
SECTION: Volcanic rocks in the Isachsen Formation, Blue Mountains
AREA: Northwestern Ellesmere Island 1984-85
GEOLOGICAL MAP # 1311A, 1:250 000, Greely Fiord West
AIR PHOTO NO. A16686-30 COORDINATES SECTION [1] (27,12)
SECTION [2] (47,59)
VOLCANIC STRATIGRAPHY: Figure A.2

GROUP 2A
SECTION: Strand Fiord Formation
AREA: Western Axel Heiberg Island 1983
TOPOGRAPHIC MAP # 59H, Strand Fiord
GEOLOGICAL MAP # 1301A, 1:250 000
TRAVERSES:
Twisted Ridge: LONG. W92°17'00" LAT. N79°25'00"
Bastion Ridge: LONG. W90°47'00" LAT. N79°21'00"
W. Glacier Fiord Syncline: LONG. W90°30'00"
LAT. N79°06'00"
VOLCANIC STRATIGRAPHY: [2], [3] and [4] on Figure 3.4
East Glacier Fiord Syncline: G.S.C. Open File Map #1147, Section RAK 32-83
VOLCANIC STRATIGRAPHY: in Ricketts et al., 1985

GROUP 2B
SECTION: Strand Fiord Formation
AREA: Northern Axel Heiberg Island 1983, 1985
GEOLOGICAL MAP # 1310A, 1:250 000, Bukken Fiord
TRAVERSES:
Celluloid Creek: AIR PHOTO NO. A16755-9 COORDINATES (50,61)
VOLCANIC STRATIGRAPHY: Figure A.3
Artharber Creek: AIR PHOTO NO. A16755-170
COORDINATES (31,50)
VOLCANIC STRATIGRAPHY: Figure 3.2

GROUP 3
SECTION: Volcanic rocks in the Hassel Formation
AREA: Northeastern Ellesmere Island 1984
TRAVERSES:
Tropical Ridge, Lake Hazen:
GEOLOGICAL MAP: See Figure 4.5
AIR PHOTO NO. A16977-27 COORDINATES (36,3)
VOLCANIC STRATIGRAPHY: Figure 4.8
Arctic Hare Mesa, Piper Pass:
GEOLOGICAL MAP: See Figure 4.6
AIR PHOTO NO. A16604-109
COORDINATES: EL84-007 NW SECTION (33,41)
EL84-010 NE SECTION (34,44.5)
VOLCANIC STRATIGRAPHY: Figure A.4

LOCATION DATA AND SAMPLING INFORMATION
INTRUSIVE ROCKS

GROUP A - *LIGHTFOOT RIVER*

AIR PHOTOGRAPHS: A = A16840-58; B = A16836-65

SAMPLE #	UNIT #	COORDINATES	H.B./T.T.*
AX85-001	SILL 2	A (66.5,46)	6 m/ 9 m
AX85-005	SILL 3	A (67,46)	6 m/ 15 + m
AX85-008	SILL 4	A (20,29)	4.75 m/ 12 + m
AX85-013	SILL 5	A (22,36.5)	4.5 m/ 5 m
AX85-015	DYKE 6	B (33.5,61)	2.5 m/ 6.5 m
AX85-019	DYKE 9	A (29,33.5)	8.0 m/ 21.5 m
AX85-020			18.5 m/ 21.5 m
AX85-026	DYKE 10	A (35.5,36)	11.5 m/ 14.5 m
AX85-027	SILL 6	A (54,47.5)	3.25 m/ 7.5 m
AX85-030	DYKE 5	B (25,40)	CM/ 60 m
AX85-031			6 m/ 60 m
AX85-032			16.5 m/ 60 m
AX85-033			18 m/ 60 m
AX85-035			43.5 m/ 60 m
AX85-036			50.5 m/ 60 m
AX85-037			CM/ 60 m
AX85-040	DYKE 4	B (14,58)	7.5 m/ 15 m
AX85-043	DYKE 3	B (7.5,50)	3 m/ 6.25 m
AX85-046	DYKE 2	B (6.0,44.5)	4.0 m/ 5.5 m
AX85-048	DYKE 1	B (5.5,33.5)	1.5 m/ 3 m

*Height from base and total measured thickness

GROUP B - *BUCHANAN LAKE, BLACKTOP RIDGE*

AIR PHOTOGRAPHS: A = A16858-29; B = A16858-30;
C = A16724-122

SAMPLE #	UNIT #	COORDINATES	H.B./T.T.
BUCHANAN LAKE			
AX85-051	SILL L	B (14,3)	0.3 m/ 1.7 m
AX85-052	SILL M	B (13.5, 2.5)	0.5 m/ E 50 m
AX85-057	SILL N	A (14.5,31.5)	0.3 m/ E 50 m
AX85-059			40 m/ E 50 m
AX85-061	SILL O	A (13,30)	2.5 m/ 5 m
AX85-062	DYKE Q	A (12,27)	CM/ 1.5 m
AX85-063			CENTRE/ 1.5 m
AX85-067	DYKE R	A (12,27)	CM/ 0.3 m
AX85-215	SILL A	B (34.5,22)	0.3 m/ 36 m
AX85-217			13 m/ 36 m
AX85-218			24 m/ 36 m
AX85-220	SILL B	B (34,12)	0.5 m/ 1.5 m
AX85-221	SILL C	B (34.12)	0.7 m/ 1.4 m
AX85-222	SILL D	B (34,12)	0.5 m/ 1.4 m

GROUP B (continued)

SAMPLE #	UNIT #	COORDINATES	H.B./T.T.
BUCHANAN LAKE			
AX85-223	SILL E	B (25,13)	1 m/ E 28 m
AX85-224			14.5 m/ E 28 m
AX85-225			17.5 m/ E 28 m
AX85-226			26.5 m/ E 28 m
AX85-227	SILL F	B (23,11)	0.25 m/ 35 m
AX85-228			7.5 m/ 35 m
AX85-230	SILL G	B (23.10)	0.7 m/ E 20 m
AX85-231	SILL H	B (16.5,5.5)	0.3 m/ E 13 m
AX85-233			6.0 m/ E 13 m
AX85-234	SILL I	B (17.5,3.5)	0.7 m/ 6.5 m
AX85-235			3 m/ 6.5 m
AX85-237	DYKE J	B (17.5,3)	4.5 m/ 8 m
AX85-238	SILL K	B (17.5,2.5)	0.7 m/ 8.5 m
AX85-239			3 m/ 8.5 m
BLACKTOP RIDGE			
EL85-201	SILL A	C (41,37)	CM/ 14 m
EL85-202			8 m/ 14 m
EL85-205	SILL B	C (43.5,33)	17 m/ 38 m
EL85-207			CM/ 38 m
EL85-208	SILL C	C (43.5,33)	CM/ 33 m
EL85-209			8.5 m/ 33 m
EL85-213	SILL D	C (45,33.5)	8.5 m/ E 24 m

GROUP C - *TANQUARY FIORD*

AIR PHOTOGRAPH A = A16788-66
B = A16788-65

SAMPLE #	UNIT #	COORDINATES	H.B./T.T.
ROLLROCK RIVER			
EL84-211	SILL 4	A (37,59)	CM/ 14 + m
EL84-218	SILL 1	A (37,59)	0.8 m/ 4.8 m
EL84-221	SILL 2	A (37,59)	8.8 m/ 9 m
EL84-222	SILL 3	A (37,59)	5.0 m/ 9 m
EL84-223	SILL 5	A (39,61)	0.2 m/ 14 m
EL84-229	SILL 6	A (39,64)	1.0 m/ 1.9 m
EL84-232	SILL 7	A (39,64)	0.7 m/ 1.0 m
EL84-235	SILL 8	A (39,64)	0.9 m/ 1.5 m

GROUP C (continued)

SAMPLE #	UNIT #	COORDINATES	H.B./T.T.
MACDONALD RIVER			
EL84-236	SILL 3	B (46,58)	1.0 m/ 23 + m
EL84-245	SILL 1	B (46,58)	3.2 m/ 3.2 + m
EKBLAW LAKE			
T-S6-14	LAYERED SILL	G.S.C.	CM/ 24.5 m

GROUP D - *LAKE HAZEN, PIPER PASS*

AIR PHOTOGRAPHS A = A16604-108
B = A16604-109
C = A16604-107
D = A166977-29

SAMPLE #	SECTION/UNIT	COORDINATES	H.B./T.T.
PIPER PASS			
EL84-015	MOUNT DOOM UPPER SILL	A (21.5,36.5)	CM/ 20 + m
EL84-023	DARK CRYSTAL	A (7.5,31.5)	CM/ 90 + m
EL84-041	ELROND RIDGE SILL B	B (7,39)	0.7 m/ 8.8 m
EL84-044	ELROND RIDGE SILL C	B (7,39)	2.0 m/ 8 m
EL84-046	STAR INTRUSIVE FEEDER B	C (24,27)	CM
EL84-050	STAR INTRUSIVE SILL 4	C (27,27)	2.5 m/ 10 m
EL84-056	STAR INTRUSIVE SILL 1	C (29,31)	CM/ 62 + m
EL84-060	CAMP SILL	C (29,16)	CM/ 37 + m
EL84-072	STAR INTRUSIVE DYKE 2 - NEAR CONTACT WITH SILL 1	C (28,30)	CM/ 2.5 m
EL84-073	PIPER PASS SILL 3	B (66,50)	1.0 m/ 12.5 + m
EL84-076	PIPER PASS SILL 1	B (68,50)	1.0 m/ 11.5 + m
EL84-110	STAR INTRUSIVE DYKE 1	C (26,30)	CM/ 60 m

GROUP D (continued)

SAMPLE #	SECTION/UNIT	COORDINATES	H.B./T.T.
LAKE HAZEN			
EL84-098	WEST CUESTA CREEK DYKE 1	D (13.5,56)	CM/ 3 m
EL84-210	COMPOSITE INTRUSION MASSIVE SILL, UNIT # 2	D (13.5,56)	CM/ 24.3 m

- OTHER SAMPLE NUMBERS REFERED TO IN THE TEXT

TANQUARY FIORD

Sample # (1)	Locality	Ref.(2)
C-082080	Sill intruding Christopher Formation	T-S1
C-082081	Sill intruding Isachsen Formation	T-S2*
C-082083	Sill intruding the Heiberg Formation	T-S3*
C-082084	Sill intruding the Isachsen Formation	T-S4*
C-082085	Sill intruding the Canyon Fiord Formation	T-S5*
Layered sill intruding the Heiberg Formation **		
C-082087	Upper chilled margin	T-S6
C-082088	Pegmatoid, subophitic gabbro in core of sill	
C-082089	Subdiabasic gabbro	
C-082082	Dyke intruding the Jurassic-Cretaceous sandstone and shale sequence, Ekblaw Lake.	T-D1
C-082086	Dyke intruding the Jurassic-Cretaceous sandstone and shale sequence, Ekblaw Lake.	T-D2

LAKE HAZEN AND PIPER PASS AREAS

C-082078	Sill intruding upper Paleozoic strata	H-S7*
C-082077	Sill intruding upper Paleozoic strata	H-S8
C-082076	Sill intruding upper Paleozoic strata	H-S9*
C-076562	Dyke intruding the Jurassic-Cretaceous sandstone and shale sequence on the Gilman River.	H-D3*
C-082910	Sample of basaltic flow; location refered to as West Tropical Ridge, this study.	H-F1*
C-082074	Sample of basaltic flow southwest of Mesa Creek.	H-F2*

OTHER SAMPLES (continued)

Sample # (1)	Locality	Ref.(2)
C-082743	Sample of basaltic flow, lower flow unit.	P-F3*
C-082746	Sample of basaltic flow, upper flow unit.	P-F4*
C-082904	Sample of basaltic flow	P-F5*
C-082750	Sample of basaltic flow	P-F6*

(1) Osadetz and Moore, in press.
(2) Localities shown in Figures 4.4, 4.5 and 4.6.
* Data quoted in text and figures.
** Sample of upper chilled margin re-analysed for this study and listed as T-S6-14 in appendices.

PETROGRAPHIC SUMMARIES
EXTRUSIVE ROCKS

Symbols and Abbreviations

1. Samples are listed according to stratigraphic height in each volcanic succession.

2. Per cent volumes, when estimated visually, are simplified according to the following scheme:

% Phenocrysts	Term used
0	Aphyric
1-2	Sparsely phyric
2-10	Moderately phyric
greater than 10	Phyric

3. Zoning:

UZ unzoned; WZ weak zoning; MZ moderate zoning; SZ strong zoning; Oscill. : concentric or oscillatory zoning; N, R normal or reverse zoning.

4. Names of mineral phases may be abbreviated as:
Plag: plagioclase
Cpx: clinopyroxene
Oliv: olivine
Op oxides: opaque oxides

5. Degree of Alteration (specific to a gabbroic assemblage):

1/3: All crystalline phases (phenocrysts and groundmass) are clear with the exception of olivine (may be partially preserved only) and volcanic glass.

2/3: The only clear, unaltered phase is pyroxene, as phenocryst or groundmass. Feldspars show incipient sericitization and olivines are completely pseudomorphed. Oxides and clays are usually abundant in the groundmass, without obliterating original textures.

3/3: All crystalline phases show some alteration. Textures are obliterated by pervasive oxidation or replacement of mineral phases and glass by clays, carbonates or zeolites.

GROUP 1A

AX85-241 Basal Flow
Fine-grained, sparsely plag-phyric, hypocrystalline basalt. Groundmass consists of an intersertal aggregate of plag-cpx-op oxides and volcanic glass altered to clays (10 %). Sparsely amygdaloidal (1mm circular vesicles filled with carbonates). Alteration 2/3.

AX85-242 Basal Flow
Fine-grained, sparsely plag-phyric, seriate, hypocrystalline basalt. Groundmass consists of an intergranular, intersertal aggregate of plag-cpx-op oxides and glass (5 %; partly replaced by green clays). Alteration 1/3.

GROUP 1B

AX85-260 Flow #1
Phenocrysts: Glomerophyric. Plagioclase (21.7%; 0.5-1.5mm) with strong normal zoning. Augite (1.5%; 0.75-1.5mm; UZ) shows partial resorption. Rare oikocrysts and pseudomorphed olivines.
Groundmass: V. fine-grained (0.1-0.2mm), holocrystalline, intergranular aggregate of plag-cpx-oliv-op oxides. Sparsely amygdaloidal (0.2-0.7mm circular vesicles filled with orange clays after glass). Alteration 1/3.

AX85-261 Flow #1
Phenocrysts: Glomerophyric, seriate. Plagioclase (16.7%; 0.2-0.7mm) shows strong zoning, resorption. Sparse augite (1.5%; 0.3-1.7mm) and olivine pseudomorphs (0.8%; 0.5-0.7mm). Monomineralic clusters predominate.
Groundmass: V. fine-grained (0.1-0.2mm), holocrystalline, intergranular aggregate of plag-cpx-oliv-op oxides. Sparsely amygdaloidal (0.5mm, circular vesicles filled with devitrified glass, clays). Alteration 1/3.

AX85-263 Flow #3
Glomerophyric, seriate, holocrystalline basalt. Phenocrysts consist of abundant plagioclase (0.3-1.2mm) with complex zoning (N, R); augite plates (0.5-2mm; UZ-WZ); and rare olivine pseudomorphs (1mm). Groundmass consists of an intergranular aggregate of plag-cpx-oliv-op oxides. Sparsely amygdaloidal (0.3-1.2mm circular vesicles filled with orange clays after glass). Alteration 1/3.

AX85-264 Flow #4
Phenocrysts: Glomerophyric, seriate. Plagioclase (12.8%; 0.15-0.7mm; SZ, R) shows partial resorption, inclusions. Augite (3%; 0.2-0.5mm) consists of clear (UZ-WZ) anhedral plates. Rare olivine pseudomorphs are present (1%; 0.5mm).
Groundmass: V. fine-grained, holocrystalline and intergranular aggregate of plag-cpx-oliv-op oxides. Sparsely amygdaloidal (1mm circular vesicles filled with clays, carbonates after glass). Alteration 1/3.

AX85-266 Flow #6
Phenocrysts: Glomerophyric, seriate. Plagioclase (9.5%; 0.25-1.2mm) shows strong zoning (N, oscill.). Clear (UZ-WZ) anhedral plates of augite (5.6%; 0.25-1mm). Rare oikocrysts (1%; 1mm).
Groundmass: V. fine-grained, holocrystalline and intergranular aggregate of plag-cpx-?oliv-op oxides. Massive. Alteration 1/3.

AX85-267 Flow #8
Phenocrysts: Microphyric, seriate. Plagioclase (5.9%; 0.5-1mm) consists of clear crystals (SZ, locally oscill.). Anhedral plates of augite (13.8%; 0.4-1mm) show a wavy extinction and poïkilitic cores.
Groundmass: V. fine-grained, holocrystalline and intergranular aggregate of plag-cpx-?oliv-op oxides. Locally sub-ophitic. Massive. Alteration 1/3.

AX85-268 Flow #9
Phenocrysts: Glomerophyric, seriate. Plagioclase (8.9%; 0.7-2mm) is subhedral (SZ, oscill.). Augites (7.3%; 0.7-1mm) are anhedral plates or oikocrysts with fritted edges and inclusions.
Groundmass: V. fine-grained, hypocrystalline aggregate of plag-cpx-?oliv-op oxides and orange clays after glass (7%). Amygdaloidal (0.3-0.5mm irregular or circular vesicles filled with altered glass). Alteration 1/3.

GROUP 1C

EL84-256A Flow #3 Section [1]
Sparsely glomerophyric, seriate, hypocrystalline basalt. Phenocrysts consist of subhedral plagioclase (0.5-1.2mm; SZ, oscill.) showing incipient sericitization; and rare, subhedral augite (0.3-0.8mm; UZ). Groundmass is an v. fine-grained, intersertal, intergranular aggregate of plag-cpx-oliv-op oxides and devitrified glass (5%). Sparsely amygdaloidal (0.5-2mm segregation vesicles filled with carbonates). Alteration 2/3.

EL84-107 Top section [2]
Sparsely phyric, seriate, hypocrystalline basalt. Phenocrysts consist of euhedral plagioclase (0.7-1.2mm, SZ rims) with poikilitic cores; and anhedral plates of augite (0.5-1mm; MZ). Groundmass is an intergranular aggregate of v. fine-grained oliv-plag-cpx-op oxides and glass (altered to orange clays and carbonates). Massive. Alteration 1/3.

GROUP 2A

BASTION RIDGE

AX83-032A, 032B Flow #1
Aphyric, holocrystalline and intergranular aggregate (0.1-0.2mm) of plagioclase, clinopyroxene, partially altered grains of olivine and opaque oxides.
Massive. Alteration 1/3.

AX83-028 Flow #2
Phenocrysts: Sparsely phyric, glomeroporphyritic. Plagioclase (1.25mm) consists of euhedral crystals (WZ,R). Augites (0.7mm) are anhedral plates (WZ) with clear cores.
Groundmass: Hypocrystalline, intergranular, intersertal aggregate of plagioclase (0.1-0.2mm), clinopyroxene (0.2mm), granular olivine (0.5mm), opaque oxides (0.1mm) and volcanic glass altered to clays (5%). Plagioclase laths show a sub-fluidal texture. Massive. Alteration 1/3.

AX83-025 Flow #3
Aphyric, hypocrystalline, intergranular and intersertal aggregate of plagioclase (seriate to 0.5mm), clinopyroxene (0.2mm), partially preserved olivine (0.2mm), opaque oxides (0.1-0.5mm) and glass (5%). The degree of alteration of the glass is variable from fresh to oxidized to complete replacement by clays (orange-brown palagonite).
Massive. Alteration 1/3.

AX83-024 Flow #4
Aphyric, holocrystalline, intergranular aggregate of plagioclase (0.1-0.3mm), clinopyroxene (0.1-0.5mm), altered olivine (0.1mm) and opaque oxides (0.1mm). Rare, larger augite oikocrysts (0.5mm).
Massive. Alteration 1/3.

AX83-023 Flow #5
Phenocrysts: Sparsely microphyric. Olivines (0.4-0.6mm) are clay pseudomorphs. Rare plagioclase and augite (0.5mm) consist of subhedral, zoned crystals. Rare augite oikocrysts (0.3-0.6mm) also occur.
Groundmass: Hypocrystalline, finely flow-banded, intergranular and intersertal aggregate (0.1-0.2mm) of plag-oliv-cpx-op oxides and oxidized volcanic glass (20-30%). Massive. Alteration 2/3.

AX83-021 Flow #5
Phenocrysts: Moderately microphyric. Phenocrysts consist of pseudomorphed olivines (0.2mm), plagioclase (seriate to 0.5mm) and magnetite (0.1mm).
Groundmass: Microcrystalline, intergranular aggregate of plag-cpx-?oliv (all crystal sizes less than 0.1mm).
Massive. Alteration 1/3.

AX83-020 Flow #5
Phenocrysts: Sparsely microphyric. Euhedral-subhedral plagioclase and augite (0.6mm).

Groundmass: Hypocrystalline, intersertal aggregate of plagioclase (0.2-0.3mm), clinopyroxene (0.1-0.2mm), altered olivine (0.2mm), opaque oxides (0.3-0.6mm) and volcanic glass replaced by clays (7-10%). Massive. Alteration 1/3.

AX83-019 Flow #6
Essentially aphyric, microcrystalline and intergranular aggregate of plagioclase laths, clinopyroxene, rare, relict olivine and granular opaque oxides. Occasional, relict and inclusion-rich oikocrysts, and interstitial glass replaced by orange clays. Alt. 1/3.

AX83-018 Flow #7
Phenocrysts: Sparsely microphyric. Partially altered plagioclase (0.2mm) and zoned augite (0.2-0.5mm).
Groundmass: Cryptocrystalline aggregate of plagioclase (seriate), clinopyroxene and opaque oxides.
Sparsely amygdaloidal (0.1-0.25mm flattened vesicles filled with green clays). Alteration 2/3.

AX83-017 Flow #8
Phenocrysts: Sparsely microphyric. Phenocrysts are plagioclase (0.8mm; WZ, N, oscill.) and anhedral, poikilitic augites (zoned and twinned; some 1mm oikocrysts).
Groundmass: Hypocrystalline, intergranular aggregate of plagioclase (0.1-0.3mm), augite, olivine, opaque oxides (0.1-0.2mm) and altered volcanic glass (7-10%).
Sparsely amygdaloidal (1-3mm circular vesicles filled with orange clays after glass). Alteration 1/3.

AX83-015 Flow #9
Aphyric, hypocrystalline, intersertal and intergranular aggregate (0.1-0.2mm) of plagioclase (sub-fluidal), clinopyroxene, granular olivine (?), opaque oxides (0.08-0.25mm; equant crystals) and glass (15% interstitial orange clays). Sparsely amygdaloidal (0.3-0.5mm elliptical vesicles filled with orange-brown clays after glass). Alteration 1/3.

AX83-013 Flow #10
Aphyric, hypocrystalline aggregate of plagioclase (0.1-0.4mm), clinopyroxene (0.1-0.2mm), rare altered olivine (less than 0.1mm), opaque oxides and interstitial glass (5%). Some augite oikocrysts (1%; 0.8mm). Massive. Alteration 1/3.

AX83-011A Flow #11 (lower cooling unit)
Aphyric, holocrystalline, intergranular aggregate of plagioclase (0.2-0.3mm), clinopyroxene (granular, less than 0.1mm), altered olivine (0.2-0.3mm) and opaque oxides (exsolution lamellae visible on 0.2-0.4mm subequant crystals). Plagioclase laths are in sub-fluidal texture. Massive. Alteration 1/3.

AX83-011B Flow #11 (upper cooling unit)
Aphyric, hypocrystalline, intersertal aggregate of sub-fluidal plagioclase (0.2-0.3mm), granular clinopyroxene, opaque oxides (0.3-0.7mm, stubby, anhedral crystals) and glass (10%, replaced by orange clays). Rare augite oikocrysts (1.5mm). Sparsely amygdaloidal (0.8mm

circular vesicles filled with layered orange brown clays after glass). Alteration 1/3.

TWISTED RIDGE

AX83-056A Flow #1
Phenocrysts: Moderately microphyric (5-10%), glomeroporphyritic. Subhedral plagioclase crystals (0.7-1mm; MZ, N/R), rare olivine pseudomorphs (0.5-0.6mm), and anhedral plates of augite (twinned; 0.3-0.5mm) with clear cores or inclusion trails (rare oikocrysts).
Groundmass: Essentially holocrystalline, intergranular aggregate of plagioclase (0.1-0.4mm), granular clinopyroxene (less than 0.1 mm), altered olivine (0.1-0.2mm), opaque oxides (0.1mm, stubby to skeletal crystals), rare glass (1-2%, interstitial; replaced by orange-brown clays) and accessory apatite (observed in feldspar).
Massive. Alteration 1/3.

AX83-057 Flow #2
Phenocrysts: Sparsely microphyric. Phenocrysts are plagioclase (0.4-0.6mm; WZ, N); and anhedral plates of augite (0.5mm; rare, distinctive oikocrysts).
Groundmass: Holocrystalline, intergranular aggregate (0.05-0.2mm) of plag-cpx-oliv-op oxides and minor interstitial glass (1-2%) altered to clays.
Massive. Alteration 1/3.

AX83-058 Flow #3
Phenocrysts: Moderately microphyric (5%). Plagioclase crystals (0.3-0.5mm) are zoned (N, oscill.), display inclusions of melt or pyroxene and are arranged in sub-fluidal texture. Augites (0.2-0.3mm) consist of anhedral, poikilitic plates that are less abundant than plagioclase. Oikocrysts are rare (1mm).
Groundmass: Holocrystalline, intergranular aggregate of plagioclase (seriate to 0.3mm), granular clinopyroxene and olivine (0.1 mm), equant grains of opaque oxides (0.1-0.2mm) and minor interstitial glass (1-2%, altered to clays).
Massive. Alteration 1/3.

AX83-059 Flow #4
Phenocrysts: Moderately microphyric. Phenocrysts consist of plagioclase (0.5mm; MZ, N); and anhedral plates of augite (0.3mm; MZ). Rare, larger oikocrysts (0.7-1.5mm) are associated with olivine pseudomorphs and magnetite.
Groundmass: Microcrystalline, intergranular aggregate (0.1mm-0.2mm) of plag-cpx-oliv-op oxides. Minute inclusions of pyroxene occur in plagioclase. Rare interstial glass replaced by clays. Sparsely amygdaloidal (0.2mm circular vesicles filled with orange clays after glass). Alteration 1/3.

AX83-060 Flow #5
Phenocrysts: Sparsely microphyric. Plagioclase (0.5mm; MZ, N); subhedral, locally bent augite crystals (1.3mm); and rare olivine pseudomorphs (0.6mm).

Groundmass: Holocrystalline, intergranular to sub-ophitic aggregate (0.1-0.2mm) of plag-cpx-oliv-op oxides. Local concentrations of interstitial glass (2-3%) altered to clays. Massive. Alteration 1/3.

AX83-062 Flow #6 (lower cooling unit)
Phenocrysts: Sparsely microphyric. Euhedral plagioclase crystals (0.7-0.8mm) show weak zoning and clear cores. Augites (0.5mm) consist of anhedral, zoned and poikilitic plates.
Groundmass: Hypocrystalline, intergranular and intersertal aggregate (0.1-0.3mm) of sub-fluidal plagioclase, cpx, oliv and op oxides. Local concentrations of glass (up to 5%, replaced by clays). Minute pyroxenes at periphery of feldspar laths. Sparsely amygdaloidal (circular vesicles filled with orange clays after glass). Alteration 1/3.

AX83-063 Flow #6 (upper cooling unit)
Phenocrysts: Sparsely microphyric. Plagioclase crystals (seriate to 1mm; SZ, N) display inclusions of glass or pyroxene. Augites (0.3-0.5mm) consist of anhedral, strongly zoned and poikilitic plates; and larger oikocrysts (0.8mm).
Groundmass: Hypocrystalline, intersertal and intergranular aggregate (0.1-0.2mm) of sub-fluidal, seriate plag; cpx, oliv and glass (35-40%; strongly oxidized).
Moderately amygdaloidal (0.6-1.7mm circular vesicles filled with green or orange clays). Alteration 1/3.

AX83-064 Flow #7
Phenocrysts: Sparsely microphyric. Plagioclase crystals (0.3-0.8mm) show variable zoning and minor resorption. Augites (0.2-0.3mm) are anhedral plates with inclusions at rims. Rare olivine microphenocrysts (0.1-0.2mm).
Groundmass: Hypocrystalline, partly cryptocrystalline aggregate of sub-fluidal plag; cpx; op oxides (in glassy areas); and interstitial, oxidized glass (up to 10%).
Sparsely amygdaloidal (0.5mm circular vesicles filled with oxidized glass and orange-brown clays). Alteration 1/3.

AX83-065 Flow #8
Phenocrysts: Sparsely microphyric. Plagioclase (0.4-0.8mm; UZ-WZ with clear cores); and rare augite (0.3-0.5mm; MZ euhedral plates with inclusions).
Groundmass: Microcrystalline, finely flow-banded, intergranular aggregate of plag-oliv-cpx-op oxides. Minor interstitial glass (2-3%). Massive. Alteration 1/3.

AX83-066 Flow #9
Phenocrysts: Moderately phyric (7-10%), seriate, glomeroporphyritic. Olivines replaced by clays (0.5mm); saussuritized plagioclase (0.4-0.8mm); anhedral, often bent poikilitic augites (0.2-0.6mm; some oikocrysts associated with oliv, plag); and rare opaque oxides (0.2mm) associated with olivine.
Groundmass: Microcrystalline, intergranular aggregate (0.1mm-0.2mm) of partially altered plag; with oliv-cpx-op oxides. Massive. Alteration 2/3.

AX85-067 Flow #9
Phenocrysts: Highly phyric (15%), glomeroporphyritic. Well-outlined olivine pseudomorphs (0.2-0.5mm). Plagioclase crystals (0.3-0.5mm; max 3mm; SZ, R, oscill.) are partially resorbed and contain melt inclusions. Augites consist of subhedral, poikilitic plates (SZ cores; 2mm oikocrysts with olivine). Opaque microphenocrysts occur in clusters of oliv+plag.
Groundmass: Microcrystalline, intergranular aggregate (0.1mm) of plag-oliv-cpx and op oxides. Sparsely amygdaloidal (1mm circular vesicles filled with layered orange clays). Alteration 1/3.

AX83-068 Flow #9
Phenocrysts: Sparsely microphyric. Anhedral plates of augite (0.15-0.3mm; clear cores).
Groundmass: Hypocrystalline, intersertal and intergranular aggregate (0.1mm) of plag-oliv-cpx-op oxides and interstitial glass (5%; altered to clays). Sparsely amygdaloidal (2-9mm flattened vesicles filled with clays after glass). Alteration 1/3.

AX83-070 Flow #10
Phenocrysts: Sparsely microphyric. Augites (0.2-0.3mm) are abundant and consist of subhedral plates with inclusions (MZ, oscill). Plagioclase crystals (0.5mm) are rare.
Groundmass: Holocrystalline, intergranular aggregate of plag-cpx-oliv-op oxides (0.1-0.3mm). Sparsely amygdaloidal (0.3mm vesicles with variable morphology, filled with orange clays). Alteration 1/3.

EAST GLACIER FIORD SYNCLINE

AX83-033 Basal Flow
Aphyric, holocrystalline, intergranular aggregate (0.1-0.2mm) of plagioclase, granular olivine (0.2mm), clinopyroxene (0.1 mm) and opaque oxides. Rare, larger augite oikocrysts (0.5-0.6mm). Local concentrations of interstitial glass (2-3%; altered to orange-brown clays).
Sparsely amygdaloidal (0.3-0.8mm vesicles with circular to irregular shapes, filled with orange clays after glass).
Alteration 1/3.

AX83-043 Top Flow
Phenocrysts: Sparsely microphyric. Rare, strongly zoned augites (0.3mm) with clear cores.
Groundmass: Holocrystalline, intergranular aggregate of plag (0.1-0.25mm; minute pyroxene inclusions), oliv (0.1-0.3mm), cpx (0.1mm) and op oxides (0.1-0.2mm). Massive. Alteration 1/3.

WEST GLACIER FIORD SYNCLINE

AX83-106 Basal Flow
Aphyric, holocrystalline, intergranular aggregate of partly sericitized plag (0.1-0.2mm), oliv (partly crystalline; 0.1-0.3mm), cpx (0.1mm) and op oxides (0.1-0.25mm). Massive. Alteration 2/3.

AX83-113 Top Flow
Phenocrysts: Sparsely phyric. Plagioclase crystals (0.5-1mm) are zoned and some contain melt inclusions. Augites (0.3-0.8mm) consist of anhedral, zoned and poikilitic plates or larger oikocrysts (0.8mm) associated with olivines. Olivines (0.3mm) are pseudomorphed.
Groundmass: Holocrystalline, intergranular aggregate (0.1-0.3mm) of plag-cpx-oliv-op oxides. Sparsely amygdaloidal (0.8mm circular vesicles filled with carbonates). Alteration 1/3.

GROUP 2B

CELLULOID CREEK

BND83-017 Flow #1
Phenocryts: Phyric, seriate, glomeroporphyritic. Plagioclase (8.4%; 0.3-1mm; MZ-SZ, N, oscill.); augite (4.5%; 0.3-1mm; clear plates, oikocrysts); pseudomorphed olivine (1%; 0.3-0.6mm).
Groundmass: Holocrystalline, intergranular aggregate (0.1-0.3mm) of plag-cpx-oliv-op oxides. Minor interstitial glass (1-2%). Massive. Alteration 1/3.

BND83-016 Flow #2
Phenocryts: Moderately phyric, seriate, glomeroporphyritic. Plagioclase (3.7%; 0.4-1.4mm; SZ, N) shows some resorption and melt inclusions. Clear, anhedral plates of augite (0.8%; 0.75-1mm; UZ). Rare olivine (0.4%; 0.8mm).
Groundmass: Holocrystalline, intergranular aggregate (0.1-0.5mm) of plag-oliv-cpx-op oxides. Minor glass altered to clays (3%). Massive. Alteration 1/3.

BND83-015 Flow #3
Phenocrysts: Moderately phyric, seriate, glomeroporphyritic. Plagioclase (7.6%; 0.5-4mm; SZ, N, oscill.) shows minor resorption. Rare pseudomorphed olivine (0.4%; 0.5mm). Rare augite (0.3%).
Groundmass: Holocrystalline, intergranular aggregate (0.5-0.2mm) of oliv (some replacement by carbonates), plag (sub-fluidal), cpx and op oxides. Sparsely amygdaloidal (0.3mm circular vesicles filled with clays and carbonates after glass). Alteration 1/3.

BND83-012 Flow #4
Phenocrysts: Moderately phyric and seriate. Subhedral plagioclase (6.2%; 0.3-1mm; UZ-WZ); augite (2%; 0.2-0.6mm) with inclusions in cores (rare oikocrysts up to 1mm); and olivine (1.2%; 0.2-0.8mm; some crystalline).
Groundmass: Holocrystalline, intergranular aggregate (0.1-0.2mm) of oliv-plag-cpx-op oxides and minor altered glass. Sparsely amygdaloidal (2mm circular vesicles filled with clays after glass). Alteration 1/3.

BND83-009 Flow #5
Phenocryts: Microphyric, glomeroporphyritic and seriate. Plagioclase (8.7%; 0.4-1.5mm; SZ, N; minor resorption); olivine (0.9%; 0.2-0.5mm;

some fresh cores); rare magnetite microphenocrysts (0.7%); rare augite (0.3-0.5mm).
Groundmass: Holocrystalline, intergranular aggregate (0.1-0.3mm) of oliv-plag-cpx-op oxides. Minor altered glass in angles between crystals. Sparsely amygdaloidal (1.2%; 1-2mm circular vesicles filled with clays and carbonates after glass). Alteration 1/3.

BND83-007 Flow #6
Massive, aphyric portion of basaltic lava.
Groundmass: Fine-grained (0.1-0.5mm), holocrystalline, intergranular aggregate of plag-cpx-oliv-op oxides. Alteration 2/3.

BND83-006 Flow #7
Phenocrysts: Sparsely phyric. Plagioclase (1mm; MZ, N, oscill.); augite (0.3-0.6mm; oikocrysts with inclusions in cores); rare pseudomorphed olivine (0.75mm).
Groundmass: Fine-grained (0.1-0.6mm), holocrystalline, seriate, intergranular aggregate of plag-cpx-oliv-op oxides. Massive. Alteration 2/3.

BND83-005 Flow #8
Phenocrysts: Sparsely phyric. Plagioclase (0.5-1mm) and olivine (1mm).
Groundmass: Holocrystalline, intergranular aggregate of plag-cpx-oliv-op oxides (0.05-0.3mm). Sparsely amygdaloidal (0.4-1mm circular vesicles filled with carbonate and clays after glass). Alteration 2/3.

ARTHARBER CREEK

AX85-074 Flow #1
Phenocrysts: Moderately phyric, seriate, glomeroporphyritic. Plagioclase (3.8%; 0.75-4mm; SZ, N, oscill.) shows some resorption at the periphery of crystals, and inclusions of oliv, cpx or glass. Augites (2.1%; 0.2-0.5mm) are uniform plates with inclusions, or oikocrysts (1-2mm). Rare olivine (0.5%; 0.3-0.75mm).
Groundmass: Fine-grained (0.1-0.4mm), microcrystalline, intergranular aggregate of plag-cpx-oliv-op oxides. Massive. Alteration 1/3.

AX85-075 Flow #1
Phenocrysts: Moderately phyric, seriate, glomeroporphyritic. Two generations of plagioclase (3.6%; 0.75-2mm): the largest crystals are clear and resorbed (SZ, N/R oscill.); plagioclase microphenocrysts (0.3-0.5mm; UZ-WZ) are overgrown by cpx (sub-fluidal texture). Augites (2.3%; 1mm) are uniform, platy crystals or oikocrysts with fritted edges. Olivines (0.4%; 0.2-0.5mm) are replaced by clays; and display a rim of oxides and finely crystalline material.
Groundmass: Microcrystalline (0.1 mm), intergranular aggregate of plag-cpx-op oxides. Minor altered glass in the interstices between phenocrysts. Massive. Alteration 1/3.

AX85-078 Flow #2
Phenocrysts: Moderately phyric, glomeroporphyritic, seriate. Large plagioclase crystals (3.8%; 0.5-2mm; SZ, N/R oscill.) are partly resorbed; microphenocrysts (0.2-0.5mm) show weak zoning. Single

crystals of augite (3.8%; 1mm) display an ophitic texture (some clear, UZ crystals in clusters with plag). Rare olivine (1.2%; 0.2-0.5mm). Groundmass: Microcrystalline, intergranular aggregate of plag-cpx-op oxides. Moderately amygdaloidal (0.3-1mm irregular, flattened vesicles filled with clays or microquartz). Alteration 1/3.

AX85-080 Flow #3
Phenocrysts: Microphyric, with bimodal distribution of sizes. Plagioclase crystals (6.6%; 0.4-1mm; N/R zoning if larger than 0.7mm) are devoid of inclusions. Augites (2.5%; seriate to 1mm) are anhedral plates with or without ophitic texture. Olivines (1%; 0.3-0.8mm) are pseudomorphed.
Groundmass: Hypocrystalline, intergranular, intersertal aggregate (0.1-0.3mm) of plag-cpx-?oliv-op oxides and altered glass (4.5%). Sparsely amygdaloidal (1-4mm circular vesicles filled with clays after glass). Alteration 1/3.

AX85-082 Flow #4
Phenocrysts: Moderately phyric, glomeroporphyritic. Plagioclase (4.7%; 0.5-2.5mm) occurs in monomineralic clusters of large crystals (SZ, R oscill.) or as microphenocryts. Melt inclusions are common. Augites (2.2%; 0.5-0.8mm) are clear plates or anhedral oikocrysts. Olivine (0.5%; 0.3-1mm) is locally overgrown by augite.
Groundmass: Hypocrystalline, intergranular, seriate aggregate (0.1-0.4mm) of plag-cpx-(rare)oliv-op oxides. Glass is altered to clays (less than 3%). Sparsely amygdaloidal (0.8mm circular vesicles filled with clays after glass). Alteration 1/3.

AX85-084 Flow #5
Aphyric to sparsely plag-microphyric. The larger plagioclase crystals (0.5mm) are euhedral and seriate (MZ, R). Groundmass: Holocrystalline, seriate, intergranular aggregate (0.1-0.5mm) of plag-cpx-(rare)oliv-op oxides. Minor interstitial glass altered to clays. Sparsely amygdaloidal (0.2-0.3mm, flattened or circular vesicles filled with brown-orange clays after glass). Alteration 1/3.

AX85-086 Flow #6
Phenocrysts: Seriate, glomeroporphyritic. Plagioclase crystals (16.3%; 0.5-2.5mm; SZ, N/R oscill.) may show resorbed edges, contain melt inclusions or be intergrown with clinopyroxenes (0.4%). Augites (2 %; 0.2-0.6mm) occur as clear plates, smaller poikilitic crystals with anhedral outlines and oikocrysts. Rare oxyhornblende phenocrysts with opaque rims (0.6%; 0.5-2.5mm) underwent resorption prior to replacement by biotite. Groundmass: Microcrystalline, intergranular aggregate (0.1-0.2mm) of plag-cpx-?oliv-op oxides. Sparsely amygdaloidal (0.75-2mm circular vesicles filled with carbonates at center, clays and oxides at rims). Alteration 1/3.

AX85-087 Flow #7
Phenocrysts: Moderately phyric, seriate, glomeroporphyritic. Plagioclase crystals (4.8%; 0.5-2mm; SZ, N/R) show melt inclusions and minor resorption. Olivines are pseudomorphed (0.7%; 0.3-0.8mm). Augites occur as oikocrysts (1.7%). Microphenocrysts are moderately abundant and include olivine, augite and an opaque phase.

Groundmass: Holocrystalline, seriate, intergranular aggregate (0.1-0.4mm) of plag-oliv-cpx-op oxides. Sparsely amygdaloidal (1-4mm circular vesicles filled with clays and carbonates after glass; 0.5%). Alteration 1/3.

AX85-091 Flow #8
Phenocrysts: Glomeroporphyritic (polymineralic clusters), seriate . Plagioclase crystals (13%; 0.5-1.75mm, SZ; R oscill./N) display melt inclusions and jagged sector zoning in resorbed, poikilitic crystals. Augites (0.3-1mm; UZ) are clear, anhedral plates (0.8%) or oikocrysts hosting plagioclase laths (1.1%; 0.5-1mm) . Minor olivine (0.3-1mm). Groundmass: Hypocrystalline, intergranular and intersertal aggregate (0.1-0.2mm) of plag-cpx-oliv-op oxides and altered glass (3%). Massive. Alteration 1/3.

AX85-094 Flow #9
Phenocrysts: Glomeroporphyritic (polymineralic clusters), seriate. Clear, glomerophyric plagioclase (10.1%; 0.5-3mm; SZ, N/R); augite (1.4%; 0.3-0.7mm; clear, UZ); and rare olivine (0.2%; 0.3-0.5mm). Euhedral microphenocrysts of olivine and an opaque phase are also present (1.6%; 0.3mm). Groundmass: Holocrystalline, intergranular aggregate
(0.1-0.2mm) of plag-cpx-oliv-op oxides (the latter consist of distinctly larger, equant to embayed crystals). Sparsely amygdaloidal (0.7mm segregation vesicles filled with green clays after glass; 0.2%). Alteration 1/3.

AX85-095 Flow #10
Phenocrysts: Sparsely microphyric, seriate. Euhedral, single crystals of plagioclase (2.8%) and olivine (2.1%; 0.3-1.25mm; iddingsitized); and anhedral plates of augite (0.9%; 0.3mm) or oikocrysts (0.6%; 0.5-1mm), some of which form small clusters with olivine, plagioclase and an opaque phase. Groundmass: Holocrystalline, intergranular aggregate (0.1-0.3mm) of plag-cpx-oliv-op oxides. Massive. Alteration 1/3.

Note: The two uppermost flows (#11 and #12) were termed "aphyric" in the field. Microscope examination indicates that these are microcrystalline to cryptocrystalline, sparsely microphyric lavas. The textures are very distinct from glomeroporphyritic, seriate and microphyric basalts from the lower part of the section.

AX85-096 Flow #11
Phenocrysts: Sparsely microphyric. Euhedral plagioclase (0.4-0.6mm; MZ); anhedral plates of augite (0.2mm; rare oikocrysts of poikilitic augite intergrown with plagioclase); and olivine (0.2-0.3mm; a few grains are euhedral and show distinct zoning between core and rims, despite the replacement by clays). Groundmass: Microcrystalline, intergranular aggregate (0.1-0.3mm) of plag-oliv-cpx-op oxides. Sparsely amygdaloidal (0.5-2mm circular vesicles filled with carbonates and dark brown clays after glass). Alteration 1/3.

AX85-097 Flow #12
Phenocrysts: Very fine-grained, seriate microphyric. Euhedral plagioclase (0.4-0.5mm;MZ); and subhedral augite (0.2-0.3mm; rare

oikocrysts are also present). Groundmass: Seriate, cryptocrystalline, intergranular aggregate of plag-oliv-cpx- and abundant op oxides. Massive. Alteration 1/3.

GROUP 3

TROPICAL RIDGE

EL84-082, -087
V. fine-grained, aphyric and holocrystalline (3% glass in -082), basalt. Groundmass is an intergranular aggregate of oliv-cpx-plag-op oxides, with an ophimottled texture. Incipient oxidation of all phases. Alteration 2/3.

ARCTIC HARE MESA

EL84-007 Top flow, NW section
As -010 below. Volcanic glass is partly devitrified and altered to orange clays. Apatite is conspicuous as euhedral prisms or needles (0.1mm). Alteration 1/3.

EL84-010 Basal Flow, NE section
V. fine-grained (0.2-0.5mm), aphyric, hypocrystalline basalt. Groundmass is an intersertal, intergranular aggregate of oliv-cpx-plag-op oxides and devitrified glass (3%). Ophimottled texture. Massive. Alteration 2/3.

PETROGRAPHIC SUMMARIES
INTRUSIVE ROCKS

Abbreviations

1. Per cent volumes, zoning and names of minerals as for extrusive rocks.

2. Grain Size: Very fine = less than 0.5 mm
Fine = less than 1 mm
Medium = 1 to 5 mm

3. Degree of Alteration:

Most of the intrusive rocks examined show a higher degree of alteration than volcanic rocks. The extent of secondary alteration can be described as follows, for a gabbroic assemblage:

1/4: Feldspar and pyroxene crystals show incipient alteration. Olivines are partly or entirely pseudomorphed. Clays are present (usually after glass) but limited to interstitial areas.

2/4: Feldspar crystals are largely unaltered, or show incipient sericitization. Pyroxenes show advanced alteration to clays. Olivines, if present, are entirely pseudomorphed. Products of deuteric alteration may be present. Textures are preserved.

3/4: Feldspar crystals are entirely replaced by clays (sericite, saussurite) while pyroxene crystals show little or no alteration by clays. Otherwise, as in 2/4.

4/4: Primary phases are completely replaced by secondary minerals (clays and carbonate; chlorite, biotite, amphibole). Textures are partially or completely obliterated.

GROUP A

LIGHTFOOT RIVER

* Description after Jollimore (1986), revised by the author.

AX85-001: Equigranular, fine-grained (less than 1 mm), intergranular aggregate of sericitized plag, cpx and op oxides. Minor interstitial quartz, brown or green clays and accessory apatite needles. Alt. 3/4.

AX85-005: Fine-grained, sparsely plagioclase-phyric, intergranular aggregate of plag, cpx, oliv and op oxides. Phenocrysts consist of euhedral, zoned crystals (1.2mm) with frequent inclusions. Alteration of olivines is limited to fractures. Interstitial green clays, rare biotite-chlorite and myrmekitic intergrowths. Alt. 1/4.

AX85-008: Fine-grained, equigranular, intergranular aggregate of sericitized plag, augitic cpx and partly corroded op oxides. Interstitial quartz, carbonate and myrmekitic intergrowths. Alt. 3/4.

AX85-013: Fine-grained, inequigranular, sparsely plagioclase-phyric, intergranular to sub-ophitic aggregate of seriate plag, cpx and partly corroded op oxides. Phenocrysts are weakly zoned, clear crystals (2 mm). Patches of altered, interstitial glass. Accessory apatite. Alt. 1/4.

* AX85-015: Medium-grained, sparsely plagioclase-phyric, inequigranular aggregate of plag (60%), cpx (20%) and op oxides (5%), with intergranular texture. Rare phenocrysts are weakly zoned crystals with frequent inclusions. Interstitial quartz and carbonate. 5% biotite associated with chlorite. Alt. 2/4.

*AX85-019: Medium-grained aggregate of sericitized plag (60%), subhedral cpx altered to chlorite (30%) and highly corroded op oxides, with sub-ophitic texture. Alt. 4/4.

* AX85-020: Medium-grained, inequigranular, intergranular aggregate of sericitized plag (50%), cpx (30%) and partly corroded op oxides (5%). Interstitial quartz and patches of carbonate. 5% biotite-chlorite. Alteration 4/4.

* AX85-026: As -020 above with 65% plag and 20% cpx.

AX85-027: Fine-grained, inequigranular aggregate of plag (0.5mm), cpx and strongly corroded op oxides, with an intergranular and sub-ophitic texture. Rare (?) olivine pseudomorphs. Interstitial quartz and minor carbonate. Rare biotite-chlorite (0.1mm).
Alt. 3/4.

* AX85-030: Fine-grained, sparsely phyric and glomeroporphyritic, intergranular aggregate of plag (55%), cpx (20%) and op oxides (15%). Phenocrysts consist of partially resorbed plagioclase (0.5-1mm, An44, N/R oscill.) in clusters with augite. Interstitial quartz, clays and minor carbonate. Alt. 1/4.

* AX85-031: Medium-grained, intergranular aggregate of plag (1-2mm; 65%; An32), augite (0.5-1mm; 20%) and partly corroded op oxides (tabular or skeletal; 5%). Interstitial quartz and biotite-chlorite after pyroxenes (2%). Alt. 2/4.

* AX85-032: As -031 above, with accessory apatite and advanced carbonatization. Alt. 4/4.

* AX85-033: As -032 above.

* AX85-035: Medium-grained, equigranular aggregate of plag (60%), cpx (30%), strongly corroded op oxides (2%) and accessory apatite, with a sub-ophitic texture. Interstitial quartz (2%), minor biotite-chlorite and myrmekitic intergrowths. Alt. 4/4.

* AX85-036: Medium-grained, intergranular aggregate of plag (65%; N/R; An50), cpx (25%) and corroded op oxides (2%). Interstitial quartz and chlorite-biotite (0.5 mm; 1%). Alt. 1/4.

* AX85-037: As -036 above; very fine-grained (less than 0.5mm) with skeletal oxides.

* AX85-040: Seriate, fine-grained aggregate of sericitized plag (0.5-1.5mm; 65%; An48), cpx (20%) and slightly corroded op oxides (5%), with an intergranular and sub-ophitic texture. Minor interstitial quartz and chlorite-biotite after pyroxenes. Alt. 3/4.

* AX85-043: As -031 above. Op oxides (10%) consist of equant, embayed crystals. Alt. 3/4.

* AX85-046: Fine to medium-grained, mineralogy as -036 above. Alt. 3/4.

* AX85-048: Fine to medium-grained, as -031 above.

GROUP B

BUCHANAN LAKE

AX85-051: Very fine-grained (less than 0.5mm), moderately glomeroporphyritic, intergranular aggregate of plag, granular cpx and partly corroded op oxides. Phenocrysts consist of subhedral, sericitized plag (0.5-1.5mm) with concentric zoning at the margins of crystals; anhedral plates of augite (0.5-0.7mm) and rare oliv pseudomorphs (0.5mm) are also present. Minor interstitial quartz and green clays. Alt. 2/4.

AX85-052: Medium-grained, equigranular, intergranular aggregate of mostly unaltered plag (N/R), cpx and op oxides (0.5-1mm, embayed). Accessory apatite. Interstitial quartz, minor chlorite-biotite and myrmekitic intergrowths. Alt. 2/4.

AX85-057: Fine-grained, equigranular portion of sill with a gabbroic assemblage. Relict intergranular texture. Saussurite after feldspars, yellow-green clays after pyroxenes and strong corrosion of opaque oxides. Interstitial quartz. Alt. 4/4.

AX85-059: Fine- to medium-grained, equigranular aggregate of sericitized plag, partially altered cpx and strongly corroded op oxides, with intergranular texture. Interstitial quartz, patches of biotite-chlorite and minor interstitial quartz. Alt. 4/4.

AX85-061: Fine-grained, inequigranular assemblage of partly sericitized plag, cpx and corroded op oxides with an embayed morphology. Intergranular to sub-ophitic texture. Interstitial quartz, carbonate and abundant green clays. Alt. 3/4.

AX85-062: Very fine-grained, sparsely plag-phyric aggregate of plag, pseudomorphed oliv, granular cpx and op oxides, with a sub-ophitic

texture. Phenocrysts consist of rare, clear plag crystals (0.5mm). Oliv typically occurs as clusters (0.2-0.3mm). Minor interstitial clays. Alt. 1/4.

AX85-063: Fine-grained, sparsely plag-oliv-phyric, glomeroporphyritic, intergranular to sub-ophitic aggregate of plag (0.1-0.5mm), altered oliv, cpx and op oxides. Phenocrysts consist of clear oliv and plag, the latter with complex sector zoning (N/R oscill.). 3% interstitial oxidized glass. Alt. 1/4.

AX85-067: As -063 above, with 3-5% oxidized glass. Plag phenocrysts display evidence of re-melting at the centre of clusters.

AX85-215: Very fine-grained, sparsely glomeroporphyritic aggregate of sericitized plag, granular cpx and op oxides (subequant to skeletal grains). Intergranular texture. Phenocrysts consist of euhedral, sericitized plag (1mm) and cpx (0.5-1mm) intergrown with feldspar. Interstitial quartz and biotite flakes. Alt. 3/4.

AX85-217: Fine- to medium-grained, inequigranular and intergranular aggregate of partly sericitized plag, cpx (with advanced replacement by clays) and partly corroded op oxides. Accessory apatite. Products of deuteric alteration include 1-2% biotite and chlorite, and secondary amphibole. Alt. 2/4.

AX85-218: Medium-grained, equigranular assemblage of plag, cpx and strongly corroded op oxides. Incipient alteration of plagioclase and augite. Interstitial quartz and carbonate. 1-2% biotite flakes associated with chlorite. Alt. 2/4.

AX85-220: Fine-grained, with primary mineralogy as -051 above. Minor interstitial glass. Alt. 2/4.

AX85-221: As -220 above. Interstitial quartz. Alt. 2/4.

AX85-222: Fine-grained (0.1-0.5mm), intergranular aggregate of zoned plag (euhedral/skeletal grains), cpx and opaque oxides. Interstitial clays. Alt. 1/4.

AX85-223: Fine-grained, inequigranular assemblage of subhedral plag, augitic cpx and strongly corroded op oxides with a sub-ophitic texture. Accessory apatite and sphene. Partial sericitization of plag. Biotite and chlorite after augite. Interstitial quartz and patches of carbonate. Alt. 2/4.

AX85-224: Fine- to medium-grained, equigranular and intergranular aggregate of plag, augitic cpx and op oxides. Sericitized plag; cpx partially replaced by chlorite. 1% biotite (0.1-0.3mm) and minor interstitial quartz. Alt 3/4.

AX85-225: Medium-grained (1-2.5mm), intergranular assemblage of sericitized and saussuritized plag, chloritized cpx and corroded op oxides. Secondary amphibole and interstitial quartz. Alt. 4/4.

AX85-226: Very fine-grained, intergranular to sub-ophitic assemblage of sericitized/saussuritized plag, cpx and op oxides. Rare interstitial quartz, carbonate and 1% biotite associated with chlorite. Alt. 3/4.

AX85-227: Very fine-grained, seriate, intergranular to sub-ophitic assemblage of partly sericitized plag, cpx and op oxides. Alt. 2/4.

AX85-228: Medium-grained, inequigranular, intergranular to sub-ophitic aggregate of partially sericitized plag, altered cpx and op oxides. 1% biotite (0.5mm) and chlorite, and minor interstitial quartz. Alt. 2/4.

AX85-230: Fine-grained, inequigranular aggregate of plag (entirely sericitized), cpx (clear) and op oxides. Chlorite and minor biotite, interstitial quartz. Alt. 3/4.

AX85-231: Fine-grained, intergranular aggregate of sericitized plag, partially altered cpx, and abundant op oxides (?oliv replaced by green clays). Alt. 3/4.

AX85-233: Fine-grained (max. 1-1.2mm), sub-ophitic assemblage of sericitized plag, clear augite and skeletal to subequant op oxides. Alt. 3/4.

AX85-234: Fine-grained, intergranular to sub-ophitic aggregate of seriate plag, augite and op oxides. Alteration consists of chlorite and biotite, and minor carbonates. Alt. 1/4.

AX85-235: Fine-grained, sparsely plag-phyric assemblage of euhedral plag and granular aggregates of cpx and op oxides with intergranular to sub-ophitic texture. Incipient sericitization of feldspars. Interstitial chlorite and biotite. Alt. 2/4.

AX85-237: As AX85-235 above.

AX85-238: Fine-grained, seriate aggregate of slightly sericitized plag, augitic cpx and op oxides with intergranular to sub-ophitic texture. Alteration consists of moderate amounts of chlorite and minor interstitial quartz and carbonate. Alt. 2/4.

AX85-239: As AX85-235 above.

EL85-201: Fine-grained, sparsely plag-phyric aggregate of seriate plag, cpx and (much smaller) op oxides. Texture is intergranular. Alt. 2/4 (chlorite + biotite).

EL85-202: Fine- to medium-grained, sparsely plag-phyric, seriate aggregate of plag, cpx, relict oliv and op oxides with intergranular texture. Alt. 2/4.

EL85-205: Fine- to medium-grained, equigranular assemblage of plag, augite and op oxides, with sub-ophitic texture. Alt. 3/4.

EL85-207: As EL85-201 above. Groundmass plag displays a skeletal morphology. Some plag phenocrysts are resorbed and poikilitic.

EL85-208: Microcrystalline, moderately phyric aggregate of plag and granular oliv, cpx and op oxides. Phenocrysts consist of partially altered, subhedral plag and cpx, and rare clay pseudomorphs after oliv (outlines preserved). Glomeroporphyritic texture. Alt. 3/4.

EL85-209: Medium-grained aggregate of plag, cpx, minor oliv and op oxides, with ophitic texture. Some olivines are preserved and cpx is clear. Alt. 3/4.

EL85-213: Medium-grained, inequigranular aggregate of plag, pyroxene and op oxides. Intergranular to sub-ophitic texture. Alt. 1/4.

GROUP C

TANQUARY FIORD

EL84-211: Fine-grained, highly altered holocrystalline and equigranular aggregate of sericitized plag, partially altered cpx (colourless) and op oxides with a sub-ophitic texture. Alt. 3/4.

EL84-218: Fine- to medium-grained, hypocrystalline aggregate of plag (incipient sericitization), cpx (russet coloured, slight pleochroism and skeletal outlines) and op oxides (strong corrosion), with intergranular to sub-ophitic texture. Accessory apatite and interstitial glass altered to clays. Alt. 2/4.

EL84-221: Fine- to medium-grained, holocrystalline aggregate of sericitized plag (51%), cpx (23%), oliv (2%) and op oxides (7%). Augites are characteristically colourless with russet-coloured margins. Secondary alteration products include clays (14%) and biotite-chlorite (3%). Alt. 3/4.

EL84-222: Medium-grained, holocrystalline aggregate of partly sericitized plag (50%), pale beige to colourless augite (18%), rare oliv (1%) and op oxides (9%), with an intergranular to sub-ophitic texture. Apatite prisms are relatively abundant (3.5%). Secondary alteration products include clays (10%), biotite (1%, associated with chlorite), carbonates (3%) and quartz (3.5%). Alt. 2/4.

EL84-223: Fine-grained, holocrystalline aggregate of partly sericitized plag (57%), colourless to russet cpx (14%, WZ), rare oliv (2%) and op oxides (10%). Accessory apatite. Secondary minerals include chlorite (11%) and amphibole (5%). Alt. 3/4.

EL84-229: Medium-grained, holocrystalline aggregate of partly sericitized plag (55%), clear anhedral plates of augite (22%; MZ), rare oliv (2%) and op oxides (10%). Groundmass texture is sub-ophitic. Secondary minerals include clays (9%) and interstitial carbonates (2%). Alt. 3/4.

EL84-232: Medium-grained, holocrystalline aggregate of clear plag (60.5%), cpx (21%; light russet colour, incipient alteration), rare oliv

(1%) and op oxides (8%). Secondary minerals include clays (6%), carbonates (2%) and minor quartz in interstitial areas. Alt. 2/4.

EL84-235: Medium-grained, holocrystalline aggregate of clear plag (53%; UZ to WZ), large plates of augite (17.5%; UZ, russet), altered oliv (7%) and op oxides (7%). Interstitial alteration products include clays (11%), carbonates (3%) adn minor quartz (1%). Alt. 2/4.

EL84-236: Fine-grained, equigranular aggregate of subhedral plag, anhedral plates of augite and partly corroded, equant op oxides. Minor relict oliv is also present. Secondary alteration products consist of brownish interstitial clays and quartz after glass. Plag are only partly sericitized and cpx contain inclusions but are largely unaltered. Intersertal, sub-ophitic texture. Alt. 1/4.

EL84-245: Medium-grained, holocrystalline aggregate of plag (54%), cpx (21%), oliv (4%) and op oxides (12%). Euhedral apatite is relatively abundant (3.5%). Interstitial clays (2%), carbonates (1%) and minor quartz. Alt. 3/4.

T-S6-14: Fine-grained, holocrystalline aggregate of sericitized plag, euhedral cpx (light rust colour, MZ, clear), and corroded op oxides. Plag entirely sericitized while cpx shows incipient alteration to clays at rims. Prisms and needles of apatite are also present. Secondary alteration products include abundant yellow-green clays and patches of carbonate. Texture is sub-ophitic. Alt. 3/4.

GROUP D

PIPER PASS, LAKE HAZEN

^: per cent volumes are estimated visually

EL84-015: Very fine-grained, hypocrystalline, intergranular aggregate of plag (48%; UZ to WZ), cpx (19%), oliv (9%), op oxides (8.5%) and devitrified glass (14%). The sample displays an ophimottled texture (augite oikocrysts). Dark green to brown clays replace interstitial glass locally. 1% carbonates in veins (0.3mm wide). Alt. 1/4.

EL84-023: Very fine-grained, intergranular aggregate of plag (36%), cpx (21%) and op oxides (12%). Secondary minerals include clays (26%) and carbonates after interstitial glass. Alt. 2/4.

EL84-041: Fine-grained, sparsely plag-cpx-phyric, hypocrystalline aggregate of plag (39%, WZ), cpx (24%), minor oliv (2%), op oxides (9%) and altered glass (21%). Accessory apatite. Phenocrysts consist of plag (0.5-0.8mm) with concentric zoning and poikilitic cores; and augite (1mm) with concentric zoning. Secondary minerals include interstitial carbonates (4%) and zeolites. Texture is intersertal, intergranular and amygdaloidal (2mm vesicles filled with carbonates). Alt. 2/4.

EL84-044: Fine-grained, hypocrystalline aggregate of plag (37%), cpx (20%), oliv (4%), op oxides (9.5%) and altered glass (25%). Accessory

apatite. Feldspars show incipient sericitization; augites display oxide rims. Fine brown clays and carbonates after glass (5%). Alt. 1/4.

EL84-046: Very fine-grained, sparsely phyric, holocrystalline aggregate of plag (47%, WZ), cpx (28%), oliv (5%) and op oxides (10%). Phenocrysts are rare and consist of plag and augite (1.5%). Secondary minerals include carbonates and clays (9%), partly after interstitial glass. Sub-ophitic, intersertal texture. Alt. 3/4.

^EL84-050: Very fine-grained, hypocrystalline, sparsely glomeroporphyritic aggregate of plag (40%, W to MZ), augitic cpx (35%, UZ), oliv (5%, pseudomorphed), op oxides (15%) and minor interstitial glass (devitrified). Phenocrysts (0.5-2mm) occur as polyminerallic clusters of plagioclase (partly resorbed with some melt inclusions, M to SZ), anhedral augites with distinctly zoned cores and partially preserved olivines. Dark green and brown clays after oliv (5%). Accessory apatite. Alt. 1/4.

EL84-056: Fine-grained, aphyric and holocrystalline aggregate of plag (52%), granular cpx (28%), op oxides (10%) and minor olivine (1%). Sub-fluidal arrangement of plag laths. Alteration products include clays after glass (9%), partly invading plag, cpx; and minor interstitial quartz. Alt. 2/4.

EL84-060: Fine-grained, hypocrystalline, sparsely plag (0.6%) and cpx (1.3%)-phyric aggregate of plag (36%), augitic cpx (25%), oliv (4%) and op oxides (9%) and interstitial, devitrified glass (24%). Alt. 3/4.

^EL84-072: Fine-grained, aphyric, massive and holocrystalline aggregate of plag (50%, WZ and incipient alteration), augitic cpx (40%, granular), relict oliv (5%, granular) and op oxides (5%, strongly embayed), with sub-ophitic texture. Accessory apatite. Oliv mantled by augite. 1-2% clays rim plag crystals and alter cpx. Alt. 3/4.

EL84-073: Fine-grained, sparsely phyric, hypocrystalline aggregate of plag (52%), augitic cpx (21%), relict grains of oliv (6%), op oxides (9%) and devitrified interstitial glass (11%). Alt. 3/4.

EL84-076: Aphyric, otherwise as EL84-073 above.

^EL84-110: Very fine-grained, holocrystalline, sparsely phyric aggregate of plag (45%), granular cpx (40%) and op oxides (15%; subangular or skeletal crystals) with intergranular texture. Accessory apatite. Phenocrysts consist of poikilitic plag (0.3-0.6mm, SZ) and anhedral cpx (0.3mm) with inclusions and frayed edges. Green clays after pyroxenes (5%), minor sericite after feldspar and interstitial quartz. Alt. 3/4.

EL84-098: Fine-grained, hypocrystalline, sparsely plag-phyric aggregate of plag (47%). augitic cpx (25%), oliv (5%), op oxides (14%) and devitrified glass (7%). 1% clays after pyroxene. Alt. 1/4.

EL84-210: Very fine-grained, holocrystalline and sparsely phyric aggregate of sericitized plag, clear granular cpx, rare pseudomorphs of oliv and op oxides, with an intergranular texture. Alt. 3/4.

APPENDIX B

MINERAL ANALYSIS

Pyroxenes, feldspars, olivines and opaque oxides were analysed at Dalhousie University using CAMBRIDGE or JEOL 733 electron microprobes operated at 15 kv with a current of 5 nanoamperes. The tables in this appendix show average analyses for groundmass minerals (G or WHOLE) and cores or rims of phenocrysts (6-12 spots per slide for each type). The term CENTRE applies to microphenocrysts only. Analyses of individual grains are available on request.

AVERAGE ANALYSES - EXTRUSIVE ROCKS

	BND83-009 olivine WHOLE	EL84-007B olivine WHOLE	EL84-010 olivine WHOLE	EL84-087 olivine WHOLE
SIO2	35.07	31.57	32.82	31.34
TIO2	0.08	0.16	0.16	0.20
AL2O3	0.00	0.04	0.02	0.02
CR2O3	0.00	0.00	0.00	0.00
FE2O3	0.00	0.00	0.00	0.00
FEO	37.72	52.68	49.33	53.88
MNO	0.45	1.23	1.10	1.26
MGO	27.59	13.94	16.91	12.30
CAO	0.35	0.40	0.41	0.34
NA2O	0.00	0.00	0.00	0.00
K2O	0.00	0.00	0.00	0.00
BAO	0.00	0.00	0.00	0.00
TOTAL	0.00	0.00	0.00	0.00

AVERAGE ANALYSES - EXTRUSIVE ROCKS

	AX83-011B feldspar G	AX83-020 feldspar G	AX83-025 feldspar CORE	AX83-025 feldspar G	AX83-025 feldspar RIM	AX83-032A feldspar G
SIO2	53.65	53.08	57.87	53.01	51.72	54.28
TIO2	0.00	0.00	0.00	0.00	0.00	0.00
AL2O3	27.14	27.98	24.97	28.08	28.04	27.76
CR2O3	0.00	0.00	0.00	0.00	0.00	0.00
FE2O3	0.00	0.00	0.00	0.00	0.00	0.00
FEO	0.93	0.85	0.61	0.88	0.67	0.00
MNO	0.00	0.00	0.00	0.00	0.00	0.00
MGO	0.11	0.10	0.06	0.09	0.08	0.00
CAO	12.00	12.42	8.22	12.35	13.23	11.23
NA2O	4.88	4.70	7.34	5.25	4.43	4.73
K2O	0.38	0.28	0.73	0.33	0.21	1.08
BAO	0.00	0.00	0.00	0.00	0.00	0.00
TOTAL	99.08	99.35	99.79	99.96	98.38	99.08

	AX83-056A feldspar G	AX83-058 feldspar CORE	AX83-058 feldspar G	AX83-058 feldspar RIM	AX83-060 feldspar G	AX85-074 feldspar CORE
SIO2	53.25	53.63	55.83	54.51	53.63	52.73
TIO2	0.00	0.00	0.00	0.00	0.00	0.00
AL2O3	28.19	28.51	28.00	28.15	28.22	28.90
CR2O3	0.14	0.00	0.00	0.00	0.00	0.00
FE2O3	0.00	0.00	0.00	0.00	0.00	0.00
FEO	0.68	0.68	0.92	0.72	0.97	0.00
MNO	0.00	0.00	0.00	0.00	0.00	0.00
MGO	0.17	0.12	0.12	0.14	0.18	0.00
CAO	12.43	11.71	10.28	11.40	12.26	13.59
NA2O	4.75	4.83	5.28	4.97	4.94	3.99
K2O	0.32	0.47	0.62	0.52	0.43	0.22
BAO	0.00	0.00	0.00	0.00	0.00	0.00
TOTAL	99.94	99.95	101.03	100.41	100.62	99.21

AVERAGE ANALYSES - EXTRUSIVE ROCKS

	AX85-074 feldspar G	AX85-074 feldspar RIM	AX85-075 feldspar CORE	AX85-075 feldspar G	AX85-075 feldspar RIM	AX85-078 feldspar CORE
SIO2	53.39	52.51	51.71	55.09	52.31	52.45
TIO2	0.00	0.00	0.00	0.00	0.00	0.00
AL2O3	27.85	28.51	29.93	26.95	29.37	30.43
CR2O3	0.00	0.00	0.00	0.00	0.00	0.00
FE2O3	0.00	0.00	0.00	0.00	0.00	0.00
FEO	0.00	0.00	0.00	0.00	0.00	0.00
MNO	0.00	0.00	0.00	0.00	0.00	0.00
MGO	0.00	0.00	0.00	0.00	0.00	0.00
CAO	12.78	13.41	13.92	10.59	13.16	13.82
NA2O	4.50	4.25	4.11	5.41	4.46	3.40
K2O	0.26	0.22	0.24	0.42	0.28	0.19
BAO	0.00	0.00	0.00	0.00	0.00	0.00
TOTAL	98.78	98.90	99.91	98.46	99.58	100.29

	AX85-078 feldspar G	AX85-078 feldspar RIM	AX85-082 feldspar CORE	AX85-082 feldspar G	AX85-082 feldspar RIM	AX85-091 feldspar CORE
SIO2	58.22	52.78	50.21	52.84	52.20	48.24
TIO2	0.00	0.00	0.00	0.00	0.00	0.00
AL2O3	25.58	29.85	30.07	27.91	28.24	32.16
CR2O3	0.00	0.00	0.00	0.00	0.00	0.00
FE2O3	0.00	0.00	0.00	0.00	0.00	0.00
FEO	0.00	0.00	0.00	0.00	0.00	0.00
MNO	0.00	0.00	0.00	0.00	0.00	0.00
MGO	0.00	0.00	0.00	0.00	0.00	0.00
CAO	8.78	13.06	14.88	12.82	13.38	16.79
NA2O	5.21	3.85	3.25	4.57	4.27	2.49
K2O	0.59	0.20	0.11	0.25	0.21	0.16
BAO	0.00	0.00	0.00	0.00	0.00	0.00
TOTAL	98.38	99.74	98.52	98.39	98.30	99.84

AVERAGE ANALYSES - EXTRUSIVE ROCKS

	AX85-091 feldspar G	AX85-091 feldspar RIM	AX85-094 feldspar CORE	AX85-094 feldspar G	AX85-094 feldspar RIM	AX85-242 feldspar CORE
SIO2	53.37	50.90	51.35	51.91	52.29	54.89
TIO2	0.00	0.00	0.00	0.00	0.00	0.00
AL2O3	28.50	30.38	29.99	29.02	29.07	25.59
CR2O3	0.00	0.00	0.00	0.00	0.00	0.00
FE2O3	0.00	0.00	0.00	0.00	0.00	0.00
FEO	0.00	0.00	0.00	0.00	0.00	0.00
MNO	0.00	0.00	0.00	0.00	0.00	0.00
MGO	0.00	0.00	0.00	0.00	0.00	0.00
CAO	12.30	14.51	13.84	13.12	12.74	11.68
NA2O	4.59	3.54	3.58	4.00	4.16	5.23
K2O	0.40	0.26	0.18	0.24	0.24	0.40
BAO	0.00	0.00	0.00	0.00	0.00	0.00
TOTAL	99.16	99.59	98.94	98.29	98.50	97.79

	AX85-242 feldspar G	AX85-242 feldspar RIM	AX85-260 feldspar CORE	AX85-260 feldspar G	AX85-260 feldspar RIM	AX85-261 feldspar CORE
SIO2	54.73	55.71	51.23	53.14	52.76	49.03
TIO2	0.00	0.00	0.00	0.00	0.00	0.00
AL2O3	26.74	25.14	30.62	28.73	30.15	31.50
CR2O3	0.00	0.00	0.00	0.00	0.00	0.00
FE2O3	0.00	0.00	0.00	0.00	0.00	0.00
FEO	0.00	0.00	0.00	0.00	0.00	0.00
MNO	0.00	0.00	0.00	0.00	0.00	0.00
MGO	0.00	0.00	0.00	0.00	0.00	0.00
CAO	11.56	10.99	14.41	12.74	13.62	15.59
NA2O	5.10	5.43	3.26	4.09	3.88	2.82
K2O	0.40	0.51	0.07	0.22	0.14	0.11
BAO	0.00	0.00	0.00	0.00	0.00	0.00
TOTAL	98.53	97.78	99.59	98.92	100.55	99.05

AVERAGE ANALYSES - EXTRUSIVE ROCKS

	AX85-261 feldspar G	AX85-261 feldspar RIM	AX85-264 feldspar CORE	AX85-264 feldspar G	AX85-264 feldspar RIM	AX85-266 feldspar CORE
SIO2	52.57	50.12	51.10	53.19	52.47	52.29
TIO2	0.00	0.00	0.00	0.00	0.00	0.00
AL2O3	28.86	30.41	30.34	28.70	29.52	30.64
CR2O3	0.00	0.00	0.00	0.00	0.00	0.00
FE2O3	0.00	0.00	0.00	0.00	0.00	0.00
FEO	0.00	0.00	0.00	0.00	0.00	0.00
MNO	0.00	0.00	0.00	0.00	0.00	0.00
MGO	0.00	0.00	0.00	0.00	0.00	0.00
CAO	13.01	14.76	14.44	12.83	13.43	13.31
NA2O	4.32	3.32	3.91	4.60	4.02	3.92
K2O	0.22	0.13	0.17	0.30	0.33	0.18
BAO	0.00	0.00	0.00	0.00	0.00	0.00
TOTAL	98.98	98.74	99.96	99.62	99.77	100.34

	AX85-266 feldspar G	AX85-266 feldspar RIM	AX85-267 feldspar CORE	AX85-267 feldspar G	AX85-267 feldspar RIM	BND83-012 feldspar G
SIO2	52.97	54.05	52.06	52.96	54.09	54.12
TIO2	0.00	0.00	0.00	0.00	0.00	0.00
AL2O3	29.46	29.63	27.88	27.52	25.89	28.04
CR2O3	0.00	0.00	0.00	0.00	0.00	0.00
FE2O3	0.00	0.00	0.00	0.00	0.00	0.00
FEO	0.00	0.00	0.00	0.00	0.00	0.00
MNO	0.00	0.00	0.00	0.00	0.00	0.00
MGO	0.00	0.00	0.00	0.00	0.00	0.00
CAO	12.68	12.02	13.29	12.78	11.61	11.82
NA2O	4.36	4.55	4.52	4.70	5.23	5.42
K2O	0.24	0.25	0.30	0.29	0.42	0.41
BAO	0.00	0.00	0.00	0.00	0.00	0.00
TOTAL	99.71	100.50	98.05	98.25	97.24	99.81

AVERAGE ANALYSES - EXTRUSIVE ROCKS

	BND83-016 feldspar CENTRE	BND83-016 feldspar CORE	BND83-016 feldspar G	BND83-016 feldspar RIM	BND83-017 feldspar CENTRE	BND83-017 feldspar CORE
SIO2	47.47	47.43	52.70	48.30	52.07	51.86
TIO2	0.00	0.00	0.00	0.00	0.00	0.00
AL2O3	33.03	32.66	28.49	31.61	29.45	28.84
CR2O3	0.00	0.00	0.00	0.00	0.00	0.00
FE2O3	0.00	0.00	0.00	0.00	0.00	0.00
FEO	0.00	0.00	0.00	0.00	0.00	0.00
MNO	0.00	0.00	0.00	0.00	0.00	0.00
MGO	0.00	0.00	0.00	0.00	0.00	0.00
CAO	17.00	16.77	12.62	16.30	13.05	13.37
NA2O	1.85	1.80	4.44	2.19	4.35	4.25
K2O	0.14	0.04	0.31	0.14	0.21	0.14
BAO	0.00	0.00	0.00	0.00	0.00	0.00
TOTAL	99.49	98.70	98.56	98.54	99.13	98.46

	BND83-017 feldspar G	BND83-017 feldspar RIM	EL84-007 feldspar G	EL84-010 feldspar G	EL84-087 feldspar CORE	EL84-087 feldspar G
SIO2	51.94	51.75	5.00	55.86	55.29	55.28
TIO2	0.00	0.00	0.00	0.00	0.00	0.00
AL2O3	29.07	29.14	27.97	26.02	27.23	27.53
CR2O3	0.00	0.00	0.00	0.00	0.00	0.00
FE2O3	0.00	0.00	0.00	0.00	0.00	0.00
FEO	0.00	0.00	0.00	0.00	0.00	0.00
MNO	0.00	0.00	0.00	0.00	0.00	0.00
MGO	0.00	0.00	0.00	0.00	0.00	0.00
CAO	13.38	13.61	10.30	10.53	10.09	10.23
NA2O	4.11	4.22	5.47	5.99	5.03	5.32
K2O	0.19	0.20	0.47	0.50	0.46	0.37
BAO	0.00	0.00	0.00	0.00	0.00	0.00
TOTAL	98.69	98.92	99.51	98.90	98.10	98.73

AVERAGE ANALYSES - EXTRUSIVE ROCKS

	EL84-087 feldspar RIM	EL84-256A feldspar CORE	EL84-256A feldspar G	EL84-256A feldspar RIM	EL85-107 feldspar G
SIO2	55.46	52.47	52.48	52.11	54.69
TIO2	0.00	0.00	0.00	0.00	0.00
AL2O3	27.47	28.98	28.15	29.09	26.95
CR2O3	0.00	0.00	0.00	0.00	0.00
FE2O3	0.00	0.00	0.00	0.00	0.00
FEO	0.00	0.00	0.00	0.00	0.00
MNO	0.00	0.00	0.00	0.00	0.00
MGO	0.00	0.00	0.00	0.00	0.00
CAO	10.34	12.90	12.68	13.20	11.07
NA2O	5.32	4.92	4.49	4.46	5.86
K2O	0.40	0.27	0.34	0.29	0.41
BAO	0.00	0.00	0.00	0.00	0.00
TOTAL	98.99	99.54	98.14	99.15	98.98

AVERAGE ANALYSES - EXTRUSIVE ROCKS

	AX83-011A pyroxene CENTRE	AX83-011A pyroxene G	AX83-011B pyroxene CORE	AX83-011B pyroxene G	AX83-011B pyroxene RIM	AX83-012A pyroxene CORE
SIO2	51.60	51.50	50.36	51.23	52.13	50.06
TIO2	0.94	0.84	1.11	0.95	0.83	1.03
AL2O3	1.63	1.78	4.91	2.37	1.75	4.52
CR2O3	0.04	0.04	0.00	0.11	0.24	0.17
FE2O3	0.00	0.00	0.00	0.00	0.00	0.00
FEO	13.26	12.29	8.75	10.97	10.58	8.02
MNO	0.17	0.13	0.00	0.12	0.08	0.00
MGO	14.19	14.57	15.47	14.59	15.33	15.46
CAO	18.92	19.20	19.59	19.89	20.22	20.08
NA2O	0.17	0.14	0.00	0.00	0.00	0.00
K2O	0.00	0.00	0.00	0.00	0.00	0.00
BAO	0.00	0.00	0.00	0.00	0.00	0.00
TOTAL	100.92	100.49	100.19	100.23	101.16	99.34

	AX83-012A pyroxene G	AX83-012A pyroxene RIM	AX83-014 pyroxene G	AX83-015 PYROXENE G	AX83-015 pyroxene CORE	AX83-015 pyroxene RIM
SIO2	51.19	51.12	51.31	51.08	51.92	50.60
TIO2	0.83	0.73	0.83	0.89	0.73	0.99
AL2O3	3.05	1.76	1.92	2.74	2.73	3.42
CR2O3	0.12	0.00	0.05	0.02	0.03	0.05
FE2O3	0.00	0.00	0.00	0.00	0.00	0.00
FEO	9.66	12.99	11.57	11.10	10.00	8.89
MNO	0.11	0.06	0.02	0.12	0.10	0.03
MGO	15.50	14.14	14.75	14.74	16.80	15.13
CAO	19.69	18.78	19.12	19.44	18.02	20.45
NA2O	0.18	0.12	0.12	0.08	0.00	0.00
K2O	0.00	0.00	0.00	0.00	0.00	0.00
BAO	0.00	0.00	0.00	0.00	0.00	0.00
TOTAL	100.33	99.70	99.69	100.21	100.33	99.56

AVERAGE ANALYSES - EXTRUSIVE ROCKS

	AX83-017 pyroxene G	AX83-020 pyroxene G	AX83-021 pyroxene G	AX83-023 pyroxene G	AX83-024 pyroxene G	AX83-025 pyroxene G
SIO2	50.60	51.24	51.56	51.61	51.21	51.95
TIO2	0.85	0.80	0.84	0.84	1.09	1.04
AL2O3	1.49	1.52	3.09	1.71	1.68	1.57
CR2O3	0.03	0.06	0.02	0.06	0.00	0.00
FE2O3	0.00	0.00	0.00	0.00	0.00	0.00
FEO	16.45	11.95	15.84	10.38	15.55	12.50
MNO	0.27	0.18	0.22	0.12	0.20	0.15
MGO	12.52	14.22	12.94	15.22	13.01	14.35
CAO	17.70	19.39	14.89	19.64	17.24	18.38
NA2O	0.17	0.01	0.54	0.11	0.15	0.25
K2O	0.00	0.00	0.23	0.00	0.00	0.00
BAO	0.00	0.00	0.00	0.00	0.00	0.00
TOTAL	100.08	99.37	100.17	99.69	100.13	100.19

	AX83-027 pyroxene CORE	AX83-027 pyroxene FERROAUG	AX83-027 pyroxene G	AX83-027 pyroxene INCLUSION	AX83-027 pyroxene RIM	AX83-031 pyroxene CORE
SIO2	48.26	48.70	51.05	50.79	50.19	52.43
TIO2	1.40	0.82	1.04	1.12	1.04	0.78
AL2O3	4.00	2.40	2.09	2.77	2.97	1.95
CR2O3	0.16	0.00	0.10	0.00	0.09	0.00
FE2O3	0.00	0.00	0.00	0.00	0.00	0.00
FEO	12.20	25.54	12.21	11.31	11.17	9.95
MNO	0.09	0.52	0.10	0.20	0.12	0.23
MGO	13.32	4.75	14.41	15.52	14.77	16.82
CAO	18.65	14.46	19.12	18.24	18.58	18.67
NA2O	0.05	2.42	0.13	0.00	0.00	0.00
K2O	0.00	0.51	0.00	0.00	0.00	0.00
BAO	0.00	0.00	0.00	0.00	0.00	0.00
TOTAL	98.13	100.12	100.25	99.95	98.93	100.83

AVERAGE ANALYSES - EXTRUSIVE ROCKS

	AX83-031 pyroxene G	AX83-031 pyroxene LOWCA	AX83-031 pyroxene RIM	AX83-032A pyroxene G	AX83-056A pyroxene CORE	AX83-056A pyroxene G
SIO2	52.22	51.92	52.40	51.60	52.72	52.12
TIO2	0.66	0.38	0.58	0.84	0.63	0.87
AL2O3	1.48	0.51	1.36	1.88	1.81	1.62
CR2O3	0.00	0.00	0.00	0.06	0.06	0.00
FE2O3	0.00	0.00	0.00	0.00	0.00	0.00
FEO	10.43	26.15	9.79	10.86	10.04	13.20
MNO	0.13	0.60	0.04	0.21	0.07	0.19
MGO	15.92	16.40	16.31	14.75	16.26	14.94
CAO	19.23	4.42	19.33	19.81	18.21	17.26
NA2O	0.00	0.00	0.00	0.36	0.02	0.12
K2O	0.00	0.00	0.00	0.00	0.00	0.00
BAO	0.00	0.00	0.00	0.00	0.00	0.00
TOTAL	100.07	100.38	99.81	100.37	99.82	100.33

	AX83-056A pyroxene RIM	AX83-057 pyroxene CORE	AX83-057 pyroxene G	AX83-058 pyroxene CENTRE	AX83-058 pyroxene CORE	AX83-058 pyroxene G
SIO2	52.42	52.61	52.61	50.04	49.94	49.96
TIO2	0.71	0.65	0.63	1.08	1.19	1.16
AL2O3	1.68	2.55	2.60	1.80	2.60	2.43
CR2O3	0.00	0.00	0.00	0.07	0.07	0.08
FE2O3	0.00	0.00	0.00	0.00	0.00	0.00
FEO	11.99	9.61	9.14	13.28	12.97	12.24
MNO	0.10	0.08	0.07	0.39	0.42	0.37
MGO	15.94	16.98	17.05	13.66	13.57	14.06
CAO	17.26	17.73	17.99	19.40	19.08	19.26
NA2O	0.07	0.08	0.06	0.26	0.33	0.32
K2O	0.00	0.00	0.00	0.00	0.00	0.00
BAO	0.00	0.00	0.00	0.00	0.00	0.00
TOTAL	100.17	100.29	100.13	99.97	100.15	99.87

AVERAGE ANALYSES - EXTRUSIVE ROCKS

	AX83-058 pyroxene RIM	AX83-060 pyroxene G	AX83-060 pyroxene HYP	AX83-103 pyroxene CENTRE	AX83-103 pyroxene CORE	AX83-103 pyroxene G
SIO2	50.30	50.21	53.95	52.36	51.92	52.34
TIO2	1.05	1.16	0.09	0.89	0.72	0.93
AL2O3	2.18	2.15	4.08	1.82	1.82	1.86
CR2O3	0.07	0.00	0.04	0.06	0.00	0.01
FE2O3	0.00	0.00	0.00	0.00	0.00	0.00
FEO	11.48	13.45	9.69	10.11	11.46	10.88
MNO	0.34	0.46	0.32	0.11	0.10	0.07
MGO	14.42	13.25	30.60	15.30	14.77	15.15
CAO	19.52	18.15	0.27	19.17	18.89	18.86
NA2O	0.29	0.31	0.05	0.14	0.31	0.25
K2O	0.00	0.00	0.00	0.00	0.00	0.00
BAO	0.00	0.00	0.00	0.00	0.00	0.00
TOTAL	99.64	99.13	99.09	99.96	99.90	100.34

	AX83-103 pyroxene RIM	AX83-106 pyroxene G	AX85-075 pyroxene CENTRE	AX85-075 pyroxene G	AX85-091 pyroxene FERROAUG	AX85-091 pyroxene G
SIO2	51.35	51.81	51.21	51.07	51.66	52.08
TIO2	1.33	1.04	1.02	0.94	0.59	0.93
AL2O3	2.90	2.85	2.84	1.70	2.98	3.00
CR2O3	0.00	0.00	0.12	0.01	0.05	0.00
FE2O3	0.00	0.00	0.00	0.00	0.00	0.00
FEO	11.07	12.19	11.21	17.07	20.73	10.88
MNO	0.09	0.13	0.27	0.43	0.50	0.28
MGO	15.19	14.70	14.86	12.71	12.22	15.23
CAO	18.05	18.32	18.41	16.35	11.09	18.25
NA2O	0.24	0.22	0.20	0.14	0.50	0.27
K2O	0.00	0.00	0.00	0.00	0.00	0.00
BAO	0.00	0.00	0.00	0.00	0.00	0.00
TOTAL	100.22	100.25	50.01	100.44	100.31	100.91

AVERAGE ANALYSES - EXTRUSIVE ROCKS

	AX85-091 pyroxene LOWCA	AX85-242 pyroxene CENTRE	AX85-242 pyroxene CORE	AX85-242 pyroxene G	AX85-242 pyroxene LOWCA	AX85-242 pyroxene RIM
SIO2	50.73	50.07	50.08	49.34	50.61	49.33
TIO2	0.55	1.39	1.18	1.06	0.64	1.31
AL2O3	0.62	3.57	3.08	1.79	1.23	2.93
CR2O3	0.00	0.21	0.14	0.11	0.05	0.07
FE2O3	0.00	0.00	0.00	0.00	0.00	0.00
FEO	29.12	10.76	11.66	18.32	23.88	12.82
MNO	0.63	0.44	0.47	0.65	0.62	0.45
MGO	11.94	15.09	14.84	11.77	14.77	13.80
CAO	5.54	17.85	17.34	15.25	6.98	17.31
NA2O	0.03	0.33	0.32	0.26	0.16	0.34
K2O	0.00	0.00	0.00	0.00	0.00	0.00
BAO	0.00	0.00	0.00	0.00	0.00	0.00
TOTAL	99.15	99.71	99.09	98.55	98.95	98.34

	AX85-261 pyroxene CENTRE	AX85-261 pyroxene CORE	AX85-261 pyroxene G	AX85-261 pyroxene RIM	AX85-264 pyroxene CORE	AX85-264 pyroxene G
SIO2	51.65	50.69	51.15	50.50	52.04	50.64
TIO2	0.73	0.75	0.87	0.78	0.60	1.12
AL2O3	2.33	2.44	2.95	2.60	1.90	3.32
CR2O3	0.16	0.36	0.03	0.46	0.17	0.13
FE2O3	0.00	0.00	0.00	0.00	0.00	0.00
FEO	8.21	7.32	9.50	7.33	8.61	11.63
MNO	0.33	0.29	0.31	0.21	0.34	0.46
MGO	16.79	16.03	15.63	15.93	16.70	16.02
CAO	19.99	21.79	18.69	21.57	18.99	16.02
NA2O	0.28	0.32	0.37	0.29	0.24	0.30
K2O	0.00	0.00	0.00	0.00	0.00	0.00
BAO	0.00	0.00	0.00	0.00	0.00	0.00
TOTAL	100.45	99.99	99.49	99.65	99.56	99.65

AVERAGE ANALYSES - EXTRUSIVE ROCKS

	AX85-264 pyroxene LOWCA	AX85-264 pyroxene RIM	AX85-266 pyroxene CORE	AX85-266 pyroxene G1	AX85-266 pyroxene G2	AX85-266 pyroxene RIM
SIO2	51.16	52.01	51.74	52.07	50.23	51.79
TIO2	0.81	0.62	0.72	0.64	0.60	0.71
AL2O3	1.61	1.87	2.87	1.48	1.65	1.55
CR2O3	0.08	0.06	0.13	0.15	0.10	0.04
FE2O3	0.00	0.00	0.00	0.00	0.00	0.00
FEO	21.44	10.02	10.32	11.99	14.83	13.99
MNO	0.59	0.35	0.35	0.37	0.41	0.49
MGO	17.03	16.85	16.12	17.84	15.74	17.02
CAO	6.57	17.69	17.00	15.94	13.52	14.38
NA2O	0.13	0.24	0.38	0.23	1.99	0.19
K2O	0.00	0.00	0.00	0.00	0.05	0.00
BAO	0.00	0.00	0.00	0.00	0.00	0.00
TOTAL	99.43	99.71	99.61	100.70	99.10	100.14

	AX85-267 pyroxene CORE	AX85-267 pyroxene G	AX85-267 pyroxene LOWCA	AX85-267 pyroxene RIM	BND83-005 pyroxene G	BND83-005 pyroxene CORE
SIO2	49.23	49.41	50.87	50.45	52.43	53.20
TIO2	1.21	1.00	0.81	0.99	0.88	0.59
AL2O3	3.76	2.65	1.30	2.22	2.34	1.91
CR2O3	0.11	0.05	0.08	0.07	0.13	0.18
FE2O3	0.00	0.00	0.00	0.00	0.00	0.00
FEO	11.27	13.07	21.15	13.26	9.82	10.71
MNO	0.46	0.52	0.68	0.51	0.15	0.19
MGO	14.33	14.48	15.39	14.70	17.30	18.68
CAO	18.46	17.02	9.42	17.10	17.54	16.23
NA2O	0.88	1.22	0.18	0.39	0.07	0.00
K2O	0.00	0.00	0.00	0.00	0.00	0.00
BAO	0.00	0.00	0.00	0.00	0.00	0.00
TOTAL	99.70	99.43	99.89	99.69	100.66	101.69

AVERAGE ANALYSES - EXTRUSIVE ROCKS

	BND83-005 pyroxene RIM	BND83-006 pyroxene CORE	BND83-006 pyroxene RIM	BND83-009 pyroxene CORE	BND83-009 pyroxene G	BND83-009 pyroxene RIM
SIO2	51.56	51.84	51.74	51.74	52.52	53.91
TIO2	1.38	0.85	0.88	1.10	0.80	0.63
AL2O3	2.45	2.61	2.85	3.64	1.84	1.61
CR2O3	0.00	0.17	0.14	0.00	0.00	0.00
FE2O3	0.00	0.00	0.00	0.00	0.00	0.00
FEO	11.25	10.63	9.95	8.55	11.17	8.93
MNO	0.30	0.09	0.05	0.00	0.09	0.12
MGO	15.16	15.31	15.22	15.58	14.59	16.88
CAO	19.14	18.53	19.23	19.86	19.24	18.69
NA2O	0.00	0.03	0.00	0.00	0.04	0.00
K2O	0.00	0.00	0.00	0.00	0.00	0.00
BAO	0.00	0.00	0.00	0.00	0.00	0.00
TOTAL	101.24	100.06	100.06	100.47	100.29	100.77

	BND83-012 pyroxene CENTRE	BND83-012 pyroxene CORE	BND83-012 pyroxene G	BND83-012 pyroxene RIM	BND83-015 pyroxene CORE	BND83-015 pyroxene G
SIO2	50.84	51.86	51.25	51.77	51.03	50.94
TIO2	1.03	1.06	0.96	1.20	0.98	0.82
AL2O3	3.16	3.33	1.50	1.68	2.61	2.82
CR2O3	0.05	0.00	0.00	0.00	0.10	0.25
FE2O3	0.00	0.00	0.00	0.00	0.00	0.00
FEO	11.25	11.66	13.79	13.34	12.02	12.65
MNO	0.29	0.17	0.38	0.31	0.15	0.11
MGO	15.49	15.88	13.08	14.42	15.48	14.48
CAO	17.84	17.12	18.86	18.11	17.55	17.89
NA2O	0.43	0.00	0.42	0.00	0.00	0.04
K2O	0.00	0.00	0.00	0.00	0.00	0.00
BAO	0.00	0.00	0.00	0.00	0.00	0.00
TOTAL	100.38	101.08	100.24	100.83	99.92	100.00

AVERAGE ANALYSES - EXTRUSIVE ROCKS

	BND83-015 pyroxene RIM	BND83-016 pyroxene CENTRE	BND83-016 pyroxene G	BND83-017 pyroxene CORE	BND83-017 pyroxene G	BND83-017 pyroxene RIM
SIO2	51.10	52.07	52.22	51.99	52.35	51.33
TIO2	0.96	0.61	0.61	0.65	0.75	0.96
AL2O3	3.31	2.46	1.49	1.57	1.59	1.20
CR2O3	0.13	0.09	0.00	0.00	0.00	0.00
FE2O3	0.00	0.00	0.00	0.00	0.00	0.00
FEO	10.13	9.46	10.81	12.38	11.33	18.13
MNO	0.07	0.09	0.08	0.13	0.23	0.40
MGO	15.52	16.29	15.88	15.57	15.88	12.47
CAO	18.04	19.29	18.88	18.16	18.59	16.25
NA2O	0.00	0.00	0.03	0.00	0.00	0.00
K2O	0.00	0.00	0.00	0.00	0.00	0.00
BAO	0.00	0.00	0.00	0.00	0.00	0.00
TOTAL	99.26	100.36	100.00	100.45	100.72	100.74

	EL84-007B pyroxene G	EL84-007B pyroxene LOWCA	EL84-010 pyroxene G	EL84-087 pyroxene CORE	EL84-087 pyroxene G	EL84-087 pyroxene LOWCACORE
SIO2	50.66	51.58	50.56	50.92	51.57	51.12
TIO2	0.98	0.68	0.98	1.18	0.77	0.71
AL2O3	1.70	1.06	1.59	1.78	1.03	0.88
CR2O3	0.02	0.01	0.04	0.00	0.00	0.00
FE2O3	0.00	0.00	0.00	0.00	0.00	0.00
FEO	15.97	20.59	16.32	14.82	17.37	22.27
MNO	0.63	0.79	0.68	0.53	0.65	0.71
MGO	13.11	15.60	13.87	14.09	15.78	16.22
CAO	16.88	9.98	15.57	16.44	12.79	7.70
NA2O	0.31	0.15	0.27	0.28	0.04	0.00
K2O	0.00	0.00	0.00	0.00	0.00	0.00
BAO	0.00	0.00	0.00	0.00	0.00	0.00
TOTAL	100.25	100.43	99.88	100.03	99.98	99.61

AVERAGE ANALYSES - EXTRUSIVE ROCKS

	EL84-087 pyroxene LOWCARIM	EL84-087 pyroxene RIM	EL84-256A pyroxene CORE	EL84-256A pyroxene G	EL84-256A pyroxene RIM	EL85-107 pyroxene CORE
SIO2	50.87	50.85	50.20	49.37	49.43	49.35
TIO2	0.76	0.92	1.17	1.35	1.26	1.43
AL2O3	1.04	1.35	2.56	2.43	2.12	3.57
CR2O3	0.00	0.00	0.16	0.02	0.08	0.06
FE2O3	0.00	0.00	0.00	0.00	0.00	0.00
FEO	18.20	17.19	13.69	14.15	15.12	11.06
MNO	0.69	0.55	0.39	0.43	0.47	0.44
MGO	12.85	13.38	12.69	13.50	12.35	14.10
CAO	15.26	15.24	19.31	18.28	19.27	18.93
NA2O	0.20	0.19	0.28	0.36	0.28	0.34
K2O	0.00	0.00	0.00	0.00	0.00	0.00
BAO	0.00	0.00	0.00	0.00	0.00	0.00
TOTAL	99.86	99.66	100.44	99.88	100.36	99.27

	EL85-107 pyroxene G	EL85-107 pyroxene RIM
SIO2	50.38	50.60
TIO2	1.01	0.78
AL2O3	2.02	1.46
CR2O3	0.10	0.10
FE2O3	0.00	0.00
FEO	13.70	14.15
MNO	0.49	0.76
MGO	13.53	13.37
CAO	17.59	17.88
NA2O	0.29	0.31
K2O	0.00	0.00
BAO	0.00	0.00
TOTAL	99.10	99.40

AVERAGE ANALYSES - EXTRUSIVE ROCKS

	AX83-060 OXIDE HEM	AX83-060 OXIDE MAG	AX85-082 OXIDE ILM	AX85-082 OXIDE MAG	AX85-242 OXIDE HEM	AX85-242 OXIDE ILM
SIO2	11.90	0.71	0.10	1.07	12.51	0.14
TIO2	38.45	21.83	51.93	27.50	34.00	44.96
AL2O3	0.36	1.81	0.09	1.44	1.29	0.32
CR2O3	0.00	0.00	0.00	0.00	0.00	0.00
FE2O3	0.00	0.00	0.00	0.00	0.00	0.00
FEO	41.25	68.13	45.80	64.54	41.65	48.54
MNO	0.64	0.95	0.49	0.91	0.45	0.48
MGO	3.89	0.21	1.26	0.26	0.87	1.15
CAO	3.05	0.11	0.13	0.05	0.42	0.07
NA2O	0.00	0.00	0.00	0.00	0.00	0.00
K2O	0.00	0.00	0.00	0.00	0.00	0.00
BAO	0.00	0.00	0.00	0.00	0.00	0.00
TOTAL	99.54	93.74	99.79	95.76	91.18	95.65

	AX85-264 OXIDE HEM	AX85-264 OXIDE ILM	AX85-264 OXIDE MAG	AX85-267 OXIDE ILM	AX85-267 OXIDE MAG	BND83-016 OXIDE ILM
SIO2	14.78	0.13	1.20	0.22	0.25	0.09
TIO2	33.73	46.02	24.27	46.65	23.97	46.61
AL2O3	2.71	0.15	2.07	0.08	1.72	0.11
CR2O3	0.00	0.00	0.00	0.00	0.00	0.00
FE2O3	0.00	0.00	0.00	0.00	0.00	0.00
FEO	38.73	47.97	64.95	46.48	67.04	46.15
MNO	0.63	0.49	0.89	0.55	0.76	0.42
MGO	0.32	0.51	0.06	0.77	0.69	1.19
CAO	0.70	0.13	0.13	0.08	0.07	0.07
NA2O	0.00	0.00	0.00	0.00	0.00	0.00
K2O	0.00	0.00	0.00	0.00	0.00	0.00
BAO	0.00	0.00	0.00	0.00	0.00	0.00
TOTAL	91.59	95.38	93.56	94.83	94.49	94.64

AVERAGE ANALYSES - EXTRUSIVE ROCKS

	BND83-016 OXIDE MAG	BND83-016 OXIDE MAG	BND83-017 OXIDE MAG	EL84-010 OXIDE ILM	EL84-010 OXIDE MAG	EL84-087 OXIDE ILM
SIO2	0.52	0.17	2.20	0.60	0.22	1.20
TIO2	25.51	26.84	24.44	45.74	23.49	44.87
AL2O3	1.91	1.85	1.82	0.30	1.88	0.19
CR2O3	0.00	0.00	0.00	0.00	0.00	0.00
FE2O3	0.00	0.00	0.00	0.00	0.00	0.00
FEO	61.70	59.89	62.66	46.93	68.85	46.49
MNO	0.72	0.76	1.17	0.72	0.66	0.81
MGO	0.48	0.41	0.64	1.29	1.01	1.31
CAO	0.07	0.11	0.16	0.06	0.09	0.11
NA2O	0.00	0.00	0.00	0.00	0.00	0.00
K2O	0.00	0.00	0.00	0.00	0.00	0.00
BAO	0.00	0.00	0.00	0.00	0.00	0.00
TOTAL	90.91	90.03	93.09	95.63	96.18	94.96

	EL84-087 OXIDE MAG	EL84-256A OXIDE ILM
SIO2	0.34	0.66
TIO2	16.76	47.80
AL2O3	1.35	0.30
CR2O3	0.00	0.00
FE2O3	0.00	0.00
FEO	75.25	47.73
MNO	0.64	0.38
MGO	0.48	0.83
CAO	0.10	0.12
NA2O	0.00	0.00
K2O	0.00	0.00
BAO	0.00	0.00
TOTAL	94.92	97.82

AVERAGE ANALYSES - INTRUSIVE ROCKS

	EL84-023 FELDSPAR G	EL84-041 FELDSPAR CORE	EL84-041 FELDSPAR G	EL84-041 FELDSPAR RIM	EL84-050 FELDSPAR CORE	EL84-050 FELDSPAR G
SIO2	54.71	51.38	51.95	52.88	52.23	53.50
TIO2	0.00	0.00	0.00	0.00	0.16	0.13
AL2O3	27.83	29.76	29.67	28.21	29.44	28.20
CR2O3	0.00	0.00	0.00	0.00	0.18	0.18
FE2O3	0.00	0.00	0.00	0.00	0.00	0.00
FEO	0.80	0.80	0.86	0.91	0.80	0.81
MNO	0.00	0.00	0.00	0.00	0.16	0.16
MGO	0.10	0.15	0.14	0.15	0.19	0.15
CAO	10.80	13.61	13.02	12.58	13.24	11.73
NA2O	5.05	3.66	3.78	4.22	4.43	5.16
K2O	0.31	0.19	0.13	0.28	0.38	0.44
BAO	0.00	0.00	0.00	0.00	0.00	0.00
TOTAL	99.58	99.54	99.53	99.22	101.19	100.45

	EL84-050 FELDSPAR RIM	EL84-056 FELDSPAR G	EL84-218 FELDSPAR CORE	EL84-218 FELDSPAR G	EL84-218 FELDSPAR RIM	EL84-222 FELDSPAR CORE
SIO2	53.53	55.75	51.87	52.49	51.61	56.25
TIO2	0.17	0.00	0.00	0.00	0.00	0.00
AL2O3	28.47	27.07	29.44	29.24	29.32	27.09
CR2O3	0.18	0.00	0.00	0.00	0.00	0.00
FE2O3	0.00	0.00	0.00	0.00	0.00	0.00
FEO	0.84	0.93	0.80	0.90	0.91	0.62
MNO	0.16	0.00	0.00	0.00	0.00	0.00
MGO	0.16	0.11	0.14	0.14	0.14	0.08
CAO	11.83	10.30	13.34	12.76	13.28	9.90
NA2O	5.14	5.25	4.39	4.58	4.18	6.29
K2O	0.41	0.53	0.35	0.41	0.28	0.36
BAO	0.00	0.00	0.00	0.00	0.00	0.00
TOTAL	100.87	99.93	100.33	100.51	99.72	100.56

AVERAGE ANALYSES - INTRUSIVE ROCKS

	EL84-222 FELDSPAR G	EL84-222 FELDSPAR RIM	EL84-232 FELDSPAR CORE	EL84-232 FELDSPAR G	EL84-232 FELDSPAR RIM	EL84-235 FELDSPAR CORE
SIO2	54.98	56.77	50.78	53.50	51.35	52.79
TIO2	0.00	0.00	0.00	0.00	0.00	0.00
AL2O3	27.70	26.84	29.50	28.30	29.09	28.79
CR2O3	0.00	0.00	0.00	0.00	0.00	0.00
FE2O3	0.00	0.00	0.00	0.00	0.00	0.00
FEO	0.63	0.55	0.87	0.92	0.92	0.75
MNO	0.00	0.00	0.00	0.00	0.00	0.00
MGO	0.08	0.06	0.17	0.14	0.18	0.16
CAO	10.72	9.37	14.11	12.03	13.55	12.16
NA2O	5.55	6.39	4.13	5.16	4.22	4.56
K2O	0.27	0.37	0.32	0.41	0.31	0.36
BAO	0.00	0.00	0.00	0.00	0.00	0.00
TOTAL	99.92	100.34	99.88	100.44	99.60	99.56

	EL84-235 FELDSPAR G	EL84-235 FELDSPAR INT	EL84-235 FELDSPAR RIM
SIO2	51.81	53.19	55.71
TIO2	0.00	0.00	0.00
AL2O3	29.67	28.71	27.01
CR2O3	0.00	0.00	0.00
FE2O3	0.00	0.00	0.00
FEO	0.79	0.77	0.63
MNO	0.00	0.00	0.00
MGO	0.13	0.13	0.10
CAO	13.44	12.03	9.95
NA2O	4.16	4.87	5.79
K2O	0.27	0.36	0.45
BAO	0.00	0.00	0.00
TOTAL	100.27	100.05	99.63

AVERAGE ANALYSES - INTRUSIVE ROCKS

	EL84-023 PYROXENE G	EL84-041 PYROXENE CORE	EL84-041 PYROXENE RIM	EL84-050 PYROXENE G	EL84-056 PYROXENE G1	EL84-056 PYROXENE G2
SIO2	51.31	48.83	49.54	50.80	50.52	51.06
TIO2	1.11	1.87	1.50	1.40	0.95	1.25
AL2O3	1.97	3.93	3.46	2.87	1.28	2.24
CR2O3	0.03	0.04	0.10	0.10	0.04	0.02
FE2O3	0.00	0.00	0.00	0.00	0.00	0.00
FEO	12.19	10.31	9.69	10.03	17.55	10.63
MNO	0.35	0.18	0.26	0.25	0.48	0.27
MGO	13.77	13.31	13.81	14.65	11.03	14.56
CAO	19.29	20.72	20.90	19.99	18.16	19.68
NA2O	0.27	0.34	0.30	0.54	0.28	0.27
K2O	0.00	0.00	0.00	0.00	0.00	0.00
BAO	0.00	0.00	0.00	0.00	0.00	0.00
TOTAL	100.28	99.51	99.56	100.62	100.28	99.97

	EL84-218 PYROXENE CORE	EL84-218 PYROXENE RIM	EL84-222 PYROXENE CORE	EL84-222 PYROXENE RIM	EL84-232 PYROXENE CORE	EL84-232 PYROXENE G
SIO2	45.83	47.24	50.61	50.30	47.83	46.64
TIO2	3.25	2.50	1.21	1.22	2.40	2.86
AL2O3	5.66	4.77	2.55	2.61	4.80	5.59
CR2O3	0.01	0.01	0.03	0.09	0.00	0.06
FE2O3	0.00	0.00	0.00	0.00	0.00	0.00
FEO	11.17	11.51	11.04	11.40	10.70	10.61
MNO	0.33	0.32	0.32	0.46	0.31	0.28
MGO	11.69	12.02	14.64	14.11	12.62	11.89
CAO	22.05	21.62	20.07	20.36	20.96	21.18
NA2O	0.49	0.54	0.35	0.34	0.45	0.50
K2O	0.00	0.00	0.00	0.00	0.00	0.00
BAO	0.00	0.00	0.00	0.00	0.00	0.00
TOTAL	100.48	100.53	100.90	100.90	100.06	99.61

AVERAGE ANALYSES - INTRUSIVE ROCKS

	EL84-232 PYROXENE RIM	EL84-235 PYROXENE CORE	EL84-235 PYROXENE RIM
SIO2	47.73	47.44	47.78
TIO2	2.20	2.50	2.32
AL2O3	4.58	5.02	4.65
CR2O3	0.00	0.01	0.05
FE2O3	0.00	0.00	0.00
FEO	10.61	10.26	10.77
MNO	0.31	0.29	0.27
MGO	12.59	12.92	12.99
CAO	21.15	21.65	21.50
NA2O	0.45	0.42	0.48
K2O	0.00	0.00	0.00
BAO	0.00	0.00	0.00
TOTAL	99.62	100.51	100.82

APPENDIX C

TABLE C-1
CHEMICAL ANALYSES USED IN ALTERATION STUDIES:
VOLCANIC ROCKS

Numbers correspond to data on Figure 5.3. Superscripts A and UA indicate "altered" and relatively "unaltered" volcanic rocks. Weight % ($H_2O_{TOT}+CO_2$) is shown for each sample. RC, relative change in weight percent after normalization to TiO_2.

Group 2A at Twisted Ridge

1^A = AX83-063 (1.76)
1^{UA} = AX83-059 (1.68)

Group 2B at Artharber Creek

2^A = AX85-082 (3.08)
2^{UA} = AX85-075 (1.13)

Group 2A at Twisted Ridge

3^A = AX83-067 (4.28)
3^{UA} = AX83-059 (1.68)

Group 1A at Geodetic Hills

4^A = AX85-241 (5.12)
4^{UA} = AX85-242 (2.50)

Group 1B at Camp Five Creek

5^A = AX85-265 (10.22)
5^{UA} = AX85-264 (2.20)

Group 2A at W. Glacier Fiord Syncline

6^A = AX83-108 (11.4)
6^{UA} = AX83-106 (1.45)

(wt%)	1^A	1^{UA}	R.C.	2^A	2^{UA}	R.C.
SiO_2	49.74	50.29	-12	51.65	49.46	+26
TiO_2	3.44	3.05	0	2.37	2.86	0
Al_2O_3	12.99	13.15	-12	13.49	14.19	+15
FeOt	16.11	15.03	-5	12.99	12.25	+28
MgO	3.95	4.37	-20	4.71	5.38	+6
CaO	8.45	9.02	-17	9.85	9.80	+21
Na_2O	3.79	3.23	+4	2.57	2.38	+30
K_2O	0.41	0.77	-53	0.47	0.50	+13
P_2O_5	0.33	0.36	-19	0.29	0.30	+17
(ppm)						
Ba	206	271	-33	204	177	+39
Rb	27	30	-20	11	11	+21
Sr	232	248	-17	220	186	+43
Y	45	43	-7	42	48	+6
Zr	216	219	-12	189	201	+13
Nb	22	23	-15	16	18	+7
Ni	28	33	-25	31	39	-4
Cr	20	25	-29	38	37	+24
Th	3.7	3.9	-16	nd	nd	nd
Hf	6.2	5.6	-2	nd	nd	nd
Ta	2.6	2.3	0	nd	nd	nd
La	21.7	22.3	-14	nd	nd	nd

TABLE C-1 (continued)

(wt%)	3^A	3^{UA}	R.C.	4^A	4^{UA}	R.C.
SiO_2	49.96	50.29	+30	53.03	52.98	-2
TiO_2	2.33	3.05	0	3.47	3.39	0
Al_2O_3	14.59	13.15	+45	13.81	13.35	+1
FeOt	12.82	15.03	+12	12.54	11.98	+2
MgO	5.31	4.37	+59	4.22	4.35	-5
CaO	10.35	9.02	+50	8.78	8.59	0
Na_2O	2.80	3.23	+13	3.16	3.12	-1
K_2O	0.59	0.77	0	0.71	0.85	-18
P_2O_5	nd	0.36	nd	0.67	0.65	+1
(ppm)						
Ba	167	271	-19	1062	1208	-14
Rb	21	30	-8	15	19	-23
Sr	242	248	+28	369	407	-11
Y	34	43	+3	53	53	-2
Zr	159	219	-5	298	289	+1
Nb	14	23	-20	33	31	+4
Ni	41	33	+63	30	32	-8
Cr	43	25	+125	34	33	+1
Th	2.4	3.9	-19	5.1	4.7	+6
Hf	4.3	5.6	0	7.3	6.8	+5
Ta	1.5	2.3	-15	2.5	2.9	-16
La	14.6	22.3	-14	36.6	36.8	-3

(wt%)	5^A	5^{UA}	R.C.	6^A	6^{UA}	R.C.
SiO_2	46.14	52.37	-20	43.28	50.86	-30
TiO_2	2.44	2.22	0	2.61	2.15	0
Al_2O_3	16.39	13.81	+8	17.42	13.78	+4
FeOt	10.40	11.62	-19	13.75	11.87	-5
MnO	0.25	0.20	+14	0.31	0.19	+34
MgO	3.06	5.82	-52	1.86	5.62	-73
CaO	18.49	10.31	+63	15.79	10.19	+28
Na_2O	2.58	2.33	+1	4.20	2.79	+24
K_2O	0.28	0.35	-27	0.44	0.93	-61
P_2O_5	0.29	0.22	+20	0.29	0.23	+4
(ppm)						
Ba	120	188	-42	124	169	-39
Rb	1	10	-91	1	32	-97
Sr	237	229	-6	240	232	+15
Y	46	40	+5	46	35	+8
Zr	217	190	+4	220	169	+7
Nb	15	13	+5	16	17	-22
Ni	50	38	+20	50	43	+4
Cr	81	56	+32	82	15	+350
Th	2.6	3.0	-21	nd	nd	nd
Hf	4.9	4.9	-9	nd	nd	nd
Ta	1.0	1.7	-46	nd	nd	nd
La	17	15.5	0	nd	nd	nd

TABLE C-2
PEARSON CORRELATION COEFFICIENTS:
GROUP 2A (ALL SECTIONS, N = 32)

	TiO_2	Al_2O_3	FeOt	MgO	CaO	Na_2O	K_2O	P_2O5
SiO_2	-0.44	0.24	-0.46	0.19	0.34	-0.35	0.13	-0.20
TiO_2		-0.75	0.82	-0.89	-0.73	0.57	-0.20	0.89
Al_2O_3			-0.73	0.72	0.52	-0.23	0.32	-0.70
FeOt				-0.74	-0.81	0.56	-0.37	0.67
MgO					0.71	-0.56	0.21	-0.83
CaO						-0.84	-0.02	-0.63
Na_2O							0.12	0.51
K_2O								-0.09

	Rb	Sr	Ba	V	Cr	Ni	Zn	Y
SiO_2	0.35	-0.10	0.17	-0.45	-0.01	0.26	-0.22	-0.15
TiO_2	0.23	-0.17	0.10	0.59	-0.33	-0.66	0.82	0.77
Al_2O_3	0.03	0.23	0.07	-0.68	0.43	0.65	-0.84	-0.69
FeOt	0.04	-0.10	-0.01	0.77	-0.32	-0.70	0.77	0.70
MgO	-0.25	0.19	-0.15	-0.57	0.39	0.74	-0.81	-0.78
CaO	-0.34	-0.02	-0.32	-0.59	0.31	0.66	-0.62	-0.60
Na_2O	0.29	0.33	0.57	0.42	-0.23	-0.48	0.45	0.52
K_2O	0.40	0.02	0.41	-0.32	0.12	0.29	-0.30	-0.13
P_2O_5	0.35	0.00	0.37	0.44	-0.32	-0.50	0.79	0.90
Rb		-0.34	0.27	-0.19	0.03	-0.01	0.08	0.24
Sr			0.68	0.09	-0.15	0.14	-0.03	0.05
Ba				-0.03	-0.22	0.00	0.12	0.34
V					-0.21	-0.56	0.73	0.57
Cr						0.63	-0.35	-0.24
Ni							-0.58	-0.42
Zn								0.78

	Zr	Nb
SiO_2	-0.03	-0.02
TiO_2	0.75	0.74
Al_2O_3	-0.59	-0.60
FeOt	0.53	0.52
MgO	-0.75	-0.76
CaO	-0.51	-0.56
Na_2O	0.50	0.54
K_2O	-0.05	-0.06
P_2O_5	0.95	0.88
Rb	0.34	0.31
Sr	0.13	0.16
Ba	0.52	0.52
V	0.37	0.31
Cr	-0.30	-0.54
Ni	-0.34	-0.53
Zn	0.69	0.74
Y	0.91	0.75
Zr		0.90

Note: Correlation coefficients with a 0.1 % level of significance are underlined (threshold values are 0.55 at N = 32; 0.80 at N = 13; 0.68 at N = 19). Standard errors are in the range 0.03-0.05 for r = 0.90; 0.13-0.21 for r = 0.50.

TABLE C-2 (continued)
GROUP 2A AT TWISTED RIDGE (N = 13)

	Th	Hf	Ta	La	Ce	Yb
SiO_2	0.60	0.01	0.09	0.33	0.34	-0.02
TiO_2	0.47	0.92	0.80	0.74	0.71	0.85
Al_2O_3	-0.42	-0.76	-0.75	-0.63	-0.62	-0.72
FeOt	0.20	0.74	0.76	0.47	0.46	0.76
MgO	-0.59	-0.89	-0.84	-0.79	-0.78	-0.85
CaO	-0.59	-0.70	-0.68	-0.70	-0.73	-0.76
Na_2O	0.43	0.63	0.58	0.60	0.62	0.76
K_2O	0.47	-0.13	-0.30	0.19	0.25	-0.23
P_2O_5	0.71	0.93	0.69	0.93	0.90	0.75
Rb	0.86	0.45	0.29	0.71	0.77	0.38
Sr	-0.16	0.14	0.16	0.13	0.02	-0.05
Ba	0.90	0.67	0.55	0.90	0.88	0.45
V	-0.01	0.47	0.74	0.22	0.20	0.55
Cr	-0.34	-0.41	-0.54	-0.38	-0.37	-0.36
Ni	-0.13	-0.32	-0.63	-0.21	-0.23	-0.47
Zn	0.37	0.74	0.76	0.59	0.58	0.68
Y	0.74	0.98	0.75	0.91	0.90	0.88
Zr	0.77	0.96	0.75	0.95	0.92	0.78
Nb	0.74	0.90	0.74	0.93	0.89	0.75
Th		0.71	0.49	0.91	0.92	0.60
Hf			0.76	0.90	0.87	0.88
Ta				0.63	0.59	0.74
La					0.99	0.73
Ce						0.73

TABLE C-2 (continued)
PEARSON CORRELATION COEFFICIENTS:
GROUP 2B (ALL SECTIONS, N = 19)

	TiO_2	Al_2O_3	FeOt	MgO	CaO	Na_2O	K_2O	P_2O_5
SiO_2	-0.28	0.15	-0.50	-0.41	-0.59	0.28	0.60	0.02
TiO_2		-0.71	0.56	-0.57	-0.50	0.41	0.08	0.91
Al_2O_3			-0.70	0.44	0.47	-0.01	0.00	-0.74
FeOt				-0.38	-0.11	0.00	-0.23	0.48
MgO					0.84	-0.61	-0.57	-0.73
CaO						-0.61	-0.78	-0.66
Na_2O							0.56	0.39
K_2O								0.22

	Rb	Sr	Ba	V	Cr	Ni	Zn	Y
SiO_2	0.64	0.43	0.68	-0.43	-0.50	-0.74	-0.44	-0.16
TiO_2	-0.18	-0.35	0.04	0.76	-0.23	0.23	0.80	0.81
Al_2O_3	0.21	0.64	-0.10	-0.67	0.29	-0.11	-0.62	-0.67
FeOt	-0.36	-0.68	-0.18	0.76	-0.12	0.50	0.61	0.56
MgO	-0.38	0.23	-0.48	-0.33	0.71	0.28	-0.32	-0.51
CaO	-0.52	-0.03	-0.55	-0.19	0.63	0.35	-0.19	-0.41
Na_2O	0.36	0.45	0.30	0.10	-0.43	-0.01	0.12	0.17
K_2O	0.70	0.30	0.35	-0.27	-0.42	-0.34	-0.24	-0.08
P_2O_5	0.08	-0.19	0.48	0.66	-0.47	-0.07	0.74	0.85
Rb		0.48	0.75	-0.21	-0.67	-0.64	-0.12	0.03
Sr			0.41	-0.57	-0.13	-0.35	-0.42	-0.37
Ba				0.09	-0.73	-0.71	0.18	0.40
V					-0.20	0.36	0.93	0.87
Cr						0.64	-0.26	-0.42
Ni							0.21	-0.02
Zn								0.93

	Zr	Nb
SiO_2	0.11	0.14
TiO_2	0.72	0.64
Al_2O_3	-0.54	-0.46
FeOt	0.29	0.12
MgO	-0.57	-0.44
CaO	-0.52	-0.51
Na_2O	0.32	0.28
K_2O	0.06	0.15
P_2O_5	0.87	0.77
Rb	0.26	0.37
Sr	-0.05	-0.02
Ba	0.65	0.64
V	0.69	0.60
Cr	-0.56	-0.52
Ni	-0.28	-0.29
Zn	0.81	0.75
Y	0.92	0.84
Zr		0.95

TABLE C-3
TRACE ELEMENT MODELLING

Hypothetical ***parental basalts*** tested for fractional crystallization and assimilation-fractionation (Table C-4) are PB1 and PB2. Trace element data (Ci) are obtained by removing 20% olivine from ***picrites*** P1 and P2. The range of values assigned to P1 and P2 are consistent with compositional data on picritic basalts reported by Krishnamurty and Cox (1977); Francis et al. (1983); and Clarke et al. (1976, 1983): Ni 600 and 1000 ppm; Cr 1000 and 2000 ppm; Th 0.05 and 0.7 ppm; and La 1.5 and 6 ppm. Nb concentrations in picrites are often below detection limits and few data are reported in the literature. The initial concentration of 10 ppm for Nb (*) is arbitrary but serves to illustrate the similar behaviour of Nb, Th and La during the AFC process. ***D***, bulk distribution coefficient calculated using partition coefficients in Table 5.12 (a).

I. Model A: Perfect Fractional Crystallization
Fractionating assemblage is 0.15 Ol + 0.35 Cpx + 0.5 Plag according to Biggar (1983).

Ni	Ci	F = 0.2	F = 0.4	F = 0.6	F = 0.8
PB1	134	107	81	54	27
PB2	80	64	48	32	16
D_{Ni} = 1.99					

Cr	Ci	F = 0.2	F = 0.4	F = 0.6	F = 0.8
PB1	268	140	61	19	2
PB2	134	70	30	9	1
D_{Cr} = 3.9					

La	Ci	F = 0.2	F = 0.4	F = 0.6	F = 0.8
PB1	1.9	2.3	2.9	4.2	7.9
PB2	7.4	9.1	11.8	17.0	31.7
D_{La} = 0.1					

Th	Ci	F = 0.2	F = 0.4	F = 0.6	F = 0.8
PB1	0.06	0.07	0.1	0.14	0.28
PB2	0.87	1.1	1.4	2.1	4.1
D_{Th} = 0.04					

Nb	Ci*	F = 0.2	F = 0.4	F = 0.6	F = 0.8
	10	12.2	15.7	22.4	41.2

TABLE C-4
TRACE ELEMENT MODELLING

II. Model B: Assimilation and Fractional Crystallization
(same fractionating assemblage as in Model A; end-member contaminants listed in Table 5.12 b).
C = Type of crustal contaminant
$[Element]_{PB2}$: Concentration of element in initial magma
$[Element]_C$: Concentration of element in contaminant
C/A: Rate of crystallization vs. assimilation

C	$[Ni]_{PB2}$	$[Ni]_C$	C/A	F = 0.2	F = 0.4	F = 0.6	F = 0.8
C1	80	135	5	64	49.5	37	28
C1	80	135	2.5	54	35	22	16
C2	80	20	5	58	39	23	10
C2	80	20	2.5	48	26	11	4

C	$[Cr]_{PB2}$	$[Cr]_C$	C/A	F = 0.2	F = 0.4	F = 0.6	F = 0.8
C1	134	235	5	65	32	19	15
C1	134	235	2.5	47	18	11.5	10.7
C2	134	35	5	58	20	6	2.5
C2	134	35	2.5	40	9	2	1.6

C	$[La]_{PB2}$	$[La]_C$	C/A	F = 0.2	F = 0.4	F = 0.6	F = 0.8
C1	7.4	11	5	9.7	13.3	20.4	40
C1	7.4	11	2.5	9.6	13.1	19.7	38
C2	7.4	30	5	10.8	16.4	27	57
C2	7.4	30	2.5	10.8	16.1	26.2	54

C	$[Th]_{PB2}$	$[Th]_C$	C/A	F = 0.2	F = 0.4	F = 0.6	F = 0.8
C1	0.87	1.06	5	1.1	1.6	2.5	5
C1	0.87	1.06	2.5	1.1	1.6	2.4	4.9
C2	0.87	10.7	5	1.7	3.1	5.9	14
C2	0.87	10.7	2.5	1.7	3.1	5.8	13.7

C	[Nb]i	$[Nb]_C$	C/A	F = 0.2	F = 0.4	F = 0.6	F = 0.8
C1	10	6	5	12.5	16.4	23.9	44
C1	10	6	2.5	12.3	16	22.8	41
C2	10	25	5	13.6	19.4	30.5	61
C2	10	25	2.5	13.5	19	29.3	57

TABLE C-5
CHEMICAL ANALYSES USED IN ALTERATION STUDIES:
INTRUSIVE ROCKS

Numbers correspond to data on Figure 6.2. Superscripts A and UA indicate "altered" and relatively "unaltered" rocks. Weight % ($H_2O_{TOT}+CO_2$) is shown for each sample. RC, relative change in weight percent after normalization to TiO_2.

Group B at Buchanan Lake

1^A = AX85-061 (3.73)
1^{UA} = AX85-051 (1.57)

Group D at Piper Pass

3^A = EL84-044 (6.96)
3^{UA} = EL84-060 (1.68)

Group D at Piper Pass

5^A = EL84-052 (14.99)
5^{UA} = EL84-050 (2.71)

Group C, Tanquary Fiord

2^A = EL84-245 (4.62)
2^{UA} = EL84-211 (2.74)

Group C, Tanquary Fiord

4^A = EL84-232 (7.68)
4^{UA} = EL84-211 (2.74)

(wt%)	1^A	1^{UA}	R.C.	2^A	2^{UA}	R.C.
SiO_2	51.79	51.12	-16	45.96	48.85	-3
TiO_2	3.06	2.53	0	3.74	3.87	0
Al_2O_3	13.03	13.17	-18	14.67	13.32	+14
FeOt	14.02	13.47	-14	13.70	14.05	+1
MgO	5.28	5.12	-15	4.95	5.35	-4
CaO	6.64	9.35	-41	9.81	7.66	+32
Na_2O	3.68	2.40	+27	2.75	4.51	-37
K_2O	0.37	0.80	-62	1.06	0.32	+243
P_2O_5	0.31	0.26	-1	0.62	0.44	+46
(ppm)						
Ba	288	269	-11	830	129	+566
Rb	11	27	-66	21	9	+141
Sr	403	248	+34	536	382	+45
Y	40	45	-26	33	32	+7
Zr	197	197	-17	181	214	-12
Nb	17	14	-17	26	29	-7
Ni	25	30	-31	33	28	+22
Cr	15	22	-44	42	22	+97

TABLE C-5 (continued)

(wt%)	3^{A}	3^{UA}	R.C.	4^{A}	4^{UA}	R.C.
SiO_2	49.75	46.89	+10	46.02	48.85	+3
TiO_2	3.63	3.78	0	3.53	3.87	0
Al_2O_3	13.63	13.42	+6	14.64	13.32	+20
FeOt	12.81	14.02	-5	13.30	14.05	+4
MgO	5.50	5.68	+1	5.36	5.35	+10
CaO	9.72	8.32	+22	10.91	7.66	+56
Na_2O	2.97	3.18	-3	2.37	4.51	-42
K_2O	0.99	1.22	-15	0.69	0.32	+136
P_2O_5	0.44	0.39	+17	0.55	0.44	+37
(ppm)						
Ba	316	625	-47	395	129	+236
Rb	19	35	-43	21	9	+156
Sr	553	462	+25	616	382	+77
Y	29	29	+4	34	32	+16
Zr	202	202	+4	208	214	+6
Nb	32	31	+7	26	29	-2
Ni	38	27	+46	40	28	+57
Cr	33	28	+23	34	22	+69

(wt%)	5^{A}	5^{UA}	R.C.
SiO_2	42.33	48.77	-27
TiO_2	4.52	3.82	0
Al_2O_3	15.68	12.63	+5
FeOt	14.56	14.01	-12
MgO	2.84	5.73	-58
CaO	14.33	9.41	+29
Na_2O	3.14	2.61	+2
K_2O	1.59	1.09	+23
P_2O_5	0.61	0.47	+10
(ppm)			
Ba	674	517	+10
Rb	40	21	+61
Sr	727	540	+14
Y	43	36	+1
Zr	343	282	+3
Nb	49	41	+1
Ni	47	68	-42
Cr	48	107	-62

TABLE C-6
PEARSON CORRELATION COEFFICIENTS:
GROUP A - LIGHTFOOT RIVER (N = 20)

	TiO_2	Al_2O_3	FeOt	MgO	CaO	Na_2O	K_2O	P_2O_5
SiO_2	-0.81	0.20	-0.63	-0.13	0.19	-0.20	0.23	-0.39
TiO_2		-0.08	0.40	-0.13	-0.36	0.29	0.07	0.58
Al_2O_3			-0.62	-0.40	-0.07	0.25	0.30	0.08
FeOt				0.06	-0.46	0.22	-0.15	0.36
MgO					0.34	-0.29	-0.61	-0.62
CaO						-0.75	-0.45	-0.46
Na_2O							0.35	0.31
K_2O								0.21

	Rb	Sr	Ba	V	Cr	Ni	Zn	Y
SiO_2	0.15	-0.37	0.01	-0.72	0.09	-0.17	0.13	-0.16
TiO_2	0.20	0.48	-0.02	0.57	0.04	0.38	-0.18	0.38
Al_2O_3	0.25	0.21	-0.23	-0.45	0.13	0.05	-0.06	0.11
FeOt	-0.17	0.21	0.24	0.67	-0.63	-0.37	0.30	0.15
MgO	-0.41	-0.05	0.06	0.30	0.47	0.20	-0.34	-0.76
CaO	-0.45	-0.63	-0.39	-0.23	0.53	0.25	-0.38	-0.31
Na_2O	0.21	0.49	0.22	0.01	-0.34	-0.28	0.43	0.09
K_2O	0.90	0.33	0.40	-0.19	-0.19	-0.16	0.15	0.31
P_2O_5	0.11	0.24	-0.04	-0.02	-0.40	0.05	0.24	0.82
Rb		0.43	0.35	0.00	-0.05	0.04	-0.12	0.21
Sr			0.55	0.27	-0.03	0.09	-0.13	0.04
Ba				0.11	-0.09	-0.18	0.32	-0.13
V					-0.14	0.09	-0.21	-0.06
Cr						0.75	-0.57	-0.30
Ni							-0.68	0.21
Zn								0.07

	Zr	Nb
SiO_2	-0.21	-0.20
TiO_2	0.60	0.46
Al_2O_3	0.19	-0.15
FeOt	0.00	0.37
MgO	-0.68	-0.44
CaO	-0.36	-0.50
Na_2O	0.29	0.37
K_2O	0.30	0.25
P_2O_5	0.79	0.69
Rb	0.25	0.12
Sr	0.26	0.19
Ba	-0.07	0.21
V	-0.06	0.08
Cr	-0.06	-0.42
Ni	0.41	-0.15
Zn	0.01	0.41
Y	0.85	0.50
Zr		0.62

Note: Correlation coefficients with a 0.1 % level of significance are underlined (threshold values are 0.55 at N = 35; 0.60 at N = 25; 0.65 at N = 20). Standard errors are in the range 0.03-0.04 for r = 0.90; 0.13-0.17 for r = 0.50.

TABLE C-6 (continued)
PEARSON CORRELATION COEFFICIENTS
GROUP B - BUCHANAN LAKE, EUREKA SOUND (N = 35)

	TiO_2	Al_2O_3	FeOt	MgO	CaO	Na_2O	K_2O	P_2O_5
SiO_2	0.04	-0.31	0.19	-0.70	-0.62	0.37	0.53	0.39
TiO_2		-0.59	0.71	-0.49	-0.58	0.48	0.28	0.74
Al_2O_3			-0.77	0.49	0.60	-0.46	-0.39	-0.57
FeOt				-0.57	-0.74	0.58	0.43	0.56
MgO					0.87	-0.70	-0.77	-0.76
CaO						-0.85	-0.70	-0.72
Na_2O							0.56	0.59
K_2O								0.54

	Rb	Sr	Ba	V	Cr	Ni	Zn	Y
SiO_2	0.28	0.02	0.32	-0.39	-0.58	-0.48	0.41	0.70
TiO_2	0.37	0.56	0.52	0.35	-0.58	-0.53	0.30	0.50
Al_2O_3	-0.41	-0.30	-0.50	-0.38	0.61	0.32	-0.39	-0.56
FeOt	0.43	0.41	0.73	0.48	-0.77	-0.60	0.47	0.48
MgO	-0.64	-0.18	-0.70	0.19	0.80	0.73	-0.61	-0.89
CaO	-0.60	-0.28	-0.79	-0.08	0.79	0.74	-0.63	-0.74
Na_2O	0.51	0.14	0.70	0.21	-0.53	-0.53	0.42	0.52
K_2O	0.85	-0.06	0.56	-0.23	-0.47	-0.54	0.60	0.67
P_2O_5	0.48	0.41	0.57	-0.16	-0.59	-0.55	0.35	0.85
Rb		-0.14	0.57	-0.05	-0.44	-0.47	0.53	0.48
Sr			0.24	0.29	-0.36	-0.30	0.05	0.21
Ba				0.21	-0.70	-0.68	0.55	0.53
V					-0.21	0.00	0.02	-0.35
Cr						0.79	-0.51	-0.65
Ni							-0.48	-0.57
Zn								0.47

	Zr	Nb
SiO_2	0.63	0.60
TiO_2	0.61	0.61
Al_2O_3	-0.57	-0.54
FeOt	0.51	0.51
MgO	-0.86	-0.77
CaO	-0.73	-0.71
Na_2O	0.52	0.52
K_2O	0.58	0.61
P_2O_5	0.86	0.81
Rb	0.41	0.39
Sr	0.46	0.51
Ba	0.52	0.54
V	-0.20	-0.14
Cr	-0.69	-0.62
Ni	-0.55	-0.59
Zn	0.43	0.31
Y	0.93	0.82
Zr		0.91

TABLE C-6 (continued)
PEARSON CORRELATION COEFFICIENTS
GROUPS C AND D - NORTHEASTERN ELLESMERE ISLAND (N = 25)

	TiO_2	Al_2O_3	FeOt	MgO	CaO	Na_2O	K_2O	P_2O_5
SiO_2	0.10	-0.37	-0.03	-0.20	0.31	0.23	0.34	-0.34
TiO_2		-0.53	0.73	0.08	-0.42	0.25	-0.29	0.35
Al_2O_3			-0.74	0.14	0.37	-0.24	-0.10	0.24
FeOt				-0.21	-0.36	0.24	-0.12	0.08
MgO					0.17	-0.28	-0.41	0.30
CaO						-0.89	-0.10	0.22
Na_2O							-0.04	-0.19
K_2O								-0.55

	Rb	Sr	Ba	V	Cr	Ni	Zn	Y
SiO_2	0.12	-0.01	-0.14	0.31	0.08	-0.20	0.06	0.02
TiO_2	-0.29	-0.18	-0.11	0.32	0.00	-0.31	-0.22	0.64
Al_2O_3	-0.12	0.21	0.41	-0.53	0.02	0.15	-0.18	-0.47
FeOt	0.04	-0.26	-0.26	0.51	-0.15	-0.32	0.11	0.58
MgO	-0.50	-0.13	-0.04	-0.23	0.35	0.62	-0.27	-0.07
CaO	-0.24	0.37	0.03	-0.59	0.07	0.52	0.33	-0.11
Na_2O	0.07	-0.48	-0.11	0.48	-0.14	-0.51	-0.17	0.03
K_2O	0.77	0.41	0.46	0.19	0.04	-0.15	0.09	-0.26
P_2O_5	-0.51	-0.21	0.26	-0.54	0.21	0.11	-0.01	0.45
Rb		0.29	0.20	0.32	-0.25	-0.40	0.04	-0.22
Sr			0.18	-0.35	-0.05	0.17	0.08	-0.07
Ba				-0.33	0.39	0.09	-0.09	-0.06
V					-0.18	-0.52	-0.34	-0.15
Cr						0.61	-0.09	0.15
Ni							0.17	0.02
Zn								0.23

	Zr	Nb
SiO_2	0.44	0.48
TiO_2	0.24	0.18
Al_2O_3	-0.71	-0.63
FeOt	0.38	0.34
MgO	-0.19	-0.40
CaO	-0.23	-0.34
Na_2O	0.06	0.15
K_2O	0.28	0.50
P_2O_5	-0.50	-0.58
Rb	0.23	0.45
Sr	0.25	0.30
Ba	-0.28	-0.21
V	0.29	0.44
Cr	0.15	0.09
Ni	0.15	-0.06
Zn	0.22	0.09
Y	0.42	0.21
Zr		0.88

TABLE C-7
CLUSTER ANALYSIS

Notes:

Cluster analysis is a multivariate statistical test to detect "natural" groupings in data. The ***K-means*** method of clustering (McQueen, 1967) splits a set of objects into a selected number of groups by maximizing ***between***-, relative to ***within***- group variation. In this way, it resembles one-way analysis of variance where the groups are unknown, and the largest F-value is sought by reassigning members to each group. The results were obtained using the SYSTAT package of statistical programs. Data for all the variables were replaced by their sample standard scores, or ***z*** scores, in order to give equal weight to all variables. The measure of similarity used in both tests is the Euclidean distance, or the distance between samples when they are plotted in poly-dimensional space with each of the element concentrations scaled along one direction.

TEST I: Cluster analysis was applied to the Group 2A basalts at Strand Fiord, in order to test the observation (Chapter 5) that basaltic lavas in the southern and eastern parts of the area (Bastion Ridge-Glacier Fiord Syncline) are relatively enriched in TiO_2, P_2O_5 and high-field strength elements, compared to basalts in successions further north (e.g. Twisted Ridge). 85 % of the 32 samples analysed are correctly classified in 4 clusters. As indicated by two-element variation diagrams (Fig. 5.8), basalts at Twisted Ridge show the greatest compositional diversity, and form 3 of the 4 clusters required by the analysis.

TEST II : The method was applied to compositional data for basic intrusive rocks in Groups B, C and D, in order to verify the presence of two main compositional types in the study area, namely: subalkaline igneous rocks of Early Cretaceous age on Axel Heiberg and western Ellesmere Islands, and mildly alkaline igneous rocks of lower Late Cretaceous age on northeastern Ellesmere Island. As expected from geochemical studies, values for SiO_2, TiO_2, Y, Zr and Nb best discriminate between the mildly alkaline gabbros and subalkaline igneous rocks (Fig. 7.6). The statistics require 3 clusters as a result of chemical variability within the group of subalkaline gabbros (Group B). The use of SiO_2 as a variable in this test introduces the problem of closure. However, a similar grouping is obtained using only TiO_2 and the high-field strength elements.

TABLE C-7 (continued)

TEST I: K-means clustering of Group 2A basalts at Strand Fiord, using TiO_2, P_2O_5, Y, Zr and Nb.
(* = misclassified; distances are euclidean)

SUMMARY STATISTICS FOR 4 CLUSTERS

VARIABLE	BETWEEN SS	D.F.	WITHIN SS	D.F.	F-RATIO
TiO_2	26.7	3	4.3	28	57.7
P_2O_5	26.7	3	3.3	27	73.1
Y	25.1	3	5.8	28	40.1
Zr	27.6	3	3.4	28	76.4
Nb	21.4	3	9.6	28	20.8

	GROUP #	SAMPLE #	DISTANCE	CLUSTER #
	2A-BR	AX83-011A	0.24	1
	2A-BR	AX83-011B	0.23	1
	2A-BR	AX83-013	0.32	1
	2A-BR	AX83-015	0.36	1
	2A-BR	AX83-018	0.55	1
	2A-BR	AX83-019	0.29	1
	2A-BR	AX83-020	0.47	1
	2A-BR	AX83-021	0.47	1
	2A-BR	AX83-023	0.50	1
	2A-BR	AX83-024	0.49	1
	2A-BR	AX83-025	0.17	1
	2A-BR	AX83-032A	0.44	1
	2A-BR	AX83-032B	0.48	1
	2A-GFS	AX83-033	0.37	1
	2A-GFS	AX83-043	0.34	1
*	2A-TR	AX83-060	0.50	1
*	2A-TR	AX83-068	0.43	1
*	2A-TR	AX83-070	0.28	1
	2A-GFS	AX83-106	0.43	1
	2A-GFS	AX83-113	0.34	1
*	2A-BR	AX83-017	0.56	2
*	2A-BR	AX83-028	0.51	2
	2A-TR	AX83-059	0.55	2
	2A-TR	AX83-062	0.76	2
	2A-TR	AX83-063	0.50	2
	2A-TR	AX83-064	0.31	2
	2A-TR	AX83-065	0.24	2
	2A-TR	AX83-058	0.00	3
	2A-TR	AX83-056A	0.30	4
	2A-TR	AX83-057	0.35	4
	2A-TR	AX83-066	0.15	4
	2A-TR	AX83-067	0.22	4

TABLE C-7 (continued)

TEST II: K-means clustering of Groups B, C and D using SiO_2, TiO_2, Y, Zr and Nb.

SUMMARY STATISTICS FOR 3 CLUSTERS

VARIABLE	BETWEEN SS	D.F.	WITHIN SS	D.F.	F-RATIO
SiO_2	28.9	2	15.1	42	40.2
TiO_2	34.2	2	9.7	42	73.7
Y	27.9	2	16.1	42	36.4
Zr	20.9	2	23.1	42	19.1
Nb	34.1	2	9.9	42	72.2

GROUP #	SAMPLE #	DISTANCE	CLUSTER #
D	EL84-015	0.32	1
D	EL84-023	0.40	1
D	EL84-041	0.41	1
D	EL84-044	0.55	1
D	EL84-046	0.27	1
D	EL84-050	1.26	1
D	EL84-056	0.29	1
D	EL84-060	0.31	1
D	EL84-072	0.28	1
D	EL84-073	0.40	1
D	EL84-076	0.38	1
D	EL84-098	0.56	1
D	EL84-110	0.47	1
D	EL84-210	0.55	1
C	EL84-211	0.34	1
C	EL84-218	0.52	1
C	EL84-221	0.72	1
C	EL84-222	0.70	1
C	EL84-223	0.82	1
C	EL84-229	0.35	1
C	EL84-232	0.55	1
C	EL84-235	0.97	1
C	EL84-236	0.28	1
C	EL84-245	0.60	1
C	T-S6-14	0.76	1
B	AX85-051	0.72	2
B	AX85-052	0.08	2
B	AX85-057	0.56	2
B	AX85-062	0.35	2
B	AX85-063	0.52	2
B	AX85-067	0.39	2
B	AX85-223	0.12	2
B	AX85-227	0.48	2
B	AX85-230	0.70	2
B	AX85-234	0.73	2
B	AX85-238	0.61	2

TABLE C-7 (continued)

GROUP #	SAMPLE #	DISTANCE	CLUSTER #
B	EL85-201	0.47	2
B	EL85-207	0.42	2
B	EL85-208	0.42	2
B	EL85-213	1.51	2
B	AX85-215	0.46	3
B	AX85-220	0.26	3
B	AX85-221	0.30	3
B	AX85-222	0.51	3
B	AX85-231	0.21	3

ANALYTICAL METHODS

SAMPLE PREPARATION

Samples for all rock units were broken into small fragments with a hydraulic press and a ceramic jaw crusher. 30-50 g of powder were recovered after grinding of the rock chips in a carbide tungsten container secured on a swing mill. The powders were homogenized in a twin shell dry blender. Splits were made of samples from coarse sill or dyke interiors.

WHOLE-ROCK GEOCHEMICAL ANALYSIS

SiO_2, TiO_2, Al_2O_3, Fe_2O_3 total, MnO, MgO, CaO, Na_2O and K_2O were determined using one of three methods listed in Table C-8.

- Electron microprobe analysis of glass beads mounted on epoxy (according to Mackay, 1981). MnO values are not reported because of low precision. Most of the Group 2 samples were analysed by this method. Unlike all the other data reported in this Appendix, major element analyses for these samples are shown as volatile-free. Totals were therefore not included in the tables of analyses.

- Analysis of 10 major and minor elements at the X-Ray Fluorescence Facility, St-Mary's University. Determinations were carried out on fused glass discs analysed on a Philips PW1400 sequential x-ray fluorescence spectrometer using a Rh anode x-ray tube. Loss on ignition was determined by heating the sample for $1^{1/2}$ hours at 1050 ^{o}C in an electric furnace. L.O.I values are shown in the H_2O^+ row in the tables of analyses, if separate H_2O and CO_2 determinations are not available (see Table C-8).

- Analysis of major elements by Atomic Absorption.

P_2O_5 Determinations

These were done separately for samples analysed by electron microprobe. Colorimetry, after Jeffery, 1970.

H_2O and H_2O^- Determinations

Penfield tube technique, modified after Volborth, 1969.

CO_2 Determinations

Automatic CO_2 titration method, Bouvier et al., 1972.

Trace Elements

TiO_2, Ba, Rb, Sr, Y, Zr, Nb, Th, Pb, Ga, Zn, Cu, Ni, Cr, Pb and Ga abundances were determined at St-Mary's University by x-ray fluorescence analysis of pressed powder pellets.

Rare earth elements (La, Ce, Sm, Eu, Tb, Yb and Lu), Cs, Sc, Co, Hf, Ta and more precise values of Th were obtained at the geochemical division of the Hahn-Meitner Institut, Berlin.

Chemical Procedures, Sr and Nd Isotopic Analysis

Sr and Nd isotopic analyses were performed by the author at the Laboratoire de Géochimie Isotopique, Université de Montréal. Calibrated Rb/Sr and Sm/Nd spikes were available (ROCMESS 1 and SMND 1) and used separately in the determination of Sr and Rb concentrations, or Sm and Nd concentrations and Nd isotopic analysis. Sr isotopic analyses were performed on unspiked samples. The technique is after Richard et al. (1976). Between 0.05 and 0.2 g of rock powder is dissolved in 3-8 ml of a 4:1 mixture of HF and HNO_3, in PTFE beakers covered with a teflon watchglass. Perchloric acid is then added and dried down to drive out fluorides and ensure proper homogenization for concentration runs. A first elution on a cation exchange column separates Rb, Sr and the REE's. The latter fraction is then eluted with diluted HCl on a column of HDEHP-coated teflon beads, and an Sm-free Nd fraction is obtained. Perchloric acid is added to Sr elutions for drying. The sample is then converted to nitrate form and run on a single W filament. H_2SO_4 is added to Rb samples after evaporation, and repeated evaporations with H_2O are done before loading of the sample on a single W filament. Nd and Sm elutions are evaporated and the elements run as metals on a Ta filament with an ionizing Re filament. The samples were analysed using a 12" National Bureau of Standards, 60° sector, solid source mass spectrometer equipped with a Faraday Cup detector. Nd isotopic ratios are normalised to $^{144}Nd/^{146}Nd = 0.7219$, and Sr isotopic ratios to $^{86}Sr/^{88}Sr = 0.1194$. Pure element standards used were E&A for Sr and JMC 321 for Nd. The BCR-1 standard was analysed repeatedly for Nd and Sm concentrations and Nd isotopic composition.

The data are reported in Table C-9. Ages used in the determination of eNd values (Fig. 7.3) were:
Group 1 basalts, 113 Ma
Group 2 basalts, 95 Ma
Group 3 basalts, 92 Ma

PRECISION AND ACCURACY*

WT%	W-2 (1)	W-2 (2)	W-2 (3a)	(3b)	W-2 (4)	BIR-1 (5)	BIR-1 (6)
SiO_2	52.37	53.10	52.39	0.08	52.68	48.32	48.04
TiO_2	1.38	1.07	1.05	0.01	1.06	0.90	0.96
Al_2O_3	15.69	15.57	15.17	0.06	15.45	15.93	15.56
Fe_2O_3T	12.05	10.88	10.27	0.14	10.80	11.98	11.35
MnO	-	0.17	0.16	-	0.17	-	0.17
MgO	6.26	6.42	6.49	0.17	6.37	9.52	9.72
CaO	10.91	10.94	10.97	0.06	10.86	13.06	13.34
Na_2O	2.37	2.22	2.29	0.19	2.20	1.74	1.82
K_2O	0.51	0.63	0.63	0.01	0.63	-	0.03
P_2O_5	-	0.14	0.13	0.01	0.14	-	0.02
T.V.			0.30		0.80		

PPM	W-2 (7a)	(7b)	W-2 (8)
Ba	186	6	174
Rb	18	4	21
Sr	192	6	192
Y	21	1	23
Zr	94	2	100
Nb	8	1	6.8
Ga	19	2	16.8
Zn	80	5	80
Cu	92	15	106
Ni	54	15	70
V	262	6	259
Cr	88	8	92

PPM	W-2 (9)	W-2 (10)	BCR-1 (11)	BCR-1 (12)
La	10.3	10.4	25.3	25
Ce	22	23	49	53.7
Sm	3.4	3.3	6.9	6.6
Eu	1.14	1.1	2.11	1.96
Tb	-	0.66	0.88	1.05
Yb	2.3	2.1	3.5	3.39
Lu	0.29	0.33	0.48	0.51
Hf	2.6	2.6	5.0	4.9
Ta	-	0.5	0.70	0.79
Th	2.2	2.4	5.7	6.04
Sc	38.2	36	35.2	33

* Key on following page

PRECISION AND ACCURACY (continued)

Major Elements

(1) Analysis of fused glass sample by electron microprobe

(2) Standard analysis, volatile-free

(3a), (3b) Average and standard deviation for 8 analyses (single pellet) obtained by X-Ray Fluorescence between 1985 and 1988. T.V. = Loss on Ignition

(4) Standard analysis, "as is", T.V. = (H_2O_T+CO_2)

(5) As in (1)

(6) As in (2)

Trace Elements (XRF)

(7a), (7b) Average and standard deviation for 6 analyses (single pellet) obtained between 1983 and 1987.

(8) Standard analysis

REE's and HFSE (INAA)

(9) and (11) Results from our analysis

(10) and (12) Standard analysis

ALL ANALYSES OF STANDARDS FROM GOVINDARAJU, 1984.

TABLE C-8

Key to symbols:

x = analysed for this study.

MAJORS:

1 = Fused sample, analysed by electron microprobe.
Dalhousie University, M-C. Williamson, analyst.

2 = Powder pellet, analysed by XRF.
St-Mary's University, XRF Facility, K. Cameron, analyst.

3 = Analysed by Atomic Absorption.
Dalhousie University, M. Parikh, analyst.

"WET": H_2O and CO_2 determinations available.
See "Analytical Methods".
Dalhousie University, M. Parikh, analyst.

TRACES: See "Analytical Methods".
St-Mary's University, XRF Facility, K. Cameron, analyst.

REE's: See "Analytical Methods".
Hahn-Meitner Institut, Berlin, under the supervision of Dr. Peter Dulski.

RB-SR,
SM-ND: See "Analytical Methods".
ic = isotopic composition.
id = element concentration obtained by isotopic dilution technique.
Université de Montréal, M-C. Williamson, analyst.

TABLE C-8
GEOCHEMISTRY

	MAJORS	"WET"	TRACES	REE'S	RB-SR	SM-ND
GROUP 1 - Isachsen Formation						
AX85-241	2	x	x	x		
AX85-242	2	x	x	x	id/ic	id/ic
AX85-260	2	x	x	x		
AX85-261	2	x	x	x	ic	
AX85-263	2	x	x	x		
AX85-264	2	x	x	x	id/ic	
AX85-266	2	x	x	x		
AX85-267	2	x	x	x	id/ic	id/ic
AX85-268	2	x	x	x		
EL84-256A	2	x	x	x	id/ic	id/ic
EL85-107	2	x	x			
GROUP 2A - Strand Fiord Formation, type area						
AX83-011A	1	x	x			
AX83-011B	1	x	x			
AX83-013	1	x	x			
AX83-015	1	x	x			
AX83-017	1	x	x			
AX83-018	1	x	x			
AX83-019	1	x	x			
AX83-020	1	x	x			

	MAJORS	"WET"	TRACES	REE'S	RB-SR	SM-ND
AX83-021	1	x	x			
AX83-023	1	x	x			
AX83-024	1	x	x			
AX83-025	1	x	x			
AX83-028	1	x	x			
AX83-032A	1	x	x			
AX83-032B	1	x	x			
AX83-033	2	x	x			
AX83-043	2	x	x			
AX83-106	2	x	x			
AX83-113	2	x	x			
AX83-056A	1	x	x	x	id/ic	
AX83-057	1	x	x	x		
AX83-058	1	x	x	x	ic	
AX83-059	1	x	x	x		
AX83-060	1	x	x	x	id/ic	id/ic
AX83-062	1	x	x	x		
AX83-063	1	x	x	x		
AX83-064	1	x	x	x		
AX83-065	1	x	x	x		
AX83-066B	1	x	x	x		
AX83-067	1	x	x	x		
AX83-068	1	x	x	x		
AX83-070	1	x	x	x		

	MAJORS	"WET"	TRACES	REE'S	RB-SR	SM-ND
GROUP 2B - Strand Fiord Formation, Bunde Fiord						
BND83-005	1	x	x	x		
BND83-006	1	x	x	x		
BND83-007	1	x	x	x	ic	
BND83-009	1	x	x	x		
BND83-012	1	x	x	x	id/ic	
BND83-015	1	x	x	x		
BND83-016	1	x	x	x	id/ic	id/ic
BND83-017	1	x	x	x	ic	
AX85-075	2	x	x			
AX85-078	2	x	x			
AX85-080	2	x	x			
AX85-082	2	x	x			
AX85-084	2	x	x			
AX85-086	2	x	x			
AX85-087	2	x	x			
AX85-094	2	x	x			
AX85-095	2	x	x			
AX85-096	2	x	x			
AX85-097	2	x	x			
GROUP 3 - Hassel Formation						
EL84-082	3	x	x			
EL84-087	3	x	x	x	ic	

	MAJORS	"WET"	TRACES	REE'S	RB-SR	SM-ND
EL84-007B	2	x	x			
EL84-010	2	x	x	x	id/ic	id/ic

GROUP A - LIGHTFOOT RIVER

AX85-001	2	x	x			
AX85-005	2	x	x			
AX85-008	2	x	x			
AX85-013	2	x	x			
AX85-015	2	x	x	x		
AX85-019	2	x	x	x		
AX85-020	2	x	x	x		
AX85-026	2	x	x	x		
AX85-027	2	x	x			
AX85-030	2	x	x			
AX85-031	2	x	x	x		
AX85-032	2	x	x			
AX85-033	2	x	x			
AX85-034	2	x	x			
AX85-035	2	x	x	x		
AX85-036	2	x	x	x		
AX85-037	2	x	x			

	MAJORS	"WET"	TRACES	REE'S	RB-SR	SM-ND
GROUP B - BUCHANAN LAKE, EUREKA						
AX85-051	2	x	x			
AX85-052	2	x	x			
AX85-057	2		x			
AX85-059	2	x	x			
AX85-061	2	x	x			
AX85-062	2		x		ic	
AX85-063	2	x	x			
AX85-067	2	x	x			
AX85-215	2		x			
AX85-217	2	x	x			
AX85-218	2		x			
AX85-220	2	x	x			
AX85-221	2	x	x			
AX85-222	2	x	x			
AX85-223	2		x			
AX85-224	2	x	x			
AX85-225	2	x	x			
AX85-226	2	x	x			
AX85-227	2		x			
AX85-228	2	x	x			
AX85-230	2	x	x			
AX85-231	2		x			
AX85-233	2	x	x			

	MAJORS	"WET"	TRACES	REE'S	RB-SR	SM-ND
AX85-234	2		x			
AX85-235	2	x	x			
AX85-237	2	x	x			
AX85-238	2		x			
AX85-239	2	x	x			
EL85-201	2		x			
EL85-202	2	x	x			
EL85-205	2	x	x			
EL85-207	2		x			
EL85-208	2		x			
EL85-209	2	x	x			
EL85-213	2	x	x		ic	
GROUP C						
EL84-211	3	x	x	x		
EL84-218	3	x	x	x		
EL84-221	3	x	x			
EL84-222	3	x	x			
EL84-223	3	x	x			
EL84-229	2	x	x			
EL84-232	3	x	x			
EL84-235	3	x	x	x		
EL84-236	2	x	x			
EL84-245	3	x	x			
T-S6-14	2	x	x			

	MAJORS	"WET"	TRACES	REE'S	RB-SR	SM-ND
GROUP D - TANQUARY FIORD						
EL84-015	3	x	x			
EL84-023	3	x	x	x		
EL84-041	3	x	x			
EL84-044	2	x	x			
EL84-046	3	x	x			
EL84-050	3	x	x	x	id/ic	id/ic
EL84-056	3	x	x	x		
EL84-060	3	x	x			
EL84-073	3	x	x			
EL84-076	3	x	x			
EL84-098	3	x	x			
EL84-110	3	x	x			
EL84-210	2	x	x	x		

TABLE C-9
ISOTOPIC DATA

SAMPLE #	$^{143}Nd/^{144}Nd_C$	+/-	Nd (ppm)	Sm (ppm)
AX83-060	0.512568	.000024	27.28	6.65 6.61
BND83-016	0.512482	.000021	18.91	4.87
EL84-010	0.512416	.000019	47.09	9:91
EL84-256A	0.512477	.000014	29.09	6.92
AX85-242	0.512738	.000018	49.17	11.28
AX85-267	0.512697 0.512748	.000016 .000015	36.04	8.14
EL84-050	0.512853	.000020	42.55	10.40

SAMPLE#	$^{87}Sr/^{86}Sr_C$	+/-	Rb (ppm)	Sr (ppm)
AX85-242	0.70711	.000033	19.22	406.67
AX85-261	0.70611 0.70553	.000055 .000030	b.d.l.	320
AX85-264	0.70604	.000031	10	238.62
AX85-267	0.70563	.000027	22.86	239.51
EL84-256A	0.70652	.000030	27.67	277.65
AX83-056A	0.70733	.000027	36	186.25
AX83-058	0.70799	.000029	60	229
AX83-060	0.707848	.000029	42.96	240.39
BND83-007	0.70589	.000027	22	205
BND83-012	0.70768	.000028	21.64	197.59
BND83-016	0.70913	.000024	51	238
BND83-017	0.70718	.000025	11	171

b.d.l.: Below detection limit

TABLE C-9 (CONTINUED)

SAMPLE#	$^{87}Sr/^{86}Sr_C$	+/-	Rb (ppm)	Sr (ppm)
EL84-010	0.70716	.000030	41.10	519.46
EL84-087	0.70721	.000043	38	550
AX85-215	0.70669	.000036	40	262
EL85-213	0.70480	.000028	13	195
AX85-062	0.70526	.000031	16	183
EL84-050	0.70450	.000039	21	507.54

STANDARDS

Eimer and Amend $SrCO_3$ standard

SAMPLE#	$^{87}Sr/^{86}Sr_C$	+/-	DATE OF ANALYSIS
E&A	0.707887	.000045	March 15 1985 / MCW
E&A	0.707836	.000023	June 10 1985 / MCW
E&A	0.707892	.000037	September 15 1986 / PT
E&A	0.707848	.000028	May 5 1987 / MCW

BCR-1 and JMC 321 standards

SAMPLE#	$^{143}Nd/^{144}Nd_C$	+/-	DATE OF ANALYSIS
BCR-1 spiked	0.512664	.000044	June 27 1986
BCR-1 us	0.512704	.000027	June 28 1986
BCR-1 spiked	0.512658	.000035	October 1st 1986
BCR-1 us	0.512610	.000055	October 1st 1986
JMC 321	0.511870	.000018	January 8 1986
JMC 321	0.511861	.000031	January 20 1986

Mass Spectrometry Blanks

Sr	10.3 nanograms	May 5 1987
Nd	384 picograms	May 6 1987

CHEMICAL ANALYSES - GROUPS 1A AND 1C

	AX85-241	AX85-242	EL84-256A	EL85-107
SiO2	50.47	51.68	46.57	47.00
TiO2	3.30	3.31	3.00	3.24
Al2O3	13.14	13.02	12.33	12.57
Fe2O3(T)	13.27	12.99	15.97	13.59
MnO	0.19	0.20	0.25	0.20
MgO	4.02	4.24	4.22	4.78
CaO	8.36	8.38	9.28	10.24
Na2O	3.01	3.04	2.35	2.71
K2O	0.68	0.83	0.77	0.70
P2O5	0.64	0.63	0.32	0.34
H2O+	1.69	1.31	1.04	5.60
H2O-	0.89	0.72	0.69	0.00
CO2	2.54	0.47	5.67	0.00
TOTAL	102.20	100.82	102.46	100.97
Rb	14	15	22	15
Cs	6.20	11.00	1.00	0.00
Sr	351	416	279	307
Ba	1009	1208	384	312
Sc	36.5	36.1	35.2	0.0
V	327	317	441	430
Cr	32	33	37	21
Co	49.0	69.6	55.2	0.0
Ni	29	32	25	29
Cu	25	31	44	58
Zn	188	138	128	126
Ga	22	24	24	22
Y	50	53	39	42
Zr	283	289	195	206
Hf	7.30	6.80	5.50	0.00
Nb	31	31	20	23
Ta	2.50	2.90	1.70	0.00
Pb	11	11	5	0
Th	5	4	4	0
U	0.00	0.00	0.00	0.00
La	36.60	36.80	23.40	0.00
Ce	80.80	75.50	56.00	0.00
Nd	0.00	0.00	37.00	0.00
Sm	12.40	12.10	7.80	0.00
Eu	3.80	3.56	2.26	0.00
Tb	1.70	1.80	1.60	0.00
Yb	4.80	5.30	3.90	0.00
Lu	0.69	0.66	0.57	0.00
SUMREE	140.8	135.7	95.5	0.0

CHEMICAL ANALYSES - GROUP 1B

	AX85-260	AX85-261	AX85-263	AX85-264	AX85-266	AX85-267
SiO2	49.56	49.75	49.88	51.24	49.76	50.99
TiO2	2.33	2.26	2.32	2.17	2.05	2.66
Al2O3	14.22	14.30	14.33	13.51	13.16	12.96
Fe2O3(T)	12.52	12.06	11.93	12.63	14.24	14.31
MnO	0.20	0.18	0.17	0.20	0.22	0.21
MgO	5.80	5.81	5.87	5.69	4.89	4.57
CaO	10.88	11.00	10.76	10.09	9.94	8.77
Na2O	2.28	2.34	2.30	2.28	2.32	2.59
K2O	0.33	0.23	0.24	0.34	0.74	0.68
P2O5	0.21	0.22	0.21	0.22	0.22	0.29
H2O+	2.27	1.18	1.16	0.69	0.37	1.47
H2O-	0.19	1.40	1.27	1.16	0.46	0.94
CO2	0.58	0.39	0.00	0.35	3.25	0.00
TOTAL	101.37	101.12	100.44	100.57	101.62	100.44
Rb	7	0	3	10	19	19
Cs	0.00	0.00	0.00	0.00	0.00	0.00
Sr	311	320	326	229	201	243
Ba	263	223	252	188	190	276
Sc	36.6	37.3	37.3	44.2	41.9	43.4
V	324	327	329	376	345	495
Cr	85	89	87	56	66	17
Co	61.5	62.4	64.1	70.0	66.7	72.5
Ni	46	47	40	38	40	25
Cu	105	106	106	133	125	147
Zn	98	95	99	114	106	119
Ga	19	22	22	20	18	17
Y	33	33	29	40	38	49
Zr	161	161	159	190	183	253
Hf	3.90	4.10	4.10	4.90	4.90	6.30
Nb	12	12	14	13	12	33
Ta	0.00	1.40	1.20	1.70	1.60	3.50
Pb	2	3	8	9	8	8
Th	0	0	0	1	0	3
U	0.00	0.00	0.00	0.00	0.00	0.00
La	13.10	12.70	12.70	15.50	15.60	31.30
Ce	30.30	30.00	28.50	34.70	33.40	63.30
Nd	0.00	0.00	0.00	0.00	0.00	0.00
Sm	6.00	6.20	6.10	7.00	6.90	8.60
Eu	2.07	2.02	2.14	2.29	2.14	2.56
Tb	1.10	0.95	1.20	1.20	1.40	1.50
Yb	3.00	3.20	3.20	4.20	3.90	5.70
Lu	0.35	0.38	0.37	0.56	0.56	0.72
SUMREE	55.9	55.5	54.2	65.5	63.9	113.7

CHEMICAL ANALYSES - GROUP 1B

	AX85-268
SiO2	50.83
TiO2	2.32
Al2O3	13.11
Fe2O3(T)	14.31
MnO	0.20
MgO	4.86
CaO	9.77
Na2O	2.41
K2O	0.36
P2O5	0.23
H2O+	1.35
H2O-	0.93
CO2	0.19
TOTAL	100.87
Rb	12
Cs	0.60
Sr	196
Ba	142
Sc	47.1
V	416
Cr	33
Co	72.2
Ni	33
Cu	156
Zn	107
Ga	20
Y	42
Zr	169
Hf	4.30
Nb	13
Ta	1.20
Pb	6
Th	0
U	0.00
La	13.70
Ce	32.00
Nd	0.00
Sm	6.60
Eu	2.14
Tb	1.20
Yb	4.20
Lu	0.53
SUMREE	60.4

CHEMICAL ANALYSES - GROUP 2A

	AX83-011A	AX83-011B	AX83-013	AX83-015	AX83-017	AX83-018
SiO2	51.29	52.63	51.73	52.28	49.67	50.27
TiO2	2.06	2.05	2.01	1.99	2.90	2.07
Al2O3	14.18	14.31	14.16	14.21	12.98	14.69
Fe2O3(T)	14.20	14.30	13.99	13.93	18.27	14.86
MnO	0.00	0.00	0.00	0.00	0.00	0.33
MgO	5.11	5.22	5.28	5.19	4.37	5.34
CaO	10.21	10.88	10.61	10.47	8.84	8.39
Na2O	2.97	2.62	3.04	3.04	3.18	4.20
K2O	0.44	0.40	0.55	0.48	0.52	1.13
P2O5	0.25	0.25	0.24	0.25	0.29	0.26
H2O+	0.75	1.22	1.24	1.11	0.91	1.57
H2O-	0.89	1.18	1.17	0.79	1.20	0.43
CO2	0.00	0.00	0.00	0.04	0.00	0.00
TOTAL	102.35	105.06	104.02	103.78	103.13	103.54
Rb	39	23	18	31	10	26
Cs	0.00	0.00	0.00	0.00	0.00	0.00
Sr	234	262	254	259	239	355
Ba	212	214	240	237	162	456
Sc	0.0	0.0	0.0	0.0	0.0	0.0
V	334	326	316	326	472	367
Cr	33	29	25	27	0	30
Co	0.0	0.0	0.0	0.0	0.0	0.0
Ni	46	44	43	42	23	42
Cu	57	63	68	68	64	71
Zn	119	117	112	114	142	119
Ga	23	23	21	22	26	20
Y	39	39	40	40	45	41
Zr	189	187	189	192	197	197
Hf	0.00	0.00	0.00	0.00	0.00	0.00
Nb	18	18	18	18	18	19
Ta	0.00	0.00	0.00	0.00	0.00	0.00
Pb	10	10	11	8	10	10
Th	3	3	6	5	6	7
U	0.00	0.00	0.00	0.00	0.00	0.00
La	0.00	0.00	0.00	0.00	0.00	0.00
Ce	0.00	0.00	0.00	0.00	0.00	0.00
Nd	0.00	0.00	0.00	0.00	0.00	0.00
Sm	0.00	0.00	0.00	0.00	0.00	0.00
Eu	0.00	0.00	0.00	0.00	0.00	0.00
Tb	0.00	0.00	0.00	0.00	0.00	0.00
Yb	0.00	0.00	0.00	0.00	0.00	0.00
Lu	0.00	0.00	0.00	0.00	0.00	0.00
SUMREE	0.0	0.0	0.0	0.0	0.0	0.0

CHEMICAL ANALYSES - GROUP 2A

	AX83-019	AX83-020	AX83-021	AX83-023	AX83-024	AX83-025
SiO2	51.53	51.56	50.64	51.26	51.43	51.68
TiO2	1.96	2.07	2.46	1.97	1.99	2.03
Al2O3	14.13	14.21	13.96	14.04	14.00	14.09
Fe2O3(T)	13.96	13.92	14.93	13.57	13.59	14.13
MnO	0.00	0.00	0.00	0.00	0.00	0.00
MgO	5.00	5.37	5.14	5.33	5.37	5.29
CaO	10.40	10.55	9.90	10.46	10.48	10.36
Na2O	2.94	2.78	3.04	2.89	2.91	3.07
K2O	0.85	0.65	0.88	0.54	0.51	0.51
P2O5	0.24	0.23	0.25	0.23	0.23	0.24
H2O+	0.70	0.90	0.62	1.04	0.80	0.83
H2O-	0.78	1.00	0.71	0.70	0.70	0.73
CO2	0.00	0.00	0.00	0.00	0.00	0.00
TOTAL	102.49	103.24	102.53	102.03	102.01	102.96
Rb	18	12	32	27	27	21
Cs	0.00	0.00	0.00	0.00	0.00	0.00
Sr	252	246	233	243	243	247
Ba	237	207	218	198	206	235
Sc	0.0	0.0	0.0	0.0	0.0	0.0
V	323	318	336	331	316	333
Cr	26	56	55	58	52	53
Co	0.0	0.0	0.0	0.0	0.0	0.0
Ni	44	51	48	48	41	44
Cu	62	85	110	81	86	88
Zn	111	114	117	114	111	112
Ga	24	20	23	20	23	22
Y	39	37	39	38	37	38
Zr	191	176	183	174	175	182
Hf	0.00	0.00	0.00	0.00	0.00	0.00
Nb	18	14	15	14	14	16
Ta	0.00	0.00	0.00	0.00	0.00	0.00
Pb	12	8	12	11	10	8
Th	5	3	5	4	2	3
U	0.00	0.00	0.00	0.00	0.00	0.00
La	0.00	0.00	0.00	0.00	0.00	0.00
Ce	0.00	0.00	0.00	0.00	0.00	0.00
Nd	0.00	0.00	0.00	0.00	0.00	0.00
Sm	0.00	0.00	0.00	0.00	0.00	0.00
Eu	0.00	0.00	0.00	0.00	0.00	0.00
Tb	0.00	0.00	0.00	0.00	0.00	0.00
Yb	0.00	0.00	0.00	0.00	0.00	0.00
Lu	0.00	0.00	0.00	0.00	0.00	0.00
SUMREE	0.0	0.0	0.0	0.0	0.0	0.0

CHEMICAL ANALYSES - GROUP 2A

	AX83-028	AX83-032A	AX83-032B	AX83-033	AX83-043	AX83-056A
SiO2	50.04	51.23	51.40	50.08	50.49	51.92
TiO2	2.77	2.04	2.10	2.09	2.05	2.06
Al2O3	13.15	14.17	14.72	13.46	13.62	14.06
Fe2O3(T)	16.96	13.88	11.52	12.68	12.40	14.73
MnO	0.00	0.00	0.00	0.19	0.17	0.00
MgO	4.44	5.69	4.88	5.32	4.84	5.08
CaO	8.85	10.22	10.66	10.23	10.17	9.51
Na2O	3.44	3.04	3.12	2.80	2.97	2.89
K2O	0.42	0.81	0.87	0.35	0.85	0.92
P2O5	0.32	0.23	0.23	0.23	0.24	0.21
H2O+	1.04	0.84	0.89	1.18	0.79	1.02
H2O-	0.73	0.60	1.11	1.12	0.89	1.59
CO2	0.00	0.07	0.00	0.00	0.00	0.00
TOTAL	102.16	102.82	101.50	99.73	99.48	103.99
Rb	15	31	30	8	20	36
Cs	0.00	0.00	0.00	0.00	0.00	0.00
Sr	248	229	244	293	244	194
Ba	212	207	212	277	265	184
Sc	0.0	0.0	0.0	0.0	0.0	42.8
V	383	330	335	328	311	322
Cr	27	64	61	12	34	31
Co	0.0	0.0	0.0	0.0	0.0	79.8
Ni	23	49	51	39	43	32
Cu	29	90	83	55	52	101
Zn	141	117	116	118	113	115
Ga	25	20	23	24	24	20
Y	47	36	37	35	38	36
Zr	208	171	175	175	192	149
Hf	0.00	0.00	0.00	0.00	0.00	4.50
Nb	19	15	14	18	19	13
Ta	0.00	0.00	0.00	0.00	0.00	1.60
Pb	16	13	9	11	8	8
Th	7	4	3	3	1	2
U	0.00	0.00	0.00	0.00	0.00	0.00
La	0.00	0.00	0.00	0.00	0.00	16.40
Ce	0.00	0.00	0.00	0.00	0.00	38.00
Nd	0.00	0.00	0.00	0.00	0.00	0.00
Sm	0.00	0.00	0.00	0.00	0.00	6.10
Eu	0.00	0.00	0.00	0.00	0.00	1.77
Tb	0.00	0.00	0.00	0.00	0.00	1.10
Yb	0.00	0.00	0.00	0.00	0.00	3.60
Lu	0.00	0.00	0.00	0.00	0.00	0.53
SUMREE	0.0	0.0	0.0	0.0	0.0	67.5

CHEMICAL ANALYSES - GROUP 2A

	AX83-057	AX83-058	AX83-059	AX83-060	AX83-062	AX83-063
SiO2	51.26	52.08	49.45	52.33	50.10	48.87
TiO2	1.93	3.39	2.99	2.31	2.62	3.38
Al2O3	13.99	13.61	12.93	14.09	13.40	12.76
Fe2O3(T)	13.68	15.51	16.43	14.83	15.11	17.61
MnO	0.00	0.00	0.00	0.00	0.00	0.00
MgO	5.06	4.02	4.30	4.58	4.35	3.88
CaO	9.10	8.61	8.87	8.69	8.65	8.30
Na2O	3.32	3.61	3.18	3.47	3.35	3.72
K2O	0.89	1.04	0.76	0.69	0.58	0.40
P2O5	0.20	0.42	0.35	0.28	0.27	0.32
H2O+	0.80	1.33	0.97	1.20	1.44	1.05
H2O-	0.89	0.89	0.66	0.77	0.88	0.48
CO2	0.10	0.00	0.05	0.00	0.00	0.23
TOTAL	101.22	104.51	100.94	103.24	100.75	101.00
Rb	34	60	30	43	29	27
Cs	0.00	1.00	1.00	0.00	1.00	2.00
Sr	227	229	248	240	244	232
Ba	213	365	271	265	240	206
Sc	39.3	32.8	34.5	31.9	31.7	33.6
V	305	306	368	329	357	382
Cr	15	26	25	36	34	20
Co	80.8	70.8	68.5	69.4	70.2	71.3
Ni	30	37	33	27	29	28
Cu	87	130	114	50	47	33
Zn	108	135	145	114	132	157
Ga	20	25	22	24	21	26
Y	33	51	43	38	39	45
Zr	151	272	219	190	194	216
Hf	4.10	7.10	5.60	4.90	4.90	6.20
Nb	16	27	23	19	21	22
Ta	1.70	3.20	2.30	1.50	2.50	2.60
Pb	6	13	12	6	7	9
Th	1	7	8	3	3	2
U	0.00	0.00	0.00	0.00	0.00	0.00
La	17.30	30.40	22.30	21.10	19.80	21.70
Ce	40.00	66.00	48.00	48.00	42.00	48.00
Nd	0.00	40.00	0.00	25.00	0.00	0.00
Sm	5.70	9.30	7.60	6.30	6.60	8.10
Eu	1.68	2.33	2.19	1.92	2.01	2.46
Tb	1.00	1.30	1.60	1.30	0.95	1.50
Yb	3.30	4.50	3.60	3.50	3.80	4.30
Lu	0.48	0.66	0.54	0.51	0.51	0.66
SUMREE	69.5	114.5	85.8	82.6	75.7	86.7

CHEMICAL ANALYSES - GROUP 2A

	AX83-064	AX83-065	AX83-066B	AX83-067	AX83-068	AX83-070
SiO2	49.15	49.89	47.68	47.82	49.37	49.52
TiO2	3.13	3.07	2.24	2.23	2.35	2.19
Al2O3	12.89	13.10	14.51	13.97	13.92	13.79
Fe2O3(T)	17.33	17.20	13.90	13.64	14.44	14.27
MnO	0.00	0.00	0.00	0.00	0.00	0.00
MgO	3.97	3.96	5.33	5.08	4.69	4.91
CaO	8.33	8.49	9.67	9.91	9.73	9.53
Na2O	3.42	3.52	3.32	2.68	3.20	2.95
K2O	0.37	0.35	0.66	0.56	0.43	0.65
P2O5	0.32	0.30	0.20	0.00	0.24	0.23
H2O+	1.51	1.40	1.26	2.65	1.54	1.17
H2O-	0.71	0.53	0.84	1.50	1.28	1.17
CO2	0.00	0.00	0.06	0.13	0.03	0.00
TOTAL	101.13	101.81	99.67	100.17	101.22	100.38
Rb	26	30	23	21	18	21
Cs	1.00	1.00	0.00	0.00	1.00	1.00
Sr	239	243	237	242	253	248
Ba	201	258	180	167	212	230
Sc	33.0	31.1	36.9	0.0	33.5	33.9
V	379	420	308	308	315	308
Cr	22	17	49	20	20	21
Co	84.3	110.0	57.2	57.1	62.5	73.0
Ni	22	18	41	33	33	33
Cu	23	48	57	63	63	66
Zn	142	145	83	123	123	103
Ga	30	26	26	24	24	22
Y	45	42	34	34	37	36
Zr	213	212	157	159	184	181
Hf	6.20	5.80	4.40	4.30	5.10	5.00
Nb	22	21	14	14	19	18
Ta	2.80	4.10	1.20	1.50	1.80	1.90
Pb	9	6	8	9	9	14
Th	1	1	3	3	3	5
U	0.00	0.00	0.00	0.00	0.00	0.00
La	21.60	20.60	15.40	14.60	19.30	19.10
Ce	48.00	44.00	34.00	32.00	41.00	40.00
Nd	0.00	0.00	0.00	25.00	25.00	0.00
Sm	8.00	7.10	6.00	5.70	6.40	6.50
Eu	2.43	2.19	1.95	1.73	1.90	1.90
Tb	1.60	1.20	0.82	1.10	1.10	1.60
Yb	4.50	4.10	3.60	3.00	3.70	3.30
Lu	0.67	0.53	0.47	0.47	0.50	0.52
SUMREE	86.8	79.7	62.2	58.6	73.9	72.9

CHEMICAL ANALYSES - GROUP 2A

	AX83-106	AX83-113
SiO2	50.12	49.94
TiO2	2.12	2.11
Al2O3	13.58	13.61
Fe2O3(T)	12.99	11.69
MnO	0.19	0.20
MgO	5.54	4.88
CaO	10.04	11.31
Na2O	2.75	2.71
K2O	0.92	0.87
P2O5	0.23	0.25
H2O+	0.66	0.74
H2O-	0.79	0.45
CO2	0.00	1.45
TOTAL	99.93	100.21
Rb	32	20
Cs	0.00	0.00
Sr	232	249
Ba	169	249
Sc	0.0	0.0
V	336	309
Cr	15	21
Co	0.0	0.0
Ni	43	30
Cu	58	54
Zn	113	114
Ga	24	22
Y	35	37
Zr	169	186
Hf	0.00	0.00
Nb	17	19
Ta	0.00	0.00
Pb	7	6
Th	4	2
U	0.00	0.00
La	0.00	0.00
Ce	0.00	0.00
Nd	0.00	0.00
Sm	0.00	0.00
Eu	0.00	0.00
Tb	0.00	0.00
Yb	0.00	0.00
Lu	0.00	0.00
SUMREE	0.0	0.0

CHEMICAL ANALYSES - GROUP 2B

	AX85-075	AX85-078	AX85-080	AX85-082	AX85-084	AX85-086
SiO2	48.90	51.23	51.01	50.09	52.61	50.86
TiO2	2.83	2.27	2.46	2.30	1.79	1.62
Al2O3	12.33	13.34	12.78	13.08	13.62	15.00
Fe2O3(T)	15.60	13.53	13.99	14.00	12.21	10.98
MnO	0.30	0.23	0.19	0.19	0.20	0.16
MgO	5.32	4.83	4.69	4.57	4.77	5.36
CaO	9.69	8.92	9.16	9.55	8.47	10.22
Na2O	2.35	2.39	2.44	2.49	2.79	2.44
K2O	0.49	1.03	0.56	0.46	0.94	1.00
P2O5	0.30	0.25	0.27	0.28	0.20	0.18
H2O+	0.50	0.58	1.48	1.79	1.18	0.76
H2O-	0.63	1.10	0.73	1.29	1.10	1.05
CO2	0.00	0.00	0.00	0.00	0.03	0.00
TOTAL	99.24	99.70	99.76	100.09	99.91	99.63
Rb	11	38	14	11	32	34
Cs	0.00	0.00	0.00	0.00	0.00	0.00
Sr	186	193	183	220	214	213
Ba	177	186	202	204	230	162
Sc	0.0	0.0	0.0	0.0	0.0	0.0
V	413	342	370	305	297	264
Cr	37	25	37	38	10	60
Co	0.0	0.0	0.0	0.0	0.0	0.0
Ni	39	25	27	31	24	32
Cu	277	80	170	167	108	87
Zn	138	106	108	103	90	93
Ga	24	22	19	22	21	21
Y	48	41	42	42	37	33
Zr	201	181	185	189	163	133
Hf	0.00	0.00	0.00	0.00	0.00	0.00
Nb	18	18	15	16	14	13
Ta	0.00	0.00	0.00	0.00	0.00	0.00
Pb	3	5	8	1	9	1
Th	0	7	4	0	7	0
U	0.00	0.00	0.00	0.00	0.00	0.00
La	0.00	0.00	0.00	0.00	0.00	0.00
Ce	0.00	0.00	0.00	0.00	0.00	0.00
Nd	0.00	0.00	0.00	0.00	0.00	0.00
Sm	0.00	0.00	0.00	0.00	0.00	0.00
Eu	0.00	0.00	0.00	0.00	0.00	0.00
Tb	0.00	0.00	0.00	0.00	0.00	0.00
Yb	0.00	0.00	0.00	0.00	0.00	0.00
Lu	0.00	0.00	0.00	0.00	0.00	0.00
SUMREE	0.0	0.0	0.0	0.0	0.0	0.0

CHEMICAL ANALYSES - GROUP 2B

	AX85-087	AX85-094	AX85-095	AX85-096	AX85-097	BND83-005
SiO2	50.13	50.75	49.82	51.15	52.37	48.49
TiO2	2.26	1.95	1.32	1.69	2.28	2.73
Al2O3	13.74	14.26	14.32	13.77	13.22	13.23
Fe2O3(T)	13.31	12.41	10.72	12.00	13.52	14.40
MnO	0.19	0.21	0.16	0.16	0.20	0.18
MgO	5.02	5.21	7.04	5.40	4.10	5.48
CaO	9.27	9.82	11.20	9.38	7.44	9.74
Na2O	2.46	2.72	2.14	2.78	2.87	2.60
K2O	1.02	0.97	0.45	1.16	1.83	0.60
P2O5	0.25	0.23	0.15	0.20	0.29	0.24
H2O+	0.94	0.56	0.88	0.95	0.66	1.19
H2O-	0.99	0.77	1.54	1.21	0.92	1.02
CO2	0.06	0.00	0.00	0.06	0.05	0.00
TOTAL	99.64	99.86	99.74	99.91	99.75	99.90
Rb	37	32	2	46	77	15
Cs	0.00	0.00	0.00	0.00	0.00	0.00
Sr	214	218	223	236	220	185
Ba	195	177	133	208	290	131
Sc	0.0	0.0	0.0	0.0	0.0	49.1
V	321	274	234	283	338	412
Cr	37	41	162	7	2	72
Co	0.0	0.0	0.0	0.0	0.0	69.1
Ni	30	24	50	29	25	60
Cu	85	150	69	72	73	213
Zn	102	99	78	91	109	126
Ga	22	24	23	21	24	20
Y	41	37	27	31	45	43
Zr	169	156	107	144	212	170
Hf	0.00	0.00	0.00	0.00	0.00	4.40
Nb	14	13	10	14	21	17
Ta	0.00	0.00	0.00	0.00	0.00	1.70
Pb	8	3	5	10	7	11
Th	6	0	0	6	3	3
U	0.00	0.00	0.00	0.00	0.00	0.00
La	0.00	0.00	0.00	0.00	0.00	13.00
Ce	0.00	0.00	0.00	0.00	0.00	30.00
Nd	0.00	0.00	0.00	0.00	0.00	0.00
Sm	0.00	0.00	0.00	0.00	0.00	6.10
Eu	0.00	0.00	0.00	0.00	0.00	1.86
Tb	0.00	0.00	0.00	0.00	0.00	1.00
Yb	0.00	0.00	0.00	0.00	0.00	3.80
Lu	0.00	0.00	0.00	0.00	0.00	0.55
SUMREE	0.0	0.0	0.0	0.0	0.0	56.3

CHEMICAL ANALYSES - GROUP 2B

	BND83-006	BND83-007	BND83-009	BND83-012	BND83-015	BND83-016
SiO2	48.17	51.51	49.13	52.15	51.22	52.18
TiO2	2.50	3.67	2.33	2.39	2.06	1.53
Al2O3	13.16	12.89	14.53	13.56	14.43	14.62
Fe2O3(T)	15.23	15.69	13.67	14.79	13.30	12.39
MnO	0.14	0.00	0.00	0.14	0.00	0.00
MgO	5.67	4.01	4.80	4.18	5.45	5.63
CaO	10.18	8.24	10.08	8.11	9.81	10.39
Na2O	2.67	3.02	3.05	3.01	2.65	2.53
K2O	0.38	0.94	0.74	1.56	0.72	0.37
P2O5	0.23	0.41	0.21	0.29	0.21	0.00
H2O+	1.14	0.63	1.21	0.68	0.44	1.04
H2O-	1.21	0.63	1.19	0.95	0.80	1.13
CO2	0.10	0.00	0.02	0.00	0.00	0.00
TOTAL	100.78	101.64	100.96	101.81	101.09	101.81
Rb	7	22	27	23	20	51
Cs	0.00	0.00	1.00	1.00	0.00	1.00
Sr	187	205	246	214	215	238
Ba	131	241	171	157	181	290
Sc	47.5	39.1	37.7	33.0	41.5	41.0
V	410	509	330	295	347	348
Cr	75	25	49	52	87	11
Co	64.2	69.9	61.8	67.5	56.3	74.8
Ni	58	43	48	51	42	24
Cu	213	135	65	101	115	48
Zn	120	153	105	88	106	114
Ga	23	22	23	19	21	21
Y	43	60	36	32	38	42
Zr	164	275	164	127	158	204
Hf	4.20	7.50	4.40	5.80	4.20	3.50
Nb	15	25	13	10	14	19
Ta	1.40	1.90	1.10	2.10	1.40	1.40
Pb	4	11	10	6	14	11
Th	1	5	2	7	8	6
U	0.00	0.00	0.00	0.00	0.00	0.00
La	11.90	22.60	15.30	23.80	14.60	13.70
Ce	31.00	55.00	36.00	50.00	32.00	29.00
Nd	0.00	0.00	23.00	0.00	0.00	0.00
Sm	5.50	8.60	5.80	7.60	5.50	5.10
Eu	1.69	2.57	1.79	2.05	1.66	1.44
Tb	1.20	1.90	0.98	1.40	0.00	1.00
Yb	3.70	5.00	3.50	3.30	3.70	2.90
Lu	0.57	0.81	0.55	0.56	0.48	0.39
SUMREE	55.6	96.5	63.9	88.7	57.9	53.5

CHEMICAL ANALYSES - GROUP 2B

	BND83-017
SiO2	50.10
TiO2	1.66
Al2O3	13.62
Fe2O3(T)	18.16
MnO	0.00
MgO	5.33
CaO	10.95
Na2O	2.21
K2O	0.35
P2O5	0.19
H2O+	0.57
H2O-	0.88
CO2	1.99
TOTAL	106.01
Rb	11
Cs	0.00
Sr	171
Ba	148
Sc	44.0
V	405
Cr	60
Co	64.2
Ni	55
Cu	199
Zn	108
Ga	22
Y	39
Zr	129
Hf	3.30
Nb	9
Ta	1.00
Pb	17
Th	6
U	0.00
La	11.40
Ce	25.00
Nd	0.00
Sm	4.40
Eu	1.40
Tb	0.00
Yb	3.80
Lu	0.53
SUMREE	46.5

CHEMICAL ANALYSES - GROUP 3

	EL84-007B	EL84-010	EL84-082	EL84-087
SiO2	49.65	50.11	50.15	47.15
TiO2	3.49	3.37	3.20	3.22
Al2O3	12.41	12.52	12.90	12.87
Fe2O3(T)	15.16	15.14	16.22	16.10
MnO	0.26	0.26	0.29	0.29
MgO	3.75	3.88	3.93	3.76
CaO	7.48	7.79	7.80	7.92
Na2O	2.54	2.68	2.92	2.90
K2O	1.65	1.59	1.38	1.41
P2O5	1.21	1.15	1.10	1.11
H2O+	1.35	0.80	0.65	0.80
H2O-	0.60	0.00	0.54	0.58
CO2	0.07	0.00	0.00	1.05
TOTAL	99.62	99.29	101.08	99.16
Rb	41	37	38	38
Cs	0.00	0.00	0.00	0.00
Sr	554	513	540	550
Ba	1139	1060	1125	1167
Sc	0.0	26.7	0.0	28.3
V	164	185	172	172
Cr	0	0	3	3
Co	0.0	54.3	0.0	62.0
Ni	14	14	8	8
Cu	21	18	23	20
Zn	141	135	141	142
Ga	29	21	25	25
Y	36	32	34	34
Zr	188	180	176	175
Hf	0.00	4.50	0.00	4.60
Nb	26	26	26	26
Ta	0.00	2.50	0.00	3.20
Pb	3	9	8	9
Th	0	5	0	5
U	0.00	0.00	0.00	0.00
La	0.00	31.30	0.00	33.30
Ce	0.00	74.00	0.00	72.00
Nd	0.00	44.00	0.00	48.00
Sm	0.00	9.90	0.00	11.00
Eu	0.00	5.32	0.00	5.65
Tb	0.00	0.00	0.00	1.70
Yb	0.00	1.30	0.00	2.50
Lu	0.00	2.30	0.00	0.38
SUMREE	0.0	124.1	0.0	126.5

CIPW NORMS, "DRY": EXTRUSIVE ROCKS

	AX83-011A	AX83-011B	AX83-013	AX83-015	AX83-017	AX83-018
Q	1.91	4.08	1.01	2.11	0.54	0.00
Or	2.60	2.36	3.25	2.84	3.07	6.68
Ab	25.13	22.17	25.72	25.72	26.91	33.06
An	24.06	26.11	23.37	23.71	19.61	17.89
Ne	0.00	0.00	0.00	0.00	0.00	1.34
Di	20.79	21.84	23.04	22.13	18.86	18.37
Hy	17.77	17.61	17.01	17.11	20.76	0.00
Ol	0.00	0.00	0.00	0.00	0.00	15.42
Mt	2.83	2.84	2.78	2.77	3.64	2.96
Il	3.91	3.89	3.82	3.78	5.51	3.93
Ap	0.58	0.58	0.56	0.58	0.67	0.60

	AX83-019	AX83-020	AX83-021	AX83-023	AX83-024	AX83-025
Q	0.97	1.83	0.00	1.73	1.85	1.24
Or	5.02	3.84	5.20	3.19	3.01	3.01
Ab	24.88	23.52	25.72	24.46	24.62	25.98
An	22.85	24.38	21.85	23.74	23.63	23.16
Ne	0.00	0.00	0.00	0.00	0.00	0.00
Di	22.65	21.98	21.36	22.13	22.29	22.18
Hy	16.54	17.43	17.15	16.97	16.98	17.45
Ol	0.00	0.00	0.46	0.00	0.00	0.00
Mt	2.77	2.77	2.97	2.70	2.70	2.81
Il	3.72	3.93	4.67	3.74	3.78	3.86
Ap	0.56	0.53	0.58	0.53	0.53	0.56

	AX83-028	AX83-032A	AX83-032B	AX83-033	AX83-043	AX83-056A
Q	0.49	0.00	1.10	2.77	1.62	1.87
Or	2.48	4.79	5.14	2.13	5.08	5.44
Ab	29.11	25.72	26.40	24.29	25.56	24.46
An	19.20	22.63	23.59	23.63	21.70	22.68
Ne	0.00	0.00	0.00	0.00	0.00	0.00
Di	19.02	22.03	22.97	22.15	23.27	19.30
Hy	19.34	16.73	12.54	16.43	14.12	19.15
Ol	0.00	1.17	0.00	0.00	0.00	0.00
Mt	3.36	2.75	2.29	2.58	2.51	2.93
Il	5.26	3.87	3.99	4.06	3.95	3.91
Ap	0.74	0.53	0.53	0.56	0.56	0.49

CIPW NORMS, "DRY": EXTRUSIVE ROCKS

	AX83-057	AX83-058	AX83-059	AX83-060	AX83-062	AX83-063
Q	0.29	1.81	0.94	2.01	1.68	0.00
Or	5.38	6.15	4.55	4.08	3.49	2.42
Ab	28.60	30.55	27.33	29.36	29.02	32.07
An	21.02	17.86	19.11	20.83	20.30	17.22
Ne	0.00	0.00	0.00	0.00	0.00	0.00
Di	19.69	18.55	19.57	17.11	18.29	19.04
Hy	18.16	15.65	18.20	18.75	17.88	17.14
Ol	0.00	0.00	0.00	0.00	0.00	0.80
Mt	2.75	3.09	3.32	2.94	3.07	3.55
Il	3.74	6.44	5.79	4.39	5.09	6.53
Ap	0.46	0.97	0.83	0.65	0.65	0.76

CIPW NORMS, "DRY": EXTRUSIVE ROCKS

	AX83-064	AX83-065	AX83-066	AX83-067	AX83-068	AX83-070
Q	1.37	1.44	0.00	0.08	0.29	0.89
Or	2.25	2.13	4.02	3.49	2.60	3.90
Ab	29.62	30.38	28.69	23.69	27.84	25.56
An	19.13	19.25	23.24	25.50	23.01	23.02
Ne	0.00	0.00	0.00	0.00	0.00	0.00
Di	17.70	18.26	20.30	21.48	20.89	19.87
Hy	19.21	18.71	3.74	17.53	17.28	18.26
Ol	0.00	0.00	10.88	0.00	0.00	0.00
Mt	3.51	3.47	2.81	2.84	2.96	2.91
Il	6.08	5.94	4.35	4.43	4.60	4.25
Ap	0.76	0.72	0.49	0.00	0.58	0.56

	AX83-106	AX83-113	AX85-075	AX85-078	AX85-080	AX85-082
Q	0.85	1.46	3.35	5.60	6.95	5.56
Or	5.50	5.26	2.95	6.21	3.37	2.78
Ab	23.61	23.52	20.14	20.56	21.07	21.75
An	22.33	23.01	21.87	23.02	22.80	23.89
Ne	0.00	0.00	0.00	0.00	0.00	0.00
Di	22.12	27.22	20.66	16.94	18.22	19.28
Hy	17.15	11.56	19.63	18.47	17.81	17.50
Ol	0.00	0.00	0.00	0.00	0.00	0.00
Mt	2.62	2.38	3.13	2.73	2.84	2.87
Il	4.08	4.12	5.43	4.39	4.79	4.50
Ap	0.53	0.60	0.70	0.58	0.65	0.67

CIPW NORMS, "DRY": EXTRUSIVE ROCKS

	AX85-084	AX85-086	AX85-087	AX85-094	AX85-095	AX85-096
Q	6.16	2.89	3.45	1.99	1.81	2.05
Or	5.67	6.03	6.15	5.79	2.72	7.03
Ab	24.20	20.99	21.24	23.36	18.53	24.03
An	22.36	27.55	23.92	24.15	28.84	22.16
Ne	0.00	0.00	0.00	0.00	0.00	0.00
Di	16.07	18.90	17.71	19.65	22.14	19.94
Hy	17.91	16.53	18.32	17.04	19.59	17.43
Ol	0.00	0.00	0.00	0.00	0.00	0.00
Mt	2.48	2.22	2.70	2.49	2.19	2.44
Il	3.48	3.13	4.39	3.76	2.56	3.29
Ap	0.46	0.42	0.60	0.53	0.35	0.46

	AX85-097	AX85-241	AX85-242	AX85-260	AX85-261	AX85-263
Q	4.68	6.67	6.91	3.26	3.55	4.09
Or	10.99	4.20	5.02	2.01	1.42	1.48
Ab	24.71	26.74	26.40	19.89	20.39	19.97
An	18.07	21.40	19.91	28.42	28.64	28.73
Ne	0.00	0.00	0.00	0.00	0.00	0.00
Di	14.68	14.82	15.34	21.23	21.46	20.16
Hy	17.61	16.05	15.48	17.76	17.12	17.48
Ol	0.00	0.00	0.00	0.00	0.00	0.00
Mt	2.73	2.77	2.64	2.57	2.46	2.42
Il	4.41	6.59	6.44	4.56	4.43	4.52
Ap	0.67	1.55	1.51	0.51	0.53	0.51

CIPW NORMS, "DRY": EXTRUSIVE ROCKS

	AX85-264	AX85-266	AX85-267	AX85-268	BND83-005	BND83-006
Q	6.19	3.78	6.25	6.06	1.23	0.00
Or	2.07	4.55	4.14	2.19	3.60	2.30
Ab	19.72	20.39	22.42	20.90	22.51	23.19
An	26.19	24.26	22.25	24.49	23.15	23.36
Ne	0.00	0.00	0.00	0.00	0.00	0.00
Di	19.42	21.31	16.98	19.68	20.43	22.29
Hy	18.55	18.40	18.32	18.27	18.91	19.41
Ol	0.00	0.00	0.00	0.00	0.00	0.36
Mt	2.57	2.94	2.91	2.91	2.93	3.10
Il	4.22	4.05	5.17	4.52	5.30	4.86
Ap	0.51	0.53	0.70	0.56	0.58	0.56

CIPW NORMS, "DRY": EXTRUSIVE ROCKS

	BND83-007	BND83-009	BND83-012	BND83-015	BND83-016	BND83-017
Q	5.30	0.00	2.92	2.80	4.29	1.15
Or	5.56	4.49	9.22	4.26	2.19	2.07
Ab	25.56	26.49	25.47	22.42	21.41	18.70
An	18.84	24.34	18.88	25.35	27.44	26.21
Ne	0.00	0.00	0.00	0.00	0.00	0.00
Di	16.24	21.21	16.33	18.18	19.93	22.59
Hy	16.66	13.31	17.93	18.68	18.00	23.16
Ol	0.00	2.21	0.00	0.00	0.00	0.00
Mt	3.12	2.78	2.94	2.65	2.46	3.61
Il	6.97	4.54	4.54	3.91	2.91	3.15
Ap	0.95	0.51	0.67	0.49	0.00	0.44

	EL84-007B	EL84-010	EL84-082	EL84-087	EL84-256A	EL85-107
Q	6.35	5.49	3.86	1.06	2.32	0.80
Or	9.93	9.46	8.27	8.57	4.91	4.37
Ab	21.92	22.85	24.96	25.13	21.32	24.20
An	17.96	17.59	18.23	18.38	22.34	21.21
Ne	0.00	0.00	0.00	0.00	0.00	0.00
Di	9.97	11.57	11.51	12.20	20.88	24.94
Hy	19.45	18.84	20.83	20.20	18.46	13.77
Ol	0.00	0.00	0.00	0.00	0.00	0.00
Mt	3.07	3.03	3.26	3.28	3.41	2.84
Il	6.76	6.46	6.15	6.27	6.12	6.50
Ap	2.85	2.69	2.57	2.64	0.79	0.83

CHEMICAL ANALYSES - GROUP A

	AX85-001	AX85-005	AX85-008	AX85-013	AX85-015	AX85-019
SiO2	48.41	49.93	49.15	49.10	51.89	49.86
TiO2	4.28	2.00	3.49	2.78	2.38	2.92
Al2O3	12.33	13.55	12.04	13.13	13.34	13.40
Fe2O3(T)	14.40	13.17	15.70	14.56	12.89	14.78
MnO	0.19	0.19	0.23	0.20	0.18	0.25
MgO	5.82	6.02	4.74	5.37	5.03	4.11
CaO	7.93	10.37	8.44	9.24	8.90	7.37
Na2O	2.62	2.40	2.37	2.18	2.74	3.53
K2O	0.87	0.41	1.14	0.31	1.07	1.13
P2O5	0.47	0.24	0.43	0.29	0.28	0.58
H2O+	2.19	1.29	2.08	1.85	1.49	2.32
H2O-	0.57	0.64	0.36	0.42	0.26	0.23
CO2	0.05	0.08	0.07	0.57	0.58	0.00
TOTAL	100.13	100.29	100.24	100.00	101.03	100.48
Rb	33	8	39	9	27	22
Cs	0.00	0.00	0.00	0.00	0.50	0.00
Sr	419	225	265	302	257	313
Ba	606	101	264	156	277	500
Sc	0.0	0.0	0.0	0.0	35.5	30.9
V	437	311	489	466	332	329
Cr	77	64	9	24	58	8
Co	0.0	0.0	0.0	0.0	43.5	38.4
Ni	57	39	28	30	35	21
Cu	160	132	79	99	60	49
Zn	104	102	148	120	127	288
Ga	27	25	23	22	22	22
Y	46	39	51	40	45	51
Zr	295	149	225	188	250	276
Hf	0.00	0.00	0.00	0.00	6.50	6.50
Nb	23	12	21	20	25	26
Ta	0.00	0.00	0.00	0.00	1.70	2.20
Pb	2	2	9	3	14	11
Th	0	0	4	0	2	5
U	0.00	0.00	0.00	0.00	0.00	0.00
La	0.00	0.00	0.00	0.00	26.90	28.90
Ce	0.00	0.00	0.00	0.00	55.70	61.30
Nd	0.00	0.00	0.00	0.00	0.00	0.00
Sm	0.00	0.00	0.00	0.00	8.70	9.60
Eu	0.00	0.00	0.00	0.00	2.71	3.36
Tb	0.00	0.00	0.00	0.00	1.50	1.50
Yb	0.00	0.00	0.00	0.00	4.70	4.50
Lu	0.00	0.00	0.00	0.00	0.70	0.67
SUMREE	0.0	0.0	0.0	0.0	100.9	109.8

CHEMICAL ANALYSES - GROUP A

	AX85-020	AX85-026	AX85-027	AX85-030	AX85-031	AX85-032
SiO2	48.53	49.64	50.92	49.86	49.29	49.00
TiO2	3.53	3.82	2.18	2.93	3.77	3.52
Al2O3	12.99	12.44	12.83	12.53	14.92	14.33
Fe2O3(T)	15.43	14.93	14.05	14.77	13.23	14.08
MnO	0.23	0.18	0.21	0.22	0.17	0.18
MgO	4.89	5.21	5.27	4.46	4.87	4.00
CaO	8.15	8.32	8.67	8.55	7.93	6.85
Na2O	3.23	3.13	2.55	2.49	3.11	3.19
K2O	1.11	0.79	0.84	0.99	1.45	1.22
P2O5	0.40	0.44	0.31	0.66	0.33	0.65
H2O+	2.08	1.50	2.02	1.89	1.53	2.45
H2O-	0.27	0.18	0.36	0.29	0.34	0.49
CO2	0.05	0.00	0.14	1.26	0.34	0.51
TOTAL	100.89	100.58	100.35	100.90	101.28	100.47
Rb	32	24	24	25	47	41
Cs	0.00	0.00	0.00	0.00	0.00	0.00
Sr	399	343	415	332	469	420
Ba	582	141	723	330	386	242
Sc	35.9	36.7	0.0	0.0	34.2	0.0
V	444	415	355	273	399	372
Cr	11	38	50	12	62	8
Co	45.9	47.9	0.0	0.0	45.9	0.0
Ni	22	39	34	24	35	37
Cu	52	124	126	72	146	173
Zn	166	112	136	150	88	104
Ga	21	21	23	23	23	29
Y	39	46	45	52	42	59
Zr	220	278	222	262	227	326
Hf	5.80	7.60	0.00	0.00	5.60	0.00
Nb	22	21	18	26	17	24
Ta	1.90	2.00	0.00	0.00	1.60	0.00
Pb	12	9	7	7	5	3
Th	2	3	0	0	0	2
U	0.00	0.00	0.00	0.00	0.00	0.00
La	25.70	24.50	0.00	0.00	17.00	0.00
Ce	54.30	55.60	0.00	0.00	38.30	0.00
Nd	0.00	35.00	0.00	0.00	0.00	0.00
Sm	9.10	10.90	0.00	0.00	8.00	0.00
Eu	2.95	3.53	0.00	0.00	2.87	0.00
Tb	1.30	1.80	0.00	0.00	1.40	0.00
Yb	4.40	4.20	0.00	0.00	3.90	0.00
Lu	0.55	0.59	0.00	0.00	0.51	0.00
SUMREE	98.3	101.1	0.0	0.0	72.0	0.0

CHEMICAL ANALYSES - GROUP A

	AX85-033	AX85-034	AX85-035	AX85-036	AX85-037	AX85-040
SiO2	49.14	49.62	47.34	48.71	48.71	49.42
TiO2	3.55	3.41	4.33	4.12	4.24	3.20
Al2O3	13.60	12.18	12.47	13.30	12.74	12.06
Fe2O3(T)	14.85	10.61	15.86	14.21	14.27	15.54
MnO	0.21	0.17	0.19	0.19	0.20	0.22
MgO	3.49	2.95	4.81	4.66	4.98	4.98
CaO	7.77	10.87	8.70	9.19	8.74	8.37
Na2O	2.93	3.31	2.78	2.62	2.98	2.52
K2O	1.04	0.88	0.72	0.77	0.81	1.21
P2O5	0.62	0.87	0.61	0.49	0.46	0.41
H2O+	2.44	1.99	1.72	1.21	1.64	1.59
H2O-	0.30	0.27	0.38	0.35	0.27	0.27
CO2	0.00	5.30	0.09	0.26	0.00	0.00
TOTAL	99.94	102.43	100.00	100.08	100.04	99.79
Rb	26	21	17	21	26	36
Cs	0.00	0.00	0.70	0.00	0.00	0.00
Sr	354	435	353	311	376	325
Ba	307	184	214	139	377	616
Sc	0.0	0.0	36.6	0.0	0.0	44.5
V	367	325	502	372	428	460
Cr	6	9	44	62	45	27
Co	0.0	0.0	43.8	0.0	0.0	47.2
Ni	34	36	48	38	40	31
Cu	205	7	68	216	140	100
Zn	175	34	68	130	113	136
Ga	32	27	27	31	30	21
Y	64	74	59	50	48	51
Zr	368	427	319	293	301	229
Hf	0.00	0.00	6.90	0.00	0.00	5.50
Nb	24	28	22	21	26	22
Ta	0.00	0.00	1.70	0.00	0.00	1.60
Pb	6	0	8	2	5	7
Th	0	0	4	1	2	3
U	0.00	0.00	0.00	0.00	0.00	0.00
La	0.00	0.00	21.60	0.00	0.00	25.30
Ce	0.00	0.00	48.70	0.00	0.00	49.80
Nd	0.00	0.00	0.00	0.00	0.00	0.00
Sm	0.00	0.00	10.40	0.00	0.00	8.40
Eu	0.00	0.00	3.35	0.00	0.00	2.61
Tb	0.00	0.00	1.70	0.00	0.00	1.60
Yb	0.00	0.00	5.00	0.00	0.00	4.80
Lu	0.00	0.00	0.60	0.00	0.00	0.71
SUMREE	0.0	0.0	91.4	0.0	0.0	93.2

CHEMICAL ANALYSES - GROUP A

	AX85-043	AX85-046	AX85-048
SiO2	48.74	51.80	46.46
TiO2	3.05	2.09	3.89
Al2O3	12.27	12.51	11.94
Fe2O3(T)	15.94	14.15	17.13
MnO	0.23	0.22	0.25
MgO	5.02	5.19	6.02
CaO	7.80	8.21	6.99
Na2O	3.06	2.86	3.22
K2O	1.19	0.85	0.33
P2O5	0.33	0.21	0.46
H2O+	2.25	1.78	2.92
H2O-	0.27	0.19	0.58
CO2	0.00	0.20	0.56
TOTAL	100.15	100.26	100.75
Rb	30	28	9
Cs	0.00	0.60	0.00
Sr	410	299	402
Ba	572	275	393
Sc	37.6	41.5	39.6
V	433	364	515
Cr	10	33	11
Co	46.9	50.7	46.9
Ni	24	31	23
Cu	57	102	47
Zn	143	127	173
Ga	24	19	22
Y	43	41	42
Zr	207	195	198
Hf	5.00	4.60	4.80
Nb	22	16	24
Ta	1.70	1.20	1.90
Pb	9	9	12
Th	2	0	5
U	0.00	0.00	0.00
La	23.80	16.20	24.90
Ce	48.30	35.00	51.90
Nd	0.00	0.00	0.00
Sm	7.80	6.90	8.60
Eu	2.61	2.30	3.01
Tb	1.40	1.20	1.50
Yb	4.30	3.90	4.40
Lu	0.62	0.60	0.56
SUMREE	88.8	66.1	94.9

CHEMICAL ANALYSES - GROUP A

	AX85-033	AX85-034	AX85-035	AX85-036	AX85-037	AX85-040
SiO2	49.14	49.62	47.34	48.71	48.71	49.42
TiO2	3.55	3.41	4.33	4.12	4.24	3.20
Al2O3	13.60	12.18	12.47	13.30	12.74	12.06
Fe2O3(T)	14.85	10.61	15.86	14.21	14.27	15.54
MnO	0.21	0.17	0.19	0.19	0.20	0.22
MgO	3.49	2.95	4.81	4.66	4.98	4.98
CaO	7.77	10.87	8.70	9.19	8.74	8.37
Na2O	2.93	3.31	2.78	2.62	2.98	2.52
K2O	1.04	0.88	0.72	0.77	0.81	1.21
P2O5	0.62	0.87	0.61	0.49	0.46	0.41
H2O+	2.44	1.99	1.72	1.21	1.64	1.59
H2O-	0.30	0.27	0.38	0.35	0.27	0.27
CO2	0.00	5.30	0.09	0.26	0.00	0.00
TOTAL	99.94	102.43	100.00	100.08	100.04	99.79
Rb	26	21	17	21	26	36
Cs	0.00	0.00	0.70	0.00	0.00	0.00
Sr	354	435	353	311	376	325
Ba	307	184	214	139	377	616
Sc	0.0	0.0	36.6	0.0	0.0	44.5
V	367	325	502	372	428	460
Cr	6	9	44	62	45	27
Co	0.0	0.0	43.8	0.0	0.0	47.2
Ni	34	36	48	38	40	31
Cu	205	7	68	216	140	100
Zn	175	34	68	130	113	136
Ga	32	27	27	31	30	21
Y	64	74	59	50	48	51
Zr	368	427	319	293	301	229
Hf	0.00	0.00	6.90	0.00	0.00	5.50
Nb	24	28	22	21	26	22
Ta	0.00	0.00	1.70	0.00	0.00	1.60
Pb	6	0	8	2	5	7
Th	0	0	4	1	2	3
U	0.00	0.00	0.00	0.00	0.00	0.00
La	0.00	0.00	21.60	0.00	0.00	25.30
Ce	0.00	0.00	48.70	0.00	0.00	49.80
Nd	0.00	0.00	0.00	0.00	0.00	0.00
Sm	0.00	0.00	10.40	0.00	0.00	8.40
Eu	0.00	0.00	3.35	0.00	0.00	2.61
Tb	0.00	0.00	1.70	0.00	0.00	1.60
Yb	0.00	0.00	5.00	0.00	0.00	4.80
Lu	0.00	0.00	0.60	0.00	0.00	0.71
SUMREE	0.0	0.0	91.4	0.0	0.0	93.2

CHEMICAL ANALYSES - GROUP B

	AX85-051	AX85-052	AX85-057	AX85-059	AX85-061	AX85-062
SiO2	50.32	50.44	50.67	49.91	49.90	49.80
TiO2	2.49	2.20	2.85	3.20	2.95	1.95
Al2O3	12.96	14.39	12.69	12.61	12.56	13.35
Fe2O3(T)	14.75	13.14	13.94	15.23	15.01	13.39
MnO	0.23	0.19	0.21	0.21	0.18	0.20
MgO	5.04	5.20	4.78	4.30	5.09	6.15
CaO	9.20	9.90	7.72	7.00	6.40	10.61
Na2O	2.36	2.70	3.65	3.51	3.55	2.12
K2O	0.79	0.70	0.86	0.88	0.36	0.41
P2O5	0.26	0.25	0.28	0.35	0.30	0.19
H2O+	1.25	0.85	2.60	3.09	2.66	1.44
H2O-	0.20	0.15	0.00	0.21	0.45	0.88
CO2	0.12	0.00	0.00	0.42	0.62	0.00
TOTAL	99.97	100.11	100.25	100.92	100.03	100.49
Rb	27	22	33	25	11	16
Sr	248	247	127	195	389	183
Ba	269	138	191	276	278	93
V	380	313	494	465	479	354
Cr	22	27	15	0	15	101
Ni	30	29	35	18	24	76
Cu	219	207	48	51	88	203
Zn	211	131	188	165	148	109
Ga	22	26	22	20	23	18
Y	45	37	39	45	39	35
Zr	197	166	187	204	190	153
Nb	14	12	14	17	16	9
Pb	11	7	0	8	4	2

CHEMICAL ANALYSES - GROUP B

	AX85-063	AX85-067	AX85-215	AX85-217	AX85-218	AX85-220
SiO2	49.83	49.87	50.63	50.60	50.66	49.55
TiO2	1.80	1.88	3.29	2.47	3.52	3.84
Al2O3	14.10	13.64	12.48	13.32	12.86	12.59
Fe2O3(T)	12.80	13.13	14.82	12.87	14.71	14.00
MnO	0.18	0.19	0.20	0.18	0.21	0.18
MgO	6.14	6.48	4.40	5.63	3.69	5.48
CaO	10.89	10.97	7.88	9.36	7.65	9.30
Na2O	2.26	2.13	3.04	2.97	3.01	2.35
K2O	0.38	0.18	1.03	0.79	1.05	0.37
P2O5	0.17	0.18	0.42	0.40	0.49	0.41
H2O+	1.05	0.96	0.70	1.55	1.10	1.35
H2O-	0.48	0.39	0.00	0.15	0.00	0.20
CO2	0.23	0.43	0.00	0.00	0.00	1.41
TOTAL	100.31	100.43	98.89	100.29	98.95	101.03
Rb	12	7	40	31	39	9
Sr	190	200	262	252	258	451
Ba	65	109	210	146	247	149
V	323	350	421	315	283	429
Cr	87	102	25	101	0	34
Ni	41	49	41	48	20	33
Cu	160	168	168	139	133	159
Zn	91	107	159	117	200	138
Ga	24	22	21	24	26	25
Y	34	34	50	42	55	44
Zr	135	148	262	197	304	269
Nb	11	11	18	16	22	23
Pb	11	7	0	2	4	4

CHEMICAL ANALYSES - GROUP B

	AX85-221	AX85-222	AX85-223	AX85-224	AX85-225	AX85-226
SiO2	48.67	49.54	49.80	51.70	54.63	49.54
TiO2	3.91	3.83	2.34	3.26	2.34	2.70
Al2O3	12.66	12.70	12.16	12.16	12.20	12.95
Fe2O3(T)	13.85	13.94	13.56	14.39	13.55	14.12
MnO	0.18	0.19	0.20	0.22	0.24	0.21
MgO	5.28	5.46	6.46	4.07	3.00	5.30
CaO	9.09	9.10	10.45	7.19	6.07	9.04
Na2O	2.41	2.48	1.99	3.16	3.37	2.57
K2O	0.34	0.34	0.51	1.16	1.22	0.74
P2O5	0.40	0.42	0.23	0.37	0.58	0.30
H2O+	1.70	1.90	1.60	2.44	2.31	2.50
H2O-	2.40	0.11	0.00	0.29	0.26	0.23
CO2	0.14	1.17	0.00	0.75	1.35	0.29
TOTAL	101.03	101.18	99.30	101.16	101.12	100.49
Rb	11	20	18	38	23	29
Sr	454	229	282	284	247	321
Ba	141	176	96	157	220	160
V	426	369	419	321	135	419
Cr	27	23	94	0	1	47
Ni	39	31	47	21	26	32
Cu	144	140	93	28	22	95
Zn	128	117	125	161	173	142
Ga	23	24	26	26	26	25
Y	43	45	37	51	70	36
Zr	265	214	160	270	367	164
Nb	22	19	14	25	32	16
Pb	7	1	0	7	6	2

CHEMICAL ANALYSES - GROUP B

	AX85-227	AX85-228	AX85-230	AX85-231	AX85-233	AX85-234
SiO2	50.45	51.02	49.26	49.91	49.95	49.81
TiO2	2.17	2.08	2.79	3.47	3.34	2.55
Al2O3	12.42	13.12	12.62	12.25	11.99	12.73
Fe2O3(T)	14.26	13.70	14.86	15.09	15.18	14.51
MnO	0.21	0.20	0.22	0.23	0.23	0.22
MgO	5.80	5.82	5.38	4.52	4.81	5.15
CaO	9.53	9.30	8.04	7.37	7.88	9.09
Na2O	2.81	2.08	2.92	3.69	3.02	2.71
K2O	0.44	0.71	0.93	0.67	1.19	0.59
P2O5	0.21	0.20	0.30	0.47	0.42	0.40
H2O+	1.20	1.70	2.56	1.70	2.22	2.00
H2O-	0.00	0.38	0.19	0.00	0.34	0.00
CO2	0.00	0.26	0.54	0.00	0.14	0.00
TOTAL	99.50	100.57	100.61	99.37	100.71	99.76
Rb	20	23	25	31	37	21
Sr	240	225	318	372	290	261
Ba	225	123	190	263	311	186
V	438	387	445	449	411	382
Cr	37	43	40	16	17	35
Ni	44	31	35	28	30	40
Cu	139	140	88	77	65	124
Zn	139	154	154	122	148	137
Ga	23	24	25	25	24	22
Y	32	36	38	46	45	44
Zr	144	141	198	264	247	205
Nb	10	10	22	23	28	15
Pb	0	5	9	0	13	0

CHEMICAL ANALYSES - GROUP B

	AX85-235	AX85-237	AX85-238	AX85-239	EL85-201	EL85-202
SiO2	51.85	51.34	49.45	51.37	50.29	51.63
TiO2	1.98	2.18	2.50	2.18	2.59	2.17
Al2O3	13.09	13.27	12.55	12.99	12.96	13.40
Fe2O3(T)	12.98	13.66	14.44	13.96	13.32	12.80
MnO	0.20	0.21	0.21	0.21	0.24	0.22
MgO	5.10	4.90	5.35	4.87	5.36	4.65
CaO	9.18	8.96	9.68	9.11	9.14	8.83
Na2O	2.40	2.36	2.48	2.69	2.78	2.79
K2O	0.71	0.52	0.55	0.55	0.50	0.75
P2O5	0.24	0.26	0.38	0.26	0.33	0.28
H2O+	1.52	1.51	1.90	1.38	2.20	1.51
H2O-	0.28	0.29	0.00	0.33	0.00	0.44
CO2	1.29	1.10	0.00	0.74	0.00	0.26
TOTAL	100.82	100.56	99.49	100.64	99.71	99.73
Rb	23	18	18	10	17	26
Sr	222	233	244	409	265	248
Ba	168	160	132	145	145	222
V	328	352	366	426	380	376
Cr	29	26	36	40	85	46
Ni	34	29	38	39	43	33
Cu	113	117	118	174	67	77
Zn	122	108	133	146	164	130
Ga	21	22	22	22	22	24
Y	43	43	42	42	40	45
Zr	215	213	202	268	189	231
Nb	18	19	16	22	16	22
Pb	2	6	0	6	0	7

CHEMICAL ANALYSES - GROUP B

	EL85-205	EL85-207	EL85-208	EL85-209	EL85-213
SiO2	48.53	51.30	48.71	48.39	48.56
TiO2	2.26	1.77	2.29	2.21	1.38
Al2O3	13.50	13.16	12.86	14.12	15.61
Fe2O3(T)	13.43	12.88	13.26	12.74	11.21
MnO	0.21	0.22	0.22	0.20	0.19
MgO	6.35	6.00	6.36	6.25	6.82
CaO	10.10	9.78	11.25	10.46	11.78
Na2O	2.52	2.44	2.65	2.54	2.05
K2O	0.50	0.50	0.36	0.54	0.39
P2O5	0.24	0.18	0.22	0.26	0.14
H2O+	1.33	1.10	0.90	1.28	0.89
H2O-	0.39	0.00	0.00	0.42	0.21
CO2	0.08	0.00	0.00	0.07	0.00
TOTAL	99.44	99.33	99.08	99.48	99.23
Rb	16	17	9	15	13
Sr	233	186	200	265	195
Ba	95	89	83	129	97
V	385	365	447	354	263
Cr	104	91	128	125	184
Ni	48	59	65	53	53
Cu	221	157	141	196	157
Zn	103	182	76	129	104
Ga	26	22	27	23	21
Y	34	35	37	35	24
Zr	155	170	155	146	88
Nb	12	12	13	12	8
Pb	9	38	0	10	11

CHEMICAL ANALYSES - GROUP C

	EL84-211	EL84-218	EL84-221	EL84-222	EL84-223	EL84-229
SiO2	47.53	45.42	46.76	44.80	45.25	46.25
TiO2	3.77	3.47	3.25	4.05	3.43	3.20
Al2O3	12.96	13.59	14.49	13.05	14.38	13.69
Fe2O3(T)	15.20	14.93	13.75	15.65	13.84	12.96
MnO	0.18	0.19	0.21	0.24	0.18	0.18
MgO	5.21	5.14	5.25	5.13	5.74	5.64
CaO	7.45	10.31	7.25	9.54	9.81	10.03
Na2O	4.39	2.41	4.26	2.61	2.23	2.11
K2O	0.31	0.73	0.92	0.45	0.69	0.89
P2O5	0.43	0.94	0.63	1.01	0.97	0.52
H2O+	2.26	2.07	2.46	1.68	2.13	2.44
H2O-	0.35	0.36	0.43	0.65	0.73	0.34
CO2	0.13	1.31	0.11	0.89	0.96	2.42
TOTAL	100.17	100.87	99.77	99.75	100.34	100.67
Rb	9	20	27	15	17	23
Cs	0.00	1.00	0.00	0.00	0.00	0.00
Sr	382	485	445	524	452	523
Ba	129	576	699	317	518	461
Sc	29.9	29.0	0.0	0.0	0.0	0.0
V	399	299	328	279	313	278
Cr	22	42	63	16	59	30
Co	64.2	55.9	0.0	0.0	0.0	0.0
Ni	28	38	26	29	40	41
Cu	15	27	25	34	5	42
Zn	107	146	114	156	73	143
Ga	22	20	22	25	23	25
Y	32	30	28	37	31	30
Zr	214	164	152	190	139	195
Hf	6.00	4.30	0.00	0.00	0.00	0.00
Nb	29	24	22	26	22	25
Ta	2.60	2.10	0.00	0.00	0.00	0.00
Pb	5	14	8	9	1	11
Th	1	2	0	3	0	2
U	0.00	0.00	0.00	0.00	0.00	0.00
La	27.90	25.80	0.00	0.00	0.00	0.00
Ce	58.00	54.00	0.00	0.00	0.00	0.00
Nd	37.00	0.00	0.00	0.00	0.00	0.00
Sm	9.00	8.60	0.00	0.00	0.00	0.00
Eu	2.57	4.06	0.00	0.00	0.00	0.00
Tb	1.30	0.91	0.00	0.00	0.00	0.00
Yb	2.90	2.60	0.00	0.00	0.00	0.00
Lu	0.39	0.37	0.00	0.00	0.00	0.00
SUMREE	102.1	96.3	0.0	0.0	0.0	0.0

CHEMICAL ANALYSES - GROUP C

	EL84-232	EL84-235	EL84-236	EL84-245	T-S6-14
SiO2	42.69	42.28	47.18	43.89	46.59
TiO2	3.27	2.95	3.74	3.57	4.39
Al2O3	13.58	13.78	12.38	14.01	12.38
Fe2O3(T)	13.70	13.53	15.74	14.55	15.90
MnO	0.16	0.17	0.18	0.24	0.23
MgO	4.97	6.52	5.71	4.73	5.99
CaO	10.12	9.92	9.43	9.37	7.74
Na2O	2.20	2.00	2.59	2.63	3.34
K2O	0.64	0.57	0.73	1.01	0.58
P2O5	0.51	0.46	0.41	0.59	0.90
H2O+	2.21	2.11	1.74	0.94	2.91
H2O-	0.38	0.38	0.82	0.57	0.36
CO2	5.09	3.82	0.55	3.11	0.36
TOTAL	99.52	98.49	101.20	99.21	101.67
Rb	20	17	19	20	17
Cs	0.00	0.00	0.00	0.00	0.00
Sr	572	526	407	512	448
Ba	367	307	188	793	315
Sc	0.0	22.1	0.0	0.0	0.0
V	304	284	448	303	331
Cr	32	33	44	40	38
Co	0.0	69.9	0.0	0.0	0.0
Ni	37	66	32	32	30
Cu	36	32	43	26	21
Zn	115	113	131	125	114
Ga	22	22	20	20	22
Y	32	26	31	32	38
Zr	193	173	195	173	207
Hf	0.00	4.60	0.00	0.00	0.00
Nb	24	22	26	25	28
Ta	0.00	2.20	0.00	0.00	0.00
Pb	7	6	5	9	6
Th	1	1	2	2	4
U	0.00	0.00	0.00	0.00	0.00
La	0.00	24.20	0.00	0.00	0.00
Ce	0.00	51.00	0.00	0.00	0.00
Nd	0.00	32.00	0.00	0.00	0.00
Sm	0.00	7.70	0.00	0.00	0.00
Eu	0.00	2.66	0.00	0.00	0.00
Tb	0.00	1.00	0.00	0.00	0.00
Yb	0.00	2.40	0.00	0.00	0.00
Lu	0.00	0.28	0.00	0.00	0.00
SUMREE	0.0	89.2	0.0	0.0	0.0

CHEMICAL ANALYSES - GROUP D

	EL84-015	EL84-023	EL84-041	EL84-044	EL84-046	EL84-050
SiO2	45.51	45.69	45.30	46.52	46.55	47.47
TiO2	3.73	3.48	3.38	3.39	3.62	3.72
Al2O3	12.92	13.30	13.25	12.75	12.99	12.29
Fe2O3(T)	15.39	15.38	13.44	13.31	15.30	15.16
MnO	0.20	0.19	0.18	0.18	0.20	0.19
MgO	4.96	4.78	5.28	5.14	4.68	5.58
CaO	7.93	9.23	8.97	9.09	9.08	9.16
Na2O	4.17	2.90	2.47	2.78	2.70	2.54
K2O	1.01	1.00	0.94	0.93	0.99	1.06
P2O5	0.37	0.36	0.37	0.41	0.39	0.46
H2O+	2.43	0.77	1.56	1.07	0.89	0.85
H2O-	0.31	0.59	1.48	0.88	0.74	0.63
CO2	0.00	0.39	5.75	5.01	0.57	1.23
TOTAL	98.93	98.06	102.37	101.46	98.70	100.34
Rb	25	33	16	18	31	21
Cs	0.00	1.00	0.00	0.00	0.00	1.00
Sr	461	524	583	518	519	540
Ba	306	291	439	296	323	517
Sc	0.0	27.9	0.0	0.0	0.0	30.0
V	409	386	340	337	369	327
Cr	22	27	43	36	20	107
Co	0.0	63.7	0.0	0.0	0.0	81.2
Ni	26	22	40	31	23	68
Cu	33	50	45	43	41	104
Zn	131	109	122	109	126	135
Ga	25	25	23	20	23	21
Y	30	29	28	27	31	36
Zr	193	197	194	189	211	282
Hf	0.00	5.30	0.00	0.00	0.00	7.70
Nb	31	32	31	30	33	41
Ta	0.00	2.90	0.00	0.00	0.00	3.70
Pb	7	5	8	7	7	3
Th	1	3	1	0	4	0
U	0.00	0.00	0.00	0.00	0.00	0.00
La	0.00	25.60	0.00	0.00	0.00	34.50
Ce	0.00	51.00	0.00	0.00	0.00	70.00
Nd	0.00	0.00	0.00	0.00	0.00	31.00
Sm	0.00	7.60	0.00	0.00	0.00	10.40
Eu	0.00	2.41	0.00	0.00	0.00	3.21
Tb	0.00	1.00	0.00	0.00	0.00	1.10
Yb	0.00	2.50	0.00	0.00	0.00	3.20
Lu	0.00	0.32	0.00	0.00	0.00	0.39
SUMREE	0.0	90.4	0.0	0.0	0.0	122.8

CHEMICAL ANALYSES - GROUP D

	EL84-056	EL84-060	EL84-072	EL84-073	EL84-076	EL84-098
SiO2	47.55	46.09	47.33	48.02	48.37	48.57
TiO2	3.30	3.72	3.25	3.22	3.15	3.63
Al2O3	13.48	13.19	13.88	13.78	13.42	13.19
Fe2O3(T)	14.58	15.31	14.97	14.54	15.01	15.27
MnO	0.19	0.18	0.21	0.19	0.19	0.20
MgO	5.00	5.58	5.09	4.75	5.01	4.79
CaO	9.20	8.18	9.36	9.59	9.36	9.16
Na2O	3.09	3.13	2.87	3.03	2.88	2.66
K2O	0.98	1.20	1.10	1.02	1.09	1.07
P2O5	0.37	0.38	0.37	0.38	0.38	0.38
H2O+	0.34	1.18	0.99	0.69	0.02	0.82
H2O-	0.28	0.45	0.27	0.49	0.49	0.51
CO2	0.31	0.05	0.11	0.51	0.00	1.47
TOTAL	98.67	98.64	99.80	100.21	99.37	101.72
Rb	29	35	33	28	32	27
Cs	0.00	0.00	0.00	0.00	0.00	0.00
Sr	503	462	501	520	516	489
Ba	317	625	351	326	355	386
Sc	21.7	0.0	0.0	0.0	0.0	0.0
V	336	416	331	332	332	383
Cr	25	28	27	24	27	26
Co	78.8	0.0	0.0	0.0	0.0	0.0
Ni	30	27	34	36	33	27
Cu	47	31	55	53	56	40
Zn	127	91	169	133	152	132
Ga	25	23	25	24	22	23
Y	31	29	31	32	30	30
Zr	211	202	207	210	208	213
Hf	5.70	0.00	0.00	0.00	0.00	0.00
Nb	32	31	32	32	31	32
Ta	5.50	0.00	0.00	0.00	0.00	0.00
Pb	10	2	7	12	10	3
Th	6	1	0	2	2	3
U	0.00	0.00	0.00	0.00	0.00	0.00
La	26.80	0.00	0.00	0.00	0.00	0.00
Ce	55.00	0.00	0.00	0.00	0.00	0.00
Nd	32.00	0.00	0.00	0.00	0.00	0.00
Sm	8.10	0.00	0.00	0.00	0.00	0.00
Eu	2.64	0.00	0.00	0.00	0.00	0.00
Tb	1.20	0.00	0.00	0.00	0.00	0.00
Yb	2.40	0.00	0.00	0.00	0.00	0.00
Lu	0.33	0.00	0.00	0.00	0.00	0.00
SUMREE	96.5	0.0	0.0	0.0	0.0	0.0

CHEMICAL ANALYSES - GROUP D

	EL84-110	EL84-210
SiO2	47.21	48.79
TiO2	3.95	3.75
Al2O3	13.68	12.94
Fe2O3(T)	15.10	15.26
MnO	0.15	0.19
MgO	5.22	5.08
CaO	7.64	8.26
Na2O	3.25	3.17
K2O	0.82	1.40
P2O5	0.40	0.38
H2O+	1.28	1.45
H2O-	0.89	0.46
CO2	0.26	0.03
TOTAL	99.85	101.16
Rb	31	34
Cs	0.00	1.00
Sr	562	578
Ba	299	589
Sc	0.0	27.9
V	420	364
Cr	27	20
Co	0.0	63.5
Ni	19	23
Cu	40	38
Zn	79	109
Ga	26	23
Y	30	32
Zr	216	217
Hf	0.00	5.20
Nb	35	32
Ta	0.00	2.90
Pb	2	8
Th	0	1
U	0.00	0.00
La	0.00	26.70
Ce	0.00	55.00
Nd	0.00	0.00
Sm	0.00	7.80
Eu	0.00	2.50
Tb	0.00	1.20
Yb	0.00	2.90
Lu	0.00	0.34
SUMREE	0.0	96.4

CIPW NORMS, VOLATILE-FREE: GROUP A

	AX85-001	AX85-005	AX85-008	AX85-013	AX85-015	AX85-019
Q	3.73	2.76	4.58	5.69	4.78	1.20
Or	5.26	2.48	6.91	1.89	6.44	6.86
Ab	22.76	20.73	20.56	18.96	23.69	30.63
An	19.90	25.47	19.34	25.86	21.46	17.82
Di	14.36	21.03	17.28	16.08	18.11	13.28
Hy	20.39	19.53	19.14	21.09	17.45	19.29
Ol	0.00	0.00	0.00	0.00	0.00	0.00
Mt	2.94	2.67	3.19	2.99	2.62	3.02
Il	8.36	3.87	6.80	5.43	4.63	5.70
Ap	1.11	0.56	1.02	0.70	0.67	1.37

	AX85-020	AX85-026	AX85-027	AX85-030	AX85-031	AX85-032
Q	0.00	2.42	4.82	5.73	0.29	2.99
Or	6.74	4.73	5.08	6.03	8.75	7.45
Ab	28.01	26.91	22.09	21.83	26.91	27.92
An	18.07	17.88	21.65	20.77	22.97	21.93
Di	17.23	17.53	16.93	15.63	12.43	7.41
Hy	16.85	18.36	20.64	19.15	17.97	20.07
Ol	1.67	0.00	0.00	0.00	0.00	0.00
Mt	3.13	3.02	2.87	3.03	2.68	2.90
Il	6.88	7.37	4.25	5.75	7.31	6.91
Ap	0.95	1.04	0.74	1.58	0.79	1.55

	AX85-033	AX85-034	AX85-035	AX85-036	AX85-037	AX85-040
Q	4.68	5.18	2.24	4.15	2.55	3.42
Or	6.32	5.61	4.37	4.61	4.91	7.27
Ab	25.47	30.13	24.03	22.59	25.72	21.75
An	21.48	16.93	19.86	22.66	19.35	18.37
Di	11.76	29.07	16.80	17.00	18.01	17.68
Hy	17.43	2.67	18.21	15.79	16.05	19.62
Ol	0.00	0.00	0.00	0.00	0.00	0.00
Mt	3.03	2.26	3.22	2.89	2.90	3.15
Il	6.93	6.95	8.41	7.98	8.20	6.19
Ap	1.48	2.15	1.44	1.16	1.09	0.97

CIPW NORMS, VOLATILE-FREE: GROUP A

	AX85-043	AX85-046	AX85-048
Q	0.06	4.65	0.00
Or	7.21	5.14	2.01
Ab	26.57	24.71	28.35
An	16.63	19.20	17.88
Di	17.40	17.53	12.54
Hy	20.87	20.32	24.33
Ol	0.00	0.00	1.65
Mt	3.25	2.87	3.55
Il	5.94	4.06	7.69
Ap	0.79	0.49	1.11

CIPW NORMS, VOLATILE-FREE: GROUP B

	AX85-051	AX85-052	AX85-057	AX85-059	AX85-061	AX85-062
Q	4.64	2.28	1.41	2.46	3.37	3.45
Or	4.73	4.20	5.20	5.38	2.19	2.48
Ab	20.31	23.10	31.73	30.80	31.14	18.36
An	22.80	25.32	16.10	16.66	17.94	26.29
Di	18.25	18.79	17.72	14.23	10.80	21.77
Hy	19.56	17.84	17.75	19.64	23.52	19.96
Ol	0.00	0.00	0.00	0.00	0.00	0.00
Mt	2.97	2.64	2.84	3.15	3.10	2.71
Il	4.81	4.22	5.55	6.31	5.81	3.80
Ap	0.60	0.58	0.67	0.83	0.72	0.44

	AX85-063	AX85-067	AX85-215	AX85-217	AX85-218	AX85-220
Q	2.34	3.22	4.31	2.04	5.91	6.56
Or	2.30	1.06	6.15	4.73	6.26	2.25
Ab	19.46	18.36	25.89	25.56	25.72	20.48
An	27.68	27.60	17.49	21.05	18.70	23.38
Di	21.61	21.96	16.00	19.40	13.79	17.66
Hy	19.32	20.35	17.54	18.05	16.40	18.07
Ol	0.00	0.00	0.00	0.00	0.00	0.00
Mt	2.58	2.65	2.96	2.60	2.96	2.87
Il	3.48	3.63	6.29	4.77	6.76	7.50
Ap	0.39	0.42	0.97	0.95	1.16	0.97

CIPW NORMS, VOLATILE-FREE: GROUP B

	AX85-221	AX85-222	AX85-223	AX85-224	AX85-225	AX85-226
Q	6.19	6.24	4.41	6.14	10.92	3.44
Or	2.07	2.07	3.07	7.09	7.51	4.49
Ab	21.24	21.66	17.09	27.67	29.62	22.42
An	23.72	23.22	23.12	16.10	15.14	22.26
Di	16.97	16.95	23.13	15.33	10.36	18.22
Hy	17.88	18.37	19.48	17.21	17.45	19.45
Ol	0.00	0.00	0.00	0.00	0.00	0.00
Mt	2.87	2.86	2.74	2.96	2.80	2.89
Il	7.75	7.50	4.52	6.40	4.62	5.28
Ap	0.97	1.00	0.53	0.88	1.39	0.72

	AX85-227	AX85-228	AX85-230	AX85-231	AX85-233	AX85-234
Q	2.51	5.90	1.55	2.16	2.76	3.56
Or	2.66	4.31	5.67	4.02	7.21	3.55
Ab	24.03	18.02	25.56	31.73	26.23	23.44
An	20.22	24.93	19.19	15.16	16.10	21.24
Di	21.80	17.39	16.63	15.79	17.69	18.37
Hy	19.51	21.49	21.39	18.31	18.72	19.48
Ol	0.00	0.00	0.00	0.00	0.00	0.00
Mt	2.86	2.78	3.06	3.06	3.10	2.94
Il	4.18	4.05	5.47	6.70	6.51	4.94
Ap	0.49	0.46	0.72	1.11	1.00	0.95

	AX85-235	AX85-237	AX85-238	AX85-239	EL85-201	EL85-202
Q	6.94	7.37	3.61	5.51	4.16	5.76
Or	4.31	3.19	3.31	3.31	3.01	4.55
Ab	20.90	20.56	21.41	23.36	24.03	24.12
An	23.59	24.77	21.89	22.28	21.90	22.32
Di	18.03	16.00	20.39	18.55	18.40	17.13
Hy	18.72	19.75	18.93	18.68	18.48	17.22
Ol	0.00	0.00	0.00	0.00	0.00	0.00
Mt	2.67	2.78	2.93	2.84	2.71	2.60
Il	3.87	4.25	4.84	4.24	5.03	4.22
Ap	0.58	0.63	0.90	0.63	0.79	0.67

CIPW NORMS, VOLATILE-FREE: GROUP B

	EL85-205	EL85-207	EL85-208	EL85-209	EL85-213
Q	0.29	4.41	0.00	0.00	0.00
Or	3.01	3.01	2.13	3.25	2.30
Ab	21.75	20.90	22.59	21.92	17.52
An	24.48	23.73	22.37	25.96	32.62
Di	20.58	19.97	26.78	20.73	20.95
Hy	20.50	19.79	15.25	18.28	19.05
Ol	0.00	0.00	1.23	0.75	0.56
Mt	2.71	2.58	2.67	2.58	2.26
Il	4.37	3.40	4.39	4.27	2.66
Ap	0.56	0.42	0.51	0.60	0.32

CIPW NORMS, VOLATILE-FREE: GROUP C

	EL84-211	EL84-218	EL84-221	EL84-222	EL84-223	EL84-229
Q	0.00	0.00	0.00	0.05	0.20	1.27
Or	1.89	4.49	5.61	2.72	4.26	5.56
Ab	38.16	21.16	35.63	22.85	19.63	18.79
An	15.16	25.01	18.23	23.30	28.20	26.58
Ne	0.00	0.00	0.82	0.00	0.00	0.00
Di	16.57	18.00	12.07	15.59	13.00	18.25
Hy	4.18	17.28	0.00	20.23	21.77	18.46
Ol	11.34	1.33	15.46	0.00	0.00	0.00
Mt	3.10	3.09	2.81	3.20	2.86	2.71
Il	7.35	6.84	6.36	7.94	6.76	6.40
Ap	1.02	2.27	1.51	2.41	2.34	1.27

	EL84-232	EL84-235	EL84-236	EL84-245	T-S6-14
Q	0.00	0.00	0.23	0.00	0.00
Or	4.08	3.60	4.43	6.26	3.55
Ab	20.06	18.02	22.59	23.27	29.28
An	27.27	28.67	20.65	24.56	17.71
Ne	0.00	0.00	0.00	0.00	0.00
Di	19.27	16.87	20.58	16.69	13.22
Hy	11.88	10.81	19.74	7.11	19.19
Ol	4.26	8.98	0.00	8.28	3.17
Mt	2.94	2.86	3.23	3.02	3.28
Il	6.70	5.96	7.33	7.10	8.64
Ap	1.27	1.14	0.97	1.44	2.15

CIPW NORMS, VOLATILE-FREE: GROUP D

	EL84-015	EL84-023	EL84-041	EL84-044	EL84-046	EL84-050
Q	0.00	0.00	0.00	0.22	0.00	0.59
Or	6.15	6.26	6.44	5.85	6.21	6.62
Ab	29.49	25.89	24.29	25.13	24.20	22.59
An	13.91	21.53	25.84	20.94	21.64	20.02
Ne	3.69	0.00	0.00	0.00	0.00	0.00
Di	20.00	20.46	19.13	20.17	19.62	20.49
Hy	0.00	7.14	19.13	16.78	17.30	19.45
Ol	13.00	8.24	1.06	0.00	0.63	0.00
Mt	3.15	3.23	3.09	2.83	3.22	3.18
Il	7.27	6.72	6.95	6.89	7.03	7.26
Ap	0.88	0.86	0.93	1.02	0.93	1.09

	EL84-056	EL84-060	EL84-072	EL84-073	EL84-076	EL84-098
Q	0.00	0.00	0.00	0.00	0.00	1.57
Or	5.97	7.45	6.74	6.26	6.56	6.56
Ab	26.99	27.76	25.05	26.49	24.71	23.36
An	20.71	19.35	22.37	21.65	20.86	21.74
Ne	0.00	0.00	0.00	0.00	0.00	0.00
Di	19.99	17.17	19.11	20.75	19.88	19.11
Hy	10.70	6.04	10.42	11.18	15.23	17.89
Ol	5.07	11.23	6.14	3.96	2.01	0.00
Mt	3.00	3.20	3.06	2.97	3.03	3.15
Il	6.32	7.18	6.25	6.21	6.02	7.08
Ap	0.86	0.90	0.88	0.90	0.88	0.90

	EL84-110	EL84-210
Q	5.71	0.00
Or	5.08	8.45
Ab	29.02	27.33
An	21.49	17.27
Ne	0.00	0.00
Di	12.35	18.24
Hy	8.00	14.36
Ol	0.00	2.90
Mt	-11.40	3.09
Il	7.71	7.26
Ap	0.95	0.90

REFERENCES

Agashe, L.V. and Gupte, R.B. 1972. Mode of eruption of Deccan Trap basalts. Bulletin Volcanologique 35: 591-601.

Allègre, C.J., Treuil, M., Minster, J.F., Minster, B. and Albarède, F. 1977. Systematic use of trace element in igneous process, part I. Fractional crystallization processes in volcanic suites. Contributions to Mineralogy and Petrology 60: 57-75.

Avison, H. 1987. Ar-40/Ar-39 age studies of mafic volcanics from the Sverdrup Basin. Unpub. B.Sc. Honours Thesis, Dalhousie University, Halifax, Nova Scotia, Canada, 88 p.

Baggeroer, A.B. and Falconer, R. 1982. Array refraction profiles and crustal models of the Canada Basin. Journal of Geophysical Research 87: 5461-5476.

Balkwill, H.R. 1978. Evolution of Sverdrup Basin. American Association of Petroleum Geologists Bulletin 62 (6): 1004-1028.

Balkwill, H.R. and Haimila, N.E. 1978. K/Ar ages and significance of mafic rocks, Sabine Peninsula, Melville Island, District of Franklin. Geological Survey of Canada Paper 78-1C: 35-38.

Balkwill, H.R. and Fox, F.G. 1982. Incipient rift zone, western Sverdrup Basin, Arctic Canada; in Arctic Geology and Geophysics, Embrie, A.F. and Balkwill, H.R., eds. Canadian Society of Petroleum Geologists Memoir 8: 171-187.

Balkwill, H.R. 1983. Geology of Amund-Ringnes, Cornwall, and Haig-Thomas Islands, District of Franklin. Geological Survey of Canada Memoir 390, 76 p.

Balkwill, H.R., Cook, D.G., Detterman, R.L., Embry, A.F., Hakansson, E., Miall, A.D., Poulton, T.P. and Young, F.G. 1983. Arctic North America and Northern Greenland in The Phanerozoic Geology of the World, II The Mesozoic B. Elsevier Science Publishers: 1-31.

Bally, A.W. and Snelson, S. 1980. Realms of subsidence. Canadian Society of Petroleum Geologists Memoir 6: 9-94.

Bally, A.W. 1987. Phanerozoic basin evolution in North America. Episodes 10(4): 248-253.

Baragar, W.R.A. 1984. Pillow formation and layered flows in the Circum-Superior Belt of eastern Hudson Bay. Canadian Journal of Earth Sciences 21: 781-792.

Basaltic Volcanism Study Project. 1981. Basaltic Volcanism on the Terrestrial Planets. Pergamon Press Inc, New York.

Bates, J.L. 1986. Cretaceous (?) volcanism associated with development of the Sverdrup Basin, Ellesmere Island, Arctic Archipelago - Preliminary results from recent mapping. Abstract, Student Conference on Northern Studies, Ottawa, October 1986.

Beane, J.E., Turner, C.A., Hooper, P.R., Subbarao, K.V. and Walsh, J.N. 1986. Stratigraphy, composition and form of the Deccan Basalts, Western Ghats, India. Bulletin Volcanologique 48: 61-83.

Bhattacharji, S. 1967. Mechanics of flow differentiation in ultramafic and mafic sills. Journal of Geology 75: 101-112.

Biggar, G.M. 1983. Crystallization of plagioclase, augite and olivine in synthetic systems and in tholeiites. Mineralogical Magazine 47: 161-176.

Blackadar, R.G. 1954. Geological reconnaissance, north coast of Ellesmere Island, Northwest Territories. Geological Survey of Canada Paper 53-10, 22 p.

Blackadar, R.G. 1964. Basic intrusions of the Queen Elizabeth Islands, District of Franklin. Geological Survey of Canada Bulletin 97, 36 p.

Bouvier, J.L., Gupta, J.G. Sen and Abbey, S. 1972. Use of an "Automatic Sulphur Titrator" in rock and mineral analysis: determination of sulphur, total carbon, carbonate and ferrous iron. Geological Survey of Canada Paper 72-31, 22 p.

Brooks, C., James, D.E. and Hart, S.R. 1976. Ancient Lithosphere: Its role in young continental volcanism. Science 193: 1086-1094.

Brown, P.E., Parsons, I. and Becker, S.M. 1987. Peralkaline volcanicity in the Arctic Basin - the Kap Washington volcanics, petrology and palaeotectonics. Journal of the Geological Society of London 144: 707-715.

Bryan, W.B., Finger, L.W. and Chayes, F. 1969. Estimating proportions in petrographic mixing equations by least-squares approximation. Science 163: 926-927.

Bryan, W.B., Frey, F.A. and Thompson, G. 1977. Oldest Atlantic Seafloor: Mesozoic basalts from western North Atlantic Margin and Eastern North America. Contributions to Mineralogy and Petrology 64: 223-242.

Bugge, C. 1910. Petrographische Resultate, Der 2ten FRAM-Expedition. Report of the Second Norwegian Arctic Expedition in the FRAM, 3(22): 1-38.

Burke, K. and Kidd, W.S.F. 1980. Volcanism on Earth through Time; in The Continental Crust and Its Mineral Deposits; D.W. Strangway, ed. Geological Association of Canada Special Paper 20: 503-522.

Burke, K. 1984. Plate tectonic history of the Arctic; in Arctic Geology; reports of the 27th International Geological Congress, Moscow: 189-198.

Byerly, G. and Swanson, D.A. 1978. Invasive Columbia River basalt flows along the northwestern margin of the Columbia River Plateau, North-Central Washington. Geological Society of America Abstracts with Programs, 10(3): 98.

Cameron, B.I. 1986. The petrology, geochemistry and tectonic significance of the Permian volcanics of the Esayoo Formation, Sverdrup Basin, High Canadian Arctic. Abstract, Student Conference on Northern Studies, Ottawa, October 1986.

Camp, V.E. 1981. Geologic studies of the Columbia River Plateau: Part II. Upper Miocene basalt distribution, reflecting source locations, tectonism and drainage history in the Clearwater Embayment, Idaho. Geological Society of America Bulletin 92: 669-678.

Carey, S.W. 1955. The orocline concept in geotectonics. Royal Society of Tasmania (Proceedings) 89: 255-288.

Carmichael, I.S.E., Turner, F.J. and Verhoogen, J. 1974. Igneous Petrology. McGraw-Hill, NY, 739 p.

Carter, S.R., Evensen, N.M., Hamilton, P.J. and O'Nions, R.K. 1978. Neodymium and strontium isotope evidence for crustal contamination of continental volcanics. Science 202: 743-747.

Cas, R.A.F. and Wright, J.V. 1987. Volcanic successions, Modern and Ancient - A geological approach to processes, products and successions. Allen & Unwin, 528 p.

Christie, R.L. 1957. Geological reconnaissance of the North Coast of Ellesmere Island, Northwest Territories.

Geological Survey of Canada Paper 56-9, 40 p.

Christie, 1964. Geological reconnaissance of northeastern Ellesmere Island, District of Franklin. Geological Survey of Canada Memoir 331, 79 p.

Churkin, M. Jr., and Trexler, J.H. Jr. 1980. Circum-Arctic plate accretion - isolating part of a Pacific plate to form the nucleus of the Arctic Basin. Earth and Planetary Science Letters 48: 356-362.

Clarke, D.B. 1969. Tertiary basalts of the Baffin Bay area. Ph.D. Thesis, University of Edinburgh, 122 p.

Clarke, D.B. and Pedersen, A.K. 1976. Tertiary Volcanic Province of West Greenland; in Geology of Greenland, Escher, A. and Watt, W.S., eds., Gronlands Geologiske Undersogelse: 365-402.

Clarke, D.B. and O'Hara, M.J. 1979. Nickel, and the existence of high-MgO liquids in nature. Earth and Planetary Science Letters 44: 153-158.

Clarke, D.B., Muecke, G.K. and Pe-Piper, G. 1983. The lamprophyres of Ubekendt Ejland, West Greenland: Products of renewed partial melting or extreme differentiation? Contributions to Mineralogy and Petrology 83: 117-127.

Coish, R.A. and Taylor, L.A. 1979. The effects of cooling rate on texture and pyroxene chemistry in DSDP Leg 34 basalt: a microprobe study. Earth and Planetary Science Letters 42: 389-398.

Coombs, D.S. 1963. Trends and affinities of basaltic magmas and pyroxenes as illustrated on the diopside-olivine-silica diagram. Mineralogical Society of America Special Paper 1: 227-250.

Cox, K.G., Bell, J.D. and Pankhurst, R.J. 1979. The Interpretation of Igneous Rocks. George, Allen and Unwin Ltd., London, 450 p.

Cox, K.G. 1980. A model for flood basalt vulcanism. Journal of Petrology 21: 629-650.

Cramer, J.J. and Nesbitt, H.W. 1983. Mass-balance relations and trace-element mobility during continental weathering of various igneous rocks. Sciences Géologiques, Mémoire 73: 63-73.

DePaolo, D.J. 1981. Trace element and isotopic effects of combined wallrock assimilation and fractional crystallization. Earth and Planetary Science Letters

53: 189-202.

Devey, C.W. and Lightfoot, P.C. 1986. Volcanological and tectonic control of stratigraphy and structure in the western Deccan Traps. Bulletin Volcanologique 48: 195-207.

Dungan, M.A. and Rhodes, J.M. 1978. Residual glasses and melt inclusions in basalts from DSDP Legs 45 and 46: evidence for magma mixing. Contributions to Mineralogy and Petrology 67: 417-431.

Dutro, J.T. Jr. 1981. Geology of Alaska bordering the Arctic Ocean; in The Ocean Basins and Margins V.5: The Arctic Ocean. A.E.M. Nairn, M. Churkin Jr. and F.S. Stehli, eds. Plenum Press, New York: 21-34.

Eaton, G.P. 1982. The Basin and Range Province: Origin and tectonic significance. Annual Review of Earth and Planetary Sciences 10: 409-440.

Eggler, D.H. 1974. Effect of CO_2 on the melting of peridotite. Carnegie Institute of Washington Year Book 73: 215-224.

Elthon, D. 1984. Plagioclase buoyancy in oceanic basalts: Chemical effects. Geochimica et Cosmochimica Acta 48: 753-768.

Embry, A.F. 1986. The Mesozoic of the Sverdrup Basin. Unpublished manuscript, 10 p.

Embry, A.F. and Osadetz, K.G., in press. Stratigraphy and tectonic significance of Cretaceous volcanism in Queen Elizabeth Islands, Canadian Arctic Archipelago. Canadian Journal of Earth Sciences.

Faure, G. 1986. Principles of Isotope Geology. 2nd Edition, Wiley, 589 p.

Feilden, H.W. and de Rance, C.E. 1878. Geology of the coasts of the Arctic lands visited by the late British expedition under Sir George Nares, R.N., K.C.B., F.R.S. Quarterly Journal of the Geological Society of London 34: 556-567.

Fisher, B.F.G. 1984. Stratigraphy and structural geology of the region surrounding Bunde and Bukken Fiords, Axel Heiberg Island, Canadian Arctic; in Current Research, Part B, Geological Survey of Canada Paper 84-1B: 309-314.

Fitton, J.G. and Dunlop, H.M. 1985. The Cameroon line, West Africa, and its bearing on the origin of oceanic

and continental alkali basalt. Earth and Planetary Science Letters 72: 23-38.

Fitton, J.G. 1987. The Cameroon line, West Africa: a comparison between oceanic and continental alkaline volcanism; in Fitton, J.G. and Upton, B.G.J., eds. Alkaline Igneous Rocks. Geological Society Special Publication 30: 273-291.

Forsyth, D.A., Mair, J.A. and Fraser, I. 1979. Crustal structure of the central Sverdrup Basin. Canadian Journal of Earth Sciences 16(8): 1581-1598.

Forsyth, D.A., Morel-à-L'Huissier, P., Asudeh, I. and Green, A.G. 1986. Alpha Ridge and Iceland - Products of the same plume? Journal of Geodynamics 6: 197-214.

Fortier, Y.O. 1957. The Arctic Archipelago. Chapter 7 in Geology and Economic Minerals of Canada, Geological Survey of Canada, Economic Geology Series 1, 4th edition.

Fortier, Y.O., Blackadar, R.G., Glenister, B.F., Greiner, H.R., McLaren, D.J., McMillan, N.J., Norris, A.W., Roots, E.F., Souther, J.G., Thorsteinsson, R. and Tozer, E.T. 1963. Geology of the North-Central part of the Arctic Archipelago, Northwest Territories (Operation Franklin). Geological Survey of Canada Memoir 320, 671 p.

Foucher, J.P., LePichon, X. and Sibuet, J.G. 1982. The ocean-continent transition in the uniform lithospheric stretching model; role of partial melting in the mantle. Philosophical Transactions of the Royal Society of London A305: 27-43.

Francis, D., Ludden, J. and Hynes, A. 1983. Magma evolution in a Proterozoic rifting environment. Journal of Petrology 24: 556-582.

Fujii, T. and Scarfe, C.M. 1985. Composition of liquids coexisting with spinel lherzolite at 10 kbar and the genesis of MORBs. Contributions to Mineralogy and Petrology 90: 18-28.

Gass, I. 1970. Tectonic and magmatic evolution of the Afro-Arabian dome; in African Magmatism and Tectonics; T.N. Clifford and I.G. Gass, eds. Oliver and Boyd, Edinburgh: 285-300.

Geist, D.J., Myers, J.D. and Frost, C.D. 1988. Megacryst-bulk rocks isotopic disequilibrium as an indicator of contamination processes: The Edgecumbe Volcanic Field, SE Alaska. Contributions to Mineralogy and Petrology

99: 105-112.

Govindaraju, K. 1984. 1984 Compilation of working values and sample description for 170 International Reference Samples of mainly silicate rocks and minerals. Geostandards Newsletter 8: Special Issue.

Grantz, A., Eittreim, S. and Dinter, D.A. 1979. Geology and tectonic development of the continental margin north of Alaska. Tectonophysics 59: 263-291.

Greeley, R. 1982. The Snake River Plain, Idaho: Representative of a new category of volcanism. Journal of Geophysical Research 87: 2705-2712.

Greeley, R. 1987. The role of lava tubes in Hawaiian volcanoes; in Volcanism in Hawaii 2; R.W. Decker, T.L. Wright and P.H. Stauffer, eds. U.S. Geological Survey Professional Paper 1350: 1589-1602.

Green, D.H. 1973. Experimental melting studies on a model upper mantle composition at high pressure under water-undersaturated conditions. Earth and Planetary Science Letters 19: 37-53.

Hall, J.K. 1973. Geophysical evidence for ancient sea-floor spreading from Alpha Cordillera and Mendeleev Ridge; in Arctic Geology; M.G. Picher, ed. American Association of Petroleum Geologists Memoir 19: 542-561.

Hamilton, W. 1970. The Uralides and the motion of the Russian and Siberian Platforms. Geological Society of America Bulletin 81: 2553-2576.

Hanson, G.N. 1980. Rare earth elements in petrogenetic studies of igneous systems. Annual Review of Earth and Planetary Sciences 8: 371-406.

Harland, W.B. and Gayer, R.A. 1972. The Arctic Caledonides and earlier oceans. Geological Magazine 109: 289-364.

Harland, W.B., Gaskell, B.A., Heafford, A.P., Lind, E.K. and Perkins, P.J. 1984. Outline of Arctic post-Silurian continental displacements; in Petroleum Geology of the North European Margin. Graham and Trotman Ltd: 137-148.

Harrison, J.C. and Bally, A.W. 1988. Cross-sections of the Parry Islands Fold Belt on Melville Island, Canadian Arctic Islands. Submitted to Bulletin of the Canadian Society of Petroleum Geologists.

Hart, W.K. 1985. Chemical and isotopic evidence for mixing between depleted and enriched mantle,

northwestern U.S.A. Geochimica et Cosmochimica Acta 49: 131-144.

Hawkesworth, C.J. and Vollmer, R. 1979. Crustal contamination versus enriched mantle: 143Nd/144Nd and 87Sr/86Sr evidence from the Italian Volcanics. Contributions to Mineralogy and Petrology 69: 151-165.

Hawkesworth, C.J., Rogers, N.W., van Calsteren, P.W.C. and Menzies, M.A. 1984. Mantle enrichment processes. Nature 311: 331-335.

Helgason, J. 1983. Structural relationships and magnetostratigraphy of the volcanic succession and the Breiddalur Dyke Swarm in Reydarfjordur, Eastern Iceland. Ph.D. Thesis, Dalhousie University, Halifax, Nova Scotia, Canada, 260 p.

Hellinger, S.J. and Sclater, J.G. 1983. Some comments on two-layer extensional models for the evolution of sedimentary basins. Journal of Geophysical Research 88: 8251-8269.

Herron, E.M., Dewey, J.F. and Pitman, W.C. III. 1974. Plate tectonics model for the evolution of the Arctic. Geology 2: 377-380.

Hinz, K., Mutter, J.C., Zehnder, C.M. and the NGT Study Group. 1987. Symmetric conjugation of continent-ocean boundary structures along the Norwegian and East Greenland margins. Marine and Petroleum Geology 4: 166-187.

Holm, P.E. 1985. The geochemical fingerprints of different tectonomagmatic environments using hygromagmatophile element abundances of tholeiitic basalts and basaltic andesites. Chemical Geology 51: 303-323.

Hooper, P.R. 1982. The Columbia River basalts. Science 215: 1463-1468.

Huppert, H.E. and Sparks, R.S.J. 1985. Cooling and contamination of mafic and ultramafic magmas during ascent through continental crust. Earth and Planetary Science Letters 74: 371-386.

Irvine, T.N. 1979. Rocks whose composition is determined by crystal accumulation and sorting; in The Evolution of the Igneous Rocks, 50th Anniversary Perspective. H.S. Yoder, ed. Princeton University Press: 245-306.

Irvine, T.N. and Baragar, W.R.A. 1971. A guide to the chemical classification of the common volcanic rocks. Canadian Journal of Earth Sciences 8: 523-548.

Irving, A.J. 1978. A review of experimental studies of crystal/liquid trace element partitioning. Geochimica et Cosmochimica Acta 42: 743-770.

Irving, A.J. and Frey, F.A. 1984. Trace element abundances in megacrysts and their host basalts; constraints on partition coefficients and megacryst genesis. Geochimica et Cosmochimica Acta 48: 1201-1221.

Jackson, H.R., Forsyth, D.A. and Johnson, G.L. 1986. Oceanic affinities of the Alpha Ridge, Arctic Ocean. Marine Geology 73: 237-261.

Jackson, K.C. and Halls, H.C. 1983. A paleomagnetic study of igneous rocks of the Sverdrup Basin. Geological Association of Canada/Mineralogical Association of Canada/Canadian Geophysical Union Joint Annual Meeting, Program with Abstracts 8: 84.

James, D.E. 1981. The combined use of oxygen and radiogenic isotopes as indicators of crustal contamination. Annual Review of Earth and Planetary Sciences 9: 311-344.

Jansa, L.F. and Pe-Piper, G. 1985. Early Cretaceous volcanism on the northeastern American margin and implications for plate tectonics. Geological Society of America Bulletin 96: 83-91.

Jansa, L.F. and Pe-Piper, G. 1988. Middle Jurassic to Early Cretaceous igneous rocks along eastern North American continental margin. The American Association of Petroleum Geologists Bulletin 72: 347-366.

Jaques, A.L. and Green, D.H. 1980. Anhydrous partial melting of peridotite at 0-15 kb pressure and the genesis of tholeiitic basalts. Contributions to Mineralogy and Petrology 73: 287-310.

Jeffery, P.G. 1970. Chemical Methods of Rock Analysis. 1st Edition, Oxford-New York, Pergamon Press, 509 p.

Johnson, G.L., and Rich, J.E. 1986. A 30 million year cycle in Arctic volcanism? Journal of Geodynamics 6: 111-116.

Jollimore, W. 1986. Analyses of dyke swarms within the Sverdrup Basin, Queen Elizabeth Islands. Unpublished B.Sc. Honours Thesis, Dalhousie University, Halifax, Nova Scotia, Canada, 54 p.

Jones, P.B. 1980. Evidence from Canada and Alaska on plate tectonic evolution of the Arctic Ocean Basin. Nature

285: 215-217.

Keen, C.E. and Hyndman, R.D. 1979. Geophysical review of the continental margins of eastern and western Canada. Canadian Journal of Earth Sciences 16: 712-747.

Keen, C.E. 1985. The dynamics of rifting: deformation of the lithosphere by active and passive driving forces. Geophysical Journal of the Royal Astronomical Society 80: 95-120.

Keen, C.E. 1987. Some important consequences of lithospheric extension; in Continental Extensional Tectonics; M.P. Coward, J.F. Dewey and P.L. Hancock, eds. Geological Society Special Publication 28: 67-73.

Keen, C.E. and de Voogd, B. 1988. The continent-ocean boundary at the rifted margin off Eastern Canada: New results from deep seismic reflection studies. Tectonics 7: 107-124.

Kerr, J.W. 1981. Evolution of the Canadian Arctic Islands: a transition between the Atlantic and Arctic Ocean; in The Ocean Basins and Margins, V.5: The Arctic Ocean. A.E.M. Nairn, M. Churkin Jr. and F.G. Stehli, eds. Plenum Press, New York: 105-199.

Kille, I.C., Thompson, R.N., Morrison, M.A. and Thompson, R. F. 1986. Field evidence for turbulence during flow of basalt through conduits from southwest Mull. Geological Magazine 123(6): 693-697.

Krishnamurty, P. and Cox, K.G. 1977. Picrite basalts and related lavas from the Deccan Traps of western India. Contributions to Mineralogy and Petrology 62: 53-75.

Kushiro, I. 1973. Partial melting of garnet lherzolites from kimberlite at high pressures in Nixon P.H., ed. Lesotho Kimberlites. National Development Corporation, Lesotho: 294-299.

Langmuir, C.H., Vocke, R.D. Jr. and Hanson, G.N. 1978. A general mixing equation with applications to Icelandic basalts. Earth and Planetary Science Letters 37: 380-392.

Larochelle, A., Black, R.F. and Wanless, R.K. 1965. Paleomagnetism of the Isachsen diabasic rocks. Nature 208: 179.

Lawver, L.A. and Baggeroer, A. 1983. A note on the age of the Canada Basin. Journal of the Alaska Geological Society 2: 57-66.

Leeman, W.P. 1976. Petrogenesis of McKinney (Snake River) olivine tholeiite in light of rare-earth element and Cr/Ni distributions. Geological Society of America Bulletin 87: 1582-1586.

Leeman, W.P., Vitaliano, C.J. and Prinz, M. 1976. Evolved lavas from the Snake River Plain: Craters of the Moon National Monument, Idaho. Contributions to Mineralogy and Petrology 56: 35-60.

LeRoex, A.P., Dick, H.J.B., Erlank, A.J., Reid, A.M., Frey, F.A. and Hart, S.R. 1983. Geochemistry, mineralogy and petrogenesis of lavas erupted along the southwest Indian Ridge between the Bounvet triple junction and 11 degrees east. Journal of Petrology 24: 267-318.

Leterrier, J., Maury, R., Thonon, P., Girard, D. and Marchal, M. 1982. Clinopyroxene composition as a method of identification of magmatic affinities of paleovolcanic series. Earth and Planetary Science Letters 59: 139-154.

Long, P.E. 1978. Characterization and recognition of intraflow structures, Grande Ronde Basalt. RHO-BWI-LD-10, Rockwell Hanford Operations, Richland, Washington, 74 p.

Long, P.E. and Wood, B.J. 1986. Structures, textures and cooling histories of Columbia River basalt flows. Geological Society of America Bulletin 97: 1144-1155.

Loughnan, F.C. 1969. Chemical weathering of the silicate minerals. American Elsevier Publishing Company, New York, 154 p.

Ludden, J., Gélinas, L. and Trudel, P. 1982. Archean metavolcanics from the Rouyn-Noranda district, Abitibi Greenstone Belt, Québec, 2. Mobility of trace elements and petrogenetic constraints. Canadian Journal of Earth Sciences 19: 2276-2287.

Mackay, R.M. 1981. Whole-rock analysis using the electron microprobe. Unpublished B.Sc. (Honours) Thesis, Dalhousie University, Halifax, Canada, 84 p.

Manson, V. 1967. Geochemistry of basaltic rocks: Major elements; in Basalts. H.H. Hess and A. Poldevaart, eds. Interscience, John Wiley and Sons, New York, 862 p.

Mantovani, M.S.M., Marques, L.S., De Sousa, M.A., Civetta, L., Atalla, L. and Innocenti, F. 1985. Trace element and strontium isotope constraints on the origin and evolution of Paraŋa continental flood basalts of Santa

Catarina State. Journal of Petrology 26: 187-209.

Marsh, J.S. 1987. Basalt geochemistry and tectonic discrimination within continental flood basalt provinces. Journal of Volcanology and Geothermal Research 32: 35-49.

Mayr, U., Trettin, H.P. and Embry, A.F. 1982a. Preliminary geological map and notes, Tanquary Fiord area, District of Franklin (NTS 340D). Geological Survey of Canada Open File 834, 31 p.

Mayr, U., Trettin, H.P. and Embry, A.F. 1982b. Preliminary geological map and notes, Clements Markham Inlet and Robeson Channel map areas, District of Franklin (NTS 120E, F, G). Geological Survey of Canada Open File 833, 40 p.

McDonough, W.F., McCulloch, M.T. and Sun, S.S. 1985. Isotopic and geochemical systematics in Tertiary-Recent basalts from southeastern Australia and implications for the evolution of the sub-continental lithosphere. Geochimica et Cosmochimica Acta 49: 2051-2067.

McKenzie, D. 1978. Some remarks on the development of sedimentary basins. Earth and Planetary Science Letters 40: 25-32.

McKenzie, D. 1984. The generation and compaction of partially molten rock. Journal of Petrology 25: 713-765.

McMillan, N.J. and Dungan, M.A. 1986. Magma mixing as a petrogenetic process in the development of the Taos Volcanic Field, New Mexico. Journal of Geophysical Research 91: 6029-6045.

McQueen, J. 1967. Some methods for classification and analysis of multivariate observations. 5th Berkeley Symposium on Mathematics, Statistics and Probability 1: 281-298.

McWhae, J.R. 1986. Tectonic history of Northern Alaska, Canadian Arctic and Spitsbergen regions since Early Cretaceous. American Association of Petroleum Geologists Bulletin 70: 430-350.

Meneley, R.A., Henao, D. and Merritt, R.K. 1975. The northwest margin of the Sverdrup Basin; in Canada's continental margins and offshore petroleum exploration. C.J. Yorath, E.R. Parker and D.J. Glass, eds. Canadian Society of Petroleum Geologists Memoir 4: 531-544.

Menzies, M. and Murthy, V.R. 1980. Enriched mantle: Nd and Sr isotopes in diopsides from kimberlite nodules. Nature 283: 634-636.

Menzies, M.A., Leeman, W.P. and Hawkesworth, C.J. 1984. Geochemical and isotopic evidence for the origin of continental flood basalts with particular reference to the Snake River Plain, Idaho, U.S.A. Philosophical Transactions of the Royal Society of London A310: 643-660.

Mohr, P. 1978. Musings on continental rifts in Petrology and Geochemistry of Continental Rifts. Neumann, E-R. and Ramberg, I.B., eds. Nato Advanced Study Institute, D. Reidel Publishing: 293-309.

Morel, P. and Irving, E. 1978. Tentative paleocontinental maps for the Early Phanerozoic and Proterozoic. Journal of Geology 86(5): 535-561.

Mutter, J.C., Buck, W.R. and Zehnder, C.M. 1988. Convective partial melting 1. A model for the formation of thick basaltic sequences during the initiation of spreading. Journal of Geophysical Research 93: 1031-1048.

Myers, J.D., Sinha, A.K. and Marsh, B.D. 1984. Assimilation of crustal material by basaltic magma: Strontium isotopic and trace element data from the Edgecumbe volcanic field, SE Alaska. Journal of Petrology 25: 1-26.

Myers, J.D., Marsh, B.D. and Sinha, A.K. 1985. Strontium isotopic and selected trace element variations between two Aleutian volcanic centers (Adak and Atka): implications for the development of arc volcanic plumbing systems. Contributions to Mineralogy and Petrology 91: 221-234.

Mysen, B.O. and Boettcher, A.L. 1975. Melting of a hydrous mantle: II, Geochemistry of crystals and liquids formed by anatexis of mantle peridotite at high pressures and temperatures as a function of controlled activities of water, hydrogen, and carbon dioxide. Journal of Petrology 16: 549-593.

Nassichuk, W.W. and Christie, R.L. 1969. Upper Paleozoic and Mesozoic stratigraphy in the Yelverton Pass region, Ellesmere Island, District of Franklin. Geological Survey of Canada Paper 68-31, 31 p.

Nassichuk, W.W. and Davies, G.R. 1980. Stratigraphy and sedimentation of the Otto Fiord Formation. Geological Survey of Canada Bulletin 286, 87 p.

Nesbitt, H.W. 1979. Mobility and fractionation of rare earth elements during weathering of a granodiorite. Nature 279: 206-210.

Neumann, H., Mead, J. and Vitaliano, C.J. 1954. Trace element variations during fractional crystallization as calculated from the distribution law. Geochimica et Cosmochimica Acta 6: 90-99.

Newman, G.W., Mull, C.G. and Watkins, N.D. 1977. Northern Alaskan paleomagnetism, plate rotation, and tectonics in the relationship of plate tectonics to Alaskan geology and resources. Proc. Alaska Geological Society Symposium, C1-C7.

Nielsen, T.F.D. 1987. Tertiary alkaline magmatism in East Greenland: a review; in Alkaline Igneous Rocks; J.G. Fitton and B.G.J. Upton, eds. Geological Society Special Publication 30: 489-515.

Norry, M.J. and Fitton, J.G. 1983. Compositional differences between oceanic and continental basic lavas and their significance; in Continental Basalts and Mantle Xenoliths. C.J. Hawkesworth and M.J Norry, eds. Shiva Publishing Ltd., Nantwich: 5-19.

O'Hara, M.J. 1968. The bearing of phase equilibria studies in synthetic and natural systems on the origin of basic and ultrabasic rocks. Earth Science Reviews 4: 69-133.

O'Hara, M.J. 1977. Geochemical evolution during fractional crystallization of a periodically refilled magma chamber. Nature 266: 503-507.

O'Hara, M.J. and Mathews, R.E. 1981. Geochemical evolution in an advancing, periodically replenished, periodically tapped, continuously fractionated magma chamber. Journal of the Geological Society of London 138: 237-277.

Oldow, J.S., Ave Lallemant, H.G., Julian, F.E. and Seidensticker, C.M. 1987. Ellesmerian (?) and Brookian deformation in the Franklin Mountains, northeastern Brooks Range, Alaska, and its bearing on the origin of the Canada Basin. Geology 15: 37-41.

Oliver, H., Ewing, M. and Press, F. 1955. Crustal structure of the Arctic regions from the Lg phase. Geological Society of America Bulletin 66: 1063-1074.

O'Nions, R.K., Carter, S.R., Evensen, N.M. and Hamilton, P.J. 1979. Geochemical and cosmochemical applications of Nd isotope analysis. Annual Review of Earth and

Planetary Sciences 7: 11-38.

Osadetz, K.G. 1982. Eurekan structures of the Ekblaw Lake area, Ellesmere Island, Canada; in Embry, A.F. and Balkwill, H.R., eds., Arctic Geology and Geophysics, Canadian Society of Petroleum Geologists Memoir 8: 219-232.

Osadetz, K.G. and Moore, P.R. Basic volcanics in the Hassel Formation (mid-Cretaceous) and associated intrusives, Ellesmere Island, District of Franklin, Northwest Territories, Canada. Geological Survey of Canada Paper in press.

Pearce, J.A. and Cann, J.R. 1973. Tectonic setting of basic volcanic rocks determined using trace element analysis. Earth and Planetary Science Letters 19: 290-300.

Pearce, J.A. and Norry, M.J. 1979. Petrogenetic implications of Ti, Zr, Y and Nb variations in volcanic rocks. Contributions to Mineralogy and Petrology 69: 33-47.

Pearce, J.A. 1983. Role of sub-continental lithosphere in magma genesis at active continental margins; in Continental Basalts and Mantle Xenoliths. C.J. Hawkesworth and M.J. Norry, eds. Shiva Publishing Ltd., Nantwich: 230-249.

Perrodon, A. 1985. Géodynamique Pétrolière. Elf Aquitaine et Masson, Pau et Paris, 385 p.

Plauchut, B.D. 1971. Geology of the Sverdrup Basin. Bulletin of Canadian Petroleum Geology 19: 659-679.

Presnall, D.C., Dixon, J.R., O'Donnell, T.H. and Dixon, S. A. 1979. Generation of mid-ocean ridge tholeiites. Journal of Petrology 20: 3-35.

Richard, P., Shimizu, N. and Allègre, C.J. 1976. $^{143}Nd/^{146}Nd$ a natural tracer: an application to oceanic basalts. Earth and Planetary Science Letters 31: 269-278.

Ricketts, B.D. 1985. Volcanic breccias in the Isachsen Formation near Strand Fiord, Axel Heiberg Island, District of Franklin; in Current Research Part A, Geological Survey of Canada Paper 85-1A: 609-612.

Ricketts, B.D., Osadetz, K.G. and Embry, A.F. 1985. Volcanic style in the Strand Fiord Formation (Upper Cretaceous), Axel Heiberg Island, Canadian Arctic Archipelago. Polar Research 3: 107-122.

Roberts, D.G., Backman, J., Morton, A.C., Murray, J.W. and Keene, J.B. 1984. Evolution of volcanic rifted margins: synthesis of Leg 81 results on the west margin of the Rockall Plateau. Initial Reports DSDP 81: 883-911.

Ross, M.E. 1986. Flow differentiation, phenocryst alignment and compositional trends within a dolerite dike at Rockport, Massachusetts. Geological Society of America Bulletin 97: 232-240.

Sakuyama, M. 1981. Petrological study of the Myoko and Kurohime volcanoes, Japan: Crystallization sequence and evidence for magma mixing. Journal of Petrology 22: 553-583.

Salveson, J.O. 1978. Variations in the geology of rift basins - A tectonic model. Paper presented at the Rio Grande Rift Symposium, Santa Fe, N.M., October 1978.

Saunders, A. 1988. Putting continents asunder. Nature 332: 679-680.

Schei, P. 1904. Preliminary account of the geological investigations made during the Second Norwegian Polar Expedition in the FRAM. Appendix I in New Land, V.II, by Otto Sverdrup, 1904. London, Green & Co.

Scotese, C.R., Bambach, R.K., Barton, C., Van der Voo, R. and Ziegler, A.M. 1979. Paleozoic base maps. Journal of Geology 87(3): 217-278.

Sengör, A.M.C. and Burke, K. 1978. Relative timing of rifting and volcanism on earth and its tectonic implications. Geophysical Research Letters 5: 419-421.

Shaw, D.M. 1970. Trace element fractionation during anatexis. Geochimica et Cosmochimica Acta 34: 237-243.

Singer, B.S. and Kudo, A.M. 1986. Assimilation-fractional crystallization of Poldavera Group rocks in the Northwestern Jemez Volcanic Field, New Mexico. Contributions to Mineralogy and Petrology 94: 374-386.

Smith, A.G., Hurley, A.M. and Briden, J.C. 1981. Phanerozoic palaeocontinental world maps. Cambridge University Press, Cambridge, 102 pp.

Sobczak, L.W. and Weber, J.R. 1973. Crustal structure of Queen Elizabeth Islands and polar continental margin, Canada in Arctic Geology, American Association of Petroleum Geologists Memoir 19: 517-525.

Sobczak, L.W. and Overton, A. 1984. Shallow and deep crustal structure of the western Sverdrup Basin, Arctic Canada. Canadian Journal of Earth Sciences 21(8): 902-919.

Soper, N.J., Dawes, P.R. and Higgins, A.K. 1982. Cretaceous-Tertiary magmatic and tectonic events in North Greenland and the history of adjacent ocean basins; in Nares Strait and the Drift of Greenland: a Conflict in Plate Tectonics. P.R. Dawes and J.W. Kerr, eds. Meddelelser om Gronland, Geoscience 8: 205-220.

Spry, A. 1962. The origin of columnar jointing, particularly in basalt flows. Geological Society of Australia Journal 8(2): 191-216.

Srivastava, S.P. 1985. Evolution of the Eurasian Basin and its implications to the motion of Greenland along Nares Strait. Tectonophysics 114: 29-53.

Srivastava, S.P. and Tapscott, C.R. 1986. Plate kinematics of the North Atlantic; in Vogt, P.R. and Tucholke, B.E. eds. The Geology of North America, Volume M, The Western North Atlantic, Geological Society of America.

Steele, K.F. and Ragland, P.C. 1976. Model for the closed system fractionation of a dike formed by two pulses of dolerite magma. Contributions to Mineralogy and Petrology 57: 305-316.

Stephenson, R.A., Embry, A.F., Nakiboglu, S.M. and Hastaoglu, M.A. 1987. Rift-initiated Permian to Early Cretaceous subsidence of the Sverdrup Basin; in Sedimentary Basins and Basin-Forming Mechanisms. Canadian Society of Petroleum Geologists Memoir 12: 213-231.

Stolper, E. and Walker, D. 1980. Melt density and the average composition of basalt. Contributions to Mineralogy and Petrology 74: 7-12.

Swanson, D.A. 1967. Yakima basalt of the Tieton River area, south-central Washington. Geological Society of America Bulletin 78: 1077-1110.

Swanson, D.A., Wright, T.L. and Helz, R.T. 1975. Linear vent systems and estimated rates of magma production and eruption for the Yakima basalt on the Columbia Plateau. American Journal of Science 275: 877-905.

Swanson D.A. and Wright, T.L. 1980. The regional approach to studying the Columbia River Basalt Group. Geological Society of India Memoir 3: 58-80.

Sweeney, J.F. 1976. Evolution of the Sverdrup Basin, Arctic Canada. Tectonophysics 36: 181-196.

Sweeney, J.F. 1977. Subsidence analysis of the Sverdrup Basin. Geological Society of America Bulletin 88: 41-48.

Sweeney, J.F. 1985. Comments about the age of the Canada Basin. Tectonophysics 114: 1-10.

Sweeney, J.F. and Weber, J.R. 1986a. Progress in understanding the age and origin of the Alpha Ridge, Arctic Ocean. Journal of Geodynamics 6: 237-244.

Sweeney, J.F. 1986b. Corridor G: Somerset Island to Canada Basin, Canadian Arctic. Centennial Continent/Ocean Transect #11, Geological Society of America.

Tailleur, I.L. 1973. Probable rift origin of the Canada Basin, Arctic Ocean; in Arctic Geology. M.G. Pitcher, ed. American Association of Petroleum Geologists Memoir 19: 526-535.

Tailleur, I.L. and Brosgé, W.P. 1970. Tectonic history of northern Alaska; in Proceedings of the Geological Seminar on the North Slope of Alaska, Palo Alto, CA. W.L. Adkinson and M.M. Brosge, eds. AAPG Pacific Section: E1-E19.

Takahashi, E. and Kushiro, I. 1983. Melting of dry peridotite at high pressures and basalt magma genesis. American Mineralogist 68: 859-879.

Tarney, J. and Weaver, B.L. 1987. Mineralogy, petrology and geochemistry of the Scourie dykes: Petrogenesis and crystallization processes in dykes intruded at depth; in Evolution of the Lewisian and Comparable Precambrian High Grade Terains; R.G. Park and J. Tarney, eds. Geological Society Special Publication 27: 217-233.

Taylor, H.P. Jr. 1980. The effects of assimilation of country rocks by magmas on $^{18}O/^{16}O$ and $^{87}Sr/^{86}Sr$ systematics in igneous rocks. Earth and Planetary Science Letters 47: 243-254.

Taylor, P.T., Kovacs, L.C., Vogt, P.R. and Johnson, G.L. 1981. Detailed aeromagnetic investigation of the Arctic Basin. Journal of Geophysical Research 86: 6323-6333.

Taylor, S.R. and Gorton, M.P. 1977. Geochemical application of spark source mass spectrography - III. Element sensitivity, precision and accuracy. Geochimica et

Cosmochimica Acta 41: 1375-1380.

Taylor, S.R. and McLennan, S.M. 1985. The Continental Crust: Its Composition and Evolution. Blackwell Scientific Publications, 312 pp.

Thompson, R.N. 1982. Magmatism of the British Tertiary Volcanic Province. Scottish Journal of Geology 18: 49-107.

Thorsteinsson, R. 1974. Carboniferous and Permian stratigraphy of Axel Heiberg Island and western Ellesmere Island, Canadian Arctic Archipelago. Geological Survey of Canada Bulletin 224, 115 p.

Thorsteinsson, R. and Trettin, H.P. 1971. Geology, Tanquary Fiord, District of Franklin. Geological Survey of Canada Map 1306A, 1: 250,000.

Tomkieff, S.I. 1940. The basalt lavas of the Giant's Causeway, District of Northern Ireland. Bulletin of Volcanology 6: 89-143.

Tormey, D.R., Grove, T.L. and Bryan, W.B. 1987. Experimental petrology of normal MORB near the Kane Fracture Zone: 22o-25o N., mid-Atlantic ridge. Contributions to Mineralogy and Petrology 96: 121-139.

Tozer, E.T. 1963. Mesozoic and Tertiary stratigraphy, western Ellesmere Island and Axel Heiberg Island, District of Franklin. Geological Survey of Canada Paper 63-30, 38 p.

Tozer, E.T. and Thorsteinsson, R. 1964. Western Queen Elizabeth Islands, Arctic Archipelago. Geological Survey of Canada Memoir 332, 242 p.

Trettin, H.P. 1971. Geology of lower Paleozoic formations, Hazen Plateau and southern Grant Land Mountains, Ellesmere Island, Arctic Archipelago. Geological Survey of Canada Bulletin 203, 134 p.

Trettin, H.P. and Balkwill, H.R. 1979. Contributions to the tectonic history of the Innuitian Province, Arctic Canada. Canadian Journal of Earth Sciences 16(3): 748-769.

Trettin, H.P., Mayr, U., Embry, A.F. and Christie, R.L. 1982. Preliminary geological map and notes, part of Lady Franklin Bay map area, District of Franklin (NTS 120C). Geological Survey of Canada Open File 834, 31 p.

Trettin, H.P. 1987. Pearya: a composite terrane with

Caledonian affinities in northern Ellesmere Island. Canadian Journal of Earth Sciences 24: 224-245.

Trettin, H.P. and Parrish, R. 1987. Late Cretaceous bimodal magmatism, northern Ellesmere Island: isotopic age and origin. Canadian Journal of Earth Sciences 24: 257-265.

Trettin, H.P. 1988. Early Namurian (or older) alkali basalt in the Borup Fiord Formation, northern Axel Heiberg Island, Arctic Canada. Geological Survey of Canada Paper 88-1D: 21-26.

Trettin, H.P. Tectonic Framework; in Innuitian Orogen and Arctic Platform: Canada and Greenland. H.P. Trettin (ed); Geological Survey of Canada, Geology of Canada No. 3; in press. (Also Geological Society of America, The Geology of North America, Volume E).

Treuil, M. and Joron, J.L. 1976. Etude géochimique des éléments en traces dans le magmatisme de l'Afar. Implications pétrogénétiques et comparaison avec le magmatisme de l'Islande et de la dorsale médio-atlantique; in Afar Between Continental and Oceanic Rifting. A. Pilger and A. Roster, eds. Inter-Union Commission on Geodynamics Scientific Report 16: 26-79.

Troelsen, J.C. 1950. Contributions to the geology of Northwest Greenland, Ellesmere Island and Axel Heiberg Island. Meddelelser om Gronland 149(7), 85 p.

Van Wagoner, N.A., Williamson, M-C., Robinson, P.T. and Gibson, I.L. 1986. First samples of acoustic basement recovered from the Alpha Ridge, Arctic Ocean: New constraints for the origin of the ridge. Journal of Geodynamics 6: 177-196.

Villemant, B., Jaffrezic, H., Joron, J-L. and Treuil, M. 1981. Distribution coefficients of major and trace elements; fractional crystallizaton in the alkali basalt series of Chaine des Puys (Massif Central, France). Geochimica et Cosmochimica Acta 45: 1997 -2016.

Vogt, P.R., Taylor, P.T., Kovacs, L.C. and Johnson, G.L. 1982. The Canada Basin: Aeromagnetic constraints on structure and evolution. Tectonophysics 89: 295-336.

Volborth, A. 1969. Elemental Analysis in Geochemistry. Elsevier, Amsterdam-New York, 373 p.

Walker, D., Shibata, T. and DeLong, S.E. 1979. Abyssal tholeiites from the Oceanographer Fracture Zone II. Phase equilibria and mixing. Contributions to

Mineralogy and Petrology 70: 111-125.

Walker, G.P.L. 1972. Compound and simple lava flows and flood basalts. Bulletin Volcanologique 35: 579-590.

Watson, E.B., Ben Othman, D., Luck, J-M. and Hofmann, A.W. 1987. Partitioning of U, Pb, Cs, Yb, Hf, Re and Os between chromian diopsidic pyroxene and haplobasaltic liquid. Chemical Geology 62: 191-208.

Weaver, B.L. and Tarney, J. 1983. Chemistry of the sub-continental mantle: Inferences from Archean and Proterozoic dykes and continental flood basalts; in Continental Basalts and Mantle Xenoliths. C.J. Hawkesworth and M.J. Norry, eds. Shiva Publishing Ltd., Nantwich: 209-229.

Weber, J.R. 1986. The Alpha Ridge: gravity, seismic and magnetic evidence for a homogeneous mafic crust. Journal of Geodynamics 6: 117-136.

Wendlandt, R.F. and Eggler, D.H. 1980. The origins of potassic magmas: I, melting relations in the systems $KAlSiO_4$-Mg_2SiO_4-SiO_2 amd $KAlSiO_4$-MgO-SiO_2-CO_2 to 30 kilobars. American Journal of Science 280: 385-420.

Wernicke, B.P., Christiansen, R.L., England, P.C and Sonder, L.J. 1987. Tectonomagmatic evolution of Cenozoic extension in the North American Cordillera; in Continental Extensional Tectonics; M.P. Coward, J.F. Dewey and P.L. Hancock, eds. Geological Society Special Publication 28: 67-73.

White, R.S., Spence, G.D., Fowler, S.R., McKenzie, D.P., Westbrook, G.K. and Bowen, A.N. 1987. Magmatism at rifted continental margins. Nature 330: 439-444.

Wilkinson, J.F.G. and Binns, R.A. 1977. Relatively iron -rich lherzolite xenoliths of the Cr-diopside suite: A guide to the primary nature of anorogenic tholeiitic andesite magmas. Contributions to Mineralogy and Petrology 65: 199-212.

Williams, L.A.J. 1978. Physical aspects of magmatism in continental rifts; in Petrology and Geochemistry of Continental Rifts. Neumann, E-R. and Ramberg, I.B., eds. Nato Advanced Study Institute, D. Reidel Publishing: 193-222.

Williamson, M-C. and Van Wagoner, N.A. 1985. Volcanism at the Alpha Ridge and in the northwest Sverdrup Basin: is there a case for a common origin? Geological Association of Canada/Mineralogical Association of Canada Program with Abstracts 10: A69.

Winchester, J.A. and Floyd, P.A. 1977. Geochemical discrimination of different magma series and their differentiation products using immobile elements. Chemical Geology 20: 325-343.

Wood, D.A. 1980. The application of a Th-Hf-Ta diagram to problems of tectonomagmatic classification and to establishing the nature of crustal contamination of basaltic lavas of British Tertiary volcanic province. Earth and Planetary Science Letters 50: 11-30.

Wörner, G., Zindler, A., Staudigel, H. and Schmincke, H-U. 1986. Sr, Nd and Pb isotope geochemistry of Tertiary and Quaternary alkaline volcanics from West Germany. Earth and Planetary Science Letters 79: 107-119.

Wright, T.L. 1984. Origin of basalt plateaus, with emphasis on flood basalts; in Growth and Evolution of Volcanic Edifices. R.M. Easton and M. Gasswinkler, eds. Geological Association of Canada Short Course Notes 4: 43-60.

Wyers, G.P. and Barton, M. 1987. Geochemistry of a transitional ne-trachybasalt-Q-trachyte lava series from Patmos (Dodecanesos), Greece: Further evidence for fractionation, mixing and assimilation. Contributions to Mineralogy and Petrology 97: 279-291.

Wyllie, P.J. 1984. Constraints imposed by experimental petrology on possible and impossible magma sources and products. Philosophical Transactions of the Royal Society of London A310: 439-456.

Wynne, P.J., Irving, E. and Osadetz, K.G. Paleomagnetic results from the mid-Cretaceous Sverdrup Basin tholeiites. In press, Canadian Journal of Earth Sciences.

Young, F.G., Myhr, D.W. and Yorath, C.J. 1976. Geology of the Beaufort-Mackenzie Basin. Geological Survey of Canada Paper 76-11, 65 p.

Yuen, D.A. and Fleitout, L. 1985. Thinning of the lithosphere by small-scale convective destabilization. Nature 313: 125-128.

Zindler, A. and Hart, S. 1986. Chemical Geodynamics. Annual Review of Earth and Planetary Sciences 14: 493-571.